Third Symposium

NAVAL
HYDRODYNAMICS

HIGH-PERFORMANCE SHIPS

STANLEY W. DOROFF
EDITOR

Office of Naval Research
Department of the Navy
ACR-65
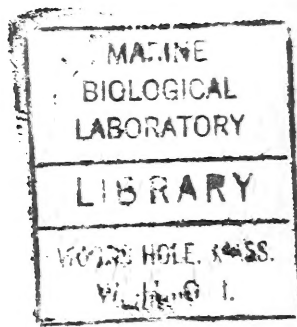
Third Symposium on

NAVAL HYDRODYNAMICS

HIGH-PERFORMANCE SHIPS

Sponsored by the

OFFICE OF NAVAL RESEARCH

and the

NETHERLANDS SHIP MODEL BASIN

September 19–22, 1960

Scheveningen, Netherlands

ACR-

OFFICE OF NAVAL RESEARCH—DEPARTMENT OF THE NAVY

Washington, D.C.

FOREWORD

In March 1960, Captain B. F. Bennett, USN of the Office of Naval Research London Branch Office contacted through the American Embassy in The Hague the Central Organization for Applied Scientific Research in The Netherlands (T.N.O.). As a result of this contact the Netherlands Ship Model Basin (NSMB), one of the institutes administered by this organization, was invited by Mr. Ralph D. Cooper, Head, Fluid Dynamics Branch, Office of Naval Research, to co-sponsor the third Symposium.

Although time for preparation was rather short the NSMB enthusiastically accepted this invitation.

The Symposium, dedicated by Dr. Th. Von Karman to Sir Thomas Havelock in recognition of his valuable contributions to naval hydrodynamics, was held at The Hague in September 1960. It was devoted to high-performance ships, such as hydrofoil boats, ground effect machines, deep diving submarines, semisubmerged ships and other special or unconventional configurations. This timely subject was of great interest to both hydrodynamicists and shipbuilders. Though the operational value of these high-performance ships appeals primarily to naval interests, it was in addition very refreshing for practical shipbuilders who deal with problems concerning commercial ships.

The size, speed and type of ships that will be used within the near future is difficult to predict. To face the possibilities within our present day technological abilities was the aim of this Symposium. In this respect the Symposium can be qualified as very successful.

It is my privilege to express the sponsors' thanks to those who have contributed to the success of the Symposium: to Professor L. Troost and Dr. Th. J. Killian who presented the addresses of welcome to the meeting, the first on behalf of the Central Organization for Applied Scientific Research in the Netherlands, the second on behalf of the USN Office of Naval Research; to the Chairmen of the Sections; to the authors and those who took part in the discussions; and to those organizations and companies who participated in demonstrations with various types of hydrofoilboats on the river "New Waterway" at Rotterdam and in front of Scheveningen Harbor, namely:

Hydrofoilboat "Sea Wings," designed and demonstrated by Dynamic Developments Inc., for the U.S. Navy;

Hydrofoilboat "Waterman" demonstrated by Aquavion Holland N. V.;

U.S. Navy Hydrofoilboat "High Pockets" developed by Baker Manufacturing Company for the U.S. Navy;

Hydrofoilboat "Shellfoil" designed by Supramar A. G.

Thanks are also due to Lips Ltd. at Drunen for the kind reception during the excursion to their Propeller Works.

The tattoo of the Marine Band of the Royal Netherlands Navy, the cocktail party given by VADM. A. H. J. van der Schatte Olivier, Flag Officer Material, Royal Netherlands Navy and the dinner speech by VADM. L. Brouwer, Chief of Naval Staff, Royal Netherlands Navy were Dutch contributions which added to the success of the social part of the meeting.

I should also like to express our gratitude towards the Board of Directors and the Staff of the Netherlands Ship Model Basin for their active help in organizing this Symposium in such a short time.

Finally I would like to add my personal thanks to those of the Board of Directors of the NSMB to the Office of Naval Research for the confidence put in our organization and the help and close cooperation we enjoyed during the preparation of the Symposium.

Wageningen, May 1962
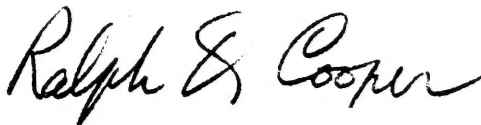Prof. Dr. Ir. W.P.A. van Lammeren
Director NSMB

PREFACE

This Symposium is the third in a series, each of which has been concerned with various aspects of Naval Hydrodynamics. The first (held in September 1956) presented critical surveys of those areas of Hydrodynamics that are of significance in naval science. Subsequent meetings were to be devoted to one or more topics selected on the basis of importance and need for research stimulation, or of particular current interest. In keeping with this objective, the second symposium (August 1958) had for its dual theme the areas of hydrodynamic noise and cavity flow.

Still continuing with the original plan, the present symposium selected for its theme the area of high-performance ships, thus emphasizing among other things the interest in the current problems and latest accomplishments associated with hydrofoil craft and ground effect machines.

The international flavor of these meetings has been preserved and, in fact, enhanced in the present case by virtue of the setting, the participation, and most particularly by the joint sponsorship by the Netherlands Ship Model Basin and the U.S. Office of Naval Research.

The background, objectives, and hopes for this meeting are more than adequately described in the speeches of welcome by Professor Troost and Dr. Killian, the dedication address by Dr. von Karman, and the foreword to this volume by Professor van Lammeren. Little remains to be said other than to echo Professor van Lammeren's expressions of gratitude to all those who contributed so much to the success of this symposium. However, taking the liberty of speaking for both the Office of Naval Research as well as the international scientific community of hydrodynamicists, I should again like to express our deepest appreciation to Professor van Lammeren and the Netherlands Ship Model Basin for their efficiency and care in managing the many varied aspects of this symposium.

Ralph D. Cooper

RALPH D. COOPER, Head
Fluid Dynamics Branch
Office of Naval Research

Sir Thomas Havelock

DEDICATION TO SIR THOMAS HAVELOCK

Theodore von Karman
Advisory Group for Aeronautical Research and Development
Paris

It is a great honor and a pleasure for me to give this address which dedicates this Third Symposium on Naval Hydrodynamics to Sir Thomas H. Havelock. Unfortunately my knowledge on wave mechanics, which was the main domain to which Sir Thomas made classical contributions, is restricted to the fundamentals. However, it is a remarkable coincidence that in the first half of our century aerodynamics and naval hydrodynamics made analogous progress, and this encourages me to talk to you on the contributions of T. H. Havelock at least from the viewpoint of an interested amateur. Also I had the good luck to obtain the support and assistance of excellent specialists through the good services of my friend J. G. Wenzel, Vice-President, General Dynamics Corporation. I would like to express my thanks to him, to Mr. Earl Uram of the General Dynamics Electric Boat Division, to Dr. Paul Wyers of Convair, and to several members of the U.S. Navy Bureau of Weapons and of the David Taylor Model Basin for helping me to obtain the necessary information. Dr. John Vannucci, Technical Information Officer of AGARD with the assistance of Mr. Francis H. Smith, Librarian, Royal Aeronautical Society, furnished me a complete list of Sir Thomas' publications.

Sir Thomas Henry Havelock was born in 1877; he is four years my senior. Incidentally we are both unmarried; according to Francis Bacon, to no wife the next best is a good wife. Sir Thomas published his first paper in 1903; the first paper published in my Collected Works is from the year 1902.

The list of the scientific papers published by Sir Thomas Havelock contains 83 items; the last item appeared in 1958. The first eight publications refer mostly to general problems of wave propagation, as for example the "Mathematical analysis of wave propagation in isotropic space at p dimensions" (Proc. London Math. Soc., 1904) or "Wave fronts considered as the characteristics of partial differential equations" (ibidem, 1904), but also to investigations in quite different fields of application, like "The dispersion of double refraction in relation to crystal structure" (Proc. Roy. Soc., 1907).

The first investigation which has relation to the problem of ship waves is his paper published in 1908: "The propagation of groups of waves in dispensive media, with application to waves on water produced by a traveling disturbance" (Proc. Roy. Soc., 1908). Then the next year Sir Thomas first called the child by its proper name: "The wave-making resistance of ships: a theoretical and practical analysis" (Proc. Roy. Soc., 1909). However his broad interest in applied mathematics and theoretical physics remained to occupy his attention at least until about 1930. We find in the list—in between papers dealing with hydrodynamics and wave resistance—dissertations like "The dispersion of electric double refraction" (Phys. Rev., 1909) and "Optical dispersion and selective reflection with application to infrared natural frequencies" (Proc. Roy. Soc., 1929).

Let us briefly review the fundamental principles of ship resistance as they were established by Froude.

Froude divided the total resistance into "frictional" and "residual" resistance. The computation of frictional resistance was based on experiments with towed flat planks and was assumed clearly dependent on viscosity and the roughness of the surface. Thus the frictional coefficient for a surface of given roughness was assumed to be a given function of the Reynolds number.

On the other hand the residual-resistance coefficient was assumed to be unaffected by viscosity and to satisfy the similarity law for an incompressible, nonviscous fluid with a free surface. From this similarity law it follows that the coefficient of the residual resistance is a function of the Froude number F only.

We have to note that in fact the residual resistance includes not only the wave-making and eddy-making resistances, but all interaction effects and especially the difference between the true frictional resistance of the ship and the frictional resistance of a flat plank of the same surface. Thus the residual resistance cannot be expected to be actually free of viscosity effects as was assumed by Froude and likewise in the conventional practice in naval architecture.

Sir Thomas Havelock is one of those rare combinations of an extremely astute mathematician with a feeling and understanding for the application of mathematics to practical ends. He is the major contributor to the theoretical hydrodynamics involved in the calculation of the resistance due to the generation of waves by moving bodies, either on the surface or submerged. Over the years, since 1908, he has published in excess of 40 papers in the field, and it is only conjecture how many publications in the field were instigated by his findings and contributions.

One of his major contributions, and, interestingly, the first one that he made to the field, was in 1908 in which he extended the work of Lord Kelvin concerning the waves produced by traveling point disturbances. Essentially, he considered the waves generated by a disturbance as a simple group or aggregate of wave trains expressed by a Fourier integral. He was able to obtain the solution for the wave group for any depth of the fluid rather than the infinite depth of Kelvin's theory. He also found that the significance of finite depth was to introduce a critical velocity above which the wave crests emanating from the source change their character from convex to concave. At the critical velocity, the transverse and divergent waves coincide and the resultant wave is normal to the path of the disturbance. This finding is completely analogous to a situation which exists in high-speed aerodynamics. As early as then, although he didn't realize it, he had developed an insight into the analogy between the shallow depth water waves generated by bodies and their shock wave patterns at supersonic speeds, which underlies modern day water table experiments.

Evidently motivated by his solution and its application to ship resistance calculations, Sir Thomas Havelock embarked on concentrated efforts in this field. Many of his contributions over the next 10 years (1908 to 1918), oddly enough, were somewhat semiempirical in nature. This is unusual for a theoretical mathematician and points up his interest in the practical application of mathematics. In the series of papers during that period, published in the Proceedings of the Royal Society, he attempted to obtain an analytical formulation for calculating the family of curves which are indicative of the "residual resistance" of ships as postulated by Froude. Initially, he considered a transverse linear pressure disturbance traveling uniformly over a water surface of infinite depth and arrived at a relation involving three universal constants (determined from experiment) and three parameters which depend upon the ship form. A major problem involved with the semiempirical

relationship was the determination or prediction of the three ship-form parameters for some arbitrary ship. Actually, the resistance relationship gives quite good agreement with experiments when experimentally determined ship-form parameters are used.

Apparently, in view of the shortcomings of the semiempirical approach and Sir Thomas' rediscovery of Michell's work, he abandoned this track and resorted to obtaining a solution to the basic formulation of wave resistance that was put forth by Michell in 1898 and which still forms the basis of all modern theoretical analyses of ship wave resistance. Michell's formulation is based on the representation of the fluid velocity in terms of a potential function which is built up of the sum of simple harmonic functions in the coordinates of the system and is coupled with several rather idealistic boundary conditions. These boundary conditions specify a slender-body ship characterized by small slopes in both the water-line and draft planes. The theory also requires that the wave slopes be small and does not allow changes of ship attitude.

Sir Thomas, over the period from 1920 to 1930, investigated the representation of ship bodies in terms of discrete and continuous source-sink or doublet distributions along the centerline plane of the ship and the ramifications and results of such an approach to the evaluation of Michell's integral. He was able to investigate the effects of straight or hollow bow lines, variations of entrance and beam for constant displacement, effect of parallel middle bodies, effect of finite draft, effects of relatively blunt and fine sterns on wave interference, and the variation of wave profile properties with systematic changes in ship form among other items important to practical ship design. In this work, he was the first to analytically determine and describe the influence of changes in water line shape on the wave resistance.

The wave resistance curves Havelock obtained as a function of Froude number have all of the characteristics of those obtained from ship model experiments. The location of the characteristic humps and hollows are depicted extremely well but their amplitudes are exaggerated in the low Froude number range (below 0.3). The agreement of the calculated resistance is excellent in cases of ship forms (especially "Michell ships") which are described by simple functions but relatively poor for actual ship forms.

In the 1930's and 1940's, Professor Havelock directed his efforts mainly toward the calculation of the wave profiles generated by two-dimensional and three-dimensional bodies as represented by source-sink or normal doublet distributions. He also derived relationships for and computed the wave drag of such bodies in terms of the energy and work in the waves.

Included in his work during this period, Havelock initiated the idea of accounting for the boundary layer effects in a real fluid by modifying the source strength function by a reduction factor which would vary with the form of the ship and with the Reynolds number. He made calculations for both two-dimensional and three-dimensional bodies and found the reduction factor had no significant effect on the bow wave but it did reduce the wave height along the side of the ship, particularly near the stern. He also investigated the effect of a modification of the lines of the ship in the stern region and found this device has the greatest influence on the wave resistance at low Froude numbers where there was greatest disagreement between theoretical and measured results. However, there still existed appreciable discrepancies between measured and theoretical curves in the low Froude number range. The effect of the modification was found to be insignificant at high Froude numbers.

Also, during the 1940's and continuing until as recently as 1956, he worked on wave drag relationships for submerged bodies of revolution (spheroids), as well as for a body traveling in the wake of another body. He was also able to account for the effects of and compute the wave motion and drag due to body acceleration or oscillations (rolling, pitching, and heaving). In addition, he investigated the characteristics of a submerged body (spheroid motion in normal and oblique wave systems) and demonstrated that pressure of the waves does not necessitate a modification of the source-sink distribution representing the body. This phase of his work gives valuable insight to problems associated with torpedoes and submarines.

The work of Havelock has been recently extended by Inui in Japan to a point where the accuracy of calculations relating to hulls of conventional width has been substantially improved and Hershey of the U.S. Naval Weapons Laboratory, Dahlgren, is using a variation of the theory to determine the wave pattern generated by a submerged body. Also, at the present time, extensive use of the generalized theory is used by the U.S. Navy's David Taylor Model Basin in the performance of numerous classified projects associated with modern submarine development.

This paper has not, and could not, do complete justice to all of Havelock's works in the limited amount of time available today. Nevertheless it is indeed an apparent and accepted fact that Havelock is a giant in his field and one feels sure that his classical contributions will be appreciated and utilized for a long time to come.

DISCUSSION

W.P.A. van Lammeren (Netherlands Ship Model Basin), after saying how much it was regretted that Sir Thomas Havelock could not be present because of illness, read the following letter, sent to the Office of Naval Research, Washington:

"I send greetings to the members of the Symposium.

I am extremely gratified by the proposal to dedicate the Symposium to myself; it is indeed a high honour, and I do not know any more pleasing compliment than to be remembered in this way by one's friends and fellow workers in the same field.

I also wish especially to thank Dr. von Karman; I am very appreciative of the great honour he has done me by giving the opening address.

I regret very much that it was not possible for me to attend the Conference myself and express my appreciation more adequately in person; but I send warmest thanks to all, and best wishes for a successful and pleasant meeting.

T. H. Havelock"

* * *

CONTENTS

ADDRESS OF WELCOME

L. Troost

Central Organization for Applied Scientific Research in the Netherlands

The joint sponsors of the Third Symposium on Naval Hydrodynamics, the U.S. Office of Naval Research and the Netherlands Ship Model Basin, have honored me by asking my assistance in the opening of this four-day Symposium in the Netherlands by delivering a brief welcome address on behalf of the host country. I am delighted to accept this invitation, in the first place because I am going to meet so many old and personal friends from the international scientific community concerned with the problems of naval hydrodynamics, in the second place because the Central Organization for Applied Scientific Research T.N.O. in the Netherlands which I represent, established by Law about 30 years ago, through its Special Organization for Industrial Research, has a very warm and active interest in applied and also more fundamental research in the field of naval architecture and marine engineering. This T.N.O. Organization brings together the interests of science, trade and industry with those of government under expert supervision, and channels research contributions of private industry and government appropriately to the areas where they are needed, encouraging, but not always attaining, a 50/50 ratio. We have the Netherlands Study Center for Naval Architecture and Navigation which is administrated by the T.N.O. Organization. This Symposium's cosponsor, however, the Netherlands Ship Model Basin, being somewhat older than the Organization itself, is an independent Foundation, self-supporting for all practical purposes, but maintaining old and friendly relations with T.N.O. in a joint and successful effort to produce more fundamental research in greater quantity and of higher quality than would otherwise be possible. It should be stated here that the research-mindedness and support of the progressive shipping and shipbuilding industries, in a centuries-old tradition in this small Low Country-by-the-Sea, are as exemplary for all T.N.O.'s industrial relations, as is the efficiency in the use of industrial and governmental research funds by the Wageningen Institute. It is believed that the Dutch build more ship tonnage per head of the population than anyone else and they are rightly proud of their maritime research facilities, including the new ones incorporated in the division of Naval Architecture of the Delft Institute of Technology.

It may be about a year and a half ago that the group of naval and marine scientists of the Massachusetts Institute of Technology, to which I then belonged, on the initiative of Professor Harvey Evans discussed the possibility of a seminar or symposium on recent developments in unusual ships like submersible and semisubmerged commercial vessels, hydrofoil, and hovering craft, under joint sponsorship of the Society of Naval Architects and Marine Engineers and M.I.T.'s corresponding Department. Through various circumstances the Society was unable to support the proposal in its then form. You may imagine my personal satisfaction in seeing it realized after my departure from the U.S., here and now, although under different sponsorship, because I consider the subjects under discussion as entirely timely in a period characteristic of almost unbelievably rapid changes in technology, in which the wild-looking idea of today may be the usual thing within 10 or 15

years. If in a Western World of undersupply of young scientists and engineers this rapid progress and the terrific amount of original thinking and imagination associated with it would stimulate a larger number of undecided students to enter the maritime sciences, and their teachers to a more and more imaginative approach of their subjects, an event as the one that is being launched today would be more than justified, quite apart from the value of its transactions of papers and discussions for the profession.

That our friends of the American Navy have considered the Netherlands as a place fit for this grand-style demonstration of progressiveness in ocean transport research, and the Wageningen Modelbasin as a worthy partner in this enterprise, is a source of deep satisfaction to the Organization I have the honor to represent here, and to the Dutch people as a whole. Traditionally devoted to welcoming foreign scholars and creative thinkers in a long history on these crossroads of European trade and traffic, science and culture, there may be few places where gratitude for assistance after World War II and for acceptance of Western World leadership have matured to such an extent of warm understanding of the ways of the American people and in general to such a degree of international orientation. These feelings of genuine friendship and hospitality prevailing here have given rise to a remarkable amount of international exchange of scientists, engineers, and students in our and other professions, not only with regard to the United States but also to the great majority of the countries whose delegates are assembled here.

Myself being an exponent of this international exchange, and having promoted it during my entire career, I have found quite some opportunity to compare the ways of engineers and scientists in our profession from this and the other side of the ocean. Let me say at once that I found them basically and on the average to be the same. Internationally seen, their characteristics, in a favorable sense, are defined by the fact that usually their road to immortality is not paved with dollars or an equivalent currency. Many of them have lately become a little more restless and inclined to change of occupation or surroundings, and not only for the above reason. But all of them have one thing in common, and also with the category of naval officers so happily represented in this audience: they have managed to marry attractive and sensible girls, who in the atmosphere of art and science have matured to the wonderful crop of gracious women here present, the unexcelled helpmates of those whose scientific productivity and creativity are so greatly dependent on these fortunate circumstances. It is to you, fair ladies, that my first word of welcome to the Netherlands goes out as well as my wishes that you may feel happily at home, but delightfully different from home, in this little country of vanishing windmills and wooden shoes, but vastly increasing industrialization. As an inveterate conference-goer I have already seen at a first glance that this one is going to be quite O.K. from the social point of view, which is at least as important, if not more, than from that of the scientific program. It is greatly dependent on your graciousness and understanding that the male attendants under your command come together in those friendly and personal shop-talking sessions which are so important to the informal scientific give-and-take and essential to those stimulating international friendships and professional relations which, even more than the formal papers and discussions, will define the lasting value of this Symposium.

To you, Officers of ONR and NSMB, sponsors of this important event, have already gone my feelings of deep appreciation for your endeavors in locating this Third Symposium in the Netherlands. Its dedication to the great Sir Thomas Havelock will be introduced by a man far more famed and worthy to this task than anybody else here present. This befits me only to the passing remark that someone has had a most wonderful idea in proposing the

incorporation of this mark of honor in the program of this Conference, at the same time giving a special tribute to that great shipbuilding and seafaring nation to which the name of our all-time scientific predecessor William Froude is forever associated. To the delegates of this and the other countries and, last but not least, to those of the great nation over the ocean that co-sponsors this Conference and that have made my and Mrs. Troost's previous nine years an unforgettable experience, goes the warmest welcome of the Dutch people, its Royal Navy, its shipping and shipbuilding community, and its T.N.O. Organization. In joining this welcome with cordial personal greetings to the many old friends and colleagues here present, I wish you all the happiest of times in our country, and a most interesting, stimulating and successful conference on the Scheveningen beach!

*   *   *

ADDRESS OF WELCOME

T. J. Killian
Office of Naval Research

It is a pleasure and a privilege to participate in opening a meeting that is a landmark in the steady growth of a truly international scientific community. Although this symposium is the third sponsored by the Office of Naval Research in the field of hydrodynamics, it is the first of a whole series, I am sure, to take place in Europe.

Certainly Europeans have made outstanding reputations for themselves in advancing hydrodynamics research. With enthusiastic support from private industry, especially in the hydrofoil area, Western European laboratories are coming forth with a steady stream of new ideas.

This week we will have the pleasure of hearing reports on recent progress and the latest approaches to the basic problems in this field. I am sure you are anticipating with great interest, as I am, the promising papers on the symposium agenda. You will hear from the top people in hydrodynamics research on both sides of the ocean. Although there will be some emphasis in the development of hydrofoils, other important areas will also be discussed.

In the case of the U.S. Navy, you will hear from specialists in the Bureau of Ships which, with the Office of Naval Research have joined together to solve the knotty problems of achieving high speed hydrofoil craft. The Office of Naval Research or ONR, as we are generally known, is also concerned with basic problems in hydrodynamics. Since ONR is a unique organization and not well understood even in the United States and as Chief Scientist of ONR, I think it would be appropriate to give you a brief review of our operation and our raison d'etre.

The U.S. Navy is well aware that the revolutionary nuclear powered, guided missile fleet of the future we now have under construction is more than anything else a product of science. We recognize that the design and production of an advanced piece of equipment does not begin until the scientist tucked away in his research laboratory has some time before worked out the principle in theory.

This search for new knowledge, which we call basic research, is one of the primary concerns of ONR. This organization was established at the end of World War II to make certain that the Navy would have the advantage of the latest scientific knowledge in designing and building its postwar fleet. At the same time, the Navy felt it was essential that much of the valuable research undertaken by civilian scientists before the war should be continued when the war ended.

Thus ONR became the first agency of the U.S. Government to be established primarily to support scientific research across the board in any discipline. It underlined the Navy's belief that all future attempts to maintain our national defense through seapower would depend in large part on the cooperation of the country's scientific community with the naval authorities.

To achieve this goal, at its inception the office established the guiding principle that it would foster fundamental research in universities and nonprofit institutions. Furthermore, we decided that such support should be given whether or not the projects might hold promise of immediately foreseeable applications for naval use. This was rather revolutionary doctrine in those days.

In other words, the Navy is quite willing to risk its funds on research projects without being certain we will get definite results for our money. The scientist himself, of course, cannot predict his results in advance, even though he starts off fully confident that he will throw some new light on his particular subject. On the other hand, it is quite possible that after a year or two of research he will discover that he has been proceeding up a blind alley. But ONR accepts the view that even negative results often have great value. The point is that uncertainty is a fact of life in scientific research. As one American scientist has stated, "the most important facts that wait to be discovered are those whose existence we do not even suspect at the present time."

There were other policies we inaugurated which were also innovations in support of academic research by the military services. For example, we insisted that the freedom of basic research from security restrictions was essential to the quality and rapid progress of the work being carried on. Today only a slight percentage, less than 1 percent, of our research contracts are classified, and these are not in the category of basic research. Our early policy also stated that the Navy should cooperate with, rather than attempt to direct and control the work of, the scientists engaged in research on its projects.

A brief summary of the administration of our contract research program today will illustrate how we have continued to carry out this early policy. About 80 percent of the funds in this program are used to support contracts in the basic research category. These contracts are awarded on the basis of proposals submitted to ONR, which are unsolicited. Normally we receive many more proposals than we could find if we had to seek them.

Selection is made by evaluating the scientific merit of the idea, and the competence of the principal investigator; finally we must have *some idea* as to how the results of the research to be undertaken could conceivably influence the Navy of the future. The size of the organization to which the investigator is attached or the type of organization, whether academic, nonprofit or industrial, is not a factor in our consideration. ONR seeks only to support the best research in any particular field.

We recognize also that few projects can be completed in one year. Therefore, research contracts let by ONR are not limited to one year; they average three years' duration or more. Not infrequently they are extended. This has made possible long-term basic research programs where several years were required to achieve fruition. In referring to the policy and operation of ONR, Dr. Nathan Pusey, President of Harvard, has said: "Backing of this kind gives the scientist confidence and frees him from the burdensome and wasteful necessity of making yearly special plans, special budgets, and special appeals for funds."

Naval research is also guided by the Naval Research Advisory Committee, which is composed of leaders in American industry as well as academic research. Utilizing the thinking of such men as Nobel prize-winner I. Rabi, we are kept alert to areas on which a greater concentration of research is needed.

ONR also recognized at the start that we would need to depend greatly on the European scientific community, and for this purpose we established our branch office in London. From there we maintain close liaison with all the important research centers in Europe and the Middle East.

Other government and military research agencies later established, such as the National Science Foundation, the Atomic Energy Commission, and the Office of Scientific Research of the U.S. Air Force, I like to feel have followed the ONR pattern to a more or less degree. In fact, the National Science Foundation even took our first chief scientist for its first and present Director.

Naturally, the Navy is proud of pioneering in the widespread, large-scale support of research by the U.S. Government: More important than that, however, is the fact that we have helped the American scientific community in producing a steady flow of brilliant ideas in recent years.

Finally, it is important to emphasize that while the products of naval research are designed primarily for military use, it is our hope, even our burning dream, that their greatest use will be their exploitation by industry to promote the peaceful progress of civilization. This dream I am sure we share with all who have joined together this pleasant morning in Scheveningen.

*   *   *

HIGH PERFORMANCE SHIPS - PROMISES AND PROBLEMS

Owen H. Oakley
Bureau of Ships, U.S. Navy

The U.S. Navy's interests in ships of maximum performance as regards speed, motions, and quietness are discussed from the point of view of design and application. A number of exploratory studies, and the designs of developmental craft, are reviewed in this light. The promise of each is considered in regard to the compromises required and the problems encountered in the course of development. It is concluded that, while no dramatic "breakthroughs" are foreseen, the accelerated pace of research in ship hydrodynamics will produce significant changes in the shape and performance capabilities of naval craft in the next few years.

INTRODUCTION

The United States Navy is currently engaged in the study of a variety of design concepts, some of which differ sharply from the conventional shape of ships. It is my purpose to describe and discuss the pattern and direction of these efforts, less from the standpoint of hydrodynamics than from the overall viewpoint of naval ship design.

If this viewpoint appears sometimes to emphasize the problems rather than the promises, it is because it is the daily experience of design that the problems are often obscured by the rosy glow of the promises.

Many of our present-day naval and merchant ships are a result of a slow process of evolution. New designs have been based on previous successful ships; small modifications were made to accomodate new needs. However, in recent years, it has become evident that a new, fresh look was desirable. Modern technology presents greater capabilities in power plants and electronic equipment. Basic research has given a better understanding of ship environment and ship behavior in that environment. The question is being raised more and more as to whether we need adhere to many of the compromises that have traditionally made up standard design procedure. The need for high performance in ships is pressing and the time is right for reappraisal of basic concepts.

Exploratory studies of the type under discussion may follow one of three paths. One approach is to select a single facet of ship behavior and try to optimize it. Necessary compromises are then made with an eye toward retaining as much of the original gains as possible. Another method is to examine closely and carefully new and hitherto neglected scientific achievements which may only lack development to bring them to the point of usefulness. The third method is to take an overall look at various ship missions, pinpoint the major problems,

outline broadly the possible solutions to these problems and then develop the most promis-
ing. The high performance ships discussed in this paper are products of all three methods.

At the risk of oversimplifying, we can state that there are three principal reasons for
exploring unusual hull forms as they apply to naval craft: to increase speed, to minimize or
control motions, and to improve stealthiness. The first two are neither new nor peculiar to
naval ships; men have been concerned with speed since the first log canoe and with motions
since the first case of mal-de-mer. The third feature, stealthiness, was concocted to cover
the functions of detection, localization, and classification of the enemy ships while remain-
ing immune to detection, localization, and classification by the enemy. One of the major
components of stealthiness is hydrodynamic quietness. This is a relatively new goal in
ship design and is, of course, important where sonar performance is concerned.

The three qualities of speed, motion, and quietness are obviously not independent, so
that changing one changes the other two. It appears, sometimes, to be a fundamental law of
nature that maximizing one quality usually results in degrading others. In a few cases this
did not occur; these are exceptions and like all good exceptions only go to prove the rule.

The phenomenon of surface waves is one of the more interesting properties of water. In
a sense it is the subject of this symposium, since it is by the avoidance or minimization of
wave effects that we hope to maximize speed and seakeeping performance. The energy
absorbed in the creation of surface waves to a large degree limits the speed of surface
ships. Likewise, it is the energy imparted to the ship by surface waves that limits other
aspects of ship performance. Quite naturally, therefore, exploratory studies have been
directed primarily at avoiding or minimizing these surface wave effects.

Fig. 1 illustrates a range of concepts and relates them to the free surface. In the top
group, two methods of avoiding the free surface are indicated, in the middle group the avoid-
ance is less complete, while in the bottom group, two surface ship hull forms are shown
which are designed to cancel wave effects rather than avoid them.
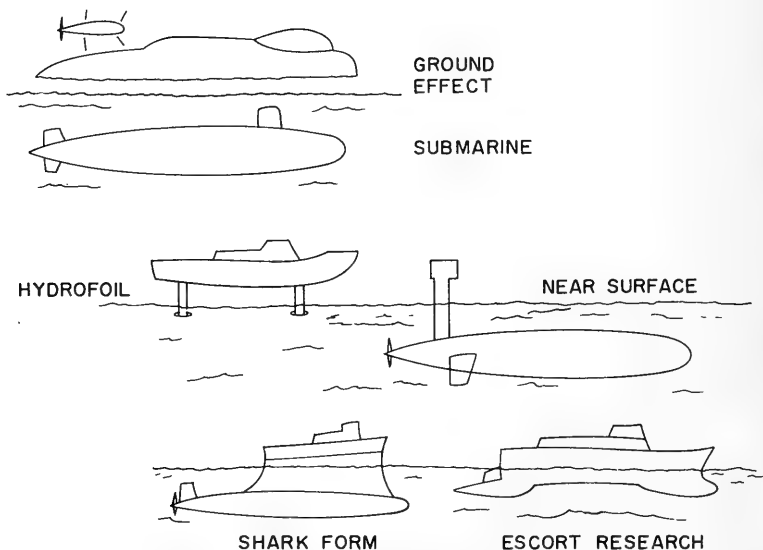

Fig. 1. Various high performance ships

This paper will discuss the potential of these concepts and some of the problems that arose in expanding certain of them into practical ship designs.

SOME HIGH-PERFORMANCE SHIPS

Ground-Effect Craft

Ground-effect craft offer the contradictory capabilities of high speed and the ability to hover above the surface. Speeds of well over 100 knots appear to be attainable and such speeds are attractive for many applications. The ability to hover has obvious advantages, for example, in amphibious operations. Recent theoretical and experimental evidence indicates that in the high speed range of operation, these craft will not respond to wave action, but can maintain level flight over ocean waves. These promises, when and if attained, indicate applications for amphibious warfare, antisubmarine warfare, aircraft carriers, missile carriers, cargo and personnel carriers, etc. The rapidly expanding literature on these ground-effect craft is a measure of their apparent promise; it is also a measure of the many problems to be resolved.

Ground-effect craft do not completely avoid the free surface, particularly the more "pedestrian" versions of this concept. Fig. 2 shows four types. Various combinations of these basic schemes are possible, and it would seem that every conceivable variation has been proposed.

RAM WING
SPEED > 100 KNOTS

PERIPHERAL JET
SPEED < 100 KNOTS

SIDEWALL
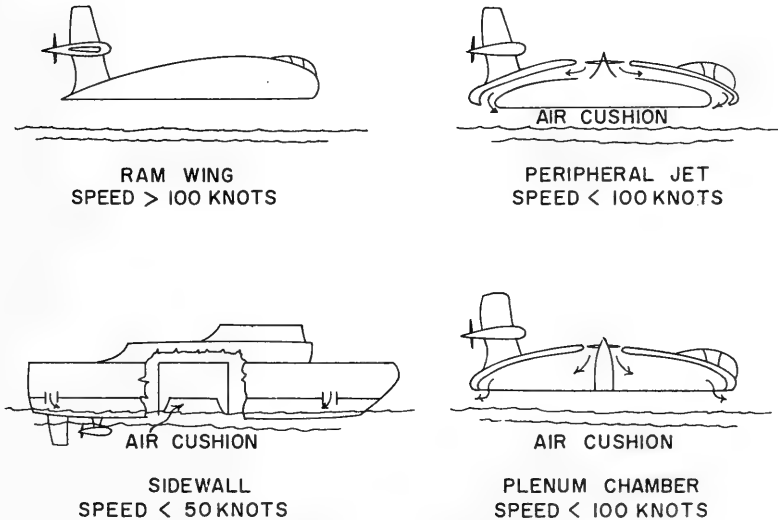SPEED < 50 KNOTS

PLENUM CHAMBER
SPEED < 100 KNOTS

Fig. 2. Four forms of ground-effect craft

The "ram wing" shown in the top of Fig. 2, is actually a low-flying aircraft. The significant reduction in induced drag achieved by flying close to surface should permit the attainment of very high lift/drag ratios at high speeds. Values as high as 60 at a chord/height ratio of 0.5 have been estimated.

The two bottom illustrations of Fig. 2 have received a great deal of attention. The literature is too extensive for complete reference here; the International Symposium at Princeton did present, however, a substantial cross section of the efforts going on in the world.

A large percentage of the research effort has been applied to the peripheral jet type. In this case, air jets are located along the periphery of the craft. When starting, the jets hit the water, and split, part of the jet goes inward and is trapped. The pressure in the air cushion is thus built up. Equilibrium is reached when the pressure in the air cushion is sufficient to bend the jets so that no more air goes inward. A simple analysis indicates that the required lift power for a particular craft depends on the weight of the craft times the velocity in the jet for a constant jet momentum. If a heavy fluid, such as water, is used instead of air, constant jet momentum implies a higher mass flow and a lower jet velocity and thus lower required lift power. Air, for the air cushion, must be supplied separately; the water curtain simply provides the seal to contain the air.

The amount of power required to supply the air cushion is a function of many parameters; among the most important is how high the craft flies and the peripheral length of air seal. Flight over water permits the use of sidewalls extending into the water (lower left in Fig. 2). The air loss can be greatly reduced by this device. The penalty for this is lower speed and loss of ability to "fly" onto a beach. The drag of the sidewalls apparently limits this type to about 50 knots, beyond which the peripheral jet offers a more efficient use of installed power. Fig. 3 shows in a highly qualitative manner the relative speed/horsepower characteristics for the four basic types.
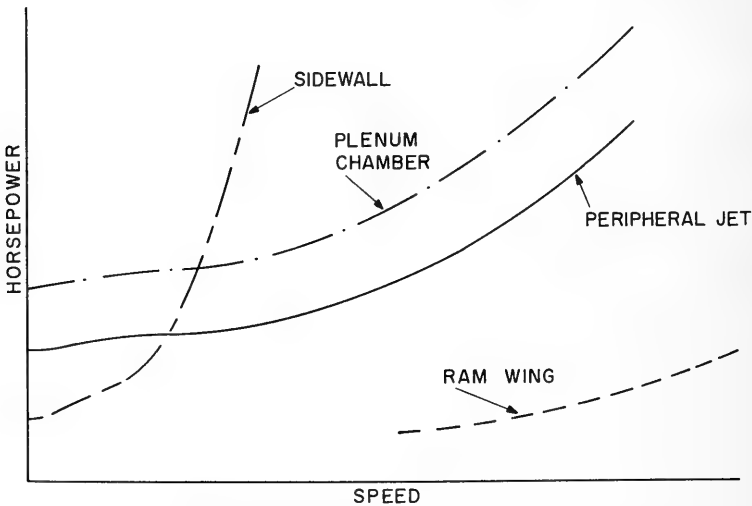

Fig. 3. Speed-power curves for the four forms of ground-effect craft

The problems to be solved are numerous. As implied by the previous discussion, most of the past efforts have gone into the determination of the mechanism and parameters affecting hovering. An examination of dynamic effects associated with forward motion has just recently begun.

The ram wing will encounter all the problems of takeoff, landing, and in-flight control of ordinary aircraft, plus the precise control required in flying close to the surface. Take-off or low-speed power requirements may well prove to be governing.

Stability and control behavior over waves is not well understood. Tests to date indicate problems associated with running trim even in calm water. Theoretical insight is being gained into the mechanisms of damping and resonant frequencies of motions over waves, but this is not complete, nor do we have as yet very much experimental experience.

The scaling laws are being carefully examined, especially in light of the British experiments with "hovercraft." Here, for example, large scale tests indicated severe spray problems, which did not arise in the small scale model tests.

The dynamics of water-wall craft have not been examined extensively. How can we reduce air leakage through this water screen? We know that the screen is relatively good at short distances down from the jet exit, but leakage is severe at substantial heights before the jet hits the free surface.

In all of these craft, a major problem is how to design the light structure required and still retain the ability to land and rest on the water in waves. Aircraft structure would be too light to meet the landing in waves requirement, while standard ship structure would be so heavy as to eliminate any payload. A blending is required.

Light-weight, high capacity air fans are required that will operate against the high cushion pressure that is needed for ground-effect craft. It is estimated that for large, operational ships this back pressure may be in the order of 150 pounds per square foot. Such fans are not shelf items.

From the designer's viewpoint, the promises are meaningful and the problems do not appear insurmountable. However, considerable expenditures of research effort and time are required. U.S. Navy work in this field, is aimed at the construction of a large ground-effect vehicle about 1963. The size and type await the results of research now underway.

Submarines

Just as the aircraft flies high and eliminates surface effects, the submarine departs from the free surface by submerging. Undesired motions are reduced rapidly with departure from the surface because wind-formed waves attenuate quickly with depth. Speed is also benefitted because it is no longer limited by the creation of surface waves. The submarine offers the ultimate in stealthiness. Thus, its principal promises are high speeds and a high degree of undetectability.

Fig. 4 shows a comparison of the power to drive two hulls of about the same displacement where one is a modern submarine and the other a destroyer hull form. Part of the submarine's advantage is its much superior propulsive efficiency. The remainder of the difference is largely attributable to the elimination of wave resistance. These two effects more than balance the greater frictional resistance of the submarine which results from its greater area of wetted surface.
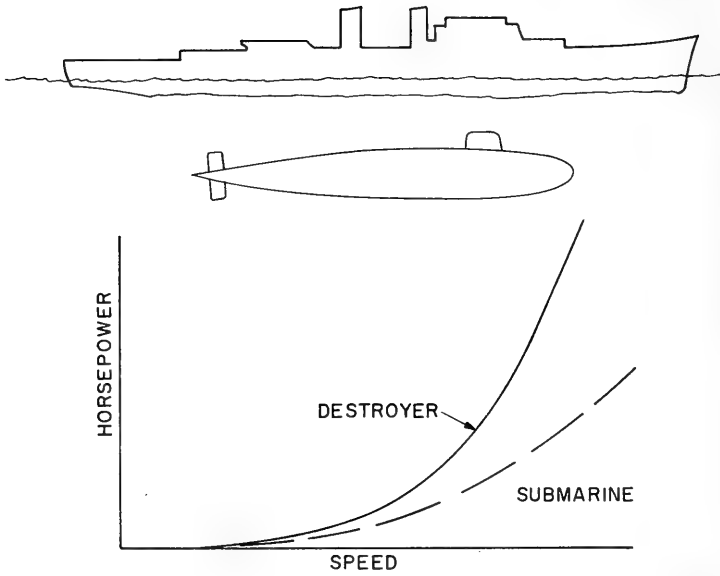
Fig. 4. Speed-power curves for a submarine and a destroyer of about the
same displacement

Fig. 5 shows a comparison between the pitching motion of a submarine on the surface in
a moderate sea state compared to the submerged pitching. The data is presented in spectral
form and shows the large decreases in motions for fairly shallow submergence. (Note, how-
ever, that the ordinate is proportional to the pitch amplitude squared.)

Fig. 5. Energy spectrum of the pitch amplitude for
a submarine

Within the past 10 years technological advances have been exploited to make the submarine the most fantastically mobile and powerful warship yet devised.

The foregoing are all promises realized, but progress in improving the performance of submarines still encounters problems. The problems essentially consist of a search for methods of improving this already powerful vehicle. The most significant improvement would be to increase speed. The most direct way, of course, is simply to increase 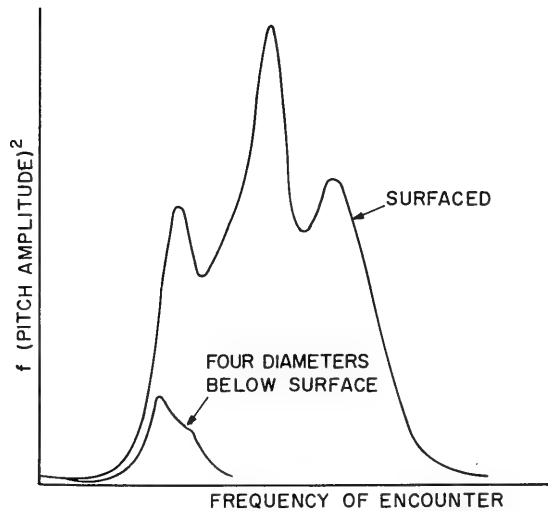the power. This would require a larger hull, so that some of the gain would be eaten up in added frictional resistance. A simplified parametric study holding payload constant and using present specific weights and volumes for machinery, indicates that a submarine would require well over 100,000 shaft horsepower to attain 50 knots. This is right at the upper bound of present technology as regards the power that can be absorbed by a single propeller. Improvements in specific weights and volumes of submarine power plants will naturally improve this situation, but it is apparent that dramatic increases in speed will be hard earned. Other methods of improvement, such as reduction of resistance by boundary layer control will be discussed in a later portion of this paper.

Near Surface Craft

The near surface craft is intended to combine the stealthiness, speed, and motion characteristics of a submarine with the air-breathing, air-communication aspects of the surface ship.

At present, nuclear power plant weights are extremely high compared with the more advanced air-breathing plant. If the submarine could be run sufficiently close to the surface to breathe air through a slender strut, and still stay far enough down to avoid excessive wave drag, a lightweight air-breathing plant could be used.

The near surface craft is intended to do this. Work on this type is currently being performed by the Davidson Laboratory. Fig. 6 shows a series of speed-power curves, as a function of depth of submergence, for an arbitrary submarine type hull form. In order to
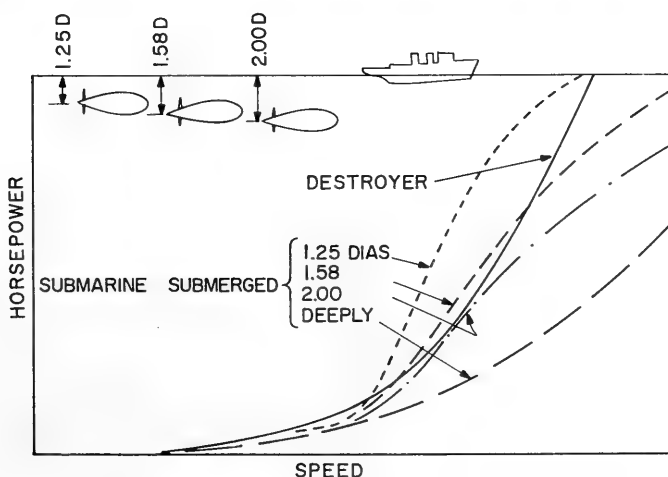

Fig. 6. Effect of the depth of submergence on the speed-power
curves for a submarine

compete with a destroyer hull form of equal displacement, the near surface craft must travel below a depth of about one and a half diameters to the axis. This implies a strut length somewhat greater than one hull diameter plus additional length in order to project some distance above the free surface to allow for waves and depth control variations. Such a strut must carry at least a periscope or closed circuit TV camera unit, communications and radar antenna and a snorkel head valve. The size of the air passages appears to govern the size of the strut. For a 20,000 shaft horsepower installation, some 80 square feet of intake, exhaust and ventilation duct is needed. This results in a strut with a chord of some 26 feet and a thickness of 6-1/2 feet, altogether not a small structure. The resistance of this strut would degrade the speed performance and affect the stability and control.

Just as the ram wing needs controls like an airplane, the near surface craft needs controls like a submarine. In fact, the controls have to be more effective to counter the effects of surface waves. Also, the structure would have to be sufficiently strong to withstand accidental deeper submergence.

Hydrofoil Craft

Hydrofoil craft promise primarily high speeds. It appears likely that speeds in excess of 100 knots are possible. In addition, motions in a seaway should be considerably less than buoyant craft of the same displacement. These craft can maintain high speed in sea conditions considerably more severe than would compel a displacement craft to slow down.

The United States Navy has maintained a hydrofoil program since shortly after World War II. Out of this has come considerable research and development, and a number of test craft embodying some promising principles. Four of these are shown in Figs. 7, 8, 9 and 10.

Fig. 7. A test hydrofoil craft, the Baker "High-Pockets"

The Baker boat, "High Pockets," exemplifies the use of surface-piercing foils (see Fig. 7). This craft has the feature of essentially equal distribution weight on the forward and the after foil systems. The Carl XCH-4 (see Fig. 8) embodies ladder foils, an "airplane" distribution of foil area fore and aft, and air screw propulsion. The Miami Shipbuilding Company's "Halobates" (Fig. 9), utilizes submerged foils in an "airplane" distribution and a right angle drive over the stern. Control in the version shown was achieved by the "Hook" system which
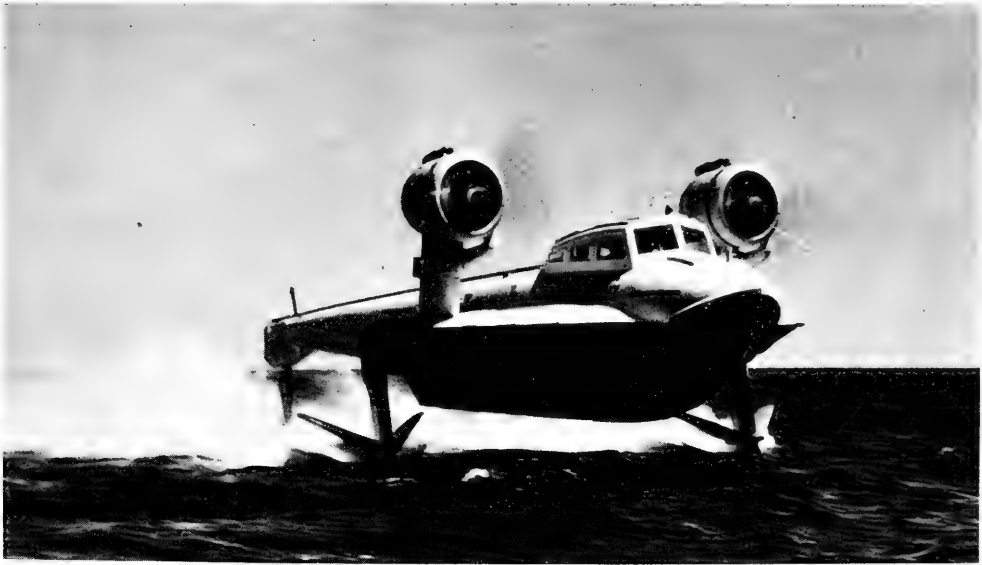

Fig. 8. A test hydrofoil craft, the Carl XCH-4
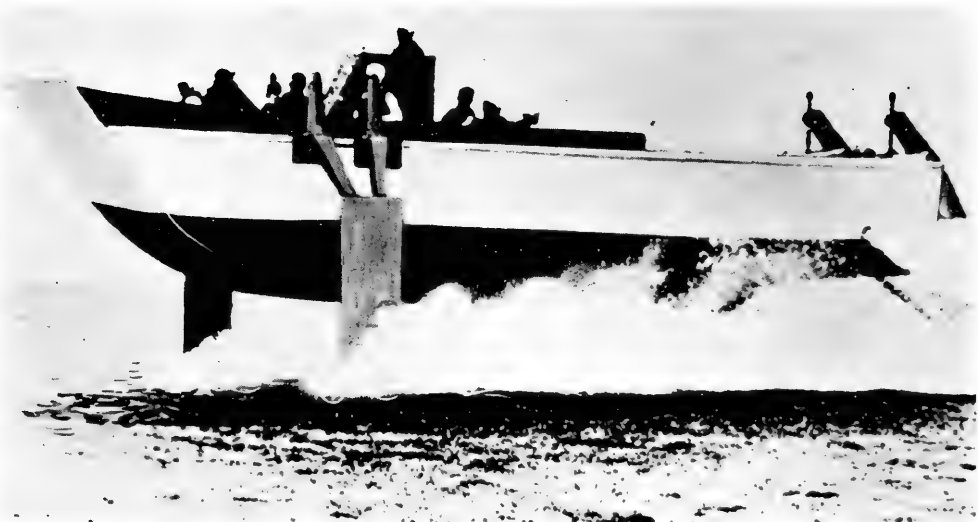
Fig. 9. A test hydrofoil craft, the Miami Shipbuilding Company's "Halobates"

used mechanical "feelers" to sense the waves ahead of the boat, and which, through linkages, adjusted the angles of attack of the forward foils. This craft was also successfully operated using a resistance height sensing device on the forward struts and an electronic "hydropilot." The most successful of these craft was "Sea Legs," by Gibbs and Cox, shown in Fig. 10. "Sea Legs" has submerged foils in a canard arrangement and a sonic height sensing system which actuates the control surfaces through an autopilot and hydraulic servos.
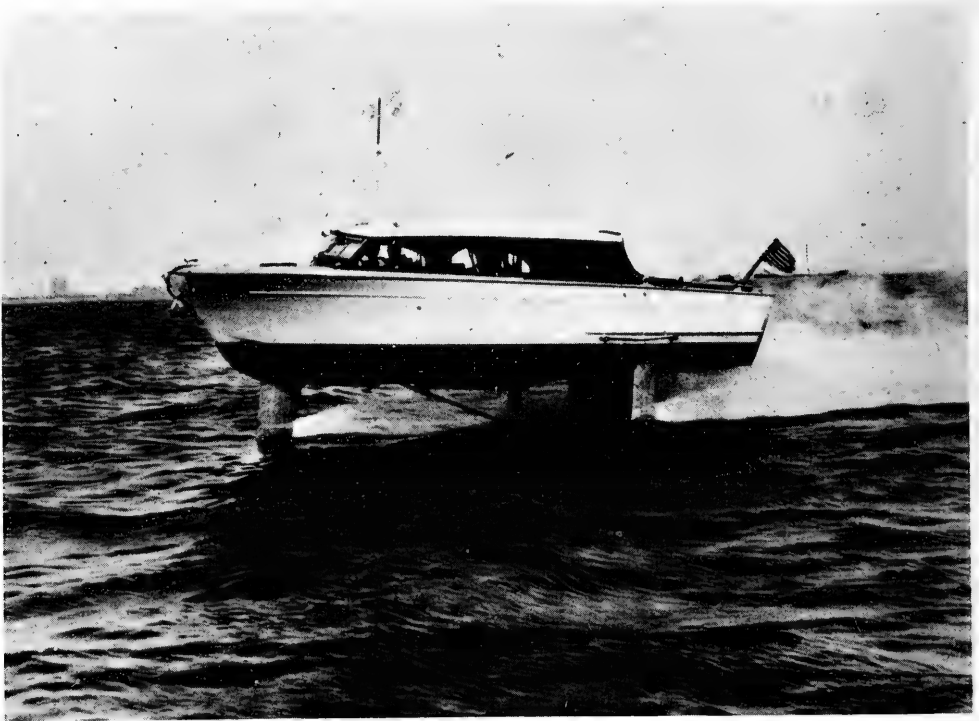
Fig. 10. A test hydrofoil craft, the Gibbs and Cox "Sea Legs"

Based on the successful performance of "Sea Legs" the submerged foils-autopilot system, was used for the antisubmarine hydrofoil craft "PC(H)." Fig. 11 shows an artist's concept of PC(H), for the construction of which a contract has recently been awarded to the Boeing Aircraft Co.

These craft are all of the subcavitating type. The maximum speed for subcavitating craft for all practical purposes is limited by cavitation to about 55 knots in calm water. It should be noted however that the XCH-4 attained a speed of about 65 knots. This craft, however, was overpowered and lightly loaded, so that any added drag due to cavitation was probably not limiting. In rough water, wave orbital velocities induce variations in the angle
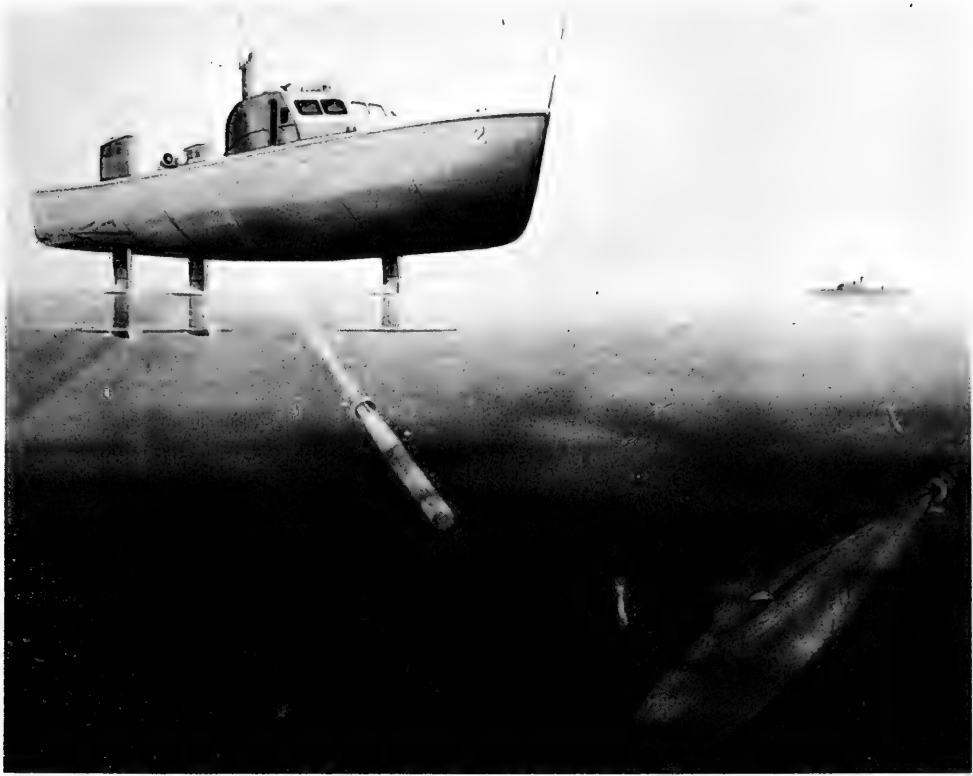
Fig. 11. Artist's concept of the antisubmarine hydrofoil craft "PC(H)"

of attack of the foils, which causes cavitation to occur at lower speeds. Fig. 12 shows the variation of angle of attack with craft speed for a state 5 sea. Fig. 13 shows the degradation of cavitation-inception speed with increasing wave height for a thin hydrofoil. Considerable work has been done on section shapes to delay cavitation, but only limited gains are possible in this direction. If we are to attain the promise of high speeds, it must be by utilizing supercavitating sections.

In the supercavitating regime we find that very high speeds or large angles of attack are required for true cavity flow. In practical foil configurations, the cavity is likely to vent to the atmosphere, either through tip vortices or down a strut. This leads to the conclusion that superventilation rather than supercavitation is the more practical mechanism to consider.

It appears that in the subcavitating range we may expect overall lift/drag ratios of about 9 to 12, and in the superventilated range, lift/drag ratios of about 5 to 7. While the lower lift/drag ratios require more power and demand more economy in structural and other weights, this does not appear to be prohibitively restrictive.

In the course of designing PC(H) a number of problems were successfully resolved on paper, while others required considerable test and reevaluation effort. For example, calculated predictions of lift and drag at top speed were in close agreement with model tests.

Fig. 12. Variation of the wave induced angle of attack for a state 5 sea and a hydrofoil 5 feet below the surface

Fig. 13. Degradation of cavitation-inception speed with increasing wave height for a thin foil submerged 6 feet and a wavelength of 100 feet
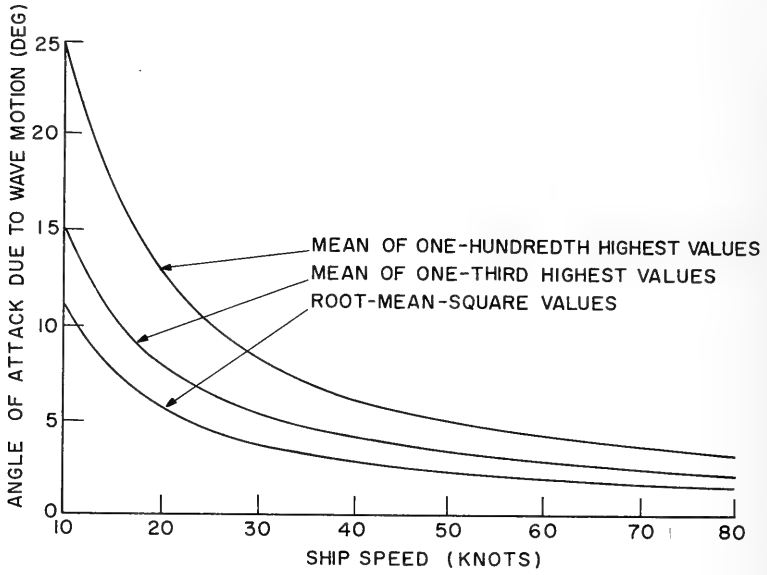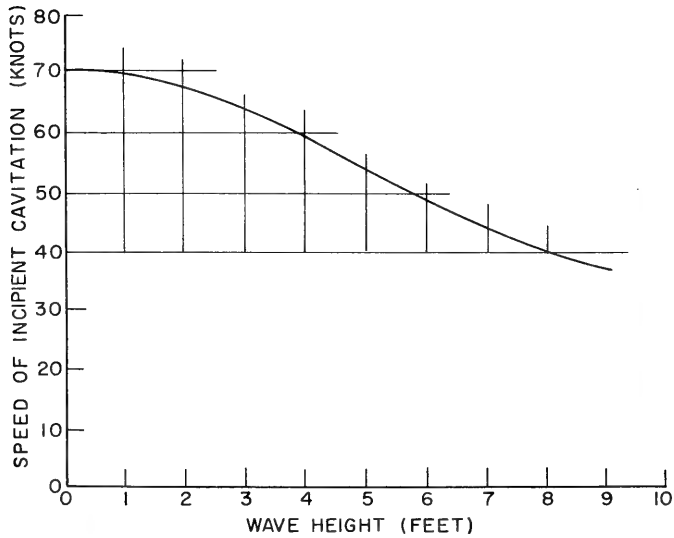
This result confirms our confidence in the use of the extensive airfoil data that are available. Model experiments in takeoff drag and available thrust indicated satisfactory margins. It was found, however, that very poor flow conditions existed at the intersection of the strut, foil, and nacelle. This poor flow was found to be cavitation and not separated flow. In analyzing the problem, aircraft technique was borrowed and simple consideration of adding pressure distributions led to small changes in configuration; the resultant clean flow was confirmed by experiment. The PC(H) represents the first hydrofoil for which the hydrodynamic coefficients were obtained experimentally at the David Taylor Model Basin. These coefficients are needed for determination of stability and autopilot gains for vertical-plane motion. Horizontal-plane and coupling effects are planned to be obtained in a similar manner in the near future.

A few problems remain to be resolved in the subcavitating regime. Probably the major one is the determination of the hydroelastic dangers, i.e., flutter and divergence. There is no adequate theory for prediction of instability speeds, and practically no experimental work in the marine range of interest. The flow problems at the intersections of strut, foil, and nacelle need to be codified. Flap effectiveness at low submergences (as determined from PC(H) tests) appears to be less than predicted by theory. These problems are all currently under study.

Flying qualities in waves are being examined. In very high speed hydrofoil craft (70 to 100 knots), the frequency of encounter with waves will be so high that it will be impossible to "contour" the surface without inducing excessive accelerations. This implies the necessity for "platforming;" that is, the craft's trajectory must remain essentially horizontal. This further implies submerged foils, because surface-piercing systems cannot platform. In addition, long struts will be needed to keep the hull clear of the water and yet insure continuous good submergences for the foils in rough water. In order to platform, the autopilot system must move the control surfaces continuously and at rapid rates in order to nullify the wave-induced disturbances. In some following seas it may not be desirable to platform and here the control system will have to permit some vertical motion. This suggests not only a wave-height sensing device, but also inputs to the autopilot from accelerometers. Roll control will require additional displacement, velocity, and acceleration inputs.

The major problems to be resolved are primarily in the supercavitating regime. Here we have theory to guide us, but systematic experimentation on the effect of geometric characteristics of foils is lacking. There are no corresponding airfoil data, of course, that are useful.

As indicated earlier, the mechanisms of ventilation are not well understood and require research starting with the basic physics of the phenomenon.

A simplified theory of hydroelastic instabilities has been developed, but there are no experimental data. This theory, incidentally, indicates a greater likelihood of hydroelastic instabilities than for a comparable all-wetted hydrofoil. Also, advances are sorely needed in materials in order that the requirements in hydrofoils for very high strength, erosion, and corrosion resistance, toughness, good fatigue life, etc., may be met.

In the supercavitating or superventilating range, takeoff may well be critical. Feasibility studies have shown that for very high speed craft, takeoff thrust requirements are incompatible with top-speed requirements. Means for achieving takeoff at lower speeds need special attention.

Foil smoothness is, of course, vital to good performance. Present tests indicate that paint (both anticorrosive and antifouling) is likely to peel off at high speeds. One promising approach is the Cox System of cathodic protection. In this method, high current densities are applied when the boat is motionless in the water. This plates out a combination of magnesium hydroxide and calcium carbonate on the foils. The idea is that the fouling will attach to this rather soft coating, and slough off at reasonably low forward speeds. A minimum value of current density is applied at all times to eliminate corrosion.

The Navy's present activity in the hydrofoil area includes an extensive research and development program directed toward a large experimental subcavitating hydrofoil ship of about 300 tons displacement and a small superventilating hydrofoil boat (about 15 tons) to be in operation by 1963.

Shark Form

If we do not try quite so hard to avoid the free surface, and if we acknowledge that certain armament and surveillance activities require topside space, then it is not a long step from the concept of near surface craft to the shark form of Fig. 1. In effect, this is simply a near surface craft with a relatively large strut piercing the surface. The shape and location of this large strut should be such as to cancel as much of the main hull's wave resistance as possible and reduce the exciting forces and moments due to sea action. Thus, the promises of the shark form are high speeds and small motions.

This concept was explored to some extent by the Germans during World War II, and this resulted in the Englemann craft. This form should have favorable motion characteristics, especially in head seas, because of the long natural periods of pitch and heave, which result from the short, fine waterline.

Fig. 14 shows a comparison of the shark form and a destroyer type hull form. At the lower Froude numbers, the shark form is quite resistful; however, at high speeds, the shark form is better than the destroyer form.

There are a number of problems to be resolved before the promises of this form can be realized.

As shown in the case of the near surface craft, the submerged hull must be located well below the free surface in order to minimize wave-making resistance and the exciting forces of the sea. In common also with the near surface craft, the shark form requires power plants of less specific volume than currently available in order to attain the speed-power advantages shown in Fig. 14.

The amount of topside weight which can be carried is limited by the low transverse stability. With very little waterplane, stability must be attained by keeping the center of gravity below the center of buoyancy. This is not easy in a form such as this, in the face of the demand for topside locations for equipment.

The shark form has, in common with the ground-effect craft, a problem of running trim in calm water. Fig. 15 compares observed trim tendencies at zero angle of attack with those calculated from Pond's theory for Rankine ovoids. This comparison is, of course, not strictly valid because of the difference in submerged hull shape and the fact that the theory does not take into account the topside shape of the shark form. Even so, the trends do
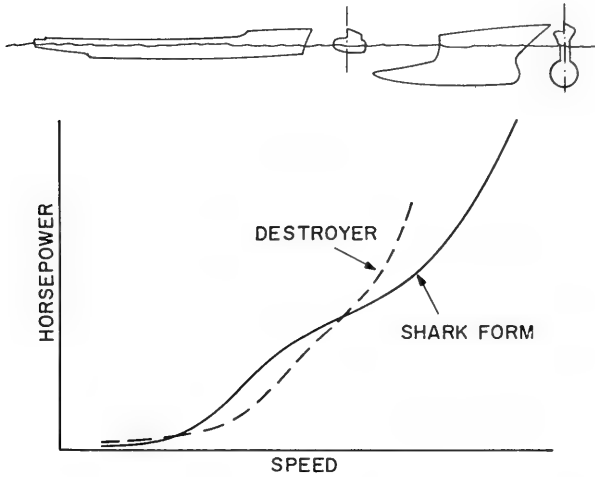
Fig. 14. Speed-power curves of a destroyer and the
shark form
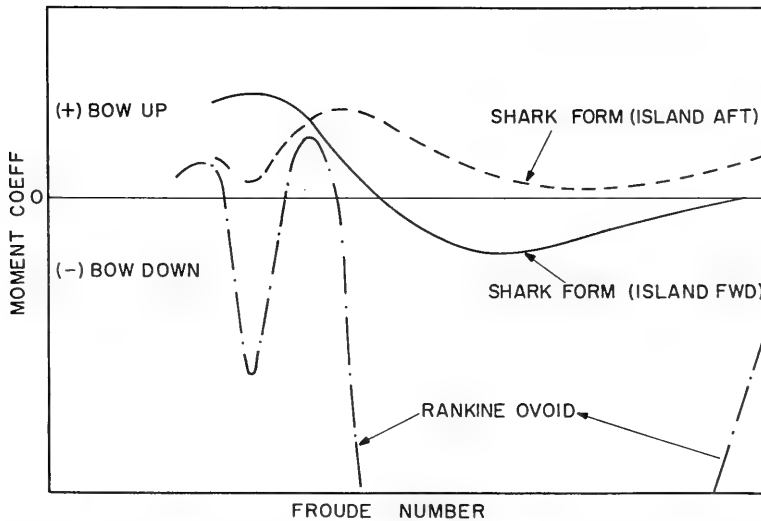
Fig. 15. Comparison of the pitching moment for the shark form with Rankine
ovoids, with the hull 1.5 diameters below the surface

appear comparable.   The pitching moments are not small and will probably require large
control surfaces to counteract them. In view of the fact that the moments vary in direction
and magnitude with speed, the control surfaces may have to be controlled by an autopilot
system.

Escort Research Ship

The escort research ship (see Fig. 1) is an actual design which was prepared to provide a research vehicle emphasizing quietness and minimum motion. Hydrodynamic quietness was sought by using a lightly loaded propeller and locating it deep and at the end of a nacelle well removed from the influence of the hull. Fig. 1 also shows the large nacelle or dome located at the bow to house sonar transducers and to provide damping and added mass which tend to produce favorable pitch characteristics.

The aim of this unusual hull form was to avoid resonance in pitch by raising the natural pitch period. It was hoped by this to permit operation in the supercritical region with attendant low pitch response. This is illustrated in Fig. 16, which shows a single degree of freedom type of response for a damped system and indicates the supercritical range in which it is desired to operate.
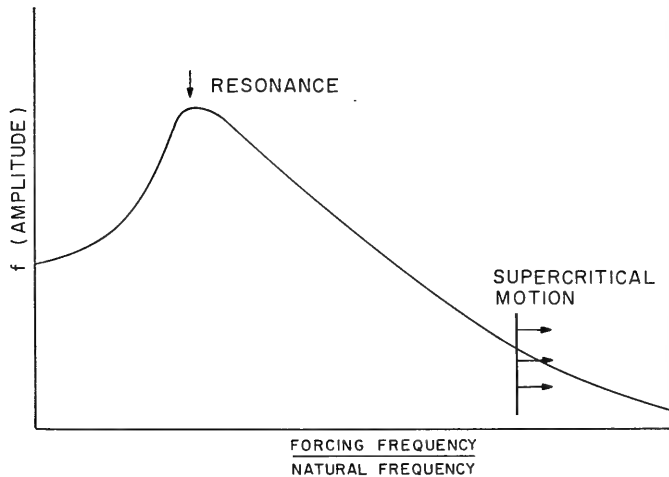
Fig. 16. The supercritical region of motion, showing the region of operation under conditions of favorable pitch characteristics

The longitudinal moment of inertia of the water plane was made small; this, combined with maximizing the longitudinal mass moment of inertia of the hull by moving heavy weights toward the ends and the added mass due to the water entrained by the nacelles, tended to produce a long pitching period.

The early models tested of this concept were largely exploratory and investigated the locations of nacelles, etc. Model tests showed excellent pitch characteristics for the configuration then under study. The short-dashed line in Fig. 17 shows the very favorable behavior in pitch. This figure shows the pitch response in regular waves and is similar to the previous figure except that the forcing frequency or period of encounter is represented as a function of speed. In this instance the wave corresponds to the maximum energy wave in a Neuman spectrum for a state 5 sea.
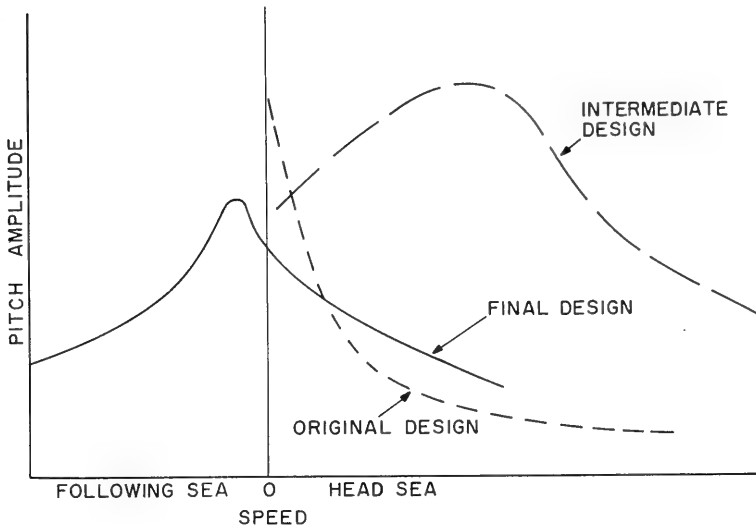
Fig. 17. Pitch behavior of various designs of the escort research ship

When firm requirements were established for the design and the design adjusted to accommodate them it was found that by designing in the new features we had also designed out the favorable pitch characteristics of the original design. The long-dashed line in Fig. 17 shows the disappointing results. The pitch period had been shortened so that resonant pitching occurred near operating speeds.

It was found that we could calculate the period of pitch, using simple single degree of freedom relationships, to agree quite well with model tests by using F. M. Lewis' data for added mass plus allowances based on simplified shapes for the end nacelles. This proved to be a useful design tool and we set about to make changes to lengthen the natural period to approach that of the original design. A period length $T/\sqrt{L}$ was chosen in accordance with Mandel's analysis which would place the design in the supercritical range for all but very low speeds.

This was accomplished by shortening and deepening the hull, shaving away the ends of the water plane to reduce longitudinal moment of inertia, and increasing the nacelle sizes. For a single degree of freedom system the natural frequency is given by

$$ f = 2\pi\sqrt{\frac{KI_{wp}}{g(I_s + I_{am})}} $$

where f is the natural frequency in pitch, I_{wp} is the moment of inertia of water plane, I_s is the mass moment of inertia of ship, and I_{am} is the mass moment of inertia of entrained water. The changes enumerated above obviously tend to lower the natural frequency.

It is not easy to alter the natural frequency of a ship while still keeping other characteristics unimpaired. For one thing the longitudinal radius of gyration in ordinary ships is about $0.22L$ or $0.25L$, not counting entrained water. In this design a value of close to

0.30L was needed. It is most difficult to relocate weights in a practical ship design to accomplish this.

By enlarging the end nacelles well beyond the size required for items of equipment, the entrained water was increased and this had the most pronounced effect in increasing the length of the pitching period.

The changes did result in moving the resonant speed back to about zero and the final design exhibited nearly as good pitch characteristics as the original, as the solid line in Fig. 17 shows.

Fig. 18 compares the escort research ship with a destroyer and a destroyer escort. This is a spectral presentation and compares the ships in the same seaway, and at the same speed. The results appear dramatic and in a sense they are, although it should be remembered that the ordinate is a function of pitch amplitude squared, which in effect exaggerates the difference in performance as regards pitch amplitude.
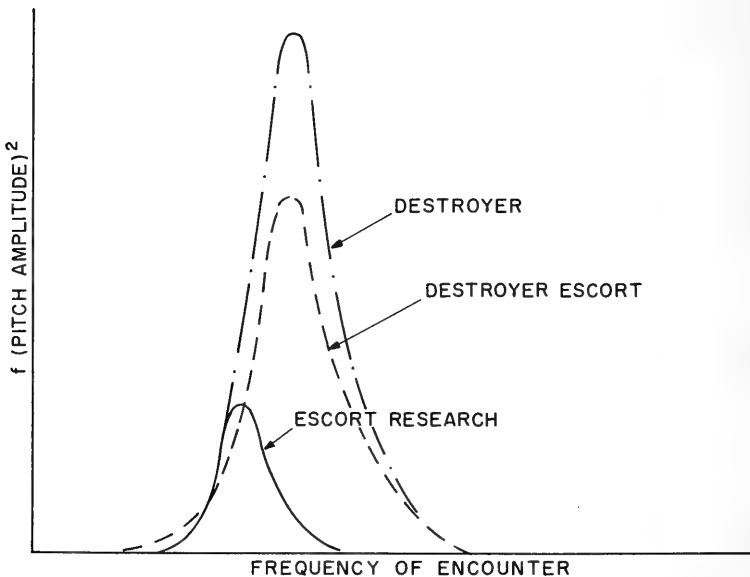
Fig. 18. Predicted pitch spectra in a state 5 sea at a ship speed of 20 knots

The problems and compromises which practical considerations impose on an ideal concept are well exemplified in our experience in this design. One facet, however, did not develop unfavorably. The speed-power relationships provided a pleasant surprise. Fig. 19 shows a qualitative comparison with a destroyer escort hull of about the same displacement. As in the case of the submarine vs destroyer comparison given previously (see Fig. 4) a significant part of the difference in power is the result of the superior propulsive coefficient of the escort research ship. Nevertheless, considering the fact that roughly a third of the displacement of the research ship resides in the nacelles it is remarkable that they cost so little in power.
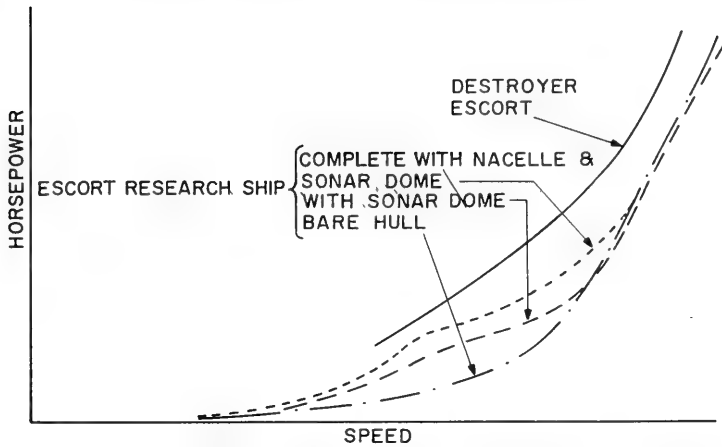
Fig. 19. Speed-power curves for an escort research ship and a destroyer
escort of about the same displacement

Some Other High-Performance Ships

Spar Ship—This craft was designed to be an effective and inexpensive sonar ship. The
principal idea was to submerge the sonar dome as deep as possible on a surface ship. It
was also desired to have minimum motions. Speed was not an important parameter. These
ideas led to a ship having a vertical distribution of displacement rather than horizontal
(see Fig. 20).
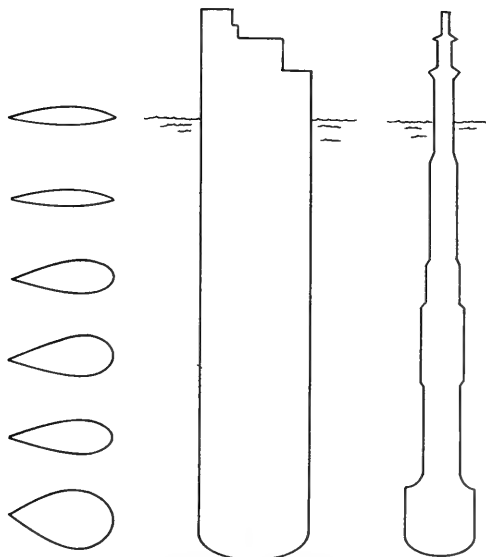
Fig. 20. A spar ship

In the course of exploring the feasibility of this concept a number of interesting problems arose. The speed was low, as expected, but model tests showed that the vertical location of the center of resistance varied considerably with speed. This caused substantial changes in running trim. The form was also highly directionally unstable as one might expect.

Natural heave periods were calculated which indicated supercritical heave motions in practically all seas. No tests were made, however. The practicability of the concept is admittedly questionable. For instance, consider the problem of taking the ship in and out of harbors. The only apparent way to do this would be to provide ballasting arrangements to permit the ship to be brought to a horizontal position. The problems of reorienting through a 90-degree angle are all too obvious and painful, but not impossible.

Catamarans (Planing and Displacement)—The yachting and small boat magazines have had many articles praising the sea-keeping characteristics of planing catamarans. This was all qualitative information. A testing program has been initiated at the David Taylor Model Basin to develop quantitative effects. There are no results at this time. This configuration has promise of allowing planing in relatively high waves, a characteristic that has not been attained with conventional planing craft. Structural problems will require careful attention.

Hulls of Minimum Wave-Making Resistance—Theory by Weinblum, Martin, Kotik and others have developed waterline shapes that should produce minimum wave-making for a given Froude Number. In the speed range of interest, a Coke-bottle form appears to be optimum. As this involves the danger of flow separation, tests are being formulated for comparison of model and theory. Motion tests are planned for the future. If the model tests check the theory, feasibility studies of practical ships will be made to determine application possibilities.


DEVICES TO INCREASE THE PERFORMANCE OF CONVENTIONAL SHIPS

To Increase Speed

In addition to unusual hull forms, there are various devices by which high speeds may be obtained. One such means might be boundary layer control to reduce frictional resistance. This could be accomplished by sucking off the boundary layer at various places along the length of the body. The objective would be to maintain laminar flow; this, ideally, would reduce frictional resistance to about 15 percent of its normal amount. The problem areas are: How much power is needed to suck in the boundary layer? If the boundary layer is drawn off through a porous outer shell, how can clogging of the pores by marine life be prevented? If slots are used, what should their size, shape and location be?

Another possibility is to enclose the body by a gas. Ideally, this would reduce the frictional resistance to about 15 percent of its normal amount. The major problem here is the stability of the gas film. If the gas goes into bubble form, experience has shown that resistance is only slightly decreased.

A third method would be to use a coating that absorbs the energy in perturbations in the water. A theory, as yet unpublished, by Boggs of the United States Rubber Company, indicates that a coating could be devised to maintain laminar flow up to very high Reynolds numbers.

These three methods of reducing frictional resistance may have application to midget submarines, and possibly to larger craft, but theoretical and experimental evidence to substantiate claims and predictions is yet to be acquired. These methods appear to have more promise in a relatively low range of Reynolds numbers than at the high Reynolds numbers at which large ships and submarines operate.

Another approach to the goal of high speed is to increase the efficiency of propulsion devices. No dramatic improvements in this area appear to be in the immediate offing. However, a number of promising new types of propulsive devices are under study and some older ideas are being refined—to name a few: supercavitating or superventilated propellers, pump jets, Kort nozzles, cycloidal propellers, oscillating fins, and two-phase flow jets. Details of these and others, would require too much space for this paper to encompass.

To Control or Minimize Motions

From the control point of view, there are a few devices that hold promise for competing with the highly efficient, standard ship rudder. One of these, the cycloidal propeller, is well known. Another is the jet flap, currently under study for aircraft. Design data, including mass flow vs rudder effectiveness, are being obtained. Yet, another competitor for the rudder is the ring airfoil developed originally for aircraft. Preliminary results indicate excellent control characteristics.

The problem of minimizing motions by using devices has been part of the research effort of the Navy and Merchant Marine for many years. For roll control, gyrostabilizers, active fins, and Frahm tanks are available. Reexamination of the last named, in recent years, has shown that by good design, passive tanks can be quite effective in reducing roll. Considerable effort has recently gone into pitch stabilizers. Fixed fins at the bow can significantly reduce pitch. Under study today are moving fins at bow and stern and flapped ducted propellers.

CONCLUSIONS

High performance ships are basic and very vital objectives of Naval Research and Development. Within the last few years, these objectives have been pursued by special attention to unusual hull forms. A number of these forms are nearing readiness to be incorporated in useful craft; notable among these is the hydrofoil craft.

Modern technical advances, especially in aerodynamics, hydrodynamics, and power plant development are exerting strong influences on ship design. For example, a hydrofoil craft was flown by Alexander Graham Bell at the end of the 19th century, but we would not be investigating, so thoroughly, the promises of hydrofoils if we did not today have high-power, lightweight machinery plants (marine gas turbines), an understanding of supercavitating foils, and strong, lightweight structure.

This is the time to look at our old compromises, and reevaluate them in the light of the new technology. We are not depending on "breakthroughs," but rather recognize that the pace of advance has quickened and the breadth of the front has widened.

The broad spectrum of craft shown in Fig. 21 illustrates the many types of marine craft, and their relative quasi-efficiencies compared to the well-known Gabrielli-Von Karman
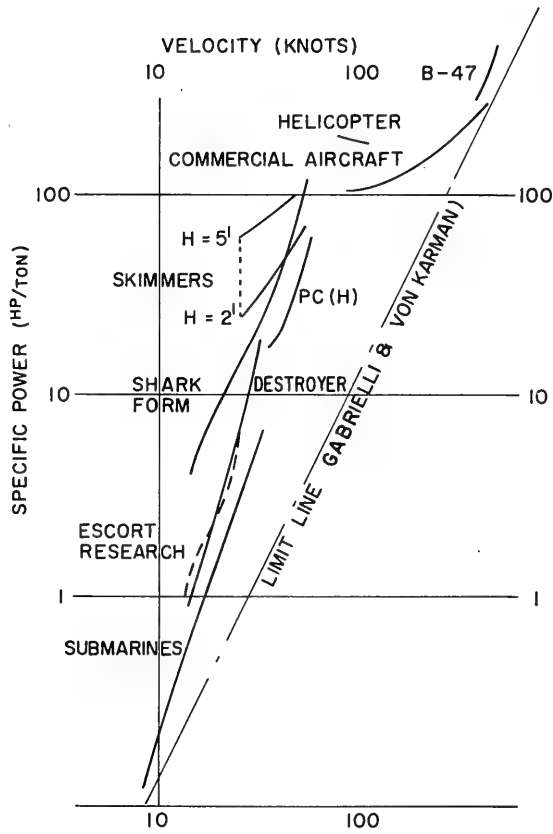
Fig. 21. Specific power curves

limit line. Of course, power per ton is not the only parameter; in the Spar Ship, for instance, this was considered of minor importance. Nevertheless, it does illustrate one facet of our high performance ships.

This paper by no means covers all the possible high performance ships. Only some of high promise have been discussed and these with the caution that for every promise there arises a multitude of problems.

DISCUSSION

(Discussion of this paper is included with that of the following paper, by J. D. van Manen.)

*   *   *

SIZE, TYPE, AND SPEED OF SHIPS IN THE FUTURE

J. D. van Manen
Netherlands Ship Model Basin

INTRODUCTION

Owners and builders of merchant ships generally view radical new ship designs with a certain amount of cautious reservation. These people frequently realize from past experience the expenses which accompany the development and application of new ideas in the field of naval architecture.

In serving naval interests, however, the situation is different. Military considerations and economic and psychological factors all play important roles. The seemingly uneconomical increases in the speed and power of tankers, and the development of nuclear propelled submarines, hydrofoil boats, and hovercraft are all projects which have been strongly stimulated by naval interests.

A speed increase of 18 to 20 knots is no longer being considered by the designers of high speed boats such as hovercraft. Indeed, speeds of 40, 60 and even 100 knots are now being discussed. Designers of these new and progressive ship types are being confronted with questions such as: How can we develop a 100-knot ship for operation on, beneath, or immediately above the surface of the water? or What is the maximum shaft power which we can install on one shaft? One might perhaps just as easily ask: What is the maximum length of a ship? The answer to this last question could, of course, be given as all the way from New York to Amsterdam, since optimum performance at sea has here been assured and guaranteed.

In all seriousness, however, the author hopes to convey that it can be nothing short of refreshing for the shipbuilder who is firmly established in mercantile construction to take an active part in and even take the very necessary initiative in the field of naval development.

If we but look carefully at the developments of the past 20 years, the following facts become unmistakably clear:

⋅ The design of ships, which has heretofore been primarily empirical in character, is clearly becoming more and more scientific and fundamental in nature. Increases in ship speeds and ship dimensions and the development of new and different types of propulsion systems have required ever more theoretical treatment.

Prior to 1940, the maximum shaft power which could be installed per shaft in merchant ships was in the order of 10,000 metric horsepower. At the present moment 16,000 shaft

23

horsepower is the normal case, and frequently 20,000-shp installations per shaft are encountered. Ship speed for tankers increased at the same time from 10 to approximately 17 knots.

The development of push boats has led to a large application of this type of transportation on inland waterways.

The rising importance of the hydrofoil boat is undeniable. The application of the hovercraft principle to marine vessels at the present time offers unknown prospects.

These imposing developments have induced several investigators to make speculative examinations of future possibilities. Gabrielli, Von Karman, Davidson, and others have kept themselves busy with more or less philosophical considerations in the field of transportation.

Representative of their ideas is the relationship between the dimensionless constant $P/V_s\Delta$ and the speed coefficient $V_s/\Delta^{1/6}$ for various means of transportation. The various ranges of this relationship are clearly presented in Fig. 1 for displacement ships, submarines, hydrofoil boats, hovercraft, and so forth.

The philosophy behind this presentation in Fig. 1 is that there will always be a requirement for new developments in a vehicle whose characteristics permit it to be placed in a blank area of the plot. In accordance with this thought process both hydrofoil boats and hovercraft are always meaningful. They may be expected to fulfill already existing and yet to be established requirements.

Supertankers

Supertankers form a type of ship which is indeed one of the most spectacular examples of increases in displacement and speed of ships. In Figs. 2a, 2b and 2c, several characteristic properties of supertankers are given on the basis of cargo carrying capacity or deadweight tonnage. The various points on these plots are derived from model tests conducted at NSMB; the curves presented are faired lines drawn through these points as accurately as possible, without any correlation analysis. Noteworthy in Figs. 2 are the following:

The increase in the beam-draft ratio, B/T, with increase in deadweight tonnage. The limitation in draft to a maximum of about 10 meters in connection with the expected depth of water in harbors thus plays an important role.

The increase in the block coefficient δ_{11} with larger deadweight tonnages is alarming by comparison with standards which still were valid 15 years ago.

Finally, the power required for ships' speeds between 15 and 17 knots and deadweight tonnages above 50,000 metric tons deserves consideration. Considered from this point of view, the development of diesel engines of 20,000 to 22,000 hp in one 10- or 12-cylinder installation is not amazing.

The large power per shaft in these extremely full ships has caused serious vibration phenomena and has led to damage. Experimental research has shown that extreme afterbodies, for the obtaining of a uniform circumferential velocity field in way of the propeller, and propellers other than the conventional screw must be taken into consideration.
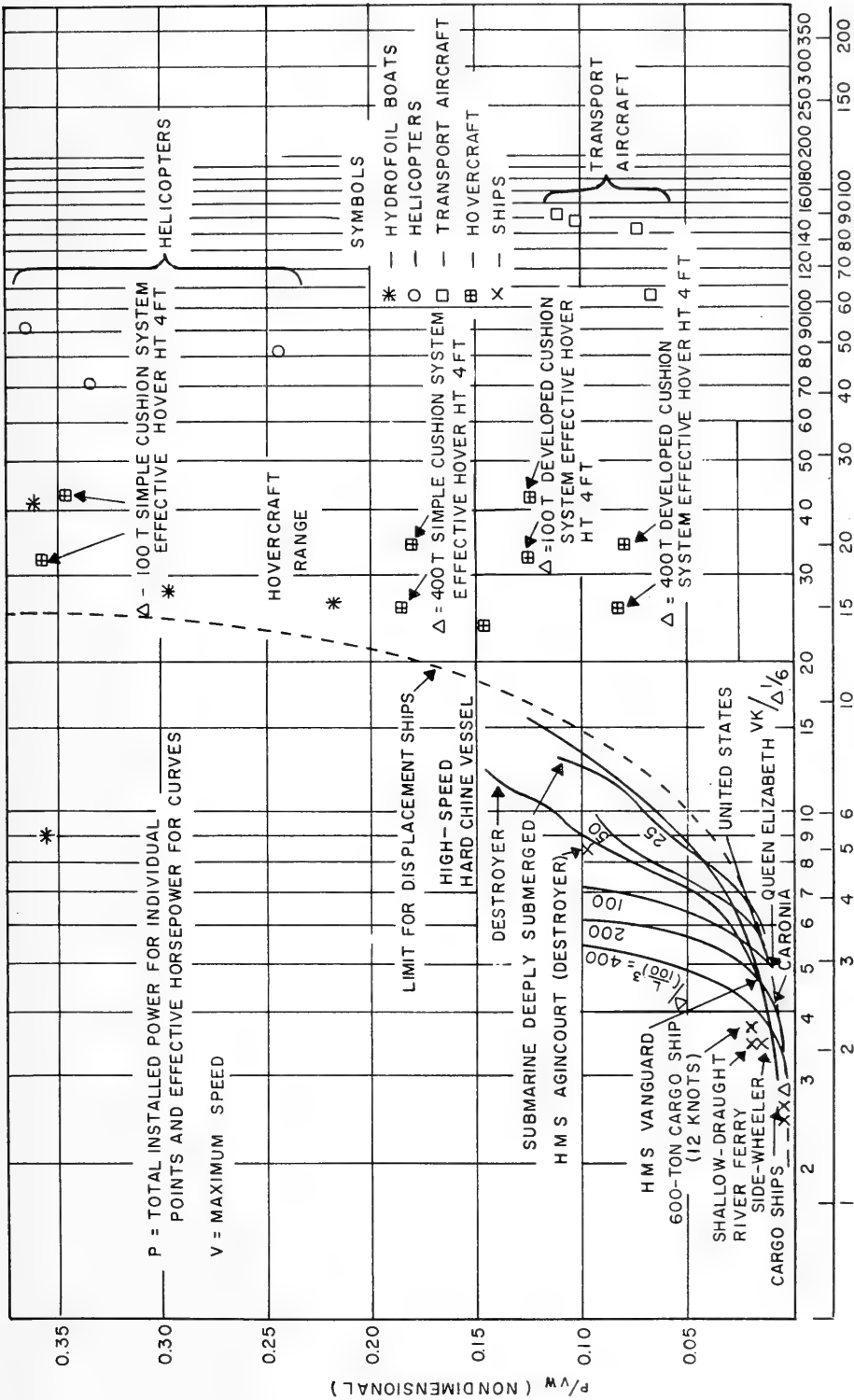
Fig. 1. Comparison between specific resistances of ships, boats, hovercraft, and aircraft (from Crewe and Eggington)
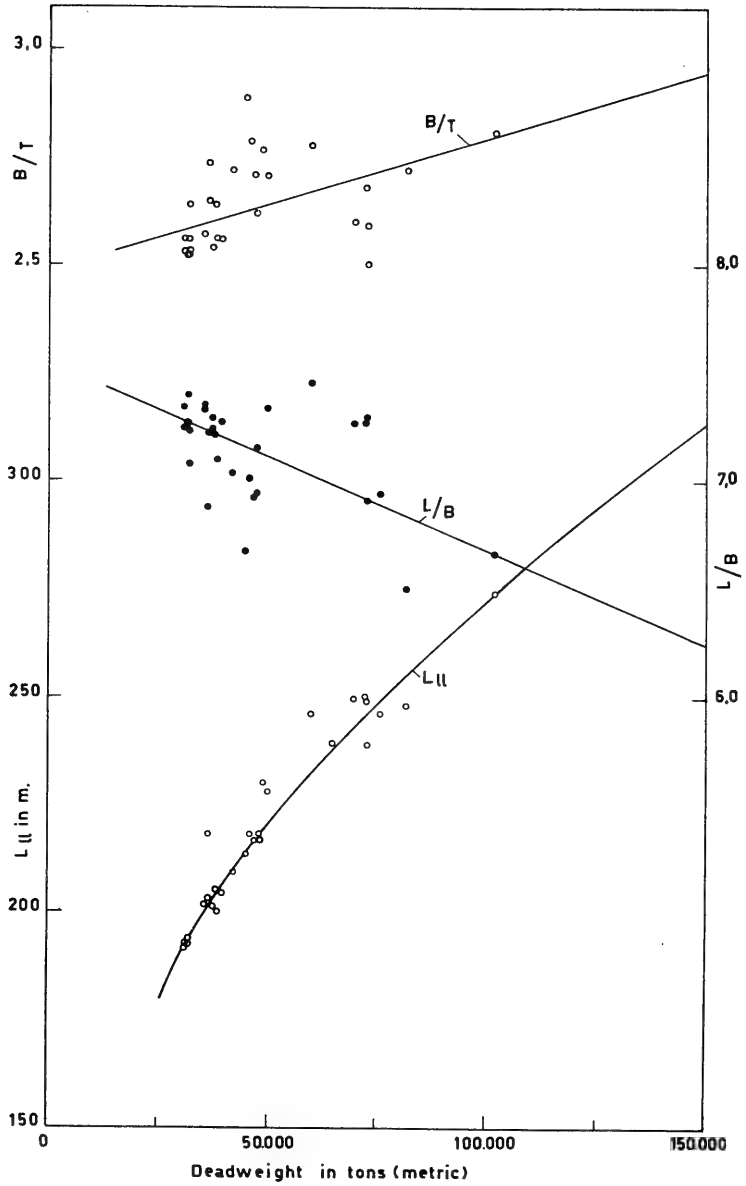
Fig. 2(a) Characteristic properties of supertankers
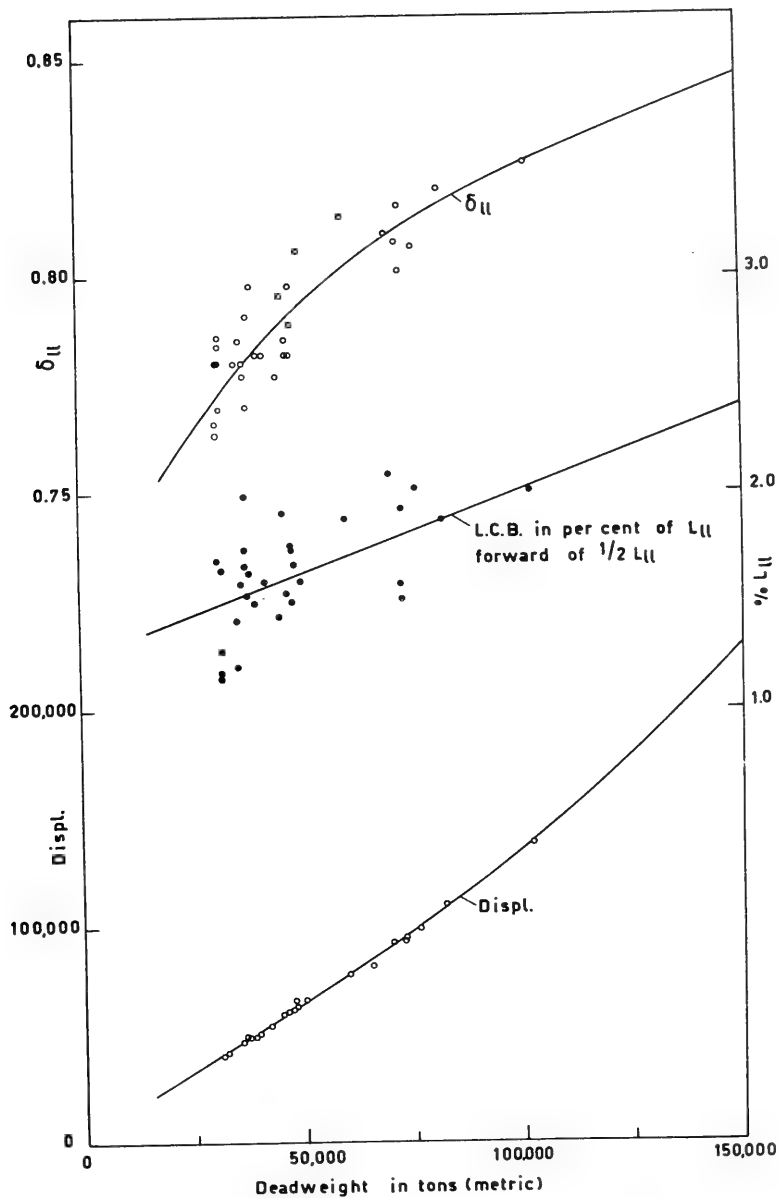
Fig. 2(b) Characteristic properties of supertankers
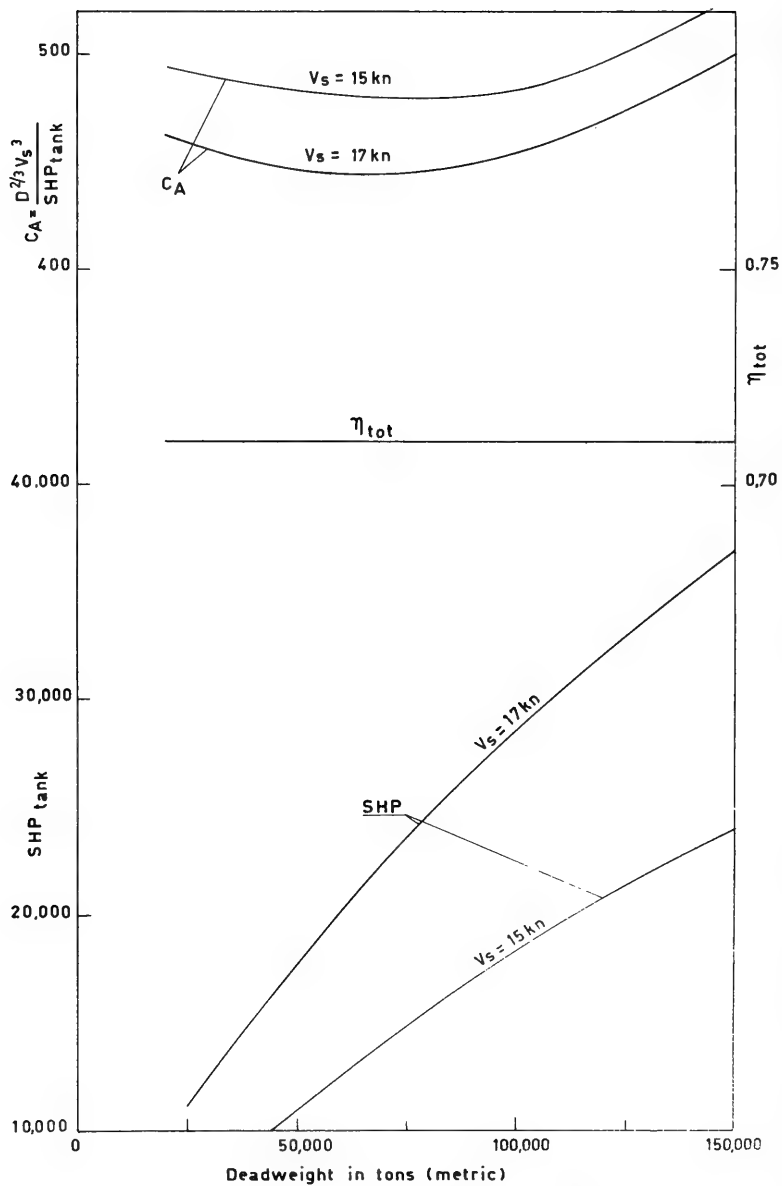
Fig. 2(c) Characteristic properties of supertankers

The 2-percent saving in shaft horsepower obtainable with the cigar-shaped Hogner afterbody provided with a complete ring nozzle propeller system becomes highly significant when considered together with the 25-percent reduction in propeller diameter obtainable over that of a conventional screw, and with the notably reduced vibration and cavitation characteristics (Fig. 3 and Table 1).

Table 1

Effect of Afterbody Shape on Propulsion

Results of Resistance and Self-Propulsion Tests on a Model of a 39,000-ton Tanker

(loaded condition; speed, 16 knots; 16,000 shp)

Afterbody	Screw	Number of Blades	Total resistance (percentages— afterbody I = 100)	DHP (percentages— afterbody I = 100)	Propulsive Coefficient
I (moderately U-shaped)	A	4	100	100	0.74
II (extremely V-shaped)	A	4	97	106	0.67
III (extremely U-shaped)	A	4	103	102	0.75
IV (Hogner form)	C	4	108	103	0.77
V (III + nozzle)	D	4	103	101	0.75
VII (twin screw)	G	3	100	105	0.70
VIII (Hogner + nozzle)	D	4	108	98	0.81
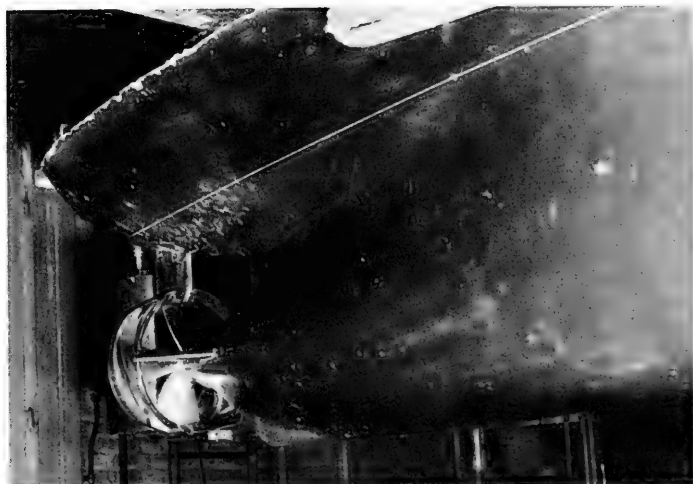
Fig. 3. Tanker model with cigar-shaped afterbody and a propeller
operating in a nozzle ring

Another question which must be asked for supertankers is: At which speeds and dead-weight tonnages does the submarine tanker, through application of nuclear propulsion, become competitive with its surface counterpart.

In general, it is to be expected that, for a cargo carrying capacity of 20,000 dwt and a speed larger than 20 to 25 knots, the submarine tanker will have a distinct advantage over the conventional tanker. The Electric Boat Division of General Dynamics Corporation has made, under contract to the Maritime Administration, a study of nuclear propelled submarine tankers for mercantile application. Neither military nor economic factors were considered in this study, which embraces 27 different designs.

The 27 designs were carried out for ship speeds of 20, 30, and 40 knots, cargo carrying capacities of 20,000, 30,000, and 40,000 dwt, and for three types of cross section, namely, rectangular, limited in draft; rectangular, unlimited in draft; and circular. The designs restricted in draft were made suitable for harbor depths of water of about 11 meters.

Of these 27 designs, two types of submarine tankers appear worthy of further development: the most conservative, and the largest and fastest.

The Most Conservative

The most conservative design would be one of rectangular cross section, limited in draft, for which the following numerical data would apply:

Cargo deadweight	21,189	tons
Speed	20	knots
Surface displacement	38,791	tons
Submerged displacement	42,671	tons
Loaded draft	35	feet
Length	583	feet
Beam	80	feet
Depth	40	feet
Total power required	35,000	shp
Number of screws	1	

The Largest and Fastest

The following design is currently considered as an upper limit in ship speed and cargo carrying capacity because of the present state of power plant technology:

Cargo deadweight	41,565	tons
Speed	37	knots
Circular cross section		
Maximum diameter	80	feet
Surface displacement	91,903	tons
Submerged displacement	101,000	tons
Loaded draft*	67	feet
Length	936	feet
Total power required	240,000	shp
Number of screws	4	

---

*Made possible by the addition of a parallel middlebody.

Noteworthy here is that Electric Boat Division currently considers 60,000 shp the maximum which can be installed per shaft.

TYPES OF PROPELLERS

After the numerical data mentioned in the preceeding section, a discussion of propulsion seems desirable.

A frequently used method of expressing the characteristics of a propeller type is the relationship between B_p- δ and η_p for optimum propeller diameter. These are defined as:

the design coefficient:

$$B_p = \frac{N\sqrt{P}}{V_a 2.5} :: K_Q^{1/2} \cdot J^{-2\frac{1}{2}}$$

the diameter coefficient:

$$\delta = \frac{ND}{V_a} :: J^{-1}.$$

This optimum relationship is given in Fig. 4 for various types of propellers, namely, (1) supercavitating propellers of the type TMB 3-50, (2) wide-blade propellers of the type Gawn 3-110, (3) propellers of the type Wageningen B 4-40, (4) propeller with nozzle rings of the type K 4-55, with a length-diameter ratio of 1/2. The range of profitable application of each type of propeller is given on the basis of B_p. The considerable difference between the optimum diameters of supercavitating and conventional screws and screws in nozzle rings is noteworthy.

Since an evaluation of types of propellers on the basis of B_p- δ can be troublesome for those who do not work with this type of data every day, a more convenient and instructive method of presentation is given in Figs. 5(a), 5(b), and 5(c) illustrating the general tendencies of the propellers discussed.

In Fig. 5(a), the power-rpm relationship is given for various speeds and diameters, as derived from the optimum relationship presented in Fig. 4, for supercavitating propellers. The cavitation thresholds, according to Tachmindji and Morgan, and the limit of efficiency $B_p = 3$, beyond which this type of propeller would not be utilized, are given for 60, 80, and 100 knot speeds. Only one line of constant propeller diameter, i.e., $D = 1$ meter, is given. Other lines of constant diameter greater than 1 meter would appear to the right in the diagram. For reasonable application of a supercavitating screw with a diameter of 1 meter, a minimum speed of 54 knots is desirable.

In Fig. 5(b), the optimum B_p- δ relationship is presented in the same manner for conventional screws of the Wageningen B 4-40 type. If the limit of 60,000 shp given by Electric Boat is adhered to for installed shaft power, then this appears to lead to inadmissably large propeller diameters for speeds of 20 knots. For 40-knot speeds with 250 rpm there still appear to be possibilities.

The same data are presented in Fig. 5(c) for the K 4-55 series operating in ducted nozzles with a length-to-diameter ratio of 1/2. The superior properties of this type of propeller with respect to maximum installed power for relatively low speeds is clearly evident.
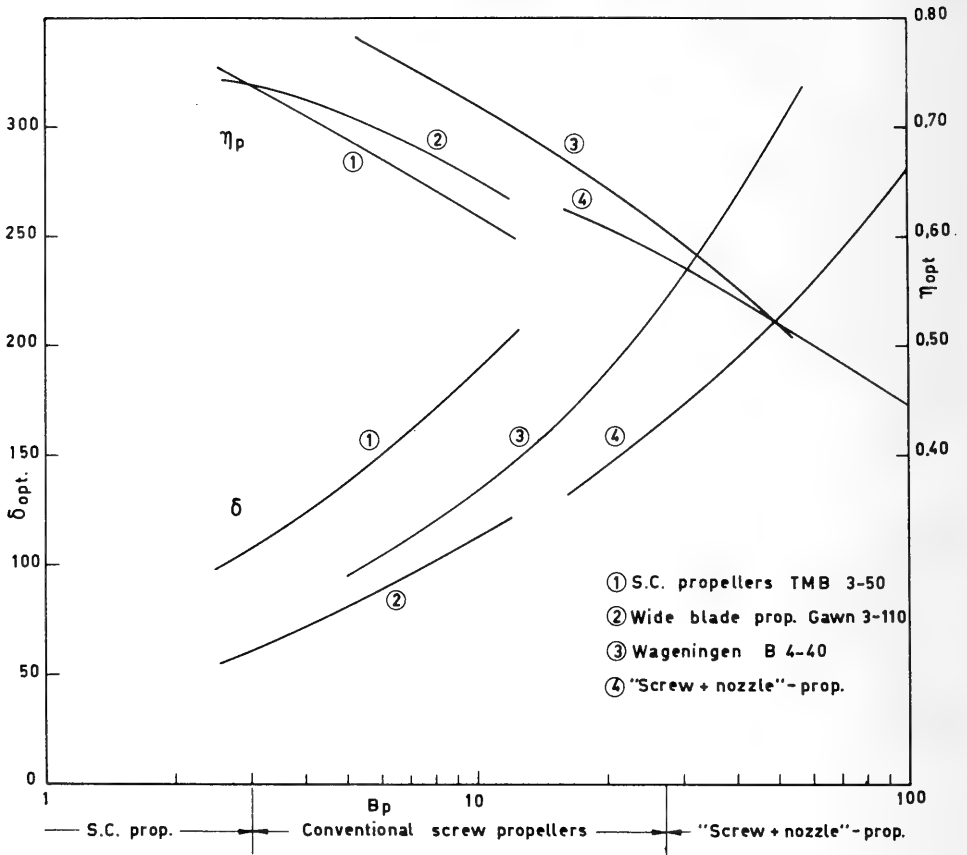
Fig. 4. Optimum relationship of B_p and δ for various types of propellers

Further investigations will have to indicate whether increasing the rpm of the ducted screw or of the supercavitating screw, or whether going to an entirely unknown field, ducted supercavitating propellers, is preferable.

GEMS AND HYDROFOIL BOATS

With the aid of Figs. 1 and 5(a) it is possible now to make estimates of size and shaft power for the design of high-speed craft such as GEMs (hovercraft) and hydrofoil boats.

Let us for the moment assume a reasonable and realistic power coefficient $P/V_s\Delta$ = 0.20. Then it follows from Fig. 5(a) that for an 80-knot hydrofoil boat with a 1-meter-diameter screw the maximum installed shaft power would be in the order of 4,000 shp, whence it follows that for a single screw craft a displacement of about 40 tons could be propelled. Therefore, for 80-knot speeds, hydrofoil boats will thus be limited, even with the installation of more screws, to cargo carrying capacities of from 40 to 120 tons.
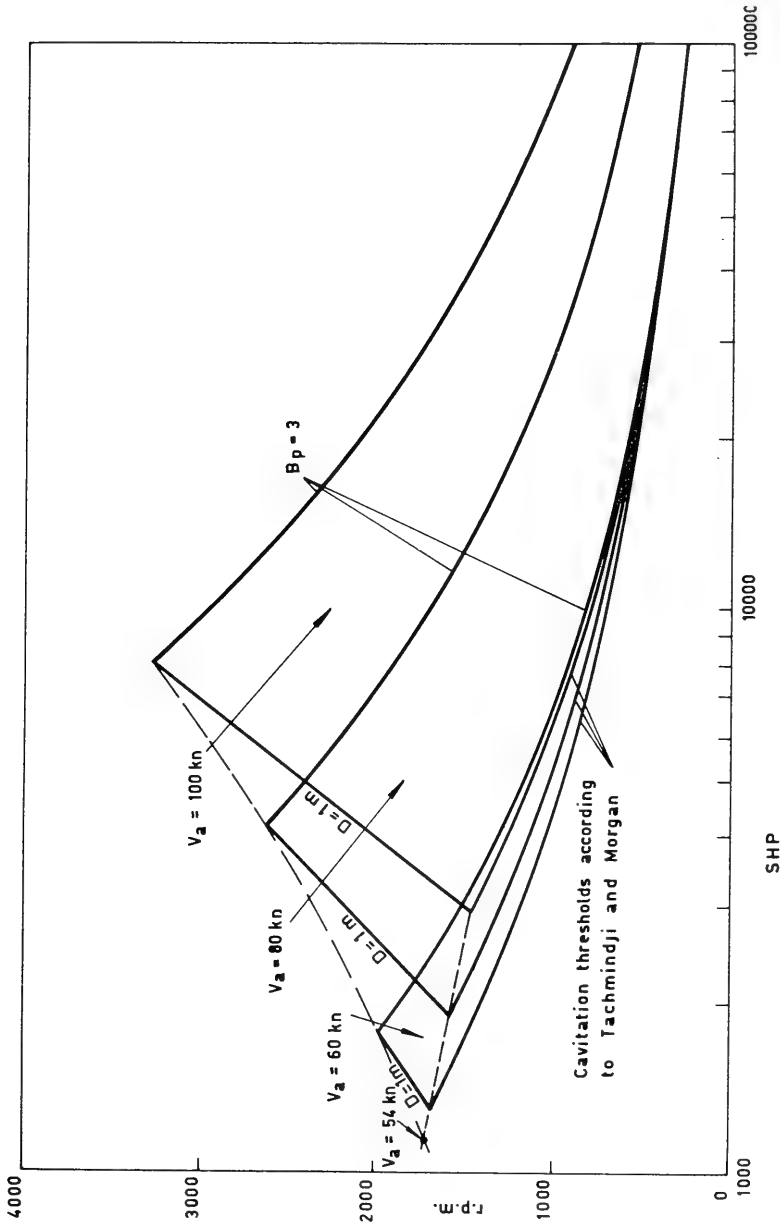
Fig. 5(a) Optimum power-rpm relationship for various speeds and diameters for supercavitating propellers
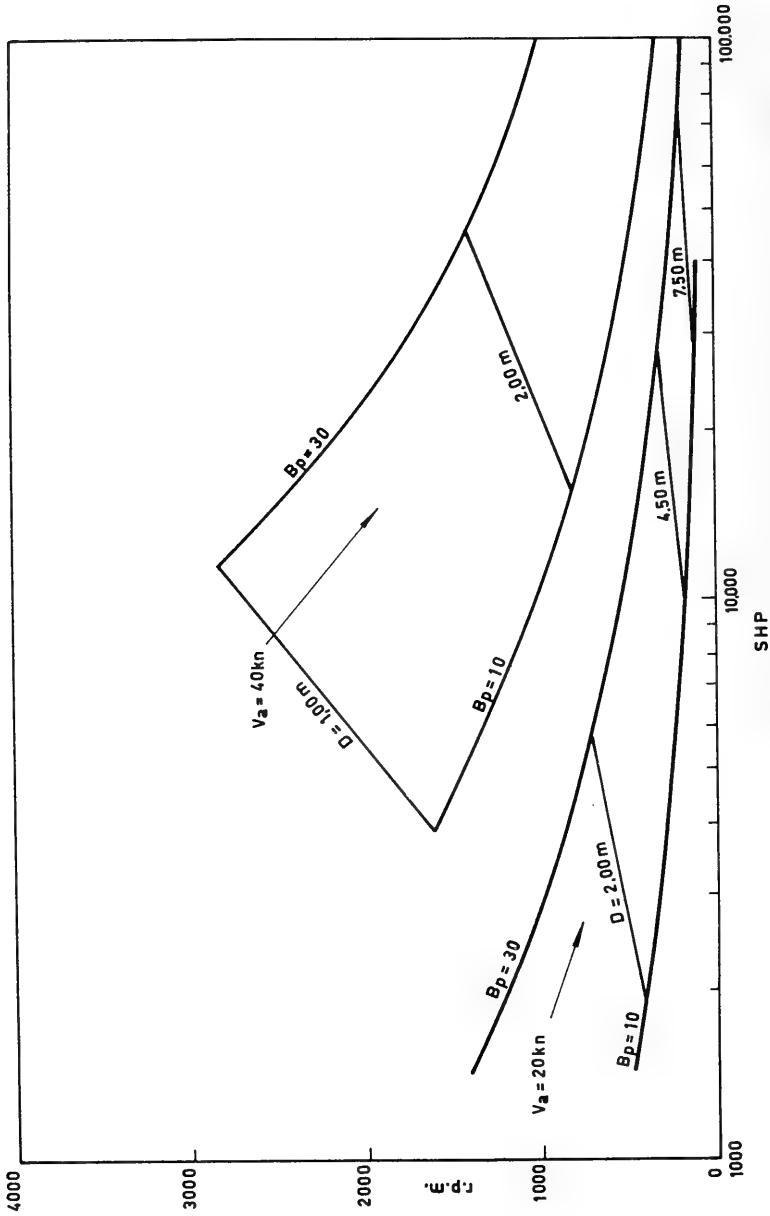
Fig. 5(b) Optimum power-rpm relationship for various speeds and diameters for conventional screw propellers
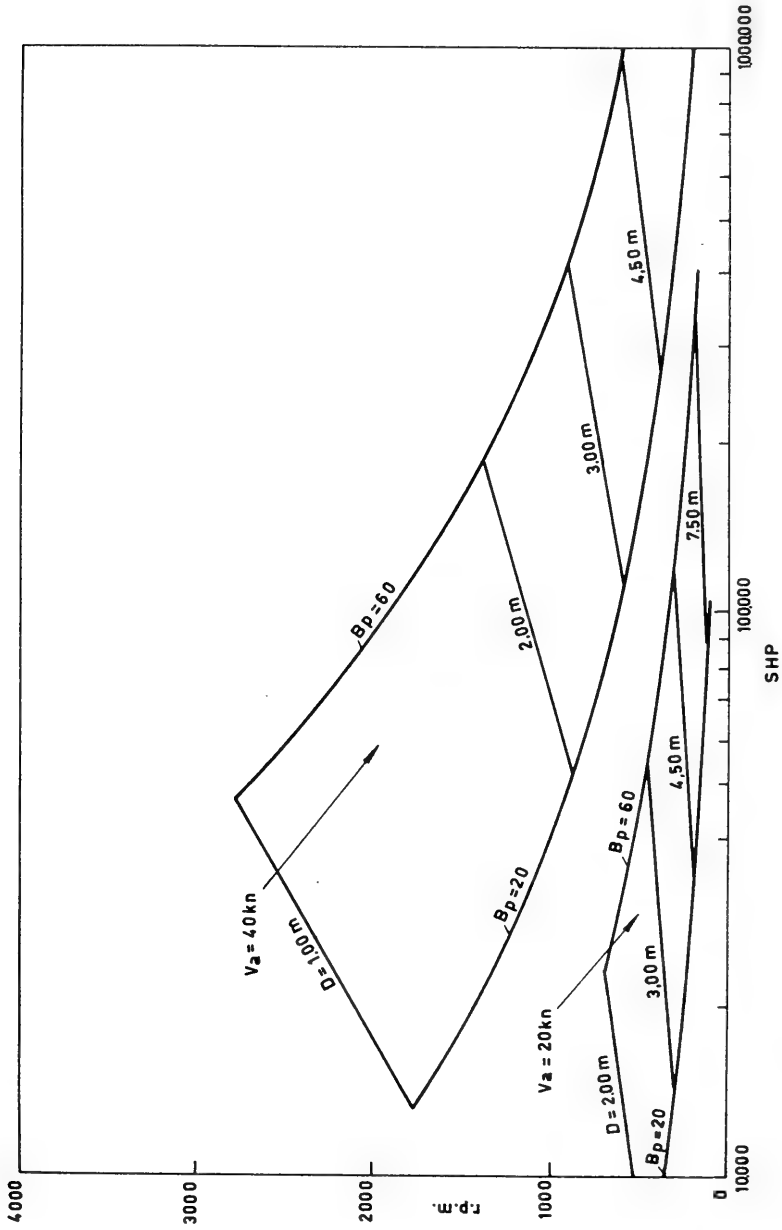
Fig. 5(c) Optimum power-rpm relationship for various speeds and diameters for "screw plus nozzle" propellers

If we continue this estimate of dimensions of prototypes in the same manner for a hover-craft, such as, for example, the 400-ton Crewe and Eggington project, then a power coefficient of $P/V_s\Delta = 0.15$ appears to have been chosen by the designers ($P = 40,000$ hp, $V_s =$ 100 knots, $\Delta = 400$ tons).

A rough weight distribution might appear as follows:

800 passengers plus 80 motor cars	160 tons
40,000-hp turbine, at 1.5 kg/hp*	60 tons
Fuel for 24 hours	130 tons
Hull	50 tons

With a diameter of 100 meters (air cushion pressure 50 kg/m²) the weight of the structure becomes 5 kg/m². A further study of the lifting mechanisms and possible structural forms will be necessary to indicate how much the hull weight has to increase at the expense of the pay load.

If the supposition is made that 50 to 60 hp per ton of displacement are required for hovering, then from 20,000 to 24,000 hp will be required to maintain the air cushion. How much special provisions such as Weiland's labyrinth seal can improve this situation remains yet to be seen. We will therefore use 20,000 to 16,000 hp to give the 400-ton GEM a 100-knot speed. The important question which then pre~nts itself for the case of a seaborne GEM is whether to use air or water propulsion. In Fig. 7 the optimum diameter and efficiency of supercavitating propellers in water and ducted propellers in air are compared against a basis of B_p. From this it appears that the diameter of the ducted propeller in air is approximately three times as great as that of a comparable supercavitating screw in water. The efficiency in air is approximately 40 percent lower than the efficiency in water.

Proceeding from an assumed propulsive efficiency of 0.75 in water and 0.45 in air, then for the available power of 20,000 hp and a speed of 100 knots, the following resistances per ton of displacement can be overcome:

55 kg/ton for water propulsion
33 kg/ton for air propulsion.

Whether it will be possible to choose the hull form and the operating height of the GEM so that these values can be reached, the future will have to show us. If we consider the water resistance negligible at these high speeds and assume the transverse sectional area of hovercraft and air cushion to be 600 m², then a resistance of 55 kg/ton in the case of water propulsion implies a drag coefficient of 0.23, which is comparable to that of an automobile.

In view of the large difference in efficiencies for water and air propulsion for a 100-knot GEM, water propulsion for a seaborne GEM should be considered. However, from these calculations for high speed GEMs one might be inclined to consider displacements, as predicted for hydrofoil boats, in the range from 40 to 120 tons to be more attractive.

Summarizing this introductory paper to this Symposium on High Performance Ships the following might be concluded.

---

*See Fig. 6.
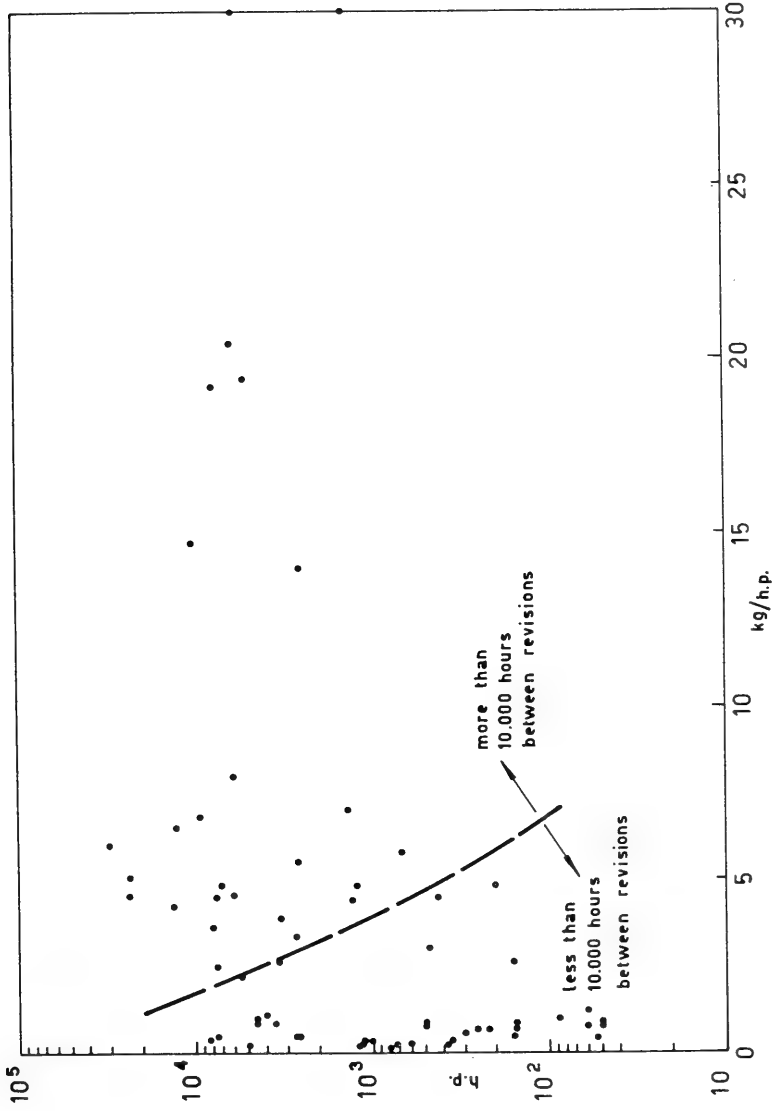
Fig. 6. Relationship of horsepower and specific weight for gas turbines for ships according to Diehl

J. D. van Manen
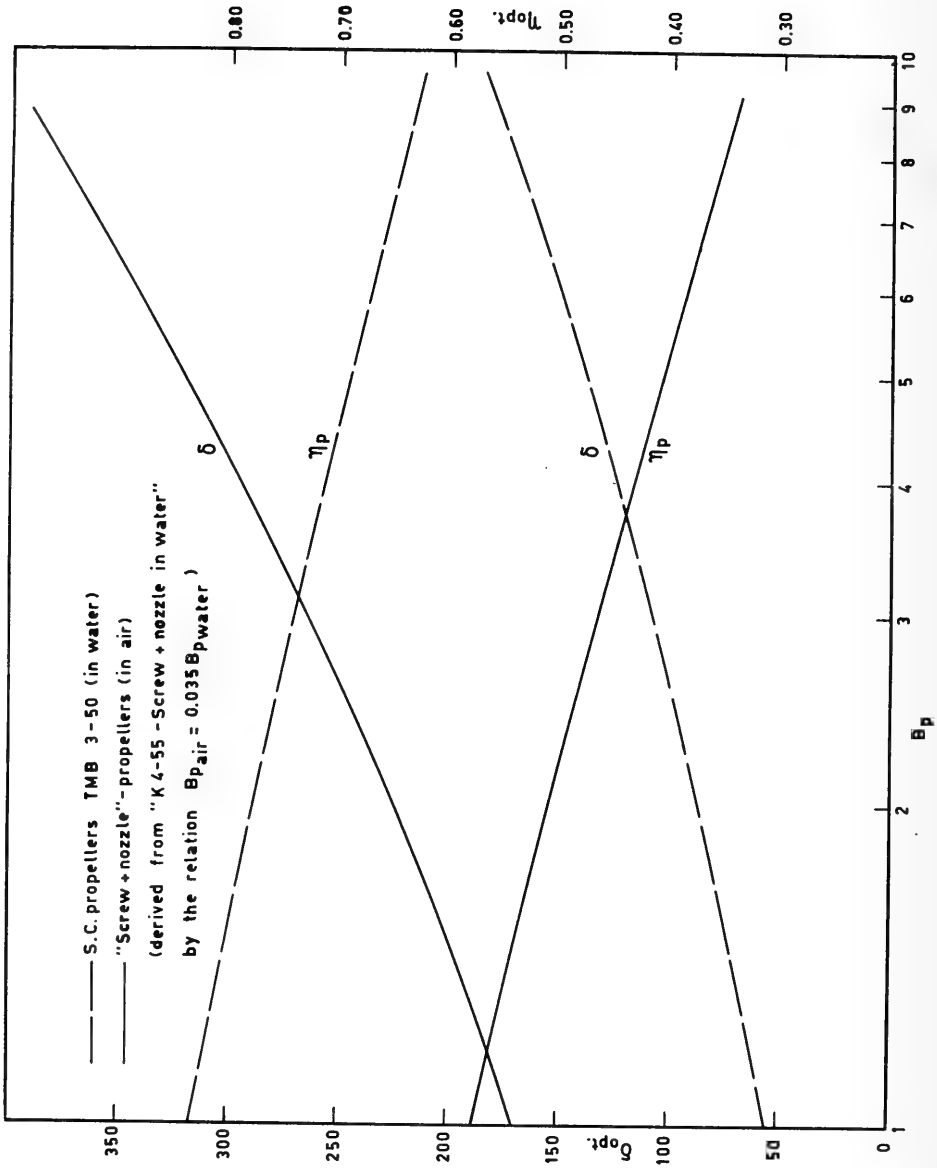
Fig. 7. Comparison of optimum diameter and efficiency of supercavitating screw propellers in water and "screw plus nozzle" propellers in air

For displacement ships (cargo), the increase in ship speed will stop between 20 and 25 knots. Above these speeds, the nuclear powered submarine will get its chance (future). The maximum draft will be limited to 10 to 11 m by harbors and docking facilities.

For submarine vessels (merchant ships), the limitations in horsepower per shaft and in available space for engines, especially athwartships, results in a maximum deadweight for submarine of 40,000 tons at a ship speed of 37 knots.

For hydrofoil boats, extremely high speeds such as 60-80 and 100 knots seem to be obtainable. The displacement of such high speed hydrofoil boats will be restricted to about 100 tons or less.

For GEMs, displacements greater than 100 tons combined with extremely high speeds (100 knots) lead to serious construction and propulsion difficulties. Propulsion in water seems to be attractive for a seaborne GEM.

DISCUSSION

R. N. Newton (Admiralty Experiment Works)

My remarks bear upon the papers presented by both Mr. Oakley and Dr. van Manen and concern those parts which deal with hydrofoil craft and hovercraft.

The considerable experience already acquired with hydrofoil craft leaves no doubt that one clear advantage of this type of craft over the orthodox displacement or planing types is the ability to maintain higher sustained speeds in a seaway. The same advantage, associated with higher speeds still, is being claimed for the more recent hovercraft or GEM.

One question which has yet to be resolved, however, is the extent to which this particular advantage applies; that is to say, it is necessary to qualify the words "in a seaway" to cast a true comparison with, say, the planing craft. The moral can be pointed, in humorous and yet serious vein in the present context, by this quotation from the writings of Hilaire Belloc:

> "The water-beetle here shall teach
> A sermon far beyond our reach;
> He flabbergasts the human race
> By gliding on the water's face
> With ease, celerity and grace;
> But if he ever stopped to think
> Of how he did it, he would sink."

Whatever form the humanly conceived "water-beetle" may take, I submit the time has arrived to think seriously as to what state of sea would force it to stop and whether it would, in fact, then sink.

Assuming no breakdown of the engines to occur the craft can be forced to land on the sea from two principal causes:

1. Encountering waves of length and height in which it is not designed to operate. Statistical or spectrum analysis of the sea conditions in the operating area can provide much data to guide the design of the craft as regards lift, stability, control, and response. It can also provide an assessment of the probability of meeting isolated severe waves, but these cannot be predicted in the true meaning of the word.

2. Impact with such isolated severe waves, or even waves over which the craft is designed to operate if, for instance, a defect develops in the control system. In this connection, it should be noted that while models of the size normally associated with ship tank work can be used to measure the external forces, an assessment of the stresses induced by these forces is a matter for the structural designer. To relate the stresses measured in the full scale craft directly to those measured in a model, the latter would need to be of the order of 1/2 to 3/4 full size. So far as I am aware, no attempt to carry out investigations of this nature has yet been made, but presumably data available from flying-boat investigations would provide valuable guidance. It is significant also to add that the structure of hydrofoils and GEMs can hardly be regarded as "robust" in comparison with displacement or planing craft.

Having been forced to land in severe conditions from any such cause as 1 or 2, or due to engine failure, the question arises: Can the craft withstand the normal bending and shear forces imposed in a seaway, or the impactive forces due to slamming? The answer to this question also has yet to be resolved but in the absence of data on the subject, it is fairly sound to assume that present designs would need to be strengthened.

It is realized these observations may be regarded by some as being very pessimistic. At the same time, it is necessary to place the possibilities of high performance craft in their proper perspective in relation to what can already be achieved by displacement craft in unexpected severe weather conditions. The simple fact is that the planing or displacement craft can successfully sustain any sea condition, and proceed, even though the speed may be considerably reduced. Actually the reduction of speed is not so serious as is sometimes implied. Comparisons can be odious and figures can be exaggerated in the absence of factual data. Nevertheless it is my opinion that, for instance, size for size, the planing craft will still be capable of proceeding at nominally high speeds in conditions when the hydrofoil or the GEM is brought virtually to a standstill. In such conditions it is the planing craft which has an overwhelming advantage. Incidentally it must not be forgotten that a planing craft to carry 50 to 60 passengers at speeds exceeding 50 knots in calm water now offers no design or constructional difficulties.

The conclusion to be drawn from these few comments on this one aspect of the possibilities of high performance surface craft is that there exists a real need for investigations to determine more precisely their limitations in irregular sea conditions. This entails not only the advancement of theory and model experiment but also correlation with full scale results in similar conditions at sea—a long and arduous task following the lines of what is already being attempted for displacement craft. Costly and time consuming though the task may be it is quite essential to carry it out if any real comparison is to be made between the orthodox and unorthodox type of craft. If it is not carried out then the risk must always remain that a craft designed for some specified state of sea will meet more severe conditions and suffer serious damage or even loss, and as so often happens with new ventures, this could cause a serious setback, if not cessation, in development.

E. V. Lewis (Davidson Laboratory, Stevens Institute of Technology)

I wish first to compliment Mr. Oakley and the Bureau of Ships on their far-sighted viewpoint in considering such a wide range of possible vehicles for military use. The escort research ship in particular I am certain will be a significant milestone in naval ship design.

In its own way the modern supertanker considered by Dr. van Manen has been a truly spectacular development. In this connection it is rather surprising to find in Fig. 2(c) that the author expects to maintain a constant overall propulsive coefficient of about 71 percent in ships up to 150,000 tons deadweight. Presumably he is assuming single screw vessels, and I would expect a reduction in efficiency as size continues to increase. My reason for expecting this trend is that for geometrical similarity the propeller diameter should go up and rpm down in order to maintain good propulsive efficiency. However, in actual ships practical considerations seem to have limited propeller diameter and prevented reduction in rpm. Dr. van Manen has apparently counted on the application of improved sterns and nozzles to maintain the efficiency of the heavily loaded propellers of larger and larger ships. Perhaps he will care to comment on this point.

J. D. van Manen

In reply to Prof. Lewis I will mention a total efficiency of about 71 percent in Fig. 2(c) is only based on statistical data.

H. Lackenby (The British Shipbuilding Research Association)

I should like to raise one or two points on Dr. van Manen's paper concerning the speeds and powers of displacement ships.

Firstly, it is stated in his Introduction that up to 1940 the maximum shaft horsepower which could be installed per shaft in a merchant ship was about 10,000. I am sure the author is referring here to single screw ships and I think perhaps that this ought to be stated. For multiple screw ships much higher powers per shaft were, of course, installed.

In this connection it is also stated that 16,000 shp is now normal and that 20,000 is frequently encountered. This is followed by the statement that at the same time tanker speeds have increased from 10 to 17 knots. This is quite true of course, but I think it might be mentioned that this speed increase was largely a natural consequence of increasing size and that in many instances it was a question of keeping the speed-length ratio about the same and increasing the speed according to the square root of the length. In other words there was a significant speed advantage in having a longer ship.

The author's references to the larger block coefficients now being associated with the high deadweight supertanker are of particular interest, and it is interesting to recall how views on this have changed, bearing in mind that between the wars one authority advised that no seagoing ship should have a block coefficient greater than 0.75. According to Fig. 2(b) we find that the largest block coefficient for the Wageningen models plotted there is about 0.825. It might be of interest to mention here that the British Shipbuilding Research Association in conjunction with Ship Division, NPL, are now endeavoring to develop oceangoing forms with block coefficients up to 0.85.

Next, a point about the economic comparison between a conventional and a submarine tanker. It is stated in the paper that for 20,000 tons deadweight and a speed of 20 to 25 knots the submarine tanker would have a distinct advantage. One has to be careful here of the basis of comparison—I think this is intended to be a surface tanker of 20,000 tons and 20 to 25 knots speed. This of course is not conventional as regards speed and would certainly be less economical than a commercial tanker of this deadweight which would have a speed round about 15 to 16 knots. I am speaking here, by the way, of economy on the basis of cost per ton-mile of cargo carried. On the other hand, from the military point of view, there may of course be some advantage in carrying the cargo at the faster speed.

J. D. van Manen

In reply to Mr. Lackenby, the 10,000 hp before 1940 refers to a single screw ship.

D. Savitsky (Davidson Laboratory, Stevens Institute of Technology)

The presentations by Mr. Oakley and Dr. van Manen on the subject of high performance ships of the future were indeed stimulating and exciting. The variety of hydrodynamic forms being considered by the authors is expressive of an open mind toward the consideration of solutions to the problem of high speed transport across the ocean.

Common to each of the vehicle forms considered by the authors is the serious problem of negotiating the rough surface of the ocean at high speed—a problem where severity appears to increase exponentially with speed. Partial solutions to the rough water problem are proposed by the use of submerged hull form, hull forms lifted clear of the water by hydrofoils and by ground effect machines flying just above the waves. In each case the roughness of the sea is still a serious disturbance, although to a lesser extent than for a displacement vessel. Clearly, the solutions proposed by each of the authors consist in a vertical displacement from the water surface.

I would like to carry this suggested solution to its logical conclusion and suggest that, for high speed transport over waves, let's leave the water surface entirely. If our mission is to transport material or people from one port to another at high speed, there is obviously no necessity for exposing the high speed vehicle to the serious disturbances of the sea for the entire length of the voyage. Obviously this suggestion leads to the rediscovery of the water based aircraft—especially designed for short range, low altitude, and relatively low speed operation (for an aircraft)—perhaps 200 to 300 miles/hr. Ordinarily I would not propose such a concept at a meeting on Naval Hydrodynamics. However, since the authors have discussed ground effect machines operating just over the waves at speeds of 100 mils/hr or more, I feel they have strayed sufficiently from the area of conventional hydrodynamic forms to allow me the freedom to do likewise. I feel that as the GEM concept is developed further and further, its appearance will be more like that of an aircraft. If this is to be the case, let us immediately consider the role of the water based aircraft for the short range transport vehicle. A well designed seaplane can easily develop a lift-drag ratio of 20 at altitude. Perhaps this can be increased by flying at low altitude (in moderate ground effect) yet out of the range of the severe wave disturbances of a sea state. To obtain equivalent lift-drag ratios, the GEM would probably need a static thrust augmentation factor of nearly 40, which would necessitate its operation at very low height-diameter ratios. For operation in a sea state of moderate severity, then, the length of the GEM would probably be upwards of 500 or 600 feet in order to achieve the required height diameter ratios

and still just clear the waves. Clearly such a large GEM craft would offer many practical design difficulties—and much research will be required to perfect its development.

On the other hand, research in the hydrodynamics of water based aircraft has been supported by the U. S. Navy for over 25 years and the success of this concept has been demonstrated time and again in the form of numerous prototypes which have been successfully designed. If the large GEM is to be considered for oceanic transport, I submit that a very hard and serious reexamination of the water based aircraft be considered for the same mission. Obviously the hovering ability of the GEM is not contained within the capabilities of a specially designed seaplane—but I have not heard the authors contend that this was an important consideration in their studies. Certainly, the GEM will find usefulness as a special purpose vehicle, but as a general working member of the family of everyday transport vehicles, perhaps other concepts will excel.

H. P. Rader (Vosper Limited)

The authors did not mention a type of high speed craft in which we are particularly interested, i.e., the hard chine planing craft. I think this may be of some interest because we have achieved speeds in excess of 50 knots with hard chine planing craft which have been in service for some time. I cannot say offhand how the performance curve of our craft compares with the performance curve of the other craft shown by the authors, because we did not have the papers in time for carrying out such a comparison. May I, therefore, submit the following table for your information and consideration. The figures quoted apply to a hard chine craft weighing about 100 tons.

Speed (knots)	Horsepower/ton
40	71
45	87
50	105
55	126

One more point concerning propellers. In the section on Types of Propellers Dr. van Manen states, "For reasonable application of a supercavitating screw with a diameter of 1 meter, a minimum speed of 54 knots is desirable." In our opinion this minimum speed is much lower, I would say between 40 and 45 knots, depending on the rate of advance or, to be more precise, on the local cavitation number at which the blade sections have to work.

J. D. van Manen

In reply to Mr. Rader, although I failed to mention the hard chine planing aircraft in my paper, I am sure they will be included in subsequent papers.

Owen H. Oakley

I agree with Mr. Savitsky that the water based seaplane operating in ground effect is a logical configuration to consider for the ram wing GEM concept. The very high L/D values which are theoretically obtainable are most intriguing, and I feel confident that this area will receive increased attention as the GEM concept develops.

For ignoring the hard chine planing craft in my discussion I apologize; it would have been of interest to make a comparison of this type with the hydrofoil and the GEM. However, I have made a rough comparison of lift over drag based on Mr. Rader's figures. For this I took the liberty of interpreting horsepower per ton as shp over displacement and applied an assumed propulsive coefficient of 0.5 to get at ehp and drag. This gave L/D values as follows: 7.8, 7.2, 6.6, 6.1. These are about in the low hydrofoil range but probably exceed what hovering GEMs may be expected to attain.

With regard to Mr. Newton's comments concerning control, motions, and performance in a seaway for all these craft, I must agree these matters are critical. I support his plea for more research in this area. The strength of ground effect craft resting on the water is of great importance. Since the weight available for structure in these craft is not great, sophisticated structures similar to those of aircraft will have to be used. Even with the advanced technology of the aircraft industry this problem promises to be formidable.

Mr. Newton quoted an appropriate piece of poetry regarding the ability of the water beetle to stay afloat as long as he did not stop to think about it. I wish to respond in kind with a verse which has a similar theme but which bears on a situation we find ourselves faced with in this delightful country, namely the quantities of delicious food we encounter:

> "Eat all kind nature doth bestow
> It will amalgamate below;
> But if you once begin to doubt
> The gastric juice will find it out."

*   *   *

ON THE EFFICIENCY OF A VERTICAL-AXIS PROPELLER

J. A. Sparenberg
Netherlands Ship Model Basin

In order to minimize the kinetic energy left behind in the wake of a vertical-axis propeller the oscillating motion of the propeller blades is discussed. The blades are assumed to be infinitely thin and infinitely long. The chord of the profiles is small with respect to the curvature of the cycloidal orbit of the blades. Also the case of a propeller with many blades or with a high rotational velocity is considered.

1. INTRODUCTION

The oscillatory motion of the blades of a vertical-axis propeller is governed by a system of rods and hinges [1]. This system prescribes the angle of incidence of the blades when they perform their rotational motion. The forces which act on the blades have been calculated by Isay [2], making approximations which give rise to some doubt and which we discuss at the end of section 6 of this paper.

One of the difficulties in a theoretical investigation is the complicated wake which is crowded with vortex layers. Another difficulty, which is discussed in section 2 is that for rigid blades with a finite chord no rigorous linearized theory for the perturbation velocities can be given. This is caused by the varying radius of curvature of the cycloidal orbits described by the blades.

In this paper we do not assume a prescribed oscillatory motion of the blades. We describe a method to construct the angle of incidence of the profile, as a function of position, in such a way that the kinetic energy which remains in the wake becomes a minimum. The following simplifying assumptions are made. The blades are infinitely thin, tip effects are ignored, and the chord of the blades is assumed to be small with respect to the smallest radius of curvature of the orbits of the blades.

The kinetic energy of the wake is expressed in terms of the bound vortices. Then by the Ritz-method this energy is minimized. The following property (section 4) of the bound vorticity of the blades, under the conditions just stated, will be proved: In order to obtain the highest efficiency, it is necessary that the sum of the bound vorticities of a blade in its two positions on a straight line parallel to the direction of translation of the propeller, be

---

constant. For instance, this constant may be taken equal to zero; then the blades pull as much as they push. It is also possible to give the constant such a value that the profiles are more active when they are in the front position.

Also the case of a vertical-axis propeller with many blades or a high-rotational velocity is considered. Here the bound vorticity and the vortex layers in the wake are approximated by continuous vortex densities. Then we find the following condition on the bound vorticity: In order to obtain the highest efficiency it is necessary and sufficient that the difference of the bound vorticity density for two points lying on a straight line parallel to the direction of translation of the propeller is a constant (section 6). In this case it is possible to write down explicitly the angle of the incidence of a blade as a function of its position.

It is intended to compare in a future paper numerical results of this theory with experimental results.

2. STATEMENT OF THE PROBLEM

We consider an unbounded fluid which is at rest relative to a Cartesian coordinate system x, y, z. In the direction of the positive x axis moves a circle with radius R (see Fig. 1). Its centre is on the x axis and has a velocity U. On the circle are M equally spaced identical blades perpendicular to the x, y plane. The blades rotate with a constant angular velocity ω around C. Besides this they execute an oscillatory motion around the point T in order to preserve the desired angle of incidence. We simplify our considerations, as stated in the introduction, by assuming each blade to be two-sided and infinitely long.

Fig. 1. Scheme of a vertical-axis propeller with M blades

The orbits of the pivotal points T of the M blades are the cycloids C_m with

$$x_m = R\left(\mu\psi + \sin\psi - \frac{2\pi m\mu}{M}\right),$$

$$y_m = R\cos\psi, \qquad \mu = \frac{U}{\omega R}. \qquad (2.1)$$

Several types of cycloids, as a function of μ, are drawn in Fig. 2.

As in lifting surface theory for airplane wings or ship screws we try to refer the profiles to a surface which moves through the fluid without disturbing it. For an airplane wing this surface is the projection of the wing on a certain adjacent flat plane with zero angle of attack. For a ship screw it is the projection of the blades on an adjacent helicoidal surface which does not disturb the incoming fluid when it rotates with the rotational velocity of the screw. In the case of a vertical-axis propeller a rigid reference surface does not exist because the curvature of the cycloids is not constant. For this reason we start with a deformable line segment $A - B$ covered with bound vorticity (Fig. 3), which moves exactly along the cycloidal orbit of the turning point T.
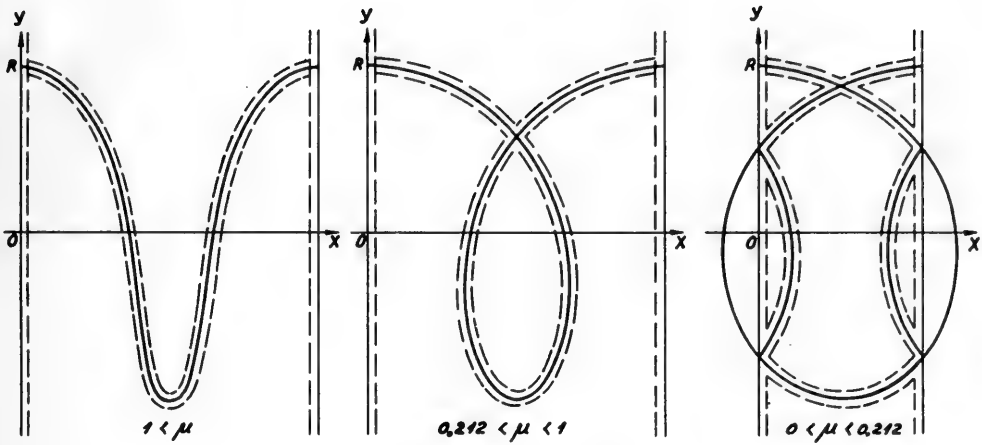
Fig. 2. Several types of cycloids
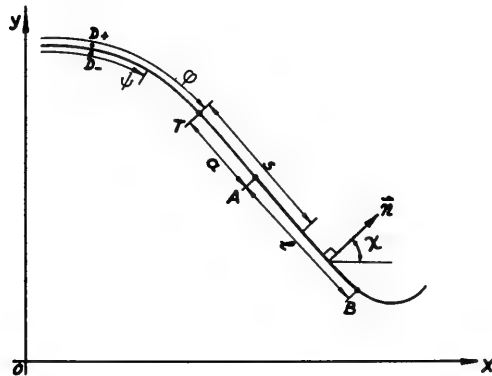
Fig. 3. The deformable profile $A - B$
along the cycloid

On this cycloid the turning point T corresponds to the parameter value $\psi = \varphi = \omega t$. Although the segment $A - B$ changes its radius of curvature we assume the distance s of some point of the profile to the point T, measured along the cycloid, to be constant. Trailing and leading edge are given by $s = a$ and $s = a + l$.

The magnitude of the velocity $V(\varphi)$ of the points of the profile is assumed to be equal to the velocity of the pivotal point T. Using the relation $\varphi = \omega t$ for the parameter of position of this point we find

$$V(\varphi) = \omega R \sqrt{1 + \mu^2 + 2\mu \cos \varphi} \ . \tag{2.2}$$

The density of the bound vortices $\Gamma(\varphi,s)$ is a function of the two variables φ and s with

$$\Gamma(\varphi, s) \neq 0, \qquad a \le s \le a + \ell. \tag{2.3}$$

In the following we will use the notation

$$\frac{\partial \Gamma(\varphi, s)}{\partial \varphi} = \dot{\Gamma}(\varphi, s), \qquad \frac{\partial \Gamma(\varphi, s)}{\partial s} = \Gamma'(\varphi, s). \tag{2.4}$$

When the elementary bound vortex $\Gamma(\varphi, s) \, ds$ changes its strength when φ increases, it leaves behind at the place φ, s free vorticity of the density

$$- \frac{\dot{\Gamma}(\varphi, s) \, ds}{R \sqrt{1 + \mu^2 + 2\mu \cos \varphi}}. \tag{2.5}$$

The total density $\gamma(\varphi, s)$ of the free vorticity which is left behind at the point φ, s by the bound vorticity of the profile which has passed this point is then given by

$$\gamma(\varphi, s) = - \int_a^{a+\ell} \frac{\dot{\Gamma}(\vartheta, \sigma) \, d\sigma}{R \sqrt{1 + \mu^2 + 2\mu \cos \vartheta}}. \tag{2.6}$$

After the partial differentiation in the integrand of (2.6) we have to consider ϑ as a function of φ, s, and σ by

$$\sigma = s + R \int_0^{\varphi} \sqrt{1 + \mu^2 + 2\mu \cos x} \, dx. \tag{2.7}$$

A necessary condition on the bound vorticity follows from the mean value K of the x component of the forces which act on the bound vortices. This mean value has to possess some prescribed value which depends on the velocity of the ship. Calculating the angle X (Fig. 3) and using the fact that the profile has the velocity $V(\varphi)$ we find for the M blades by the law of Kutta-Joukowski

$$K = \frac{\rho \omega \, RM}{2\pi} \int_0^{2\pi} \int_a^{a+\ell} \Gamma(\varphi, s) \sin \vartheta \frac{\sqrt{1 + \mu^2 + 2\mu \cos \varphi}}{\sqrt{1 + \mu^2 + 2\mu \cos \vartheta}} \, ds \, d\varphi. \tag{2.8}$$

where $\vartheta = \vartheta(\varphi, s)$ by (2.7) with $\sigma = 0$.

Another formula which will be used later on gives the difference of the value of the velocity potential $\phi(x, y)$ across the cycloid (points D_+, D_-, Fig. 3) when the profile has passed. This difference at the place ψ is

$$\phi_+(\psi) - \phi_-(\psi) = \int_a^{a+\ell} \Gamma(\vartheta, \sigma) \, d\sigma. \tag{2.9}$$

where $\vartheta = \vartheta(\psi, \sigma)$, defined by (2.7) when we put $s = 0$ and $\varphi = \psi$ in that equation. In order to use a potential for the whole fluid it is necessary that the lines covered with free vorticity

$\gamma(\varphi,a)$ do not intersect each other. This can be obtained by a simple artifice; viz., in the neighbourhood of points of intersection of the cycloids we assume that the bound vorticity of the blades becomes zero. Then the bound vorticity of the profile is left behind as free vorticity; however, a little farther, free vorticity of opposite strength is created which compensates the effect of the first one. Then (2.9) can be used with arbitrary accuracy when the distance between the two free vorticities just mentioned becomes small enough.

We now introduce two independent order quantities, viz., the length ℓ of the chord of the profile and Γ the total strength of the bound circulation of the profile at a reasonable point. We consider the case

$$\mu \neq 1 , \qquad \ell << R \frac{|1 - \mu|^2}{1 + \mu} , \qquad a \approx \mathcal{O}(\ell) \tag{2.10}$$

where $\mu \neq 1$ means that the cycloid has no cusp, and the second condition means that the chord of the profile is very small with respect to the smallest radius of curvature of the cycloid.

The function $\Gamma(\varphi,s)$ exhibits, as a function of s, large variations over the chord. In fact, it becomes infinite at the leading edge $s = a + \ell$ and zero at the trailing edge $s = a$. As a function of φ it is clear that the variations of $\Gamma(\varphi,s)$ are almost everywhere small when $\ell \to 0$ and φ changes with an amount of the order ℓ. In formulas:

$$\Gamma(\varphi,\ s + \varepsilon) \neq \Gamma(\varphi,s) + \varepsilon \Gamma'(\varphi,s),$$
$$\Gamma(\varphi + \varepsilon,\ s) \approx \Gamma(\varphi,\ s) + \varepsilon \dot{\Gamma}(\varphi,s), \qquad \varepsilon \approx \mathcal{O}(\ell) . \tag{2.11}$$

From this we can develop, with respect to ℓ and Γ, Eqs. (2.6), (2.8), and (2.9), which are important for our theory. Only lowest order terms are taken into consideration.

We find from (2.6) for the density $\gamma(\psi)$ of the free vorticity at the end of the profile, $s = a$ in (2.6), within higher order terms

$$\gamma(\psi) \overset{\text{def}}{=} \gamma(\psi,a) = - \int_a^{a+\ell} \frac{\dot{\Gamma}(\vartheta,\sigma)\ d\sigma}{R\sqrt{1 + \mu^2 + 2\mu \cos \vartheta}}$$

$$\approx - \frac{1}{R\sqrt{1 + \mu^2 + 2\mu \cos \psi}} \int_a^{a+\ell} \dot{\Gamma}(\psi,\sigma)\ d\sigma$$

$$+ \mathcal{O}(\ell\Gamma) \overset{\text{def}}{=} - \frac{\dot{\Gamma}(\psi)}{R\sqrt{1 + \mu^2 + 2\mu \cos \psi}} + \mathcal{O}(\ell\Gamma). \tag{2.12}$$

The mean value of the component K in (2.8) becomes

$$K \approx \frac{\rho\omega\,RM}{2\pi} \int_0^{2\pi} \Gamma(\varphi)\ \sin\ \varphi\ d\varphi + \mathcal{O}(\ell\Gamma), \tag{2.13}$$

while (2.9) changes into

$$\phi_+(\psi) - \phi_-(\psi) = \Gamma(\psi) + \mathbb{O}(\ell\Gamma) . \tag{2.14}$$

Hence with respect to the wake and to the mean value of K we can treat the profile with a sufficiently small chord as a concentrated vortex $\Gamma(\varphi)$. This is no longer true when we calculate the angle of incidence of the profile; then we have to take into account the variations of the induced velocities over the chord (section 5).

3. THE KINETIC ENERGY LEFT BEHIND IN THE WAKE

We want to derive the potential of the cycloidal free vortex layers with density $\gamma(\psi)$ (2.12). To this effect we start from the potential $\phi^*(x,y)$ of a row of equally spaced vortices of equal strength. The potential of such a configuration is known [3, p. 186]. Because in the remaining part of this paper we do not need the third space coordinate z, the symbol z will be used to denote the complex variable $x + iy$. We find

$$\phi^*(x,y) = Re \frac{\gamma}{2\pi i} \ln \sin \frac{\pi}{h} (z - \zeta_m), \tag{3.1}$$

where γ is the strength of the vortices, h their mutual separation distance, z the point in which the potential is considered and ζ_m the location of some vortex (see Fig. 4). It can be easily seen that this potential is not periodic, we find

$$\phi^*(x+h,y) - \phi^*(x,y) = \begin{cases} -\dfrac{1}{2}\gamma, & y > Im \ \zeta_m \\[2mm] +\dfrac{1}{2}\gamma, & y < Im \ \zeta_m \end{cases} . \tag{3.2}$$

When we take $h = 2\pi\mu R$ and let the points $\zeta_m = (\xi_m + i\eta_m)$ with $m = 1, ..., M$, describe the parts of the M cycloids lying in the interval $0 \leq x < 2\pi\mu R$, the other points of the rows describe the parts of the cycloids outside this interval. In this way we cover the whole wake of the propeller with free vortices. The potential $\phi(x,y)$ of the wake flow can be written as
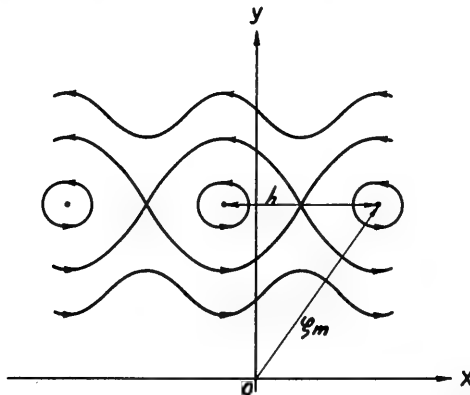
Fig. 4. Row of vortices with streamlines

$$\phi(x,y) = Re \; \frac{R}{2\pi i} \sum_{m=0}^{M-1} \int_0^{2\pi} \gamma(\vartheta) \; \ln\left(\sin\frac{(2-\zeta_m)}{2\mu R}\right)\sqrt{1+\mu^2+2\mu\cos\vartheta}\;d\vartheta \quad (3.3)$$

where

$$\zeta_m = (\xi_m + i\eta_m) = R\left(\mu\vartheta + \sin\vartheta - \frac{2\pi m\mu}{M} + i\cos\vartheta\right). \quad (3.4)$$

Because the intensity $\Gamma(\psi)$ of the bound vortex is a periodic function of ψ, the same holds for the free vortex density $\gamma(\psi)$, and besides this the mean of $\gamma(\psi)$ over a period $0 \le \psi < 2\pi$, or over an interval of length $2\pi\mu R$ in the x direction, is zero.

Then it follows from (3.2)

$$\phi(x+2\pi\mu R, y) - \phi(x,y) = 0, \qquad |y| > R. \quad (3.5)$$

When, however, $|y| < R$ we have for the mean vorticity between $y = \pm R$ and y over the period $2\pi\mu R$ in the x direction

$$\pm M\Big\{\Gamma(2\pi-\psi) - \Gamma(\psi)\Big\}, \qquad y = R\cos\psi. \quad (3.6)$$

Here by (3.2) we have

$$\phi(x+2\pi\mu R, y) - \phi(x,y) = M\Big\{\Gamma(2\pi-\psi) - \Gamma(\psi)\Big\}, \qquad |y| < R. \quad (3.7)$$

Our aim is to determine the function $\Gamma(\psi)$ in such a way that the energy left behind in the wake becomes as small as possible. To this end we consider the kinetic energy E of the fluid in the strip $0 \le x \le 2\pi\mu R$, $-\infty < y < +\infty$, which by Green's theorem can be written as

$$E = \frac{1}{2}\rho\iint\left\{\left(\frac{\partial\phi}{\partial x}\right)^2 + \left(\frac{\partial\phi}{\partial y}\right)^2\right\}dx\;dy = \frac{1}{2}\rho\int\phi\,\frac{\partial\phi}{\partial n}\,d\ell. \quad (3.8)$$

The surface integral extends over a vertical strip of width $2\pi\mu R$, the line integral along the vertical boundaries of the strip and along both sides of the cycloids (Fig. 2, dashed lines). The normal derivative is directed into the enclosed regions.

We consider first the integrals along both sides of the cycloids. These integrals for M different cycloids have the same magnitude; hence we find by (2.14) for their combined contribution E_c to the kinetic energy E,

$$E_c = -\frac{\rho R M}{2}\int_0^{2\pi}\Gamma(\psi)\;\frac{\partial\phi}{\partial n}(\psi)\sqrt{1+\mu^2+2\mu\cos\psi}\;d\psi \quad (3.9)$$

where the line of integration and the direction of the normal to this line are denoted in Fig. 5. As in (3.9) we will not mention in this and the next section the order of accuracy of the formulas. This will be considered again in section 5.

From (3.9) it follows that we have to determine the normal derivative $\partial\phi/\partial n$. The unit normal of the cycloid is
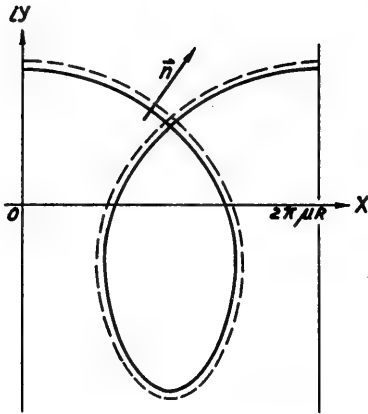
Fig. 5. The path of integration
along the cycloid for $m = 0$

$$\vec{n} = (\sin\psi,\ \mu + \cos\psi)\ \frac{1}{\sqrt{1 + \mu^2 + 2\mu\cos\psi}}. \quad (3.10)$$

The velocity $\vec{v}(x,y)$ which belongs to the potential $\phi(x,y)$ (3.3) is

$$\vec{v} = -\frac{1}{4\pi\mu}\sum_{m=0}^{M-1}\int_0^{2\pi}\gamma(\vartheta)$$

$$\cdot\left\{\begin{array}{l}\sinh\dfrac{(y-\eta_m)}{\mu R} - \sin\dfrac{(x-\xi_m)}{\mu R} \\[2mm] \cosh\dfrac{(y-\eta_m)}{\mu R} - \cos\dfrac{(x-\xi_m)}{\mu R}\end{array}\right\}$$

$$\cdot\sqrt{1 + \mu^2 + 2\mu\cos\vartheta}\ d\vartheta \quad (3.11)$$

where ξ_m and η_m are defined in (3.4). By (3.10) and (3.11) we find for the normal velocity in a point x_o, y_o of the cycloid with $m = 0$ (2.1)

$$\frac{\partial\phi}{\partial n}(\psi) = -\frac{1}{4\pi\mu}\sum_{m=0}^{M-1}\int_0^{2\pi}\gamma(\vartheta)$$

$$\cdot\left[\frac{\sin\psi\ \sinh\left(\dfrac{y_o-\eta_m}{\mu R}\right) - (\mu+\cos\psi)\ \sin\left(\dfrac{x_o-\xi_m}{\mu R}\right)}{\cosh\dfrac{(y_o-\eta_m)}{\mu R} - \cos\dfrac{(x_o-\xi_m)}{\mu R}}\right]$$

$$\cdot\frac{\sqrt{1 + \mu^2 + 2\mu\cos\vartheta}}{\sqrt{1 + \mu^2 + 2\mu\cos\psi}}\ d\vartheta. \quad (3.12)$$

By (2.12), (3.9), and (3.12) we obtain

$$E_c = -\frac{\rho M}{8\pi\mu}\sum_{m=0}^{M-1}\int_0^{2\pi}\int_0^{2\pi}\Gamma(\psi)\ \dot{\Gamma}(\vartheta)$$

$$\cdot\left[\frac{\sin\psi\ \sinh\dfrac{(y_o-\eta_m)}{\mu R} - (\mu+\cos\psi)\ \sin\dfrac{(x_o-\xi_m)}{\mu R}}{\cosh\dfrac{(y_o-\eta_m)}{\mu R} - \cos\dfrac{(x_o-\xi_m)}{\mu R}}\right]\ d\vartheta\ d\psi \quad (3.13)$$

where x_o, y_o and ξ_m, η_m are defined by (2.1) and (3.4).

Next we consider the contribution of the vertical boundaries of the strip (Fig. 2) to the line integrals (3.8) of the kinetic energy E. Because $\partial\phi(x,y)/\partial x$ is periodic for all values

of y and $\phi(x,y)$ is periodic for $|y| > R$ the contributions of the integrals cancel each other for $|y| > R$. This is no longer true for $|y| < R$. We obtain for the part E_v of E which belongs to the vertical boundaries

$$E_v = -\frac{1}{2}\rho \int_{-R}^{+R} \left\{\phi(0,y) - \phi(2\pi\mu R, y)\right\} \frac{\partial\phi(0,y)}{\partial x} \, dy \,. \tag{3.14}$$

Using (3.7) and (3.11) we find after some reduction

$$E_v = -\frac{\rho M}{8\pi\mu} \sum_{m=0}^{M-1} \int_0^{2\pi} \int_0^{2\pi} \frac{\Gamma(\psi) \, \dot{\Gamma}(\vartheta) \, \sinh \dfrac{(y-\eta_m)}{\mu R} \, \sin\psi}{\left\{\cosh \dfrac{(y-\eta_m)}{\mu R} - \cos \dfrac{\xi_m}{\mu R}\right\}} \, d\vartheta \, d\psi \,, \tag{3.15}$$

where $y = R\cos\psi$ and ξ_m and η_m are from (3.4).

Hence we find for the total kinetic energy

$$E = E_c + E_v = \int_0^{2\pi} \int_0^{2\pi} \Gamma(\psi) \, \dot{\Gamma}(\vartheta) \, L(\psi,\vartheta) \, d\psi \, d\vartheta \tag{3.16}$$

where

$$L(\psi,\vartheta) = -\frac{\rho M}{8\pi\mu} \sum_{m=0}^{M-1} \left[\frac{\sin\psi \, \sinh \dfrac{(y_o - \eta_m)}{\mu R} - (\mu + \cos\psi) \sin \dfrac{(x_o - \xi_m)}{\mu R}}{\cosh \dfrac{(y_o - \eta_m)}{\mu R} - \cos \dfrac{(x_o - \xi_m)}{\mu R}} \right.$$

$$\left. + \frac{\sinh \dfrac{(y - \eta_m)}{\mu R} \, \sin\psi}{\cosh \dfrac{(y - \eta_m)}{\mu R} - \cos \dfrac{\xi_m}{\mu R}} \right] \tag{3.17}$$

in which $y = R\cos\psi$ and x_o, y_o and ξ_m, η_m are from (2.1) and (3.4).

It can be seen that for $\varphi = \vartheta$ this function possesses a singularity of the form

$$\lim_{\psi \to \vartheta} L(\psi,\vartheta) \approx \frac{\rho M}{4\pi} \frac{1}{(\psi - \vartheta)} \,. \tag{3.18}$$

Besides this singularity there are other ones which are the points of intersection of the cycloids with themselves ($\mu < 1$), with each other ($M > 1$), or with the vertical lines $x = 2k\pi\mu R$. The first term yields besides the singularity mentioned in (3.18) also singularities for

$$y_o = \eta_m, \quad x_o - \xi_m = 2k\pi\mu R, \quad 0 \le \psi,$$

$$\vartheta \le 2\pi, \quad \psi \ne \vartheta, \quad k = 0, 1, \ldots \tag{3.19}$$

and the second term yields singularities for

$$y = \eta_m, \qquad \xi_m = 2k\pi\mu R, \qquad 0 \le \psi, \quad \vartheta \le 2\pi, \qquad k = 0, 1, \ldots \qquad (3.20)$$

where as many integers $k = 0, 1, \ldots$ have to be used as are compatible with the condition $0 \le \psi, \vartheta \le 2\pi$. The order of these latter singularities is

$$\mathbb{O}\left\{\left[(\psi_s - \psi)^2 + (\vartheta_s - \vartheta)^2\right]^{-1/2}\right\} \qquad (3.21)$$

where ψ_s s, ϑ_s denotes the singular point in the ψ, ϑ plane.

4. THE VARIATIONAL PROBLEM

We want to minimize the energy E left behind in the wake over a length of a period $2\pi\mu R$. It seems most simple to start from (3.16) by using Ritz's method. First, however, a general property of the function $\Gamma(\psi)$ will be derived.

We can split $\Gamma(\psi)$ into an even and an odd function with respect to $\psi = \pi$,

$$\Gamma(\psi) = \Gamma_e(\psi) + \Gamma_o(\psi), \qquad \Gamma_{\substack{e\\o}}(\pi+\psi) = \pm\Gamma_{\substack{e\\o}}(\pi-\psi) . \qquad (4.1)$$

The condition (2.13) then becomes

$$\frac{\rho\omega\, RM}{2\pi} \int_0^{2\pi} \Gamma_o(\psi)\, \sin\psi\, d\psi = K \qquad (4.2)$$

which does not yield any restriction on $\Gamma_e(\psi)$. Using (4.1) the kinetic energy (3.16) becomes

$$E = \int_0^{2\pi} \int_0^{2\pi} \left\{\left[\Gamma_e(\psi)\,\dot\Gamma_e(\vartheta) + \Gamma_o(\psi)\,\dot\Gamma_o(\vartheta)\right] + \left[\Gamma_e(\psi)\,\dot\Gamma_o(\vartheta)\right.\right.$$
$$\left.\left. + \Gamma_o(\psi)\,\dot\Gamma_e(\vartheta)\right]\right\} L(\psi,\vartheta)\, d\psi\, d\vartheta . \qquad (4.3)$$

From (3.17) it can be derived that

$$L(\psi,\vartheta) = -L(2\pi-\psi,\ 2\pi-\vartheta) . \qquad (4.4)$$

By this (4.3) reduces to

$$E = \int_0^{2\pi} \int_0^{2\pi} \left[\Gamma_e(\psi)\,\dot\Gamma_e(\vartheta) + \Gamma_o(\psi)\,\dot\Gamma_o(\vartheta)\right] L(\psi,\vartheta)\, d\psi\, d\vartheta . \qquad (4.5)$$

Both terms between brackets in (4.5) yield a positive contribution to E, because each of them represents the kinetic energy which belongs to some bound vortex function $\Gamma_e(\psi)$ or $\Gamma_o(\psi)$.

From this result and from (4.2) we find that we have to take

$$\Gamma_e(\psi) \equiv 0 .\tag{4.6}$$

Hence $\Gamma(\psi)$ has to be an odd function with respect to ψ. We suppose

$$\Gamma(\psi) = \Gamma_o(\psi) = \sum_{n=1}^{N} a_n \sin n\psi .\tag{4.7}$$

Condition (2.13) yields

$$a_1 = \frac{2K}{\rho\omega\,RM} .\tag{4.8}$$

Using (4.7) the energy E becomes

$$E = \sum_{p,q=1}^{N} qa_p\,a_q \int_0^{2\pi}\!\!\int_0^{2\pi} \sin p\psi \cos q\vartheta\, L(\psi,\vartheta)\,d\psi\,d\vartheta .\tag{4.9}$$

Differentiation of this expression with respect to a_n $(n = 2, ..., N)$ yields

$$\frac{\partial E}{\partial a_n} = \sum_{q=1}^{N} a_q \int_0^{2\pi}\!\!\int_0^{2\pi} (q \sin n\psi \cos q\vartheta$$

$$+\, n \sin q\psi \cos n\vartheta)\, L(\psi,\vartheta)\,d\psi\,d\vartheta = 0, \qquad (n = 2, \ldots, N).\tag{4.10}$$

These are $N-1$ linear equations for the $N-1$ unknowns $a_2, ..., a_N$.

Without altering the kinetic energy in the wake we may add a constant value to the circulation $\Gamma(\psi)$.

From the fact that the optimum bound vorticity $\Gamma(\psi)$ has to be an odd function of ψ plus an arbitrary constant we find the following property, mentioned already in the introduction,

$$\Gamma(\psi) + \Gamma(-\psi) = \text{const}.\tag{4.11}$$

5. THE DETERMINATION OF THE ANGLE OF INCIDENCE

Our aim is to derive formulas which determine the angles of incidence of the profiles as functions of their position.

Because all blades are equivalent we consider the profile whose turning point T moves along the cycloid C_o. On this profile we introduce a parameter s^* (Fig. 6) which measures the distance of a point of the profile to the turning point T; s^* is positive in the direction of $V(\varphi)$. We can calculate the normal velocities on the profile caused by the translation $V(\varphi)$ and a rotation around T, which have to be compensated by a suitable vortex distribution on the profile. Next we assume a kind of linearisation procedure which consists of compensating the normal velocities not on the real profile, but on the cycloid. The points
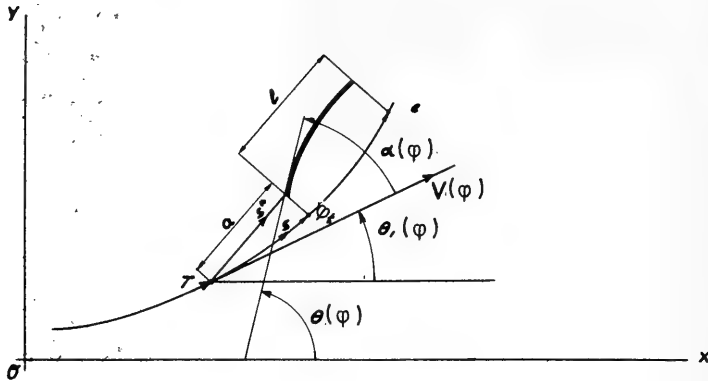
Fig. 6. The profile in the neighbourhood of the cycloid

of the real profile are represented by points on the cycloid in such a way that $s^* = s$. The leading and trailing edge of the profile are denoted on the cycloid by φ_ℓ and φ_t.

First we consider the velocities induced by the bound vorticity of the other blades and by the free vorticity along the cycloids C_m, $m = 1, ..., M - 1$. It is clear that for these velocities and hence for their resultant component $v_{n,1}(\varphi_o, s)$ normal to the profile, we have the relation

$$v_{n,1}(\varphi, s) = \mathbb{O}(\Gamma), \qquad a \leq s \leq a + \ell . \tag{5.1}$$

At the end of this section it will turn out that this information about these velocities is sufficient with respect to the accuracy with which we have approximated the basic formulas (2.6), (2.8), and (2.9).

Next we consider the velocity $\vec{v}_z(\varphi, z)$ with components $v_{x,z}$ and $v_{y,z}$ induced by the free vorticity along C_o,

$$v_{x,z} - iv_{y,z} = -\frac{1}{2\pi i} \int_{-\infty}^{\varphi_t} \frac{\Gamma(\vartheta)\, d\vartheta}{[x - \zeta(\vartheta)]}$$

$$= -\frac{1}{2\pi i} \int_{-\infty}^{\zeta(\varphi_t)} \frac{\dot{\Gamma}(\vartheta)}{[z - \zeta(\vartheta)]} \frac{d\zeta}{R(\mu + \cos\vartheta - i\sin\vartheta)} . \tag{5.2}$$

The second integral formulation has the form of a Cauchy integral. We have to consider the behaviour of this integral when z is in the neighbourhood of $\zeta(\varphi_t)$. This is a well-known problem [4, ch. 4]; we find

$$v_{x,z} - iv_{y,z} = \frac{1}{2\pi i} \frac{\dot{\Gamma}(\varphi_t)\, \ln\,[z - \zeta(\varphi_t)]}{R(\mu + \cos\varphi_t - i\sin\varphi_t)} + \psi(z) \tag{5.3}$$

where $\psi(z)$ is a bounded function for $z \to \zeta(\varphi_t)$, which is of $\mathbb{O}(\Gamma)$. Making use of (3.10) we find for the normal component $v_{n,z}(\varphi,s)$ of this velocity,

$$v_{n,z}(\varphi,s) = \frac{1}{2\pi} \frac{\dot{\Gamma}(\varphi_t) \ln (s-a)}{R\sqrt{1 + \mu^2 + 2\mu \cos \varphi_t}}$$

$$+ \mathbb{O}(\Gamma) \overset{\text{def}}{=} w(\varphi) \ln \left(\frac{s-a}{R}\right) + \mathbb{O}(\Gamma) . \tag{5.4}$$

It will be assumed that the profile is infinitely thin and cambered. On the profile we assume a vortex layer with density $\Gamma_{tot}(\varphi,s)$ which represents the sum of bound and free vorticity. Hence we have the following equation:

$$Re \left[\frac{1}{2\pi i} \int_a^{a+\ell} \frac{\Gamma_{tot}(\varphi,\sigma) \, d\sigma}{[z(s) - \zeta(\sigma)]} \cdot \vec{n}(s) \right] = - V(\varphi) [\alpha(\varphi) + f'(s)] + \omega\theta'(\varphi)s$$

$$- w(\varphi) \ln \left(\frac{s-a}{R}\right) + \mathbb{O}(\Gamma) \tag{5.5}$$

where $\alpha(\varphi)$ is the angle of incidence of the profile, $f(s)$ is the camber, and $\theta(\varphi)$ represents the angle of the profile with respect to a line of fixed direction, for instance the x axis (Fig. 6). The angle of incidence $\alpha(\varphi)$ can be defined as the angle between the tangent to the profile at the trailing edge and the velocity $V(\varphi)$. The angles α, θ, and θ_1 to be defined in (5.6) are positive in the counterclockwise direction. The angle $\theta(\varphi)$ can be split into two parts:

$$\theta(\varphi) = \theta_1(\varphi) + \alpha(\varphi) = - \tan^{-1} \frac{\sin \varphi}{\mu + \cos \varphi} + \alpha(\varphi) . \tag{5.6}$$

For small values of ℓ Eq. (5.5) can be written in the form

$$\frac{1}{2\pi} \int_a^{a+\ell} \frac{\Gamma_{tot}(\varphi,\sigma) \, d\sigma}{(s-\sigma)} = - V(\varphi) [\alpha(\varphi) + f'(s)] + [\omega\theta_1'(\varphi) + \omega\alpha'(\varphi)] s$$

$$- w(\varphi) \ln \left(\frac{s-a}{R}\right) + \mathbb{O}(\Gamma) . \tag{5.7}$$

The inversion of this integral equation is well known [4, section 88]:

$$\Gamma_{tot}(\varphi,s) = \frac{\beta(\varphi)}{\pi\sqrt{s-a} \sqrt{a+\ell-s}} + \frac{2}{\pi\sqrt{s-a} \sqrt{a+\ell-s}} \int_a^{a+\ell} \Big\{ V(\varphi) [\alpha(\varphi) + f'(\sigma)]$$

$$- [\omega\theta_1'(\varphi) + \omega\alpha'(\varphi)]\sigma + w(\varphi) \ln \left(\frac{\sigma-a}{R}\right)$$

$$+ \mathbb{O}(\Gamma) \Big\} \frac{\sqrt{\sigma-a} \sqrt{a+\ell-\sigma}}{(s-\sigma)} \, d\sigma \tag{5.8}$$

where

$$\beta(\varphi) = \int_a^{a+\ell} \Gamma_{tot}(\varphi, s) \, ds. \tag{5.9}$$

We consider the asymptotical representation of $\Gamma_{tot}(\varphi, s)$ in the neighbourhood of $s = a$. After some analysis we find from (5.8)

$$\lim_{s \to a} \Gamma_{tot}(\varphi, s) \approx \frac{\beta(\varphi)}{\pi\sqrt{\ell}\ \sqrt{s-a}} - \frac{2}{\pi\sqrt{\ell}\ \sqrt{s-a}} \left(\int_a^{a+\ell} \left\{ V(\varphi)\left[\alpha(\varphi) + f'(\sigma)\right] \right. \right.$$

$$- \left[\omega\theta_1'(\varphi) + \omega\alpha'(\varphi)\right]\sigma + w(\varphi)\ \ln\left(\frac{\sigma-a}{R}\right)$$

$$\left. \left. + \mathbb{O}(\Gamma) \right\} \frac{\sqrt{a+\ell-\sigma}}{\sqrt{\sigma-a}} d\sigma + \pi^2\ w(\varphi)\ \sqrt{\ell}\ \sqrt{s-a} \right). \tag{5.10}$$

We have to satisfy the condition that the velocity of the fluid remains finite at the trailing edge. This is equivalent to the demand that the total vorticity $\Gamma_{tot}(\varphi, s)$ for $s = a$ equals the free vorticity in the wake. Hence we find from (5.10)

$$\beta(\varphi) = 2 \int_a^{a+\ell} \left\{ V(\varphi)\left[\alpha(\varphi) + f'(\sigma)\right] - \left[\omega\theta_1'(\varphi) + \omega\alpha'(\varphi)\right] \right.$$

$$\left. + w(\varphi)\ \ln\frac{(\sigma-a)}{R} + \mathbb{O}(\Gamma) \right\} \frac{\sqrt{a+\ell-\sigma}}{\sqrt{\sigma-a}} d\sigma. \tag{5.11}$$

and

$$- 2\pi\ w(\varphi) = \gamma(\varphi_t). \tag{5.12}$$

Equation (5.11) determines $\beta(\varphi)$ in terms of the still unknown angle of incidence $\alpha(\varphi)$, while (5.12) is satisfied automatically (Eqs. (2.12) and (5.4)).

The last condition we have to satisfy states that the integral over the bound vorticity of the profile has to have the known value $\Gamma(\varphi)$. Hence first we have to calculate the bound vorticity $\Gamma(\varphi, s)$. We start from the definition of $\Gamma_{tot}(\varphi, s)$

$$\Gamma_{tot}(\varphi, s) = \gamma(\varphi, s) + \Gamma(\varphi, s) \tag{5.13}$$

where $\gamma(\varphi, s)$ is the free vorticity passing along the profile. Using (2.6) we obtain

$$\Gamma_{tot}(\varphi, s) = - \int_a^{a+\ell} \frac{\dot{\Gamma}(\varphi, \sigma)\ d\sigma}{R\sqrt{1 + \mu^2 + 2\mu\ \cos\vartheta}} + \Gamma(\varphi, s) + \mathbb{O}(\Gamma) \tag{5.14}$$

where ϑ follows from (2.7). However, the first term on the right-hand side of (5.14) is $\mathbb{O}(\Gamma)$. Hence we find, making use of (5.9),

$$\Gamma(\varphi) = \int_a^{a+\ell} \Gamma(\varphi, s) \ ds \approx \int_a^{a+\ell} \Gamma_{tot}(\varphi, s) \ ds$$

$$+ \ \mathbb{O}(\ell\Gamma) = \beta(\varphi) + \mathbb{O}(\ell\Gamma). \tag{5.15}$$

From (5.11) we obtain

$$\alpha(\varphi) - \frac{\ell\omega}{V(\varphi)} \left(\frac{a}{\ell} + \frac{1}{4}\right) \alpha'(\varphi) = \frac{\Gamma(\varphi)}{\pi\ell \ V(\varphi)} - \frac{2}{\pi} \int_0^1 f'(\sigma\ell + a) \frac{\sqrt{1-\sigma}}{\sqrt{\sigma}} d\sigma$$

$$+ \frac{\ell\omega}{V(\varphi)} \left(\frac{a}{\ell} + \frac{1}{4}\right) \theta_1'(\varphi) - \frac{\omega}{2\pi} \frac{\dot{\Gamma}(\varphi)}{V^2(\varphi)} \ln \frac{\ell}{R} + \mathbb{O}(\Gamma). \tag{5.16}$$

Because $\alpha = \mathbb{O}(\Gamma\ell^{-1})$ the second term on the left-hand side can be disregarded. Besides this by the choice $a = -(1/4)\ell$ the coefficient of this term as well as the coefficient of $\theta_1'(\varphi)$ vanishes. Then equation (5.16) changes into

$$\alpha(\varphi) = \frac{\Gamma(\varphi)}{\pi\ell \ V(\varphi)} - \frac{\omega}{2\pi} \frac{\dot{\Gamma}(\varphi)}{V^2(\varphi)} \ln \frac{\ell}{R}$$

$$- \frac{2}{\pi} \int_0^1 f' \left[\ell \left(\sigma - \frac{1}{4}\right)\right] \frac{\sqrt{1-\sigma}}{\sqrt{\sigma}} d\sigma + \mathbb{O}(\Gamma). \tag{5.17}$$

Hence, for a more easy analysis of the propeller, it can be recommended to place the turning point T at one quarter of the chord length from the trailing edge.

From this we see that, within the accuracy of the theory, we do not have to take into account the induced velocities (5.1), which give rise to a change of the angle of attack by an amount of $\mathbb{O}(\Gamma)$.

6. VERTICAL-AXIS PROPELLERS WITH AN INFINITE NUMBER OF BLADES OR QUICKLY ROTATING PROPELLERS

When the number of blades or the rotational velocity of the propeller increases, the wake of the propeller becomes crowded with free vortex layers. Hence it seems natural to replace this complicated system by a continuous distribution of free vorticity. The bound vorticity can be replaced by a continuous distribution over the circumference of the circle. We assume for its strength per unit length the function $\Gamma_c(\varphi)$, where the index c indicates a continuous distribution.

For the free vorticity per unit length in the x direction, which is left in the strips between y and $\pm R$ (see Fig. 7) we find
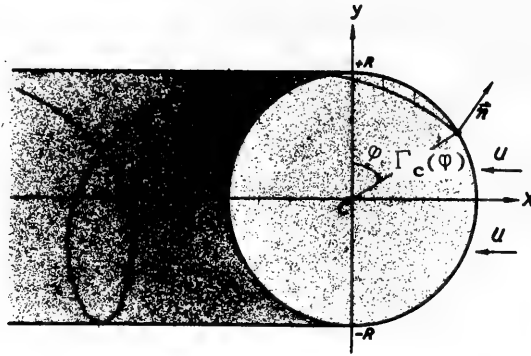
Fig. 7. The propeller with a continuous
vortex distribution

$$\mp \frac{1}{\mu} \{\Gamma_c(\varphi) - \Gamma_c(2\pi - \varphi\} , \qquad y = R \cos \varphi . \tag{6.1}$$

The velocity induced by two infinite strips with vorticity of strength given in (6.1) at $y = R \cos \varphi$ is

$$- \frac{1}{\mu} \left[\Gamma_c(\varphi) - \Gamma_c(2\pi - \varphi) \right] . \tag{6.2}$$

By this the energy in an arbitrary rectangle of unit length in the x direction between $y = \pm R$ and far behind the propeller becomes

$$E = \frac{\rho R}{2\mu^2} \int_0^\pi \left[\Gamma_c(\varphi) - \Gamma_c(2\pi - \varphi) \right]^2 \sin \varphi \, d\varphi . \tag{6.3}$$

The condition for the total component in the x direction of the force acting on the bound vorticity is

$$\rho \omega R^2 \int_0^{2\pi} \Gamma_c(\varphi) \sin \varphi \, d\varphi = K . \tag{6.4}$$

We have now to minimize (6.3) under the condition (6.4). Introducing the perturbed bound vorticity

$$\Gamma_c(\varphi) + \varepsilon_1 g_1(\varphi) + \varepsilon_2 g_2(\varphi) , \tag{6.5}$$

where $g_1(\varphi)$ and $g_2(\varphi)$ are arbitrary functions of φ, into (6.3) we have to differentiate E with respect to ε_1, while condition (6.4) must be taken into account. Applying the multiplication method of Lagrange we obtain

$$\frac{\rho R}{\mu^2} \int_0^{\pi} \left[\Gamma_c(\varphi) - \Gamma_c(2\pi - \varphi) \right] \left[g_1(\varphi) - g_1(2\pi - \varphi) \right] \sin \varphi \, d\varphi$$

$$+ \lambda \rho \omega \, R^2 \int_0^{\pi} g_1(\varphi) \sin \varphi \, d\varphi = 0 \qquad (6.6)$$

where λ is a still unknown constant.

This equation can be written in the form

$$\frac{1}{\mu^2} \left(\int_0^{\pi} - \int_{\pi}^{2\pi} \right) \left[\Gamma_c(\varphi) - \Gamma_c(2\pi - \varphi) \right] g_1(\varphi) \sin \varphi \, d\varphi$$

$$+ \lambda \omega R \int_0^{2\pi} g_1(\varphi) \sin \varphi \, d\varphi = 0 \; . \qquad (6.7)$$

Because $g_1(\varphi)$ is arbitrary we have

$$\frac{1}{\mu^2} \left[\Gamma_c(\varphi) - \Gamma_c(2\pi - \varphi) \right] = \mp \lambda \omega R, \qquad \begin{array}{l} 0 < \varphi < \pi \\ \pi < \varphi < 2\pi \end{array} . \qquad (6.8)$$

From this it follows that the only condition which we have to satisfy is: the difference of the bound vorticity at the front and the back of the circle for the same values of y is a constant. Hence we may for instance assume $\Gamma_c(\varphi) = -\Gamma_c(2\pi - \varphi) = \text{const.}$ From (6.4) it follows

$$\Gamma_c(\varphi) = \pm \frac{K\mu}{4\rho \, RU} , \qquad \begin{array}{l} 0 < \varphi < \pi \\ \pi < \varphi < 2\pi \end{array} . \qquad (6.9)$$

This agrees with the result of section 4 where it was found that the optimum bound vorticity was an odd function of φ plus some arbitrary constant. In this case of continuous vorticities it is allowed to add an arbitrary even function of φ to the distribution in (6.9).

From the above it follows that the vorticity in the wake is concentrated wholly on the lines $y = \pm R$. The strength γ per unit length in the x direction becomes

$$\gamma = \mp \frac{K}{2\rho \, RU}, \qquad y = \pm R \; . \qquad (6.10)$$

This means that the induced velocity u in the wake is, parallel to the x axis, independent of y and amounts to

$$u = - \frac{K}{2\rho \, RU} \; . \qquad (6.11)$$

This result can be checked easily by calculating the external force necessary for the increase of momentum which follows from (6.11).

Isay [2] uses a formula, Eq. (1) in his work, which is not in agreement with our formula (6.1). He gives also another formula, Eq. (12), which he thinks to be faulty, but which, in the opinion of the author, is the correct one. That something is wrong with Eq. (1) of Isay follows from the fact that in it the velocity of the incoming fluid does not occur. It is clear that when this velocity increases, the density of the free vorticity in the wake decreases, when the bound vorticity distribution remains the same.

7. THE ANGLE OF INCIDENCE IN THE CASE OF CONTINUOUS DISTRIBUTIONS

We first consider the induced velocity by the two half infinite equidistant rows of vortices which form the wake. By elementary calculations we find that the component of the velocity $v_{n,1}$, in the direction $\vec{n}$, normal to the cycloid, at some point φ of the circle (Fig. 7) amounts to

$$v_{n,1} = \frac{-K}{8\rho RU \sqrt{1 + \mu^2 + 2\mu \cos \varphi}} \left[\beta^* \sin \varphi \right.$$

$$\left. + \frac{1}{\pi} (\mu + \cos \varphi) \ln \left(\frac{1 + \cos \varphi}{1 - \cos \varphi} \right) \right],$$

$$\beta^* = \begin{matrix} 1, & 0 < \varphi < \pi \\ 3, & \pi < \varphi < 2\pi \end{matrix} . \qquad (7.1)$$

The component of the velocity normal to the cycloid, induced by the bound vorticity (6.9) on the circle, becomes

$$v_{n,2} = - \frac{K\mu}{8\pi\rho RU} \frac{(1 + \mu \cos \varphi)}{\sqrt{1 + \mu^2 + 2\mu \cos \varphi}} \ln \left(\frac{1 + \cos \varphi}{1 - \cos \varphi} \right) . \qquad (7.2)$$

Finally we write down the normal component of induced velocities by a constant density Γ_c^* of bound vorticity on the circle,

$$v_{n,3} = \frac{\Gamma_c^* \mu \sin \varphi}{2\sqrt{1 + \mu^2 + 2\mu \cos \varphi}} . \qquad (7.3)$$

The velocities (7.2) and (7.3) are the mean values of the velocity components normal to the cycloid in points just outside and just inside the circle. Hence we find for the total induced normal velocity

$$v_n = v_{n,1} + v_{n,2} + v_{n,3} . \qquad (7.4)$$

When the propeller consists of M blades, each blade has to possess a bound vorticity

$$\Gamma(\varphi) = \frac{2\pi R}{M} \left(\pm \frac{K\mu}{4\rho RU} + \Gamma_c^* \right), \qquad \begin{array}{c} 0 < \varphi < \pi \\ \pi < \varphi < 2\pi \end{array} . \tag{7.5}$$

The constant bound vorticity Γ_c^* is still arbitrary and can be used also in this case to determine the activity of the blades in the front or in the back position.

With respect to the tangent at the cycloid we obtain for the angle of incidence $\alpha(\varphi)$

$$\alpha(\varphi) = \alpha_o - \frac{v_n(\varphi)}{V(\varphi)} + \frac{\Gamma(\varphi)}{\pi V(\varphi) \, \ell} \tag{7.6}$$

where α_o is the angle of zero lift, $V(\varphi)$ follows from (2.2), and ℓ is the length of the chord of the profile. The angles $\alpha(\varphi)$ and α_o are positive when they open to the left with respect to the direction of $V(\varphi)$.

Because we have not taken into account the velocities induced by the oscillating motion of the blades we have to place the turning point T of the profiles at one quarter of the chord length from the trailing edge, as follows from the end of section 5.

REFERENCES

[1] Mueller, H. F., "Recent Developments in the Design and Application of the Vertical Axis Propeller," Trans. S.N.A.M.E., 1955

[2] Isay, W. H., "Zur Berechnung der Strömung durch Voith-Schneider-Propeller," Ing. Arch. XXIV Band, 1956

[3] Kotschin, N. J., Kibel, I. A., and Rose, N. W., "Theoretische Hydromechanik," Band I, Akademie Verlag, Berlin, 1954

[4] Muskhelishvily, N. J., "Singular Integral Equations," 2nd ed., transl. P. Noordhoff, N. V., Groningen, 1954

DISCUSSION

G. Weinblum (Institut für Schiffbau, University of Hamburg)

I wish to raise the question, who should decide when mathematicians disagree? I have not understood what you have done. Have you calculated some numerical values so that we can compare what comes out?

J. A. Sparenburg

This is a case in which mathematicians do not agree upon the interpretation of the basic formulae needed for the theory. In my opinion the taxation of the various ways of approach has to be made by executing experiments, not only of the over-all results but also of the basic formulae. We have made some calculations based on the simple theory of sections 6 and 7. Before publishing results, however, we shall compare them with results based on the more refined theory of sections 2-5 and on experiments.

W. H. Isay (Institute of Applied Mathematics of the German Academy of Science)

In reply to Dr. Sparenberg's discourse on my papers* dealing with the theory of the Voith-Schneider propeller I should like to remark the following:

Equation (12) of my paper II mentioned by Dr. Sparenberg is obtained by the usual methods of potential flow analysis if it is assumed that the free vortices move to infinity downstream of the propeller without losing their intensity. In reality, however, these vortices will decay in the real turbulent flow downstream of the propeller and both their influence and their induced velocity will decrease accordingly. The use of Eq. (12) will therefore yield grossly erroneous results, particularly for the blades on the downstream half of the propeller which are hit by the free vortices produced by the blades on the upstream half of the propeller. This is because the influence of the free vortices is greatly exaggerated by Eq. (12) of potential theory.

On the other hand, any attempt to arrive at an actually comprehensive theoretical description of the turbulent mixing and decay of the free vortices would have little chance to succeed as the process is not only different at different points but also subject to random effects. It was therefore deemed important to evolve a physically reasonable equivalent representation of the velocity field of free vortices which may be used also for numerical calculations without excessive difficulty. Equation (1) of my paper II, or Eq. (3) of my paper I, is satisfactory under this aspect though naturally different from the conventional formulae of potential theory. This formula yields useful results which are in satisfactory agreement with force measurements. A full discussion of the difference between Eqs. (1) and (12) along with numerical examples can be found in sections 2, 5, and 6 of my paper II.

The problem thus encountered will be of interest with all types of propellers and turbo equipment in which part of the blades operate within the wake vortices produced by other blades. This, however, shall not imply that the method I have shown for Voith-Schneider propellers can be applied without change to other types of hydrodynamic machinery.

Contrary to the opinion held by Dr. Sparenberg the induced velocity u_f of the free vortices decreases with increasing incoming velocity u_o also in the case of Eq. (1) of my paper II. This is caused by the resulting change in the distribution of circulation as can be readily seen from the numerical examples given in my papers. Furthermore, this reduction in u_f, for increases in u_o, is not more pronounced with Eq. (12) than it is with Eq. (1) as might erroneously be concluded when considering the initial factor $\omega R/u_o$ without at the same time observing the behaviour of the circulation. The latter becomes apparent only from the boundary condition of flow past the profile, i.e., from the integral equation.

Naturally it is possible also with my theory to determine — similarly as has been shown for the problem treated by Dr. Sparenberg in his paper — the distribution of the angle of incidence for a prescribed relationship for the change of blade circulation as the blade proceeds on the propeller circle. Also in this instance the difference between Eqs. (1) and (12) of my paper II becomes apparent. If, for example, a simple cosine law is prescribed for blade circulation (in which case the propulsive force produced by the upstream and downstream halves of the propeller would be about equal), then the incidence angle distribution obtained from

---

*(I) "Zur Behandlung der Strömung durch einen Voith-Schneider-Propeller mit kleinem Fortschrittsgrad," Ing. Arch. 23:379 (1955); (II) "Zur Berechnung der Strömung durch Voith-Schneider-Propeller," Ing. Arch. 24:148 (1956); (III) "Der Voith-Schneider-Propeller im Nachstrom eines Schiffsrumpfes," Ing. Arch. 25:303 (1957); (IV) "Ergänzungen zur Theorie des Voith-Schneider-Propellers," Ing. Arch. 26:220 (1958).

Eq. (1) is quite reasonable. In fact it is found that, apart from the obvious change in sign, the angle of incidence for the blades on the downstream half of the propeller must be about 1.3 to 1.8 the value for the upstream half, depending on the advance ratio and the total lift. On the other hand, if Eq. (12) is employed, the resulting incidence angle pattern for the downstream side is completely senseless as it includes abrupt changes and even infinities.

It must further be noted that one might consider describing the mixing and decay of the free vortices not by Eq. (1), but by introducing the known Lamb's law* describing the decay of vortices in a real liquid into Eq. (12). I have abstained from this for two reasons: First, Lamb's law holds only for isolated vortices in purely laminar flow whereas propeller flow is turbulent, and second, the mathematical realization of this method would have been rather complicated without enabling a definitely better physical description of the problem.

While this problem is discussed here to such an extent, it is scarcely considered in Dr. Sparenberg's paper. Equations (5.1), (5.2), and (5.3) used therein for angle of incidence determination will render approximate solutions for the upstream half of the propeller blade circle only. One must keep in mind that the blades on the downstream side are exposed to the free wake vortices induced by the upstream blades, and that on the downstream side the velocity field of these free vortices cannot justly be omitted from the boundary condition for the flow past the profile since it exerts a decisive influence.

In closing I should like to remark that in my opinion the theory of quickly rotating propellers evolved by Dr. Sparenberg in sections 6 and 7 with circulation (6.9) and free wake vortices (6.10) has the disadvantage of introducing excessive simplification. It is therefore probable that this theory will not render physically reasonable results. This can be seen already from the fact that Eq. (7.6) for incidence angle α yields $\alpha = \infty$ exactly for $\varphi = 0$ and $\varphi = \pi$, whereas in reality the value of α will be relatively small or even zero for these values of φ.

J. A. Sparenburg

Equation (1) in paper II by Prof. Isay is the basis of his theoretical work. This formula describes the velocities induced by free vortices which are shed by a system of rotating and periodically varying bound vortices, placed in a homogeneous stream. The density of the free vorticity decreases when the velocity of the incoming stream increases. Hence it may be expected that the induced velocities of the free vorticity decrease in this case. However, in the above mentioned Eq. (1) the incoming velocity does not occur, which is surprising. The remark of Prof. Isay, that the increase of the incoming velocity causes a decrease in the free vorticity by changing the bound vorticity, describes a secondary effect. Here the basis formula itself and not its relation to a special boundary value problem is discussed.

Prof. Isay further questions the validity of author's formulae (5.1), (5.2), and (5.3) for the downstream side of the circle. When we look at (5.2), for instance, we see that a pole of the integrand crosses the line of integration when the point z, where we consider the induced velocities, crosses the vortex layer. This means a discontinuity of the value of the integral, which corresponds to the discontinuity of the velocities at the vortex layer. Hence with respect to potential theory, this formula is valid also in the downstream region.

---

*H. Lamb, "Lehrbuch der Hydrodynamik," 2nd ed., Leipzig, 1931, p. 669

The remark of Prof. Isay that the theory for the quickly rotating propeller (sections 6 and 7 of my paper) is too crude may be true. It does not follow, however, from the fact that the angle of incidence α becomes infinite at the places $\varphi = 0$ and $\varphi = \pi$. The regions where α is large are so small that they can be neglected by the realisation of a model. As is well known in many linearised theories, there occur singularities at points where the theory does not hold, for instance, the endpoints of the range of contact by indentation problems and the leading edge by lifting surface theory. This does not affect the applicability of these theories, when the influence of the singularities is restricted within narrow limits. Moreover the results of the simple theory are not devoid of sense and show the behaviour mentioned by Prof. Isay in his contribution.

It is, as Prof. Isay stresses, highly recommendable to investigate the interaction of turbulence and free vorticity. However, in my opinion this must be done on the basis of experiments or theory and not on the basis of a law stated a priori.

*   *   *

A SOLUTION OF THE MINIMUM WAVE RESISTANCE PROBLEM

R. Timman and G. Vossers
Netherlands Ship Model Basin

INTRODUCTION

The problem of the determination of ship hulls with minimum wave resistance has been the subject of numerous investigations. The usual way of approach, based on a classical paper by Weinblum (1930) is to consider a ship hull in the form of an infinitely deep cylinder and to solve the variational problem of minimizing the resistance integral with prescribed horizontal cross section of the ship. In Weinblum's original paper a Ritz method is used; the waterline is represented by a polynomial with unknown coefficients which are determined from a minimum problem for a function of a finite number of variables. Computation of the Weinblum-functions (1955) facilitates the procedure.

The method, however, is open to some criticism, since it is not a priori clear, that it yields a good approximation to the variational problem.

It is known that Pavlenko (1934) reduced the variational problem to the solution of an integral equation of the first kind. It is known that its solution has certain singularities, which cannot properly be represented by a polynomial.

In this paper the problem is reduced to an integral equation of the second kind, obtained by the following consideration. The resistance integral in the thin ship approximation is known to be a quadratic functional of the hull function. If the additional condition is also expressed by a quadratic functional, the problem is simply equivalent to a principal axis problem and the solution exists, as is known from the general theory of quadratic functionals. Essentially, it is assumed that the cross sections of the ship are similar in shape, which (with a slight modification) produces the required result. This means, that the ship considered has a finite draft.

In order to obtain a simple integral equation, the influence of the bottom in the evaluation of Michell's integral is neglected, although a more correct treatment lies within the power of numerical methods.

MICHELL'S FORMULA FOR THE RESISTANCE INTEGRAL

We introduce a coordinate system with the x axis along the axis of the ship, the y axis athwartships, and the z axis downward. The ship hull is represented by a function

$$y = \pm f(x, z) , \qquad -L/2 < x < L/2 , \qquad 0 < z < T$$

where L is the length of the ship and T the draft. The ship is moving in the x direction with constant velocity c. The disturbance potential φ, from which the disturbance velocities $u = -\partial\varphi/\partial x$, $v = -\partial\varphi/\partial y$, $w = -\partial\varphi/\partial z$ are derived, is determined by the condition that at the hull of the ship

$$\frac{\partial\varphi}{\partial x} = c\,\frac{\partial f}{\partial x}\,.$$

The linearization, introduced by Michell consists in applying this condition at the plane of symmetry $y = 0$, in which case the potential, satisfying the Laplace equation $\nabla^2\varphi = 0$ and the free surface condition at the plane $z = 0$:

$$\varphi_{xx} - \kappa\varphi_z = 0$$

where

$$\kappa = \frac{g}{c^2}\,.$$

The solution of this boundary value problem is then

$\varphi(x,y,z)$

$$= \frac{2c}{\pi} \int_{-L/2}^{+L/2} dx_1 \int_0^T dz_1 \frac{\partial f(x_1,z_1)}{\partial x_1} \int_\kappa^\infty \frac{e^{-\frac{\alpha^2}{\kappa}(z+z_1)}\ \sin\left[\alpha(x-x_1) + y\,\frac{\alpha}{\kappa}\sqrt{\alpha^2-\kappa^2}\right]}{\sqrt{\alpha^2-\kappa^2}}\,\alpha\,d\alpha$$

$$- \frac{2c}{\pi} \int_{-L/2}^{L/2} dx_1 \int_0^T dz_1 \frac{\partial f(x_1,z_1)}{\partial x_1} \int_0^\kappa \frac{e^{-\frac{\alpha^2}{\kappa}(z+z_1) - \frac{\alpha y_1}{\kappa}\sqrt{\kappa^2-\alpha^2}}}{\sqrt{\kappa^2-\alpha^2}}\cos\alpha(x-x_1)\,d\alpha$$

$$+ \frac{2c}{\pi^2} \int_{-L/2}^{+L/2} dx_1 \int_0^T dz_1 \frac{\partial f(x_1,z_1)}{\partial x_1} \int_0^\infty \cos\alpha(x-x_1)\,d\alpha$$

$$\times \int_0^\infty \frac{e^{-\sqrt{\alpha^2+n^2}\,y}}{\sqrt{\alpha^2+n^2}}\cos(nz-\varepsilon)\cos(nz_1-\varepsilon)\,dn$$

where

$$\tan\varepsilon = -\frac{\alpha^2}{\kappa n}\,.$$

The pressure is determined by Bernoulli's equation

$$-\varphi_t + \frac{1}{2}\left[(-c+\varphi_x)^2 + \varphi_y^2 + \varphi_z^2\right] + \frac{p}{\rho} - gz = \frac{1}{2}c^2 + \frac{p_\infty}{\rho}$$

or, in linearized approximation for steady flow,

$$p - p_{\infty} = - \dot{\rho} c \, \varphi_x + \rho g z \, .$$

The force in the x direction, exerted on a surface element of the hull is

$$dK = - p \, \frac{\partial f}{\partial x} \, dx dz$$

where $dx dz$ is the projection of the element on the x, z plane. The total resistance is

$$R = - 2 \int_{-L/2}^{+L/2} \int_0^{\infty} p \, \frac{\partial f(x,z)}{\partial x} \, dx dz = 2 \dot{\rho} c \int_{-L/2}^{+L/2} \int_0^{\infty} \frac{\partial \varphi}{\partial x} \, \frac{\partial f}{\partial x} \, dx dz \, .$$

Substitution of the expression for φ gives for the resistance integral

$$R = \frac{4 \dot{\rho} c^2}{\pi} \int_{-L/2}^{+L/2} dx \int_{-L/2}^{+L/2} dx_1 \int_0^{\infty} dz \int_0^{\infty} dz_1 \frac{\partial f(x,z)}{\partial x} \, \frac{\partial f(x_1, z_1)}{\partial x_1}$$

$$\times \int_{\kappa}^{\infty} e^{-\frac{\alpha^2}{\kappa}(z + z_1)} \frac{\alpha^2 \cos \alpha \, (x - x_1)}{\sqrt{\alpha^2 - \kappa^2}} \, d\alpha \, .$$

We introduce dimensionless coordinates

$$\xi = \frac{2x}{L} \, , \qquad \eta = \frac{2y}{B} \, , \qquad \zeta = \frac{z}{T}$$

where B is the beam and T the draft of the ship. Then

$$\frac{\partial f(x,z)}{\partial x} = \frac{B}{L} \, \frac{\partial \eta(\xi, \zeta)}{\partial \xi} = \frac{B}{L} \, h(\xi, \zeta)$$

and the resistance integral takes the form

$$R = \frac{\dot{\rho} c^2 B^2 T^2 \kappa^2}{\pi} \int_{-1}^{+1} d\xi \int_{-1}^{+1} d\xi_1 \int_0^{+1} d\zeta \int_0^{+1} d\zeta_1 \, h(\xi, \zeta) \, h(\xi_1, \zeta_1)$$

$$\times \int_1^{\infty} e^{-\lambda^2 \kappa T (\zeta + \zeta_1)} \cos \frac{\lambda L \kappa}{2} (\xi - \xi_1) \frac{\lambda^2 \, d\lambda}{\sqrt{\lambda^2 - 1}} \, .$$

The volume of the ship is given by

$$V = \int_{-L/2}^{+L/2} dx \int_{0}^{T} f(x,z)\ dz\ .$$

The problem then consists in the determination of the function $f(x,z)$, which minimizes the resistance at a prescribed volume.

SIMPLIFIED TREATMENT OF THE VARIATIONAL PROBLEM

We put the condition that $f(x,z) = 0$ for $x = \pm L/2$ and transform the resistance integral by integration by parts:

$$R = \frac{\rho c^2 B^2 T^2 L^2 \kappa^4}{4\pi} \int_{-1}^{+1} d\xi \int_{-1}^{+1} d\xi_1 \int_{0}^{\infty} d\zeta \int_{0}^{\infty} d\zeta_1\ \eta(\xi,\zeta)\ \eta(\xi_1,\zeta_1)$$

$$\times \int_{1}^{\infty} e^{-\lambda^2 \kappa T(\zeta+\zeta_1)}\ \cos\frac{\lambda L \kappa}{2}\ (\xi-\xi_1)\frac{\lambda^4\ d\lambda}{\sqrt{\lambda^2 - 1}}\ .$$

In order to simplify the problem, a special class of ship hulls is considered which is so determined that both R and V appear as quadratic functionals of a function $f(\xi)$. We assume

$$f(\xi,\zeta) = f(\xi)\ g\left[\frac{\zeta\sqrt{1-\xi^2}}{f(\xi)}\right].$$

where $f(\xi)$, the waterline function, is to be determined and $g(\mu)$ is a fixed function of μ which is zero for μ greater than a certain value. If the factor $\sqrt{1-\xi^2}$ did not exist, the assumption would mean that all cross sections of the ship were similar. If $f(\xi)$ vanishes at the front and the stern of the ship, also the draft would vanish there. This is prevented by the present assumption, and moreover it will appear later that the addition of this factor actually yields functions $f(\xi)$ which vanish at these places. The volume of the ship is given by

$$V \doteq \frac{LT}{2} \int_{-1}^{+1} d\xi \int_{0}^{\infty} d\zeta\ f(\xi)\ g\left[\frac{\zeta\sqrt{1-\xi^2}}{f(\xi)}\right] = \frac{LT}{2} \int_{-1}^{+1} \frac{f^2(\xi)}{\sqrt{1-\xi^2}}\ d\xi \int_{0}^{\infty} g(\mu)\ d\mu\ .$$

The resistance is

$$R = \frac{\rho' c^2 B^2 T^2 L^2 \kappa^4}{4\pi} \int_{-1}^{+1} d\xi \int_{-1}^{+1} d\xi_1 \int_0^\infty d\zeta \int_0^\infty d\zeta_1 \ f(\xi) \ f(\xi_1) \ g\left[\frac{\zeta\sqrt{1-\xi^2}}{f(\xi_1)}\right]$$

$$\times \int_1^\infty e^{-\lambda^2 \kappa T(\zeta + \zeta_1)} \cos\frac{\lambda L \kappa}{2}(\xi - \xi_1) \frac{\lambda^4 \ d\lambda}{\sqrt{\lambda^2 - 1}}.$$

In order to obtain a simple integral expression, we neglect the dependence of g on ζ and assume infinite depth. An estimate of the validity of this procedure is obtained by considering the case, where the cross sections are rectangular:

$$\begin{cases} g(\mu) = 1, & 0 < \mu < 1 \\ g(\mu) = 0, & \mu > 1. \end{cases}$$

Then

$$\int_0^\infty d\zeta \ g\left(\frac{\zeta\sqrt{1-\xi^2}}{f(\xi)}\right) e^{-\lambda^2 \kappa T \zeta} \ d\zeta = \int_0^{\frac{f(\xi)}{\sqrt{1-\xi^2}}} e^{-\lambda^2 \kappa T \zeta} \ d\zeta$$

$$= \frac{1}{\lambda^2 \kappa T}\left[1 - e^{\frac{-\lambda^2 \kappa T f(\xi)}{\sqrt{1-\xi^2}}}\right]$$

which integral is simply replaced by $1/\lambda^2 \kappa T$.

If necessary, the method can be refined, yielding more complicated integrals which can be treated by numerical methods. The simplified expression for R is

$$R = \frac{\rho' c^2 B^2 L^2 \kappa^2}{4\pi} \int_{-1}^{+1} d\xi \int_{-1}^{+1} d\xi_1 \ f(\xi) \ f(\xi_1) \int_1^\infty \frac{\cos \gamma_o(\xi - \xi_1)\lambda}{\sqrt{\lambda^2 - 1}} \ d\lambda$$

or, using the formula

$$Y_o\left[\gamma_o(\xi - \xi_1)\right] = -\frac{2}{\pi}\int_1^\infty \frac{\cos \gamma_o(\xi - \xi_1)\lambda}{\sqrt{\lambda^2 - 1}} \ d\lambda,$$

$$R = -\frac{\rho' c^2 B^2 L^2 \kappa^2}{8} \int_{-1}^{+1} d\xi \int_{-1}^{+1} d\xi_1 \ f(\xi) \ f(\xi_1) \ Y_o\left[\gamma_o(\xi - \xi_1)\right],$$

where

$$\gamma_o = \frac{\kappa L}{2} = \frac{gL}{2c^2} = \frac{1}{2F^2}$$

depends on the Froude number. We introduce variables ϑ and ϑ_1 by $\cos \vartheta = \xi$, $\cos \vartheta_1 = \xi_1$ and have to minimize the integral

$$J = \int_0^\pi d\vartheta \int_0^\pi d\vartheta_1 \ f(\vartheta) \ f(\vartheta_1) \ \sin \vartheta \ \sin \vartheta_1 \ Y_o\Big(\gamma_o|\cos \vartheta - \cos \vartheta_1|\Big) = J(f,f)$$

with the condition

$$\int_0^\pi f(\vartheta^2) \ d\vartheta = C.$$

REDUCTION TO AN INTEGRAL EQUATION OF THE SECOND KIND

Suppose that $f(\vartheta)$ is the minimal function and consider a neighbouring function

$$f(\vartheta) + \varepsilon h(\vartheta)$$

where ε is a small parameter. Then

$$J(f + \varepsilon h) = J(f,f) + 2\varepsilon J(f,h) + \varepsilon^2 J(h,h)$$

and

$$V(f + \varepsilon h) = V(f,f) + 2\varepsilon V(f,h) + \varepsilon^2 V(h,h).$$

Since $J(f,f)$ must be a minimum for f, with constant V, we consider

$$J(f + \varepsilon h) - \lambda V(f + \varepsilon h)$$

where λ is a Lagrangian multiplier. The expression

$$J(f + \varepsilon h) - \lambda V(f + \varepsilon h) = J(f,f) - \lambda V(f,f) + 2\varepsilon [J(f,h) - \lambda V(f,h)]$$
$$+ \varepsilon^2 [J(h,h) - \lambda V(h,h)]$$

can only be an extremum if

$$J(f,h) - \lambda V(f,h)$$

vanishes for any choice of h. This means that f must be such that

$$\int_0^\pi d\vartheta \int_0^\pi d\vartheta_1 \; f(\vartheta) \; h(\vartheta_1) \; \sin \vartheta \; \sin \vartheta_1 \; Y_o\Big[\gamma_o(\cos \vartheta - \cos \vartheta_1)\Big]$$

$$- \lambda \int_0^\pi f(\vartheta) \; h(\vartheta) \; d\vartheta = 0$$

for all functions $h(\vartheta)$, or

$$\int_0^\pi h(\vartheta_1) \; d\vartheta_1 \left\{ \sin \vartheta_1 \int_0^\pi f(\vartheta) \sin \vartheta \; Y_o\Big[\gamma_o(\cos \vartheta - \cos \vartheta_1)\Big] \, d\vartheta - \lambda f(\vartheta_1) \right\} = 0.$$

This can only be true, if $f(\vartheta)$ satisfies the integral equation of the second kind:

$$\lambda f(\vartheta_1) = \int_0^\pi f(\vartheta) \; \sin \vartheta \; \sin \vartheta_1 \; Y_o\Big[\gamma_o(\cos \vartheta - \cos \vartheta_1)\Big] \, d\vartheta.$$

Since the kernel is integrable, this is an ordinary Fredholm equation and the functions $f(\vartheta)$ are the eigenfunctions of the corresponding equation, while λ is the corresponding eigenfunction. Apparently the solutions vanish for $\vartheta = 0$ and $\vartheta = \pi$, as was required. Moreover, the eigenvalue λ is the value of the quotient $J(f,f)/V(f,f)$ for the eigenfunction. For the ship hull only the first eigenfunction, which has no zeros, will come into consideration.

SOLUTION OF THE INTEGRAL EQUATION

The integral equation

$$\lambda f(\vartheta_1) = \int_0^\pi f(\vartheta) \; \sin \vartheta \; \sin \vartheta_1 \; Y_c\Big(\gamma_o|\cos \vartheta - \cos \vartheta_1|\Big) \, d\vartheta$$

resembles an integral equation satisfied by the Mathieu functions. Therefore, at first a solution in terms of a Fourier series in ϑ, with coefficients depending on γ_o was looked for. This method, however, is only feasible for very small values of γ_o. For this reason, a direct numerical approach was used.

* * *

ON THE PROBLEM OF MINIMUM WAVE RESISTANCE
FOR STRUTS AND STRUT-LIKE DIPOLE DISTRIBUTIONS

Samuel Karp,* Jack Kotik, and Jerome Lurye
Technical Research Group, Inc.
Syosset, New York

In this paper we consider the problem of minimizing the wave resistance of a strut of fixed length and volume-per-unit depth at a given Froude number. The work of others has shown that a satisfactory solution of the problem within the framework of the classical linearized theory is not possible. In this paper we show that by regarding the dipole distribution rather than the form as the unknown function, and by correcting the classical thin-ship relation between the dipole distribution and the form, a satisfactory solution can be found. The universal minimum curve of C_w vs f is shown, as well as C_w vs f for a number of optimum and non-optimum forms. Among the problems left unanswered in this paper are the influence of three-dimensional effects and other corrections to the linearized theory.

1. INTRODUCTION

The linearized theory of ship wave resistance has been developed by a series of students beginning with Michell [1]. Accounts of this theory together with extensive bibliographies will be found in Refs. 2-4. Based on the assumption that the fluid is inviscid and that the ship is thin enough to generate only waves of small amplitude, the theory imposes the linearized free surface condition on the velocity potential that characterizes the flow. By means of these assumptions, the problem is made mathematically tractable and expressions for the wave resistance are derived. The expressions have the form of integrals involving either the functions that define the shape of the hull or the functions that define the distribution of sources and sinks by which the hull is generated. Consequently, if we wish to find the hull of minimum wave resistance within the linear approximation, we have to solve a problem in the calculus of variations. Specifically, a quadratic functional (the integral representing wave resistance) is to be minimized subject to a suitable side condition. The need for imposing some constraint on the minimization process becomes apparent upon observing, for example, that a hull of zero beam has zero wave resistance.

Previous studies have been of two types. One type depends on the fact that Michell's integral for the wave resistance can be evaluated in terms of tabulated functions for ship

forms defined by a certain class of polynomials. The wave resistance is then a function of the polynomial coefficients, and minima can be found by simple computations (see Ref. 5). The other type of investigation has been concerned with minimization within the class of vertical struts of infinite depth having fixed length, fixed volume-per-unit depth, and an otherwise arbitrary form. The latter problem, with which this paper is concerned, has been considered by a number of authors. Their results have been unsatisfactory for one or more of the following reasons:

    1. The problem was found to have no solution at all.

    2. The shapes obtained were infinitely wide at bow and stern.

    3. Shapes (which in some cases have negative width) were obtained by solving an integral equation numerically without regard for the fact that solutions of the equation are known to be (in general) singular.

The cause of these difficulties is a nonuniformity in the accuracy of the perturbation procedure used to linearize the problem. As in the case of thin air foils (see Ref. 6) for fixed position along the air foil the results are arbitrarily accurate for sufficiently small thickness. However, the convergence is not always uniform with respect to position, the difficulty occurring at the ends of the foil.

In this paper the problem is formulated with dipole density instead of strut shape as the unknown function. The dipole density satisfies one of the integral equations studied by previous workers, and is generally singular at the ends of the interval in which it is defined. The associated shape, defined by the closed streamlines in the flow generated by the dipoles, is approximately proportional to the dipole density (as in the usual theory) except at the ends. The shape has the required length and volume-per-unit depth, to first order in the perturbation parameter, and finite positive width. Hence, although refinements can still be made in the method of calculating the shape the basic problem is regarded as solved.

In Section 2 we formulate the problem and derive the integral equation for the dipole density. In Section 3 we discuss the optimum shape for large Froude number. In Section 4 we describe the numerical solution of the integral equation. In Section 5 we determine the shape of the optimum form. In Section 6 we compare the shape and wave drag of various forms.

2. FORMULATION AND THE INTEGRAL EQUATIONS

We reproduce here the usual theory of the thin strut of minimum wave resistance in order to motivate the formulation given later in this section. Throughout the discussion, the fluid is assumed to be incompressible and inviscid and the flow to be irrotational. Referring to Fig. 1, we introduce a right-handed rectangular coordinate system $(\hat{x}, \hat{y}, \hat{z})$. The $\hat{x}$-$\hat{z}$ plane $(\hat{y} = 0)$ represents the upper surface of the fluid, the acceleration of gravity is downwards and the flow velocity is in the $+\hat{x}$-direction.

It is convenient also to introduce the dimensionless coordinates x, y, z defined by

$$\hat{x} = Lx, \qquad \hat{y} = Ly, \qquad \hat{z} = Lz \tag{1}$$

where L is the length of the strut's horizontal section in the $\hat{x}$-direction.

Fig. 1. Coordinate system fixed in a thin strut. The $\hat{x} - \hat{z}$ plane ($\hat{y} = 0$) represents the upper surface of the fluid, the acceleration of gravity is downward and the flow velocity is in the $+\hat{x}$ - direction.
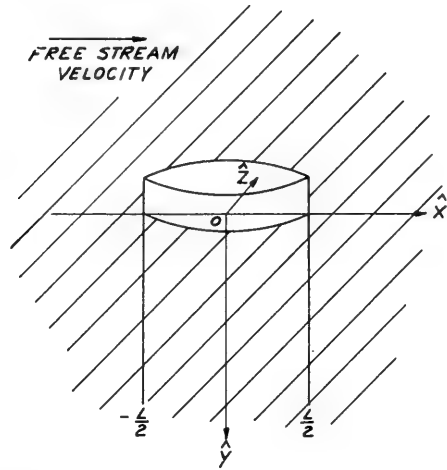
Now let the strut be represented by the equation

$$\hat{z} = \pm \hat{\zeta}(\hat{x}). \text{*}$$ (2)

The extremities of the strut are given by $\hat{x} = \pm L/2$, so that $\hat{\zeta}(\pm L/2) = 0$. Since we wish to perform a perturbation about the strut of zero thickness, we introduce $V/2L$ as a perturbation parameter, where V is the volume-per-unit depth, and write

$$\hat{\zeta}(\hat{x}) = \frac{V}{2L} \hat{\zeta}_1(\hat{x}).$$ (3)

Since V is the cross-sectional area, $V/2L$ is the average half-beam. The wave resistance of the strut is given by

$$R_w = \frac{1}{2} \rho c^2 \left(\frac{V}{2L} \right)^2 C_w$$ (4)

where C_w is the wave resistance coefficient. Michell's theory gives [3, p. 115]

$$C_w = 4 \int_{-L/2}^{L/2} \int_{-L/2}^{L/2} \frac{d\hat{\zeta}_1(\hat{x})}{d\hat{x}} \frac{d\hat{\zeta}_1(\hat{x}')}{d\hat{x}'} K\left[\nu(\hat{x} - \hat{x}') \right] d\hat{x} d\hat{x}'$$ (5)

where $\nu = g/c^2$ and the function $K(t)$ is defined by

$$K(t) = \frac{2}{\pi} \int_1^\infty \frac{\cos \lambda t}{\lambda^2 \sqrt{\lambda^2 - 1}} d\lambda .$$ (6)

*The strut is supposed symmetrical about the $\hat{x} - \hat{y}$ plane.

If we introduce the dimensionless variables x and x' into (5), we get

$$C_w = 4 \int_{-1/2}^{1/2} \int_{-1/2}^{1/2} \frac{d\zeta(x)}{dx} \frac{d\zeta(x')}{dx'} K\left[F(x-x')\right] dx' dx \tag{7}$$

where $\zeta(x)$ is defined by

$$\zeta(x) = \hat{\zeta}_1(Lx) \tag{8}$$

and

$$F = \nu L = \frac{1}{f^2} . \tag{9}$$

The quantity f is called the Froude number.

The problem is to find the function $\zeta(x)$ that minimizes Eq. (7) subject to a suitable constraint. In the case of a strut, a natural constraint is the requirement that a strut of given length L have a given volume V per unit draft. The side condition is thus

$$\int_{-L/2}^{L/2} 2\hat{\zeta}(\hat{x}) \, d\hat{x} = V . \tag{10}$$

In terms of $\zeta(x)$, this becomes

$$\int_{-1/2}^{1/2} \zeta(x) \, dx = 1 . \tag{11}$$

The problem therefore is to minimize Eq. (7) among all functions $\zeta(x)$ that satisfy the following conditions:

1. $d\zeta/dx$ must be integrable in $-1/2 \le x \le 1/2$ (otherwise Eq. (7) would be meaningless).

2. $\zeta(x)$ must satisfy Eq. (11).

3. $\zeta(\pm 1/2) = 0$.

It is at this point that the central difficulty of the problem appears, in that the minimizing $\zeta(x)$ will now be shown to obey an integral equation that has no solution. Using standard procedures in the calculus of variations, we have at once that if $\zeta(x)$ satisfies the three above conditions, it must also satisfy the equation

$$\int_{-1/2}^{1/2} \frac{d\zeta(x')}{dx'} K(F|x-x'|) \, dx' = kx \tag{12}$$

where the constant k is determined by Eq. (11). Differentiation of Eq. (12) twice with respect to x yields

$$\int_{-1/2}^{1/2} \frac{d\zeta(x')}{dx'} \; Y_0(F|x-x'|) \; dx' = 0 \tag{13}$$

where $Y_0(t)$ is the Bessel function defined by

$$Y_0(t) = -\frac{2}{\pi} \int_1^\infty \frac{\cos \lambda t \; d\lambda}{\sqrt{\lambda^2 - 1}} \; .$$

From Eq. (6)

$$\frac{d^2 K(t)}{dt^2} = Y_0(t) \; .$$

Dorr [7] has solved Eq. (13) with an arbitrary given right-hand side; i.e., he has solved

$$\int_{-1/2}^{1/2} h(x') \; Y_0(F|x-x'|) \; dx' = p(x). \tag{14}$$

The change of variables $x = -1/2 \cos \beta$, $x' = -1/2 \cos \beta'$ converts Eq. (14) into

$$\int_0^\pi H(\beta') \, Y_0\left(\frac{F}{2}|\cos \beta - \cos \beta'|\right) \; d\beta' = P(\beta) \tag{15}$$

where $H(\beta') = (1/2 \sin \beta') \, h(-1/2 \cos \beta')$ and $P(\beta) = p(-1/2 \cos \beta)$.

Dorr then proves that the eigenfunctions of Eq. (15) are the even Mathieu functions of integral order, $ce_n(\beta, F^2/4)$. Since over the integral $(0,\pi)$ these are closed [8], and the kernel $Y_0(F/2|\cos \beta - \cos \beta'|)$ is quadratically integrable over the square $0 \leq \beta' \leq \pi$, $0 \leq \beta \leq \pi$, it follows [9] that there is at most one solution to Eq. (15) in L_2. Moreover, there are no solutions to Eq. (15) not in L_2, as may be deduced from the work of MacCamy [10], who has shown that the only singularities of $h(-1/2 \cos \beta')$ in the interval $0 \leq \beta' \leq \pi$ occur at $\beta' = 0$ or π, these singularities being of the form $1/\sin \beta'$. Thus

$$H(\beta') = \left(\frac{1}{2} \sin \beta'\right) \, h\left(-\frac{1}{2} \cos \beta'\right)$$

is bounded in the interval $0 \leq \beta' \leq \pi$ and is therefore in L_2.

Summarizing, we have that Eqs. (15), (14), and (13) all have at most one solution. It follows that the unique solution of Eq. (13) is zero. Since any solution of Eq. (12) is a

solution of Eq. (13), we conclude finally that Eq. (12) has no solution at all.* Thus, the seemingly natural way in which the problem of the strut of minimum wave resistance has been formulated turns out to be inadequate. We will show that the functions $\zeta(x)$ satisfying the conditions 1, 2, and 3 comprise a class which is too severely restricted for the minimizing $\zeta(x)$ to be found within it.

The problem can also be approached as follows. Since we require $\zeta(\pm 1/2) = 0$, two integrations by parts in Eq. (7) lead to

$$C_w = -4F^2 \int_{-1/2}^{1/2} \int_{-1/2}^{1/2} \zeta(x) \ \zeta(x') \ Y_0(F|x-x'|) \ dx'dx, \qquad (16)$$

and the corresponding integral equation is

$$\int_{-1/2}^{1/2} \zeta(x') \ Y_0(F|x-x'|) \ dx' = \alpha \ \text{ on } \left[-\frac{1}{2}, \frac{1}{2}\right] \qquad (17)$$

where α is determined so that Eq. (11) holds. As mentioned above it is shown in Ref. 10 that the solutions of Eq. (17) are generally infinite at $x = \pm 1/2$, so that the derivation of Eq. (16) is suspect and the solution physically unacceptable. Nevertheless Pavlenko [12] has solved Eq. (17) numerically by replacing it by a set of algebraic equations and imposing $\zeta(\pm 1/2) = 0$. According to Wehausen, for Froude numbers $f < 0.325$ he finds negative ordinates near the ends. For higher Froude numbers his solutions are fairly good except at the ends, as we shall see. Shen and Kern [13] solved Eq. (17) numerically by assuming that $\zeta(x)$ was a polynomial with three undetermined coefficients. Their results are discussed in Section 6.

We now show that Eqs. (16) and (17), suitably interpreted, are still the correct equations. Let $\hat{\psi}(\hat{x}, \hat{y}, \hat{z}; V/2L)$ be the potential for the flow generated by a strut advancing into still water. Assuming the strut to be fixed and the free stream directed along the positive $\hat{x}$ axis with velocity c, we have $c\hat{x}$ as the potential of the free stream.[†] Then

$$\hat{\psi}\left(\hat{x}, \hat{y}, \hat{z}; \frac{V}{2L}\right) = \frac{V}{2L} \hat{\phi}(\hat{x}, \hat{y}, \hat{z}) + c\hat{x} \qquad (18)$$

where $V\hat{\phi}/2L$ is the "perturbation potential" expressing the amount by which the strut disturbs the free stream. The well-known [3, p. 113] linearized boundary conditions on $\hat{\phi}$ for a thin strut are

$$\frac{\partial^2 \hat{\phi}(\hat{x}, 0, \hat{z})}{\partial \hat{x}^2} = \frac{g}{c^2} \ \frac{\partial \hat{\phi}(\hat{x}, 0, \hat{z})}{\partial \hat{y}} \qquad (19)$$

at the mean free surface $\hat{y} = 0$ and

---

*The exceptional case $k = 0$ in Eq. (12) leads to the nontrivial solution $\zeta = $ constant, but this fails to satisfy the condition $\zeta(\pm 1/2) = 0$ unless $\zeta = 0$. Sretenskii [11] has concluded that there are no square-integrable solutions, but his reasoning has been criticized by Wehausen [3].
[†]The flow velocity, $\bar{v}$, is given by $\bar{v} = \text{grad } \psi$.

$$\frac{\partial \hat{\phi}(\hat{x}, \hat{y}, 0\pm)}{\partial \hat{z}} = \pm c \frac{d\hat{\zeta}_1(\hat{x})}{d\hat{x}} \qquad (19a)$$

along the longitudinal center section of the strut, defined by the half-strip $-L/2 \leq \hat{x} \leq L/2$, $\hat{y} \geq 0$, $\hat{z} = 0$.

In terms of the dimensionless variables x, y, z, and the function $\phi(x,y,z) = \hat{\phi}(Lx, Ly, Lz)$, Eqs. (19) and (19a) become

$$\frac{\partial^2 \phi(x, 0, z)}{\partial x^2} = F \frac{\partial \phi(x, 0, z)}{\partial y} ; \qquad y = 0 \qquad (20)$$

$$\frac{\partial \phi(x, y, 0\pm)}{\partial z} = \pm c \frac{d\zeta(x)}{dx} ; \quad -\frac{1}{2} \leq x \leq \frac{1}{2} , \quad y \geq 0, \quad z = 0 . \qquad (20a)$$

ϕ is thus determined by the potential Eqs. (20) and (20a), and the usual conditions at infinity.

We introduce next a Green's function $G(x,y,z; x',y',z')^*$ representing the potential at (x,y,z) of a point sink at (x',y',z') in a uniform flow under a free surface. Then G satisfies Eq. (20) in the variables x,y,z and x',y',z', and the potential $\phi(x,y,z)$ can be expressed in terms of G as follows:

$$\frac{V}{2L} \phi(x, y, z) = \frac{c}{4\pi} \frac{V}{2L} \int_0^\infty dy' \int_{-1/2}^{1/2} -2\zeta'(x') \; G(x,y,z; x',y',0) \, dx' . \qquad (21)$$

ϕ as given by Eq. (21) satisfies Eq. (20) because G does. It can also be directly verified to satisfy Eq. (20a). Thus the flow around a thin strut in Michell's theory is characterized by the potential

$$\psi \left(x, y, z; \frac{V}{2L} \right) = cLx + \frac{V}{2L} \phi(x, y, z) \qquad (22)$$

where ϕ is defined by Eq. (21).

Note that the ship form associated with the potential ϕ is not really $V\zeta(x)/2L$, which is only the approximate form to first order in $V/2L$; the actual ship form is defined by the surface of closed streamlines of the full flow whose potential is the ψ of Eq. (22). Thus if we denote the actual form by

---

*The coefficient of the singularity in G is unity, i.e., $G = [(x-x')^2 + (y-y')^2 + (z-z')^2]^{-1/2}$ plus a regular function. This coefficient is positive for a sink and negative for a source in contrast to the usual situation, because we take for the flow velocity the gradient of the potential, rather than the negative of the gradient.

$$\hat{z} = \pm s\left(x, y; \frac{V}{2L}\right),$$ (23)

its expansion in powers of $V/2L$ is assumed to be (see, for instance, Ref. 14)

$$s\left(x, y; \frac{V}{2L}\right) = \frac{V}{2L} \zeta(x) + \text{smaller terms}.$$ (24)

Equation (24) reflects the fact that the so-called strut is a strut only to the first order in $V/2L$. The actual shape as determined by the closed streamlines of Eq. (22) has a depth dependence; however, we expect that the shape approaches a strut as a limiting form for great depths.*

At this point it is important to observe that the leading term in the approximation to C_w for the shape $s(x, y; V/2L)$, as $V/2L \rightarrow 0$, is given by Eqs. (7) and (16).

The basic idea, on which all our results depend, is to consider a class of potentials more extensive than that defined by Eq. (21) but including the latter as a subclass. Specifically, let

$$\frac{V}{2L} \mu(x, y, z) = \frac{c}{2\pi} \frac{V}{2L} \int_0^\infty dy' \int_{-1/2}^{1/2} g(x') \frac{\partial G(x, y, z; x', y', 0)}{\partial x'} dx'$$ (25)

where $g(x)$ is integrable and satisfies Eq. (11), i.e.,

$$\int_{-1/2}^{1/2} g(x) \, dx = 1.$$ (26)

Otherwise $g(x)$ is to be arbitrary. Equation (25) resembles Eq. (21) integrated by parts. Evidently, μ satisfies Eqs. (20) and (20a) with $d\zeta/dx$ replaced by dg/dx. The derivative dg/dx need not be integrable, and $g(\pm 1/2)$ need not vanish; hence the potentials μ form a larger class than the potentials ϕ, since the functions $\zeta(x)$ appearing in Eq. (21) were assumed to have integrable first derivatives and to vanish at $x = \pm 1/2$. (Obviously, the class of function $\zeta(x)$ is included in the class $g(x)$.) Our expectation is that among the ship forms defined by this larger class of potentials there will be found one with a minimum wave resistance. That this is so will be established shortly.

As in the case of the forms $s(x, y; V/2L)$ associated with ϕ, the extended class of forms, $\sigma(x, y; V/2L)$ say, associated with μ, are made up of the closed streamlines[†] of the flow

---

*For instance a depth equal to a wavelength of a surface wave having velocity c.
†Although we have not proved it rigorously, we believe that there will always be a closed body (i.e., a surface of closed streamlines) formed in the flow defined by Eqs. (25) and (27) whenever the total moment of the dipole distribution on the x axis is negative. Since, as discussed above, the density of the distribution is $-(c/2\pi)(V/2L) g(x)$, the assertion is that there will be a closed body if

$$\int_{-1/2}^{1/2} g(x) \, dx > 0.$$

We now observe that all the distributions considered satisfy this latter condition because they all satisfy Eq. (26), the right side of which is always positive. Thus, all the flows defined by Eqs. (25) and (27), subject to Eq. (26), lead to closed bodies.

whose potential is $\theta(x,y,z; V/2L)$ where

$$\theta\left(x,y,z;\frac{V}{2L}\right) = cLx + \frac{V}{2L}\mu(x,y,z).$$ (27)

If we could expand $\sigma(x,y; V/2L)$ in powers of $V/2L$, we would expect to find

$$\hat{z} = \pm\,\sigma\left(x,y;\frac{V}{2L}\right) = \frac{V}{2L}\,g(x) + \text{ smaller terms } = \sigma_1\left(x,y;\frac{V}{2L}\right) + \cdots$$ (28)

analogous to Eq. (24).

Just as $V\zeta(x)/2L$ in Eq. (21) is the first order approximation to $s(x,y; V/2L)$, as shown in Eq. (24), so $Vg(x)/2L = \sigma_1$ in Eq. (25) is the first-order approximation to $\sigma(x,y; V/2L)$, as shown in Eq. (28). However, in contrast to $\zeta(x)$, $g(x)$ need merely be integrable and can therefore have integrable singularities, so that the first-order approximation $\sigma = Vg/2L$ is not always uniform in x. On the other hand, in spite of the nonuniformity, we expect that the integral in Eq. (26) when multiplied by $V/2L$ still gives, to first order, the volume-per-unit draft.

Before we can find the function $g(x)$ in Eq. (25) that minimizes the first-order drag coefficient of the shape σ we need an expression for this coefficient. (Equations (7) and (16) apply to the restricted class of shapes, $s(x,y; V/2L)$ but not necessarily to the extended class, $\sigma(x,y; V/2L)$.) To obtain the drag coefficient for σ, we note that $-\partial G(x,y,z;x',y',0)/\partial x'$ in Eq. (25) gives the potential of an x-directed dipole located at $(x',y',0)$.* Therefore, we may interpret μ in Eq. (25) as arising from a distribution of such dipoles over the half-strip $-1/2 \le x' \le 1/2$, $y' \ge 0$, $z' = 0$, the density of the distribution being $-(c/2\pi)(V/2L)g(x')$.

It is possible to calculate the force exerted on any one of the above dipoles by the combination consisting of the remaining dipoles and the uniform flow. The force on the entire distribution, i.e., the wave resistance, is then the product of the density function, $-(c/2\pi)$ $(V/2L)g(x')$, and the force on a single dipole, integrated over the distribution. When the integration is carried out and the integral divided by $(\rho c^2/2)(V/2L)^2$, the drag coefficient of the distribution and therefore of the shape $\sigma(x,y; V/2L)$ is

$$C_w = -4F^2 \int_{-1/2}^{1/2} \int_{-1/2}^{1/2} g(x)\ g(x')\ Y_0(F|x-x'|)\ dx'dx.$$ (29)

This result is proved in Appendix A.

Comparison of Eq. (29) with Eq. (16) shows that the expression for the wave drag of the shape $\sigma(x,y; V/2L)$ has the same form as that for the drag of the shape $s(x,y; V/2L)$ with the restricted functions $\zeta(x)$ replaced by $g(x)$. Note, however, that Eqs. (7) and (16), which were equivalent for the restricted class $\zeta(x)$, are no longer so when ζ is replaced by g. Indeed, if dg/dx is not integrable, such replacement makes Eq. (7) meaningless. Thus, only Eqs.

---

*Recall that G is the potential of a sink.

(16) or (29) represent valid formulas for the drag of the extended class of shapes $\sigma(x,y; V/2L)$.*

To minimize this drag among all shapes $\sigma(x,y; V/2L)$, we must determine a function $g(x)$ that minimizes C_w in Eq. (29), subject to the side condition Eq. (26). This is a straightforward problem in the calculus of variations and leads to the following integral equation for the minimizing function $g(x)$:

$$\int_{-1/2}^{1/2} g(x') \; Y_0(F|x-x'|) \; dx' = \lambda \tag{30}$$

where λ is a (constant) Lagrange multiplier whose value is determined by the use of Eq. (26). It is easily shown that Eq. (30) is the necessary and sufficient condition for $g(x)$ to minimize Eq. (29).

Once Eq. (30) has been solved, subject to Eq. (26), the resultant $g(x)$ is substituted into Eq. (25) and the potential $\mu(x,y,z)$ obtained. The minimizing shape, $\sigma(x,y; V/2L)$, is then given by the set of closed streamlines associated with the potential $cLx + (V/2L)$ $\mu(x,y,z)$. As already noted, such a shape will not be a true strut; it is a strut only to the first order in $V/2L$.

It has been proved [10] that any solution to the integral Eq. (30) must become singular at the endpoints $x = \pm1/2$, the singularity being of the form

$$\frac{1}{\sqrt{\frac{1}{4} - x^2}}.$$

Thus the solution cannot have a first derivative which is integrable over the closed interval $-1/2 \leq x \leq 1/2$, and therefore cannot belong to the set of functions $\zeta(x)$. It is for this reason that we introduced the extended class of functions $g(x)$.

Since the minimizing $g(x)$, i.e., the solution to Eq. (30), becomes infinite at $x = \pm1/2$, it may seem that such a function can have little to do with the actual minimizing shape, $\sigma(x,y; V/2L)$. However, Eq. (28) indicates that $(V/2L) g(x) = \sigma_1$ is the first-order (in $V/2L$) approximation to σ. The explanation is that the approximation of σ by σ_1 is not uniform in x, and gets worse and worse toward the endpoints $x = \pm1/2$. Thus, even for very small $V/2L$, the shape will be well approximated by σ_1 only if x is not too near the ends. The shape is determined by a set of streamlines, as stated above, and its complete determination is discussed in Sections 3 and 5.

We have interpreted $g(x)$ as a measure of the density, $-(c/2\pi)(V/2L) g(x)$, of the dipole distribution that gives rise to the shape $\sigma(x,y; V/2L)$. In this view, the minimization process consists in the following: among all distributions of x-directed dipoles in the half-strip already defined, whose density is a function of x only and satisfies Eq. (26), we choose that

---

*Note that if $g(x) = $ const. the body in an infinite fluid would be a Rankine oval, and delta function singularities would have been necessary in Eq. (7).

distribution which has (and hence produces a shape $\sigma(x,y; V/2L)$ which has) the least wave resistance.*

Since the minimizing density is infinite at the endpoints $x = \pm 1/2$, the stagnation points of the flow defined by Eq. (27) lie outside the interval $-1/2 \le x \le 1/2$. Hence the minimizing shape $\sigma(x,y; V/2L)$ actually extends beyond the limits of this interval. However, as $V/2L \to 0$ the stagnation points approach $\pm 1/2$, as shown in Sections 3 and 5.

Finally, we remark that any solution of Eq. (30) is an even function of x, so that if free surface effects are disregarded the minimizing struts may be said to be symmetrical fore and aft. The above discussion summarizes our formulation of the problem of the strut of minimum wave resistance.

3. THE MINIMIZING SHAPE FOR LARGE FROUDE NUMBER

When the Froude number is large, it is possible to derive an algebraic expression for the limiting form assumed by the minimizing shape at great depths. In this section we indicate briefly how this can be done.

For large Froude number the parameter F is small, so that the kernel in the integral Eq. (30) can be approximated in the usual way by the formula

$$Y_0(F|x-x'|) \cong \frac{2}{\pi} \log\left(\frac{1}{2}\gamma'F|x-x'|\right) \tag{31}$$

where $\log \gamma' = \gamma$ = Euler's constant = 0.577... .

Thus, the integral equation becomes

$$\frac{2}{\pi}\int_{-1/2}^{1/2} g(x') \log\left(\frac{1}{2}\gamma'F|x-x'|\right) dx' = \lambda . \tag{32}$$

The solution to this equation is an elementary function. Specifically, we have [15]

$$g(x) = \frac{A}{\sqrt{\frac{1}{4} - x^2}} \tag{33}$$

where A is a constant that depends on λ and F, i.e., it depends on the side condition Eq. (26) and on the Froude number, f. Naturally, when $\lambda = \lambda(F)$ is chosen so that $g(x)$ satisfies Eq. (26) then A = constant independent of F. Wehausen [3] regards the singularity at $|x| = 1/2$ as depriving the solution of physical reality. This criticism is valid in the context

---

*We recall, that, to first order in $V/2L$, Eq. (26) fixes the volume-per-unit draft. Thus within the limitations of first-order theory, the minimization is still being performed among all struts having a given carrying capacity per unit draft.

of Pavlenko's theory in which $g(x)$ represents the form of the strut. In the present theory $g(x)$ represents a dipole density and the criticism does not apply.

Now, according to the procedure developed in the previous sections, we can obtain the minimizing shape σ by substituting $g(x)$ from Eq. (33) into Eq. (25) and determining the closed streamlines of the potential defined by Eq. (27). However, this procedure can be by-passed if we desire only the limiting form assumed by σ at large depths. At such depths, the flow is very nearly two-dimensional (horizontal) and can therefore be characterized by a complex velocity potential

$$\Omega(\tau) \;=\; cL\tau \;+\; \frac{V}{2L}\, w(\tau) \tag{34}$$

where $\tau = x + iz$ and w is the complex perturbation potential arising from the presence of the strut.

In terms of its real and imaginary parts,

$$w(\tau) \;=\; \mu(x,z) \;+\; i\xi(x,z) \tag{35}$$

where μ is the real perturbation potential of Eqs. (25) and (27) and ξ is the associated real stream function.

We now verify that w has the specific form

$$w(\tau) \;=\; \frac{iK}{\sqrt{\dfrac{1}{4} - \tau^2}} \,. \tag{36}$$

In Eq. (36), K is a real constant to be determined. The definition of w is completed by stipulating that the τ plane be slit along the x axis from $-1/2$ to $+1/2$, with the square root given the positive determination on the side of the slit for which $z = 0+$.

Differentiating Eq. (36) with respect to z, we get

$$\frac{\partial w}{\partial z} \;=\; \frac{dw}{d\tau}\,\frac{\partial \tau}{\partial z} \;=\; \frac{iK\tau}{\left(\dfrac{1}{4} - \tau^2\right)^{3/2}} \,\frac{\partial \tau}{\partial z}\,. \tag{37}$$

Letting $z \to 0+$ in Eq. (37) and introducing Eq. (35), we have

$$\frac{\partial \mu(x,0+)}{\partial z} \;+\; i\,\frac{\partial \xi(x,0+)}{\partial z} \;=\; -\,\frac{Kx}{\left(\dfrac{1}{4} - x^2\right)^{3/2}} \,. \tag{38}$$

It follows that

$$\frac{\partial \mu(x,0+)}{\partial z} = -\frac{Kx}{\left(\frac{1}{4} - x^2\right)^{3/2}}, \qquad -\frac{1}{2} < x < \frac{1}{2}.$$

(39)

On the other hand, differentiation of $g(x)$ with respect to x in Eq. (33) gives

$$\frac{dg}{dx} = \frac{Ax}{\left(\frac{1}{4} - x^2\right)^{3/2}}.$$

(40)

Now we set $K = -Ac$. Then, upon comparing Eqs. (39) and (40), we get

$$\frac{\partial \mu(x,0+)}{\partial z} = c \frac{dg}{dx}$$

(41)

which is what Eq. (20) becomes when ϕ is replaced by μ and ζ by g. (The process $z \to 0-$ reproduces Eq. (41) with a negative sign on the right, in agreement with Eq. (20).)

We conclude that for large Froude numbers and at large depths, the perturbation potential, μ, of Eqs. (25) and (27) is given by

$$\mu(x,z) = \text{Re} \frac{-iAc}{\sqrt{\frac{1}{4} - \tau^2}} = \text{Im} \frac{Ac}{\sqrt{\frac{1}{4} - \tau^2}}.$$

(42)

The associated perturbation stream function, ξ, is therefore

$$\xi(x,z) = \text{Re} \frac{-Ac}{\sqrt{\frac{1}{4} - \tau^2}}.$$

(43)

We recall that the constant A appearing in Eqs. (42) and (43) is determined by the Froude number and the side condition Eq. (26). But

$$\int_{-1/2}^{1/2} \frac{A}{\sqrt{1/4 - x^2}} \, dx = 1 \quad \text{implies} \quad A = \pi^{-1}.$$

From Eqs. (34) and (43) it follows that the stream function, $\Gamma(x,z)$, for the total flow at large depths and large Froude number has the form

$$\Gamma(x,z) = cLz + \frac{V}{2L} \zeta(x,z) = cLz - \frac{V}{2L} \text{Re} \frac{c\pi^{-1}}{\sqrt{\frac{1}{4} - \tau^2}}.$$

(44)

The closed streamline defining the minimizing shape, σ, is given by

$$\Gamma(x, z) = 0 . \tag{45}$$

To see this, note that the flow is symmetrical about the x-y plane, so that the part of the x axis outside the shape σ belongs to the streamline in question. Now as $x \to \infty$ (which implies $r \to \infty$), $\Gamma(x,z) \to cLz$, as is evident from Eq. (44). But $cLz = 0$ on the x axis, proving that the desired streamline is defined by Eq. (45).

Thus the limiting form assumed by the minimizing shape, σ, at large depths and for large Froude number, is represented by

$$cLz - \frac{V}{2L} \text{ Re } \frac{c\pi^{-1}}{\sqrt{\frac{1}{4} - \tau^2}} = 0 \qquad (\tau = x + iz). \tag{46}$$

If we define a thickness parameter $\epsilon = V/2L^2 = \bar{B}/2L,$* where $\bar{B}$ is the average (full) width, we can rewrite Eq. (46) as

$$z = \frac{\epsilon}{\pi} \text{ Re } \left(\sqrt{\frac{\frac{1}{2} + \tau}{\frac{1}{2} - \tau}} + \sqrt{\frac{\frac{1}{2} - \tau}{\frac{1}{2} + \tau}} \right) . \tag{47}$$

In bipolar coordinates[†] ξ and θ we have

$$z = \frac{\frac{1}{2} \sin \theta}{\cosh \xi + \cos \theta} \quad \text{and} \quad x = \frac{\frac{1}{2} \sinh \xi}{\cosh \xi + \cos \theta}$$

letting the line $\theta = 0$ have length 1. Also

$$\frac{\frac{1}{2} + \tau}{\frac{1}{2} - \tau} = e^\xi (\cos \theta + i \sin \theta)$$

and Eq. (47) becomes

$$\frac{\frac{1}{2} \sin \theta}{\cosh \xi + \cos \theta} = 2 \frac{\epsilon}{\pi} \cosh \frac{\xi}{2} \cos \frac{\theta}{2} .$$

---

*ϵ is also equal to the horizontal-plane area coefficient multiplied by $B/2L$, where B is the usual maximum beam.

†See, for example, Morse and Feshbach, "Methods of Theoretical Physics," New York: McGraw-Hill, 1953, p. 1210.

Finally,

$$\sin \frac{\theta}{2} = \frac{\pi}{8\epsilon \, \cosh \frac{\xi}{2}} \left(-1 + \sqrt{1 + \frac{64\epsilon^2}{\pi^2} \cosh^4 \xi} \right) \tag{48}$$

which is a convenient form for computation. It is easily seen that $\xi = 0$ corresponds to $x = 0$. In order to get an idea of the range of ξ we observe that at the stagnation points we have $y = 0$, $|x| > 1/2$, and hence $\theta = \pi$. Solving Eq. (48) with $\theta = \pi$ approximately for ξ_{max}, the value of ξ at the stagnation point, we find

$$\xi_{max} \cong 2 \, \cosh^{-1} \left[\frac{\pi}{4\epsilon} + \left(\frac{\pi}{4\epsilon} \right)^{1/3} \right]^{1/3} \tag{49}$$

and

$$|x_{max}| \approx \frac{1}{2} + \left(\frac{\epsilon}{2\pi} \right)^{2/3} .$$

The midship beam is given to first order by

$$z(0) \approx \frac{2\epsilon}{\pi} .$$

Since $2\epsilon/\pi$ is the beam given by the Michell theory it is interesting to compare $z(0)$ with $2\epsilon/\pi$. Table 1 shows that the relative error is less than 0.008 for $\epsilon < 0.10$.*

<div align="center">

Table 1

Comparison of $z(0)$ and $2\epsilon/\pi$

</div>

ϵ	$\dfrac{2\epsilon}{\pi}$	$z(0)$	$\dfrac{z(0) - \dfrac{2\epsilon}{\pi}}{z(0)}$
0.005	0.00318	0.00318	0.0000
0.01	0.00637	0.00637	0.0000
0.02	0.1273	0.1273	0.0000
0.05	0.03183	0.03177	-0.0019
0.10	0.06366	0.06316	-0.0079

The values of x_{max} indicate the extent to which the form fails to have the preassigned length. Figure 2 shows the optimum forms for five values of ϵ ranging from 0.005 to 0.100. They resemble dogbones.

---

*Typical values of ϵ are 0.04 for a destroyer and 0.048 for a tanker, based on the waterplane section in each case.
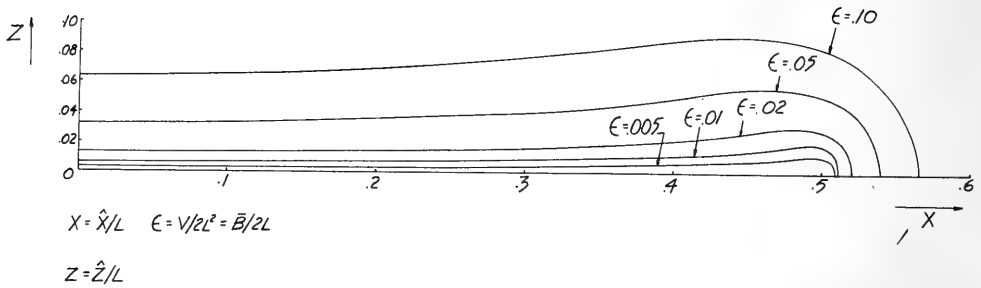
Fig. 2. The optimum shape (at large depth) for large Froude number for various values of the thickness parameter ϵ. This form is obtained by considering the streamfunction of Eqs. (47) and (48). We have Eq. (48), where $z = (1/2) \sin \theta /(\cosh \xi + \cos \theta)$ and $x = (1/2) \sinh \xi /(\cosh \xi + \cos \theta)$.

Equation (28) implies that

$$\int_{-1/2}^{1/2} \hat{z}(x) \; dx \cong \int_{-1/2}^{1/2} \sigma_1(x) \; dx = \int_{-1/2}^{1/2} \frac{V}{2L} \, g(x) \; dx = \frac{V}{2L} \qquad (50)$$

or

$$\int_{-1/2}^{1/2} z(x) \; dx \cong \epsilon.$$

To see how well the approximate side condition specifies the volume we have compared

$$\int_{-x_{max}}^{x_{max}} z(x) \; dx,$$

computed by numerical integration, with ϵ, for various values of ϵ. The results are as follows:

ϵ	0.0050	0.0100	0.0200	0.050	0.100
$\int_{-x_{max}}^{x_{max}} z(x) \, dx$	0.0047	0.0093	0.0177	0.044	0.082

Expansion of the exact volume for small ϵ yields

$$\int_{-1/2}^{1/2} z(x) \; dx \cong \epsilon \left[1 - 0.44 \, \epsilon^{1/3} \right] \qquad (50a)$$

in which the coefficient 0.44 is approximate. The general form (specifically the minus sign) of this relation is in agreement with the theorem of G. I. Taylor relating the dipole moment, the volume, and the added mass in the x-direction, for a line dipole distribution in a flow without free surface.

4. NUMERICAL SOLUTION OF THE INTEGRAL EQUATION

Equation (30), with $\lambda = -1$, was solved by numerical methods as described in Appendix B. The solution depends on Froude number and is denoted by $g_o(x)$ or $g_o(x;f)$. Solutions for other values of λ are given simply by $\lambda g_o(x)/-1$. The desired solution $g(x)$ which satisfies Eq. (26) is given by

$$g(x;f) = \frac{g_o(x;f)}{I_o(f)} \tag{51}$$

where

$$I_o(f) = \int_{-1/2}^{1/2} g_o(x;f) \, dx. \tag{52}$$

$I_o(f)$ and $g(x;f)$ have been computed from $g_o(x;f)$. As indicated in Appendix B

$$g(x) = \frac{h(x)}{\sqrt{\frac{1}{4} - x^2}} \tag{53}$$

where $h(x)$ is a bounded function. The behavior of $h(\pm 1/2)$ as a function of f (see Fig. 5) is of interest since when $h(\pm 1/2)$ is large (small) the bulge in the shape at bow and stern is also large (small), as shown in Section 5. Figure 4 shows $g(x;f)$ for various values of f. Figure 5 shows $h(x;f)$ for various values of f. Figures 3, 4, and 5 show that bluntness is a predominant feature at high speed, but less so at low speeds. However, the forms appear to have bulbs at all values of f yet examined ($f > 0.3$). Note that (in Fig. 3) $h(\pm 1/2) \to \pi^{-1} \cong$ 0.3183, as $f \to \infty$, in agreement with Eq. (43) et seq.

The function $h(x)$ (Fig. 5) is of some interest. We have $h(x) \to \pi^{-1}$ as $f \to \infty$, as explained in Section 3. Hence one can qualitatively define a high-speed range as that in which $h(x) \sim \pi^{-1}$. Figures 4 and 5 suggest that $f > 0.6$ is a reasonable definition of the high-speed range. Below $f = 0.6$ there is a rapid transition from the dogbone shape characteristic of high speed to shapes whose maximum beam is amidship.

Let $C_w^{f'}(f)$ be the wave resistance coefficient at Froude number f of the form which is optimum at Froude number f'. $C_w^f(f)$, shown in Fig. 6, is then a universal optimum for struts. Note that $C_w^f(f)$ is a maximum at $f = 0.65$. In Fig. 6 we show also $C_w^{1.0}(f)$ and $C_w^{0.5}(f)$. $C_w^f(f)$ and $C_w^{1.0}(f)$ are very close for $f > 0.6$, which substantiates our identification of $f > 0.6$ as the high-speed range. The divergence of $C_w^f(f)$ and $C_w^{1.0}(f)$ below $f = 0.6$ is substantial. $C_w^f(f)$ and $C_w^{0.5}(f)$ are close in the range $0.46 < f < 0.6$.
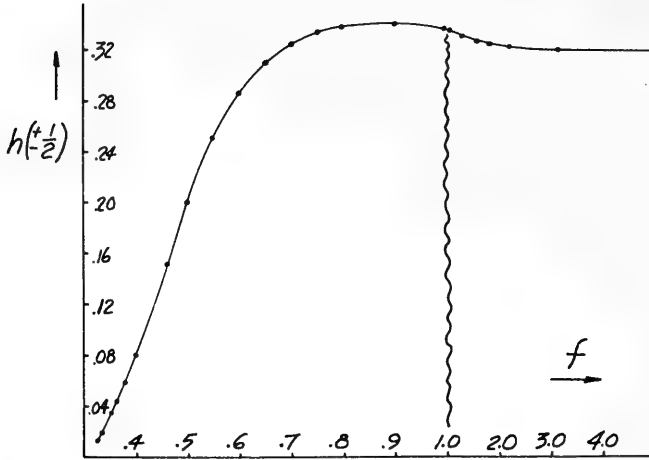
Fig. 3. Graph of $h(\pm 1/2)$ vs f. The optimizing dipole distribution has the form $-(c/2\pi)\,h(x)/(1/4 - x^2)^{1/2} = -cg(x)/2\pi$; see Eq. (53). $h(\pm 1/2)$ is the coefficient of the edge singularity, and is important in determining the shape at the ends.

As indicated in Appendix B the interval of integration (half a boat-length) was divided into six subintervals (seven points). One of the factors affecting the accuracy of the numerical scheme with seven points is the value of F, since as F increases the number of oscillations of $Y_o(F|x|)$ increases. We believe that all our numerical results for $f < 0.4$ should be regarded as questionable. For some lower values of f the numerical solution of the integral equation and the wave resistance coefficient had the wrong sign. Figure 3 shows $h(\pm 1/2)$ decreasing rapidly for $0.3 < f < 0.4$, with intentions of becoming negative. Also, a separate computer program was written for calculating C_w for any strutlike dipole distribution. The mesh in this program was variable, and it was found that seven points was not sufficient to calculate C_w for $f = 0.4$ with an accuracy of the order of 5 percent whereas seven points gave an accuracy of better than 1 percent for $f = 0.5$. A more powerful computer program is in preparation for work on the three-dimensional problem, and we expect that it will allow us to extend the range of accurate calculation to lower values of f.

5. DETERMINATION OF THE SHAPE NEAR THE ENDS

Having found the optimum dipole distribution we are left with the problem of finding the form. While digital methods were available and will play a role in future work we preferred to determine the shape approximately by analytic means. We expect that $z = Vg(x)/2L$ should be a good approximation to the true shape away from the ends, at least for sufficiently small $V/2L^2 = \epsilon$ and sufficiently far from the free surface. Figure 7 shows the exact shape and the linearized shape $g(x)$ in the case of $f = \infty$, for $\epsilon = 0.05$. The agreement even away from the ends is not as good as one would like[*] but no attempt will be made to improve this aspect of the theory.

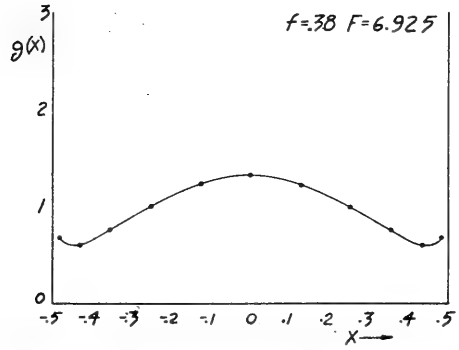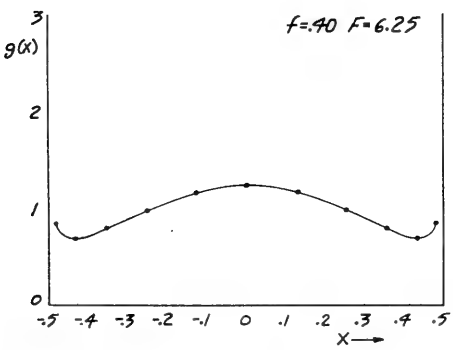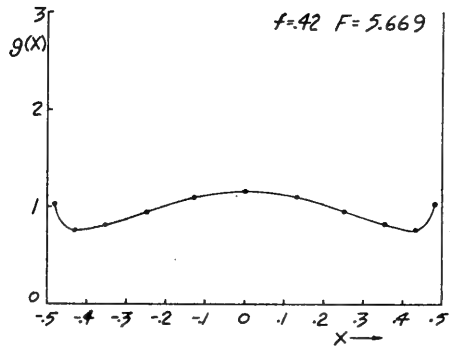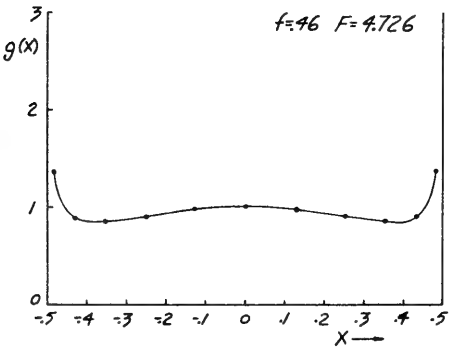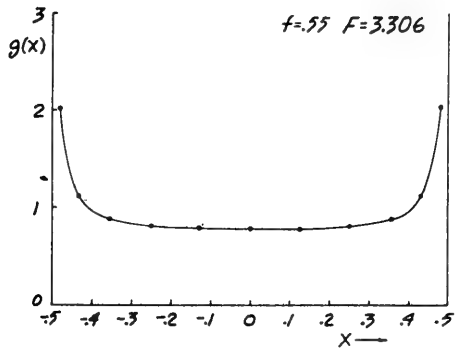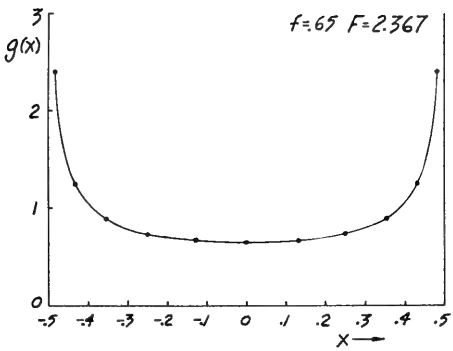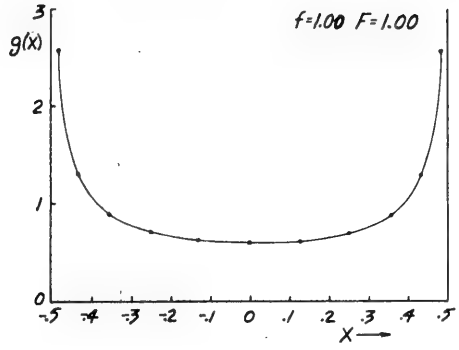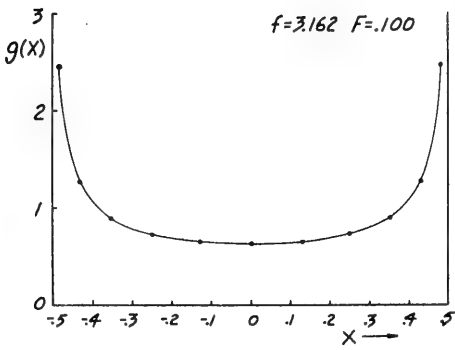[*]See also Fig. 10. For additional discussion see Section 6.

Fig. 4. Graphs of $g(x)$ vs x for eight values of f. $-cg(x)/2\pi$ is the optimum dipole distribution.
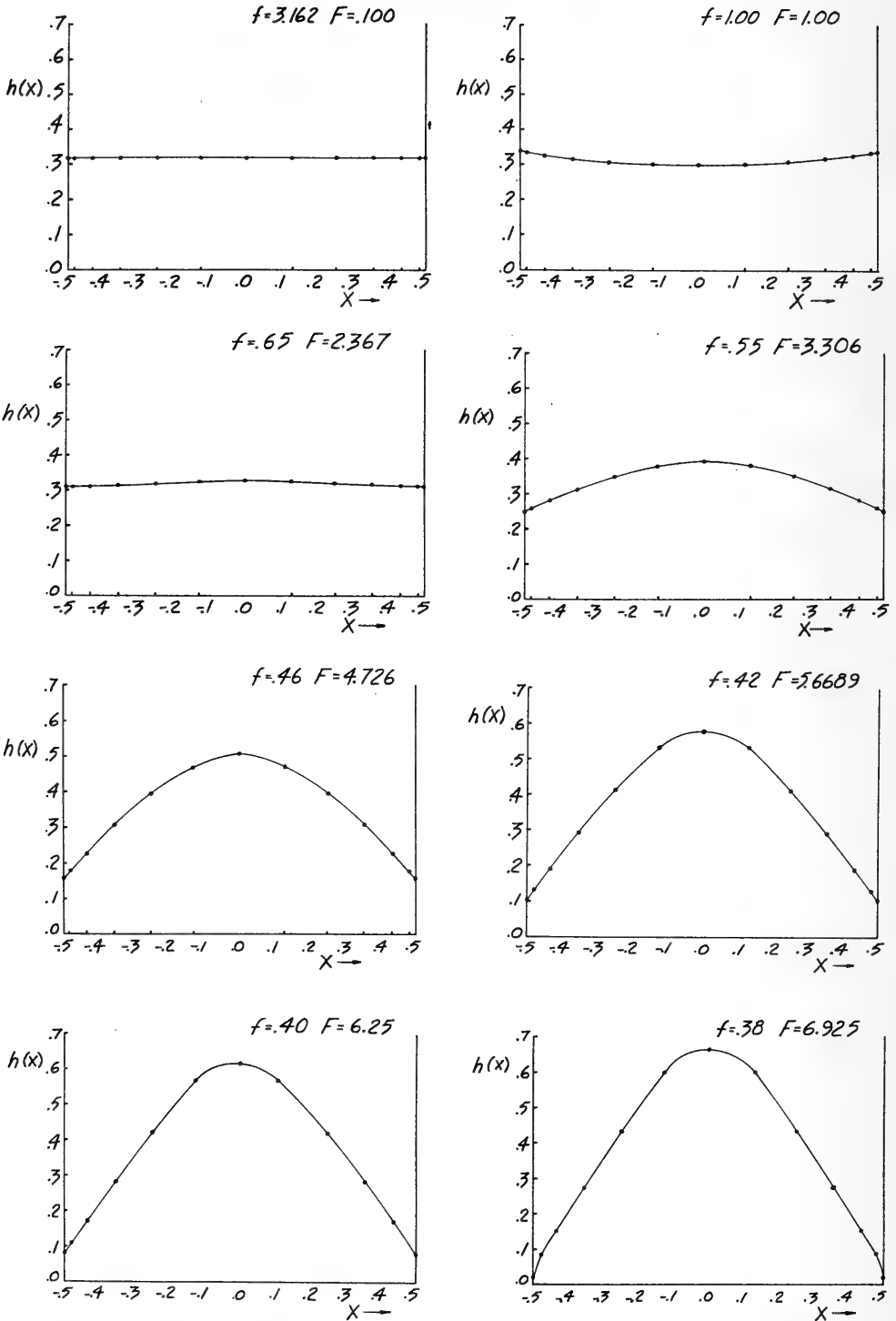
Fig. 5. Graphs of $h(x)$ vs x for eight values of f. $h(x) = g(x)(1/4 - x^2)^{1/2}$. Note that $h(x)$ for $f > 0.65$ is almost independent of f.
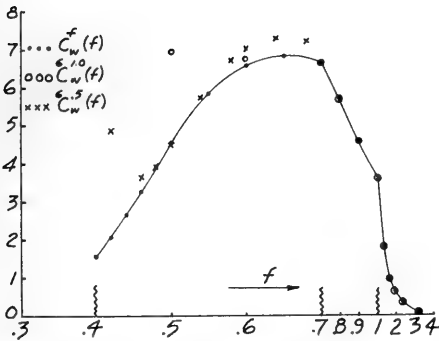
Fig. 6. $C_w^f(f)$, $^6C_w^{1.0}(f)$ and $^6C_w^{0.5}(f)$ vs f. Notice the changes of f-scale at $f = 0.7$ and 1.0. $C_w^f(f)$ is the universal minimum curve. The figure shows that a dipole distribution which is optimal for $f = 1$ performs well for $0.6 < f < \infty$, but ceases to do so as f decreases. Likewise, a strut which is optimal for $f = 0.5$ performs well in the range $0.46 < f < 0.6$.
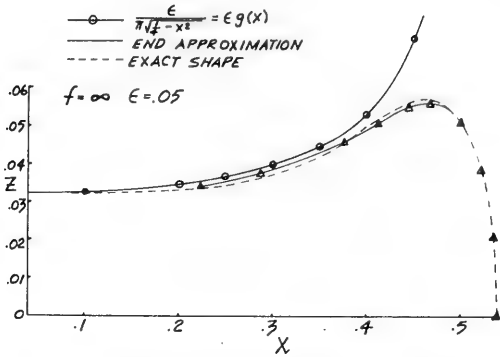
Fig. 7. Graphs of the exact optimum shape, $\epsilon g(x)$, for $f = \infty$ and an approximation to the shape. The figure shows the extent to which the approximate shape at the ends matched the linearized shape, and the way in which we joined the two.

We now prove that the shape at each end is determined by the singularity of $g(x)$ at that end in the following sense. Suppose we have a distribution of x-directed dipoles whose strength is 0 for $x' > 0$ and $-q(x')/\pi(x')^{1/2}$ for $x' > 0$, where $x' = x + L/2$ and

$$q(x') = \frac{V}{2L} (A_0 + A_1 x' + A_2 (x')^2 + \ldots).$$ (54a)

If we let $\hat{x}' = \hat{r} \cos \theta$ and $\hat{z}' = \hat{r} \sin \theta$, the stream function of the two-dimensional flow is given by

$$\hat{\xi} = c\hat{r} \sin \theta - \frac{V}{2L} \left(\frac{A_0}{\hat{r}^{1/2}} \cos \frac{\theta}{2} + A_1 \hat{r}^{1/2} \cos \frac{\theta}{2} + A_2 \hat{r}^{3/2} \cos \frac{3\theta}{2} + \ldots \right).$$ (55)

Let us introduce dimensionless variables $r = \hat{r}/L$, $\xi = \hat{\xi}/L$, so that the dipole density is

$$- \frac{q(x')}{\pi \sqrt{x'}} = - \frac{L\epsilon c}{\pi \sqrt{x'}} (B_0 + B_1 x' + \ldots)$$ (54b)

where

$$B_0 = \frac{A_0}{cL^{1/2}}$$

$$B_1 = \frac{A_1 L^{1/2}}{c}$$

and the dimensionless stream-function is given by

$$\xi = c \left[r \sin \theta - \epsilon \left(\frac{B_0 \cos \theta/2}{r^{1/2}} + B_1 r^{1/2} \cos \frac{\theta}{2} + \ldots \right) \right]. \qquad (56)$$

If we solve Eq. (54b) when $\xi = 0$ (the streamline passing through the stagnation point) for r as a function of θ we obtain the following expansion of r in terms of θ and ϵ:

$$r = B_0^{2/3} \left(\frac{\epsilon}{2 \sin \theta/2} \right)^{2/3} + \frac{2}{3} B_0^{1/3} B_1 \left(\frac{\epsilon}{2 \sin \theta/2} \right)^{4/3} + \ldots \qquad (57)$$

where the successive terms involve ascending powers of ϵ.[*] We conclude that for small ϵ the shape at one end is determined mainly by the singularity of the dipole distribution at that end. The series $A_0 + A_1 \hat{x}' + \ldots$ will have a radius of convergence equal to L, the distance to the other singularity. In order to use Eq. (57) to find the approximate shape at the ends we relate the coefficients B_0 and B_1 to the solution $g(x)$ of the integral equation. Since $\epsilon g(x)$ generates the desired unnormalized shape shrunk by a factor of L in the x-direction, and since the dipole density corresponding to $\epsilon g(x)$ is $-Lc\epsilon g(x)/\pi$, we have from Eq. (54b)

$$- \frac{Lc}{\pi} \epsilon g(x) = - \frac{Lc}{\pi} \epsilon \frac{h(x)}{\sqrt{\frac{1}{4} - x^2}} = - \frac{Lc}{\pi} \epsilon \frac{h(x')}{\sqrt{x'(1 - x')}}$$

$$= - \frac{L\epsilon c}{\pi \sqrt{x'}} (B_0 + B_1 x' + \ldots) \qquad (58)$$

from which

$$h(x') = (B_0 + B_1 x' + \ldots) \sqrt{1 - x'} \qquad (59)$$

and therefore

$$h(x' = 0) = h\left(x = -\frac{1}{2}\right) = B_0 \qquad (60a)$$

and

$$\left. \frac{dh}{dx'} \right|_{x'=0} = \left. \frac{dh}{dx} \right|_{x=-1/2} = -\frac{1}{2} B_0 + B_1. \qquad (60b)$$

These equations determine B_0 and B_1 in terms of $h(x)$. Since we have only a digital approximation to $h(x)$ we were only able to determine B_0 and B_1 approximately. Figure 7 shows the extent to which the approximate shape at the ends matched the linearized shape, and the way in which we joined the two. This example is for $f = \infty$ but it is fairly typical. Figure 8 shows the resulting shapes for a number of values of f.

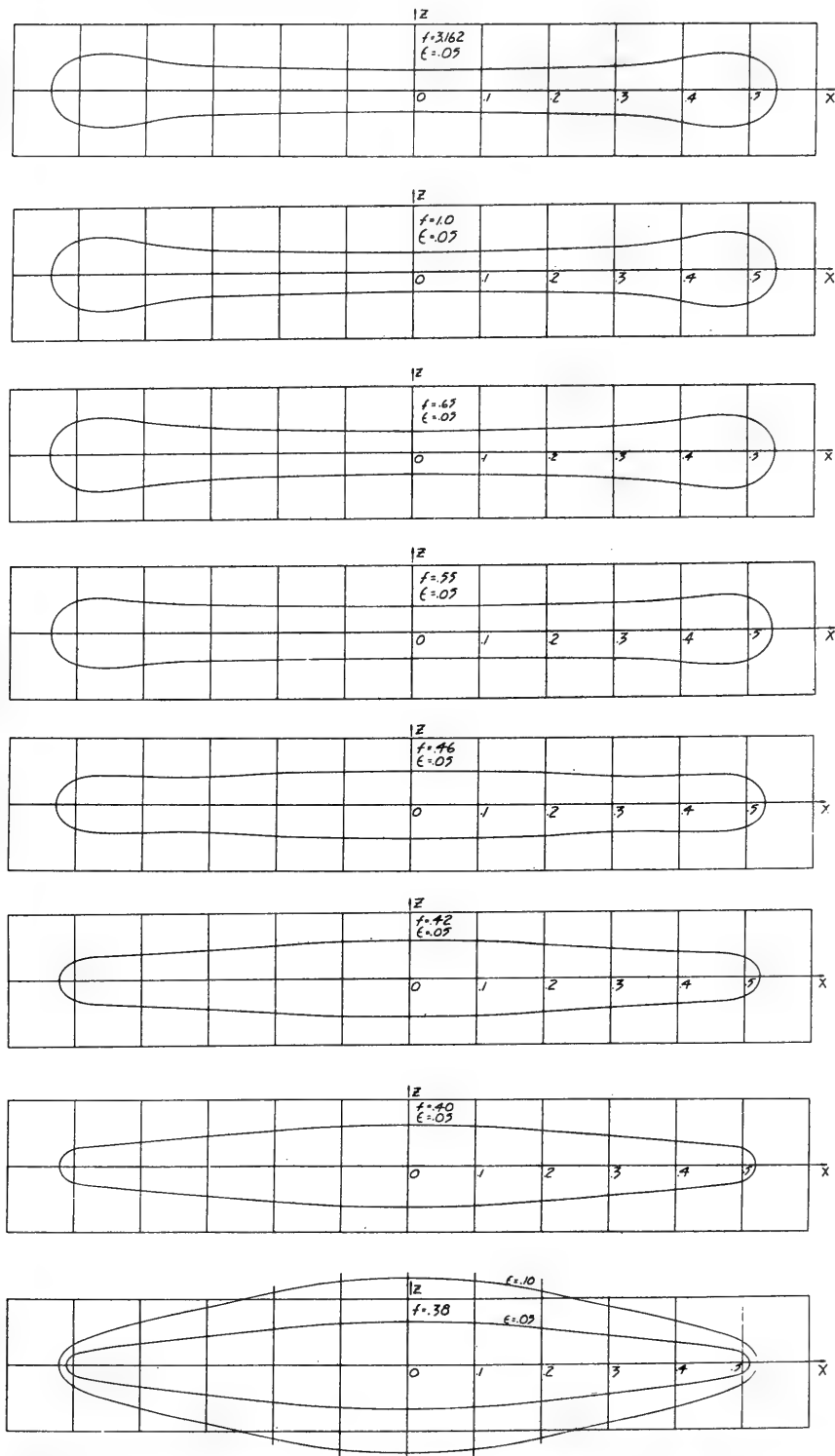[*]The next term involves all the B_i.

Fig. 8. Approximate optimum shapes at sufficiently large depth for eight values of f.

6. COMPARISON OF VARIOUS FORMS

In Section 4 we examined the resistance of some optimum dipole distributions. We now compare these with some others. Figure 9 shows the universal minimum $C_w^f(f)$, $C_w^{0.5}(f)$ and $C_w(f)$ for a parabolic dipole distribution vanishing at the ends (labeled $C_w^P(f)$). It is known that a dipole distribution $-cg(x)/2\pi$, where

$$g(x) = \frac{-\dfrac{2}{p}\sin\dfrac{2\pi}{p}(1-4x^2)^{2/p}}{(1+2x)^{4/p} + (1-2x)^{4/p} - 2(1-4x^2)^{2/p}\cos\dfrac{2\pi}{p}} \tag{61}$$

generates (in two-dimensional flow) a lens given by

$$z(x) = \frac{1}{2}\left(\sqrt{\csc^2\frac{p\pi}{2} - 4x^2} + \cot\frac{p\pi}{2}\right). \tag{62}$$

For $p = 1.812$ the full interior lens angle is $(2-p)\pi = 0.188\pi$, while

$$\int_{-1/2}^{1/2} z(x)\,dx = 0.05 \quad \text{and} \quad \int_{-1/2}^{1/2} g(x)\,dx = 0.057.$$

Figure 9 shows $C_w(f)$ for a dipole distribution $-cg(x)/2\pi$ (labeled $C_w^{LD}(f)$) and also $C_w(f)$ for a dipole distribution $-cz(x)/2\pi$ (labeled $C_w^{LS}(f)$). This last quantity is Michell's wave resistance for the shape $z(x)$, since $-cz(x)/2\pi$ is the linearized dipole distribution defined by the shape $z(x)$. Figure 10 shows $g(x)$ and $z(x)$, and we see that even for these thin forms the approximation $g(x) \sim z(x)$ is not very accurate. Comparing $C_w^{LD}(f)$ with $C_w^{LS}(f)$ in Fig. 9 we find a discrepancy of up to 25 percent. We notice that $C_w^{0.5}(f)$ is about half of $C_w^P(f)$, $C_w^{LD}(f)$, or $C_w^{LS}(f)$ over a considerable range of f.

Some information on Pavlenko's work was obtained from Refs. 4 (p. 115) and 12. The forms shown by Pavlenko are reminiscent of ours, and show the same trend as a function of f (for $f \leq 0.43$, the maximum f considered in these references). Shen and Kern [13] solved the integral equation approximately, by determining three coefficients in a polynomial approximation to the solution. They carried out the computations for $F = 0.1, 0.2, 0.4, 0.6$
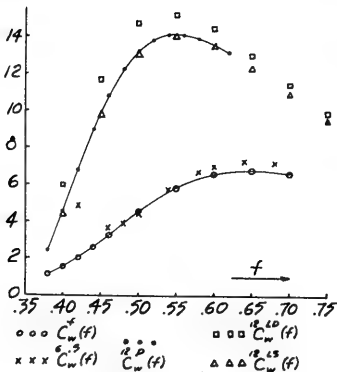
Fig. 9. Graphs of

$$C_w^f(f),\ {}^6C_w^{0.5}(f),\ {}^{12}C_w^P(f),\ {}^{12}C_w^{LD}(f),\ \text{and}\ {}^{12}C_w^{LS}(f)$$

vs f. The upper curve and the points nearby show $C_w(f)$ for a parabolic dipole distribution

$$\left(-\frac{c}{2\pi}\left[\frac{1}{6}\left(\frac{1}{4}-x^2\right)\right]\right),$$

for the dipole distribution generating a lens (in an infinite fluid), and for the linearized dipole distribution defined by the lens. The lower curve and nearby points show the universal minimum $C_w^f(f)$ and also $C_w(f)$ for the dipole distribution which is optimum at $f = 0.5$. A reduction in $C_w(f)$ by 50 percent has been achieved.
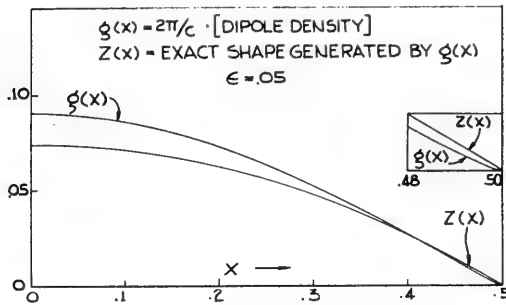
Fig. 10. Graphs of the shape function for a lens and $-2\pi/c$ times the exact dipole distribution which generates it in an infinite fluid.

($f = 3.162$, 2.236, 1.581, 1.292). The forms shown by them are somewhat reminiscent of ours. The forms of Pavlenko and of Shen and Kern differ from ours in having finite entrance angles.

In a series of pioneering papers Weinblum has considered the problem of minimizing the wave resistance of more realistic, three-dimensional forms. He has defined various families of polynomials, imposed constraints on the coefficients by specifying some geometrical properties of the form, and used the remaining degrees of freedom to minimize the resistance. Again, in spite of these differences in approach, our forms show the same general variation with Froude number as his waterplane sections.

(It should be noted that all wave resistance coefficients of dipole distributions are normalized with respect to dipole moment (multiplied by $-2\pi/c$) rather than volume. Hence to the extent that volume differs from dipole moment (multiplied by $-2\pi/c$) a comparison of wave resistance coefficients does not provide an exact comparison of resistance values based on equal volume. This discrepancy, like the length discrepancy for optimum forms, does not affect our theoretical results, which are asymptotically valid for $\epsilon \to 0$.)

7. SUMMARY

A universal curve of minimum wave resistance for infinite strutlike dipole distributions has been found (see Fig. 6). The optimizing distributions have been found, and turn out to be infinite at the ends. Despite this last mentioned feature the corresponding shapes, at large depths, are determined. The shapes are blunt at the ends, which extend beyond the interval on which the dipoles are distributed (see Fig. 8). Attention is called to the distinction between shape and dipole distribution, a distinction which is of fundamental importance in the present context. Attention is also called to the discrepancy between the wave resistances calculated using Michell's approximate dipole distribution proportional to shape and the exact dipole distribution yielding that shape, especially for ships with nonzero entrance angle (see Figs. 9 and 10). Some of the objectionable features of the analysis given by previous investigations have been removed.

ACKNOWLEDGMENT

We wish to acknowledge the valuable contributions of Mr. V. Mangulis, who helped us in some of the analytical calculations, Mr. D. Cope, who heads the computer group at TRG, and Mr. G. Weinstein, who wrote the main digital computer programs.

Appendix A

PROOF OF THE WAVE RESISTANCE FORMULA

We wish to show that Eq. (29) gives the correct formula for the drag coefficient of a distribution of horizontal dipoles in the half-strip $-1/2 \leq x \leq 1/2$, $0 \leq y < \infty$, $z = 0$, the density of the distribution being $-(c/2\pi)(V/2L) f(x)$ with $f(x)$ integrable but not necessarily bounded.

In what follows, we revert temporarily to the unnormalized variables $\hat{x}$ and $\hat{y}$. Consider first a finite number, n, of sources located in the above half-strip at the points $(\hat{x}'_s, \hat{y}'_s, 0)$ $(s = 1, 2, \ldots, n)$ and having strengths $q_s (s = 1, 2, \ldots, n)$. Then the wave resistance, R, of such an assemblage in a steady stream flowing in the $\hat{x}$ direction with velocity c, is shown by Lunde [2] to be

$$R = 16\pi\rho\,\nu^2 \int_0^\infty \left(I_n^2 + J_n^2 \right) \cosh^2 u \; du \tag{A1}$$

where ρ is the fluid density, $\nu = g/c^2$, and

$$I_n = \sum_{s=1}^n q_s \cos (\nu\hat{x}'_s \cosh u) \; e^{-\nu\hat{y}'_s \cosh^2 u} \tag{A2}$$

$$J_n = \sum_{s=1}^n q_s \sin (\nu\hat{x}'_s \cosh u) \; e^{-\nu\hat{y}'_s \cosh^2 u} . \tag{A3}$$

We now evaluate I_n and J_n when the source collection is arranged to form a finite set of $\hat{x}$-directed dipoles. For the purpose, we must assume that n is even, and we locate the dipoles at the points $(\hat{x}_p, \hat{y}_p, 0)$ $(p = 1, 2, \ldots, n/2)$. The coordinates $\hat{x}_p, \hat{y}_p$ are related to $\hat{x}'_s, \hat{y}'_s$ by the equations

$$\left. \begin{array}{ll} \hat{x}_p = \hat{x}'_s & (s = 2p - 1) \\[2mm] \hat{x}_p + \hat{h} = \hat{x}'_s & (s = 2p) \\[2mm] \hat{y}_p = \hat{y}'_s & (s = 2p - 1 \text{ or } 2p) \end{array} \right\} \; p = 1, 2, \ldots, \frac{n}{2} . \tag{A4}$$

The quantity $\hat{h}$ is a small distance which will eventually approach 0.

The dipole moments, m_p, are related to the source strengths, q_s, by

$$\frac{m_p}{\hat{h}} = q_s \qquad (s = 2p - 1)$$

$$-\frac{m_p}{\hat{h}} = q_s \qquad (s = 2p) .$$

(A5)

Introducing Eqs. (A4) and (A5) into (A2) and (A3), we obtain

$$I_n = \frac{1}{\hat{h}} \sum_{p=1}^{n/2} m_p \left\{ \cos(\nu \hat{x}_p \cosh u) - \cos\left[\nu(\hat{x}_p + \hat{h}) \cosh u\right] \right\} e^{-\nu \hat{y}_p \cosh^2 u} \qquad (A6)$$

$$J_n = \frac{1}{\hat{h}} \sum_{p=1}^{n/2} m_p \left\{ \sin(\nu \hat{x}_p \cosh u) - \sin\left[\nu(\hat{x}_p + \hat{h}) \cosh u\right] \right\} e^{-\nu \hat{y}_p \cosh^2 u} . \qquad (A7)$$

For small $\hat{h}$,

$$\cos\left[\nu(\hat{x}_p + \hat{h}) \cosh u\right] \approx \cos(\nu \hat{x}_p \cosh u)$$
$$- \hat{h}\nu \cosh u \sin(\nu \hat{x}_p \cosh u) \qquad (A8)$$

$$\sin\left[\nu(\hat{x}_p + \hat{h}) \cosh u\right] \approx \sin(\nu \hat{x}_p \cosh u)$$
$$+ \hat{h}\nu \cosh u \cos(\nu \hat{x}_p \cosh u). \qquad (A9)$$

Therefore in the limit, as $\hat{h} \to 0$,

$$I_n = \nu \cosh u \sum_{p=1}^{n/2} m_p \sin(\nu \hat{x}_p \cosh u) e^{-\nu \hat{y}_p \cosh^2 u} \qquad (A10)$$

$$J_n = -\nu \cosh u \sum_{p=1}^{n/2} m_p \cos(\nu \hat{x}_p \cosh u) e^{-\nu \hat{y}_p \cosh^2 u} . \qquad (A11)$$

These equations represent the forms assumed by I_n and J_n when the original sources (and sinks) are combined so as to form a collection of $n/2$ $\hat{x}$-directed dipoles in the $\hat{x}$-$\hat{y}$ plane, the dipole moments being m_p ($p = 1, 2, \ldots, n/2$). The wave resistance of such a collection is obtained by substituting Eqs. (A10) and (A11) into (A1). Before substituting, we go to the limit of an infinite number of dipoles of infinitesimal strength, continuously distributed with a density $m(\hat{x})$ in the half strip $-L/2 \le \hat{x} \le L/2$, $0 \le y < \infty$, $\hat{z} = 0$. To this end, it is convenient first to imagine the $n/2$ dipoles arranged in a rectangular array of r rows each containing q dipoles. Then (A10) and (A11) can be replaced by the double sums

$$I_n = \nu \cosh u \sum_{i=1}^{q} \sum_{j=1}^{r} m_i \sin (\nu \hat{x}_i \cosh u) \ e^{-\nu \hat{y}_j \cosh^2 u} \qquad \text{(A12)}$$

$$J_n = -\nu \cosh u \sum_{i=1}^{q} \sum_{j=1}^{r} m_i \cos (\nu \hat{x}_i \cosh u) \ e^{-\nu \hat{y}_j \cosh^2 u}. \qquad \text{(A13)}$$

Passing to the continuous case with the $\hat{y}$ integration extended to infinity, we get, instead of (A12) and (A13),

$$I = \nu \cosh u \int_{-L/2}^{L/2} \int_{0}^{\infty} m(\hat{x}) \ \sin (\nu \hat{x} \cosh u) \ e^{-\nu \hat{y} \cosh^2 u} \ d\hat{y} d\hat{x} \qquad \text{(A14)}$$

$$J = -\nu \cosh u \int_{-L/2}^{L/2} \int_{0}^{\infty} m(\hat{x}) \ \cos (\nu \hat{x} \cosh u) \ e^{-\nu \hat{y} \cosh^2 u} \ d\hat{y} d\hat{x}. \qquad \text{(A15)}$$

Note that in Equations (A14) and (A15), we have assumed only the integrability of $m(\hat{x})$ and not its boundedness.

The $\hat{y}$ integration can be performed separately, so that (A14) and (A15) become

$$I = \frac{1}{\cosh u} \int_{-L/2}^{L/2} m(\hat{x}) \ \sin (\nu \hat{x} \cosh u) \ d\hat{x} \qquad \text{(A16)}$$

$$J = -\frac{1}{\cosh u} \int_{-L/2}^{L/2} m(\hat{x}) \ \cos (\nu \hat{x} \cosh u) \ d\hat{x}. \qquad \text{(A17)}$$

Finally, we reintroduce the normalized variable $x = \hat{x}/L$. Then

$$I = \frac{L}{\cosh u} \int_{-1/2}^{1/2} M(x) \ \sin (Fx \cosh u) \ dx \qquad \text{(A18)}$$

$$J = -\frac{L}{\cosh u} \int_{-1/2}^{1/2} M(x) \ \cos (Fx \cosh u) \ dx. \qquad \text{(A19)}$$

In these equations, $M(x)$ is defined to be $m(Lx)$, while $F = L = gL/c^2$ as before.

According to (A1) and the above discussion, the wave resistance of a continuous distribution of x-directed dipoles in the aforementioned half-strip is

$$R = 16\pi\rho\nu^2 \int_0^\infty (I^2 + J^2) \cosh^2 u \; du \qquad \text{(A20)}$$

where I and J are given by (A18) and (A19).

Squaring (A18) and (A19), we get

$$I^2 = \frac{L^2}{\cosh^2 u} \int_{-1/2}^{1/2} \int_{-1/2}^{1/2} M(x) \; M(x') \; \sin (Fx \cosh u)$$

$$\cdot \; \sin (Fx' \cosh u) \; dx dx' \qquad \text{(A21)}$$

$$J^2 = \frac{L^2}{\cosh^2 u} \int_{-1/2}^{1/2} \int_{-1/2}^{1/2} M(x) \; M(x') \; \cos (Fx \cosh u)$$

$$\cdot \; \cos (Fx' \cosh u) \; dx dx'. \qquad \text{(A22)}$$

Thus

$$I^2 + J^2 = \frac{L^2}{\cosh^2 u} \int_{-1/2}^{1/2} \int_{-1/2}^{1/2} M(x) \; M(x')$$

$$\cdot \; \cos \left[F(x-x') \cosh u \right] dx dx'. \qquad \text{(A23)}$$

Substituting from (A23) into (A20), we have

$$R = 16\pi\rho F^2 \int_0^\infty \int_{-1/2}^{1/2} \int_{-1/2}^{1/2} M(x) \; M(x')$$

$$\cdot \; \cos \left[F(x-x') \cosh u \right] dx dx' du. \qquad \text{(A24)}$$

We perform the u integration first, using the identity

$$\int_0^\infty \cos (t \cosh u) \; du = -\frac{\pi}{2} Y_o(|t|). \qquad \text{(A25)}$$

Then (A24) becomes

$$R = -8\pi^2 \rho F^2 \int_{-1/2}^{1/2} \int_{-1/2}^{1/2} M(x) \ M(x') \ Y_o(F|x-x'|) \ dxdx'. \qquad \text{(A26)}$$

Now let the density $M(x) = -(c/2\pi)(V/2L) f(x)$, as in Eq. (25) of the text. Then

$$R = -2\rho c^2 \left(\frac{V}{2L}\right)^2 F^2 \int_{-1/2}^{1/2} \int_{-1/2}^{1/2} f(x) \ f(x') \ Y_o(F|x-x'|) \ dxdx'. \qquad \text{(A27)}$$

The drag coefficient, C_w, is obtained by dividing R by

$$\frac{1}{2} \rho c^2 \left(\frac{V}{2L}\right)^2 .$$

Thus, the final result is

$$C_w = -4F^2 \int_{-1/2}^{1/2} \int_{-1/2}^{1/2} f(x) \ f(x') \ Y_o(F|x-x'|) \ dxdx' \qquad \text{(A28)}$$

in agreement with Eq. (29).

Appendix B
NUMERICAL SOLUTION OF THE INTEGRAL EQUATION

The equation to be solved is Eq. (30) of the text, viz.,

$$\int_{-1/2}^{1/2} g_o(x') \ Y_o(F|x-x'|) \ dx' = -1. \qquad \text{(B1)}$$

It is easily shown that $g_o(x) = g_o(-x)$, so that (B1) can be written

$$\int_{0}^{1/2} g_o(x') \left\{ Y_o(F|x-x'|) + Y_o[F(x+x')] \right\} dx' = -1 . \qquad \text{(B2)}$$

As already noted, MacCamy has proved [10] that $g_o(x)$ has the form

$$g_o(x) = \frac{1}{\sqrt{1/4 - x^2}} h(x) \tag{B3}$$

where $h(x)$ is a regular function in $-1/2 \le x \le 1/2$. The singularity in $g_o(x)$ at $x = 1/2$ introduces a loss of accuracy into the numerical solution of (B2); we therefore convert (B2) into an equation for the regular function, h, by means of the following change of variables:

$$x = 1/2 \sin \beta, \qquad x' = 1/2 \sin \beta'. \tag{B4}$$

Equation (B2) then becomes

$$\int_0^{\pi/2} H(\beta') \left\{ Y_o\left(\frac{F}{2} |\sin \beta - \sin \beta'|\right) \right.$$

$$\left. + Y_o\left[\frac{F}{2}(\sin \beta + \sin \beta')\right] \right\} d\beta' = -1 \tag{B5}$$

where $H(\beta) = h(1/2 \sin \beta)$. Thus the unknown in (B5) is a regular function.

To perform the integration in Eq. (B5) numerically, we first divide the interval of integration, $0 \le \beta' \le \pi/2$, into an even number, n, of equal subintervals of length $\pi/2n$. We denote the values assumed by β' at the endpoints of these subintervals by $\beta_j (j = 1, 2,..., n + 1)$. Then $\beta_1 = 0$ and $\beta_{n+1} = \pi/2$. We further denote by H_j the values of the unknown function $H(\beta')$ at β_j, i.e., $H_j = H(\beta_j)$. Finally, we allow the variable β to assume the values $\beta_i (i = 1, 2, \ldots, n + 1)$. We thereby obtain $n + 1$ linear algebraic equations for the $n + 1$ unknowns H_j, each equation corresponding to a different value of the index, i. These equations are constructed as follows:

The part of the integration in (B5) that involves $Y_o[F/2 (\sin \beta + \sin \beta')]$ can be performed at once by Simpson's rule:

$$\int_0^{\pi/2} H(\beta') Y_o\left[\frac{F}{2}(\sin \beta_i + \sin \beta')\right] d\beta' \approx \frac{\pi}{6n} \left\{ H_1 Y_o\left[\frac{F}{2}(\sin \beta_i + \sin \beta_1)\right] \right.$$

$$+ 4H_2 Y_o\left[\frac{F}{2}(\sin \beta_i + \sin \beta_2)\right] + 2H_3 Y_o\left[\frac{F}{2}(\sin \beta_i + \sin \beta_3)\right]$$

$$\left. + \ldots H_{n+1} Y_o\left[\frac{F}{2}(\sin \beta_i + \sin \beta_{n+1})\right] \right\} \quad (i = 2, 3, \ldots n + 1). \tag{B6}$$

(We have excluded the case $i = 1$ in (B6) because it is discussed separately below.)

On the other hand, the logarithmic singularity in Y_o prevents the remaining integral in (B5) from being represented by a formula like that of (B6); when $i = j$, the expression $Y_o(F/2|\sin \beta_i - \sin \beta_j|)$ is meaningless. We therefore break up the integral and write (when $i = 1$ or $n + 1$)

$$\int_0^{\pi/2} H(\beta') \, Y_o\left(\frac{F}{2}|\sin \beta_i - \sin \beta'|\right) d\beta'$$

$$= \int_{\beta_1}^{\beta_{i=1}} H(\beta') \, Y_o\left(\frac{F}{2}|\sin \beta_i - \sin \beta'|\right) d\beta'$$

$$+ \int_{\beta_{i-1}}^{\beta_{i+1}} H(\beta') \, Y_o\left(\frac{F}{2}|\sin \beta_i - \sin \beta'|\right) d\beta'$$

$$+ \int_{\beta_{i+1}}^{\beta_{n+1}} H(\beta') \, Y_o\left(\frac{F}{2}|\sin \beta_i - \sin \beta'|\right) d\beta' \qquad (i = 2, 3, \ldots, n). \quad \text{(B7)}$$

Since the total number of subintervals, n, is even, the first and third integrals on the right of (B7) (these contain no singularity) either both extend over an even or both extend over an odd number of subintervals. In the even case, the integrals are evaluated by Simpson's rule. In the odd case, they are evaluated by the trapezoidal rule over the first subinterval and by Simpson's rule over the rest. (Note that when $i = 2$, the first integral on the right of (B7) vanishes, while when $i = n$, the third integral vanishes.)

The second integral on the right of (B7) is approximated by first writing

$$\int_{\beta_{i-1}}^{\beta_{i+1}} H(\beta') \, Y_o\left(\frac{F}{2}|\sin \beta_i - \sin \beta'|\right) d\beta'$$

$$\approx H_i \int_{\beta_{i-1}}^{\beta_{i+1}} Y_o\left(\frac{F}{2}|\sin \beta_i - \sin \beta'|\right) d\beta'. \qquad \text{(B8)}$$

This approximation is sufficiently accurate for our purpose when $n \geq 6$. The integral on the right of (B8) is evaluated by expanding the Bessel function about the point $\beta' = \beta_i$. The result is

$$\int_{\beta_{i-1}}^{\beta_{i+1}} Y_o\left(\frac{F}{2}|\sin \beta_i - \sin \beta'|\right) d\beta' \approx \frac{2}{n}\left[\log\left(\frac{\pi\gamma'F}{8n}\cos \beta_i\right)\right]\left(1 - \frac{\pi^2 F^2 \cos^2\beta_i}{192 n^2}\right)$$

$$- \frac{2}{n}\left[1 + \frac{\pi^2}{n^2}\left(\frac{1}{72} + \frac{1}{96}\tan^2\beta_i\right) - \frac{\pi^2 F^2 \cos^2\beta_i}{144 n^2}\right] \qquad (i = 2, 3, \ldots, n) \quad \text{(B9)}$$

where $\log \gamma' = \gamma = $ Euler's constant $= 0.577 \ldots$.

By these procedures, we can perform numerically the integration on the left side of (B7) for $i = 2, 3, \ldots, n$. Adding the result to the right side of (B6) and (in accordance with the integral equation (B5)) equating the entire sum to -1, we obtain $n - 1$ linear algebraic equations for the $n + 1$ unknowns $H_j (j = 1, 2, \ldots, n + 1)$, each equation corresponding to one of the i values, $i = 2, 3, \ldots, n$.

The remaining two equations, associated with $i = 1$ and $i = n + 1$, are arrived at separately. When $i = 1$,

$$Y_o \left(\frac{F}{2} \left| \sin \beta_1 - \sin \beta' \right| \right) = Y_o \left(\frac{F}{2} \left| \sin \beta_1 + \sin \beta' \right| \right)$$

since $\beta_1 = 0$; thus (B5) becomes

$$\int_0^{\pi/2} 2H(\beta') Y_o \left(\frac{F}{2} \sin \beta' \right) d\beta' = -1 \qquad (i = 1). \qquad (B10)$$

This equation can be rewritten

$$\int_{\beta_1}^{\beta_2} 2H(\beta') Y_o \left(\frac{F}{2} \sin \beta' \right) d\beta' + \int_{\beta_2}^{\beta_{n+1}} 2H(\beta') Y_o \left(\frac{F}{2} \sin \beta' \right) d\beta' = -1. \quad (B11)$$

The first integral on the left is approximated by setting $H(\beta') = H_1$ and expanding Y_o about $\beta' = 0$. The result is

$$\int_{\beta_1}^{\beta_2} 2H(\beta') Y_o \left(\frac{F}{2} \sin \beta' \right) d\beta' \approx \frac{2H_1}{n} \left[\log \left(\frac{\pi \gamma' F}{8n} \right) \right] \left(1 - \frac{\pi^2 F^2}{192 n^2} \right)$$

$$- \frac{2H_1}{n} \left[1 + \frac{\pi^2}{n^2} \left(\frac{1}{72} - \frac{F^2}{144} \right) \right]. \qquad (B12)$$

The second integral in (B11), which is free of singularities, extends over an odd number of subintervals and is therefore evaluated by the combination of the trapezoidal and Simpson's rules already described. Upon adding the result to the right side of (B12) and substituting into (B11), we obtain the algebraic equation corresponding to $i = 1$. Finally, when $i = n + 1$, (B5) becomes

$$\int_{\beta_1}^{\beta_{n+1}} H(\beta') Y_o \left(\frac{F}{2} \left| \sin \beta_{n+1} - \sin \beta' \right| \right) d\beta'$$

$$+ \int_{\beta_1}^{\beta_{n+1}} H(\beta') Y_o \left[\frac{F}{2} \left(\sin \beta_{n+1} + \sin \beta' \right) \right] d\beta' = -1 \qquad (i = n + 1). \quad (B13)$$

The second integral on the left of (B13) is given by (B6) with $i = n + 1$. The first integral in (B13) can be written (since $\sin \beta_{n+1} = 1$)

$$\int_{\beta_n}^{\beta_{n+1}} H(\beta') \, Y_o \left(\frac{F}{2} \left| 1 - \sin \beta' \right| \right) \, d\beta' = \int_{\beta_1}^{\beta_n} H(\beta') \, Y_o \left(\frac{F}{2} \left| 1 - \sin \beta' \right| \right) \, d\beta'$$

$$+ \int_{\beta_n}^{\beta_{n+1}} H(\beta') \, Y_o \left(\frac{F}{2} \left| 1 - \sin \beta' \right| \right) \, d\beta'. \qquad \text{(B14)}$$

The first integral on the right of (B14) contains no singularities and extends over an odd number of subintervals; we therefore evaluate it by the combination of the trapezoidal and Simpson's rules. The second integral must be specially dealt with because the first derivative of $1 - \sin \beta'$ with respect to β' vanishes at $\beta' = \beta_{n+1} = \pi/2$. If we are to maintain consistency in order of accuracy to which the integral is evaluated, we cannot merely replace $H(\beta')$ by H_{n+1} in the interval $\beta_n \leq \beta' \leq \beta_{n+1}$. Rather, a linear approximation to $H(\beta')$ must be employed, viz.,

$$H(\beta') \approx H_n + \frac{H_{n+1} - H_n}{\beta_{n+1} - \beta_n} (\beta' - \beta_n)$$

$$= H_n + \frac{2n}{\pi} (H_{n+1} - H_n) \left(\beta' + \frac{\pi}{2n} - \frac{\pi}{2} \right) \qquad (\beta_n \leq \beta' \leq \beta_{n+1}). \qquad \text{(B15)}$$

Upon substituting from (B15) into the integral and expanding Y_o about the point $\beta' = \pi/2$, we obtain the following approximation:

$$\int_{\beta_n}^{\beta_{n+1}} H(\beta') \, Y_o \left(\frac{F}{2} \left| 1 - \sin \beta' \right| \right) \, d\beta' \approx \frac{H_n}{2n} \left[\log \left(\frac{\gamma' F \pi^2}{32n^2} \right) - 1 - \frac{\pi^2}{96n^2} \right]$$

$$+ \frac{H_{n+1}}{2n} \left[\log \left(\frac{\gamma' F \pi^2}{32n^2} \right) - 3 - \frac{\pi^2}{288n^2} \right]. \qquad \text{(B16)}$$

Addition of this result to the first integral on the right of (B14), followed by substitution from (B14) into (B13), gives the final algebraic equation for the quantities H_j. This equation corresponds to $i = n + 1$. All our calculations were made with $n = 6$.

Having obtained $g_o(x)$ the computer finds

$$I_o(f) = \int_{1/2}^{1/2} g_o(x; f) \, dx$$

and $g(x) = I_o^{-1}(f) g_o(x; f)$. The wave resistance is found easily from

$$C_w^f(f) \;=\; 4F^2 I_o^{-1}(f) \;,\tag{B17}$$

which follows from (29) and (B1). Since one can prove that Eq. (29) is a positive definite expression it follows that $I_o(f) > 0$, which is not obvious from the integral equation (B1).

REFERENCES

[1] Michell, J.H., "The Wave Resistance of a Ship," Phil. Mag. (5) 45:106-123 (1898)

[2] Lunde, J.K., "The Linearized Theory of Wave Resistance and Its Application to Ship-Shaped Bodies in Motion on the Surface of a Deep, Previously Undisturbed Fluid," Technical and Research Bulletin 1-18, The Society of Naval Architects and Marine Engineers, New York, July 1957

[3] Wehausen, J.V., "Wave Resistance of Thin Ships," in Proceedings of the Symposium on Naval Hydrodynamics, Publication 515, National Academy of Sciences-National Research Council, pp. 109-137, 1957

[4] Birkhoff, G., Korvin-Kroukovsky, B.V., and Kotik, J., "Theory of the Wave Resistance of Ships," Trans. Soc. Naval Arch. Marine Engrs. 62:359-396 (1954)

[5] G. Weinblum, "Schiffe Geringsten Widerstandes," Proc. Third Internat. Congr. Appl. Mech., Stockholm, pp. 449-458, 1930; also "Schiffe Geringsten Widerstandes," Jahrbuch der Schiffbautechnischen Gesellschaft, Vol. 51, 1957

[6] Lighthill, M.J., "A New Approach to Thin Aerofoil Theory," Aero Quart., vol. 3, p. 3, Nov. 1951

[7] Dorr, J., "Zwei Integralgleichungen erster Art, die sich mit Hilfe Mathieuscher Funktionen losen lassen," Zeits. angew., Math. Physik 3:427-439 (1952)

[8] Erdelyi, A., et al., "Higher Transcendental Functions," vol. 3, NewYork:McGraw-Hill, p. 132, 1955

[9] Tricomi, F.G., "Integral Equations," New York:Interscience, pp. 143-144, 1957

[10] MacCamy, R.C., "On Singular Integral Equations with Logarithmic or Cauchy Kernels," J. Math. and Mech. 7:355-375 (May 1958)

[11] Sretenskii, L.N., "Sur un Probleme de Minimum Dans la Theorie du Navire," C.R. (Dokl.) Acad. Sci. USSR (N.S.) 3:247-248 (1935)

[12] Pavlenko, G.E., "The Resistance of Water to the Motion of a Ship," State Publishing House for Water Transport, Moscow, pp. 188-192, 1953 (in Russian)

[13] Shen, Y.C. and Kern, G.E., "Development Study of a Subsurface Ship," Aerojet-General Corp. Report 1535, 1958

[14] Stoker, J.J., and Peters, A.S., "The Motion of a Ship, as a Floating Rigid Body, in a Seaway," Institute of Mathematical Sciences, New York University, Report IMM-NYU 203, 1954

[15] Magnus, W., and Oberhettinger, F., "Formulas and Theorems for the Functions of Mathematical Physics," Chelsea, 1949

[16] Yourkevitch, V., "The Form of Least Resistance," A.T.M.A., 31:687 (1932); see also the Shipbuilder and Marine Engine Builder, p. 235, Apr. 1933

[17] Karp, S., Kotik, J., and Lurye, J., "On Ship Forms Having Minimum Wave Resistance," TRG, Inc., Report TRG-119-SR-1, 1959

DISCUSSION

C. Wigley (London)

Unfortunately advance copies of these papers were only available yesterday. This prevents any criticism of the mathematical work, but there are some points of importance which should be mentioned regarding the practical use of these calculations of forms of minimum resistance.

Firstly the wave resistance as calculated by the Michell or equivalent formulas is that wave resistance which would exist in a perfect fluid.

Secondly it is assumed that for a ship the wave resistance is to be simply added to another resistance due to viscosity which does not change greatly with a change of form.

Regarding the first point raised, in fact, except at very high speeds where the Froude number is above 0.4, the effects of viscosity on the wave formation are serious, causing a decrease in the efficiency of the afterbody as a wavemaker.

Regarding the second point, the nonwave resistance may be considered as consisting of the sum of two terms, the first term depending only on the wetted surface and speed and being some 90 to 95 percent of the total, and the second term, sometimes called the form resistance, depending as well on the shape of the form. Very little is known as to the variation of this form resistance with speed, although its value at very low speed is shown by the difference between the calculated frictional resistance and that actually measured, since the wave resistance can be neglected at such speeds. It is suggested by M. Guilloton (see Trans. I.N.A., London, vol. 1952, pp. 352 and 353) that the form resistance is increased at the higher speeds owing to the effect of the wave motion on the flow round the form, a symptom of this influence being the change of attitude of the form during motion.

The effects of these considerations on the actual minima of resistance are well shown by the simple question of the optimum position for the center of buoyancy. From the mathematical theory, as given by these papers today, the optimum position of the center of buoyancy would be amidships at all speeds. In practice, it is found that, at the lower speeds up to a Froude number of about 0.25 where the wave resistance is small the optimum position of the center of buoyancy lies forward of amidships, since the form resistance is thus diminished. As the speed increases the optimum position moves aft and lies aft of amidships for

a range of Froude number up to about 0.4, owing to the lower efficiency in wavemaking of the afterbody, which evidently causes an advantage when displacement is moved from the forebody to the afterbody. At still higher speeds the best position tends to agree with the theoretical position at amidships.

It may be of some interest to compare the results for struts of infinite draft found by Messrs. Kotik, Karp, and Lurye with some experimental and calculated results for bulbous bows I published in the Proceedings of the North-East Coast Institution of Engineers & Shipbuilders in 1936. These calculations were made for a spheroid added to a calculable ship form, and the experiments were made with a fairing between the spheroid and the form which would tend to diminish any additional form resistance. Also the change of form was hoped to be insufficient to change appreciably the frictional correction to the wave resistance. Under these precautions the calculated and experimental curves showed, for the best position and size of the bulb, a definite decrease in resistance over a range of Froude number from 0.25 to 0.5.

The conclusion of these comments is that, owing to the uncertainty of the application of such results as those in the papers under discussion, it is advisable that they should be checked by actual measurements before any practical use be made of them.

G. Weinblum (Institut für Schiffbau, Hamburg)

May I express my sincerest thanks to the authors of this paper and of the preceding paper for the aesthetic pleasure presented to me. Some general remarks may be to the point:

1. It is a well-known proposition that ship theory can become too difficult for naval architects.

2. It is therefore advisable for naval architects to love mathematicians.

3. This love, however, should not be unreciprocated.

4. The present speaker feels much obliged that his mathematic colleagues have given such a kind credit to his earlier work. Obviously these attempts were formally rather poor; nonetheless, they embrace some physical and technical ideas which have proved to be fruitful in the further development. Besides the authors mentioned, Dr. Guilloton has contributed to the discussion of the problem which is thrilling both from the point of view of ship hydrodynamics as well as mathematics.

Twenty-five years ago a contribution was made by Prof. von Karman at the 4th International Congress in Cambridge, England, in which he pointed out difficulties encountered when dealing with the exact solution of the minimum problem. Among other things, he found curves with infinite horns shown in the paper by Prof. Karp and others. This finding caused a lot of confusion in the professional world. Unfortunately, Prof. von Karman has forgotten to publish these interesting investigations.

A decisive progress has been made in the meanwhile by distinguishing between the shape of the singularity distribution and the actual body form. Although this difference is well known and has been clearly illustrated by Havelock, e.g., in the case of the general ellipsoid, no use was made of this fact in many earlier publications on our subject. I suggested in vain a thesis on this topic some 12 years ago but it was not completed. So we are

essentially indebted to Prof. Inui, because he has dealt with the problem at stake in a consequent and efficient if approximate manner. His severe remark that Wigley and I have hampered the progress in wave resistance research by neglecting the distinction between hull form and distribution is perhaps too hard since our conclusions are primarily based on the sectional area curve and this, fortunately, is less affected by the difficulties mentioned than that of the actual ship form.

I am dwelling at some length on this subject as a warning example: one should not proceed too long in a well-established groove of thought and therefore lose the connection with facts.

Prof. Timman and Mr. Vossers have, as far as I understand, rigorously remained within the concept of the Michell ship. We are looking forward for explicit results. Prof. Karp and colleagues have followed rather the way indicated by Havelock, distinguishing between body form and distribution. Although the results apply to a rather restricted case of a deeply submerged strut, they are in principle extremely interesting. The optimum cross sections plotted correspond to some extent to those which have been derived by approximate methods, except, however, that they all are more exaggerated and show a rounded nose which could not be obtained by the low degree polynomials used before. It would be interesting to have similar cross sections for Froude numbers below 0.38.

This lower range appears to have important practical consequences. Using my earlier work my collaborator Kracht has investigated the influence of the bulbous bow (and stern). Contrary to experimental results and earlier findings by Mr. Wigley and myself he has established that moderate bulbs may have a beneficial influence on wave resistance even at low Froude numbers. We are continuing with these investigations. To get an independent check, wholly submerged bodies of revolution moving in the vicinity of the free surface have been considered. I have already treated this problem several times earlier. However, while in the case of the Michell surface ship it is plausible from physical reasoning to assume zero end ordinates for the distributions, there is no need to introduce this restriction for bodies of revolution. Therefore, together with Dr. Eggers and Mr. Sharma, I have investigated singularities systems which include continuous line doublet distributions, concentrated sources, and, following Wigley, doublets located on the axis of the body.

The plots in Fig. D1 show the optimum longitudinal distribution calculated for a constant area coefficient $\varphi = 0.60$ (except for plot (g)), three depths of immersion ratios $2f/L$, and two Froude numbers.

The symbol $<2, 4, 6, 8\ D>$ indicates the powers of the polynomial terms; D stands for concentrated dipoles at the ends of the axis with a doublet moment a_D.

Computations have been made under three assumptions:

1. The end ordinates of the dipole distribution, $\eta(\pm 1) = 0$.

2. End ordinates $-\eta(\pm 1)$ are not prescribed but $a_D = 0$; a result $\eta(\pm 1) > 0$ means a concentrated source at the ends.

3. The dipole moment $a_D \neq 0$. In this case the area of the circle at the ends of the axis represents the dipole moment to the scale of the distribution curve.

Figures D1(a)-(c) show the optimum doublet distributions for $\gamma_o = 1/2F^2 = 6$, $F = 0.289$. These distributions coincide sometimes nicely for different $2f/L$ (Fig. D1(a)), sometimes
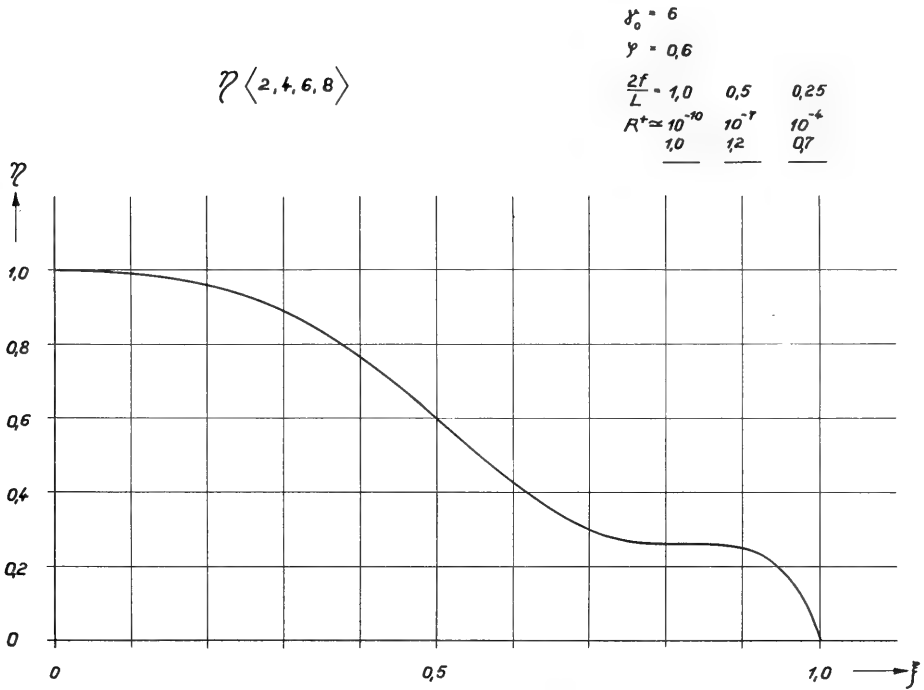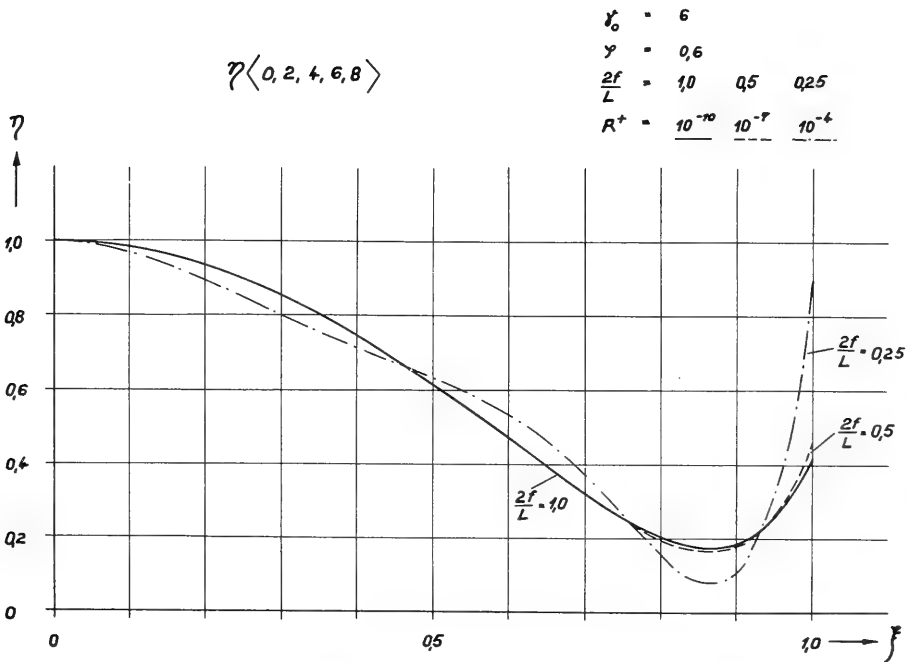
Fig. D1(a). Optimum longitudinal distribution

Fig. D1(b). Optimum longitudinal distribution

$$\gamma_o \quad \cdot \quad 6$$
$$\gamma \quad \cdot \quad 0,6$$

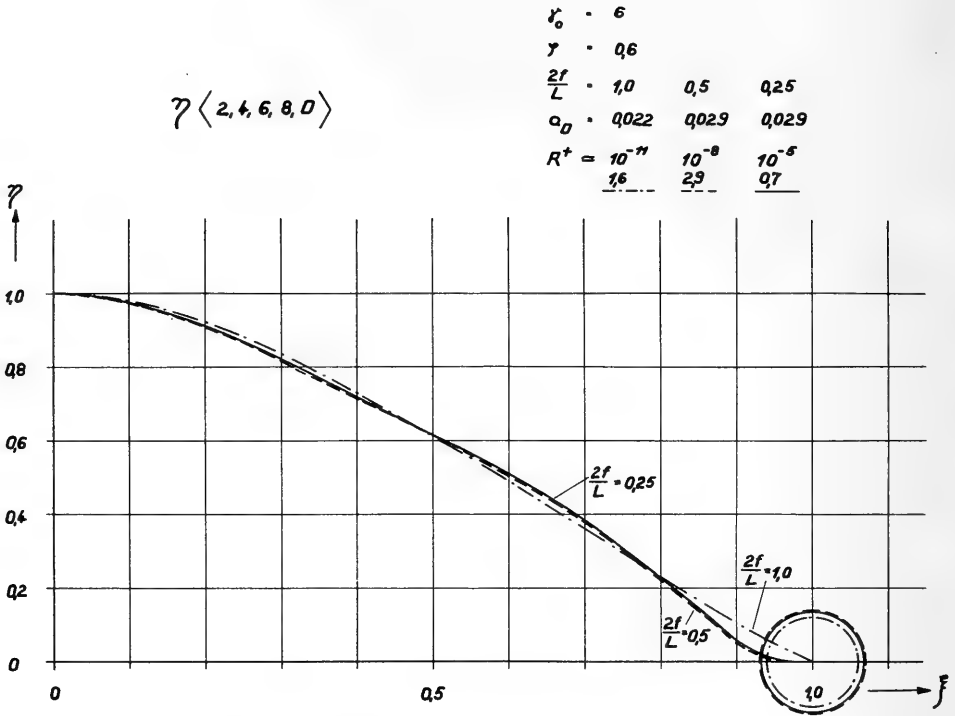|		
$\frac{2f}{L}$ $\cdot$ 1,0	0,5	0,25
a_D $\cdot$ 0,022	0,029	0,029
R^+ $=$ 10^{-11}	10^{-8}	10^{-6}
1,6	2,9	0,7

$\eta \langle 2, 4, 6, 8, 0 \rangle$

Fig. D1(c). Optimum longitudinal distribution

they differ. Occasional erratic behavior has been disregarded for present purposes. We are primarily interested in the variation of the shape with the three assumptions listed. Figure D1(a) ($\eta(\pm 1) = 0$, $a_D = 0$) shows the well-known swan-neck form; the curve for $2f/L = 0.25$ in Fig. D1(b) may be doubtful.

In the range of low Froude numbers $\gamma_o = 15$, $F = 0.183$ we find in Fig. D1(d) the orthodox hollow distribution ($\eta(\pm 1) = 0$, $a_D = 0$); in Figs. D1(e) and D1(f) we see the relatively small end ordinates and doublets respectively.

Figure D1(g) finally shows the optimum forms for a high prismatic $\varphi = 0.80$ and $\gamma_o = 1/2F^2 = 15$. In general the results do not present great surprises except for the appearance of a concentrated doublet at small F and the large reduction in resistance due to the former as compared with the assumption $a_D = 0$. An explanation can be found by comparing the generated body shapes which display marked differences. The resulting forms and data for other Froude numbers will be the subject of a more elaborate report.

The numbers R^+ stand for dimensionless wave resistance values. Obviously, they indicate that the latter is negligible for $2f/L = 1$ and in some cases for $2f/L = 0.5$ at the Froude numbers considered. Thus the investigations presented by the authors have contributed to clarify a basic problem of ship theory. For purpose of practice we shall be forced to investigate more general forms than the Michell ship. E.g., in the range of higher Froude numbers conclusive experiments have shown that by using a flat stern a definite improvement can be reached. A further step in this direction may be the investigation of the so-called Hogner interpolation formula although some essential difficulties must be overcome.

$$\gamma_o = 15$$
$$\gamma = 0.6$$
$$\frac{2f}{L} = 1.0 \quad 0.5 \quad 0.25$$
$$R^+ \simeq 10^{-20} \quad 10^{-12} \quad 10^{-8}$$
$$3.0 \quad 0.8 \quad 1.6$$
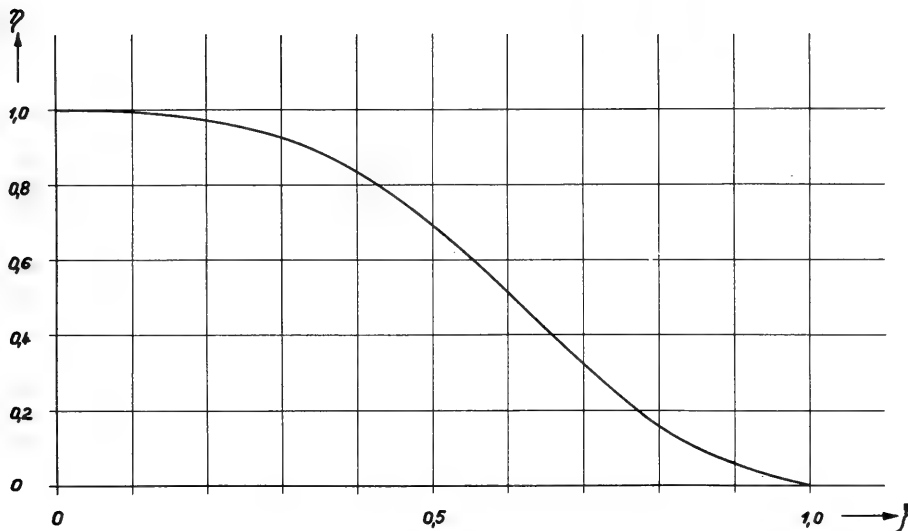
$$\eta \langle 2, 4, 6, 8 \rangle$$

Fig. D1(d). Optimum longitudinal distribution

$$\gamma_o = 15$$
$$\gamma = 0.6$$
$$\alpha_0 = 0$$
$$\frac{2f}{L} = 0.5 \quad 0.25$$
$$R^+ = 10^{-11} \quad 10^{-7}$$

$$\eta \langle 0, 2, 4, 6, 8 \rangle$$
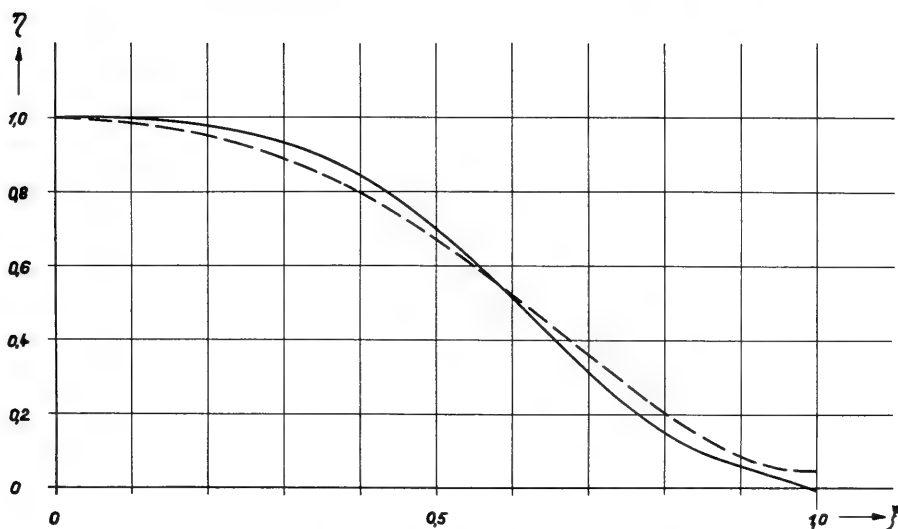
Fig. D1(e). Optimum longitudinal distribution

$$\eta \left\langle 2, 4, 6, 8, D \right\rangle$$

$\gamma_0 = 15$

$\gamma = 0.6$

$\frac{2f}{L}$ =	1.0	0.5	0.25
a_D =	0.005	0.003	0.002
$R^+ \propto$	10^{-20}	10^{-13}	10^{-9}
	0.9	1.6	2.1
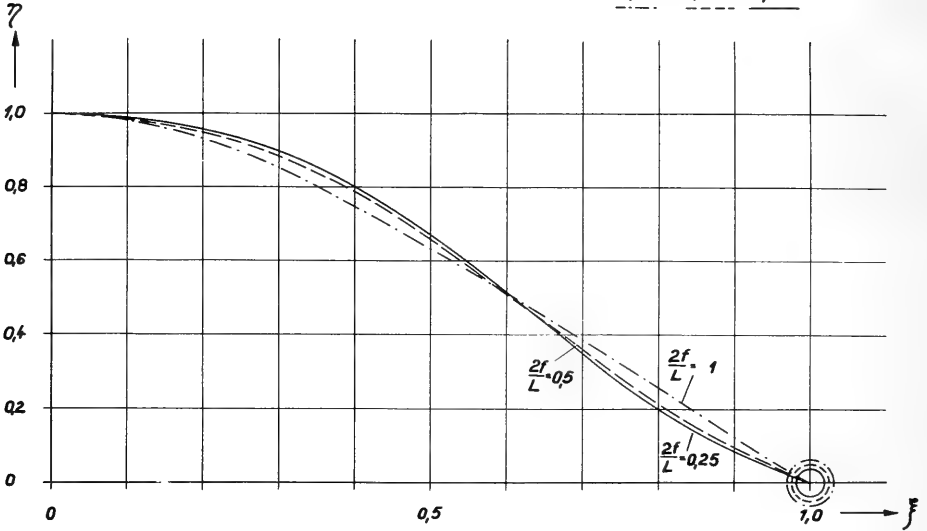
Fig. D1(f). Optimum longitudinal distribution

$$\eta \left\langle 2, 4, 6, 8, D \right\rangle$$

$\gamma_0 = 15$

$\gamma = 0.8$

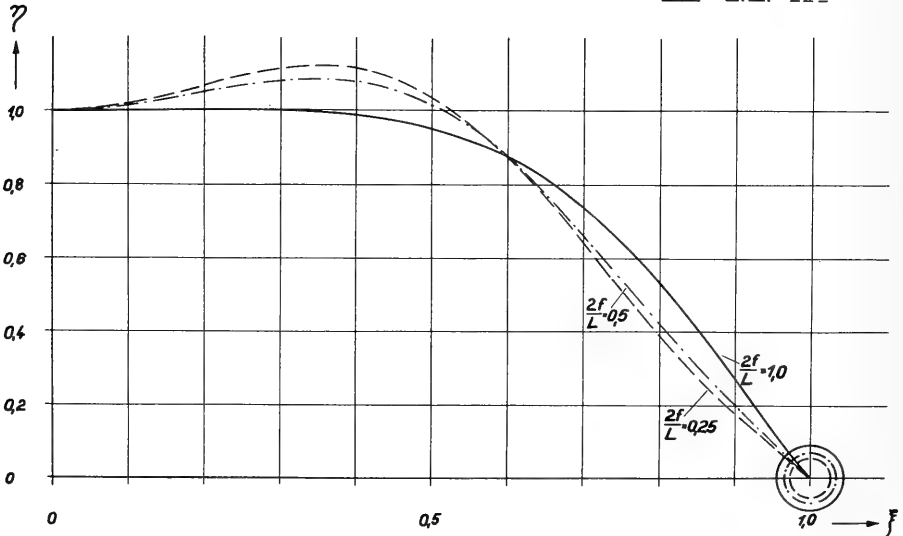| $\frac{2f}{L}$ =	1.0	0.5	0.25
a_D =	0.012	0.006	0.004
$R^+ \propto$	10^{-20}	10^{-12}	10^{-8}

Fig. D1(g). Optimum longitudinal distribution

J. Kotik

Dr. Weinblum has asked a question as regards an arithmetical error in Fig. 10. The parameter ϵ is defined as the average half-beam divided by the length, rather than the average beam. Perhaps this factor of 2 will accommodate Prof. Weinblum's doubts. In reference to Dr. Weinblum's descriptions of his work on the wave resistance of submerged boats, or of dipoles distributed on a submerged horizontal line segment, I have the following comment. It turns out that if one fixes the length and submergence of this horizontal line segment, distributes dipoles on it, and tries to minimize the wave resistance within the family of dipole distributions having a fixed dipole moment (or approximately a fixed volume), one is led to an integral equation which has no solution. We cannot say at present why this apparently well-posed problem has no solution.

S. Karp

I would like to ask Prof. Timman whether the solution of the integral equations were Mathieu functions.

R. Timman

There is still a big gap between the mathematical approach to the problem of minimum resistance and the engineering point of view. With regard to the influence of viscosity, I am quite sure that the purely mathematical approach is not feasible.

T. Inui (University of Tokyo)

I should like to make some general remarks regarding future possible developments in our "practical" study of wavemaking resistance.

Firstly, I wish to point out the necessity of improving our measuring techniques such as so-called stereophotography for recording the actual wavemaking phenomena which we can observe in our daily model basin work. Figure D2 is one example of such stereo slides. It is more than five years since I first tried to take a picture of model waves at the Tokyo University Tank.

Secondly, I should like to point out the special importance of coordination between theory and experiment in our study of wavemaking resistance. If we had no theoretical basis, we could not go any further in our study, even if we have succeeded in taking beautiful pictures of model waves. In this connection, Sir Thomas Havelock's contribution in the field of wavemaking theory is most valuable.

Thirdly and finally, I wish to mention our desire of having an international panel to make use of high speed computers for preparing many kinds of mathematical tables which may be valuable not only to our basic studies but also to our practical design work.
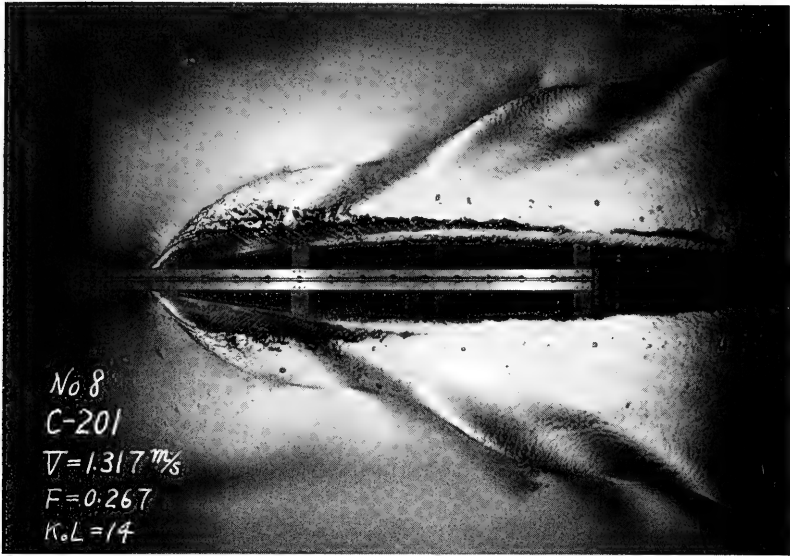
Fig. D2. A black-and-white reproduction of a colored stereo slide

John M. Ferguson (John Brown and Co., Glasgow)

The authors of these two preceding papers must be admired for the ease and sureness of handling the complicated mathematics of this problem of minimum wave resistance. Yet the feeling of admiration is tempered with a little disappointment. In what way do these papers, as they stand, assist the practical designer in his daily work of producing the best form for a given set of conditions.

A typical example is as follows: A form is designed. To this form a model is made and tested. The form may not come up to expectation. In what way can this model be altered to improve its performance? Somewhere in R. E. Froude's published work he states that the quality of performance of a model depends mainly on the shape of the sectional area curve and the load water plane. If the mathematicians could devise some method of analyzing the sectional area curve so that the analysis could indicate the features of performance and thereby suggest the manner in which the area curve could be modified for the better, then their mathematics would be really worthwhile.

The mathematician has all the time he needs. The practical designer often has to produce the answer today, if not sooner.

Some years ago, a young colleague of mine was interested in this problem. He devised a method in which a sectional area curve was analyzed by Runge's scheme into a sine and cosine series. It was found that the coefficients of the sine series could be related to certain values of the speed-length base and that the humps and hollows of the coefficients bore some close relationship to the humps and hollows of the typical resistance curve. If a hump on the resistance curve occurred at, say a trial or contract speed and there was a hump in the Runge coefficient at that point, it was suggested that a reduction of the hump in the resistance curve might result from a reduction in the value of the nearest Runge coefficient. The series would then be rearranged to give the original value of the prismatic coefficient

of the sectional area curve. This rearrangement of the series then resulted in an alteration in the sectional area curve from a rebuilding of the series. In two or three cases where this was tried there was some improvement in performance, but there were some failures as well.

In one particular example where a drastic change was made in the sines with the intention of completely removing a large hump in the resistance curve, a reversal of the analysis gave a sectional area curve with a large hollow in it at or about midships. From the practical point of view this was laughable. Yet some work by Prof. Weinblum and others have produced such sectional area curves.

An intriguing thought pertaining to this hollow is provided by the fact that the sectional area curve for the model in motion, taking the wave profile into account, can show such peculiar hollows.

I throw these thoughts to the mathematicians in the hope that they may be able to adapt their powerful mathematical methods to the daily needs of the less expert practitioners. It might be better if these experts could recognize the needs of their humbler brethren — said in all sincerity. On the other hand it would be as helpful if we more practical people paid greater attention to the more general but more fundamental work of the mathematicians.

*   *   *

THE HYDRODYNAMICS OF HIGH-SPEED HYDROFOIL CRAFT

Marshall P. Tulin
Hydronautics, Incorporated
Rockville, Maryland

A general discussion of some important hydrodynamic problems associated with the operation of high-speed hydrofoil craft is presented. The difficulties that arise from the necessity to either avoid cavitation or design for supercavitating operation, and at the same time to deal with those high-gust loadings that accompany flight in a seaway are emphasized. Theoretical results pertaining to the effect of a seaway on foil loadings and cavitation inception are given, as well as results describing the influence of the free surface on inception speed. The importance of flaps is stressed and new theoretical results concerning flap effectiveness in both sub- and supercavitating flows are presented. Finally, the effect of near-surface operation on the lift-drag ratio of supercavitating foils is discussed and some new theoretical results are given.

INTRODUCTION

I should like at the very beginning to state two warnings. The first concerns the title of this paper which was poorly and immodestly selected. Rather than "*The* Hydrodynamics of High-Speed Hydrofoil Craft" it should read "*Some* Hydrodynamics of High-Speed Hydrofoil Craft." In excluding from discussion many important problems, I have sought to emphasize others which are, in my opinion, most needy of discussion at this time. The second warning is addressed to the very small number of you who not only expect from me but even look forward to highly mathematical content. I am sorry to announce that not a single integral sign is to be displayed here. For this reason, I have already been accused of a kind of scientific degeneracy. Such a charge must, of course, be vigorously denied and I hasten to point out that between the lines and behind the figures lies, I think, enough mathematics to satisfy all but the most jaded theoretician.

The hydrofoil boat together with the airplane has been evolving now for over 50 years. It has appeared in many and varied configurations and performed with mixed success; until recently its future as a marine vehicle remained uncertain. The inevitably growing need for high-speed transport over water would seem to be well enough recognized at this time, however, so that the serious and continued development and use of the hydrofoil boat may be considered safely assured.

The advantages of the hydrofoil craft over displacement or planing craft for high Froude number operation is well-known. Only the edge jet vehicle (or hydroskimmer or ground effect machine as it is sometimes called) offers competitive performance and then, we believe, only in large sizes, say several thousand tons displacement. In Fig. 1 are outlined on a
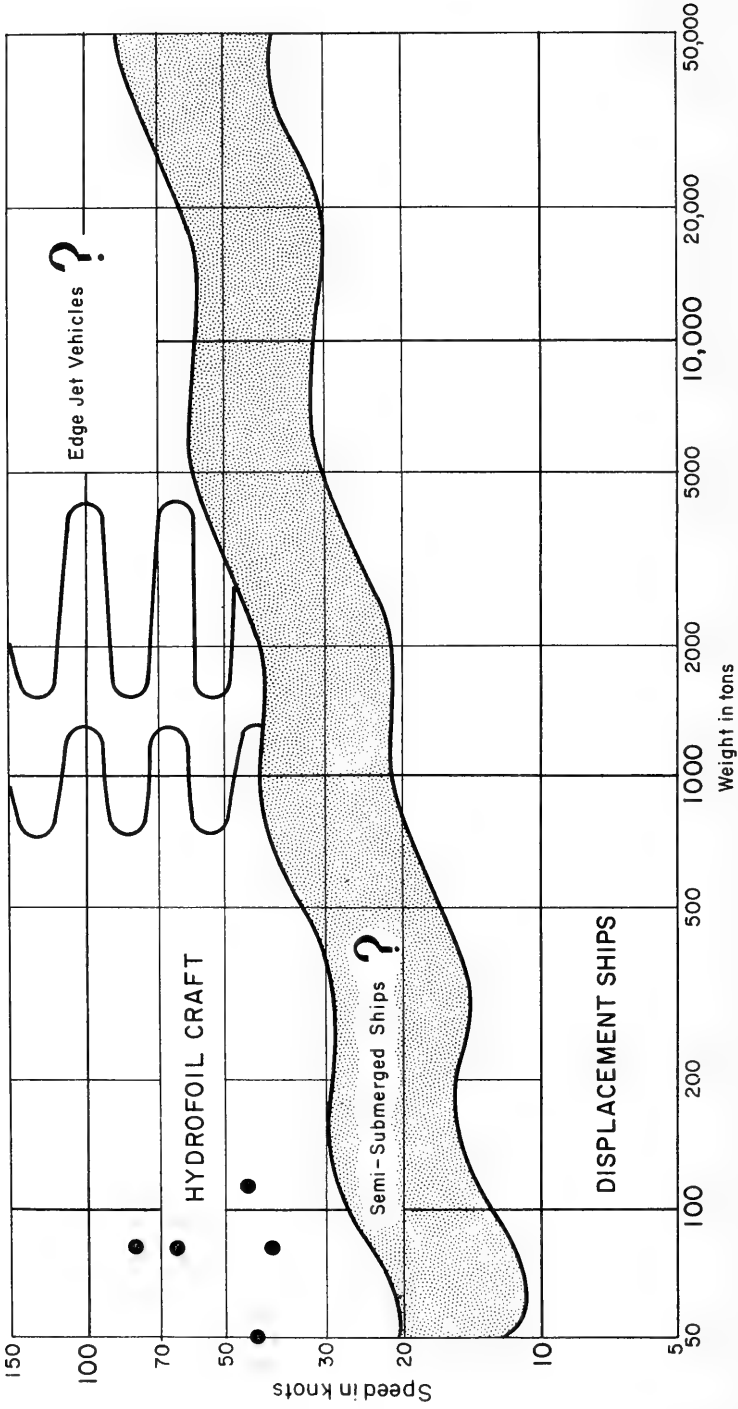
M. P. Tulin

Fig. 1. Optimum operating regimes for seagoing vehicles

speed versus displacement diagram the regions in which various marine vehicles, including semisubmerged ships in addition to those already mentioned above, would seem to offer optimum powering performance. This diagram is based on available data [1, 2] and powering calculations we have carried out at Hydronautics, Incorporated. Also shown are design points for various hydrofoil boats that have been constructed or are under construction. Study reveals that both with regard to needs and capability, the hydrofoil boat seems particularly fated for high-speed operation, that is for speed in excess of 40 and perhaps as high as 120 knots.

The engineering problems involved in the design and construction of high-speed hydrofoil boats are exceedingly severe with respect to power plant, transmission, structure, and hydrodynamic aspects. It is the purpose of the present paper to discuss some of the important hydrodynamic considerations involved, to underline certain problems, and generally to give perspective to the situation that the hydrodynamicist faces.

Both sub- and supercavitating craft intended for sustained operation at sea are considered. It is emphasized that high-speed craft involve very high static foil loadings and additional severe seaway loadings. The hostility of the sea environment is strikingly illustrated through comparison with the atmospheric environment through which the airplane flies. The problem of preventing cavitation on subcavitating craft is discussed and the effect of seaway motions on inception is predicted. The importance of flaps for loads and motion control is underlined and some new theoretical results relating to the effect of the free surface on two-dimensional flap effectiveness for both sub- and supercavitating foils are presented. Other new theoretical results pertaining to the effect of the free surface are also given and, in particular, its beneficial influence on lift-drag ratios of two-dimensional supercavitating foils is revealed.

Many staff members of Hydronautics, Incorporated, have participated in the preparation of the results indicated above.

WING LOADINGS

Considering the essential similarity between the hydrofoil boat and the airplane, it is natural to compare the problems that have faced their development and, of course, to take maximum advantage of mutually useful and pertinent information and experience. This last statement will almost universally be translated as meaning that the naval architect should take advantage of the knowledge of the aeronautical engineer—as, most naturally, he often does. Of course, seacraft and aircraft operate in vastly different environments. Whereas air is so light that it is still a matter of amazement to many that anything substantial can support itself therein, every successful hydrodynamicist early acquires a great deal of respect for the weightiness of his own particular subject. A consequence of this difference in densities is illustrated in Fig. 2. In interpretation of this figure it is useful to recall that the wing or foil loading (displacement over foil area) equals the wing lift coefficient (C_L) multiplied by the dynamic pressure q, $(\rho U_0^2/2)$, and that the optimum lift coefficient for a given design depends primarily upon hydrodynamic considerations relating to minimum powering requirements; practical design lift coefficients for both seacraft and aircraft lie in the range 0.1 to 0.35. The very much larger wing loadings experienced by high-speed seacraft in comparison to those for supersonic aircraft are apparent from the figure. It is striking that the wing loadings of 60-knot-plus seacraft are at least one and almost two orders of magnitude larger than for aircraft of contemplated design. At the same time, the hydrodynamic demands for thinness of underwater structures are just as severe as in the
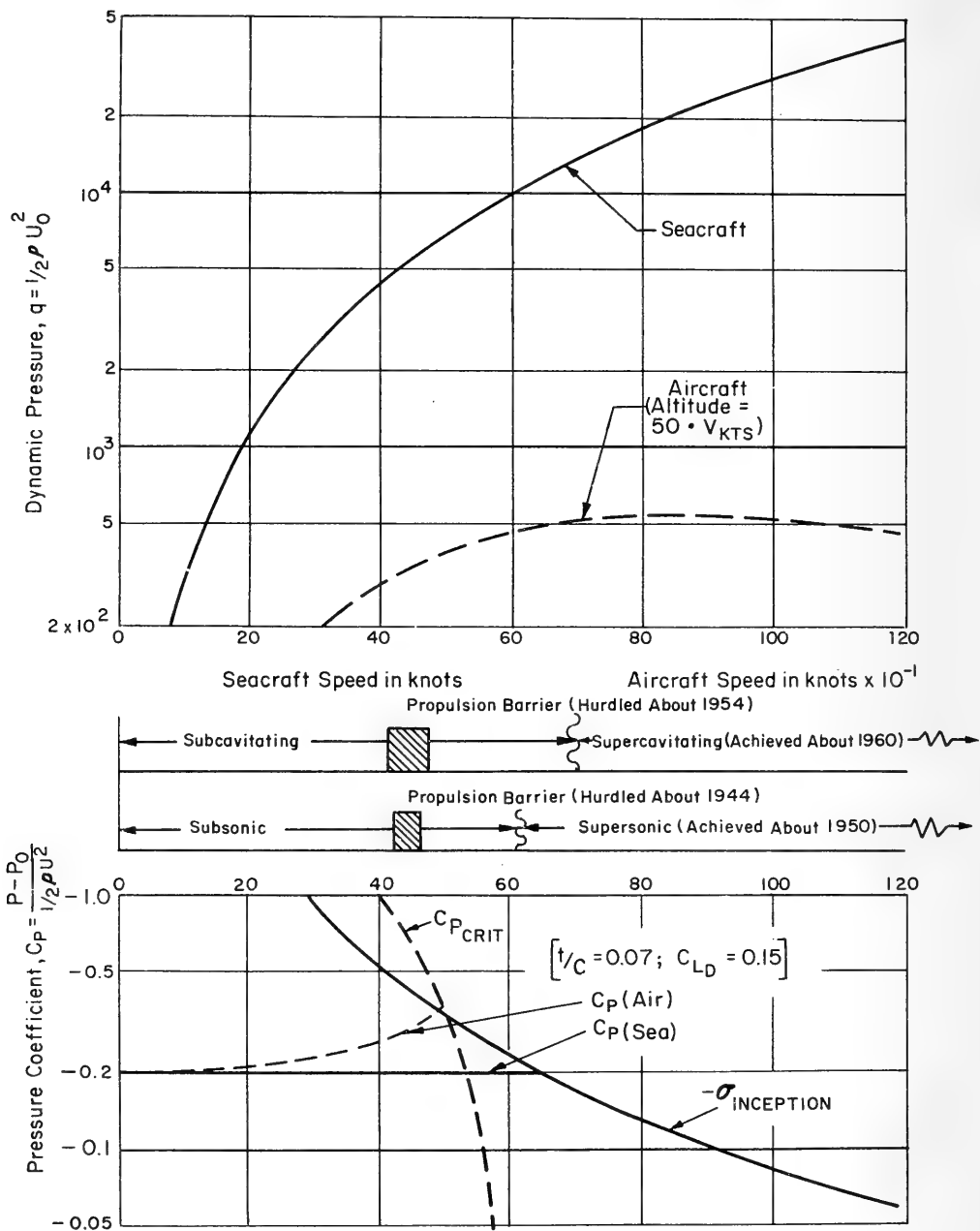
Fig. 2. A comparison of some parameters for seacraft and aircraft

case of aircraft; for either a supercavitating or supersonic foil of given length, drags are incurred proportional to the square of the foil thickness. It is rather difficult to put this comparison on a quantitative basis, but suffice it to say that a 5 percent diamond-shaped strut has the same drag coefficient (about 0.1 based on thickness) operating at mach number 2.3 in air, as when operating at 60 knots and 5 feet submergence in water while ventilated to the atmosphere.

Similarly, for subsonic or subcavitating foils a great premium is placed on structural slenderness, since the speeds which may be attained in either case without impairment in operation increase with thinness of structure. An attempt is made to illustrate this fact in Fig. 2 (bottom) where the critical pressure coefficient for aircraft and inception cavitation number for seacraft are plotted, together with the minimum pressure coefficient for a wing of about 7 percent thickness ratio and 0.1 lift coefficient. Such a wing would encounter, according to Fig. 2, drag rise and buffeting difficulties at 500 knots plus in air and 65 knots plus in calm water. However, a wing of 4 percent thickness and 0.1 lift coefficient could probably achieve about 530 knots in air and 80 knots in calm water before impairment of operation. The crucial observation to be made is that the seacraft structural designer must thin his wings at design dynamic pressures and wing loadings some 20 to 50 times greater than would exist in the case of an aircraft.

It is interesting, having put the static loading problem in some perspective, to note some analogies between propulsion and hydrodynamic problems for the airplane and hydrofoil boat. In these analogies, which it will be immediately recognized cannot be taken too literally, high-speed problems incurred in air due to the finite speed of sound become equivalent to difficulties caused by cavitation in water. In both media, screw propellers are commonly used at low speeds, with their use being finally impaired unless radical change in form is made at speeds of the order of 400 knots in air and 40 knots in water. The propulsion barriers that existed as a consequence, have both been successfully hurdled at this time, by the introduction of jet propulsion in one case, and of the supercavitating propeller in the other [3, 4]. It is taken for granted that high-speed hydrofoil craft will utilize supercavitating propellers with efficiencies at design in the range 0.65 to 0.72.

At speeds somewhat higher than those at which the low-speed screw propeller runs afoul of efficiency loss and severe vibration, the supporting foils of vehicles in both media begin to suffer those same difficulties, and at speeds in excess of 750 knots in air and 75 knots in water, it is almost essential that the design of wings and foils be based on entirely different principles than for low speeds. As is indicated in Fig. 2, the first hydrofoil craft utilizing supercavitating foils is being test flown this year (1960); it has been designed and constructed by Dynamic Developments, Inc., of Babylon, New York, under contract to the Office of Naval Research of the U.S. Navy. The cavities attached to these foils are not, of course, filled with water vapor, but are ventilated through the free surface to the atmosphere.

THE HOSTILE SEA

In a very important respect and in addition to considerations of static wing loading, the sea is a much more difficult, even hostile, environment in which to fly than the atmosphere. Most naval designers and ship's passengers have acquired an appreciation for the severity of the wind-driven motions which must statistically be expected to exist near and on the ocean's surface; and all of us who allow ourselves to be transported from place to place in aircraft have awareness of the turbulence in the atmosphere—we may even have observed

that such turbulence is generally much more intense near the ground than at high altitudes.
I do not think, however, that ever before has a quantitative comparison of gust intensities
just beneath the surface of the sea, and in the atmosphere been made. In Fig. 3, the hori-
zontal axis represents the root-mean-square of the vertical velocities (in feet per
second) either in air or water, and the vertical axis the probability of exceeding a given
value of root mean square velocity. Shown plotted are curves for the North Atlantic at a 5-
foot depth averaged the year around and curves for averages for the atmosphere at low alti-
tudes (0 to 10,000 feet) and moderate altitudes (30 to 50,000 feet). The values for air have
been taken from Ref. 5. The values for the North Atlantic at 5-foot depth were theoreti-
cally derived from experimental all-year observations of significant wave heights in the North
Atlantic made by the U.S. Weather Bureau, and have been taken from Ref. 6. It will be
observed that a root-mean-square value of 1 foot per second is exceeded only 17 percent of
the time at moderate altitudes in the atmosphere, 53 percent of the time at low altitudes, and
89 percent of the time at a depth of 5 feet in the North Atlantic. For an rms value of 3 feet
per second, the respective percentages are 3, 16, and 28 percent. Only for high-intensity
gusts (which occur infrequently) is the atmosphere at low altitudes statistically gustier
than the ocean. The intensity of motions in the sea of course varies with depth of submer-
gence, and in Fig. 4 this dependence is shown for a sea generated by a 20-foot-per-second
wind, which about corresponds to a state 3 sea. It is to be noted that the rms vertical
velocity is about twice as great at the surface as it is at 5-foot submergence and is further
reduced about 50 percent as the depth increases to 10 feet.

The motion of the environment induces loads on the vehicle structure and subsequent
rigid body motions and structural flexing. The seacraft, operating as it does in such close
proximity to the sea surface must maintain its altitude relative to the instantaneous sea
surface within very strict limits lest the hull impact or the foils and propeller broach. For
that reason it is generally desirable for the craft to "follow" or respond to waves which are
as long or longer than the craft itself. Both surface-piercing and variable-incidence foils
are designed with such response in mind. Of course, the actual response of the vehicle to
a certain sea will particularly depend on the frequency with which it encounters the waves
that compose that sea. It so happens that the spectrum of a real, fully-risen, wind-gen-
erated sea seems to be sharply peaked, most of the energy residing in waves traveling with
a celerity close to the wind speed and with corresponding lengths [7]. The consequence of
this fact is that a boat traversing such a sea will sense a dominant frequency of encounter,
which will depend on the wind speed that generated the sea, the boat's speed, and its direc-
tion relative to the wind. In Fig. 5 is plotted this frequency of encounter versus boat speed
from motion into (to the left) and with (to the right) the wind, for wind speeds from 7 to 23.5
knots, corresponding to sea states from 2 through 5. These curves are based on studies
made by F. Turpin and M. Martin [8]. It is to be noted that a response to frequencies, ω,
in excess of 2.5 radians per second or about 0.4 cps (averaging the "with" wind and "into"
wind encounters) is required for a 60-knot boat operating in state 5 sea, and even more
rapid responses for faster craft. The rms accelerations experienced by a boat responding
to such a sea are 0.707 $\omega^2 H_0$, where H_0 is the semiamplitude of the vehicle's heaving
motion relative to fixed axes.

Such accelerations must themselves be limited especially on account of human comfort
limits. It turns out, in fact, that our tolerance to vertical accelerations is quite small.
Shown in Fig. 6 are curves based on recent studies of factors influencing hydrofoil boat
handling qualities by P. Eisenberg [9] which delimit acceleration and frequency ranges for
which vertical motions are perceptible, uncomfortable, and intolerable. If an rms acceleration
of 0.15 g is taken as an upper design limit, then in a state 5 sea, H_0 could not exceed
about 6 inches. However, the rms wave semiamplitude in the same sea is about 3 feet and
the 10 percent highest waves have an rms semiamplitude of 5.4 feet. It would seem that
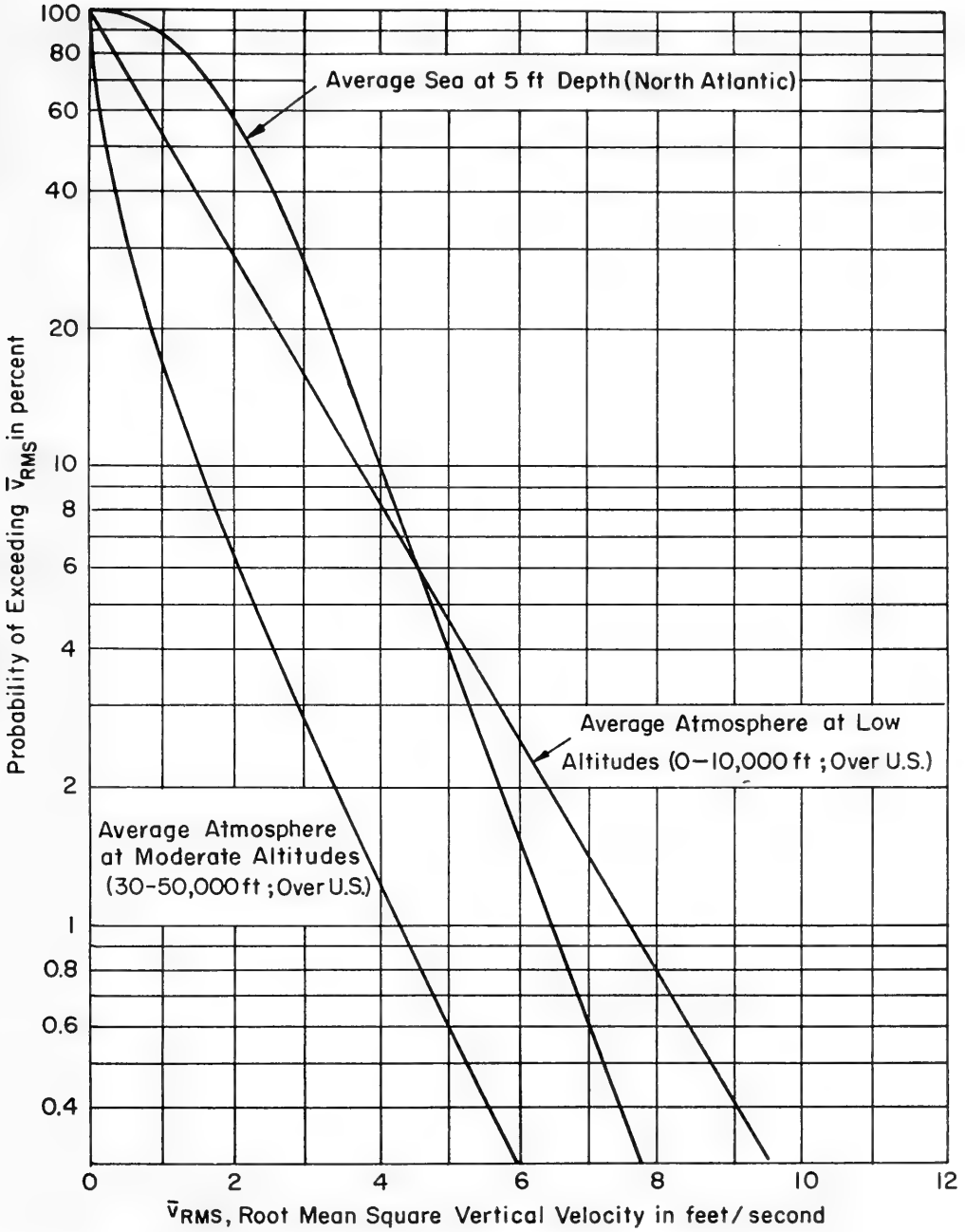
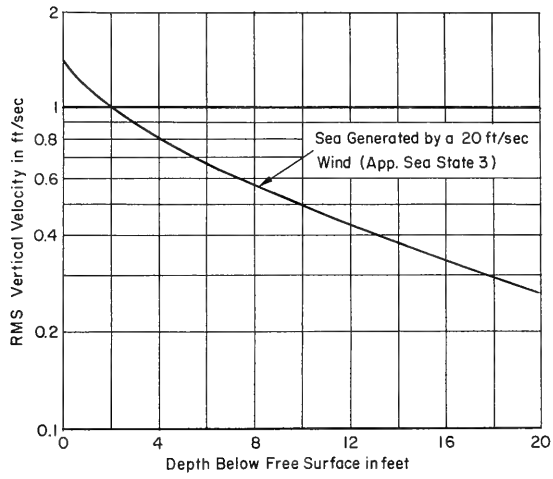Fig. 3. Statistical vertical velocities at sea and in the atmosphere

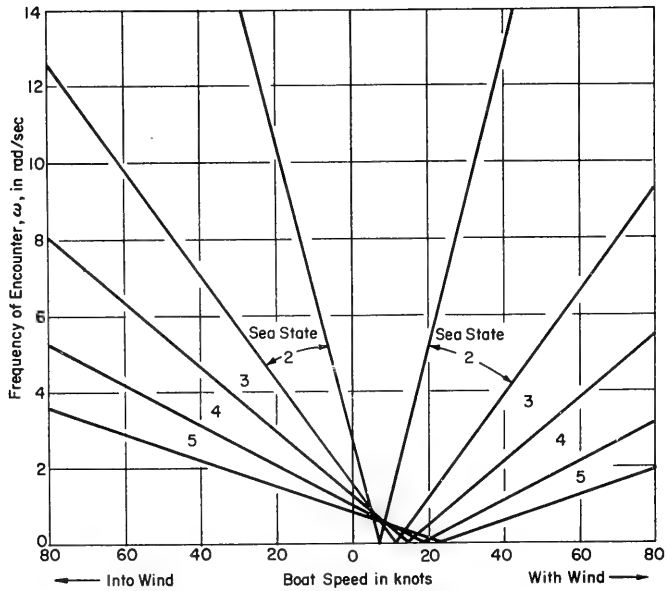Fig. 4. Effect of depth on vertical velocities
in a seaway

Fig. 5. Frequencies with which a boat encounters waves of
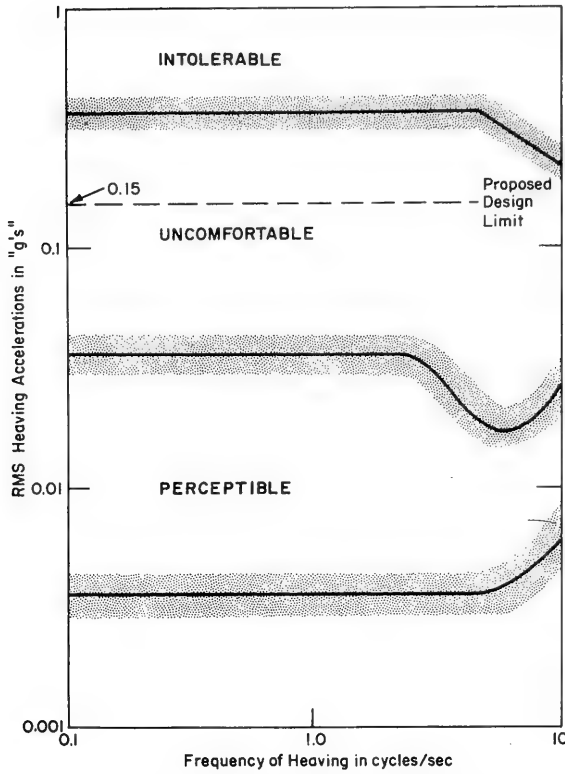various sea states corresponding to various wind speeds

Fig. 6. Human sensitivity to heaving oscillations

such a sea cannot, for reasons of comfort alone, be followed to any extent, but must be plowed. Such an effort, of course, requires a boat with sufficient hull clearance and foil submergence for the hull to pass over crests and the foil system to extend under wave troughs. Variable incidence foil systems particularly recommend themselves for plowing, since a typical surface-piercing foil would during such motions experience fluctuations in load due not only to the orbital subsurface velocities associated with waves, but also to changes in wetted area.

It is of interest to calculate the fluctuating loads acting on a plowing fully submerged foil system, without trim changes, flap or spoiler actuation (in other words, a passive foil system), in order that the problem of controlling these loads by one or another of the means just mentioned can be properly assessed. These loads will actually depend on the rigid body motions of the vehicle and the structural flexing. Aircraft experience [10, 11] would lead us to believe that such dynamic effects tend to increase the loads calculated on the basis of a rigid structure and quasi-static analysis such as we make here. Thus, alarming as our results may be, they are probably not to be relieved by more rigorous calculations, but only through a relaxing of the sea conditions that we have referred to. The dynamic g loadings (in addition to static loadings) induced by the seaway on a fully submerged wing are, according to quasi-static and rigid-body theory, approximately equal to

$$(C_{L_\alpha}/C_L U_0)\bar{v}$$

where C_{L_α} is the foil lift curve slope, C_L is the equilibrium lift coefficient, U_0 is the speed of advance, and $\bar{v}$ is the seaway-induced vertical velocity. If rms g loadings are desired, then rms values of $\bar{v}$ are to be used in computation. The quantity

$$C_{L_\alpha}/C_L U_0$$

at design speed is a characteristic of the craft, while the quantity $\bar{v}$ depends on the environment. Clearly, if minimum dynamic loadings are desired, then the parameter

$$C_{L_\alpha}/C_L U_0$$

should be minimized in design.

In Fig. 7 are shown calculated values of this parameter as a function of speed, for a family of subcavitating and supercavitating hydrofoil wings. The former was selected with wing lift coefficients, thickness ratios, and aspect ratios varying from 0.35, 0.11, and 7 (respectively) at 45 knots to 0.15, 0.05, and 3.3 (respectively) at 70 knots and in such a way as to maintain approximately constant wing stress and satisfy cavitation inception considerations at each speed. The operating depth of submergence is for all wings taken as one mean foil chord. The supercavitating wings were taken in two versions, utilizing in one case thin low-drag foil sections ($t/c \approx 0.08$) with aspect ratios and lift coefficients ranging from 5 and 0.18 respectively at 60 knots to 3.4 and 0.16 respectively at 90 knots, and in the other case thicker foil sections ($t/c \approx 0.16$) with aspect ratios and lift coefficients ranging from 8.1 and 0.26 at 60 knots to 5.6 and 0.23 at the higher speed. All of the supercavitating wings considered are designed for approximately equal maximum nominal stress and are optimized with respect to lift-drag ratios.

The dynamic loads parameter is seen to be generally larger for subcavitating wings, mainly as a result of the higher sectional lift curve slopes of subcavitating foils relative to supercavitating sections. It will be recalled that at infinite depth, the former are about
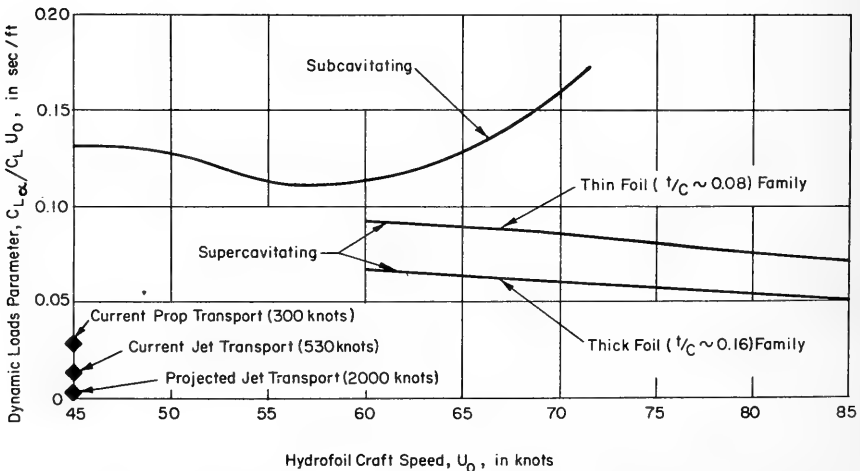

Fig. 7. Dynamic loads parameter $C_{L_\alpha}/C_L U_0$ for a family of hydrofoil craft

four times the latter in value. The proximity of the free surface tends to reduce this ratio, however, and for the wings considered, the C_{L_α} were in an average ratio of about two to one. The increase in the dynamic loads parameter for subcavitating craft between 60 and 70 knots is entirely due to the decrease in lift coefficients demanded in order to prevent cavitation inception. For the optimized supercavitating wing families a general decrease in dynamic load parameter accompanies and is due to increasing speed. The family with thicker foil sections enjoys a smaller value of the parameter because of higher optimum lift coefficients. The values of

$$C_{L_\alpha}/C_L U_0$$

for three transport aircraft [12] are also shown on the vertical ordinate and are seen to be considerably smaller in value than for the best supercavitating wing at 85 knots; the speed of these aircraft range from 300 to 2,000 knots.

The results of the calculation of the dynamic loads parameter shown in Fig. 7 and which have just been discussed, are combined with earlier statistical results, Fig. 3, relating to the character of the North Atlantic and of the atmosphere, to determine the probability that a particular craft with passive foil system (no load alleviation) will suffer dynamic rms g loadings exceeding a certain level. These new results are shown in Fig. 8. The extremely marked effect of decreasing values of dynamic loads parameter,

$$C_{L_\alpha}/C_L U_0$$

in reducing the probability of high g loadings is to be noted. As this parameter varies from a value of 0.04, which is a little less than for the best supercavitating wing at 90 knots, to a value of 0.12 which is a little less than for the subcavitating wing at 65 knots, the probability of exceeding an rms g loading of 0.2 increases from 4 to 70 percent.

The results for aircraft utilizing the low-altitude gust probability curve of Fig. 3 for the propeller transport and the high-altitude curve for the jet are interesting in themselves, but they have been especially included in order to afford through comparison a striking illustration of the magnitude of the dynamic loads problem that must be faced by the designer of seagoing high-speed hydrofoil craft.

LOAD ALLEVIATION AND FLAPS

The results shown in Fig. 8 make it abundantly clear that extremely effective load-alleviating devices must be provided if the design limit of 0.15 g rms vertical acceleration set according to comfort criteria is to be met. These devices must counter vertical orbital velocities in both upward and downward directions and for 60-knot plus craft at encounter frequencies of the order of 2.5 radians per second and higher. If load alleviation is sought through tail foil trim control, then angular accelerations leading to vertical accelerations in excess of the design limit would, according to our calculations, seem to be implied. As an alternative, control of lift at the main foils without essential change of trim suggests itself and has the additional advantage of affording more rapid response than in the case of trim control.

The use of flaps has especially been considered, and in that connection we present here the results of recent calculations on the behavior of two-dimensional flaps for both subcavitating and supercavitating foils, both operating at very high forward speeds. It must
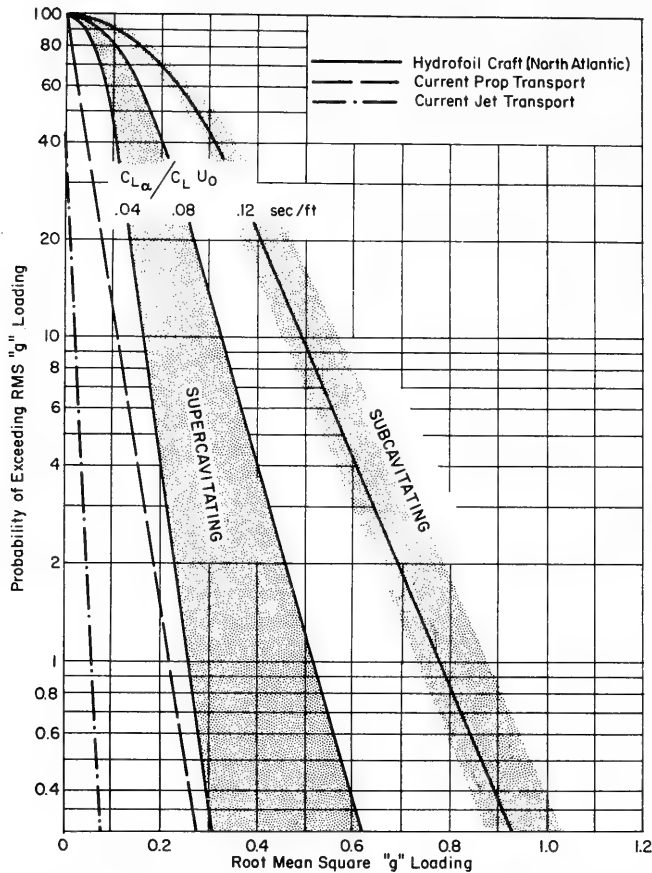
Fig. 8. Statistical dynamic loading for seacraft and aircraft

be understood that the values of flap effectiveness and hinge moments shown must be suit-
ably modified in practice to take into account real fluid and finite aspect ratio effects;
these results do, however, show the magnitude of the effect of near surface proximity.

In Fig. 9 (left) are given curves of subcavitating flap effectiveness versus flap-chord
ratio for depth-chord ratios from zero to infinity. A composite curve for a range of flap-
chord ratios, graphically illustrating the near surface effect is also given in Fig. 9 (right).
The important conclusion is that theory predicts about a 4-percent loss in flap effectiveness
relative to infinite depth at one chord submergence, and a 13-percent loss at 1/2 chord
depth. The loss at zero submergence in the planing condition is 50 percent. These calcu-
lations assume that no cavitation occurs on the foil in the vicinity of the hinge; such occur-
rence would of course lead to loss in flap effectiveness. The results for surface effect on
subcavitating flap effectiveness were obtained by my colleague C. F. Chen in a very inter-
esting way. He determined that a particular flow reversal theorem which had previously
been derived for flows without free surfaces [13] was applicable in the present case, and he
was thus able to calculate the force on a flapped foil in terms of the flow about a flat plate
at incidence under the free surface; the latter flow is exactly the flow about the lower foil
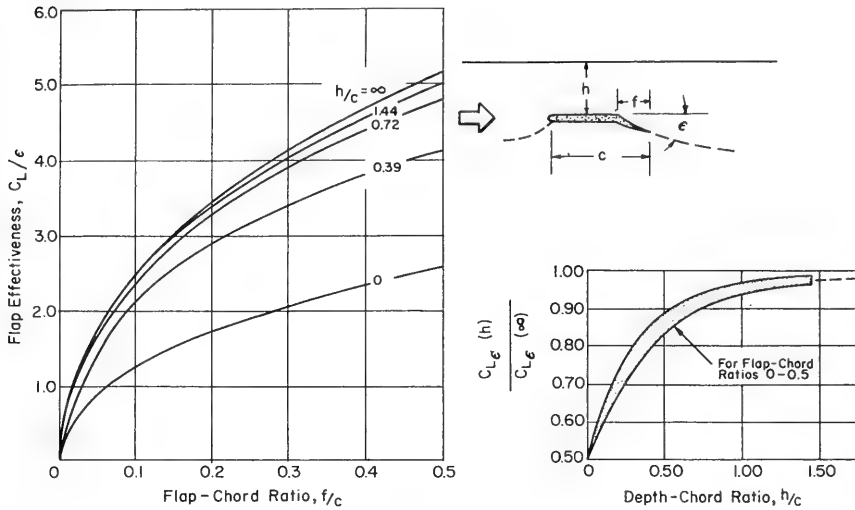
Fig. 9. Free surface effect on two-dimensional subcavitating flap effectiveness

of a two-dimensional biplane and has been known for decades [14]. This calculation constituted the first application to my knowledge of flow reversal theorems for flows with a free surface.

The flap effectiveness of supercavitating flaps at a given depth and for a particular flap-chord ratio is less than that of subcavitating flaps, but the difference in effectiveness decreases with depth and finally disappears at zero submergence. This situation corresponds to the fact that subcavitating flap effectiveness decreases as the free surface is approached whereas supercavitating flaps become more effective. J. Auslaender [15] has recently developed pertinent theory and calculated the performance of supercavitating flaps including the effect of the free surface. In Fig. 10 are presented curves of flap effectiveness versus flap-chord ratio for depth-chord ratios of 0, 1, and infinity. The results for infinite submergence had been obtained previously [16], at which time it was observed that supercavitating flaps at infinite depth reached a maximum value of flap effectiveness for flap-chord ratios less than one. It will be observed in Fig. 10 that for a flap-chord ratio of 0.25, the supercavitating flap gains 17 percent in effectiveness at 1 chord submergence (relative to infinite depth) and 47 percent at 0 submergence in the planing condition. Also, presented as Fig. 11 are hinge moment coefficients for supercavitating foils composed of a forward flat section operating at various angles of incidence δ, followed by a 25-percent flap, all operating at a depth of 1 chord. These results and many more of the same nature have been obtained by Auslaender using linearized theory for zero cavitation number [16-19]. It is presumed that practical foils will be ventilated to the atmosphere and thus operate at a cavitation number close to zero, so that the present results are meaningful practically.

The action of flaps or other load alleviation devices must, of course, be supervised by a suitable sensing and control system. Such systems, involving acoustic wave sensors and similarly sophisticated devices—plus the ubiquitous black box or two—are apparently under active development. I will not dare to say anything about these things, but it is perhaps worth speculating in the present context that high-speed boats must mainly plow through rather than respond to the sea, and that the alleviation of dynamic loads, rather than the
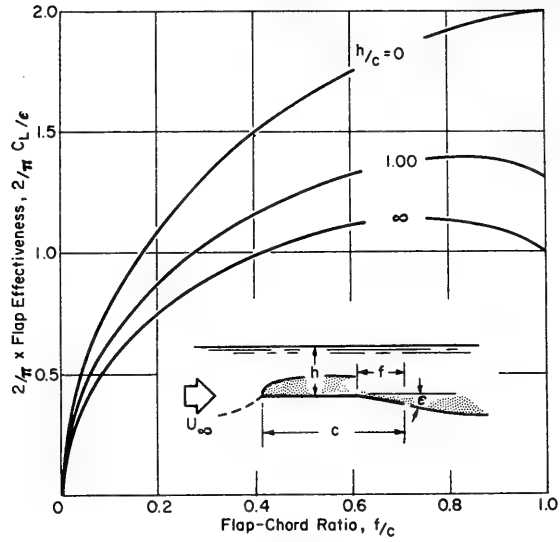
Fig. 10. Free surface effect on two-dimensional
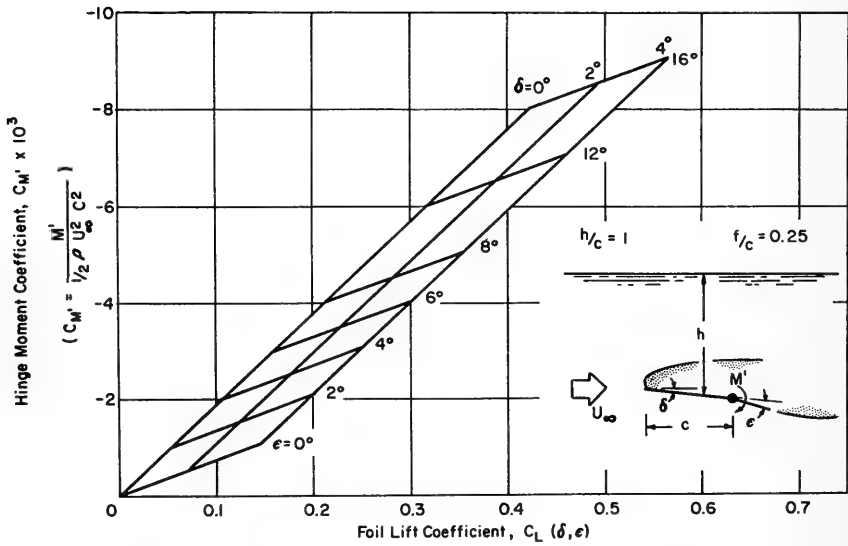supercavitating flap effectiveness

Fig. 11. Supercavitating hinge moment coefficient

control of motions, becomes the task that must be successfully accomplished by the flaps, black boxes, etc.

CAVITATION SUPPRESSION

As boat speeds increase beyond 40 knots the danger of cavitation occurrence on foils, vertical struts, and propulsion nacelles rapidly increases. Because of the erosive effects of cavitation it does not seem attractive to design for operation with small regions of local cavitation occurring on the underwater structure, nor does it seem really feasible to allow extensive cavitation short of supercavitation because of the buffeting that very often accompanies such "transcavitating" flows [20]. The designer must thus strive to suppress cavitation, a process which as earlier mentioned leads to underwater structures which become increasingly thin.

A great deal has been written about the estimation of minimum pressure coefficients on hydrodynamic bodies, and I will here only add several small straws to the camel's back. The first concerns the point that it would seem to us generally dangerous in design, even in the earliest stages, to consider the inception properties of components by themselves rather than in combination. This might seem to be a rather obvious remark, but nevertheless there has been considerable discussion of the inception properties of components, and very little on combined configurations. In Fig. 12 are shown theoretical inception speeds for a modified spheroidal nacelle and a NASA 16 series strut both separately and in combination, as a function of pod length-diameter ratio. The strut maximum thickness was assumed to be 1/6 of the nacelle diameter and its length 67% of the nacelle length; since such a nacelle may at times operate in practice right up to the free surface, the calculations were made for zero depth although the relieving effect of the free surface was not taken into account. These calculations were made for illustrative purposes only, and although thought to be realistic, do not necessarily represent optimum configurations; further they neglect the influence of the propeller and horizontal foils should they be called for, and the additional influence of pitch and yaw. Even so the relation between component and configuration inception speeds is indicated.

In considering the inception speeds of components it would seem very important that the effect of wave motions be taken into account, for the minimum pressure coefficients of high-speed foil and strut sections are very sensitive to incidence and yaw. Shown as Fig. 13 is an estimation of the probability that local cavitation will occur on a hydrofoil wing of aspect ratio 4, with Series 16 sections of 4-percent thickness and a design lift coefficient of 0.15, while operating at 5-foot depth in the average North Atlantic environment described in Fig. 3; it was assumed that cavitation occurs during motions involving fluctuating angles of attack for values of rms angle of attack equal to steady inception angles, and this is believed to be a conservative assumption. It is observed that this wing, which could according to theory make 70 knots in calm water, will cavitate over 50 percent of the time during year-round operation at speeds as low as 50 knots, and over 75 percent of the time at 60 knots. These predictions of average performance do not, of course, show how inception speed varies with sea state, so in Fig. 14 is presented (solid line from the left) a curve of inception speed versus sea states (and corresponding wind speed) for the wing described above, assuming again that the rms angle of attack corresponds to the steady inception angle. The dashed curves are based on the slightly different assumptions that the average of one-third highest and maximum angles of attack in the seaway correspond to the steady inception angle. It is of interest to know how much faster than inception speed a wing may be driven before the cavity grows long enough to cause serious buffeting, and the right-hand
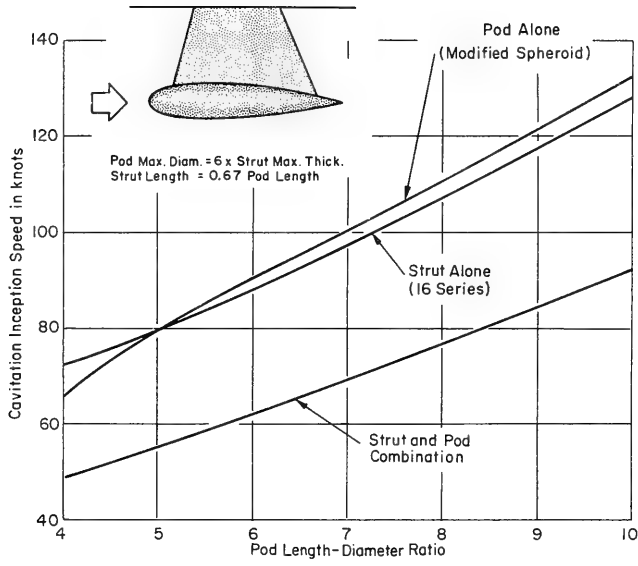
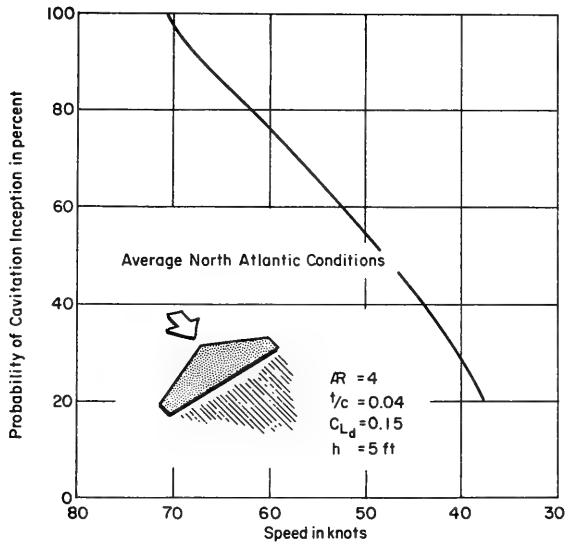Fig. 12. Cavitation inception speeds for streamlined pods and struts

Fig. 13. Probability of cavitation inception vs speed for North Atlantic operation
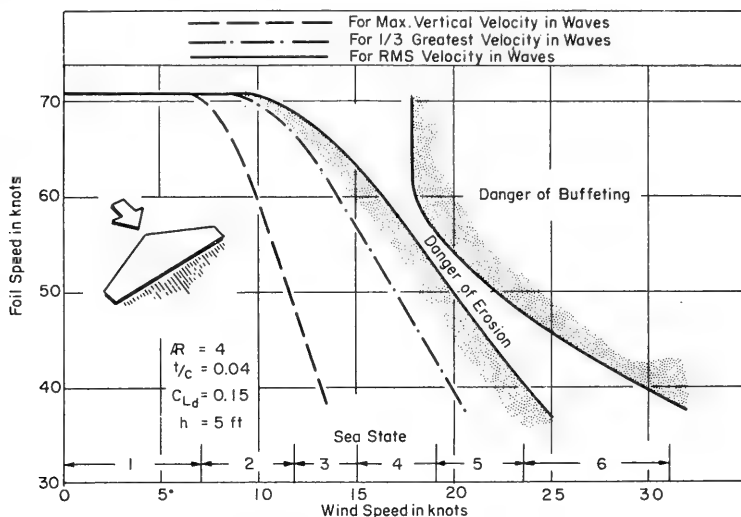
Fig. 14. Wing cavitation inception vs sea state

boundary in Fig. 14 outlines the region of forward speeds and sea state wherein severe foil vibrations might be expected; this prediction is entirely theoretical as far as operation in a seaway is concerned, being based on observations under steady angles of attack [20].

In order not to end this discussion of cavitation suppression on too despairing a note, I would like to present as Fig. 15 the results of calculations that we have carried out on the effect of the proximity of the free surface on the minimum pressures due to the thickness portion of a thin plane wing, and on the minimum pressures acting on spheroidal bodies of revolution. For the smaller depth-diameter ratios, the latter refer particularly to the pressures on the upper portion of the body. These calculations indicate that very modest gains in inception speed may result in practical cases due to the proximity of the free surface.

SUPERCAVITATING OPERATION

It has already been pointed out that the propulsion of high-speed hydrofoil boats depends upon the utilization of supercavitating propellers, and it would seem clear, in addition, that the 70-knot-plus potential of these craft will depend upon the utilization of super-cavitating foils and struts. A great deal has recently been written about practical bodies operating in cavity flow, and particularly good references to this work are the collective papers presented at the second Office of Naval Research Symposium on Naval Hydrodynamics (1958), which was the immediate predecessor of the present Symposium.

The Langley Laboratory of the (U.S.) National Aeronautics and Space Administration have in the past conducted especially valuable theoretical and experimental studies of supercavitating wings and struts operating in ventilated condition [17-19, 21]. These results provide at least a lower bound to the values of lift-drag ratios to be attained for high-speed craft, and it is believed that further significant increases in foil efficiency will be realized, if at all, only as the result of detailed and intensive research.
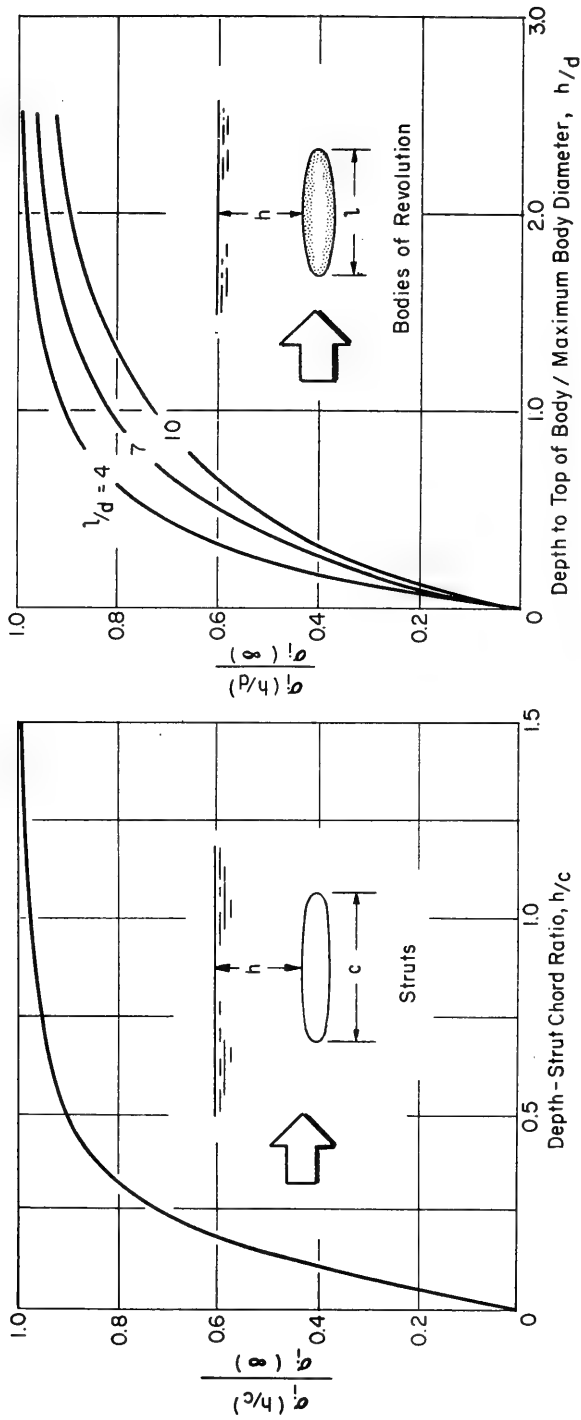
Fig. 15. Inception cavitation coefficients, σ_i, as affected by the near surface

For foils of optimum design, the sum of induced and cavity drags seems to be considerably greater than the friction drag. The division of induced and cavity drag depends very much on the wing aspect ratio, the cavity drag being generally larger and thus more important for aspect ratios of 2 or 3 and higher.

Theoretical studies [16, 17], now confirmed by experiments [18, 22], have led to the design of low-drag supercavitating foils such as are used in propeller design. We have recently developed a theory and made calculations to reveal the effect of near-surface proximity on the shape of optimized low-drag foils, and on the resulting lift-cavity drag (L/D_c) ratios. It may be recalled that I had some time ago shown that, according to linearized theory, there exist for supercavitating foils at infinite submergence, optimum values of L/D_c, inversely proportional to the foil lift coefficient. These ideal optimum ratios are not realized in practice partly because of the necessity to design foils of sufficient strength, and thus develop lift from incidence as well as camber; nevertheless, these ratios do provide information as to the efficiency with which lift can be developed through camber. In Fig. 16 are shown together with previous results for infinite submergence, theoretical two-dimensional foil efficiencies at a submergence of one chord. The optimum ratios of L/D_c are seen to be almost four times higher at this moderately shallow submergence than for deep submergences, but for various reasons these same ratios for practical foils and lift coefficients are reduced to about 1.5. As a caution against any undue optimism that might be generated by this finding, it should be recalled that active load-alleviation devices such as the supercavitating flaps earlier discussed will, it seems safe to predict, inevitably extract their own penalty in terms of increased cavity drag.
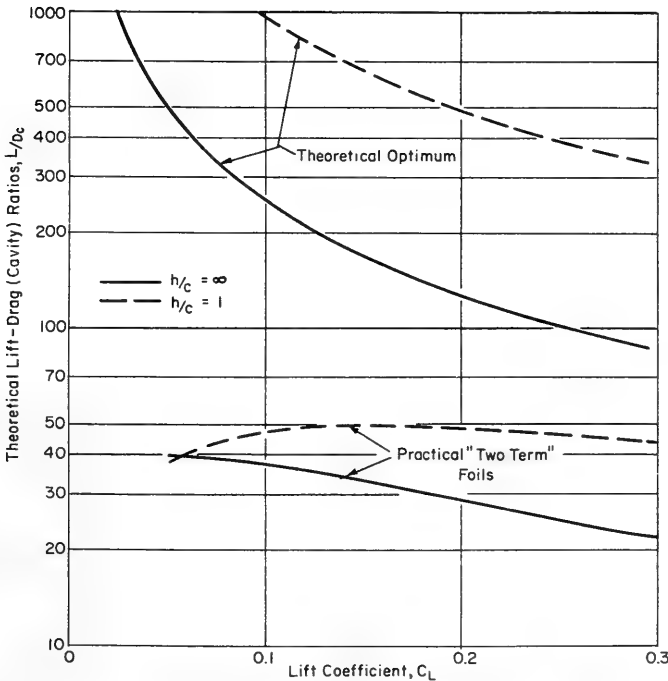

Fig. 16. Theoretical two-dimensional lift-drag (cavity) ratios

CONCLUSION

The subject of the hydrodynamics of high-speed hydrofoil craft has been far from exhaustively discussed here, even with regard to a cataloging of important problems. An effort has been made, however, to provide a little perspective as to the task that faces the designer and, in particular, to emphasize the problem of seaway induced dynamic loads, the related problem of load alleviation, certain problems connected with cavitation suppression—especially in a seaway, and, finally, the problem of the varied effects of near-surface proximity on foil performance. An attempt has also been made to provide some new and useful information relating to these problems; it will be understood that much of this information is based on theoretical developments and calculations carried out by the staff of Hydronautics, Inc., which are themselves the subjects of separate papers, and could not for reasons of space be gone into in any greater detail here; it is a pleasure to acknowledge that a good many of these results that I have just referred to were obtained under a research program sponsored by the U.S. Navy's Bureau of Ships.

Finally, lest some of the conclusions that have been arrived at are interpreted as throwing some doubt on the feasibility of high-speed ocean-going hydrofoil craft, let us affirm our personal conviction that such craft will inevitably be successfully developed and will before too much time passes find their unique place in the transportation scheme of things.

REFERENCES

[1] Saunders, H.E., "Hydrodynamics in Ship Design," Vol. II, New York: The Society of Naval Architects and Marine Engineers, 1957

[2] Geyer, L.A., and Wennagel, G.J., "A Feasibility Study of Hydrofoil Seacraft," Presented before The Chesapeake Bay Section of the Society of Naval Architects and Marine Engineers, 1958

[3] Tachmindji, A.J., Morgan, W.B., Miller, M.L., and Hecker, R., "The Design and Performance of Supercavitating Propellers," David Taylor Model Basin Report C-807, 1957

[4] Tachmindji, A.J., and Morgan, W.B., "The Design and Estimated Performance of a Series of Supercavitating Propellers," p. 489 in "Second (1958) Symposium on Naval Hydrodynamics," Washington: Office of Naval Research, 1960

[5] Press, H., Meadows, May T., and Hadlock, I., "A Reevaluation of Data on Atmospheric Turbulence and Airplane Gust Loads for Application in Spectral Calculations," NASA Technical Report 1272, Washington, 1956

[6] Brooks, R.L., and Jasper, N.H., "Statistics on Wave Heights and Periods for the North Atlantic Ocean," David Taylor Model Basin, Sept. 1957

[7] Neumann, G., and Pierson, W.J., "A Comparison of Various Theoretical Wave Spectra," Proceedings of the Symposium on the Behaviour of Ships in a Seaway (25th Anniversary of the NSMB), H. Veenman and Zonen, Wageningen, The Netherlands, 1957

[8] Turpin, F.J.,and Martin, M., "The Effect of Surface Waves on Some Design Parameters of a Hydrofoil Boat," Hydronautics, Inc., Technical Report 001-3, Jan. 1961

[9] Eisenberg, P., "Considerations of Hydrofoil Boat Handling and Motions Qualities," Hydronautics, Inc., Technical Report 001-4, Oct. 1960

[10] Bisplinghoff, R.L., "Some Structural and Aeroelastic Considerations of High-Speed Flight (Nineteenth Wright Brothers Lecture)," Journal of the Aeronautical Sciences 23 (No. 4), Apr. 1956

[11] Bennett, F.V., and Pratt, K.G., "Calculated Responses of a Large Sweptwing Airplane to Continuous Turbulence with Flight-Test Comparisons," NASA Technical Report R-69, Washington, 1960

[12] The Staff of the Langley Research Center, "The Supersonic Transport—A Technical Summary," NASA Technical Note D-423, Washington, June 1960

[13] Heaslet, M.A., and Spreiter, J.R., "Reciprocity Relations in Aerodynamics," NACA Technical Note 2700, Washington, 1952

[14] Glauert, H., "The Elements of Aerofoil and Airscrew Theory," New York: Macmillan, 1st ed., 1944

[15] Auslaender, J., "The Behaviour of Supercavitating Foils with Flaps Operating at High Speed Near a Free Surface," Hydronautics, Inc., Technical Report 001-2, 1960

[16] Tulin, M.P., and Burkart, M., "Linearized Theory for Flows about Lifting Foils at Zero Cavitation Number," David Taylor Model Basin Report C-638, Feb. 1955

[17] Johnson, V.E., Jr., "Theoretical Determination of Low-Drag Supercavitating Hydrofoils and Their Two-Dimensional Characteristics at Zero Cavitation Number," NACA RM L57G11a, Washington, 1957

[18] Johnson, V.E., Jr., "Theoretical and Experimental Investigation of Arbitrary Aspect Ratio, Supercavitating Hydrofoils Operating Near the Free Water Surface," NACA RM L57I16, Washington, 1957

[19] Johnson, V.E., Jr., "The Influence of Submersion, Aspect Ratio, and Thickness on Supercavitating Hydrofoils Operating at Zero Cavitation Number," p. 317 in Proceedings "Second (1958) Symposium on Naval Hydrodynamics," Washington: Office of Naval Research, 1960

[20] Numachi, F., Tsudoda, K., and Chida, I., "Cavitation Tests on Six Profiles for Blade Elements," Inst. High Speed Mech., Tohoku Univ., Report 8, pp. 25-46, 1957

[21] Wadlin, K.L., "Ventilated Flows with Hydrofoils" (NASA), Presented at the Twelfth General Meeting of the American Towing Tank Conference, Berkeley, California, Sept. 1959

[22] Waid, R.L., and Lindberg, Z.M., "Water Tunnel Investigations of a Supercavitating Hydrofoil," California Institute of Technology, Hydrodynamics Laboratory Report 47-8, Apr. 1957

DISCUSSION

S. F. Hoerner (Gibbs and Cox, Inc., New York)

The Froude number is generally used in the consideration of displacement-type ships. As far as hydrofoil boats are concerned, it is known that such craft will be able to operate efficiently at higher Froude numbers. The size of hydrofoil craft is limited, accordingly, and to mention a number, the limit might be in the order of 500 tons. However, there is also an upper limit to the Froude number as far as hydrofoil craft are concerned. To explain this briefly, consider a craft of 200 tons operating at 50 knots, which is believed to be feasible. We may now put into that craft heavier machinery, propelling it at 100 knots, which is twice the original speed. As a consequence, to support the same weight, we will only need 1/4 the original foil area. The size of the struts supporting the weight of the hull above the foils is, on the other hand, a function of the hull weight and of drag and other forces such as impact which are more or less proportional to that weight. In other words, the struts remain the same size as those of the original craft. Since struts are roughly accountable for half the drag of a foil system, the faster boat will have higher drag. This result can be said to be the consequence of high Froude number. The argument applies to plain configurations of hull plus foil system, while cavitation is not yet taken into account.

Marshall P. Tulin

It is certainly true that all studies of the speed and power of hydrofoil craft have revealed that there is a maximum practical Froude number beyond which hydrofoil craft may not be economically or otherwise feasible. Such studies, of course, include those made by Dr. Hoerner himself—which have proved very valuable to students of hydrofoil craft during the last few years. The actual value of a maximum Froude number depends on structural and power plant weights and its existence is not to be argued, but I would like to suggest that this Froude number may be an increasing function of time and that its estimation is thus not particularly easy. I might further comment on Dr. Hoerner's remark with regard to the drag of struts. In particular, I don't think I can agree that the strut drag is simply about half of the foil system drag; I believe that very much depends upon the configuration of the foil system and that the strut drag may be considerably less than half of the total for certain systems.

S. F. Hoerner

My statement that strut drag is roughly half the foil system drag applies to fully submerged foil systems at maximum speed. Generally, struts in such systems represent approximately 1/2 the *parasitic* drag, which mean approximately 1/4 the total drag, at maximum-range speed.

F. S. Burt (Admiralty Research Laboratory)

I endorse the point Mr. Tulin made that there is a considerable shortage of systematic data of components in association with one another. It is more important that tests on these associated systems should be carried out at the correct cavitation number than at the correct Froude number. In fact you are in the usual difficulty; you want all your numbers right,

which can only be achieved at full-scale, and under these conditions it is very difficult to get really systematic measurements under completely controlled conditions. There are very few facilities available which can run at sufficient speed to get the correct cavitation number and a reasonable approximation to the Froude and Reynolds numbers. We have, in fact, been doing some work in the rotating-beam channel at the Admiralty Research Laboratory because we can run at large scale and very high speeds, up to 100 knots. There are available in the world quite a number of seaplane tanks which are going into disuse at the moment and I would suggest that these are ideal facilities for this type of work, particularly as a lot of them have the ability to make tests in simple wave systems, which is a very vital part of the whole problem. I suggest that more use might be made of these facilities by our various governments for hydrofoil craft experiments.

Marshall P. Tulin

I am very happy to hear Mr. Burt's comment on the effects of interactions on inception based upon his own experience and presumably on experimental measurements of cavitation inception. With regard to facilities, he has an admirable point with regard to the utilization of seaplane tanks where they exist. As I mentioned in my talk, the Hydrodynamics Division of the former National Advisory Committee for Aeronautics, now the National Aeronautics and Space Administration (NASA), carried out most valuable research on supercavitating hydrofoils and other related problems very pertinent to the development of hydrofoil craft; we all hope in the United States that those fine facilities which are no longer being used for seaplane research will continue to be put to use for high-speed hydrofoil and other marine testing.

Glen J. Wennagel (Dynamic Developments, Inc., Babylon, New York)

Mr. Burt talked on the further use of existing high-speed towing tanks and certainly these should be used. In fact, with the decrease in interest in high-speed seaplanes in recent years, perhaps hydrofoils have given these tanks a new lease on life. However, it is not always easy to test in the existing towing tank facilities. Sometimes they are far away and scheduling difficulties exist. Also, they are expensive. We went, about a year ago, to facilities like the Whirling tank and the Pendulum in order to have something relatively cheap in our own back yard, where we could use relatively inexpensive small models, make changes quickly and put ourselves in the right ball park on a hydrofoil or strut design. Then we would look forward to using some of the high-speed tanks, such as those at Langley Field, Virginia, after a foil design has been optimized. Let me give you an idea of the dollars and cents involved here. The whirling tank is worth about 100,000 dollars. You can use that amount of money up rather quickly in testing with larger scale models. To get the accuracies we wanted, a single model tested at Langley Field was worth about 12,000 dollars. You do not have to build many of those to use up the cost of a smaller facility.

P. Kaplan (Technical Research Group, Inc., Syosset, New York)

I have some questions as to the validity of the simple gust-load formula for the g loading of a hydrofoil system. The numbers appear to be too pessimistic, at least from my quick judgement of them, and we must remember the fact that the real hydrofoil craft is a coupled

system where there is important effect of pitch and you have really two foils at different positions relative to the center, but quite different from a simple aircraft and what I have done was to compute some values of this gust-load factor according to the quasi-steady formula and then compare that with some values obtained from some experiments at the Model Basin. This bore out the fact that the original formulation appears to be quite pessimistic. However, the Model Basin tests were at a rather low Froude number, so perhaps that may cover some of the difference. Also, Mr. Tulin mentioned that he did not cover all of the various problems associated with the hydrodynamics of high-speed craft, and in particular I would like to put forward the fact that in this case of high-speed and supercavitating foils it appears that there may be a rather distinct possibility of the hydroelastic instability, that is, flutter. Some theoretical results carried out about a year ago at Stevens indicated that there is a greater possibility of obtaining a hydroelastic instability, that is, flutter, for supercavitating foils as compared to fully wetted foils. This sort of problem should be looked into very carefully in the design of these craft.

Marshall P. Tulin

With regard to Dr. Kaplan's question about the calculation of g loadings (which were admittedly based on the simplest sort of analysis), there is no question that very much more sophisticated calculations for hydrofoil craft should be carried out. In my paper I refer to several sophisticated calculations carried out for aircraft and I would suggest that these calculations should serve as a model with regard to hydrofoil investigations. To say that coupled motions are involved in such calculations is a gross understatement. In the case of a recent aircraft investigation, five degrees-of-freedom were considered, including torsion and bending of the wing, which are very important for high-speed aircraft and should certainly be as important in the case of the hydrofoil craft with its high wing loadings. It was particularly this aircraft investigation which prompted me to make the remark in my paper that the simplest kind of analysis leads, if anything, to conservative results regarding load estimations. Of course, the damping of hydrofoil craft motions is not necessarily the same as in the case of an aircraft, and for that reason alone we cannot come to any rigorous conclusions from aircraft experience. I hope that the kind of calculations, as I have indicated above, will be carried out; I can say that we plan to make some calculations ourselves.

Problems of hydroelastic phenomena are well-known to be important for high-speed supercavitating foils whether used in hydrofoil craft or in propellers. Such problems, particularly with regard to leading edge flutter, have already been experienced, and some stopgap solutions have been obtained. Certainly research on the subject of flutter and on strut divergence, which may be very important for high-speed craft, should be the subject of future investigations.

Edward V. Lewis (Davidson Laboratory, Stevens Institute of Technology)

Mr. Tulin has pointed out some of the serious problems of hydrofoil craft design for rough sea conditions. He expresses optimism regarding the possibility of solving these problems and suggests possible solutions.

I should like to return to a more basic problem of the hydrofoil boat which pertains to fundamental limitations on this type of craft. For this purpose we may compare a hydrofoil boat with an airplane, in which the boat hull and airplane fuselage are comparable, but the hydrofoil wings are in water instead of air. At any particular speed the increased density

of water makes it possible for the wing area to be proportionately reduced for the hydrofoil boat. The total drag and hence overall L/D would be about the same as an airplane for an idealized hydrofoil craft in which resistance of appendages and supports is neglected. However, the increased density of water makes it possible with the proper "wing" area to obtain sufficient dynamic lift for the hydrofoil boat to "fly" at lower speeds than the airplane in air. When the hydrofoil craft is then designed to operate at a speed intermediate between that of an airplane and a ship, there should theoretically be a reduction in hull or fuselage resistance in air which is proportional to the square of the speed. Hence, the initial appeal of the hydrofoil boat was the hope that it could fill the speed gap between ships and airplanes, with a higher L/D or lower P/WV than the airplane. Unfortunately, the strut system required to put the wings in the water adds more to the resistance than is saved by the reduced speed. Hence, even the most enthusiastic hydrofoil man does not expect as good an L/D for the hydrofoil craft as for the airplane.

An important difference remains between the hydrofoil boat and the airplane. At its lower speed, the hydrofoil craft requires much less power, which should be advantageous. But the lower speed is less efficient for propulsion, and the drive system becomes very complex. Hence, no gain in payload from reduced power requirements can be expected in practice. Insofar as fuel is concerned, for the same specific fuel rate the total fuel consumed for equal distances is the same or greater.

Hence, it appears that the goal of the hydrofoil boat designer is simply to equal the performance of aircraft, but at reduced speed. The possibility of doing this in terms of L/D and gross weight (payload) appears remote. In short, a seaplane can outperform a hydrofoil boat, and attain higher speed at the same time. We must recognize therefore that the hydrofoil craft is inherently a special purpose vehicle.

I realize that it is dangerous in this company to appear antihydrofoil, hence, I hasten to add that I am enthusiastic about this development. My reason is simply that it is already stimulating technical progress in naval architecture, bringing advanced hydrodynamics, better structures, and more efficient power plants into the picture. No matter what happens to the hydrofoil itself, naval architecture will never be the same again.

*   *   *

ON HYDROFOILS RUNNING NEAR A FREE SURFACE

S. Schuster and H. Schwanecke
Versuchanstalt für Wasserbau und Shiffbau
Berlin Towing Tank

For the steady state of flow the results of pressure distribution measurements dependent on speed, depth of submergence, angle of attack, and roll angle—both for a flat and for a dihedral hydrofoil—are presented, as well as the results of six-component measurements for two dihedral foils. Below the Froude depth number 1, related to the depth of submergence, the flow and hence the pressure distribution changes according to the shallow water laws; above this figure no significant speed dependency exists. Here the pressure distribution is influenced only by the distance between the hydrofoil and the surface in relation to its profile length. For this situation, which is normal for hydrofoil boats under service conditions, simple theoretical rates for calculating the hydrodynamic forces are given, as well as the results of these calculations in the case of a parallel submerged hydrofoil of great span. By analyzing the separate influences the relation to results of wind tunnel tests can be set up. By means of the results from theoretical and experimental examinations, relations are derived for the vertical and the lateral stability both of flat and dihedral hydrofoils as well as for the influence of sideslip motion.

INTRODUCTION

One of the most important suppositions for the design of hydrofoil boats is the precise knowledge of the flow forces occurring on the foils under given service conditions. There is no doubt that many conceptions are transferable from aerodynamic research but some essential properties like lift distribution and all values of driving performance and running behavior connected herewith will be more or less influenced by the proximity of the water surfaced. During the last twenty years this problem has been treated very often, but further treatment, based on new experiments in the Versuchsanstalt für Wasserbau und Schiffbau (the Berlin Towing Tank), may be expected to clarify and complete the picture. During these examinations the pressure distribution both for completely submerged hydrofoils and for those piercing the water surface, the deformation of the surface, and the flow forces have been measured as well as theoretically treated, all angles being varied.

PRESSURE DISTRIBUTION MEASUREMENT

Two brass hydrofoil models with special borings have been used for measuring the pressure distribution, one of them being a flat hydrofoil and the other a dihedral hydrofoil (V-form), both idealized with circle segment profiles of constant length without distortion (Fig. 1). On the starboard side the flat foil was fitted with 68 borings and the dihedral foil with
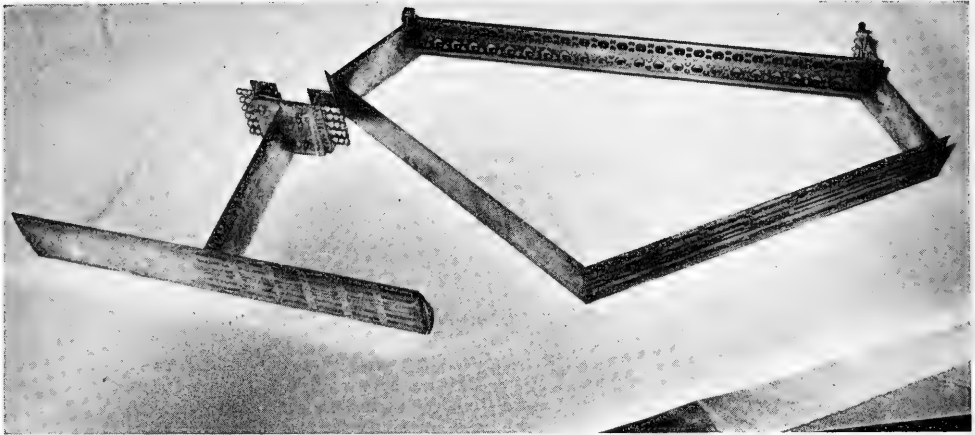
Fig. 1. Hydrofoil models simplified for pressure distribution measurement

49 borings of 1.5-mm diameter. The holes were arranged in sections parallel to the longitudinal axis and connected to each other parallel to the lateral axis. For measurement all the sets of holes but one have been covered with thin plastic strips. Thus, successively, the pressure distribution around the profile for 6 cross sections for the flat foil and 7 cross sections for the dihedral foil has been measured and photographically recorded during each run in the deepwater channel. For the flat foil the angle of attack has been varied from −1 degree to +6 degrees, and the depth of submergence from 30 mm to 240 mm at a speed of $u_0 = 3.7$ m/sec; for a special series the speed was also varied, from 0.4 to 3.7 m/sec. For the dihedral foil the angle of attack has been kept constant at +1 degree while the rolling angle has been varied from 0 to 33 degrees, one arm of the hydrofoil being parallel to the water surface when the rolling angle was 33 degrees. The measured pressure in relation to the ram pressure has been plotted versus the profile length for every section. Integration of the pressure curves results in the local lift coefficients, which in turn by integration over the span supply the total coefficient. For checking these values and for finding the drag three component tests have been made.

Flat Foil

The variation with speed for the flat foil first of all confirmed the shallow water effect as found by Laitone [1], Parkin, Perry, and Wu [2] and Plesset and Parkin [3], which occurs especially at the critical speed $u_0 = \sqrt{gh}$ (Fig. 2), where h denotes the distance between the trailing edge and the undisturbed water surface.* At a speed sufficiently above this value the ratio between depth of submergence and length of profile only is authoritative for the course of the pressure curve. Samples are shown in Figs. 3 and 4. Herein the characteristics of the diagrams versus h/c and α are different. The local lift coefficients indeed change in the same sense as depth of submergence and angle of attack, but in the first case the pressure distribution is unchanged, while it is varying much in the second case. Therefore, approaching the surface cannot be substituted by a reduction of the angle of attack.

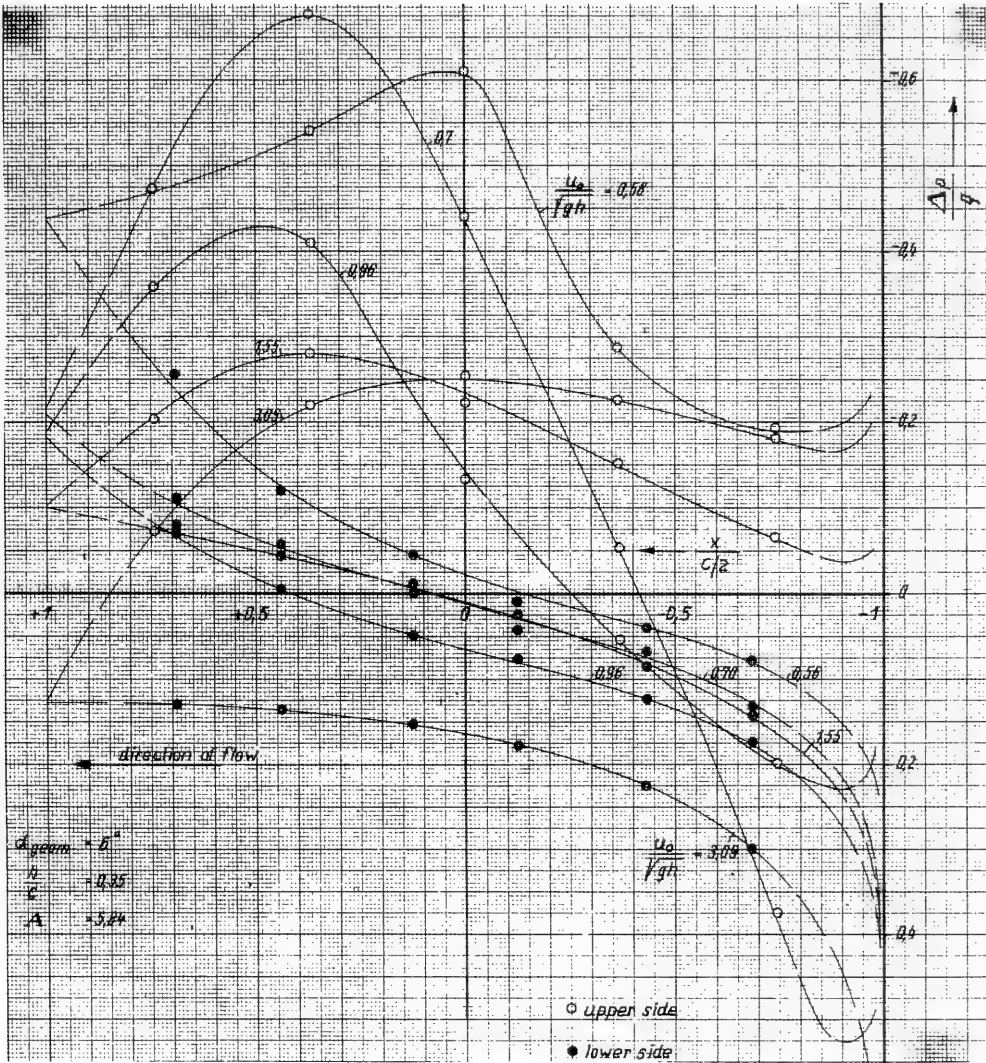*A nomenclature list is given at the end of the paper.

Fig. 2. Pressure data for the flat foil of circle segment profile
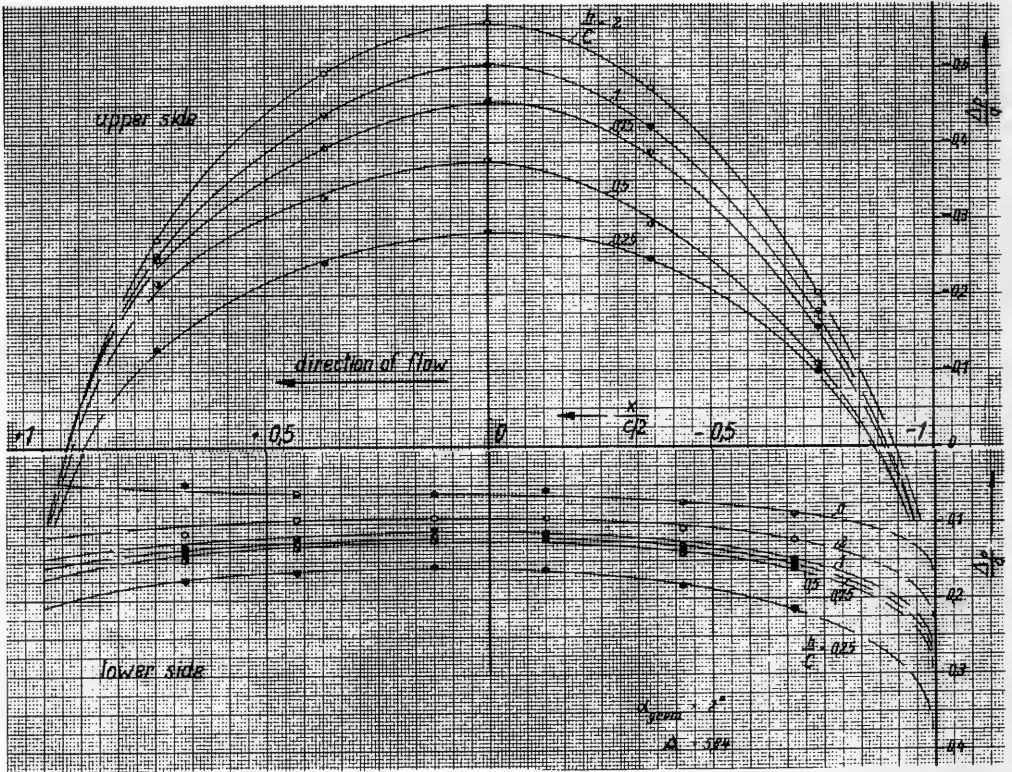at subcritical and supercritical velocity

Fig. 3. Pressure distribution for $\alpha = 2$ degrees and varying h/c ratios for the flat foil
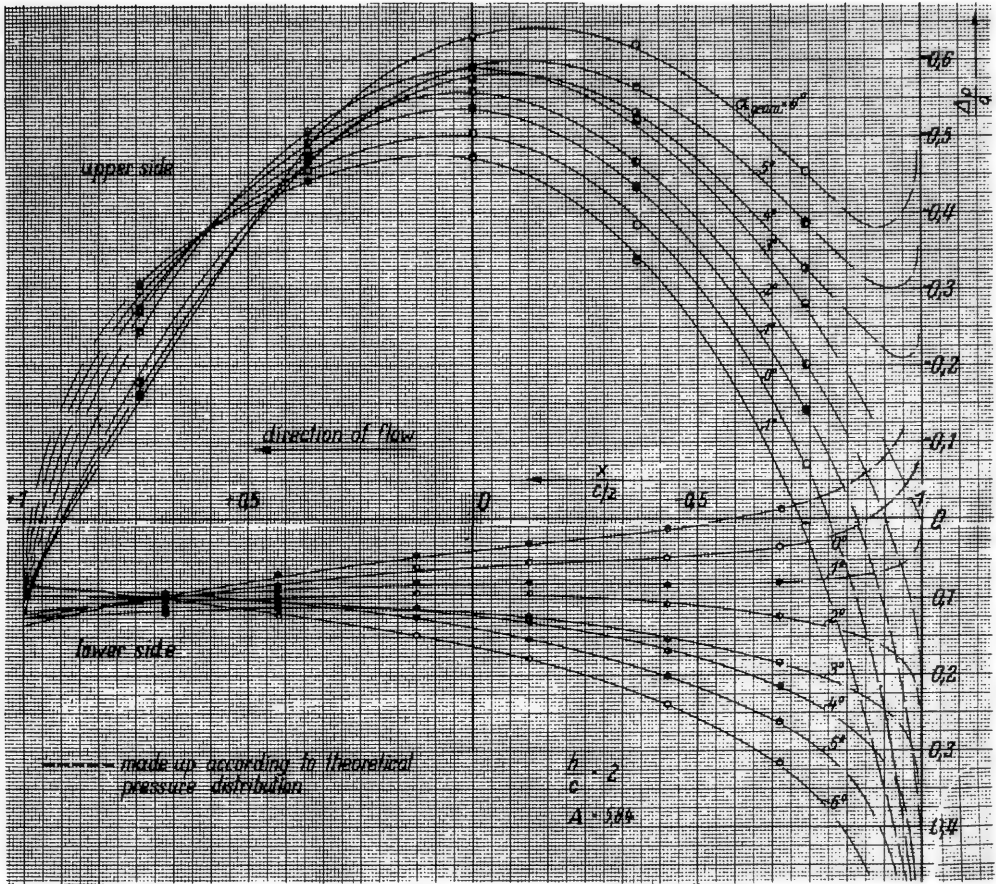
Fig. 4. Pressure distribution for $h/c = 2$ and
varying angles of attack for the flat foil

The lift distribution over the span can be seen in Fig. 5, the lift coefficients for the complete hydrofoil are shown in Fig. 6, and the components of the suction side as well as those of the pressure side and the ratio between these components are shown in Figs. 7 to 9, where the C_L values are related to conditions in great depth (infinite medium). In approaching the water surface the lift of the foil running at supercritical speed decreases nearly along a parabola with the depth of submergence, especially for $h/c < 2$, the effect of the suction side being diminished and the effect of the pressure side being augmented. This change will decrease for increasing angles of attack. It is remarkable that the drag coefficient is decreasing with the decrease of depth in spite of the increasing waves (Fig. 10).

Summing up, the results of these tests with the flat foil were as follows:

1. Owing to the proximity of the water surface an additional velocity is induced which is contrary to the direction of flow. This results in an increase of the lift component on the pressure side and in a decrease on the suction side. Due to the suction side's greater part of the total lift in the deep submerged position, a diminution of lift thus results. Owing to the minor flow velocities at both sides the profile resistance decreases.

2. Owing to the curvature of flow along the upper side the effective profile curvature is diminished. Thus the angle of zero lift will be shifted toward positive values, and the effective angle of attack and thereby the lift coefficient will become less. Relatively this influence decreases with increasing angle of attack.

3. Owing to the continual lift diminution in the range $2 > \bar{h} > 0$ a submergence stabilizing seems to be possible even for hydrofoils not piercing the water surface.

Dihedral Foil

The measured lift distribution for the dihedral foil can be seen in Fig. 11. The pressure distribution over the profile is similar to that for the flat, fully-submerged hydrofoil. The joint of the two foil halves at the keel point, as well as that between foil and struts, causes an increase of lift on the suction side, and in the first case simultaneously decreases the pressure at the lower side. When piercing the surface a diminution of the local lift occurs within the region of the surface approach in such a manner as though the results of flat parallel submerged foils had been transferred stripwise.

Figure 12 shows the lift decrease of both foils plotted versus the relative submergence. This diagram shows also the test results of Land [4], which were found at substantially higher speeds.

The lift diminution for the complete dihedral hydrofoil caused by the surface effect can be found by integration of the local values

$$C_L/C_{L_\infty}$$

within the range of $\bar{h} = 0$ to $\bar{h} = \bar{h}_{keel}$. The mean of (C_L/C_{L_∞}) amounts to approximately 0.5 for $\bar{h}_{keel} = 0.5$, to 0.8 for $\bar{h}_{keel} = 1.5$, and to 0.9 for $\bar{h}_{keel} = 5$.

Summing up, it follows from the tests with the dihedral hydrofoil that:
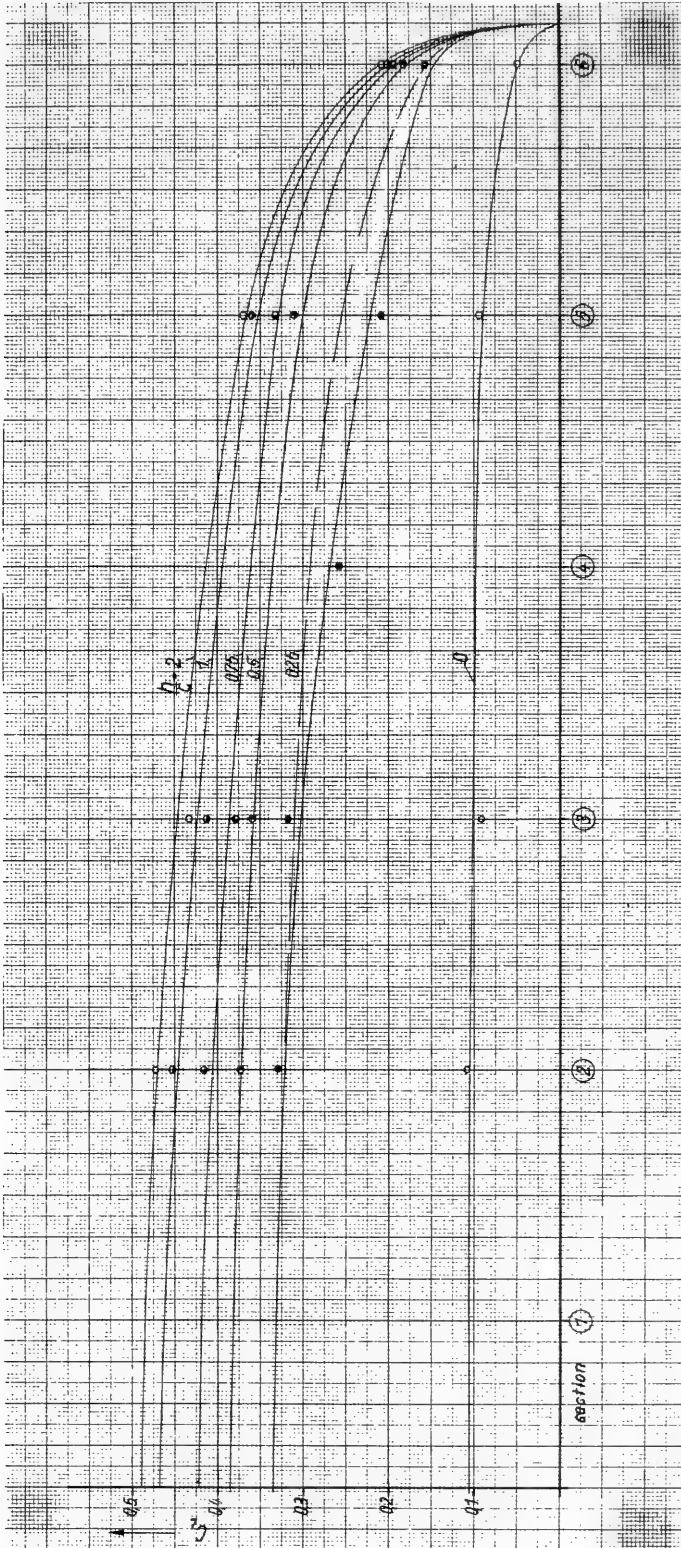
Fig. 5. Lift distribution over the span of the flat foil for varying h/c ratios
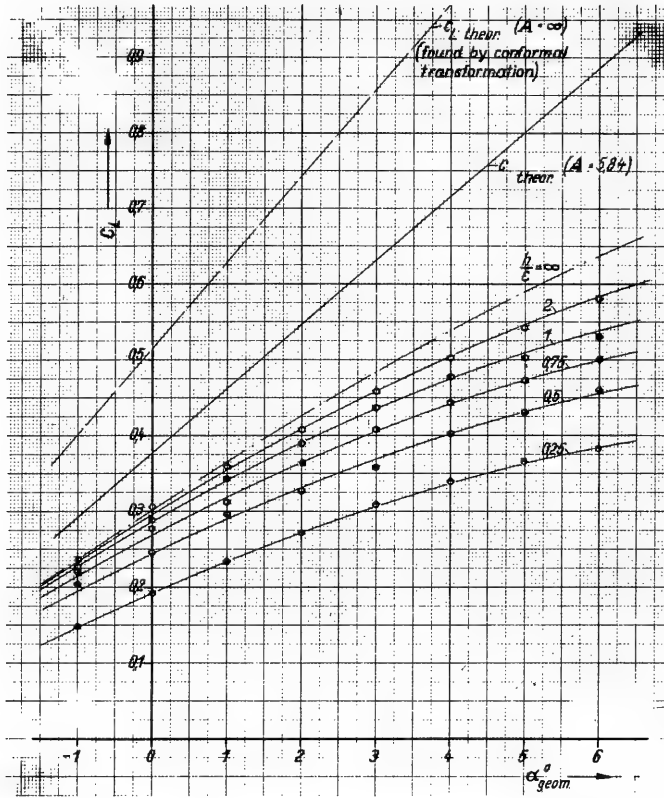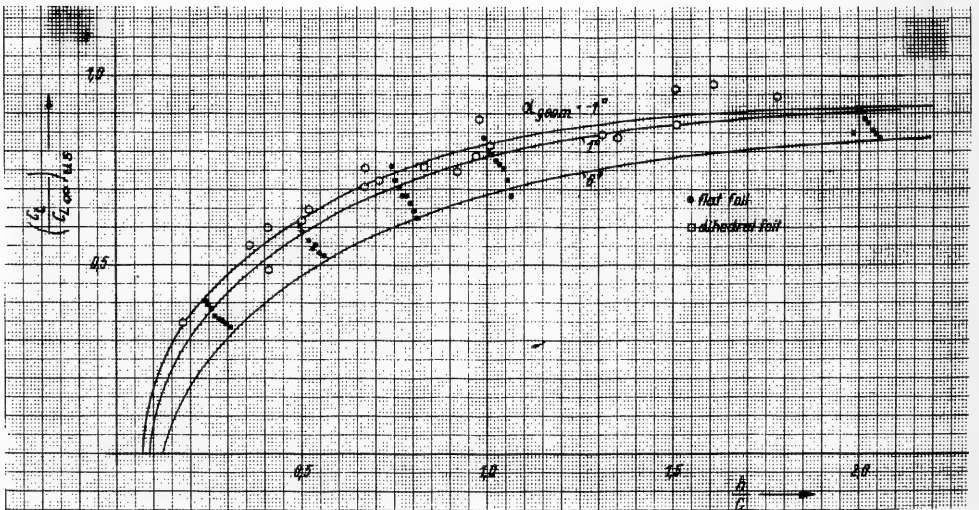
Fig. 6. Lift coefficients of the flat foil

Fig. 7. Lift coefficients of the upper sides
of the flat dihedral foils
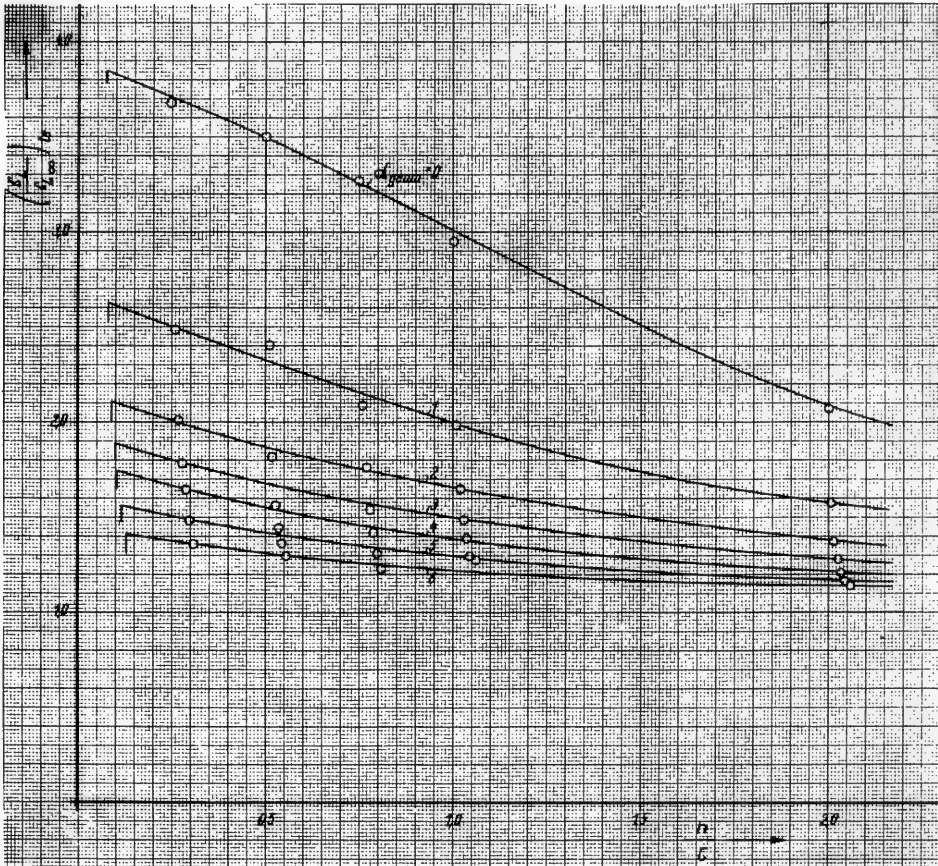
Fig. 8. Lift coefficients of the lower side of the flat foil
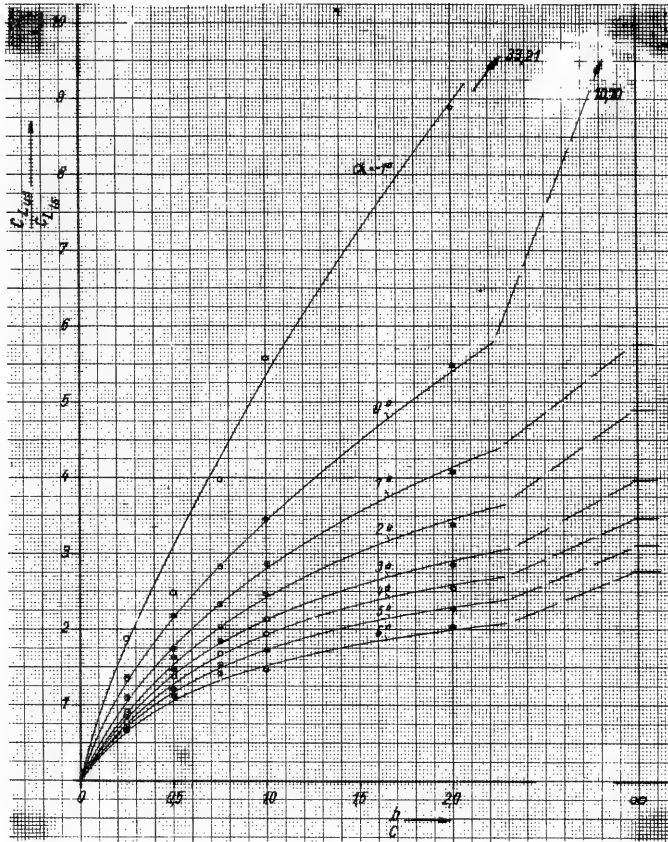
Fig. 9. Relation between lift of the upper side
and the lower side of the flat foil
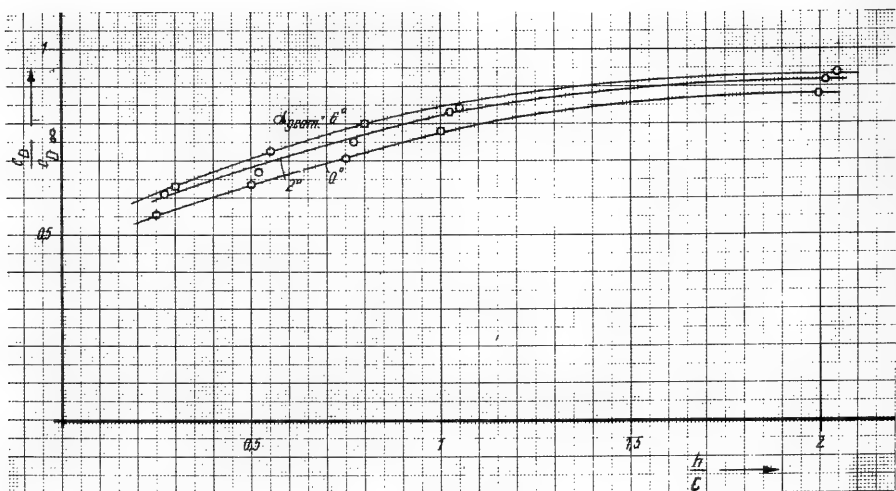
Fig. 10. Drag coefficients of the flat foil
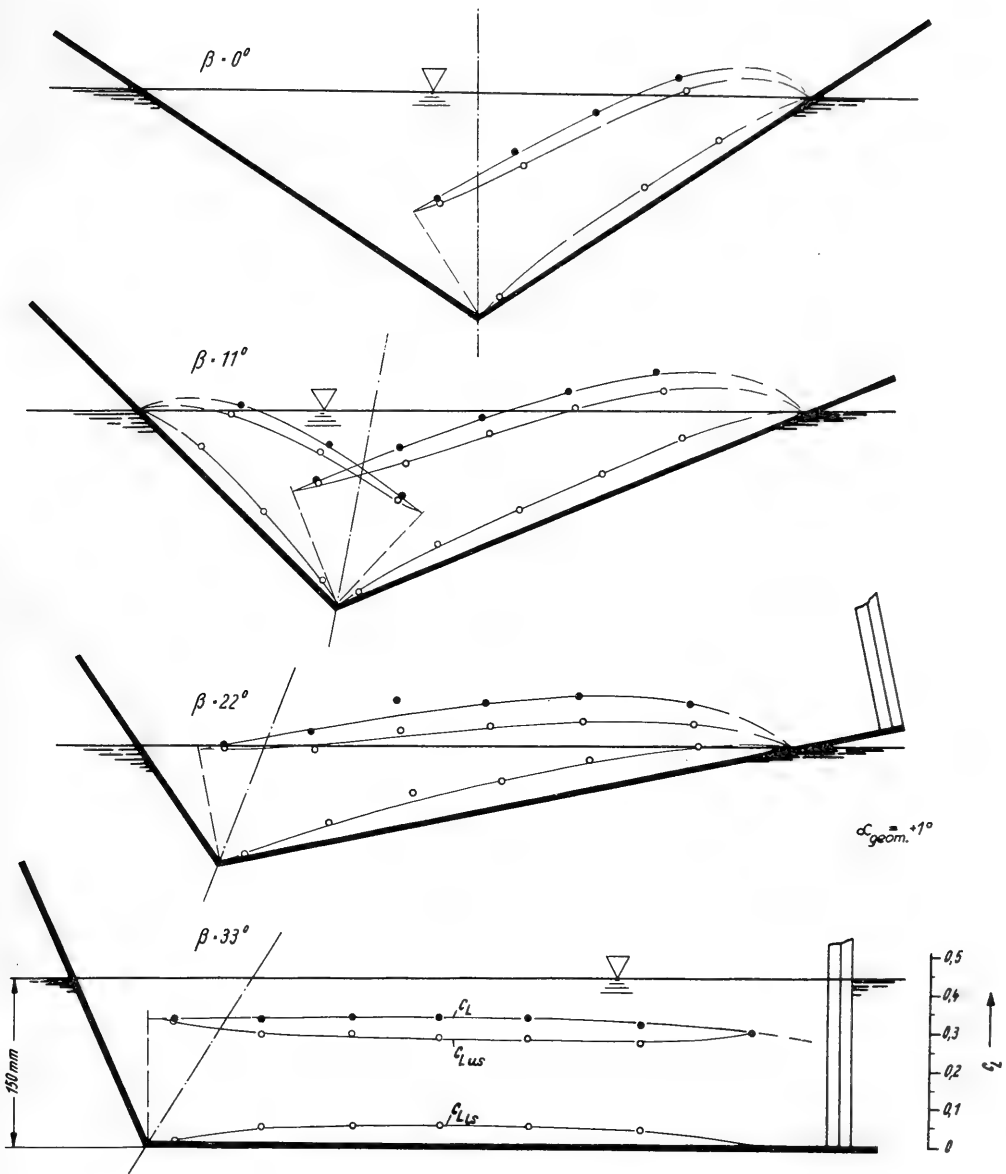
Fig. 11. Lift distribution for the dihedral foil
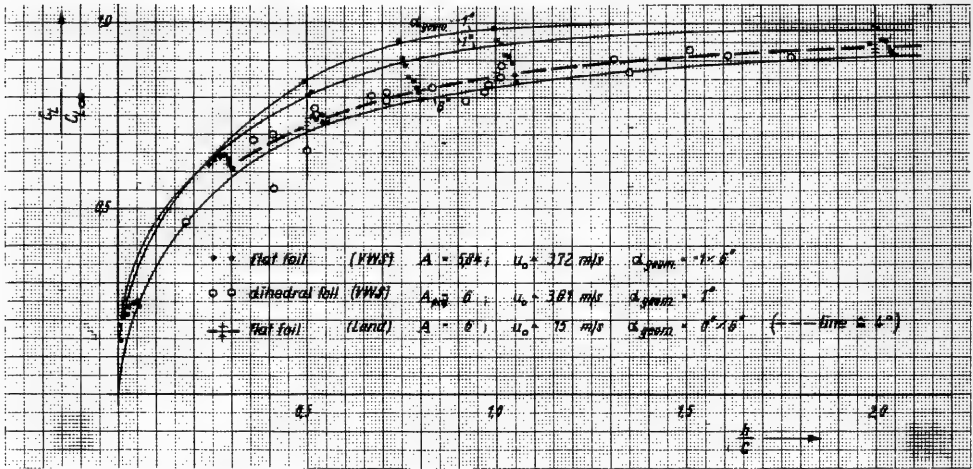
Fig. 12. Comparison of lift coefficients versus relative depth

1. The test results of fully submerged flat foils can be transferred to emerging foils by means of the strip method. The lift decrease toward the outer regions becomes also measurable for $h/c < 2$ and essential for $h/c < 1$. Enlarging the profile length in the outer regions therefore seems to be less practical since the h/c value will be smaller and the influence of the water surface will be extended to larger regions of the span. According to item 2 in the summing up for the preceding subsection, it would be better to increase the angle of attack, i.e., to distort the foil.

2. Since the strip method can be used for the rolling dihedral hydrofoil too, there is no special need for investigating the influence of the roll angle. Even for hydrofoils in a side-slip motion the measurement of the pressure distribution can be retained, for in this case only the local angles of attack are changed, the influence of which has been determined for the flat parallel submerged foil.

STATE OF FLOW EXAMINATION

If the existence of a shallow water effect could be concluded from the pressure measurement, then the transition from the subcritical to the supercritical range of the Froude depth number must be perceptible by a change of the surface deformation. Tests with a flat parallel submerged hydrofoil, extending sideways to the walls of a circulating water channel, proved that there is indeed a transition from a steady flow to a rapid flow with a hydraulic jump between. With regard to the speed increment above the foil and to the slope of the water surface connected herewith, a local Froude depth number

$$F_{h'} = \frac{u_0}{\sqrt{gh'}} \left(1 + \frac{\pi}{2} \alpha\right)^{3/2}$$

where h' denotes the minimum depth above the foil, can be defined as a barrier. The deformation corresponds to pictures shown in the publication of Parkin, Perry, and Wu [2].

Below $F_h{}' = 1$, i.e., in the subcritical speed range, the depth of submergence of any foil plays a similar part for the circulation as the water depth does for the orbital velocity of waves in shallow water. Thus correspond the C_L reduction on the upper side and the wave speed reduction

$$\frac{C_{Lh}}{C_{L\infty}} \;\hat{=}\; \frac{u_h}{u_\infty} = \sqrt{\tanh \frac{gh}{u_\infty^2}} \;\hat{=}\; \sqrt{\tanh \frac{(C_L/C_{L\infty})^2}{F_h^2}} \;.$$

Hence

$$F_h^2 \;=\; \left(\frac{C_L}{C_{L\infty}}\right)^2 \Big/ \tanh^{-1}\left(\frac{C_L}{C_{L\infty}}\right)^2$$

follows.

To be sure, this can be seen exactly only at small depths, for example for $h/c = 0.37$ as in Fig. 13. For larger depths the transition is smoothed at $F_h = 1$ and disappears gradually in the same manner as it does in deep water. Above $F_h = 2$ no dependency of the Froude depth number exists. Hydrofoil boats generally run by dynamic lift at a speed more than 25 knots and at a submergence less than 2 m. This corresponds to a smallest Froude depth number of about 3.

Summing up, the results of examination of the state of flow are as follows:

1. The hydrofoil is susceptible to the shallow water effect. For operating conditions of hydrofoil boats the flow pattern is a supercritical one. For theoretical considerations by analogy from wave theory, rapid flow is presumed in the direct neighborhood of the hydrofoil in place of orbital motion for waves.

2. For individual hydrofoils no critical speed barrier can exist as it does for displacement ships in shallow water, given by speed and depth. But for the complete craft fitted with several hydrofoils such a barrier, of course, can exist, since the wave formation behind the hydraulic jump follows the Froude depth number given by the water depth and changes the flow against the next hydrofoil in line.

3. The only significant quantity for the influence of the water surface on the circulation around a hydrofoil in the supercritical range is the relative depth of submergence of the foil element, $\bar{h} = h/c$. It is independent of the configuration and speed of the hydrofoil.

FLOW FORCES MEASUREMENT

In 1941 six component tests on hydrofoils already had been made in the circulating water tunnel of the firm Gebr. Sachsenberg AG., Berlin, under the direction of G. Weinblum. The results were published at that time only for a restricted number of persons.

In one case a model of a dihedral foil with a constant circle segment profile of a constant length $\ell = 96$ mm and a thickness $t = 6.4$ mm was used [6]. The dihedral angle could
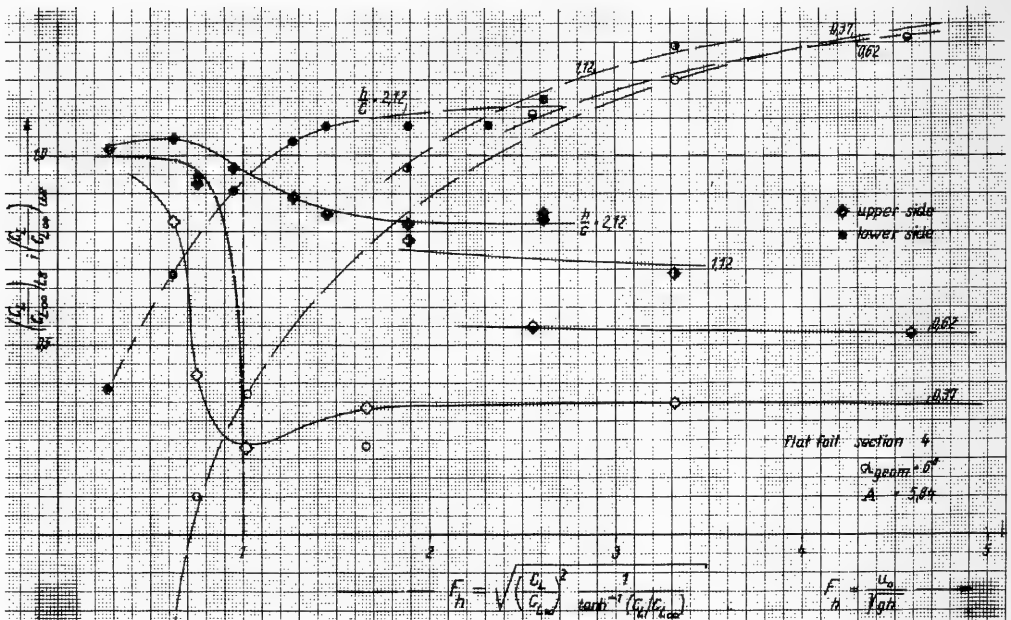
Fig. 13. Local lift coefficients of the upper and lower sides of
the flat foil for different h/c ratios

be changed between 15 degrees and 50 degrees. Variations of span from 200 to 600 mm, of roll angle from 0 to 10 degrees, and of angle of attack from –5 to +7 degrees were made. All the values of C_L, C_D, and C_{M_x} were measured for a constant speed of 4 m/sec. For example such diagrams could be drawn as can be seen in Figs. 14 and 15 for lift and drag, or in Figs. 16 and 17 for the roll moment. The results for the mean span of 400 mm were $C_{L_{max}} =$ 0.36, $dC_L/d\alpha = 2.72$ to 3.14 related to the effective angle of attack, $\alpha(C_L = 0) = -4.5$ degrees, $C_{D_{min}} = 0.015$, and $\varepsilon_{min} = 0.07$.

A comparison of the results for the different variations showed with regard to lift, drag, drag-lift ratio, and lateral stability:

1. The aspect ratio $A = b^2/F$ possibly should be chosen not less than 4. Raising it beyond 5 will give but little additional profit.

2. As long as the proximity of the surface does not influence the complete foil, i.e., as long as $\bar{h}_{max} > 1$, the $dC_{mx}/d\alpha$ value will increase for decreasing dihedral angles, for $\bar{h}_{max} < 1$ the ratio diminishes rapidly. For the aspect ratio 4.15 the maximum relative depth is 1 for a dihedral angle of 27 degrees. The optimal dihedral angle for this aspect ratio is around 30 degrees.
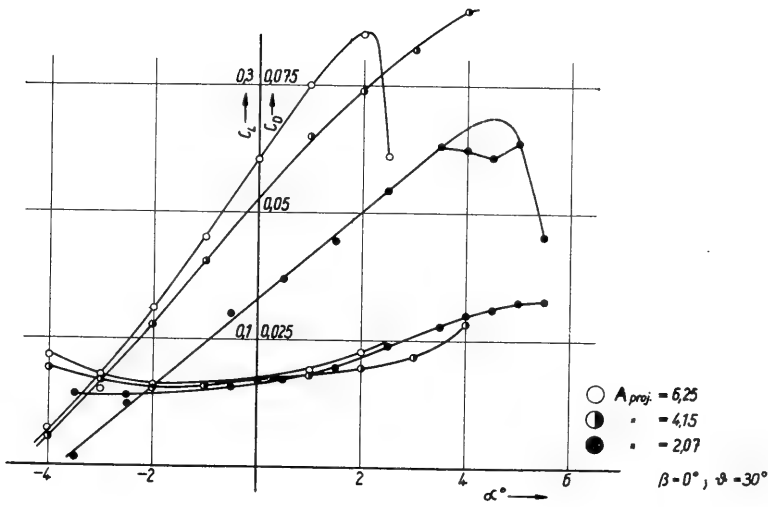
Fig. 14. Influence of the aspect ratio on the lift coefficients (upper curves)
and drag coefficients (lower curves) of a dihedral foil
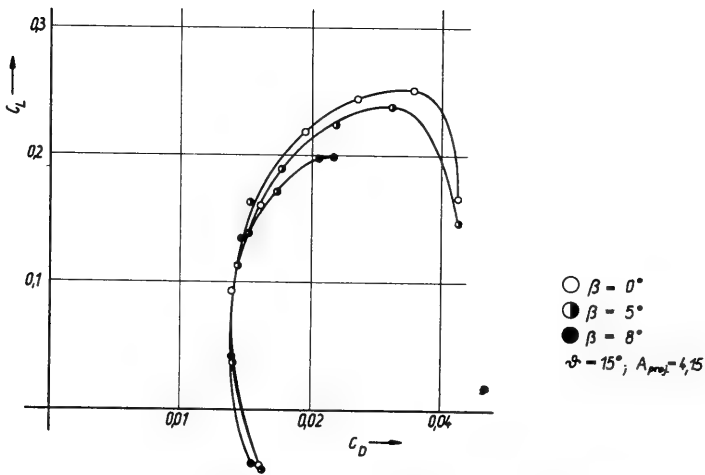
Fig. 15. Influence of the rolling angle on a dihedral foil
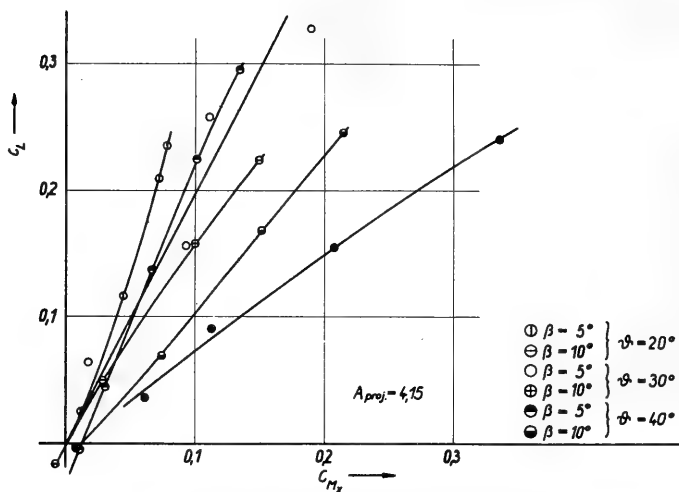
Fig. 16. Influence of the dihedral and rolling angles
on the rolling moment
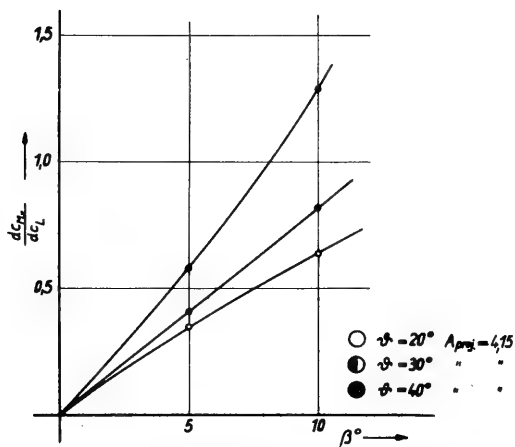
Fig. 17. Lateral stability of dihedral foils

3. By rolling, the flow, being symmetrical before, becomes nonsymmetrical. When the span is kept equal the aspect ratio and the angle of inclination between foil and water surface increase for one part as much as they decrease for the other. Indeed rolling has the same effect as superposing the influences of aspect ratio and dihedral angle. At small roll angles C_L and C_D are only slightly changed. At greater angles lift and ascent of lift drop more and more and the resistance increases.

The results of this first test series were complemented in 1958 by six component measurements in the circulating water tunnel of the VWS [7]. The dihedral hydrofoil model already described for the measurements of the pressure distribution with a fixed dihedral angle ϑ = 33 degrees was used. The flow speed was about 2 m/sec. The influence of rolling and sideslipping in particular were examined.

First of all Fig. 18 shows the geometrical variation of the effective angle of attack of the pressure-side chord along with the roll angle and with the sideslip angle. For instance if such a hydrofoil is running straight-on with α = 1 degree, then for the profiles, 0.8 degree is the effective angle. If there does exist a sideslip angle of γ = 10 degrees toward starboard — for instance when turning to port — the effective angle of attack will increase on the starboard side to +6 degrees while on the port side it will decrease to –4 degrees. If there is an additional roll angle of about β = +20 degrees toward the center of the turning circle, then this angle of attack difference will be increased to +8 degrees and –7 degrees respectively. For a rolling angle of β = –20 degrees to the outside, a diminution of the effective angles of attack to +2.5 degrees and –1.5 degrees respectively will result. An augmentation of the sideslip angle causes a nearly linear augmentation of these angles of attack.

Since therefore for hydrofoil boats under service conditions the angle of attack can spread over a very wide range, the course of the coefficients for lift, drag, and pitching moment has been measured for a 45-degree variation of the angle of attack (Fig. 19). Here the flow separated at about +8 degrees on the upper side and at about –10 degrees on the lower side. The lift coefficient will increase, of course, after such a sudden breakdown but the drag-lift ratio $\varepsilon = C_D/C_L$ then will be three times as high as it was before (Fig. 20). The fact that relatively high negative lift values can be obtained is of no importance for practice. In turning circles for the inner side, i.e., on the port side when turning to port, a decrease of lift may, of course, be desired, even down to zero. But it should not reach negative values, since an adequate raising of lift on the outer side beyond twice the value as before seems to be unlikely considering the augmentation of drag, the diminution of speed, and the smaller submerged area of the outer foil, which is reduced by rolling. For running with a following sea — a situation when negative angles of attack will occur easily — such a negative lift also will be dangerous even if it occurs only for a short period.

Figures 21 and 22 demonstrate the variation of forces and moments versus the sideslip angle and the roll angle. The coefficients for lift, drag, and roll moment are practically constant; the coefficient for the yawing moment is insignificant. The coefficients for lateral force and roll moment increase linearly from zero upward with increasing sideslip angle and roll angle. For instance a sideslip of +8 degrees toward starboard causes a lateral force toward port of eight times the value brought about by –8 degrees rolling toward starboard; the roll moment due to a sideslip is 70 percent higher. Both roll moments relative to the keel point are stabilizing, i.e., any rolling will reduce itself and a sideslip will produce a rolling toward the inside of the curve.

Simultaneous systematic variations of the angles of attack, of rolling, and of sideslip produced only unessential differences relative to drag and lateral forces compared with the separate variations. But the situation deteriorated relative to the lift. For a sideslip angle around 10 degrees the flow separated throughout. Lift then broke down much more completely as the additional rolling increased (Fig. 23).

Summing up, it can be stated:

1. The range of the angle of attack of the profiles of a dihedral foil with a circle segment characteristic which can be utilized is about –4 degrees < α < +6 degrees.
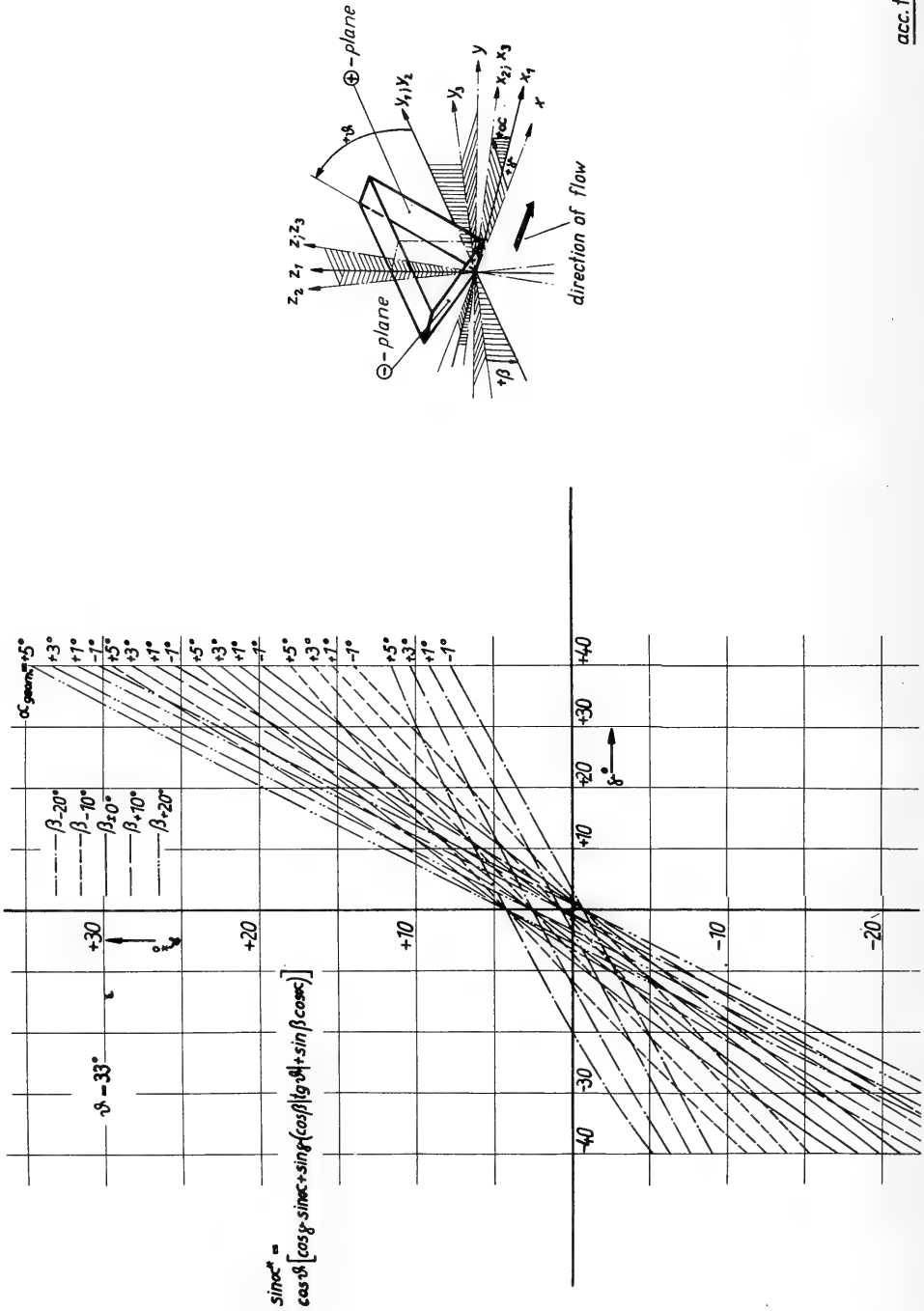
Fig. 18.   Effective angle of attack of the chord
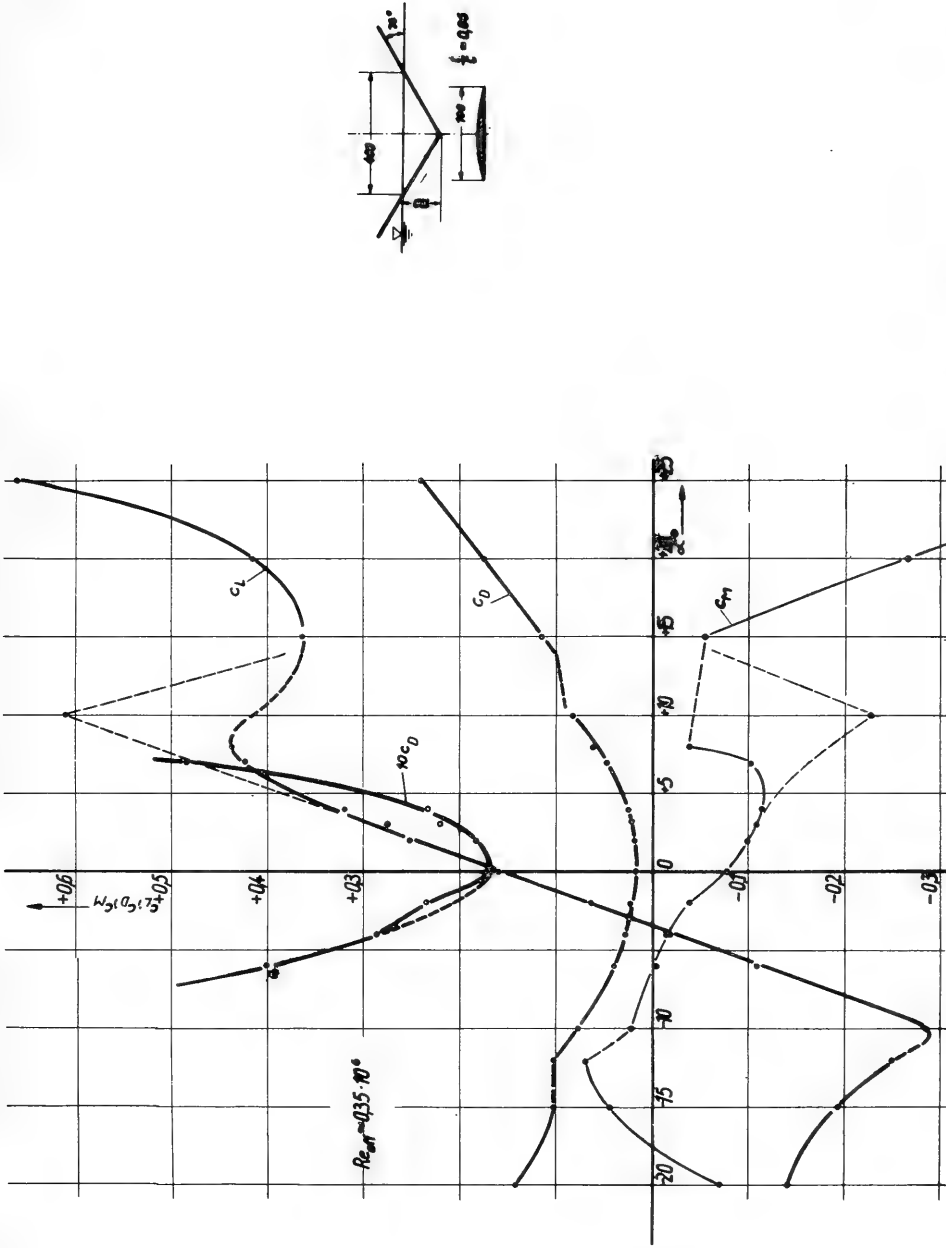
Fig. 19. Lift, drag, and pitching moment for a dihedral foil in a symmetrical flow
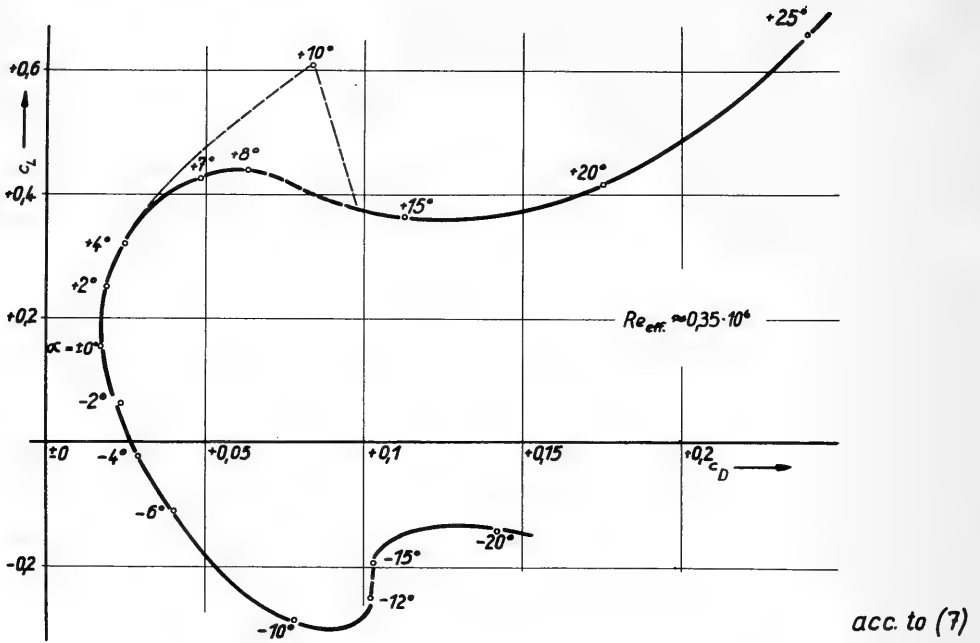
Fig. 20.   Polar of a dihedral foil in a symmetrical flow

2. Lateral stabilizing can be brought about much more effectively by the moment due to sideslip than by that due to rolling. While the rolling is less dangerous for the lift, a range of only +8 degrees can be admitted for a sideslip angle.

3. Additional rolling of a dihedral foil in a sideslip motion acting in the same sense as the moment due to sideslip will raise the risk of a lift breakdown.

EXAMINATION OF ROTARY INSTABILITY

With a model of a dihedral foil the relation between rolling and sideslip has been tested thoroughly in a small VWS tank using a special device (Fig. 24). For a constant lift, the model at u_o = 4 m/sec could immerse freely. Relative to rotary motions both about the longitudinal and the vertical axis the model could either be fixed or set free.

The sideslip angle was measured each time when the lift collapsed. For free rolling, sideslip angles up to 11 degrees could be brought about; rolling angles then amounted to about 10 degrees acting in the same direction as the moment due to the sideslip. Enlarging the sideslip angle to 11 degrees caused a lift breakdown at the foil which had been more emerging and a rotary instability was the result. This procedure is not reversible, i.e., the sideslip angle has to be totally reduced to regain the flow and to start with sideslip again. For a fixed rolling of 20 degrees, sideslip angles of 16 degrees and 9 degrees could be obtained; the smaller sideslip angle is conjugated to rolling in the same sense as the moment due to sideslip, the other one is conjugated to rolling in the opposite direction.
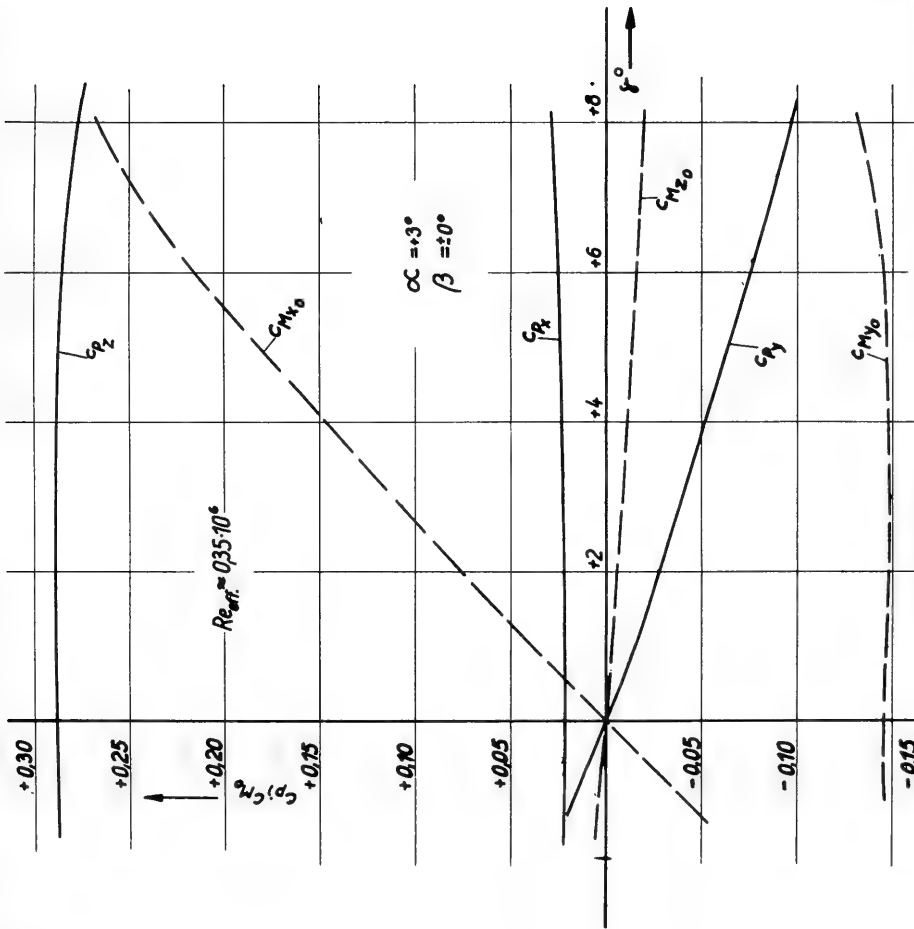
Fig. 21. Forces and moments for small sideslip angles.
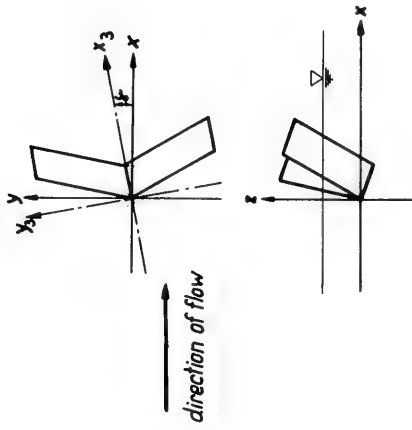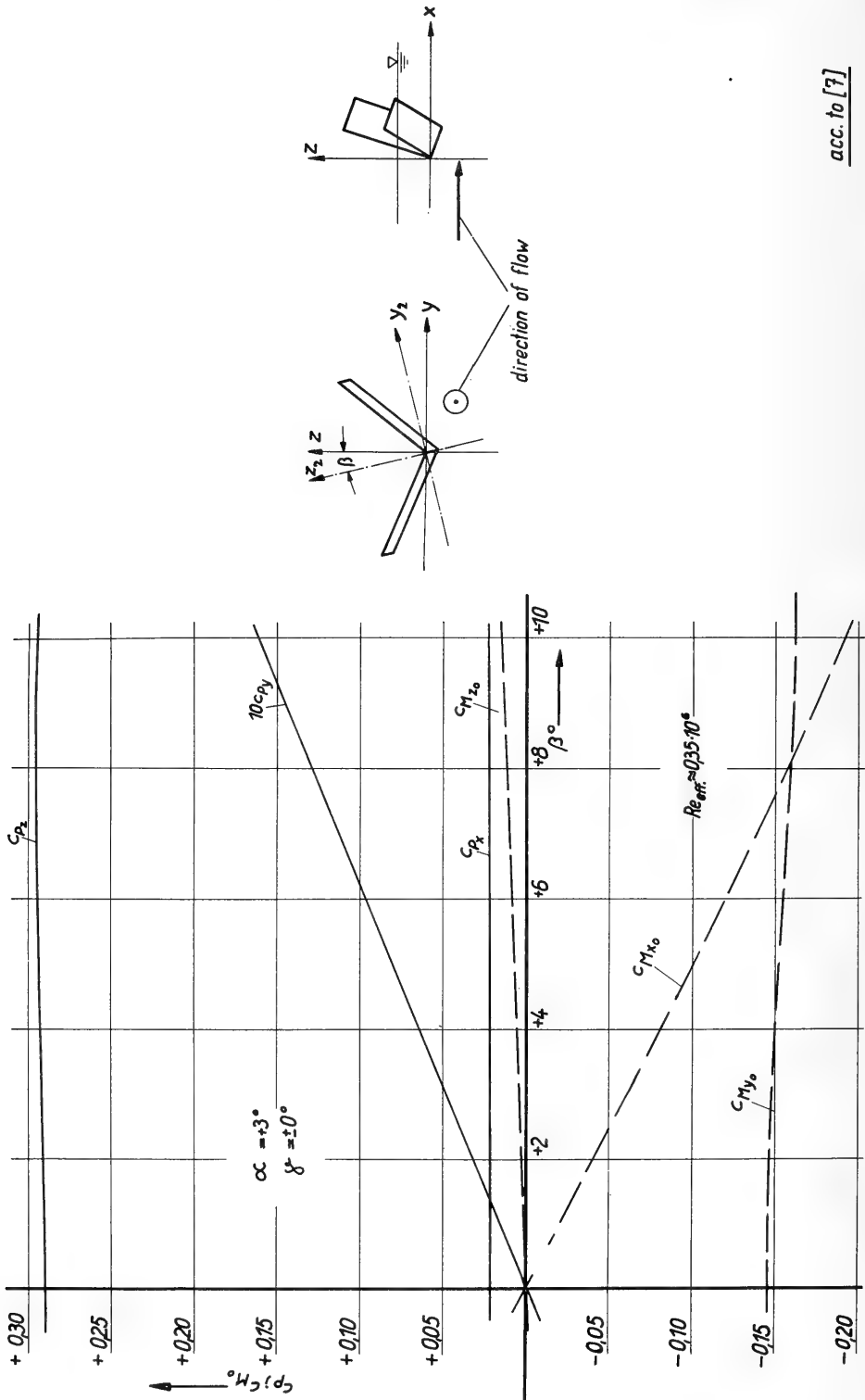
Fig. 22. Forces and moments for small roll angles
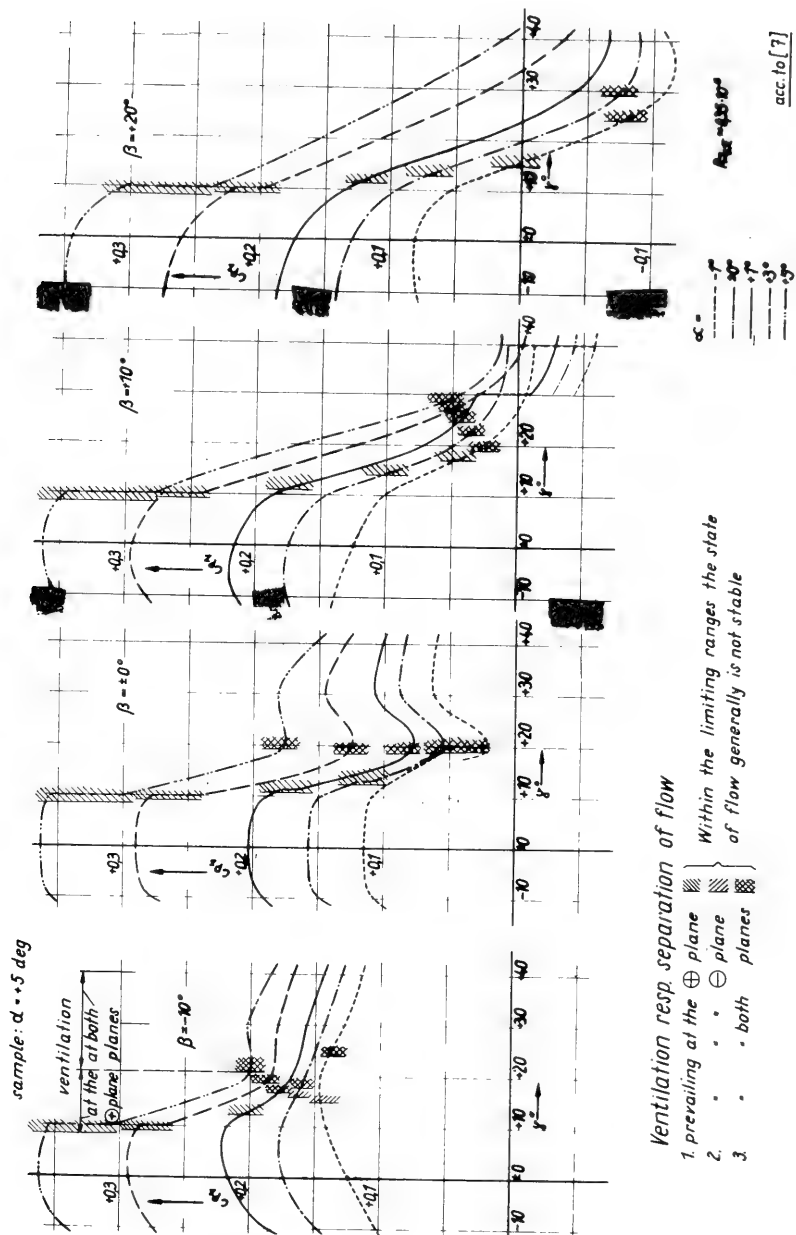
Fig. 23. Dimensionless lift C_{P_x}
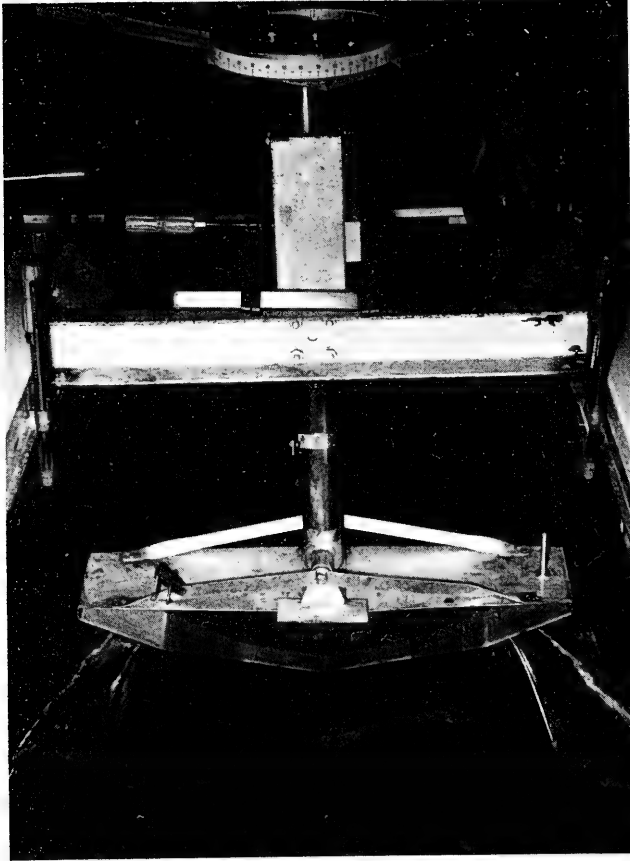
Fig. 24.   Arrangement for rotary instability tests
of a dihedral foil

To sum up:

1. Rolling into the inside of the curve for hydrofoil boats as well as for planing craft
and airplanes such that the principal plane coincides with the apparent perpendicular is
more disadvantageous relative to security than is rolling into the outside of the curve as
occurs with displacement craft.

2. Hydrofoils already rolling to the outside at the beginning of the curve will run a
tighter circle (with higher sideslip angles) than those rolling to the inside.

3. The preceding result contradicts the conception that in a circle a foil rolling to the
outside will stall easier because of the higher load. Therefore the whole situation needs a
thorough investigation.

THEORETICAL CONSIDERATIONS

The velocity field of a hydrofoil of great span running at the depth $\bar{h} = h/c = h^*/2$ beneath the undisturbed water surface in deep water can be represented by the well-known relations (for instance, Ref. 8)

$$\frac{u(x,z)}{u_0} = 1 + \frac{u_1(x,z)}{u_0}$$

$$= 1 + \frac{1}{2\pi} \int_{-1}^{+1} f(\xi) \frac{z + h^*}{(x-\xi)^2 + (z+h^*)^2} d\xi$$

$$+ \frac{1}{2\pi} \int_{-1}^{+1} f(\xi) \frac{z - h^*}{(x-\xi)^2 + (z-h^*)^2} d\xi \tag{1}$$

$$+ \frac{g}{u_0^2} \exp\left[-\frac{g}{u_0^2}(h^* - z)\right] \int_{-1}^{+1} f(\xi) \, G_1\left(\frac{g}{u_0^2}, x, \xi, z, h^*\right) d\xi \tag{1a}$$

$$\frac{w(x,z)}{u_0} = \frac{w_1(x,z)}{u_0}$$

$$= -\frac{1}{2\pi} \int_{-1}^{+1} f(\xi) \frac{x - \xi}{(x-\xi)^2 + (z+h^*)^2} d\xi$$

$$- \frac{1}{2\pi} \int_{-1}^{+1} f(\xi) \frac{x - \xi}{(x-\xi)^2 + (z-h^*)^2} d\xi$$

$$- \frac{g}{u_0^2} \exp\left(-\frac{g}{u_0^2}[h^* - z]\right) \int_{-1}^{+1} f(\xi) \, G_2\left(\frac{g}{u_0^2}, x, \xi, z, h^*\right) d\xi \tag{1b}$$

where u_o denotes the running speed and $f(\xi)$ the pressure distribution over the profile length. At the free surface the velocity field fulfils the boundary condition resulting from the linearized Bernoulli law

$$\frac{u_0^2}{g} \frac{\partial u_1(x,0)}{\partial x} + w_1(x,0) = 0. \tag{2}$$

The shape of the surface results as well from the Bernoulli law by linearization to

$$z_w(x) = -\frac{u_0 u_1(x,0)}{g} \; . \tag{3}$$

The pressure distribution at the profile, i.e., the function $f(\xi)$ with $f(x)$ being the meanline of the profile, can be found from the relation

$$u(x,-h^*) \; f'(x) = w(x,-h^*) \tag{4}$$

with u and w taken from Eq. (1).

The boundary condition (2) and hence the velocity field (1) is valid for smooth water above the foil as well as ahead and aft, i.e., for a condition which permits the existence of deep water waves.

Within the technically interesting range of the Froude depth number $F_h = u_o \sqrt{gh}$ there is as shown by experimental investigations rapid flow prevailing above the foil with the exception of the direct neighborhood of the leading edge. For this case the boundary condition (2) and therewith the terms for the velocity field (1) are no longer valid. Behind the foil, with the exception of the direct neighborhood of the trailing edge, the flow is tranquil again, for here the physical suppositions for rapid flow are missing due to the water presumed as being deep. For this range Eqs. (1) and (2) are valid again.

The consequence of the rapid flow is that the water surface above the foil remains smooth, while for small distances between foil and water surface the water flows parallel to the upper side of the profile, whereby the well-known apparent camber reduction results. That means above the foil there is, dependent on the Froude depth number, at relative low speeds already a state of flow which will occur behind the foil only at considerably higher speeds. Therefore for the range of the foil $(-1 > x > +1)$ in Eqs. (1) the terms containing g/u_o^2 may equal 0. The equations simplify to

$$\frac{u(x,z)}{u_0} = 1 + \frac{1}{2\pi} \int_{-1}^{+1} f(\xi) \; \frac{(z+h^*) \; d\xi}{(x-\xi)^2 + (z+h^*)^2}$$

$$+ \frac{1}{2\pi} \int_{-1}^{+1} f(\xi) \; \frac{(z-h^*) \; d\xi}{(x-\xi)^2 + (z-h^*)^2} \tag{5a}$$

$$\frac{w(x,z)}{u_0} = -\frac{1}{2\pi} \int_{-1}^{+1} f(\xi) \; \frac{(x-\xi) \; d\xi}{(x-\xi)^2 + (z+h^*)^2}$$

$$- \frac{1}{2\pi} \int_{-1}^{+1} f(\xi) \; \frac{(x-\xi) \; d\xi}{(x-\xi)^2 + (z-h^*)^2} \; . \tag{5b}$$

At the surface $(z = 0)$ the additional velocity u_1 in Eqs. (5) disappears, so that in the case of rapid flow at the upper side of the profile the boundary condition

$$\frac{u(x,0)}{u_0} = 1 \tag{6}$$

will be satisfied.

By inserting the velocity components (5) into (4) the following integral equation for determining the pressure distribution $f(\xi)$ results:

$$-2\pi f'(x) = \int_{-1}^{+1} f(\xi) \left[\frac{1}{x - \xi} + \frac{(x - \xi) - 2h^* f'(x)}{(x - \xi)^2 + 4h^{*2}} \right] d\xi . \tag{7}$$

The integral

$$\int_{-1}^{+1} f(\xi) \frac{d\xi}{x - \xi}$$

is the known relation for the downwash of a thin profile in an infinite medium. The part of the relation (7) dependent on the depth of submergence h^* represents the influence of the surface, which results in a diminution of the effective angle of incidence for the profile.

For the solution of Eq. (7) the following function with unknown coefficients will be chosen:

$$f(\xi) = 2a_0 \sqrt{\frac{1 - \xi}{1 + \xi}} + 4a_1 \sqrt{1 - \xi^2} + 4a_2 \xi \sqrt{1 - \xi^2} . \tag{8}$$

The coefficients a_n will be found by complying with Eq. (7) for three points of the chord. For these points $x = \pm c/4$ and $x = \pm 0$ may be chosen. By means of the a_n, which are a function of h^*, the lift of the profile follows from the known relation

$$C_L \equiv C_L(h^*) = 2\pi \left[a_0(h^*) + a_1(h^*) \right] . \tag{9}$$

If the distance h^* is considerable, i.e., if the profile is deeply submerged, it then follows from (7) that

$$-2\pi f'(x) = \int_{-1}^{+1} f(\xi) \frac{d\xi}{x - \xi} , \tag{7a}$$

that is, the Ackermann-Birnbaum integral equation for evaluating the pressure distribution of thin profiles in infinite flow. If the distance h^* disappears, i.e., if the profile runs at the surface, it then follows from (7) that

$$-\pi f'(x) = \int_{-1}^{+1} f(\xi) \frac{d\xi}{x - \xi} . \tag{7b}$$

The lift then has only one-half the magnitude it has in great depth; that means in this case only the lift of the lower side is effective.

Now a curved profile may be considered, for instance a circle segment profile with camber m and angle of incidence α_{geom} of the chord. For this the contour of the chord is given by

$$f(x) = f_0 x + f_1 x^2 . \tag{10}$$

Then

$$f'(x) = f_0 + 2f_1 x \tag{11}$$

where f_0 and f_1 may be of small values:

$$f_0 = -\alpha_{geom}$$

$$f_1 = -2m .$$

For this case Eq. (1) can be written

$$-2\pi' f_0 = \int_{-1}^{+1} f(\xi) \left[\frac{1}{x-\xi} + \frac{(x-\xi) - 2h^* f_0}{(x-\xi)^2 + 4h^{*2}} \right] d\xi \tag{12a}$$

$$-4\pi' f_1 x = \int_{-1}^{+1} f(\xi) \left[\frac{1}{x-\xi} + \frac{(x-\xi) - 4h^* f_1 x}{(x-\xi)^2 + 4h^{*2}} \right] d\xi . \tag{12b}$$

Equation (12a) gives the lift of a flat plate,

$$C_{L_0}(h^*) = 2\pi \left[a_{00}(h^*) + a_{10}(h^*) \right]$$

and Eq. (12b) gives the additional lift produced by the camber,

$$C_{L_1}(h^*) = 2\pi \left[a_{01}(h^*) + a_{11}(h^*) \right] .$$

The total lift then amounts to

$$C_L(h^*) = C_{L_0}(h^*) + C_{L_1}(h^*)$$

and is shown in Fig. 25 for a flat plate as well as for a circle segment profile.

For the profile approaching the surface an apparent camber reduction at the upper side occurs whereby the lift of the profile, already reduced by the proximity of the surface, will be reduced further. In the actual case of a circle segment profile the lower side is flat; it is therefore equal to the lower side of a flat plate and delivers a lift taken as independent of the depth h^*:
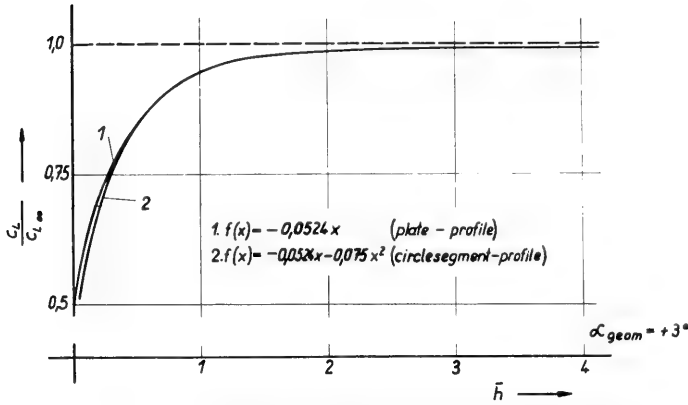
Fig. 25. Decrease of lift near the surface without regard
to the apparent camber reduction

$$C_L(h^*)\Big|_{\ell s} = C_{L_0}(\infty)\Big|_{\ell s} = 2\pi \frac{a_{00}(\infty)}{2} , \qquad (13)$$

$$\frac{C_L(h^*)}{C_L(\infty)}\Big|_{\ell s} = 1 .$$

The lift of the upper side can be written

$$C_L(h^*)\Big|_{us} = C_{L_0}(h^*)\Big|_{us} + C_{L_1}(h^*)\Big|_{us}$$

$$= 2\pi \left\{ a_{00}(h^*) - \frac{a_{00}(\infty)}{2} + a_{10}(h^*) \right.$$

$$\left. + \sigma\left(\frac{h^*}{2}\right) \left[a_{01}(h^*) + a_{11}(h^*) \right] \right\} , \qquad (14)$$

$$\frac{C_L(h^*)}{C_L(\infty)}\Big|_{us} = \frac{1}{0,5\, a_{00}(\infty) + a_{11}(\infty)} \left\{ a_{00}(h^*) - \frac{a_{00}(\infty)}{2} + a_{10}(h^*) \right.$$

$$\left. + \sigma\left(\frac{h^*}{2}\right) \left[a_{01}(h^*) + a_{11}(h^*) \right] \right\}$$

where $\sigma(h^*/2)$ stands the apparent camber reduction. The total lift of the profile then
amounts to

$$C_L(h^*) = C_L(h^*)\Big|_{us} + C_L(h^*)\Big|_{ls}$$

$$= 2\pi\left\{a_{00}(h^*) + a_{10}(h^*) + \sigma\left(\frac{h^*}{2}\right)\left[a_{01}(h^*) + a_{11}(h^*)\right]\right\} , \qquad (15)$$

$$\frac{C_L(h^*)}{C_L(\infty)} = \frac{a_{00}(h^*) + a_{10}(h^*) + \sigma\left(\dfrac{h^*}{2}\right)\left[a_{01}(h^*) + a_{11}(h^*)\right]}{a_{00}(\infty) + a_{11}(\infty)}$$

where

$$a_{00}(\infty) = \alpha = -f_0$$

$$a_{11}(\infty) = 2m = -f_1 .$$

In Eq. (15) only the factor $\sigma(h^*/2)$ is unknown. It can be calculated theoretically, but then separate mathematical operations will be necessary. By experiment this camber reduction factor can be found easily from the reduction of the no-lift angle occurring in an approach to the surface

$$\sigma \frac{h^*}{2} \equiv \sigma(\bar{h}) = \frac{\alpha_0(\bar{h})}{\alpha_0(\infty)} = \frac{m(\bar{h})}{m(\infty)} , \qquad (16)$$

where independence of the shape of the profile can be supposed. Figure (26) shows the factor $\sigma(\bar{h})$ as found by experiments. With the aid of this factor the lift reduction of the profile can be found as a function of the depth $\bar{h}$ from Eq. (15) as shown in Fig. 27.

    Figure (28) shows the calculated lift of the upper side and of the lower side of the considered profile dependent on the depth $\bar{h}$, as well as the corresponding values taken by measurement. The actual increase of lift of the lower side and the decrease of lift of the upper
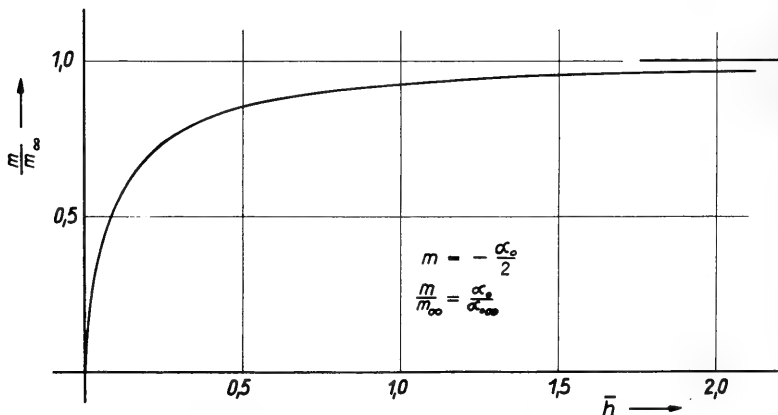
Fig. 26. Apparent camber reduction of a circle segment profile
as found experimentally
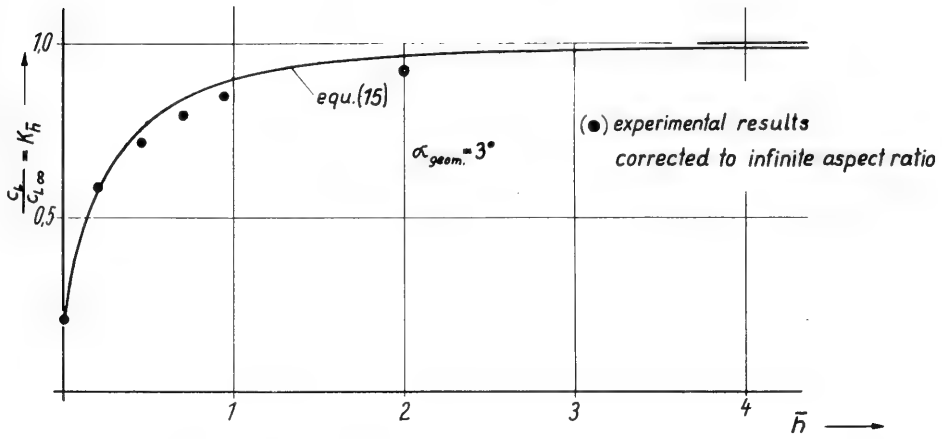
Fig. 27. Decrease of lift for a circle segment profile near the free surface
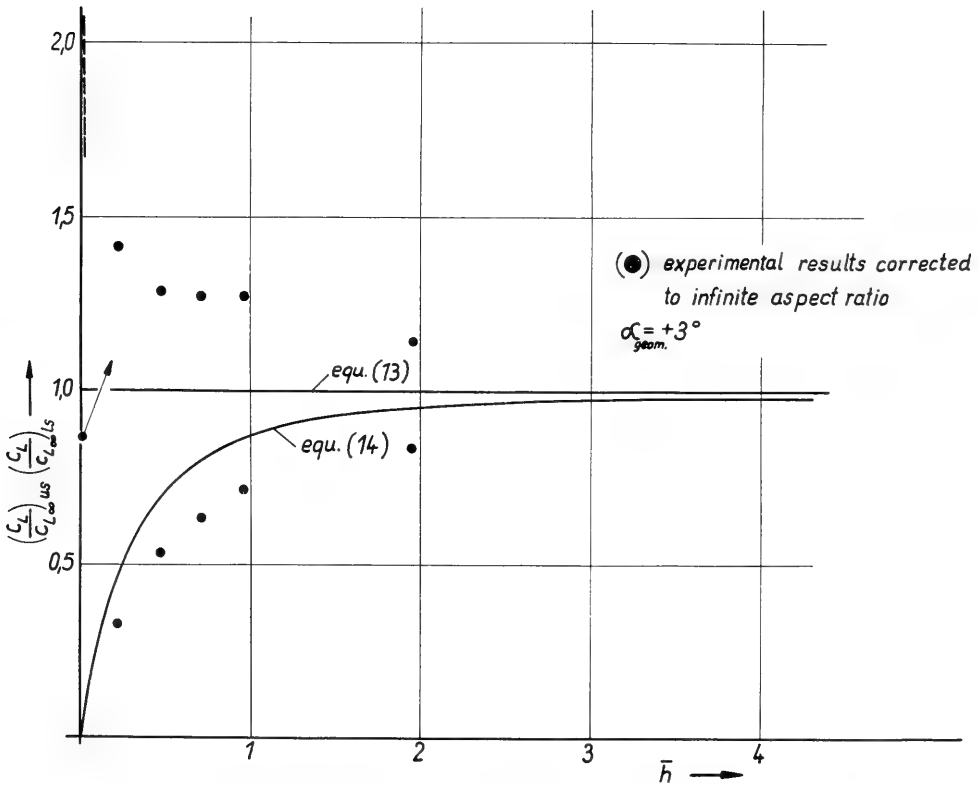
Fig. 28. Lift coefficients of the upper and lower sides of a circle segment profile.

side, being higher than calculated, cannot be represented by these simple formulas. But since these influences compensate each other for the most part, the calculated total lift nearly equals the measured lift. For calculating the total lift, therefore, this method may be used as an approximation.

INTRODUCTION OF THE MAIN PARAMETERS

Laying out foils for hydrofoil boats needs not only information about the decrease of lift due to the free surface but also about the influence of the aspect ratio and eventually of the dihedral angle. The above-mentioned measurements proved that for supercritical flow above the foils the spanwise distribution of lift is only slightly dependent on the depth $\bar{h}$. For supercritical flow, therefore, it is possible to consider the influences of the surface and of the aspect ratio separately without being greatly mistaken. Moreover this gives the possibility of calculating the lift decrease of dihedral foils.

The main parameters will be introduced now. The influence of the finite aspect ratio will be covered by the relation found by Weinig [9] by means of the cascade theory:

$$\frac{dC_L}{d\alpha} = K_A \ 2\pi \ . \tag{17}$$

The factor K_A is shown in Fig. 29. The aspect ratio of a dihedral foil has to be taken as the wetted aspect ratio, i.e.,
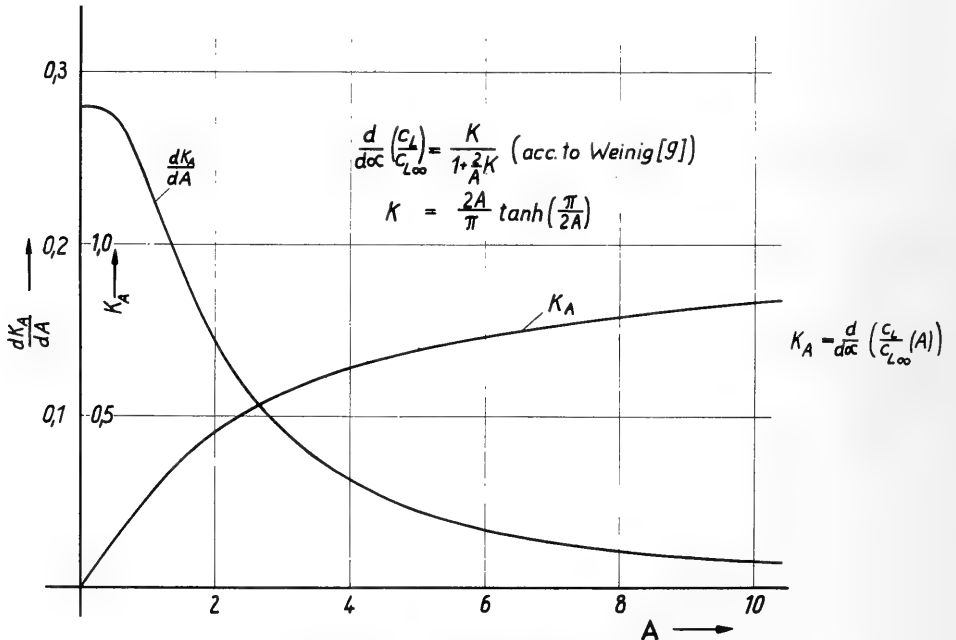
Fig. 29. Dependence of the lift gradient and the increase
of the lift gradient on the aspect ratio

$$A = \frac{A_{proj}}{\cos \vartheta} \, .$$

The parameter for the influence of the water surface $K_{\bar{h}}$ for parallel submerged foils equals the term

$$\frac{C_L}{C_{L_\infty}} (\bar{h})$$

as shown in Fig. 30. For dihedral foils or slanting flat foils of constant profile length, the tips of which run at the depths $\bar{h}_1$ and $\bar{h}_2$ $(\bar{h}_2 > \bar{h}_1)$, a mean value valid for the whole foil can be found by integration of the term

$$\frac{C_L}{C_{L_\infty}} (\bar{h})$$

over the depth of submergence:

$$K_{\bar{h}_m} = \frac{1}{\bar{h}_2 - \bar{h}_1} \int_{\bar{h}_1}^{\bar{h}_2} \frac{C_L}{C_{L_\infty}} (\bar{h}) d\bar{h}. \qquad (18)$$
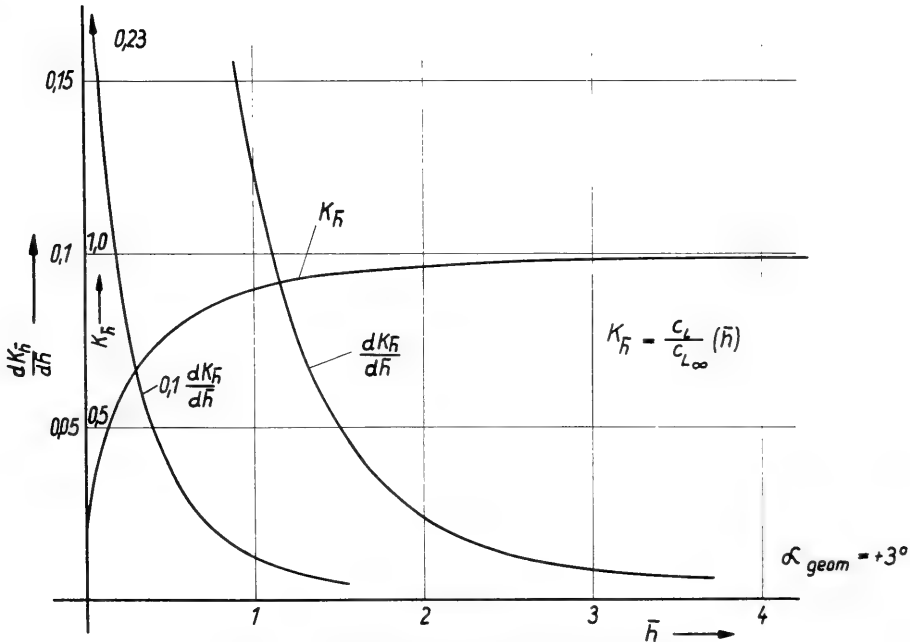
Fig. 30. Dependence of the decrease of lift and the gradient of the lift decrease on the depth ratio

In case the foil pierces the surface, $\bar{h}_1 = 0$ and the term shown in Fig. 31 is found to be

$$K_{\bar{h}_m} = \frac{1}{\bar{h}_2} \int_0^{\bar{h}_2} \frac{C_L}{C_{L\infty}} (\bar{h}) \, d\bar{h} . \tag{18'}$$

One more parameter takes care of the difference between the geometrical angle of incidence α_{geom} generally defined for a system moving with the foils and the geometrical angle of incidence α^*_{geom} actually existing in a system fixed relative to flow. It may be stated (see Fig. 18)

$$K_\alpha = \frac{\alpha^*_{geom}}{\alpha_{geom}} = \frac{\cos \vartheta}{\sin \alpha_{geom}} \left[\cos \gamma \sin \alpha_{geom} + \sin \gamma (\cos \beta |\tan \vartheta| \right.$$
$$\left. + \sin \beta \cos \alpha_{geom}) \right] . \tag{19}$$

For a nonrolling and nonsideslipping dihedral foil with the dihedral angle ϑ,

$$K_\alpha = \cos \vartheta .$$

Together with the known profile efficiency factor K_P the increase of lift for a hydrofoil becomes

$$K_{\bar{h}_m} = \frac{C_L}{C_{L\infty}}(\bar{h}) \bigg|_m - \frac{1}{\bar{h}_2} \int_0^{\bar{h}_2} \frac{C_L}{C_{L\infty}}(\bar{h}) d\bar{h}$$

$\frac{C_L}{C_{L\infty}}(\bar{h})$ acc. to equ. (15)

$\alpha_{geom} = +3°$
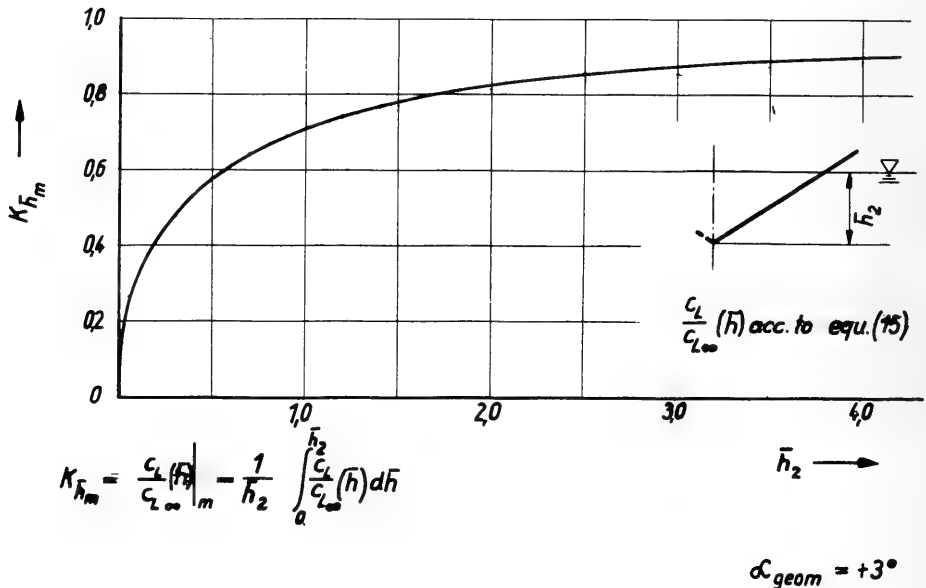
Fig. 31. Decrease of lift for a dihedral foil

$$\frac{dC_L}{d\alpha} = 2\pi \ K_A \ K_{\bar{h}} \ K_\alpha \ K_P \ . \tag{20}$$

By means of this relation the results of wind-tunnel tests or of theoretical calculations can be compared with the results of hydrofoil measurements.

VERTICAL STABILITY OF HYDROFOILS

For the sake of good driving properties a suitable vertical stability of hydrofoils is very important. However, it should again not be too great since the foils then will respond to minor disturbances, for instance to small waves on a surface otherwise calm; that means such foils will run stiff. Therefore not too steep a dL/dh curve is desirable.

For a nonrolling surface-piercing foil, the lowest point of which is at depth $\bar{h}_2$ with wetted aspect ratio A, the total change of lift

$$dL\bigg|_{A_1 \bar{b}_1 \bar{h}_2} = \frac{\partial L}{\partial A}\bigg|_A \ dA + \frac{\partial L}{\partial \bar{b}}\bigg|_{\bar{b}} \ d\bar{b} + \frac{\partial L}{\partial \bar{h}}\bigg|_{0,\bar{h}_2} \ d\bar{h} \tag{21}$$

is dependent on the variations of aspect ratio, span, and depth of submergence. From the geometry of the foil it follows that

$$dA = \frac{d\bar{h}}{\sin \vartheta} = d\bar{b}$$

so that

$$\frac{dL}{d\bar{h}}\bigg|_{A_1 \bar{b}_1 \bar{h}_2} = \frac{\partial L}{\partial A}\bigg|_A \ \frac{1}{\sin \vartheta} + \frac{\partial L}{\partial \bar{b}}\bigg|_{\bar{b}} \ \frac{1}{\sin \vartheta} + \frac{\partial L}{\partial \bar{h}}\bigg|_{0,\bar{h}_2} \ .$$

From

$$L = \rho u_0^2 \ bc \ C_{L\infty} K_\alpha \ K_P \ \cos \ \vartheta \ K_A \ K_{\bar{h}_m} \tag{22}$$

it follows that for each panel of the foil

$$\frac{\partial L}{\partial A}\bigg|_A = \frac{1}{2} \ \rho u_0^2 \ bc \ C_{L\infty} K_\alpha K_P \ \cos \ \vartheta \ \frac{\partial K_A}{\partial A}\bigg|_A \ K_{\bar{h}_m}\bigg|_{\bar{h}_2} \tag{23a}$$

$$\frac{\partial L}{\partial \bar{b}}\bigg|_{\bar{b}} = \frac{1}{2} \ \rho u_0^2 \ bc \ C_{L\infty} K_\alpha K_P \ \cos \ \vartheta \ \frac{1}{\bar{b}} K_A\bigg|_A \ K_{\bar{h}_m}\bigg|_{\bar{h}_2} \tag{23b}$$

$$\frac{\partial L}{\partial \bar{h}}\bigg|_{0,\bar{h}_2} \doteq \frac{1}{2} \ \rho u_0^2 \ bc \ C_{L\infty} K_\alpha K_P \ \cos \ \vartheta \ K_A\bigg|_A \ \frac{\partial K_{\bar{h}_m}}{\partial \bar{h}}\bigg|_{0,\bar{h}_2} \ . \tag{23c}$$

The quantity $\partial K_A / \partial A$ may be taken from Fig. 29. Furthermore

$$\frac{\partial K_{\bar{h}_m}}{\partial \bar{h}} = \frac{\partial}{\partial \bar{h}} \left(\frac{1}{\bar{h}_2} \int_0^{\bar{h}_2} K_{\bar{h}} \, d\bar{h} \right) = \frac{1}{\bar{h}_2} \left(K_{\bar{h}} \Big|_{\bar{h}_2} - K_{\bar{h}_m} \Big|_{\bar{h}_2} \right)$$

with $K_{\bar{h}}$ and $K_{\bar{h}_m}$ being as given by Figs. 30 and 31. Herewith the heaving gradient becomes

$$\frac{dL}{d\bar{h}} \bigg|_{A_1 \bar{b}_1 \bar{h}_2} = \rho u_0^2 \, b \, c \, C_{L\infty} K_\alpha K_P \cos \vartheta \left[\frac{\partial K_A}{\partial A} \bigg|_A \frac{K_{\bar{h}_m} \big|_{\bar{h}_2}}{\sin \vartheta} + K_A \bigg|_A \frac{K_{\bar{h}_m} \big|_{\bar{h}_2}}{\bar{b} \sin \vartheta} \right.$$

$$\left. + K_A \bigg|_A \frac{1}{\bar{h}_2} \left(K_{\bar{h}} \bigg|_{\bar{h}_2} - K_{\bar{h}_m} \bigg|_{\bar{h}_2} \right) \right]$$

(24a)

and

$$\frac{dC_L}{d\bar{h}} \bigg|_{A_1 \bar{b}_1 \bar{h}_2} = C_{L\infty} K_\alpha K_P \cos \vartheta \left\{ \frac{\partial K_A}{\partial A} \bigg|_A \frac{K_{\bar{h}_m} \big|_{\bar{h}_2}}{\sin \vartheta} + K_A \bigg|_A \left(\frac{K_{\bar{h}_m} \big|_{\bar{h}_2}}{\bar{b} \sin \theta} \right. \right.$$

$$\left. \left. + \frac{K_{\bar{h}} - K_{\bar{h}_m}}{\bar{h}} \bigg|_{\bar{h}_2} \right) \right\}$$

(24b)

with $C_{L\infty} = 2\pi \sin (\alpha + 2m)$.

In the case of a submerged dihedral foil or a flat parallel submerged foil the change of lift due to changes of submergence will be remarkably less than for the surface-piercing dihedral foil, because the first two terms of Eq. (24b) disappear. For a flat foil running at depth $\bar{h}_0$ the depth-gradient becomes

$$\frac{dL}{d\bar{h}} \bigg|_{A_1 \bar{b}_1 \bar{h}_0} = \rho u_0^2 \, b \, c \, C_{L\infty} K_P K_A \bigg|_A \frac{\partial K_{\bar{h}}}{\partial \bar{h}} \bigg|_{\bar{h}_0} \qquad (K_\alpha = 1)$$

(25a)

and

$$\frac{dC_L}{d\bar{h}} \bigg|_{A_1 \bar{b}_1 \bar{h}_0} = C_{L\infty} K_P K_A \bigg|_A \frac{\partial K_{\bar{h}}}{\partial \bar{h}} \bigg|_{\bar{h}_0} .$$

(25b)

It can be seen here that for the range of a small depth of submergence ($\bar{h}_0 \leq 1$) a vertical stabilization of a flat foil is quite possible as confirmed by experiments made in the Berlin Towing Tank with such a foil in a seaway. The submerged dihedral foil proved to be much more unfavorable since only those parts running near the surface are strongly influenced by the surface effect. In this case with the lowest point of the foil at depth $\bar{h}_2$ and the highest point at depth $\bar{h}_1$,

$$\frac{dL}{d\bar{h}}\bigg|_{A_1\bar{b}_1\bar{h}_1,\bar{h}_2} = \rho u_0^2\, b\, c\, C_{L\infty} K_\alpha K_P \cos\vartheta\, K_A\bigg|_A \frac{\partial K_{\bar{h}_m}}{\partial\bar{h}}\bigg|_{\bar{h}_1,\bar{h}_2}. \qquad (26a)$$

Thus

$$\frac{\partial K_{\bar{h}_m}}{\partial\bar{h}}\bigg|_{\bar{h}_1,\bar{h}_2} = \frac{\partial}{\partial\bar{h}}\left(\frac{1}{\bar{h}_1-\bar{h}_2}\int_{\bar{h}_1}^{\bar{h}_2}K_{\bar{h}}\,d\bar{h}\right) = \frac{1}{\bar{b}\,\sin\vartheta}\left(K_{\bar{h}}\big|_{\bar{h}_2} - K_{\bar{h}}\big|_{\bar{h}_1}\right).$$

This gives

$$\frac{dC_L}{d\bar{h}}\bigg|_{A_1\bar{b}_1\bar{h}_1,\bar{h}_2} = C_{L\infty}K_\alpha K_P\cos\vartheta\,K_A\bigg|_A \frac{K_{\bar{h}}\big|_{\bar{h}_2} - K_{\bar{h}}\big|_{\bar{h}_1}}{\bar{b}\,\sin\vartheta}. \qquad (26b)$$

An improvement for the submerged dihedral foil will be possible by arranging horizontal auxiliary foils at the upper ends as near as possible to the surface such that they are within the range of substantial $\partial K_{\bar{h}}/\partial\bar{h}$ (Fig. 30).

ROLLING STABILITY

A surface-piercing nonrolling dihedral foil with the dihedral angle ϑ, constant profile length, and wetted aspect ratio A may be examined now. For an inclination $d\beta$ a differential stabilizing moment relative to the lowest point is produced according to

$$dM_x\bigg|_{A_1\bar{b}_1\bar{h}_2} = \frac{\partial M_x}{\partial A}\bigg|_A dA + \frac{\partial M_x}{\partial\bar{b}}\bigg|_{\bar{b}} d\bar{b} + \frac{\partial M_x}{\partial\bar{h}}\bigg|_{0,\bar{h}_2} d\bar{h}. \qquad (27)$$

The differentials dA, $d\bar{b}$, and $d\bar{h}$ can be obtained from the geometry of the foil:

$$d\bar{b} = \mp\, d\beta\,\frac{1}{\tan\vartheta} = dA$$

$$d\bar{h} = \mp\, d\beta\,\bar{b}\,\bar{\eta}\,\cos\vartheta$$

with the dimensionless distance from the lowest point $\bar{\eta} = \eta/b$. For evaluating $\partial M_x/\partial A$, $\partial M_x/\partial\bar{b}$, and $\partial M_x/\partial\bar{h}$ the spanwise lift distribution will be given by the term $f(\bar{\eta},\bar{h}) = f(\bar{\eta})\,f(\bar{h})$, where with sufficient accuracy an elliptical law may be chosen for the function $f(\bar{\eta})$:

$$f(\bar{\eta}) = C_L(\bar{\eta}) = C_{L\infty}\,K_A\,\frac{4}{\pi}\sqrt{1-\bar{\eta}^2}.$$

The function $f(\bar{\eta})$ takes care of the depth of submergence, i.e.,

$$f(\bar{h}) = \frac{C_L}{C_{L\infty}} = K_{\bar{h}}$$

where

$$\bar{h} = \bar{h}_2(1 - \bar{\eta})$$

$$= \bar{h}_2 - \bar{b}\,\bar{\eta}\,\sin\vartheta\,.$$

Herewith the moment M_x may be written as

$$M_x = \rho u_0^2\, b\, c^2\, C_{L\infty} K_\alpha K_P \bar{b} K_A \frac{4}{\pi} \int_0^1 \bar{\eta}\sqrt{1 - \bar{\eta}^2}\, K_{\bar{h}}\Big|_{\bar{\eta}}\, d\bar{\eta}\,. \tag{28}$$

The derivatives of the moments relative to the single parameters are

$$\frac{\partial M_x}{\partial A}\bigg|_{A_1 \bar{b}_1 \bar{h}_2} = \frac{1}{2}\rho u_0^2\, b\, c^2\, C_{L\infty} K_\alpha K_P \bar{b}\, \frac{\partial K_A}{\partial A}\bigg|_A \frac{4}{\pi} \int_0^1 \bar{\eta}\sqrt{1-\bar{\eta}^2}\, K_{\bar{h}}\Big|_{\bar{\eta}}\, d\bar{\eta} \tag{29a}$$

$$\frac{\partial M_x}{\partial \bar{b}}\bigg|_{A_1 \bar{b}_1 \bar{h}_2} = \frac{1}{2}\rho u_0^2\, b\, c^2\, C_{L\infty} K_\alpha K_P K_A\bigg|_A \frac{8}{\pi} \int_0^1 \bar{\eta}\sqrt{1-\bar{\eta}^2}\, K_{\bar{h}}\Big|_{\bar{\eta}}\, d\bar{\eta} \tag{29b}$$

$$\frac{\partial M_x}{\partial \bar{h}}\bigg|_{A_1 \bar{b}_1 \bar{h}_2} = \frac{1}{2}\rho u_0^2\, b\, c^2\, C_{L\infty} K_\alpha K_P \bar{b}\, K_A\bigg|_A \frac{4}{\pi} \int_0^1 \bar{\eta}\sqrt{1-\bar{\eta}^2}\, \frac{\partial K_{\bar{h}}}{\partial \bar{h}}\bigg|_{\bar{\eta}}\, d\bar{\eta}\,. \tag{29c}$$

Herewith the total change of moment relative to the lowest point of the dihedral becomes

$$\frac{\partial M_x}{d\beta}\bigg|_{A_1 \bar{b}_1 \bar{h}_2} = -\rho u_0^2\, b\, c^2\, C_{L\infty} K_\alpha K_P \cos\vartheta\,\bar{b}^2\, \frac{4}{\pi}\left[\frac{\partial K_A}{\partial A}\bigg|_A \frac{F_1}{\sin\vartheta}\right.$$

$$\left. + K_A\bigg|_A \left(\frac{2F_1}{\bar{b}\,\sin\vartheta} + F_2\right)\right] \tag{30a}$$

and

$$\frac{dC_{M_x}}{d\beta}\bigg|_{A_1 \bar{b}_1 \bar{h}_2} = -C_{L\infty} K_\alpha K_P \cos\vartheta\,\bar{b}^2\, \frac{4}{\pi}\left[\frac{\partial K_A}{\partial A}\bigg|_A \frac{F_1}{\sin\vartheta} + K_A\bigg|_A \left(\frac{2F_1}{\bar{b}\sin\vartheta} + F_2\right)\right] \tag{30b}$$

with

$$F_1 = \int_0^1 \bar{\eta} \sqrt{1 - \bar{\eta}^2} \, K_{\bar{h}} \Big|_{\bar{\eta}} \, d\bar{\eta}$$

$$F_2 = \int_0^1 \bar{\eta}^2 \sqrt{1 - \bar{\eta}^2} \, \frac{\partial K_{\bar{h}}}{\partial \bar{h}} \Big|_{\bar{\eta}} \, d\bar{\eta} .$$

Together with the stabilizing moment a lateral force is effective, the magnitude of which is

$$dP_y = \frac{\partial P_y}{\partial A} \, dA + \frac{\partial P_y}{\partial \bar{b}} \, d\bar{b} + \frac{\partial P_y}{\partial \bar{h}} \, d\bar{h} . \tag{31}$$

The general term for the lateral force is given by

$$P_y \Big|_{A_1 \bar{b}_1 \bar{h}_2} = \rho u_0^2 \, b \, c \, C_{L\infty} K_\alpha K_P \, \sin \vartheta \, K_A \Big|_A \frac{4}{\pi} \int_0^1 \sqrt{1 - \bar{\eta}^2} \, K_{\bar{h}} \Big|_{\bar{\eta}} \, d\bar{\eta} . \tag{32}$$

With the differentials

$$dA = \mp d\beta \, \frac{\bar{b}}{\tan \vartheta} = d\bar{b}$$

$$d\bar{h} = \mp d\beta \, \bar{b} \, \bar{\eta} \, \cos \vartheta$$

and

$$\frac{\partial P_y}{\partial A} \Big|_{A_1 \bar{b}_1 \bar{h}_2} = \frac{1}{2} \rho u_0^2 \, bc \, C_{L\infty} K_\alpha K_P \, \sin \vartheta \, \frac{\partial K_A}{\partial A} \Big|_A \frac{4}{\pi} \int_0^1 \sqrt{1 - \bar{\eta}^2} \, K_{\bar{h}} \Big|_{\bar{\eta}} \, d\bar{\eta} \tag{33a}$$

$$\frac{\partial P_y}{\partial \bar{b}} \Big|_{A_1 \bar{b}_1 \bar{h}_2} = \frac{1}{2} \rho u_0^2 \, bc \, C_{L\infty} K_\alpha K_P \, \sin \vartheta \, \frac{1}{\bar{b}} K_A \Big|_A \frac{4}{\pi} \int_0^1 \sqrt{1 - \bar{\eta}^2} \, K_{\bar{h}} \Big|_{\bar{\eta}} \, d\bar{\eta} \tag{33b}$$

$$\frac{\partial P_y}{\partial \bar{h}} \Big|_{A_1 \bar{b}_1 \bar{h}_2} = \frac{1}{2} \rho u_0^2 \, bc \, C_{L\infty} K_\alpha K_P \, \sin \vartheta \, K_A \Big|_A \frac{4}{\pi} \int_0^1 \sqrt{1 - \bar{\eta}^2} \, \frac{\partial K_{\bar{h}}}{\partial \bar{h}} \Big|_{\bar{\eta}} \, d\bar{\eta}, \tag{33c}$$

the resulting change of lateral force is found to be

$$\frac{dP_y}{d\beta}\bigg|_{A_1 \bar{b}_1 \bar{h}_2} = \rho u_0^2\, bc\; C_{L\infty} K_\alpha K_P\; \cos\vartheta\; \bar{b}\left[\frac{\partial K_A}{\partial A}\bigg|_A K_{\bar{h}_m}\bigg|_{\bar{h}_2} + K_A\bigg|_A \left(\frac{1}{b} K_{\bar{h}_m}\bigg|_{\bar{h}_2}\right.\right.$$

$$\left.\left. + \frac{4}{\pi} \sin\vartheta\; F_3\right)\right] \tag{34a}$$

and

$$\frac{dC_{P_y}}{d\beta}\bigg|_{A_1 \bar{b}_1 \bar{h}_2} = C_{L\infty} K_\alpha K_P\; \cos\vartheta\; \bar{b}\left[\frac{\partial K_A}{\partial A}\bigg|_A K_{\bar{h}_m}\bigg|_{\bar{h}_2} + K_A\bigg|_A \left(\frac{1}{b} K_{\bar{h}_m}\bigg|_{\bar{h}_2}\right.\right.$$

$$\left.\left. + \frac{4}{\pi} \sin\vartheta\; F_3\right)\right] \tag{34b}$$

with

$$F_3 = \int_0^1 \bar{\eta}\sqrt{1-\bar{\eta}^2}\; \frac{\partial K_{\bar{h}}}{\partial \bar{h}}\bigg|_{\bar{\eta}}\; d\bar{\eta}\,.$$

Using the terms $dC_{M_x}/d\beta$ and $dC_{P_y}/d\beta$ the position of the initial lateral metacenter above lowest point can be found [7]:

$$z_0 = -C\; \frac{dC_{M_x}}{d\beta}\; \frac{1}{C_L + \dfrac{dC_{P_y}}{dy}}\bigg|_{\beta=0}\,. \tag{35}$$

Analogously, stabilizing moment and lateral force for any inclination β can be found. The different values K_A and dK_A/dA have to be taken [7] considering the wetted breadth for both panels relative to the profile length. In addition to that a dependence on β appears, i.e., for the moment there has to be written:

$$dM_x = \frac{\partial M_x}{\partial A}\, dA + \frac{\partial M_x}{\partial \bar{b}}\, d\bar{b} + \frac{\partial M_x}{\partial \bar{h}}\, d\bar{h} + \frac{\partial M_x}{\partial \beta}\, d\beta.$$

For the case of the submerged dihedral foil as well as of a submerged flat foil all the terms taking care of the change of the aspect ratio and of the breadth will disappear. The rolling stability of submerged foils therefore is principally less than that of dihedral foils piercing the surface.

As in the case of vertical stabilization, a lateral stabilization might be possible for submerged foils as well if the depth of submergence is low or if horizontal stabilizing plates are arranged near the free surface.

For a submerged dihedral foil the lowest point of which is running at the depth $\bar{h}_2$ with the upper ends at the depth $\bar{h}_1$ the gradient of the rolling moment in the upright position becomes

$$\frac{dC_{M_x}}{d\beta}\bigg|_{A_1\bar{b}_1\bar{h}_1,\bar{h}_2} = -C_{L\infty}K_\alpha K_P \cos\vartheta\ \bar{b}^2\ \frac{4}{\pi}\ K_A\bigg|_A \int_0^1 \bar{\eta}^2\sqrt{1-\bar{\eta}^2}\ \frac{dK_{\bar{h}}}{d\bar{h}}\bigg|_{\bar{\eta}}\ d\bar{\eta} \quad (36)$$

and the gradient of the lateral force becomes

$$\frac{dC_{P_y}}{d\beta}\bigg|_{A_1\bar{b}_1\bar{h}_1,\bar{h}_2} = C_{L\infty}K_\alpha K_P \cos\vartheta\ \sin\vartheta\ \bar{b}\ \frac{4}{\pi}\ K_A\bigg|_A \int_0^1 \bar{\eta}\sqrt{1-\bar{\eta}^2}\ \frac{dK_{\bar{h}}}{d\bar{h}}\bigg|_{\bar{\eta}}\ d\bar{\eta} \quad (37)$$

with

$$\bar{h}_1 \le \bar{h}(\bar{\eta}) \le \bar{h}_2 .$$

For a parallel submerged foil running at the depth $\bar{h}_0$,

$$\frac{dC_{M_x}}{d\beta}\bigg|_{A_1\bar{b}_1\bar{h}_0} \doteq -C_{L\infty}K_P\ \bar{b}^2\ \frac{4}{\pi}\ K_A\bigg|_A\ \frac{dK_{\bar{h}}}{d\bar{h}}\bigg|_{h_0} \int_0^1 \bar{\eta}^2\sqrt{1-\bar{\eta}^2}\ d\bar{\eta}$$

$$= -C_{L\infty}K_P\ \bar{b}^2\ \frac{1}{4}\ K_A\bigg|_A\ \frac{dK_{\bar{h}}}{d\bar{h}}\bigg|_{\bar{h}_0} \quad (38)$$

and

$$\frac{dC_{P_y}}{d\beta}\bigg|_{A_1\bar{b}_1\bar{h}_0} = 0 \qquad (dA = d\bar{b} = 0). \quad (39)$$

The lateral stabilization due to sideslipping will not be developed here since this can be done in a manner corresponding to the treatment of the vertical and of the rolling stability.

NOMENCLATURE

b semispan of the hydrofoil

$b_{proj} = b\cos\vartheta$

c chord length

$\bar{b} = b/c$

h depth of submergence of the foil

h' minimum local water depth above the foil

$\bar{h} = h/c$

$h* = h/(c/2)$

$A = 2b/c$ aspect ratio

$S = 2bc$ area of the hydrofoil

u_0 running speed

u_1 induced velocity in the direction of the undisturbed flow

w_1 induced velocity perpendicular to the direction of the undisturbed flow

$F_h = u_0/\sqrt{gh}$ Froude depth number

α_{geom} geometrical angle of attack of the chord

α_0 no-lift angle

m camber

$C_L = L/\rho u_0^2 bc$ lift coefficient

C_D drag-coefficient

C_P transverse-force coefficient

$C_{M_x} = M_x/\rho u_0^2 bc^2$ rolling-moment coefficient

ϑ dihedral angle

β rolling angle

γ sideslip angle

$\varepsilon = C_D/C_L$ drag-lift ratio

REFERENCES

[1] Laitone, E.V., "Limiting Pressure on Hydrofoils at Small Submergence Depths," J. Appl. Phys. 25:623 (1954)

[2] Parkin, B.R., Perry, B., and Wu, Y.T., "Pressure Distribution on a Hydrofoil Running Near the Water Surface," J. Appl. Phys. 27:232 (1956)

[3] Plesset, M.S., and Parkin, B.R., "Hydrofoils in Noncavitating and Cavitating Flow," Cavitation in Hydrodynamics, Nat. Phys. Lab., 1955

[4] Land, N.S., "Characteristics of an NACA 66, S-209 Section Hydrofoil at Several Depths," NACA W.R.L.-757, 1943

[5] Schuster, S., and Schwanecke, H., "Über den Einfluss der Wasseroberfläche auf die Auftriebsverteilung von Tragflügeln," Schiffstechnik 4:117 (1957)

[6] Schuster, S., and Logothetopoulos, J., "Sechskomponentenmessungen an einer Wasser-tragfläche zur Untersuchung der Einflüsse von Streckung, Kielung und Krängung," Versuchs-Abtlg. d. Gebr. Sachsenberg AG. No. 5a, 1942 (unpublished)

[7] Schwanecke, H., "Über Sechskomponenten-Messungen an einem V-Wassertragflügel bei symmetrischer und unsymmetrischer Anströmung," Schiffstechnik 6:93 (1957)

[8] Isay, W.H., "Zur Theorie der nahe der Wasseroberfläche fahrenden Tragflächen," Ingenieur-Archiv 27:295 (1959/60)

[9] Weinig, F., "Beitrag zur Theorie des Tragflügels endlicher, insbesondere kleiner Spannweite," Luftfahrt-Forschung 13:405 (1936)

DISCUSSION

P. Kaplan (Technical Research Group, Inc., Syosset, New York)

I noticed, or it appeared to me, that the influence of roll was only static. I wonder if you have considered or done any work, not reported here, as to the effect of the roll damping, that is, what happens when the foil is performing not just a static roll, deflection, but is actually performing a roll angular motion? This is important since it is the roll damping that determines the major behavior of the roll motion. According to the results of the free motion studies, there was quite different behavior of the system as compared to an aircraft, so I wonder just what influence a dihedral will have on the roll damping and if any consideration was given to this problem.

S. Schuster

Our results given here of the tests and formulas are valid only for the steady state. Even the test for finding the point of breaking down of the lift shows only the beginning of the motion. Damping forces and moments can only be found during the motion itself. We are beginning the investigation for the unsteady problems, especially for hydrofoils in waves, but at present we are not able to give you an answer to these special questions. I think that damping is higher for rolling than for yawing, but for the whole system of two or more hydrofoils, we have to consider sideslip motion too. Perhaps there will be something to report after finishing our investigations on oscillations of a propeller in the axial direction and in the rotational direction.

* * *
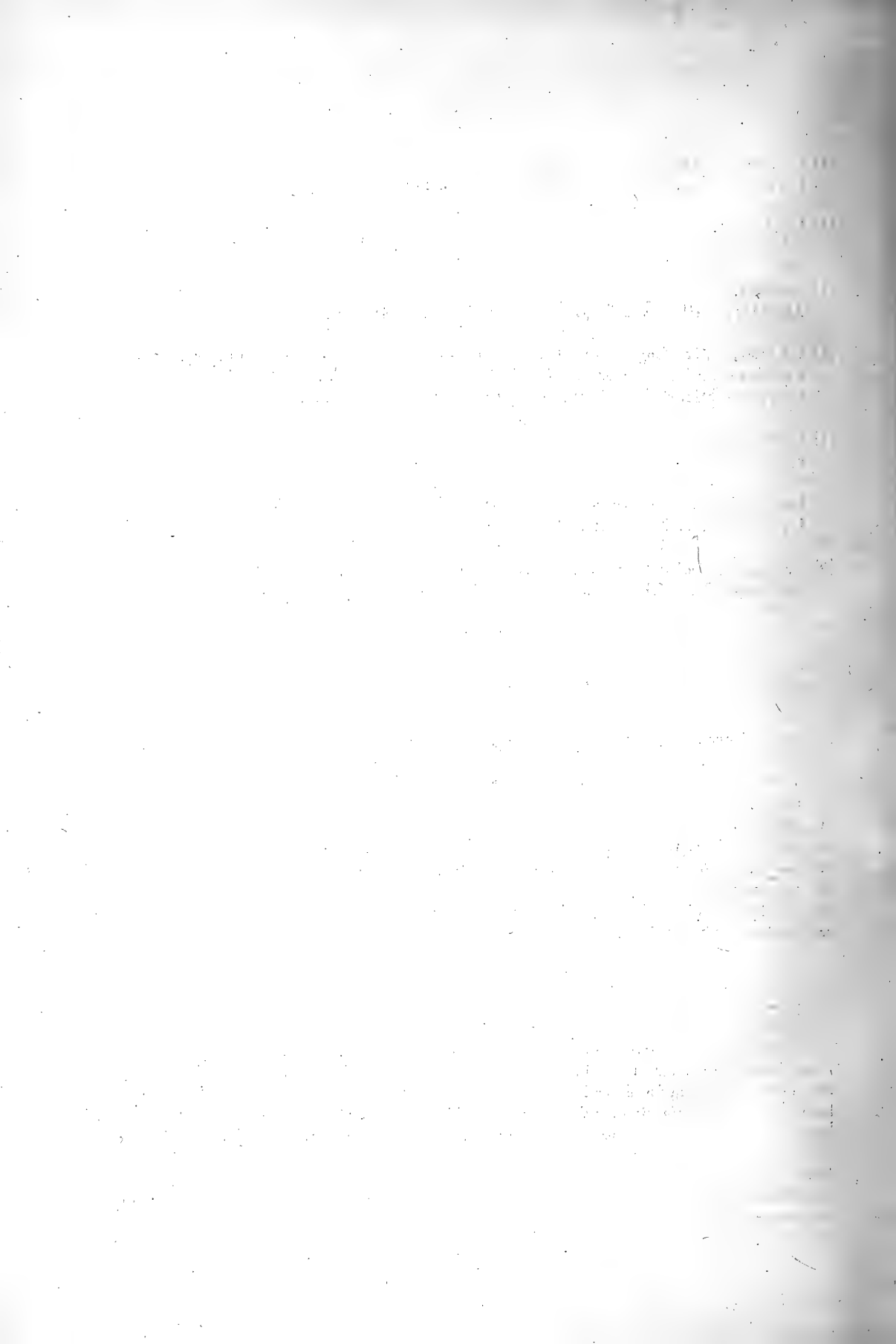
THE EFFECT OF SIZE ON THE SEAWORTHINESS OF HYDROFOIL CRAFT

A. Hadjidakis
Aquavion Holland N.V., The Hague

The pitching movements and the vertical accelerations of hydrofoil craft with surface-piercing foils are studied in a very simplified way to show the effect of size as a function of wave parameters, and speed or Froude number. Considerations are given to variations of static pitch angle, heave, natural frequency, and damping ratio—the latter based on a linearized equation of motion. The analysis indicates that at wave lengths of 2/3 and 3/2 of the length of the hydrofoil craft, extreme values of vertical accelerations are to be expected, which decrease rapidly with increasing length of the craft, or decreasing speed, which leads to the conclusion that the seaworthiness increases with the length of the hydrofoil craft.

INTRODUCTION

The seaworthiness of hydrofoil craft is sometimes doubted, while the comfort offered to the passengers is often considered to be insufficient, when going on a seaway [1-7]. The purpose of this paper is to give in the most simple way some insight into the behavior of hydrofoil craft on sea, and to determine the most unfavorable conditions, which are compared for craft of different sizes.

This, of course, needs some explanation. The high cost involved in constructing big hydrofoil craft makes it necessary to obtain experience regarding seaworthiness, stability, and comfort, as well as structural loadings and other technical aspects, by means of scale models or small prototypes. It is therefore desirable to prove that the results obtained in this way can be interpreted for craft of greater size.

Today a hydrofoil craft does not present problems on relatively smooth water. Its behavior under unfavorable conditions is thus decisive for its suitability for passenger transport at sea.

Therefore it is necessary to gather the existing knowledge which may contribute to a prediction of the properties of a big hydrofoil craft, based on the known performance and behavior of a small craft, so that a project for a seaworthy passenger ferry can be started in full confidence.

The following considerations and calculations have been formulated in a general way, making them valid for a large number of existing hydrofoil systems. However, they are not valid for systems which cannot be compared to a spring-and-mass system. Thus they do not

191

apply to hydrofoil craft with fully submerged foils, lacking a definite position of equilibrium relative to the water surface. Their stability depends only on a human or electric brain, controlling the lift developed by the different foils. The behavior in a seaway of this latter category depends merely on the degree of intelligence of its governor.

Furthermore, only the most unfavorable conditions have been considered. Going against the waves, the vertical accelerations were found to be critical; when going with the waves, this was the case with the maximum negative pitch angle.

Both critical values depend on design characteristics of the different hydrofoil systems, as there are: the lift reserve of the forward foils, the natural frequencies for pitch and heave, the damping ratio, etc. These design characteristics, being independent of size, will not be discussed in this paper.

The many purposely introduced simplifications, of course, create deviations. Thus it is necessary to apply the results only to two or more craft of the same hydrofoil system, differing essentially in a scale factor only, for it is only in that case that the deviations are in the same sense for all units, so that they will largely compensate each other.

THE SEAWAY

The waves are assumed to be of sinusoidal shape, where the waveheight H is equal to σ times the wavelength λ, and σ indicates the rate of steepness of the waves. The craft's speed V forms an angle γ with the vector of the speed of wave propagation c. Then the forced frequency or excitation frequency of the forces, trying to disturb the craft from its equilibrium position, is

$$\omega = 2\pi \left| \frac{c - V\cos\gamma}{\lambda} \right|, \quad \text{where} \quad c = \sqrt{\frac{g\lambda}{2\pi}} \tag{1}$$

The amplitude of the static pitch angle on a given wave pattern can be determined as follows: The maximum static pitch angle ψ_0 is attained in the position shown in Fig. 1. Its value is

$$\psi_0 = \frac{\sigma\lambda}{\ell} \sin\left(\pi\frac{\ell\cos\gamma}{\lambda}\right) \tag{2}$$

which can never exceed $\pi\sigma$.
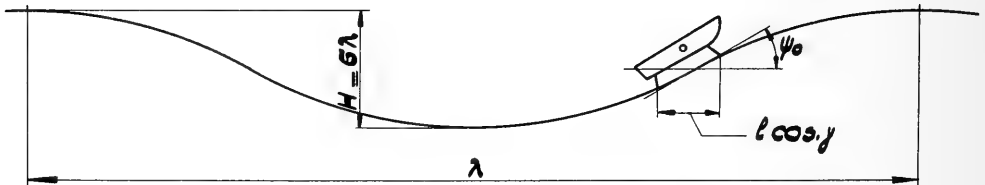
Fig. 1. Maximum static pitch angle

Similarly, the amplitude of the static roll angle is found to be

$$\varphi_0 = \frac{\sigma \lambda}{b} \sin\left(\pi \frac{b \sin \gamma}{\lambda}\right) . \qquad (3)$$

The vertical movements of the center-of-gravity of a hydrofoil craft can also be determined: The dimensionless static amplitude of the center of gravity is (see Fig. 2)

$$\frac{Z_0}{\ell} = \frac{\sigma \lambda}{2\ell} \cos\left(\pi \frac{\ell \cos \gamma}{\lambda}\right) . \qquad (4)$$
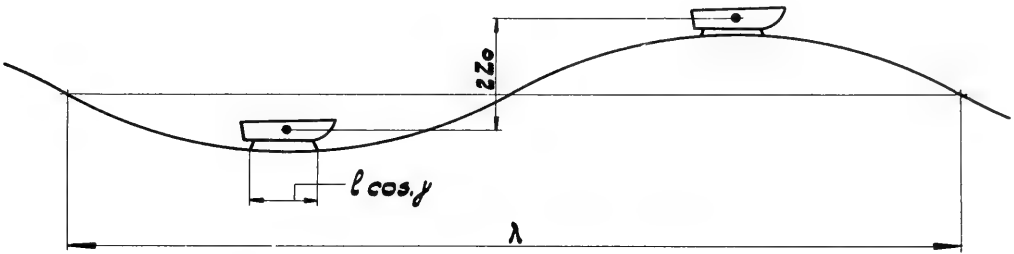
Fig. 2. Static amplitude of the center of gravity

Both values are shown in Fig. 3 as a function of wavelength divided by craft length. The scales for ψ_0 and Z_0/ℓ are valid for $\sigma = 0.05$. For other values of σ the scales have to be adjusted.

The roll angle φ will not be discussed in more detail, because experience has shown that rolling is not a critical factor. Moreover it can be treated in the same way as the pitch angle.

Figure 3 shows both the static pitch amplitude ψ_0 and the dimensionless static vertical amplitude of the center of gravity Z_0/ℓ as a function of the relative wavelength $\lambda/\ell \cos \gamma$. If

$$\frac{\lambda}{\ell \cos \gamma} = \frac{2}{2} , \frac{2}{4} , \frac{2}{6} , \text{ etc., then } \psi_0 = 0$$

but Z_0/ℓ shows an extreme value, while if

$$\frac{\lambda}{\ell \cos \gamma} = \frac{2}{1} , \frac{2}{3} , \frac{2}{5} , \text{ etc., then } Z_0/\ell = 0$$

and ψ_0 attains its extreme values. The effect of these parameters on the craft's behavior will be discussed later.

It should be noted that the values of the excitation frequency resulting from Eq. (1) should be regarded with some reserve. Practice has shown results to be sufficiently accurate when going against or with the waves, but when going along the waves higher values of ω are actually found due to the irregularity of the seaway [8].
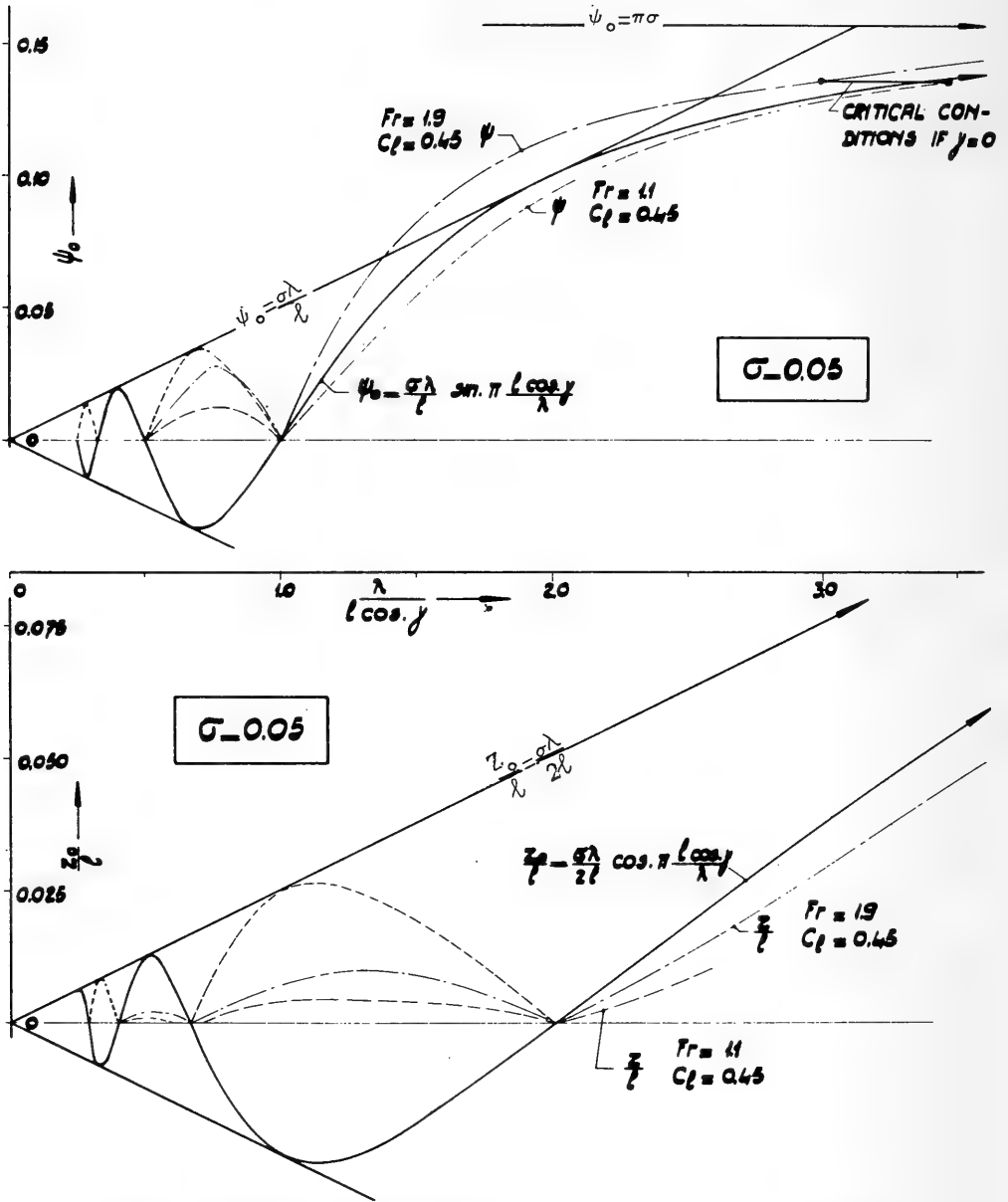
Fig. 3. Wave characteristics as shown in Figs. 1 and 2 (a list of symbols is given at the end of the paper)

THE HYDROFOIL CRAFT

The seaworthiness of a craft might be specified as a combination of characteristics which guarantee safety and comfort for passengers and crew while traveling at sea. Some of those characteristics are: static stability, dynamic stability, constructional properties, proper means of navigation, and lifesaving equipment. Variation of size of a certain type

of hydrofoil craft will not affect its static stability. Constructional properties, proper means of navigation, and lifesaving equipment are (although very important) not to be discussed.

Hence the following will be limited to the dynamic stability and its influence on the comfort of hydrofoil craft. The main factors which define the movements are: static amplitude, (already discussed), excitation frequency, (already discussed), natural frequency, and damping ratio.

The motions of hydrofoil craft are defined by a number of basic equations. There is equilibrium when the weight of the craft equals the combined lift forces of the foils:

$$mg = \Sigma L .$$

The lift force of a foil is proportional to dynamic pressure, lift coefficient, and submerged foil area:

$$L = \frac{1}{2}\rho V^2 C_l \, F . \tag{6}$$

A deviation in pitch from the equilibrium position creates an extra lift ΔL which tries to restore the craft to its original position. The restoring moment is called R. It will be clear that: $\Delta L :: mg$ since $L :: mg$ (Eq. (5)), so $R :: mgl$. Further, for the moment of inertia, $I :: ml^2$ if the mass distribution can be supposed to be similar. Thus the natural frequency of the craft can be calculated:

$$w_{n_p} = \sqrt{\frac{R}{I}} \quad :: \sqrt{\frac{mgl}{ml^2}}$$

where the index p is used for pitch, or

$$w_{n_p} = k_{w_p} \sqrt{\frac{g}{\ell}} . \tag{7}$$

In an analogous way the natural frequency for heaving motions can be found to be

$$w_{n_h} = k_{w_h} \sqrt{\frac{g}{\ell}} . \tag{8}$$

The dimensionless damping ratio in case of pitch, d_p, is the damping N divided by the critical damping:

$$d_p = \frac{N}{2\sqrt{IR}} \text{ where } N :: D_p \ell \frac{1}{\dot{\psi}} \quad . \tag{9}$$

In this equation D_p is the damping force:

$$D_p = \frac{1}{2}\rho V^2 \Delta C_l \, F_d \tag{10}$$

in which $\Delta C_l = W/V$ and $W :: \ell\dot{\psi}$ so $N :: V\ell^2 F_d$.

The foil area F_d, contributing to the damping, is of course proportional to the foil area F:

$$N :: V\ell^2 F .$$ (11)

It was already stated that $I :: ml^2$ and $R :: mgl$, so

$$d_p :: \left(\frac{V\ell^2 F}{\sqrt{ml^2 mgl}} = \frac{VF\sqrt{\ell}}{m\sqrt{g}} \right) .$$ (12)

Combining Eqs. (5) and (6) with (12) leads to

$$d_p = \frac{k_{d_p}}{C_l Fr} .$$ (13)

Similarly it can be found that in case of heave

$$d_h = \frac{k_{d_h}}{C_l Fr}$$ (14)

Consequently the damping ratio is inversely proportional to the lift coefficient and the Froude number for both types of motion.

This result might seem unexpected, the damping being proportional to speed, while the damping ratio is inversely proportional to the Froude number. The explanation is simple: an increase of speed of 10 percent corresponds with a decrease of submerged foil area of 20 percent, if the lift coefficient remains constant (see Eq. (6)). For similar hydrofoil craft of differing size, k_{w_h}, k_{w_p}, k_{d_p}, and k_{d_h} are constant values. They may vary, however, for different hydrofoil systems.

All elements necessary to calculate the motions of a hydrofoil craft are now available if the craft may be considered as a damped linearized spring and mass system. The dynamic amplitudes are then determined by the equations

$$\psi/\psi_0 = \frac{1}{\sqrt{(1 - w/w_{n_p}^2 +)^2 + 4d_p^2 w/w_{n_p}^2}}$$ (15)

$$Z/Z_0 = \frac{1}{\sqrt{(1 - w/w_{n_h}^2)^2 + 4d_h^2 w/w_{n_h}^2}} .$$ (16)

These equations have been plotted in Fig. 4 for various damping ratios.

It is now possible to determine the vertical accelerations at a certain point of the craft. This point has been chosen near the bow at a distance from the center of gravity of $l/3$, no passengers or crew being expected to be carried at a more forward point. The resulting accelerations have been calculated by adding vectorially the vertical acceleration caused by a variation of the pitch ψ and the vertical acceleration caused by a variation of heave Z. This is based on the assumption that pitch and heave are entirely independent of each other, which, although not correct, gives very acceptable results, as has been shown by Abkowitz [9].

$$\frac{z}{z_0} = \frac{\psi}{\psi_0} = \frac{1}{\sqrt{(1-\omega/\omega_n^2)^2 + 4d^2\omega/\omega_n^2}}$$
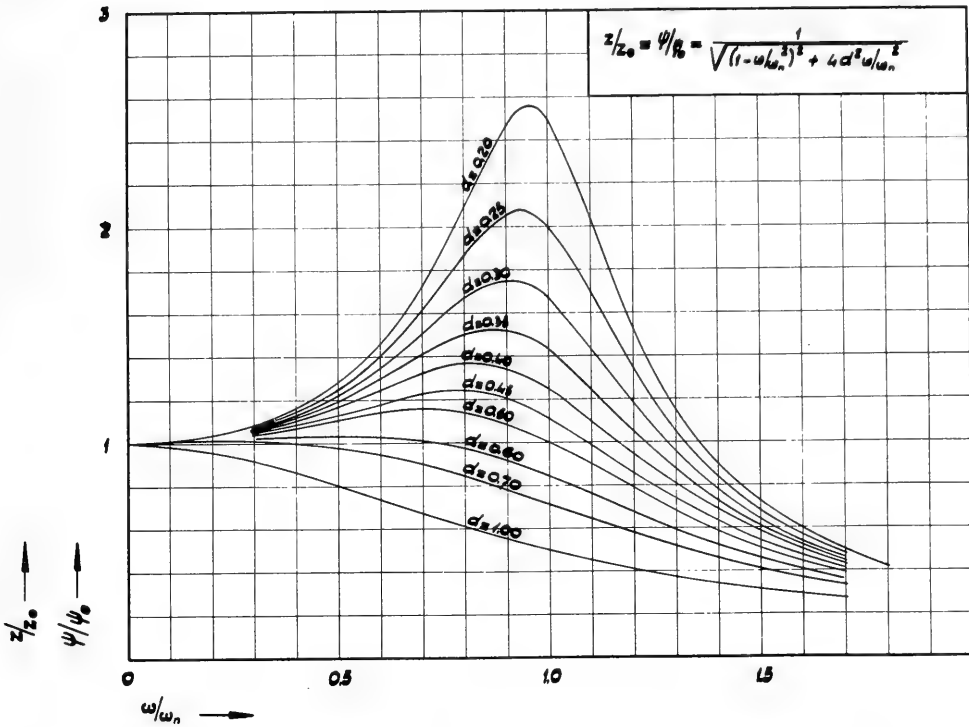
Fig. 4. Amplitudes of forced vibrations for various degrees of damping

BEHAVIOR OF THE CRAFT

Concerning the course of a hydrofoil craft relative to the waves, experience has shown two conditions to be of decisive importance for its seaworthiness. The first occurs if $\gamma = 0$, i.e., on a following sea. In that case, the extreme value of ψ plays a dominant role.

Figure 5 shows the influence of the orbital motion of water particles in a following sea. This orbital motion creates a moment which tries to pull the nose of the craft down.
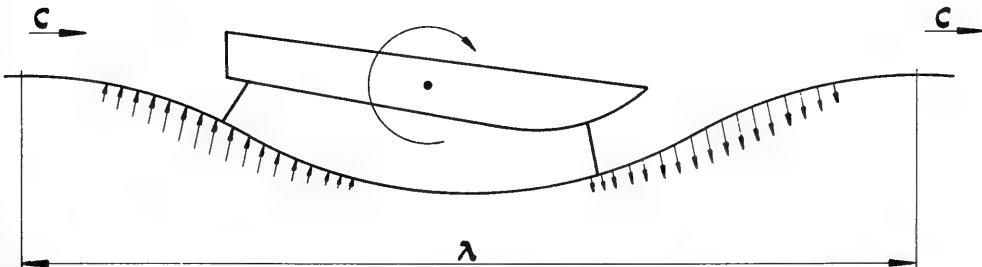
Fig. 5. Influence of the orbital motion of water particles in a following sea

As the pitch increases with increasing wave height, it will be clear that at a certain wave height the combination of a high value of negative pitch, combined with the orbital effect, makes the bow touch water. This phenomenon introduces a braking effect which causes the craft to slow down, so this wave height represents the limit up to which the craft can remain foilborne on a following sea. The lift reserve of the bow foils of a certain hydrofoil system evidently determines the limiting wave height.

However, in Fig. 3 the dynamic pitch amplitudes of two similar hydrofoil craft differing only in size have been indicated as functions of the relative wavelength. The critical condition for the craft with the lower Froude number is seen to occur at a greater relative wavelength. Consequently, of two similar craft the bigger one (having the lower Froude number) will encounter its critical condition on a following sea on relatively higher waves.

When going along the waves, i.e., when $\gamma = \pi/2$, a hydrofoil craft will attain its greatest roll angle φ. However, experience has shown that this is not a critical condition at all; therefore it will not be discussed in more detail.

When the craft is going against the waves, i.e., $\gamma = \pi$, the pitch amplitude is not critical, because the orbital moment will help to surmount the next wave, but the maximum value of the excitation frequency is obtained. Therefore this can be called a critical condition as far as vertical accelerations are concerned, these accelerations being proportional to the square of the excitation frequency. While discussing vertical accelerations, γ will henceforth be assumed to be equal to π.

Applying the foregoing theory to an example, a comparison is made between an existing small hydrofoil craft ($l = 6.73$ m, $V = 30$ knots) and a designed bigger craft ($l = 36$ m, $V = 45$ knots). Of the existing craft (Fig. 6), the natural frequencies for pitch and heave and the damping ratio are known. With the aid of Figs. 3 and 4 a curve could be obtained indicating the vertical acceleration at the bow as a function of the relative wavelength. The natural frequencies and the damping ratio of the designed bigger craft have been calculated according to Eqs. (7), (8), (13), and (14), which made it possible to establish an equivalent curve for the bigger craft. Both curves are shown in Fig. 7.

It will be noted that there are two critical values of the relative wavelength λ / l where the vertical acceleration at the bow Z_b/g attains peak values. These critical wavelengths correspond with 2/3 and 3/2 times the craft's length.

Contrary to what might be expected, Fig. 7 shows that critical values of acceleration are not to be expected at a relative wavelength of more than two. This means that vertical acceleration decreases with increasing wavelength. In other words, the comfort of the small craft will be much better on waves with a length of 20 m and a height of 1 m, than on waves with a length of 10 m and a height of 0.5 m.

Similarly, the big craft will be more comfortable on waves of 100-m length and 5-m height, than on waves of 50-m length and a height of 2.5 m, although the comfort in the latter case is much better than the best that can be obtained with the small craft.

In reality the wave pattern is never found to be so regular as the theory supposes it to be. On a seaway, wavelengths vary considerably, which tends to level off the extreme accelerations. Furthermore small waves are always superimposed on the longer waves, which will tend to raise the maximum accelerations to be found for values of λ /l higher than two. These two effects have been taken into account in the dashed curves shown in Fig. 7.

Fig. 6. Small hydrofoil craft
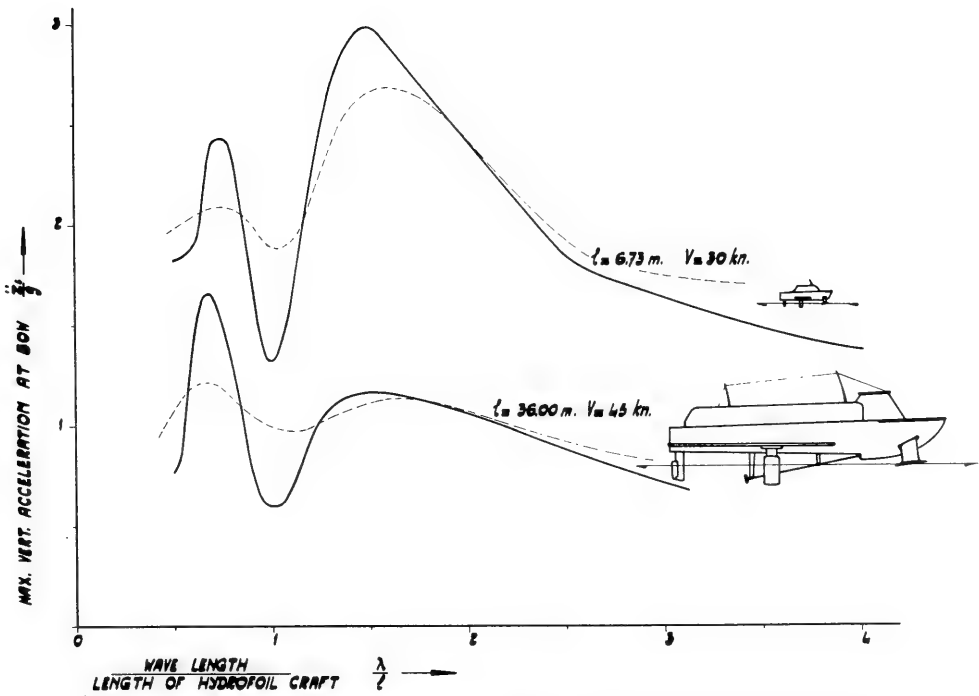
Fig. 7. Maximum vertical acceleration at the bow of a small hydrofoil craft and
a larger hydrofoil craft

As the behavior of a hydrofoil craft in the most unfavorable conditions is of decisive importance for its seaworthiness and comfort, the critical accelerations at $\lambda/l = 2/3$ and $\lambda/l = 3/2$ have been plotted in Fig. 8 as a function of craft length. This graph is valid for one speed only, i.e. 30 knots, which makes it possible also to show the variation of the Froude number with the craft length. The vertical acceleration at the bow for $\lambda/l = 1$ is also shown.
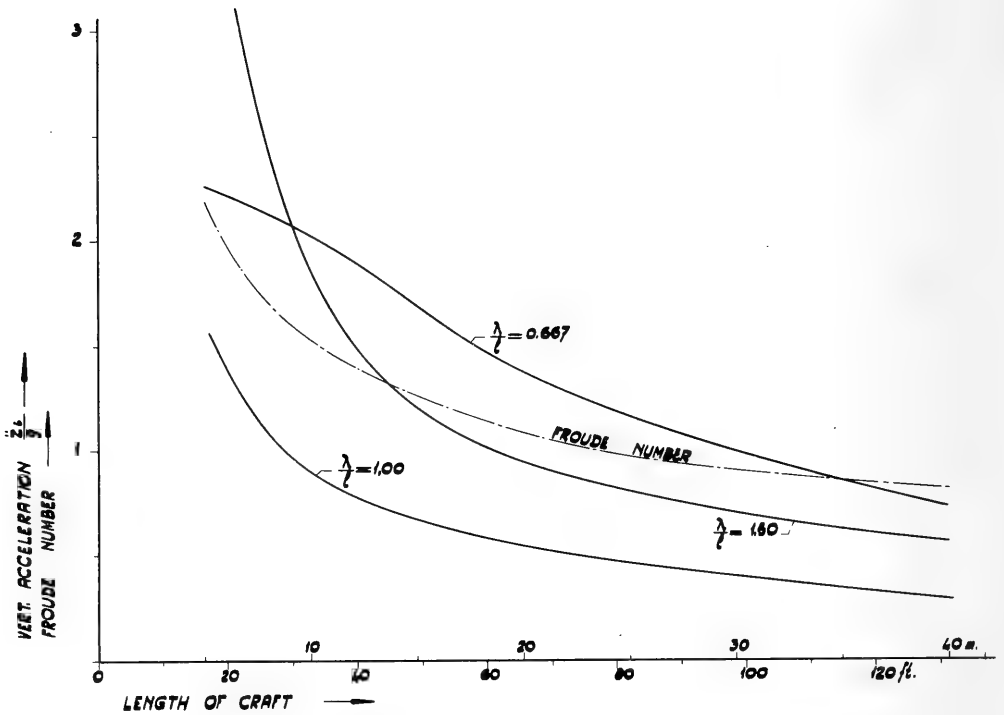
Fig. 8. Maximum vertical acceleration at the bow for critical values of λ/l as a function of craft length l at a constant speed of 30 knots

Of these curves the one for $\lambda/l = 3/2$ is the most important, because the critical accelerations at $\lambda/l = 2/3$ occur at relatively higher frequencies and can therefore be more easily attenuated or even eliminated by means of foil suspension or similar improvements.

The influence of the speed of the craft is shown in Fig. 9, where the curve for $\lambda/l = 3/2$ has been drawn for five different speeds. Evidently the vertical acceleration is approximately proportional to the square of the speed for a given craft length.

Thus it can be stated that vertical accelerations decrease rapidly with increasing length of the hydrofoil craft, which means that the comfort, depending on the frequency of variation of the accelerations (jerk), improves even more rapidly.
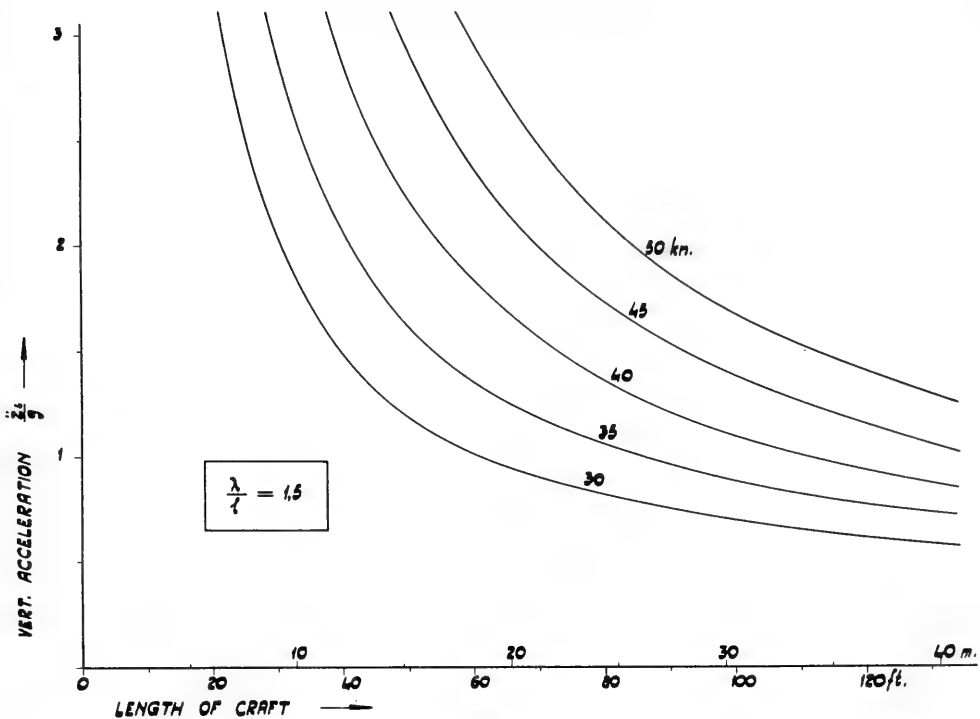
Fig. 9. Influence of the speed on the maximum vertical acceleration at the bow as a function of craft length for the critical value $\lambda/l = 1.5$

CONCLUSIONS

Assuming that the wavelength and height are proportional to the length of the hydrofoil craft, in other words, that a craft of double length is running on waves which are twice as long and high, it may be concluded that:

1. On a following sea, where maximum pitch is the critical factor, the seaworthiness is nearly unaffected by size. Actually the seaworthiness improves slightly with decreasing Froude number, i.e., increasing length.

2. When going against the waves, vertical accelerations are critical, which, with increasing length of the craft, decrease more than proportionally with the Froude number.

Consequently the seaworthiness increases with the length of the craft, the more so when the comfort is taken into consideration.

LIST OF SYMBOLS

a =   angle of attack (effective)
b =   maximum span of hydrofoils
C_l =   lift coefficient
c =   speed of wave propagation

γ = course angle relative to wave propagation
D = damping force
d = damping ratio
F = submerged foil area (effective)
Fr = Froude number
F_d = submerged foil area, contributing to damping
φ_0 = static roll amplitude (radians)
φ = roll amplitude (radians)
g = acceleration of gravity
H = waveheight
h = index for heave
I = moment of inertia
k = design constant
L = lift force
l = craft's length
λ = wavelength
m = mass of the craft
N = damping
w = excitation frequency
w_n = natural frequency
p = index for pitch
ψ_0 = static pitch amplitude (radians)
ψ = pitch amplitude (radians)
R = redressing moment (per radian)
ρ = density
σ = steepness of waves
V = craft's speed
w = relative vertical speed
Z_0 = static heave amplitude
Z = heave amplitude.

REFERENCES

[1] Buermann, T.M., Leehey, P., and Stillwell, J.J., "An Appraisal of Hydrofoil Supported Craft," Trans.of the Soc. of Naval Arch. and Marine Eng., New York, 1953

[2] Crewe, P.R., "The Hydrofoil Boat; Its History and Future Prospects," Trans. of the Institution of Naval Arch., London, 1958

[3] Büller, K.J., "Neue und noch gröszere Tragflügelboote,"Schiff und Hafen, 1959, p. 802

[4] Schertel, H. von, "Tragflächenboote," Handbuch der Werften, Band II, Schiffahrts-Verlag Hansa, Hamburg, 1952

[5] Schertel, H. von, "Tragflügelboote," V.D.I. Zeitschrift, Band 98, No. 36, p. 1955, Postverlagsort Essen, Düsseldorf, 1956

[6] Reinecke, H., "Tragflügelboote," Schiffbautechnik, 8 Jahrgang, Heft 4, Berlin, 1958

[7] Berentzik, H., "Vergleich der theoretisch errechneten Beschleunigungen eines Trag-flügelbootes im Seegang mit den experimentell ermittelten Werten," Schiffbautechnik, 10 Jahrgang, Heft 7, Berlin, 1960

[8] Höer, C.C., "Ergebnisse von Beschleunigungsmessungen an einem 10-m—Tragflügelboot-Groszmodell im natürlichen Seegang der Ostsee," Schiffbautechnik, 9 Jahrgang, Heft 11 and 12, Berlin, 1959

[9] Abkowitz, M.A., "The Effect of Antipitching Fins on Ship Motions," Trans. of the Soc. of Naval Arch. and Marine Eng., New York, 1959

DISCUSSION

P. Kaplan (Technical Research Group, Inc., Syosset, New York)

I want to know if the results just depend upon the assumption that the system is a simple spring-mass system. It appears that hydrofoils alone as simple spring-mass systems are overdamped in free motion as a single-degree-of-freedom. You have no such thing as a natural frequency in many cases. Also, I would like to know if the result that vertical accelerations are maximum at ratios of wavelength to craft length equal to two-thirds and three-halves is true for all cases or just for the particular designs chosen for illustration.

A. Hadjidakis

I said at the beginning of my lecture that what I have done was done in a very general way and in a very simple way, because, otherwise, one would need a computer and would have to go into very difficult calculations. I have chosen this very simple spring and mass system to get some quick results and to make it clear that in any case the seaworthiness of bigger craft would be better than that of small craft. I meant, indeed, in all cases, except fully submerged foil systems.

I might say now concerning what one should take for the characteristic length of the craft; one had perhaps better take the distance of the extreme foils, or something like that, to obtain better results. I do not pretend the diagrams I have shown are very accurate, but the main thing I wanted to prove is the direction wherein we are going if we make craft bigger. What you said about the damping ratios, that hydrofoil craft are overdamped, I do not agree. Damping, as far as heave is concerned, is very high indeed, but damping on pitch depends on what sort of hydrofoil system you have. With our one-foil system, on very small craft we find damping ratios as small as 0.4, so in that case one can feel on different wavelengths what is approximately the critical frequency of the craft. If you look at Fig. 4 it will be clear that this critical frequency is not a well-defined thing; you cannot measure it very exactly.

P. Kaplan

You said that in following seas the important characteristic of seaworthiness is pitching. I think that heave is rather important, and that you get large possibilities of settling in the water just due to that motion as well.

A. Hadjidakis

I don't agree, because although the heave is there, of course, the pitch will be more important, making the craft nosedive. In that case the angle of attack of the foils decreases, which means that lift decreases too (Fig. 5). Quite a big lift reserve on the forward foils is then needed to take the craft up again for the next wave, because otherwise the nose will touch that wave and then what we call seaworthiness in that particular case is finished and one cannot go at full speed. That is what I meant; I insist on the pitch being the most important factor on a following sea because, if you would go down horizontally, which is the case when heave is the main factor, you still have the same lift-coefficient, and it would be a very poor design if the craft wouldn't go up then in time.

P. Kaplan

I want to know just how you get better performance from a small craft to a large one. You did not just increase the size, you also changed the speed. Now with Froude scaling we get the same relative values. Is there any particular way in which you did this or do you see any particular optimum way of carrying out this change in size and speed to obtain an improvement in the craft?

A. Hadjidakis

The speed of 45 knots was chosen for the big craft with a capacity of about 400 passengers because of economic and efficiency reasons, and in my opinion it is not necessary to have higher speeds. The owner of the passenger-carrying craft will generally not gain more money by a somewhat higher speed and I think the passengers will not even realize the small time gains they will have in that case. Hence the number of 45 knots was not chosen for some physical reason. There is, however, another aspect to this matter. We have experience with all sorts of craft of different sizes and the biggest one could carry about 70 passengers. We found weight is not going up as the cube of the length of the craft, but somewhat less than that. It is logical to give a bigger craft a higher speed, which helps a lot in keeping the foil dimensions and weight down. In our designs the foil weight is about 5 to 8 percent of the total displacement weight.

*   *   *

DESIGN AND INITIAL TEST OF ONR
SUPERCAVITATING HYDROFOIL BOAT XCH-6

Glen J. Wennagel
Dynamic Developments, Inc.
Babylon, New York

INTRODUCTION

The Grumman Aircraft Engineering Corp. and its affiliate, Dynamic Developments, Inc., are engaged in research and development programs directed toward practical, high-speed hydrofoil systems. Emphasis is placed on application to vehicles with water speeds between 50 and 100 knots. Three of the test programs which assist in this effort are considered to be of special interest to the Third Symposium on Naval Hydrodynamics. The first of these programs utilizes a whirling tank facility which enables hydrodynamic and hydroelastic tests on waterborne or underwater devices up to speeds of 100 knots. The second program utilizes a pendulum facility wherein hydrodynamic models swing through a water tank of variable water temperature and, consequently, variable vapor pressure.

The third test program utilizes a research and test craft with supercavitating surface-piercing hydrofoils, a supercavitating propeller and a gas turbine power plant. This vehicle has been chosen as the subject for discussion herein. Construction and initial tests have been performed under Contract Nonr 2695(00) with the Office Of Naval Research. The purpose of this test program is to determine the hydrodynamic efficiencies of the propeller and hydrofoil system over a speed range between 0 and 60 knots, and to investigate corrosion preventive measures for gas turbine engines operating in a marine environment.

GENERAL CHARACTERISTICS

General characteristics of the craft are shown in Figs. 1, 2a, 2b, and 2c. Overall length, with foils extended, is 23.3 feet. Clearance between the keel and the 60.0-knot water line is 2.08 feet. Takeoff gross weight, with one pilot, is 2550 pounds. Table 1 gives a complete weight statement.

HULL

The hull has been constructed from an aluminum sport boat manufactured by Grumman Boats, Inc. Three primary modifications have been made to the basic hull. The first is the addition of Lockfoam covered with three layers of fiberglass cloth to the forebody bottom. The new forebody lines were established through the addition of ribs installed external to

205

Fig. 1. The ONR supercavitating hydrofoil boat

the original hull. This addition increases forebody deadrise, so as to minimize wave impact loads on the hull, and forms a step on the hull bottom. Vertical tubes are installed within the boat and through the hull bottom aft of the step, to facilitate step ventilation. A second modification is an aluminum box aft of the transom of the basic boat which gives the craft a desired overall length and provides support for the tail hydrofoil and strut assembly. The third modification is an opening for the engine exhaust in the starboard side-skin near the aft end of the basic hull. Stainless steel sheet is used as a doubler around this cutout to provide strength over a region affected by the high temperatures of the exhaust.

The basic hull skin is fabricated by stretch-forming two pieces of sheet which are joined together at the keel. Riveted construction is employed to attach hull and box extension skins to ribs and longitudinal stiffeners. All the aluminum is 61S-T6 alloy.
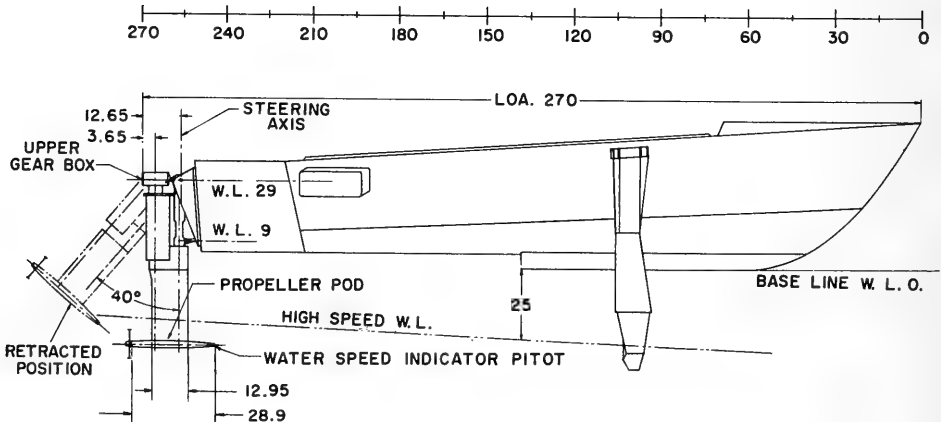
Fig. 2a. Side view of the ONR supercavitating hydrofoil boat (all dimensions in inches)
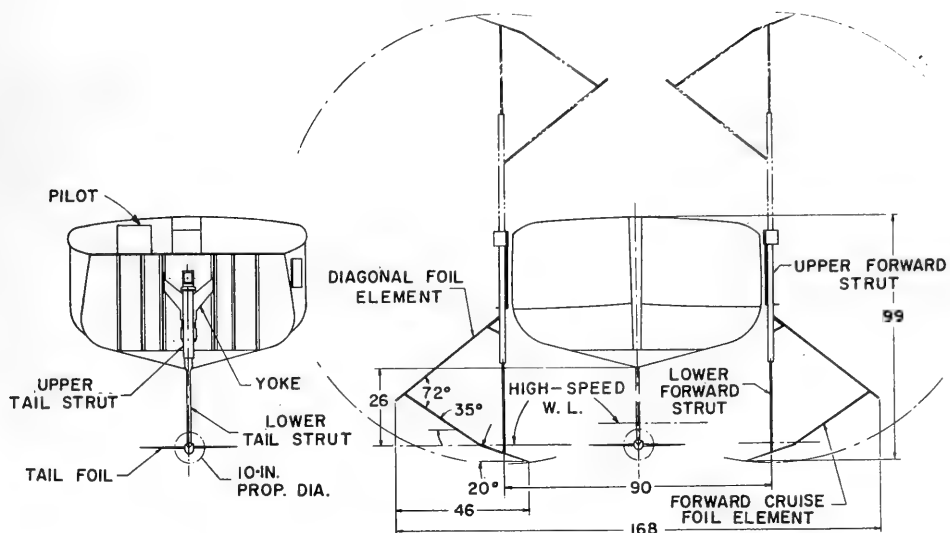
Fig. 2b. Front and rear views of the ONR supercavitating hydrofoil boat
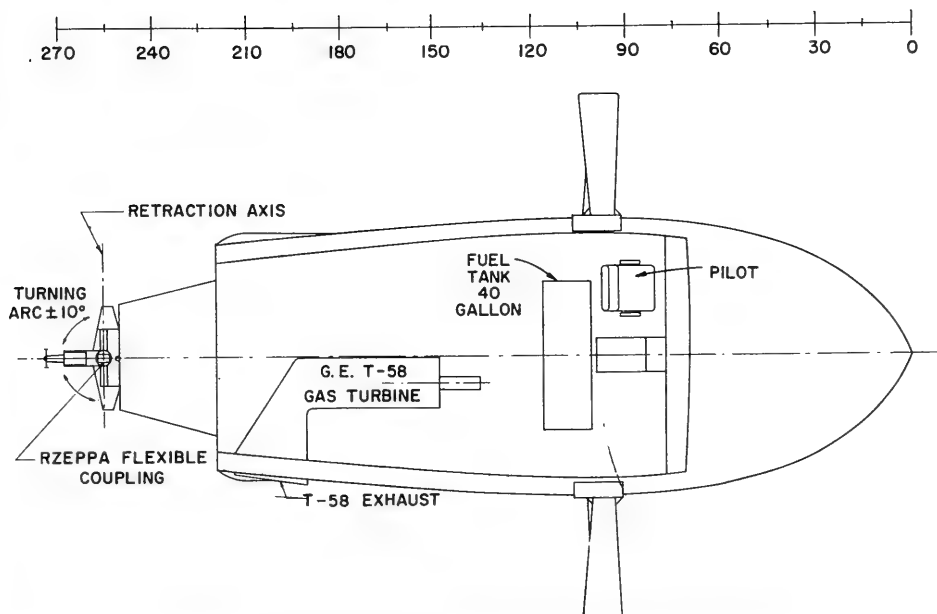
Fig. 2c. Top view of the ONR supercavitating hydrofoil boat

Table 1
Weight Statement

Item		Weight (lb)
Hull:		709
Basic Boat	425	
Forebody Bottom Addition	130	
Aft Box Extension	105	
Step Vent Tubes	14	
Pilot Seat and Supports	35	
Forward Foil Assemblies and Supports:		392
Support Fittings and Structure	80	
Upper Struts	94	
Lower Struts	64	
Diagonal Foils	84	
Cruise Foils	70	
Tail Foil Assembly:		155
Tail Strut	43	
Yoke	32	
Strut and Yoke Support Fittings	37	
Propeller Pod	25	
Upper Gear Box	12	
Tail Foil	6	
Transmission (All Gears, Shafting, Bearings, Seals, Couplings):		117
Powerplant:		598
General Electric T-58 and Reduction Box	375	
Engine Mounts	78	
Exhaust Duct and Hull Supports	60	
Bellmouth and Screen	10	
Cowl and Supports	15	
Throttle Control and Supports	15	
Tachometers and Throttle Slave	10	
Engine Instruments and Panel	35	
Lubrication and Fuel System:		211
Pumps	19	
Fuel and Oil	92	
Fuel Tank and Supports	10	
Oil Tanks (2) and Supports	41	
Fuel and Oil Lines	34	
Fuel (1) and Oil (2) Filters	15	
Steering System		42
Lear Actuator (For Tail Strut Incidence Adjustment)		13
Pilot and Equipment		210
Torquemeter		15
Air Bleed System		15
Battery		53
Propeller		10
Miscellaneous		10
Total		2550

HYDROFOIL SYSTEM

Two surface-piercing hydrofoils (one on each side of the boat) are located forward of the vehicle center of gravity and one fully submerged foil is located aft of the transom. Approximately 77.0 percent of the vehicle weight is supported on the forward hydrofoils.

As seen in Fig. 3, each of the forward hydrofoil assemblies incorporates a vertical strut supported to the hull in its upper region. A cruise foil element is attached to the lower end of each strut. A portion of this element is cantilevered so as to extend inboard of the strut bottom. In addition, it extends outboard and up from the lower end of the strut with positive dihedral. The upper end of each cruise foil is joined to the upper region of the strut by a diagonal foil element with negative dihedral.
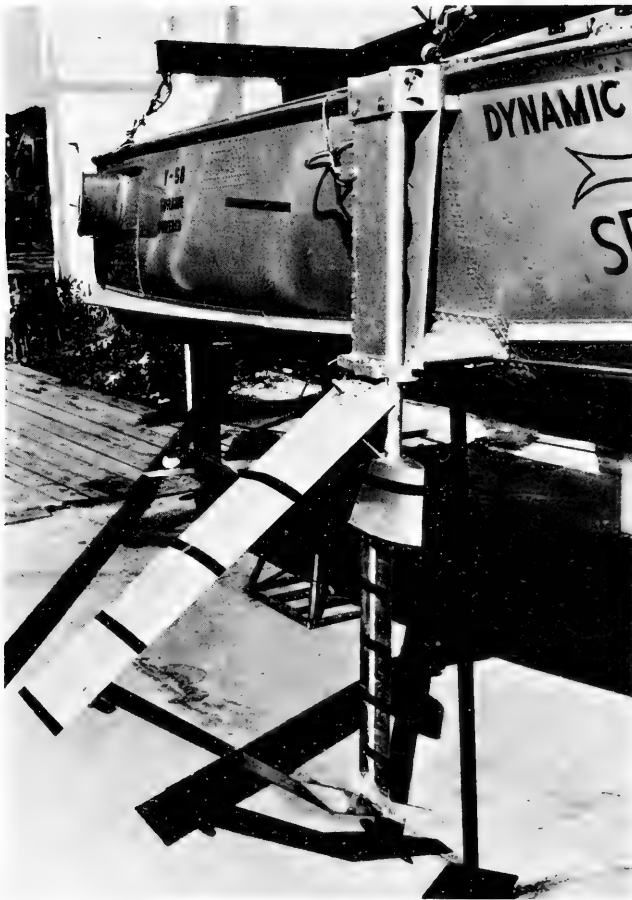
Fig. 3. A forward hydrofoil assembly

Cross sections of the foil and strut elements of the forward foil assembly are shown in Fig. 4. The cruise foil elements embody a basic supercavitating section which has a circular-arc bottom shape, a flat upper contour, a sharp leading edge, and a blunt trailing

T ⊢ ⎯⎯⎯⎯⎯⎯⎯⎯⎯⎯⎯⎯⎯⎯⎯⎯⎯⎯⎯ C ⎯⎯⎯⎯⎯⎯⎯⎯⎯⎯⎯⎯⎯⎯⎯⎯⎯⎯⎯

3°45′

└─ CIRCULAR ARC   LEADING EDGE RADIUS = 0.0.15 IN.

FORWARD CRUISE FOIL SECTION
R = RADIUS OF UPPER SURFACE CONTOUR

LOCATION	C IN.	T IN.	R IN.
OUTBOARD END	11.940	0.811	177.733
DIHEDRAL BREAK	8.394	0.578	124.688

⎯⎯⎯⎯⎯⎯ 12.0 IN. ⎯⎯⎯⎯⎯ ⌐ T

0.460

└─ CIRCULAR ARC   LEADING EDGE RADIUS = 0.015 IN.

FORWARD DIAGONAL FOIL SECTION
R = RADIUS OF UPPER SURFACE CONTOUR

LOCATION	T IN.
OUTBOARD TIP	0.72
INBOARD END	1.20

┌─ PARABOLA

⌐T   ┌─ 0.375 IN.

0.50 IN. ┘

⊢⎯⎯⎯ 2.75 IN. ⎯⎯⎯⊣⎯⎯⎯⎯ 4.0 IN. ⎯⎯⎯⎯

TRAILING EDGE RADIUS = 0.062 IN.

LOWER FORWARD STRUT SECTION

PERCENT CHORD	T IN.
60. I	0.375
81.5	0.375
92.7	0.260

Fig. 4. Cross sections of the elements of a forward hydrofoil assembly

edge. Over the lower regions of this element, a tapered afterbody is added to the basic section. At low speeds, prior to cavity formation, this afterbody reduces the drag which would exist for the basic section. At higher speeds, after cavity formation, the afterbody is essentially unwetted but still contributes to section strength and stiffness. The diagonal foil elements, which are wetted only during low-speed operation, employ a subcavitating cross section with a vented base. This section employs a flat bottom, a circular-arc upper

contour, a sharp leading edge, and a blunt trailing edge. The strut cross section employs a parabolic forebody and a tapered afterbody; the two regions of this section are separated by a step.

The tail hydrofoil (Fig. 5) employs zero dihedral and is supported on the forward half of the propeller pod; the pod is supported by a single strut. Figure 6 illustrates the strut and foil cross sections. The tail hydrofoil section is of symmetrical, subcavitating design and incorporates a low thickness ratio. A parabolic cross section with a blunt base is used on the tail strut. Propeller pod fineness ratio is approximately 8.5.
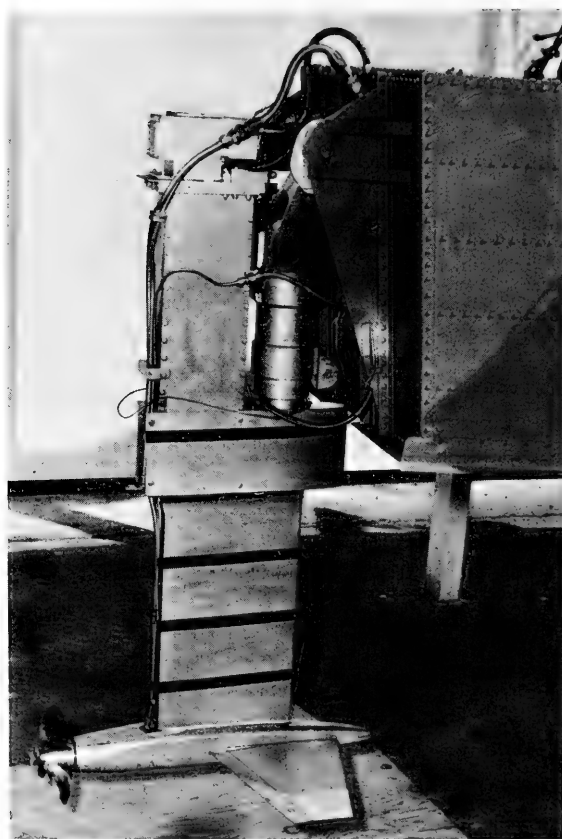
Fig. 5. The tail strut, propeller, and hydrofoil

The forward, cruise foil elements and lower struts are fabricated from solid stainless steel. Upper regions of the forward and tail struts are fabricated from heavy-gage aluminum plate. Diagonal foils, tail foil, lower tail strut, and propeller pod are machined from solid aluminum.

Each forward, cruise foil element is attached to its supporting strut by flush-head bolts which are inserted from the bottom side of each foil element and which extend into tapped holes of the struts. Diagonal to cruise element attachment is similar, with bolt

G. J. Wennagel
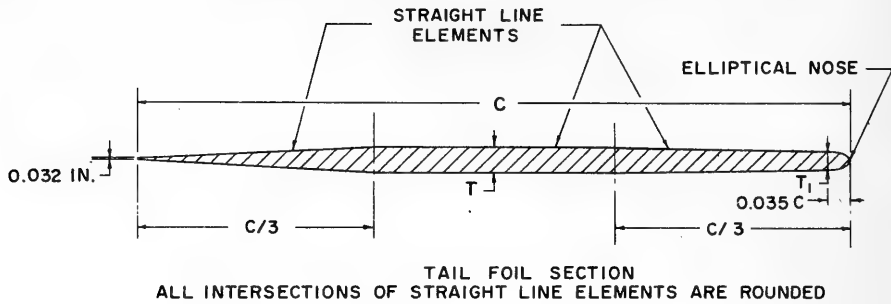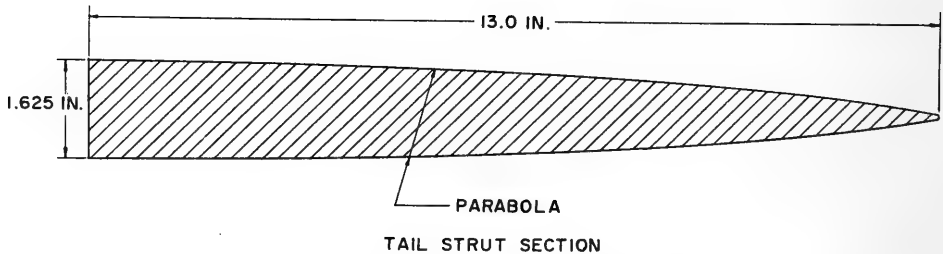
Fig. 6. Cross sections of the tail strut and hydrofoil

insertion from the upper side of each diagonal and with tapped holes in each cruise foil element. These intersections are thus maintained hydrodynamically clean without resort to bodies of revolution. Diagonal to upper strut connection on each forward foil assembly involves one fitting and connecting bolts. Each of the two lower struts extends up into an adjoining, hollow, upper strut; attaching bolts connect the mating segments. This design enables easy replacement or modification of any of the four, separate components which make up each forward hydrofoil assembly.

The propeller pod is split along a horizontal plane so as to form an upper half and a lower half. Suitable machining allows for the insertion of a one-piece tail foil between the upper and lower halves of the pod. Attaching bolts, which are externally flush, connect these three structural elements. Thus, emphasis has been placed on obtaining a design which allows easy replacement or modification of the tail hydrofoil.

A welded connection is employed between the upper half of the pod and the tail strut. This welding extends around the entire perimeter of the strut cross section and has been hand polished to obtain a smooth finish. Rigid and fixed connection between these two elements was a design requirement so as to allow subsequent, internal machining of both strut and pod in a manner that could guarantee proper alignment of transmission components.

An upper tail strut, of hollow construction, attaches to the top of the lower strut, and provides support at its upper end for a right-angle gear box. Gear box and lower strut attachment is by bolts to allow easy disassembly and inspection of internal transmission components.

All aluminum components are 61S-T6 alloy; all steel elements are 416 stainless alloy with an ultimate tensile strength of 150,000 psi. The struts, which employ constant cross section, were externally contoured by a single pass through a Whaley Machine of 14-inch diameter. A Keller BL Model C Machine was used for obtaining the more complicated external contours of the forward cruise hydrofoils.

CONTROLS AND RETRACTION

The boat is steered by rotation in yaw of the entire tail strut-pod-foil assembly. Tail foil incidence with respect to the keel is adjustable while foilborne, and a trailing edge trim tab is provided on the cruise foil element of one forward hydrofoil assembly. Each of the three hydrofoil assemblies is separately retractable.

Tail assembly retraction, steering, and incidence adjustment in pitch are accomplished by means of a unique, structural yoke. The yoke is an aluminum casting with machined surfaces. As shown in Fig. 2a, the yoke provides support to the tail strut at two, vertically separated locations. Both of these supports are through sleeve bearings on cylindrical portions of the yoke structure. The bearings, in turn, support an aluminum tube which is rigidly bolted to the strut assembly at both support points. The sleeve bearings allow rotation of the tail assembly in yaw, about the tube and steering axis. This axis, extended, coincides with the 20.0-percent chord line of the lower strut. Each of the bearings can transmit loads in a horizontal plane. Up and down loads are transferred from the tube to the yoke at the lower and upper bearing supports, respectively. The upper end of the tube and the top of the strut are joined by a fitting. This fitting supports the upper gear box and has an arm extending out on its port side. Connected to the arm is a fore and aft push-pull rod of the steering system. Rod loads establish equilibrium of the tail assembly in regard to moments applied about the steering axis and motion of the rod provides steering action. Strut displacement in yaw is limited by stops to plus or minus 6.0 degrees. The remainder of the steering system provides for mechanical, irreversible control from the pilot's wheel. At high speed, only small strut rotations are required; a wheel-to-strut rotation ratio of 54.5 to 1.0 is employed.

Yoke support to the hull is provided at three pickup points. Two points at the upper end of the yoke, separated athwartship, are hinged on a lateral axis. Rotation about this axis allows for both retraction and for tail foil incidence adjustment. Each of the two upper support points can transmit loads in all directions. The third support point is at the bottom of the yoke and is attached to the hull through an electrically operated, linear actuator manufactured by Lear, Inc., Instrument Division, Stamford, Connecticut (Model No. 434-AJ). Variable length of this support, in the fore and aft direction, allows incidence change in pitch while foilborne. This attachment is designed to take only axial (fore and aft) loads.

The vertical steering axis and the lateral retraction axis intersect at a point on the vehicle vertical plane of symmetry. Also passing through this point is the centerline of longitudinal, transmission shafting. A Rzeppa coupling in the transmission, at this three-axis intersection, allows for simultaneous transmission of power, tail assembly incidence change in pitch, and tail assembly steering. Manufacture of the flexible coupling is by Dana Corp., Con-Vel Division, Detroit, Michigan (Model No. OR).

Three pickup points on the hull support each upper strut of the forward foil assemblies. Two points on top of each strut, separated in the fore and aft direction, are hinged on a longitudinal axis. Each of these supports can take loads in all directions. A third support

on each strut is located at the chine. It consists of a manually operated, locking handle which can take loads in the lateral direction only. When this latter support is unlocked, each forward foil assembly can be retracted by rotation outboard and up.

Provision has been made to avoid damage to the primary hull structure in case the hydrofoils strike a solid object. On the forward foil assemblies, shear pins which attach the support fittings, on top of the upper struts, to the upper struts are designed to fail under specific loads. In the event of a failure, the affected forward assembly can leave the vehicle in the aft direction; the support at the locking handle, near the chine, allows this motion without restraint. On the tail assembly, retraction can occur, under a crash condition, by means of a shear pin incorporated in the lower yoke support and designed to fail under a specified load. In the event of such failure, damage would be localized to the Rzeppa coupling in the longitudinal transmission shafting.

A manually operated, trailing edge trim tab is installed on the cruise foil element of the starboard forward foil assembly. It allows trim of the vehicle in roll.

TRANSMISSION

Line shafting runs aft from the engine to the upper gear box, down through the tail strut to the propeller pod and then aft to the propeller. The transmission arrangement is shown in Fig. 7. Precise design and manufacture has achieved a rigid design criteria of minimum frontal area on the strut and pod. At 200 hp and at the maximum output speed of the engine reduction box, 6000 rpm, gears and bearings are designed for a 50-hour life. Design and manufacture was by the Medium Steam Turbine and Gear Division, General Electric Company, Lynn, Massachusetts.

Shafting between the engine and upper gear box incorporates a torque sensor, a torque limiting shear pin and couplings with bearing supports. At the intersection of the transmission, retraction, and steering axes, a Rzeppa coupling allows both angular misalignment and parallel offset of shaft centerlines.

Upper gear box and pod each contain a right-angle, spiral bevel gear set of 1.0 to 1.0 ratio wherein each gear incorporates a 35-degree spiral angle and a 20-degree pressure angle. They are of 3.0-inch pitch diameter and 7.0 diametral pitch. All gears are keyed to their respective shafts except for the pod pinion which has a major diameter fit fixed spline and a rear face which shoulders against its drive shaft. Material is AISI-9310 aircraft quality stock. Teeth were case-carburized to 60-63 RC after generating and then finish ground. The gears were developed with proper contact patterns on both sides of the teeth so that a single grinder set up could produce the gearing for both the upper and pod bevel sets.

Connection between the upper gear box and the pod pinion drive shaft is made by a free-floating, internally splined quill shaft in the upper strut. A ball bearing carries the thrust reaction of the pod pinion, and this bearing has been located in an area well above the high-speed water line where sufficient housing volume is available without detrimental effect on drag. The length of the drive shaft between the thrust bearing and the pod pinion is approximately 26.0 inches. Pod pinion radial reactions are carried by precision needle bearings. The pinion drive shaft is induction-hardened and ground in the locale of these needle bearings to serve as integral bearing races; this feature acts to further reduce frontal area. The pod pinion's axial load component was selected to be of minimum value

1 LOCKNUT
2 LOCKWASHER
3 ROLLER BEARING
4 SNAP RING
5 WASHER
6 SPACER
7 LOCKNUT
8 LOCKWASHER
9 BEVEL GEAR
10 KEY
11 KEY
12 BEARING RETAINER
13 BALL BEARING
14 SPACER WASHER
15 SPACER WASHER
16 MACHINE SCREW
17 LOCKNUT
18 LOCKWASHER
19 SHAFT SEAL
20 UPPER DRIVE SHAFT
21 MACHINE SCREW
22 SNAP RING
23 SHIMS
24 SPACER WASHER
25 SNAP RING

26 UPPER VERTICAL SHAFT
27 BALL BEARING
28 MACHINE SCREW
29 ALIGNMENT WASHER
30 METAL PLUG
31 VERTICAL DISTANCE PIECE
32 SOLID RING
33 SPLIT RING
34 SHIM
35 SHIM
36 SHAFT SEAL
37 LOWER VERTICAL SHAFT
38 NEEDLE BEARING
39 NEEDLE BEARING
40 BEVEL GEAR
41 SPACER
42 SPLIT WASHER
43 ROLLER BEARING
44 LOCKWASHER
45 LOCKNUT
46 BEVEL GEAR
47 SNAP RING
48 SPACER WASHER
49 ROLLER BEARING
50 SHIMS

51 BEARING GREASE SEAL
52 BEARING RETAINER
53 SPACER WASHER
54 SHAFT SEAL
55 PROP KEY
56 WASHER
57 BALL BEARING
58 WASHER
59 SPLIT WASHER
60 BEARING RETAINER
61 BEARING LOCK PLATE
62 ALIGNMENT CUP
63 SHIM
64 BEARING RETAINER
65 ROLLER BEARING
66 BEVEL GEAR

FIGURE NO 6
TRANSMISSION ARRANGEMENT

DWG 7492E81 GENERAL ELECTRIC
POWER TRANSMISSION, PHOTO NO.8125104

NOTES:
KEYS TO BE FITTED AT ASSEMBLY
BEVEL GEARS SHIMMED FOR PROPER
CONTACT AT ASSEMBLY

Fig. 7. The transmission arrangement

while the gear's axial component is of maximum value. The hand of the spiral angle is such that the gear's axial reaction is out of mesh, or to the rear, in direct opposition to the propeller thrust. This allowed for the use of relatively small propeller shaft thrust bearings, since the net bearing thrust load is the difference of these forces. Two thrust bearings are employed just forward of the propeller shaft seals. Two roller bearings straddle-mount the gear to provide radial reactions.

Shafting in the upper gear box and the quill shaft are of 4340 stock with induction-hardened splines. The pod pinion drive shaft is of 4350 stock while the propeller shaft is of forged and age-hardened K-monel. The areas of seal contact on the transmission input shaft and propeller shaft are built up with a copper flash followed by a nickel flash and a hard chrome plate.

Seals are of the double lip type and made of Sirvene 7080, a material chosen for its sea-water resistance. A single seal is used at the drive input with system lube oil depended upon for lubrication. Tandem seals packed with a sea-water-resistant grease are used on the propeller shaft. An interesting feature is that the pod structure is split horizontally along its longitudinal axis and bolted together on assembly. The pod machinery area is sealed by filling a machined groove, which runs along the periphery of each half, with a room-temperature self-curing, silicone rubber compound.

Damage due to galvanic action has been controlled by careful selection of materials exposed to sea water. Like the propeller shaft, the pod seal carrier is of K-monel. A locking ring, used to retain the seals, is cadmium plated. All lube and scavenge fittings and lube oil supply lines and grease fittings are of aluminum. To date, there is no evidence of erosion due to galvanic action.

The lubricant used conforms to specification MIL-0-6086 (light). This is a petroleum-base aircraft gear oil containing extreme pressure additives. An electric pump in the lube supply system delivers two quarts of oil per minute at 20 psig. A pressure sensing switch has been incorporated in the supply line. If the pressure falls below 15 psig, this switch opens a return line from the engine fuel control to the fuel tank and engine shutdown is thereby automatic. A panel light then goes on to inform the pilot of the reason for engine shutdown. Total oil flow is divided by a tee located at the boat transom so that one quart per minute is supplied both to the upper gear set and to the pod gearset. Gear mesh and input shaft thrust bearings are pressure-lubricated in the upper gear box. Oil mist and oil flow by gravity lubricate the remaining gear box bearings, the spline couplings of the quill shaft, and the thrust bearing of the pod pinion drive shaft. A single lip seal directly beneath the pod pinion thrust bearing prevents leakage of oil to the pod. An oil scavenge port is located at the level of this seal to allow the return of the lubricant to the lube system. Needle bearings for radial load reaction on the pod pinion drive shaft are grease packed on assembly, and a grease fitting is provided to the uppermost of these bearings. A spray nozzle, to pressure lubricate the pod gearset, is located at the aft end of the pod-strut juncture. Oil mist is depended upon to lubricate the propeller shaft roller bearings. The pod is bored to give the effect of a shroud about the driven bevel gear. Dual channels run axially from below the gear to a sump just forward of the foremost roller bearing. This sump is shrouded to break up windage effects from a roller bearing locknut. The lubricant is then scavenged through drilled passageways up through the strut where connection to the lube scavenge system is made. Propeller shaft thrust bearings are grease packed and are provided with ring seals. Wash out of the grease packing by lube oil is prevented by slinger rings on the propeller shaft. Scavenge lines are joined at the transom into one line which continues forward. An electric scavenge pump returns the lubricant to a reservoir. An oil cooler has been found unnecessary and is not used.

Magnetic drain plugs are employed in the strut and in the pod to provide indication of gear or bearing wear.

ENGINE

Power is supplied by a General Electric YT-58-2 free turbine engine. Maximum turbine output speed is 19,500 rpm. An engine gear box with a 3.25-to-1.0 ratio reduces the output shaft speed to a maximum of 6000 rpm. At this speed, the engine has a guaranteed normal continuous rating of 900 hp on a 59°F day and 765 hp at 80°. Although available power is greatly in excess of vehicle requirements, its light weight and desirable output speed make the T-58 particularly well suited for this application. Engine fuel and lubrication systems are in accord with normal practice for this engine, with 5-micron and 25-micron filters installed in the engine fuel and gear box oil supply lines, respectively.

A goal of this program has been to determine the location and degree of corrosion effects on engine components and to test thereafter various coatings and changes in material so as to systematically accomplish a final marinization of the YT-58-2 engine. Accordingly, initial installation utilized a standard engine, No. SN-200-103, without any special component protection, external cowling, or maintenance procedure.

External corrosion was first observed on small, unpainted areas of the engine's magnesium front frame and of the magnesium reduction gear box. Further corrosion was then prevented in these locations by a grease coating. Thereafter, stiffness became apparent in the linkage motion of the variable stator system. This stiffness was then corrected by periodic application of oil. Subsequent corrosion occurred on other exterior components. Again, after observation for a suitable period of time, further corrosion was halted in each locale by regular application of grease or oil.

Engine operation was continued, with inlet exposure to direct salt-water spray, until the turbine inlet temperature reading at idle had increased to approximately 100° C higher than normal. Removal of the compressor casing revealed a significant amount of corrosion throughout the entire compressor, with the effects of corrosion increasing toward the later stages. Although the aerodynamic configuration of the higher stage blading had been materially affected, engine starting difficulty had not been encountered. The compressor rotor was cleaned by hand using large, gun barrel brushes; blades were removed and cleaned with an aluminum oxide blast. The engine was reassembled and a cowling was installed to protect the inlet from direct salt-water spray. In addition, engine washdowns were begun whereby 2.5 gallons of fresh water were sprayed into the inlet just prior to engine shutdown after each test period. A second period of operation, equivalent to the first, was completed and internal engine components were again inspected. It was found that the simple procedures then adapted had essentially halted the spread of further corrosion. Engine temperatures and operation remained normal over the observation period.

A second engine, No. SN-200-102, has recently been installed and is currently being used during test operations. It is a modified engine intended to test the effectiveness of certain coatings in preventing corrosion of engine components. Table 2 gives a list of these components and their coatings. Prior to installation, test-stand operation was completed by the General Electric Company to determine the effects of these modifications on aerodynamic characteristics. They have been found small, and guaranteed performance ratings remain unchanged. Vehicle operation will continue to use engine washdowns, exterior oil application and inlet cowling. While no effects of corrosion have yet been observed with this engine, insufficient operating time has been accumulated to allow proper conclusions.

Table 2
Marinization Changes to the YT-58-2 Engine

Engine Dash No.*	Engine Item	Material and Specification No.	Coating or Treatment
102 and 101	Front Frame	Magnesium AMS 4434	Nubelon S
102 and 101	Compressor Casing	Steel, G. E. SAED B50T1131	Nickel Plate
102 and 101	Compressor Rear Frame	Steel, G. E. SAED B50T1131	Nickel Plate
102	Compressor Spool & Blade Assy	Steel AMS 6451	Nubelon S
102 and 101	Compressor Sta. Vanes & Rings	Steel AISI 405	. . . .
	Stages 1 thru 7	. . . .	Nubelon S
	Stages 8 and 9	. . . .	Heresite
	Stage 10 and Exit Vanes	. . . .	Silicone Alum.
102 and 101	Combustion Chamber Casing	Steel, G. E. SAED B50T1131	Nickel Plate
101	Variable Stator Actuating Rings	Steel AISI 410	Chrome Plate
101	Variable Stator Actuator Levers	Steel AMS 5120	Nickel Plate
101	Main Reduction Gear Case	Magnesium AMS 4434	Replace with Aluminum, Alodine
101	All Magnesium Engine Components	Magnesium AMS 4434	Replace with Aluminum, Alodine
101	Compressor Spool	Steel AM-355	Nubelon S

*This column identifies the changes as applying to the second engine, No. SN-200-102, or to the third engine, No. SN-200-101.

A third engine, No. SN-200-101, is being modified for later installation and test. It includes all of the coatings incorporated in the second engine, with additional changes as given in Table 2. It is hoped that this engine, after test-stand operation and waterborne service with suitable operating procedures, will represent a final marinization of the YT-58-2 engine.

PROPELLER

The propeller is located on the aft end of the propeller pod behind the tail foil and strut. It has been designed and manufactured by personnel of the David Taylor Model Basin for zero cavitation number and in accordance with the DTMB three-bladed, supercavitating propeller series. This series is fully described in Refs 1-3. Propeller diameter is 10.0 inches; pitch ratio at the 70.0 percent radius is 1.61; expanded area ratio is 0.457; blade thickness fraction is 0.024; rotation is clockwise looking forward. Propeller material is

stainless steel with an ultimate tensile strength of 140,000 psi. A design feature is a nylon liner between the propeller hub and the propeller shaft. The shaft is tapered and propeller attachment is by means of a locknut and a brass key. Friction between the hub and shaft is reduced, by the nylon liner, to a very low value. This reduced friction, together with a torque limit on the locknut, has enabled specification of key size such that key failure in shear occurs at a predetermined value of propeller torque. Protection to transmission components is thereby provided for a condition wherein the propeller might strike floating debris or some solid object. Laboratory tests were undertaken to determine proper key size; failure of the key occurs at a torque of 2500 inch-pounds.

INSTRUMENTATION

Instrumentation has been incorporated to provide cockpit indication of water speed, propeller torque, propeller rotative speed, propeller thrust, keel trim in pitch, tail foil incidence in pitch with respect to the keel, tail strut position in yaw, transmission and engine oil temperatures and pressures, compressor and power turbine speeds and temperatures, and fuel pressure.

The propeller torque measuring device is installed in the horizontal transmission shaft aft of the engine gear box. It is a torque transducer, Model No. TG-5-3000A, manufactured by the Crescent Engineering and Research Company, El Monte, California. The core or sensor section of the transducer incorporates a solid shaft which acts as a torsional spring. It is splined at its ends to mating sections of the drive shaft, and is enclosed by a cylindrical, fixed pickup unit. Cylindrical crowns are attached to the shaft of the sensor section at two locations which are separated along its longitudinal axis. The crowns have intermeshing teeth which extend around the center region of the solid shaft. Torque causes a change in the size of air gaps which exist between the intermeshed teeth of the two crowns, and this change modifies the magnetic reluctance. The variation in reluctance effects proportional changes of impedance in two coils of the enclosing pickup unit. The coils perform as two legs of an ac bridge to reflect electrical unbalance which is proportional to torque. This unbalance is amplified, demodulated and applied to a microammeter which reads torque directly.

Propeller thrust is calculated by employing strain gages affixed to the linear actuator which attaches the lower yoke support point to the hull. Data is recorded on a portable oscillograph. Measured compression loads in the actuator enable the calculation of propeller thrust, as required for moment equilibrium about the retraction axis, based on estimated tail foil lift and tail assembly drag components, together with associated centers of pressure. The calculation of thrust is therefore approximate at the present time. It is planned to perform towing-tank tests of the tail assembly to accurately measure estimated quantities and to thereby provide more accurate calculation of propeller thrust.

FLOW CONDITIONS

Flow conditions involve cavities over the upper surface and behind the blunt base of each forward cruise foil, behind the blunt base of each forward diagonal foil, along the afterbody sides of the forward struts, and behind the blunt base of the tail strut. All other regions of foils and struts experience subcavitating flow.

Hydrofoil and strut design provides several air paths to cavity regions. Forced ventilation is provided through tubes to the blunt base of the tail strut and to the blunt trailing edge regions of the diagonal and cruise foil elements of each forward hydrofoil assembly. Air supply for this purpose is obtained from two bleed ports located aft of the compressor section

of the gas turbine power plant. Air flow utilized from each port is approximately 0.20 lb/ sec. Natural paths, for air flow from the atmosphere, are also provided. The blunt base of the tail strut extends through the water surface. Similarly, air can flow from the atmosphere to the sides of the afterbody on the forward two struts. At high speed, therefore, only the parabolic forebodies of the forward struts are wetted. The cavities along the afterbody sides can interconnect with cavities on the upper surface of the forward cruise foil elements. A natural air path to the cavity regions of the forward cruise foil elements is also provided along the blunt trailing edges of the diagonal and cruise foils. These blunt bases are connected to each other at the intersection of the two foil elements. In addition, the cavity regions of the cruise foils, at high speed, open directly to the atmosphere since these elements are surface piercing and this forms their primary source of air under cruise conditions. A further possibility for air supply to these regions is through vortices from the foil inboard tips which can extend aft and up to the water surface.

Air from the atmosphere flows to cavity regions with velocity and associated pressure drop. Resultant cavity pressures are thus intermediate between vapor and atmospheric pressures.

A goal of testing at Grumman Aircraft and Dynamic Developments, Inc. is to develop hydrofoil systems which can make a smooth and stable load transition from subcavitating conditions at low speeds to cavity flow conditions at high speeds. Each type of flow is thereby utilized over the speed range where it best affords maximum lift-to-drag ratio. Both surface-piercing and fully submerged foil systems are envisioned which can accomplish this smooth flow transition, and it is expected that several foil arrangements will eventually be tested on the XCH-6.

PERFORMANCE

Curves of estimated vehicle drag and thrust available are plotted vs velocity in Fig. 8. These are typical curves which pertain to current vehicle operation at a gross weight of 2550 pounds. In practice, both thrust available and drag curves can be altered.
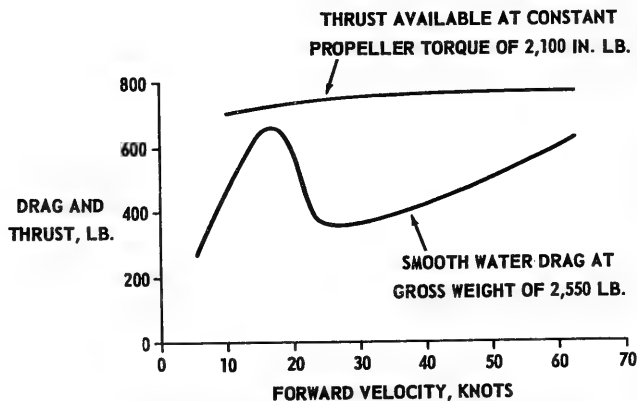
Fig. 8. Estimated smooth water drag and thrust available

Thrust available is dependent upon the size of the shear pin located in the horizontal transmission shafting, aft of the engine gear box. These pins are hollow. The choice of inside diameter and pin material alloy allows selection of maximum transmission and propeller torque. This, in turn, determines available propeller thrust at each forward speed. Normal vehicle operation utilizes a shear pin which is designed to fail when propeller torque reaches 2100 inch-pounds.

Component drag prediction for operation in smooth water has been based upon methods outlined in Refs. 4 and 5. Such prediction appears to be in good agreement with test results obtained to date. The total smooth water drag values given in Fig. 8 can be considered to correspond to normal operation, but the low-speed region can be altered depending upon pilot adjustment of tail foil incidence in pitch with respect to the keel. Minimum takeoff speed, the speed at which the keel just clears the smooth water surface, is approximately 20.0 knots at a gross weight of 2550 pounds.

The propeller was designed to develop 774.0 pounds of thrust at a speed of 62.0 knots and at the maximum rotative speed of 6000 rpm. Predicted propeller efficiency, under these conditions, is 73.9 percent. Associated propeller torque is 2100 inch-pounds.

For operation in smooth water at 60.0 knots, the total drag is estimated to be 660.0 pounds. Only 20.0 percent of this value corresponds to drag due to lift; 8.0 percent is attributed to spray drag; 16.0 percent is due to air drag; the remaining 56.0 percent is due to friction plus pressure drag of wetted elements. This distribution of drag is important when considering vehicles of much larger size with the same cruise speed. Larger craft can be expected to incorporate suitable aerodynamic streamlining, not employed on the XCH-6, and will benefit from considerably reduced friction drag coefficients associated with larger chords and consequently higher Reynolds numbers.

INITIAL TRIALS

Several features of the present configuration have resulted from initial testing.

The nylon liner between the propeller shaft and the propeller hub was provided after an early run wherein the propeller struck a piece of floating debris. The transmission was protected by a shear pin in the drive shaft for conditions of excessive torque from the engine. When excessive torque was suddenly applied from the propeller, however, the inertia of transmission components allowed the bevel gears within the pod to feel the overload prior to shear-pin failure. The result was a tooth failure on one of the bevel gears. Damage to the propeller, consisting of a few nicks on blade leading edges, was very slight and easily corrected by filing.

A reduction in drag, associated with forced air ventilation, was first established by providing air to the blunt base of the tail strut. It allowed the maintenance of given forward velocities with reduced propeller speeds. Provision for forced air supply was then extended to include the blunt base regions of the forward hydrofoils.

During initial trails, a slight porpoising was encountered at approximately 40.0 knots. The oscillation was of constant amplitude, without either build up or decay. It was theorized that ventilation behind the blunt base of the tail strut extended over the sides of the pod near its aft end so as to cause a small decrease in total lift of the tail assembly. This change in lift caused a small increase in vehicle trim and a corresponding increase in pod

immersion. At the increased immersion, the flow again reseated on the affected region of the pod, initial lift and trim were restored, and the process would then repeat itself, causing a mild and steady oscillation. A small plate was added on top of the pod and behind the strut so as to limit the extent of the air cavity. This change eliminated further oscillation.

Forward foil design has successfully provided a smooth and stable manner of cavity formation over the cruise foils. It is significant that the vehicle has never experienced adverse roll due to uneven extent of ventilation, one side to the other. Further, it has never experienced abrupt changes in pitch as might be caused if ventilation or flow reseating occurred abruptly. This is true for both smooth and rough water operation, and for running at either a constant heading or during turning maneuvers.

CONCLUSIONS

1. Forced air ventilation, into regions behind the blunt base of a strut or foil, is a practical means of drag reduction.

2. Within the limits of completed testing, predicted propeller and ventilated hydrofoil efficiencies have been confirmed.

3. Ventilated hydrofoil systems can be designed to allow cavity formation in a smooth and stable manner. They offer the elimination of abrupt loss in lift associated with some subcavitating foil systems when ventilation occurs. Complete flow stability has been demonstrated over a wide variety of sea conditions and turning maneuvers.

4. Supercavitating foil sections, as compared to subcavitating types, exhibit a reduced lift curve slope which minimizes incremental lift changes associated with orbital velocities within waves. This feature, together with satisfactory hydrodynamic efficiencies, appears to offer an important field for future development.

ACKNOWLEDGEMENTS

REFERENCES

[1] Tachmindji, A.J., Morgan, W.B., Miller, M.L., and Hecker, R., "The Design and Performance of Supercavitating Propellers," David Taylor Model Basin Report C-807, Feb. 1957

[2] Tachmindji, A.J., and Morgan, W.B., "The Design and Estimated Performance of a Series of Supercavitating Propellers," p. 489 in "Second (1958) Symposium on Naval Hydrodynamics," Washington: Office of Naval Research, 1960

[3] Caster, E.B., "TMB 3-Bladed Supercavitating Propeller Series," David Taylor Model Basin Report 1245, Aug. 1959

[4] "Study of Hydrofoil Seacraft," Vol. I, Bethpage, New York: Grumman Aircraft Engineering Corp. and Dynamic Developments, Inc., Oct. 1958

[5] Johnson, V.E., Jr., "Theoretical and Experimental Investigation of Arbitrary Aspect Ratio, Supercavitating Hydrofoils Operating Near the Free Water Surface," NACA RM L57I16 (NASA, Washington), Dec. 1957

DISCUSSION

H. P. Rader (Vosper Limited, Portsmouth)

With my compliments to Mr. Wennagel and also to Mr. Tulin I should like to make just a few remarks concerning the practical application of supercavitating sections. Recently we have tested two propellers with supercavitating blade sections of wedge-shaped thickness distribution. The efficiency of both propellers under noncavitating conditions was rather poor. On analyzing the results according to the method of the equivalent polar curve as devised by Prof. Lerbs we found that the drag coefficients of the equivalent blade sections were much higher than those of supercavitating sections with quasi-elliptic or elliptic-parabolic thickness distribution. In fact the drag coefficients agreed very closely with values published in Dr. Hoerner's excellent book "Fluid Dynamic Drag." The drag coefficient ratios for various thickness-chord ratios are approximately as follows:

Thickness-chord Ratio	C_D Wedge/C_D Ellipse
0.04	2.5
0.06	4.0
0.08	5.5
0.10	7.1

When we design supercavitating hydrofoils and propellers we must not forget that the boat fitted with the equipment has to pass through the noncavitating speed range. This is particularly important for hydrofoil boats which have a pronounced hump in their resistance curve at a speed where supercavitating conditions may not be obtainable unless artificial ventilation is used. Even with ventilation the drag coefficients of wedge-shaped sections would be higher than those of quasi-elliptic or elliptic-parabolic sections under noncavitating conditions. I noticed in Mr. Wennagel's interesting paper (or rather in Fig. 8) that at the hump the resistance-displacement ratio of the craft described by him is approximately 0.26, which is rather high.

Marshall P. Tulin

With regard to Mr. Rader's comments on the efficiency of supercavitating sections with blunt bases operating in fully cavitating flow, it is, of course, certainly true that such sections are not particularly efficient because of the blunt base, which causes a drag that is proportional to the square of the base thickness. In fact, it was with some surprise that the

David Taylor Model Basin tests of supercavitating propellers revealed that the efficiency of such propellers at design advance ratio was essentially independent of cavitation number, implying that the efficiency was a little bit less at high cavitation number, that is, under fully wetted conditions, than it was in supercavitating operation, and thus indicating that very little price was being paid because of the drag incurred by the blunt section operating under fully cavitating conditions. With regard to the future, I would not care to speculate on what shapes practical supercavitating foils, designed for high performance craft, will take. Certainly in the case of fully submerged foils, flaps and perhaps other such devices will be included; and I think that we must be patient to see how foil shapes will evolve.

Glen J. Wennagel

In regard to Mr. Rader's comment on the ONR boat, the drag hump during takeoff is due in good part to the foil and strut blunt trailing edges. The design gross weight as stated was 2550 pounds. With a 2100-in./lb shear pin, which corresponds to 200 hp at 6000 rpm, we reach a point where the boat will not take off when the gross weight reaches about 3000 pounds. This is without forced air. If the pilot turns on the air, the reduction in drag is apparent and the boat will take off.

T. G. Lang (U.S. Naval Ordnance Test Station)

My comments are directed toward both Mr. Tulin's paper and Mr. Wennagel's paper.

The development of high-speed hydrofoil craft having surface-piercing hydrofoils or struts requires a detailed knowledge of the effects of air ventilation on hydrodynamic forces. The U.S. Naval Ordnance Test Station has conducted a series of experiments on hydrofoil models in which air was forcibly exhausted through ports in the hydrofoil surface. These experiments were conducted in the high-speed water tunnel at the California Institute of Technology in 1958 and 1959. The objectives of the studies were to investigate the use of forced ventilation for the purposes of control and of improving hydrofoil performance characteristics.

Figure D1 shows a model of one hydrofoil used in the tests in which a spanwise series of small holes can be seen just behind the leading edge. In this study, the chordwise location of the holes was varied and the spanwise length changed.

Figure D2 is a top view of this model mounted in the water tunnel showing air being exhausted through the series of holes, while Fig. D3 is a side view. The air did not spring forward of the exhaust point unless extensive cavitation occurred behind the leading edge or unless the hydrofoil was placed at an angle of attack above its fully-wetted stall angle. Figure D4 is a top view of this model placed at the stall angle of attack. The air is seen to ventilate forward of the holes.

Figure D5 is a top view of another model having the same contour in which a small amount of air is exhausted through a single hole in the upper surface. The angle at which the air diverged outward increased as the angle of attack increased. Figure D6 shows this same model at the same angle of attack but with an increased air-flow rate. It is noted that the sides of the air cavity are more distinct in the latter case and the thin, patchy type of ventilation which was seen in the previous figure has disappeared.
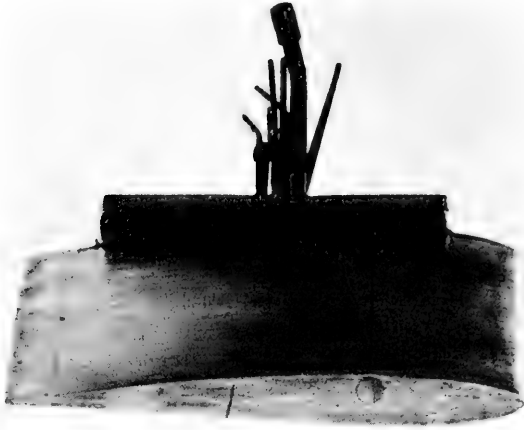
Fig. D1. Hydrofoil model

Fig. D2. Top view of the model shown in Fig. D1
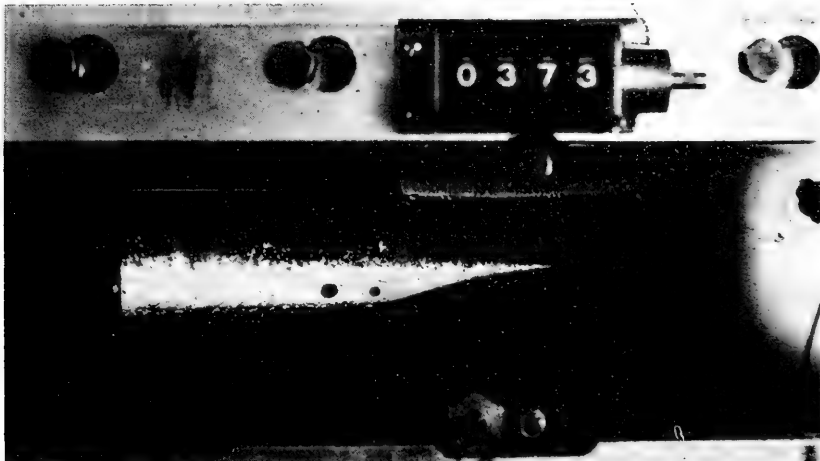
Fig. D3. Side view of the model

Fig. D4. Top view of the model at the stall angle of attack
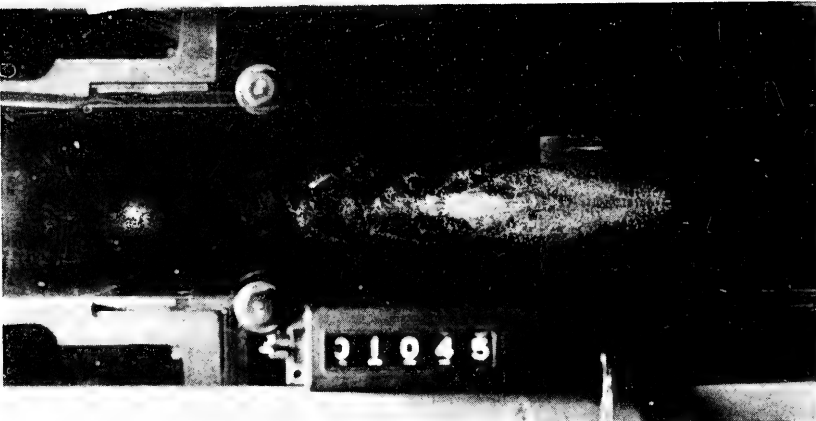
Fig. D5. Top view of a model with a single hole
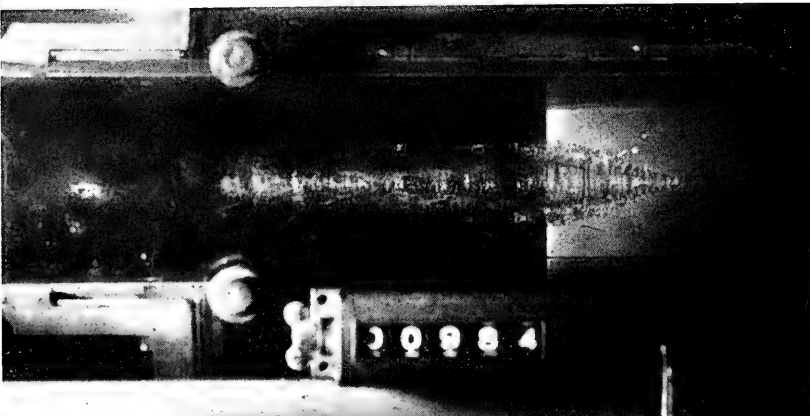
Fig. D6. Same model as Fig. D5 with increased air flow

Figure D7 is a plot of the lift coefficient versus angle of attack. The upper curve refers to fully-wetted flow and the lower curve to vented flow. Note the large decrease in
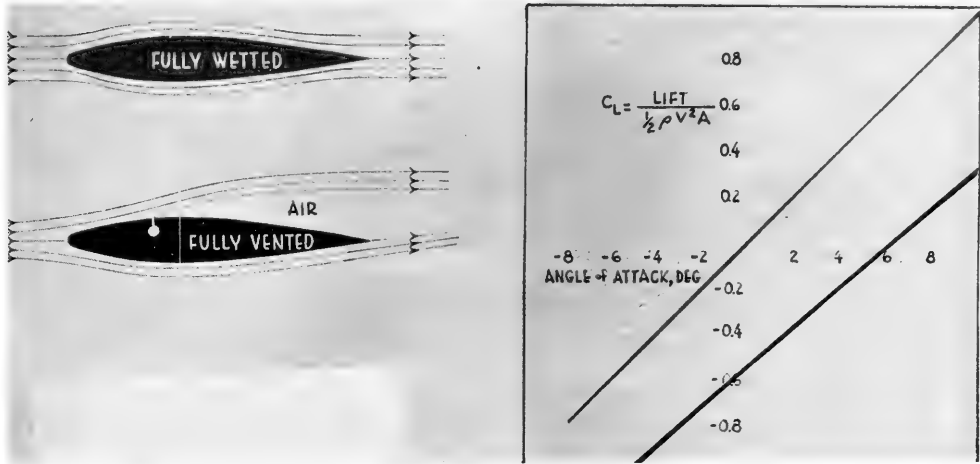
Fig. D7. Lift coefficient of (top curve) fully wetted and (bottom curve) vented hydrofoil

lift when the hydrofoil is forcibly vented. This type of ventilation can be induced by exhausting air through a port at any position on a hydrofoil and therefore may be used as a means of controlling the hydrodynamic forces developed by the hydrofoil. It should also be noted that the slope of the lift coefficient curve is reduced by ventilation. The references cited at the end of this discussion include theoretical work which predicts the lift and drag of two-dimensional hydrofoils of arbitrary shape vented at arbitrary chordwise locations for the case of zero ventilation number. Good agreement is shown with experiment.

Figure D8 shows top and side views of a hydrofoil model having a cambered parabolic cross section wherein air was exhausted through a hole in the trailing edge. The effective
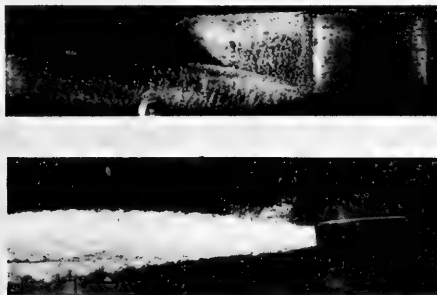
Fig. D8. Top and side views of a cambered parabolic hydrofoil with air exhausted through a hole in the trailing edge

aspect ratio in this photograph is 1.44. Note the shape of the air cavity at the tip. As in the previous test series, the air was not seen to ventilate forward of the trailing edge unless a region of separated water existed, such as that caused by stall, extensive cavitation, or boundary layer separation. Figure D9 shows this same hydrofoil in two-dimensional flow with a very small airflow rate. The vortex pattern seen behind the trailing edge disappears when the airflow rate is increased.

$Q' = 0.024, \alpha = 4°, R = \infty$
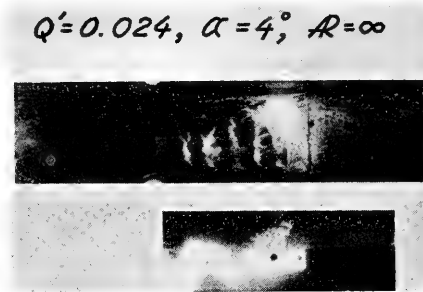
Fig. D9. Hydrofoil of Fig. D8, but
with a very small airflow rate

Figure D10 is a plot of the lift-to-drag ratio of the two-dimensional parabolic hydrofoil. The lift-to-drag ratio approaches 25 as the airflow rate increases. Higher ratios could have been obtained if tunnel blockage had not limited the minimum ventilation to $K \gtrless 0.14$.

SYMBOL V_∞, FT/SEC
o   30
△   20

SHADED SYMBOL-FULLY WETTED
CLEAR SYMBOL-VENTED

$R = \infty$
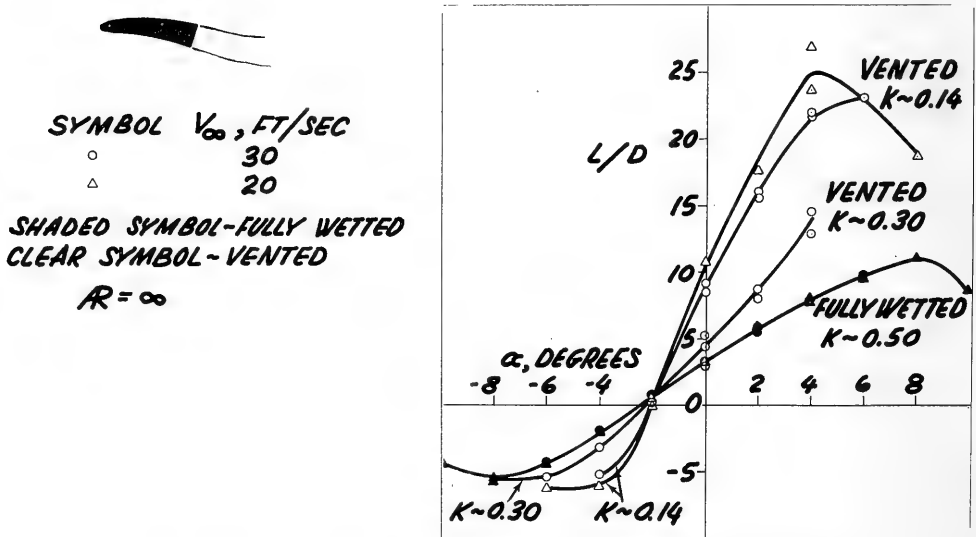
Fig. D10. Experimental lift-to-drag ratios of the two-dimensional, cambered, parabolic hydrofoil

Figure D11 is a table showing an analytical comparison at noncavitating speeds of a fully-wetted NACA 16-series hydrofoil and a base-vented parabolic hydrofoil. It is seen

that the cavitation-free speed at the surface may be increased from 20 to over 50 percent by use of the parabolic cross section. The lift-to-drag ratio, however, is decreased.

NACA 16-SERIES — **CAMBERED PARABOLA**

HYDROFOIL	PARAMETERS		RESULTS			
	c_L	t/c	c_D	l/D	$6i$	V_{cr} AT WATER SURFACE (KNOTS)
16-SERIES PARABOLA	.50	.15	.0101 .0166	49 30	.67 .32	33 48
16-SERIES PARABOLA	.25	.15	.0101 .0166	25 15	.51 .16	38 68
16-SERIES PARABOLA	.50	.10	.0094 .0117	53 43	.55 .32	37 48
16-SERIES PARABOLA	.25	.10	.0094 .0117	27 21	.39 .16	43 68
16-SERIES PARABOLA	.50	.05	.0086 .0088	58 57	.44 .32	41 48
16-SERIES PARABOLA	.25	.05	.0086 .0088	29 28	.28 .16	51 68

ASSUMPTIONS:

1. TURBULENT FLOW
2. $Re = 2 \times 10^6$, $C_f = .0039$
3. EQUAL c_L AND t/c
4. CIRCULAR ARC CAMBER LINE
5. $K \ll 1.0$
6. $\alpha = 0°$
7. $AR = \infty$
8. NO SWEEPBACK

Fig. D11. Comparison of hydrofoils having equal lift coefficients and thickness-to-chord ratios

Figure D12 shows a vented hydrofoil which is designed for optimum efficiency. It is constructed by first designing a strut having a thickness distribution and cutoff trailing edge which provides zero cavity drag in accordance with Tulin's linearized cavity theory for zero cavitation number. This strut is then cambered in such a manner that the pressure on the

ASSUMPTIONS: $K=0$, $\alpha=0°$, CIRCULAR ARC CAMBER LINE, $AR = \infty$,

TURBULENT FLOW, $C_f = 0.0039$

c_L	l/D	$6i$
1.0	128	1.28
.8	114	1.02
.6	96	0.77
.5	86	0.64
.4	73	0.51
.3	59	0.38
.2	42	0.26
.1	23	0.13

CUT-OFF FOR $C_{d_c} = 0$ AT $K = 0$

$C_P = 0$

CUT-OUT TO REDUCE FRICTIONAL DRAG

$$l/D = \frac{c_L}{C_f(1 + c_L)}$$
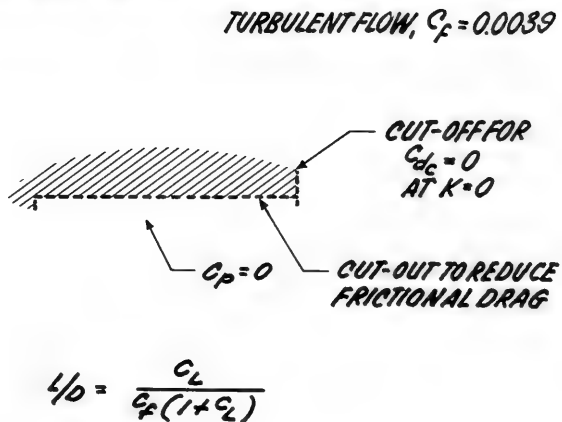
Fig. D12. Base-vented hydrofoil having optimum efficiency

lower side is static depth pressure. Once this is accomplished, the lower surface can be ventilated in order to reduce frictional drag. In this manner, all the lift is generated by the upper surface and the lift-to-drag ratio is optimized.

Figure D13 is a theoretical plot of the lift-to-drag ratio versus cavitation number of several hydrofoil shapes. The strength and lift of each of the hydrofoils was assumed to be equal to that of an NACA 16-510 hydrofoil. As the cavitation number was reduced, the chord length and thickness of each hydrofoil was varied to prevent cavitation. The assumptions were two-dimensional flow, a fully turbulent boundary layer, zero angle of attack, circular-arc camber line, and cavity pressure equal to depth pressure.
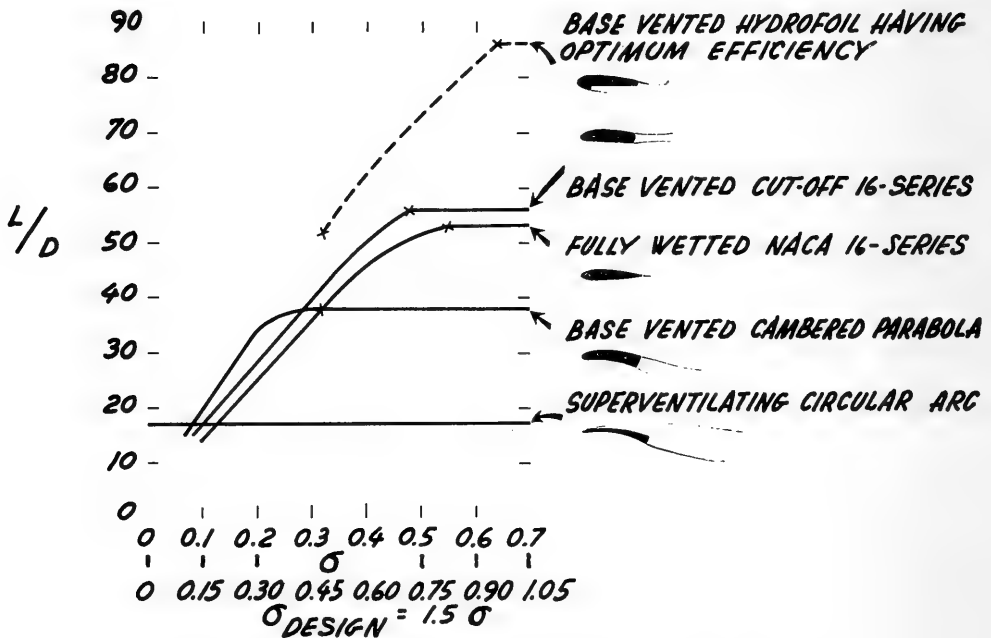
Fig. D13. Comparison of hydrofoils having equal strength and lift

The following reports published at the U.S. Naval Ordnance Test Station include more detailed results of these studies:

1. Lang, T.G., "Base Vented Hydrofoils," NavOrd Report 6606, Oct. 19, 1959
2. Fabula, A.G., "Theoretical Lift and Drag on Vented Hydrofoils for Zero Cavity Number and Steady Two-Dimensional Flow," NavOrd Report 7005, Nov. 4, 1959
3. Lang, T.G., and Daybell, Dorothy A., Smith, K.E., "Water Tunnel Tests of Hydrofoils With Forced Ventilation," NavOrd Report 7008
4. Lang, T.G., and Daybell, Dorothy A., "Water Tunnel Tests of a Base-Vented Hydrofoil Having a Cambered Parabolic Cross Section," NavWeps Report 7584, Oct 10, 1960
5. Fabula, A.G., "Application of Thin Airfoil Theory to Hydrofoils With Cut-Off, Ventilated Trailing Edge," NavWeps Report 7571, Sept. 13, 1960

Marshall P. Tulin

We should all thank Mr. Lang of the Naval Ordnance Test Station for presenting us with his recently obtained experimental information on base- and side-ventilated foils. Work of this kind is most important to continue. I might perhaps mention at this time that the idea of using a fully-wetted but base-ventilated hydrofoil for high-speed operation was, to the best of my knowledge, originated at the Langley Laboratory of the NASA by Mr. Virgil E. Johnson, Jr. These foils are very promising in certain respects, but are also probably very sensitive, cavitation wise, to angle of attack. As was mentioned in the paper, we believe that supercavitating foils intended for use on seagoing boats must be capable of operating without cavitation under a reasonable range of design angles of attack; that range may be larger than is possible with fully-wetted, base-ventilated, parabolic foils.

W. Graff (Versuchsanstalt für Binnenschiffbau, Duisburg, Germany)

The project of a full-cavitating hydrofoil is a proposal of mine made 24 years ago. About 12 years ago I constructed and tested such a boat. The boat was driven by an airscrew of 800 hp. The system of foil was somewhat similar to that shown by Mr. Wennagel and had forward foils piercing the surface and a full-submerged foil aft. The trials of the boat raised serious difficulties. Running on smooth water with full-cavitating foils we got self-excited heaving and pitching oscillations, known as porpoising, such that it was impossible to reach the full speed. Unfortunately, I could not finish these trials. The calculations made on this matter seemed to show that the distance of the foils on high speed was the most important factor in this problem. It was of interest to hear that Mr. Wennagel also observed these phenomena and that he was able to eliminate them.

*   *   *
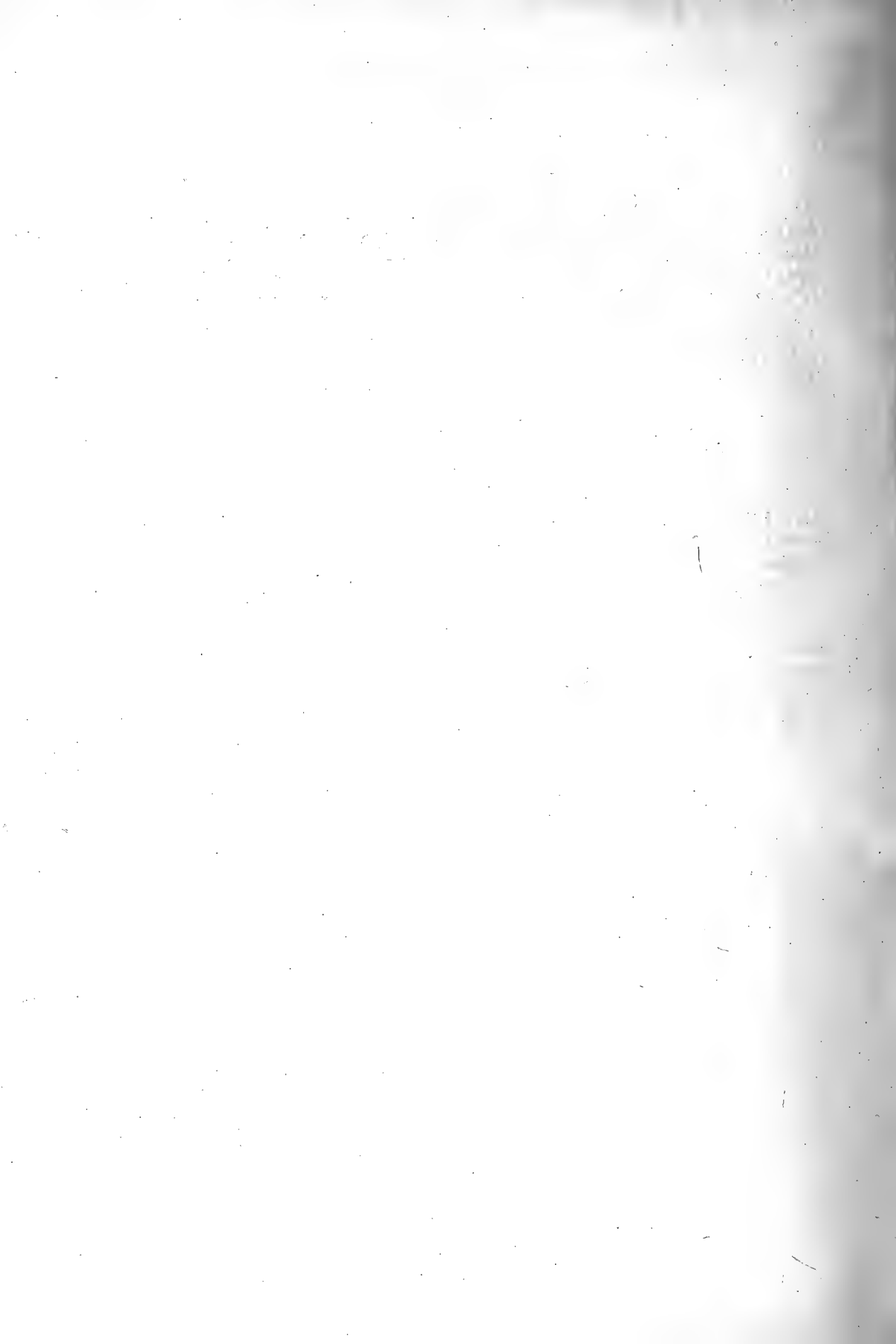
DESIGN AND OPERATING PROBLEMS
OF COMMERCIAL HYDROFOILS

H. Von Schertel
Supramer A.G., Lucerne, Switzerland

Development of modern means of transportation undoubtedly trends towards a progressive increase of speed in combination with an improved riding comfort. Speed on the water is still far behind the speeds already achieved with road or rail vehicles and aircraft.

Conventional types of watercraft cannot attain the speed of land vehicles under economically acceptable conditions. The solution of the problem by means of the hydrofoil boat is examined and the specific qualities are discussed by which the requirements are fulfilled.

The paper then deals with the fundamental physical aspects of the foil system as the most important design problem, and comparison is made between the surface-piercing foil and the fully submerged foil in relation to drag-lift ratio and behavior in a seaway. The section ends with a review of the practical adaptability of these two basic foil systems.

In the second part of the paper the commercial application of hydrofoil boats is discussed. Technical data are given about the types which are already being operated in regular passenger service. After a short review about the introduction of the hydrofoil boat in public transportation, follows an enumeration of the various existing hydrofoil passenger lines.

Finally the economic transportation problems are dealt with and data are given about the profitableness of hydrofoil passenger services. The field of application of commercially operated hydrofoil craft within the framework of modern communications and their limitations as regards speed is investigated.

INTRODUCTION

Development of modern means of transportation undoubtedly trends toward a progressive increase of speed in combination with improved riding comfort. Considering the progress achieved in passenger vehicles on road, on rail, and in the air from their first use in public service until the present, one finds that their speeds have increased about tenfold. The first railroad between Stockton and Darlington inaugurated in 1825 attained a speed of 10 miles per hour, while European express trains nowadays run at top speeds of 100 mph. The first serviceable automobiles reached about 12 mph, which in the course of time was stepped up in normal passenger cars to 120 mph. The passengers of the first commercial aircraft were carried at speeds between 60 to 75 mph. Today we cross the Atlantic at nearly 600 mph.

Conditions in waterborne transportation are very different. Already in 1860 the "Great Eastern," the largest vessel of its time, attained a speed of 14.5 knots whereas the cruising speed of the fastest passenger ship of today, the "United States," surpasses this hardly 2-1/2 times. On inland waters the increase of speed has been by no means greater. The

most modern and fastest ships on European lakes surpass their 100 years older predecessors only by twice their speed. The reason for this lagging behind of waterborne craft compared with other means of transportation lies in the well-known large increase of drag with augmented speed.

It is, therefore, not surprising that inventors, engineers, and scientists of several nations have been endeavoring for many decades to find solutions which will result in comparable speeds on the water. Conviction that the shape of modern displacement bodies can hardly be further improved, and that the solution can only be found in a reduction of the immersed volume and of the wetted surface, led to the development of gliding or planing vessels (V-bottom boats), in which dynamic lifting forces take the place of the static displacement lift, and later on to the construction of hydrofoil boats in which the hull is finally lifted completely out of the water.

The planing boats did not solve the problem of attaining the travelling times of land vehicles under economically acceptable conditions and with good behavior in a seaway. The reason for this must be attributed to the relatively high drag/weight ratio at the required speed and to the extremely hard buffeting to which planing boats are exposed and which the passengers cannot be expected to endure.

SPECIFIC CHARACTERISTICS OF HYDROFOIL BOATS IN COMPARISON WITH OTHER FAST WATER CRAFT

Drag, Speed, and Economy

In Fig. 1 in which the specific power requirements of various water- and aircraft are plotted against speed, displacement boats, planing vessels, and hydrofoil boats are compared
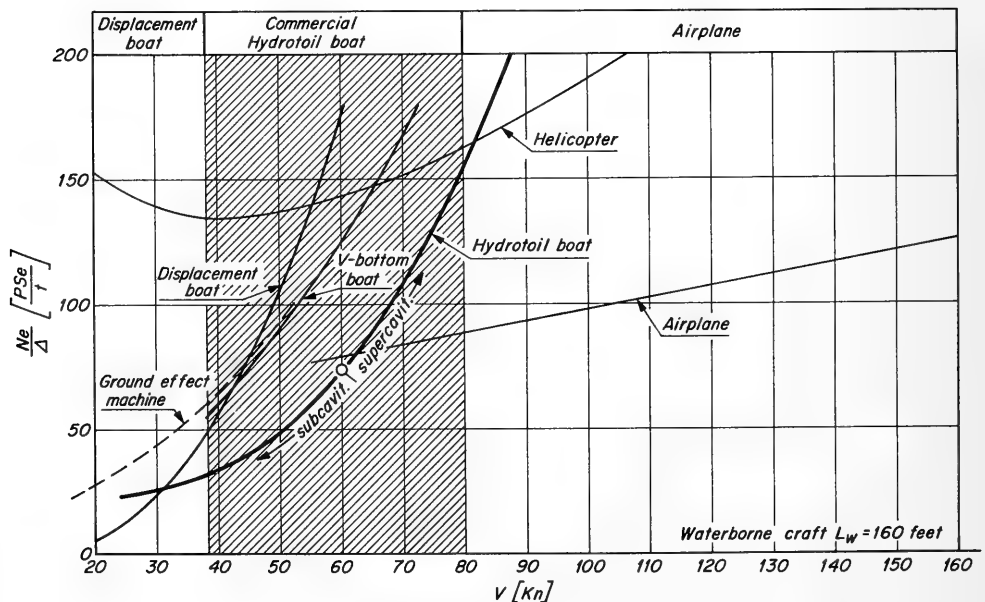
Fig. 1. Power coefficient of various craft

with each other, all of them having—with regard to the Froude number—the same length of 160 feet, representing vessels of about 300-ton displacement.* It can be seen that hydrofoil boats in the interesting speed range between 40 and 60 knots require only about 55 percent of the propelling power of planing vessels, which shows that foil-supported craft can be designed for comparatively high speeds and that they can operate at such speeds with reasonable efficiency. This is to say that at high Froude numbers, hydrofoil systems are known to function at drag/weight ratios below these of conventional motorboats. In conclusion, hydrofoil boats must be expected to be comparatively economical within certain size and speed ranges where other types of waterborne craft cannot operate effectively.

To illustrate this last statement we show in Fig. 2 the earning power of the hydrofoil boat Type PT 20 in relation to speed. PT 20 represents a type of boat which today is operating in regular passenger service in many parts of the world. This particular diagram will be referred to in detail later on. It is shown that under the given service conditions an interest of more than 50 percent on the invested capital can be achieved. The diagram, which is based on actual experiences, reveals that the hydrofoil boat has succeeded in
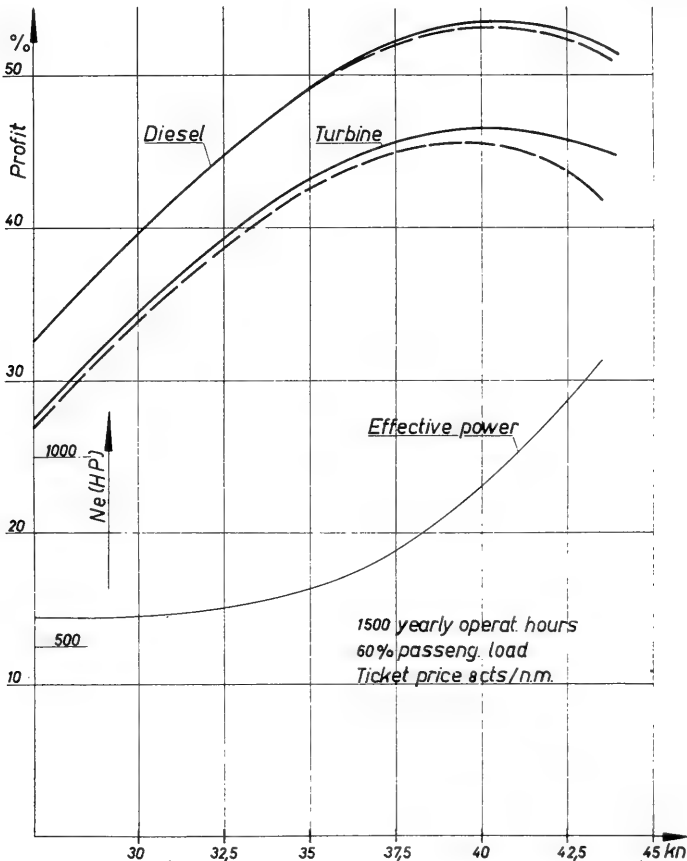
Fig. 2. Earning power of the PT 20 type
hydrofoil boat in relation to speed

---

*Some of the notations used in the text and figures are listed at the end of the paper.

attaining economically the present-day speeds of land vehicles, since the average speed of
fast trains in highly developed countries lies at 43 knots and at 32 for the whole world. But
in favor of the hydrofoil boat it should be mentioned that regular passenger services and
experimental trips along coastlines have demonstrated a further advantage, inasmuch as it
can reach certain destinations in an appreciably shorter time than land vehicles, which —
travelling with equal speed — must of necessity follow the more or less irregular coastline.
Such conditions for example prevail in Scandinavia.

Even better results can be obtained with a projected 300-ton Supramar hydrofoil boat.
In Fig. 3 is shown the obtainable profit for this type versus speed. Best results are
achieved at a speed of 50 knots yielding an interest on the invested capital of 57 percent.
When this project is realized, hydrofoil boats will show a clear superiority over land vehi-
cles with respect to travelling time whenever they operate between the same points on the
coast. This diagram also will be discussed in detail later on.
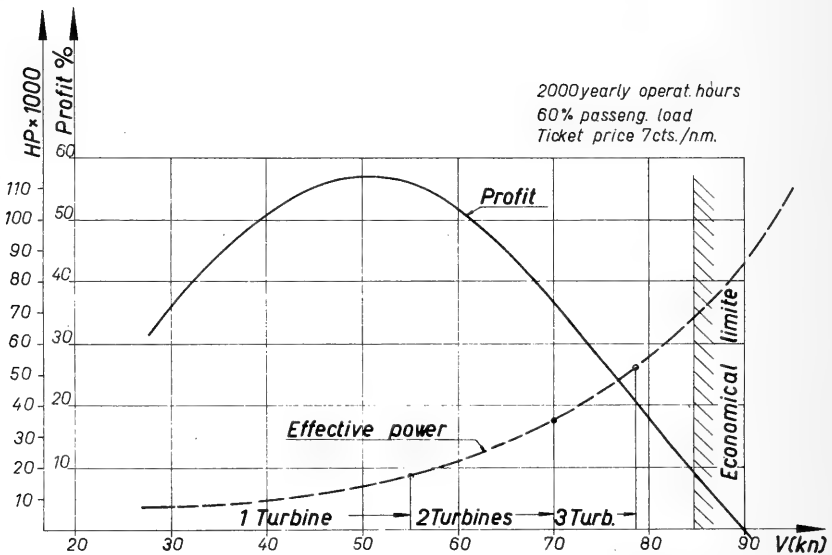
Fig. 3. Earning power of the PT 300 type hydrofoil boat (length = 160 feet)

Another quality distinguishes the hydrofoil boat from conventional craft. At higher
speeds, displacement and V-bottom boats cause the formation of a wave system of consider-
able amplitude in their wake which can interfere with the safe operation of other craft and
damage river banks. For this reason the speed of such boats is generally restricted in nar-
row waterways. Since hydrofoil boats develop only comparatively small wave-resistance
the disturbance of the water surface is so slight that the boats can maintain high speeds on
smaller lakes, rivers, and canals and in congested waters without endangering any other
craft or shore installations.

Considering now the airplane as the most serious competitor, we can derive from Fig. 1
that the airplane can attain much higher speeds with lower specific propulsion power than
the hydrofoil boat. Therefore aircraft represents a very economical means of transportation.
However its commercial use requires an extensive and very expensive ground organization,

and it is well-known that aircraft operation over short distances does not pay very well. Consequently hydrofoil craft may successfully compete with airplanes over short distances because of their lower costs of operation and maintenance and of their point-to-point rather than of airport-to-airport performance. Conditions may be such that a passenger choosing the hydrofoil boat will arrive in less time at his destination than he would when choosing the airplane. Although the airplane develops many times the speed of the hydrofoil boat the journey by air involves the trip to and from the air terminals, which are often far away from the original point of departure and destination. Over fairly short distances the helicopter might be expected to be a serious competitor of hydrofoil craft. However, as shown in Fig. 1, it requires rather high powered engines and its operation and maintenance costs are several times those of the hydrofoil boat. Thus in many cases the prevailing conditions will favor the use of hydrofoil craft instead of airborne means of transportation.

Sea-Riding Qualities and Passenger Comfort

Rapid connection between two points becomes meaningless unless the passenger can rely on the timetable: in other words transportation must be regular and not be subject to frequent interruptions on account of bad weather. Also the movements and accelerations of a vessel caused by adverse weather conditions must be considered. If they assume proportions which affect the passenger's comfort, speed must be reduced.

It has already been stated that the problem of rapid transportation on the water cannot be solved by planing boats on account of their buffeting in a seaway. At the cruising speeds which are here under consideration accelerations of 6 g and more have been measured in such vessels, accelerations which may be endured for a short time by the crew of a naval craft but which exclude the use of such boats in commercial operation.

Principally it can be stated that hydrofoil boats are able to maintain a higher speed level in a seaway than any other waterborne craft of similar size. Based on practical experiences, Fig. 4 shows the approximate size of waves in which hydrofoil boats of the Schertel-Sachsenberg system can still remain foilborne. The lower curve represents wave amplitudes at which the boats can operate at full power; the upper curve shows wave sizes at which a somewhat reduced cruising speed can be maintained while still keeping the vessel in foil-borne condition. The diagram permits the estimation of the size of hull required for operation in waves of known sizes. With a new type of foil system presently being developed the limits indicated in the diagram will be considerably widened.

Riding comfort in any watercraft is of course affected by the extent of its movements in a seaway. Pitching, heaving, and rolling motions of hydrofoil boats are generally much smaller than those of similar-sized conventional boats. It can also be stated that the amplitude of these motions as well as the degree of submergence in the waves decrease with the increase of speed and of the frequency with which waves are encountered. This phenomenon in the performance of hydrofoil boats is due to a reduction of the influence of the waves on the vessel's inertia and of the orbital wave velocity on the foil's angle of incidence with the frequency of wave encounter. On the other hand, however, vertical accelerations increase with speed. In accordance with the linear theory they increase also in proportion to the slope of the waves.

Some indication of the extent of motion in a seaway may be gained from Fig. 5, which is based on the latest tests undertaken with a 90-foot boat in waves estimated to have reached a height of 5 to 6.5 feet and a length of 100 to 150 feet. The diagram depicts the average
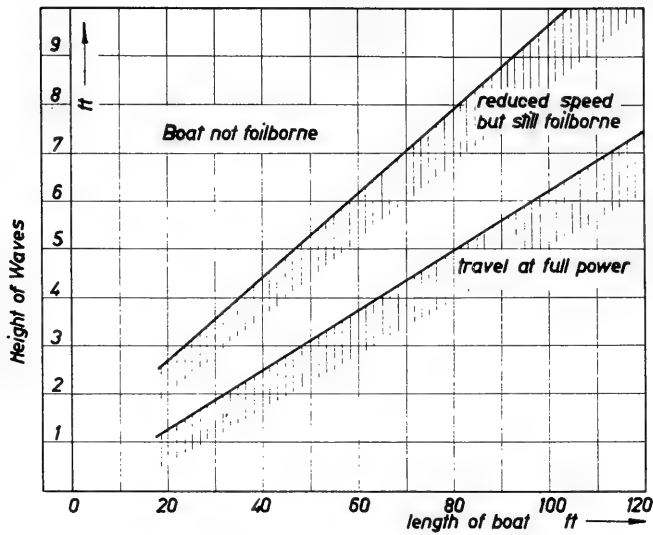
Fig. 4. Limits of seaworthiness of Supramar boats

readings of the maxima taken during a period of 4 minutes. The roll angle is, of course, at its maximum in a beam sea. Compared with displacement boats of similar size, however, that angle is still small and the angle of pitch is very small indeed.

Figures 6 and 7 show the influence of speed or Froude number respectively and of wavelength on the vertical accelerations of a surface-piercing front foil. These diagrams are taken from a hitherto unpublished theory developed by Mr. de Witt of the scientific staff of Supramar. For the accelerations shown in the figures the most unfavorable course of the boat in relation to the direction of the waves was assumed in each case. The thick curve
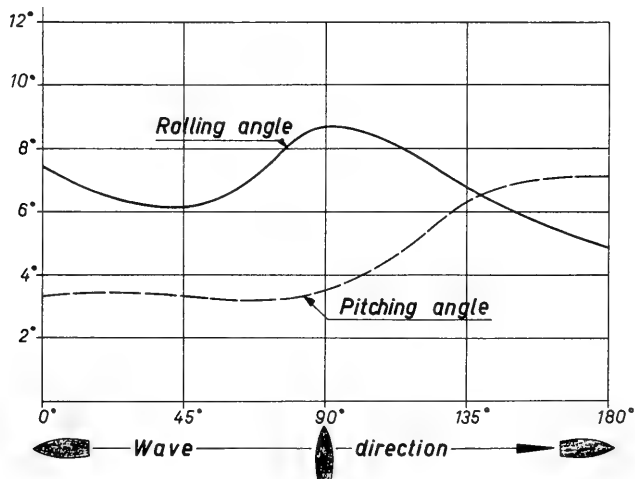
Fig. 5. Mean values of pitching and rolling in rough water for the PT 50 (wave height, 5 to 6-1/2 feet; wavelength, 100 to 150 feet)
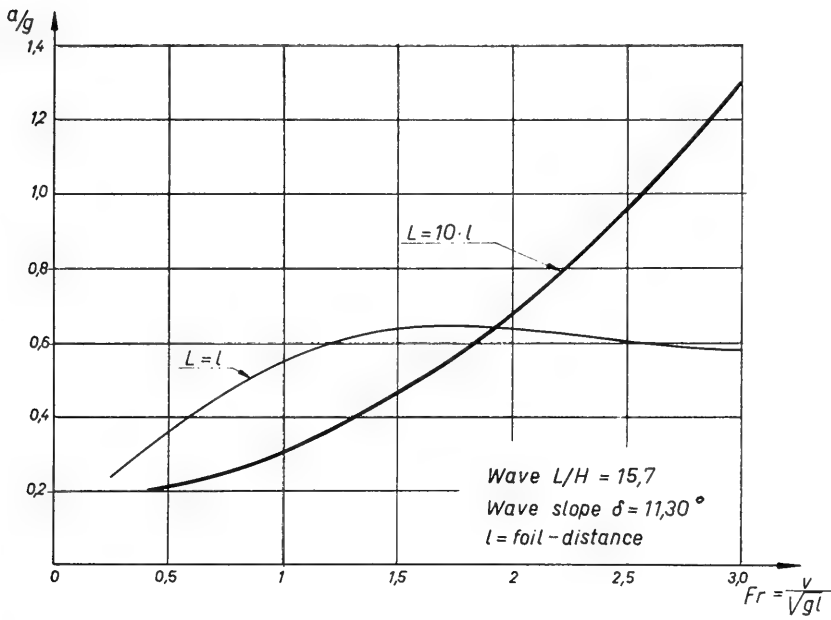
Fig. 6. Influence of the Froude number on vertical accelerations
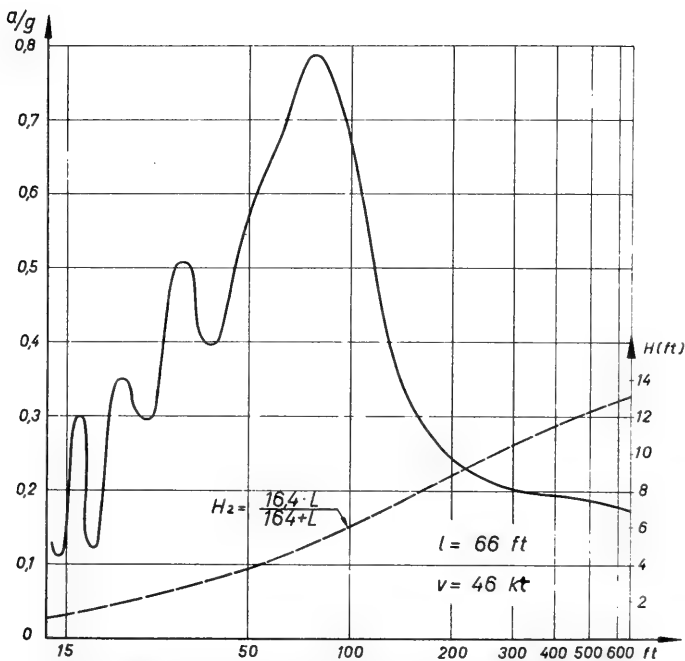
Fig. 7. Influence of the wavelength on vertical accelerations

in Fig. 6 corresponding to an extremely long wave of ten times the foil distance shows the typical increase of acceleration with increasing Froude number. Accelerations in medium waves, however, equaling the foil distance, are less dependent on the Froude number as may be seen from the thin curve. The calculations represented in Fig. 7 are based on a foil distance of 66 feet and a speed of 46 knots. The wave height for each respective wavelength is shown by the dashed curve. Figure 7 shows that under the assumed conditions the vertical accelerations increase only up to wavelengths approximately equal to the foil distance and decrease beyond that size, which is due to the decrease of the slope of the wave with its increasing length.

Figure 8 shows the influence on vertical accelerations of the direction of travel with regard to the wave direction for two different relations of wavelength to foil distance. Under
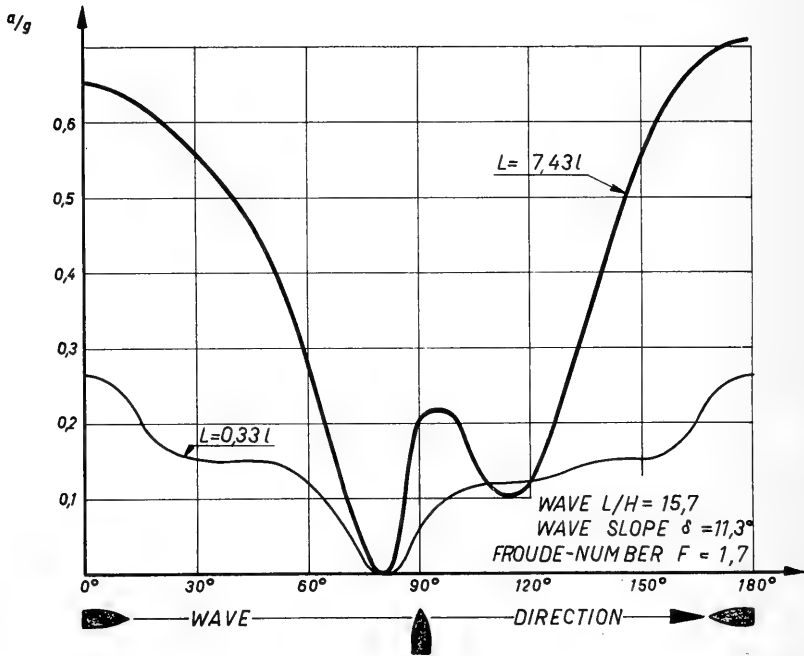
Fig. 8. Influence of the wave direction on vertical accelerations

the given conditions (L/H = 15.7, F = 1.7) the maximum values are attained against the sea and with a following sea, while at a course of about 80 degrees the boat remains at the same place in the wave, which results in the disappearance of accelerations.

TECHNICAL CHARACTERISTICS OF THE TWO BASIC FOIL SYSTEMS

Having examined the suitability of hydrofoil craft for commercial transportation in general, we shall now consider the main design problem in hydrofoil engineering, i.e., the foil system itself, as it naturally has a decisive influence on the all-round performance of the craft. Since it is not the purpose of this paper to present a survey of all the various designs

already in existence we shall limit the discussion to the two basic foil systems which during recent years frequently formed the subject of discussions and led to differences of opinions between the experts:

1. Surface-piercing hydrofoil systems—The surface-piercing systems consist either of single V-shaped foils or of a combination of smaller foils arranged one on top of the other like rungs of a ladder. A deviation from the equilibrium of the craft causes a change of the wetted lift-producing area of the foil and automatically creates restoring forces. The system therefore is automatically stable.

2. Fully-submerged hydrofoil systems—Fully-submerged foils have no inherent self-stability. Depth of immergence must be maintained by means of mechanical, electrical, or other controlling devices which—measuring either the distance between the hull and the water surface or the foil submergence—give signals to contrivances which in turn affect the lift by changing the angle of incidence of the foil or of flaps at its trailing edge.

We shall now compare drag and compare behavior of the two basic foil systems, and shall consider their possible future application.

Drag/Lift Ratio

We shall assume equal speed (45 knots), equal aspect ratio of $A = b/c = 8.3$, and a suitable foil section for either type. An average submergence ratio of $h = 1.2c$ is provided for the dihedral surface-piercing foil (lowest point $h = 2c$) in accordance with the boats which are at present in operation, and a lift coefficient of only $C_L = 0.22$ with respect to aeration.

The fully-submerged foil, however, requires a submergence ratio of not less than $h = 2c$ in order to avoid an excessive approach to wave-troughs but it is permissible to apply a lift coefficient of 0.26, since this foil is not exposed to air-entrainment, and only cavitation by influence of orbital motion has to be considered.

The total drag of a hydrofoil system may be expressed as

$$D = C_D S q$$

where S is the projected foil area and q is the dynamic pressure. The drag coefficient is composed of four main components:

$$C_D = C_{D_i} + C_{D_o} + C_{D_w} + C_{D_{pa}}.$$

The first component is $C_{D_i} = C_L{}^2/\pi A$ = minimum induced drag for infinite submergence. When approaching the water surface the second component has to be considered:

$$C_{D_o} = C_{D_f} + C_{D_{pr}} = \text{section drag.}$$

The frictional component C_{D_f} is strongly dependent on roughness of foil surface. For smooth conditions and the applicable section thickness ratios of 0.05 to 0.10 skin friction drag amounts to over 90 percent of section drag, so that the pressure drag $C_{D_{pr}}$ is very small. For the determination of section drag mostly results of experiments are used.

C_{D_o} of a V-shaped foil with an dihedral angle ϑ is increased to

$$C_{D_o} = C_{D_o}/\cos\vartheta$$

due to the increased length of wetted surface. The third component

$$C_{D_w} = \text{wave drag}$$

is negligibly small for high Froude number hydrofoil boats. The fourth component

$$C_{D_{pa}} = \text{parasitic drag}$$

refers in this case to the foil struts, piercing the water surface. V-shaped foils with their tips above the water surface during travel permit the use of relatively narrow struts since the produced transverse forces can be taken up by structural elements which remain above the water surface when the boat is travelling in foilborne condition. Because the struts are only little immersed at cruising speed the parasitic drag of the foil is small. The fully-submerged foil however requires very long struts which in view of the existing bending moments must also be rather wide. Therefore a considerable parasitic drag is caused which offsets the more favorable hydrodynamic qualities of the straight fully-submerged foil.

Calculation of the four drag components for the given example and on the assumptions stated above yields a drag/lift ratio for the surface-piercing foil of 6.9 percent and for the fully-submerged foil of 6.7 percent. Towing tank results obtained from two model foils of the two systems confirm the theoretical analysis. They both produced drag/lift ratios of approximately 7 percent. In conclusion, we can thus consider the two basic foil systems as being equally favorable in regard to resistance at design cruising speed. In travelling beyond cruising speed, however, the conditions change in favor of the surface-piercing foil system. The area of the fully-submerged foil is determined by the capacity of takeoff at the attainable $C_{L\,max}$ value. The lift coefficient decreases then with the square of speed and as a rule attains an unfavorably small value at top speed. On the other hand, when speed of the surface-piercing foil exceeds cruising speed the wetted areas of the foil as well as that of the appendages (struts emerge completely) are reduced to such an extent that their frictional drag becomes less than that of the fully-submerged foil.

Experiments carried out recently with a 1-ton test boat originally fitted with surface-piercing foils which were later replaced by a new system of automatically controlled submerged foils also confirmed these inherent characteristics of the two types. Figure 9 shows that cruising speed of the boat of about 50 km/h (27 knots) is reached with any of the two foils at the same engine speed whereas the top speed attained with the surface-piercing foil is 65 km/h (35 knots) as against 59 km/h (about 32 knots) with the fully-submerged foil.

Behavior in Sea Waves

The behavior of a hydrofoil vessel in sea waves is essentially the result of two functions. The first one, called the "wing characteristic Z" indicates the stabilizing variation (dL/dh); thus

$$Z = (dL/L_o) / (dh/b_o)$$

where L_o = lift when travelling at normal waterline
          b_o = normal wetted span of foil between surface-piercing points
          h = depth of submergence.
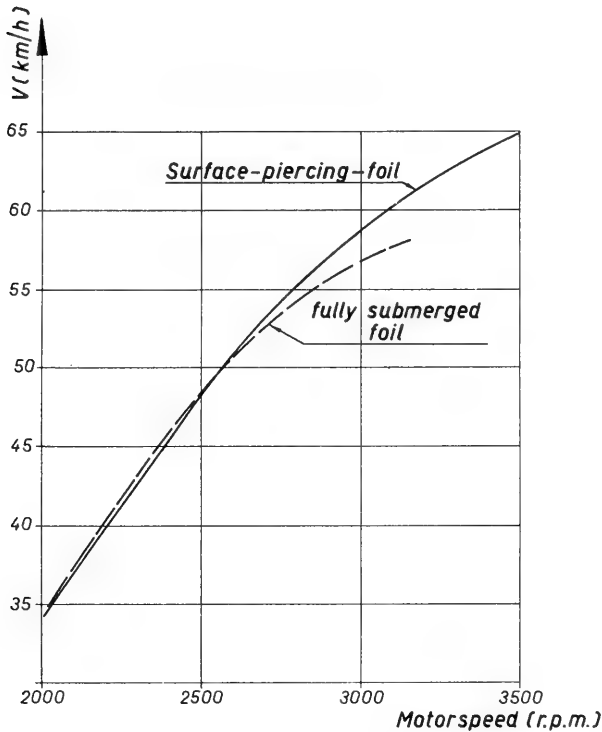
Fig. 9. Comparison of the two foil systems on a test boat

The wing characteristic obtained with a surface-piercing foil in the Saunders-Roe towing tank and measurements carried out on the 60-ton Supramar craft (dotted line) is presented in Fig. 10. The hump in the curve of the 60-ton boat is produced by the stern-heavy trim of the boat at low speed.

In designing a surface-piercing hydrofoil the value of the characteristic Z can be influenced to a certain extent by selection of the dihedral angle, by suitable variation of foil chord, foil camber, and angle of incidence in the vicinity of the piercing points. High values of Z provide for efficacious stabilization but involve hard riding in a choppy sea. Vice versa, reducing the slope of the curve shown in Fig. 10 leads to gentler behavior in a seaway but low stability. In order to achieve better riding comfort it is obvious that the wing characteristic should be adapted to wave heights and wavelengths; this, however, presents difficulties with this type of foil. Nevertheless, trials which have been recently undertaken in this respect with a smaller craft and an adjustable front foil of rather simple design gave very encouraging results.

In order to make a vessel with fully-submerged foils stable, variations of lift as a function of h must be provided by proper variation of the angle of incidence of the foil or
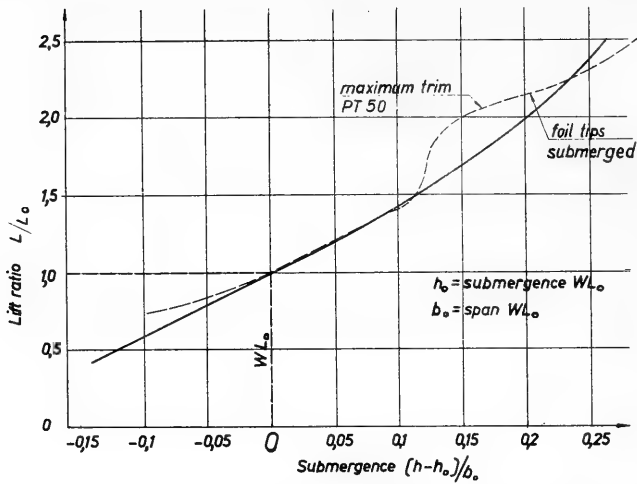
Fig. 10. Wing characteristic of a surface-piercing V-foil

its flaps. The respective control device must be designed in such a way that it reacts to a change of submergence, corresponding to the same value of Z as for surface-piercing foils. The fully-submerged hydrofoil, however, has a significant advantage over the surface-piercing type inasmuch as the value of Z can be changed at will whenever desirable and inasmuch as a damping or filtering function can be introduced in such a manner that the foil does not react to short waves and follows the contours of longer waves only insofar as to keep the hull clear from the water surface. Furthermore, lift is being gradually modified in conformity with the signal, whereas in the case of the surface-piercing foil, lift-variation occurs more or less suddenly with an impact when travelling in waves. Consequently boats with fully-submerged foils give better riding comfort. In rough sea conditions it is possible to differentiate submergence against time and to modify the foil angle reaction accordingly. The control device may also respond to accelerations; pitch and rolling angles can be reduced by means of a gyroscope stabilizer. Such control is difficult to materialize for surface-piercing foils because of their high autostability.

The second characteristic of a foil in a seaway is its reaction to orbital motion indicated by

$$W = (dC_L/d\alpha)/C_{L_o} = \frac{1}{\alpha - \alpha_0}$$

where $dC_L/d\alpha$ = lift-curve slope. A high value of W means that a foil has a tendency to react strongly to orbital velocites in waves. To make a foil less susceptible to these motions, it would be desirable to make the lift-curve slope as small as possible and the design-lift coefficient C_{L_o} as high as possible. Since the lift-curve slope is primarily a function of aspect ratio, its reduction is bound to increase the drag, and since, on the other hand, the lift coefficient C_{L_o} is limited by considerations of cavitation and ventilation, the value of this parameter W cannot be reduced effectively.

Rigid hydrofoils are, therefore, always subjected to the influence of orbital wave motions. This fact is without practical consequence when running against the sea, but the influence of orbital motion is a very undesirable reality in a following sea. In such

conditions a maximum reduction of lift occurs when approaching a wave crest, and, on the other hand, when approaching a wave trough, orbital motions have the tendency to increase the foil's lift. Consequently the phase of the foil travel is shifted under the effect of inertia in relation to the wave contour (by about 120 degrees) and moves against it. Under unfavorable conditions the hull may be forced into the crest of the waves, thereby reducing the speed of the craft considerably.

The amplitude of orbital motions reduces at a progressive rate, with increasing submergence. A fully-submerged foil is therefore exposed to a smaller amplitude than the average encountered by a comparable surface-piercing foil. Since, as already explained, the maximum lift coefficient will also be usually higher, a fully-submerged foil suffers less from orbital motion. Apart from that, the control device can be adapted to compensate the orbital influence by corresponding variation of lift.

Conclusion Regarding Practical Applications

After having discussed the characteristics of the two basic hydrofoil systems we can make the following statements in conclusion of the first part of this paper:

Boats of the surface-piercing hydrofoil type have sufficiently low drag/lift ratios to justify their use for high-speed commercial passenger service. Under equal conditions and having equal cruising speed they can be expected to reach a higher top speed than vessels provided with fully-submerged foils. Natural stability, simplicity of construction, operational reliability, ease of handling and maintenance, and, last but not least, a remarkable invulnerability of the foil-system have contributed to the acceptance of hydrofoil boats as a means of commercial passenger transportation. It can be taken for granted that the described qualities will lead to a preference for this type for use on inland waters, in coastal regions, and within protected sea areas.

Fully submerged foil-systems are in the same drag/lift bracket as the surface-piercing type. They possess superior seariding qualities and offer higher riding comfort because of their smaller and smoother heave and pitch response to sea waves. However, the complexity of the height- and stability-control which is needed for this type of boat must be considered to constitute a serious drawback of this system. No doubt the electronically controlled hydrofoil boats, which have been developed in the U.S., have shown excellent riding qualities. In spite of this fact there remains for the traditional shipbuilder the unusual conception that stability, naturally inherent to any properly built ship from historical times, should now be subjected to the faultless functioning of a number of complicated gadgets. In case of a failure of such a control system, there may not remain sufficient time to cut off the automatic and to "land" the boat by hand as is possible with an airplane. Although an unexpected sudden tilting of a commercial vessel will not necessarily result in any catastrophic situation, such an incident is liable to destroy the confidence of passengers. In consequence the introduction of the fully-submerged hydrofoil system in public service still presents problems and meets opposition of orthodox shipowners.

Therefore the requirement exists to maintain the stability of the fully-submerged foil type directly by dynamic forces, similar to the surface-piercing foil, without inserting bulky and vulnerable mechanical devices or electronic appliances. Based on ideas and experiments carried out 15 years ago by the author, a new self-controlling system is in development which — not being dependent on servo power sources and amplifiers etc. — can be expected to offer sufficient reliability. In heavy seas the system can perform in the manner

described in the preceding subsection and there can also be introduced an additional simpli-
fied gyroscope control. A trial boat equipped with this new system is at present undergoing
tests conducted by the Supramar company, and has, so far, been successful.

Undoubtedly boats with fully-submerged foils will have a large field of application in
the future in less protected sea areas and as long-distance ferry boats on open sea. But
their range of operation will always be restricted by their faster competitor, the airplane, to
which preference will be given in all cases where its travelling time between two points,
including airport feeder service time, is considerably shorter.

PRESENT TYPES OF COMMERCIAL PASSENGER BOATS

In the second part of the paper we will deal with commercial application of hydrofoil
boats. We shall first regard the type of passenger boats which are at present in operation.
It is known that the first hydrofoil design which was used in scheduled commercial passen-
ger services was the Schertel-Sachsenberg type. The reason for the advanced technical
stage of this system lies in its structural simplicity and the reliability of the surface-
piercing foils used in this type. Another reason for the perfection of these boats is the fact
that they are the result of organized development efforts which began with the author's
experiments in the thirties and which were continued through the following years without
interruption. Design and construction have always been accompanied by extensive theo-
retical and experimental research as well as by trials with full-scaled craft. With the con-
struction of 16 different types and a total of nearly 60 hydrofoil boats to this date, of which
26 are passenger ferries, experience has accumulated to such an extent that Supramar's
engineering staff is in the position to go ahead with the design of larger and faster economi-
cal passenger craft.

The predecessors of the present commercial boats were built during World War II. Out
of the six types which were designed for speeds up to 60 knots we shall mention the 80-ton
type VS 8 launched in 1943. This craft deserves attention because it was the largest hydro-
foil boat ever constructed and has not been surpassed even today. It was designed as a
high-speed long-range cargo carrier for operation between Sicily and Africa. The 105-foot-
long hull was constructed in light metal alloy. A maximum speed of 40 knots was obtained
using a twin arrangement of Mercedes-Benz Diesel engines with a combined output of
3600 hp. Although the corresponding ratio of 45 hp/ton is considered to be marginal for
satisfactory operation, the boat was nevertheless able to run at 37 knots against seawaves
up to 6 feet in height and 150 feet in length.

To date two prototypes find application in established passenger lines, the PT 20
(a 27-ton boat for 75 passengers) and the PT 50 (a 60-ton boat for 140 passengers). The
first PT 20 was built in 1955 in the Rodriquez Shipyard at Messina. This craft (Fig. 11)
turned out to be the first of a series of very successful boats, 19 of which have been built
or are nearing completion.

The light-metal alloy materials used in building the PT 20 hulls are Al-Mg and
Al-Mg-Si. Watertight compartments are provided below the passenger decks and in other
parts of the hull. Several of these compartments are filled with foam-type plastic which
makes these boats practically unsinkable.

The engines installed in the PT 20 are supercharged 1350 Daimler-Benz Diesel engines
of the type MB 820 Db. The reversible gear, placed between the engine and drive shaft,
represents a special type developed by Zahnradfabrik Friedrichshafen. A 110-hp auxiliary

engine is located in the stern of the hull for emergency operation. Driving a small separate propeller, this engine can be used to maneuver the boat in displacement condition.

Fig. 11. The PT 20 hydrofoil boat

The general arrangement of the PT 20 type is shown in Fig. 12. The boat is operated and the machinery controlled entirely from the bridge which is located above the engine room. Forty-five passengers can be accomodated in the forward cabin, while the rear cabin is somewhat smaller and can take 30 passengers.

Together with the struts and a horizontal girder each foil forms a uniform framework which, apart from giving static advantages, facilitates the exchange of the foil structure. The foils themselves are made from medium steel as shells welded at the seams. The forward foil can be tilted with narrow limits by means of a hydraulic ram acting on the girder across the hull. It is therefore possible to adjust the angle of attack of that foil during operation, thus counteracting the effect of larger variations in passenger loads and to ensure optimum behavior in seawaves.

The PT 20 can be considered to be the smallest type of foilborne craft suitable for passenger-carrying coastal service. In view of its novel and unconventional characteristics the first boat of its class was originally licensed as "experimental" and restricted to operation in a 6-mile zone off the coast of Italy. After frequent inspections and supervision of the service, the Registro Italiano Navale extended the license in 1958 to operation within a 20-mile coastal zone and in 1960 within a 50-mile limit. Today the PT 20 as well as the PT 50 have been classed by the authorities of several countries.

Technical data which have an influence on the profitable operation of the type PT 20 are presented in Fig. 13. The shaft power of the engine was measured during operation by means of a torque meter. The propeller was model-tested, thereby taking proper account of the influence of shaft inclination. The drag/lift ratio was then derived from net power. This
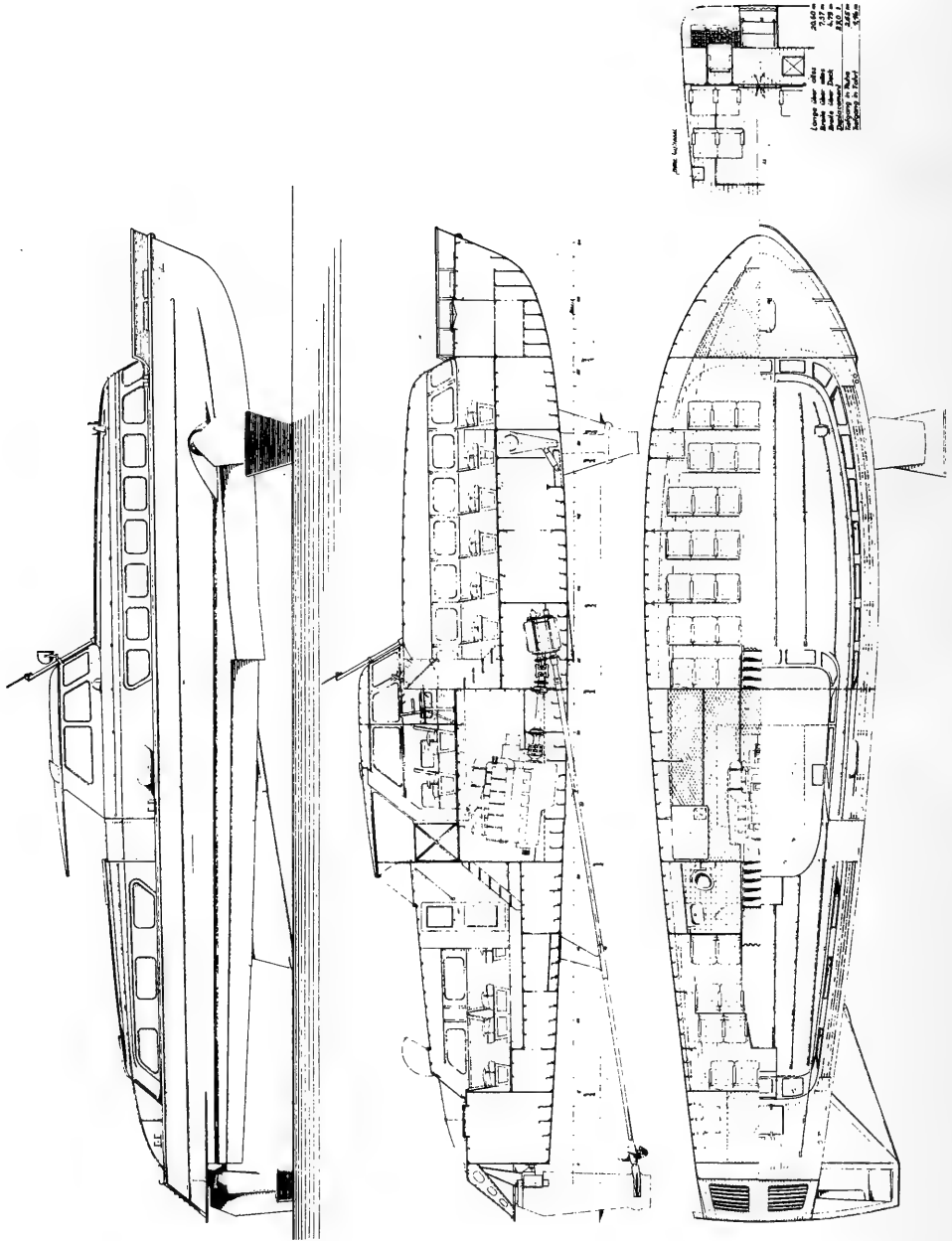
Fig. 12. The PT 20 hydrofoil boat
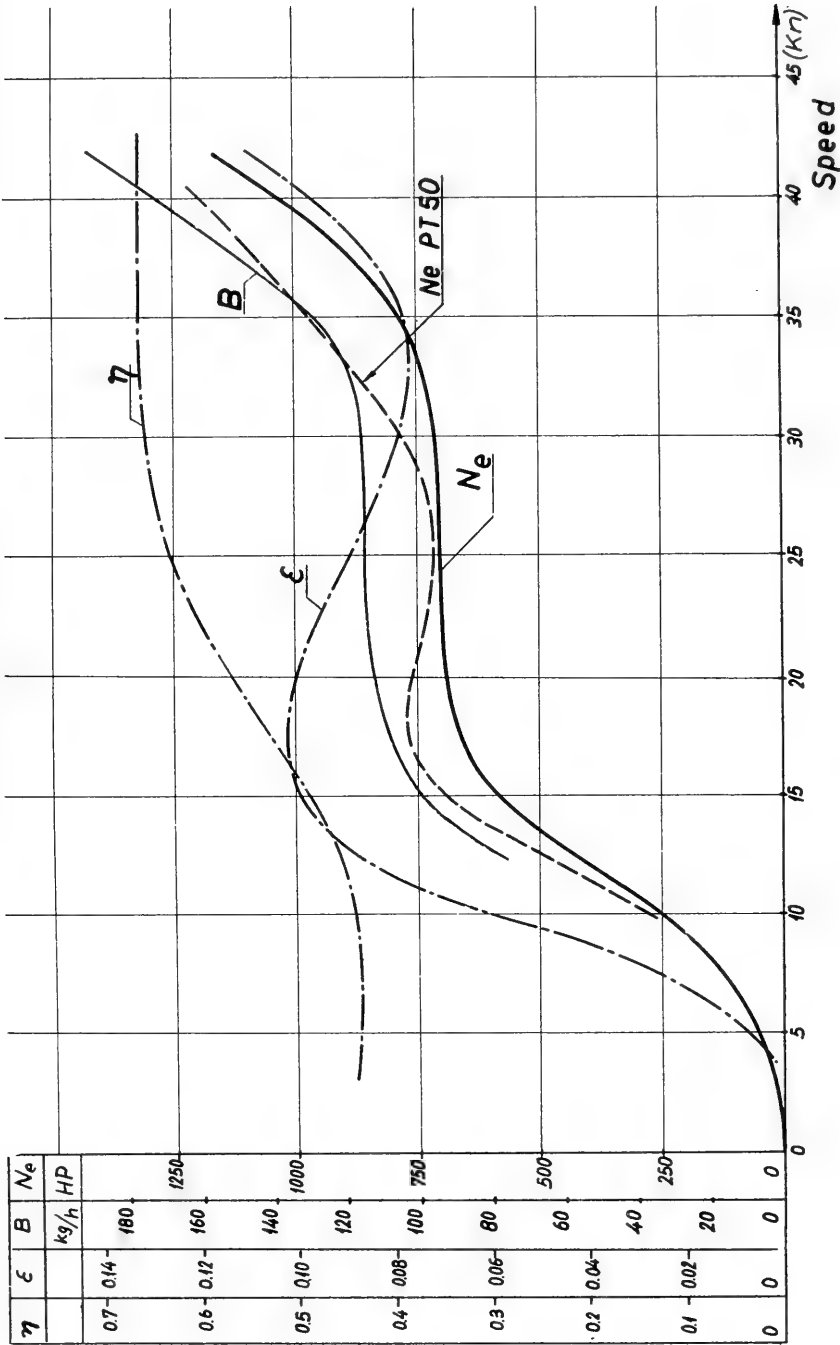
Fig. 13. Performance of the PT 20

ratio is D / W = 8.6 percent at cruising speed (38 knots) and its minimum is 7.7 percent at a speed of 34 knots. The corresponding maximum lift/drag is W / D = 14.3.

A special type of PT 20 was designed for the transportation of engineers and workers to offshore oil-drilling and pumping stations for oil-producing organizations in tropical waters (Fig. 14). In this type, bridge and engine room have been arranged in the foreship in order to obtain better vision since tropical waters have an occasional influx of driftwood.
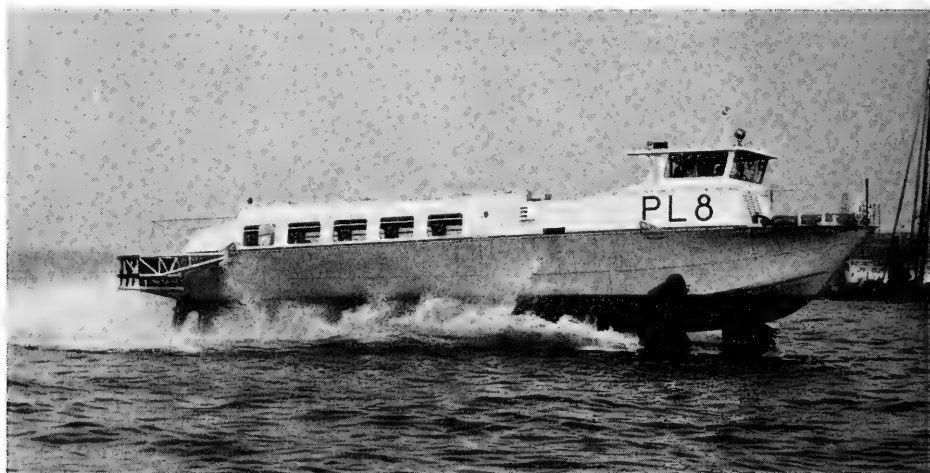
Fig. 14. A special type of PT 20 for oil-workers in tropical waters

Tropical conditions were taken into consideration in the design and installment of the engine plant, and the propeller has been placed in a specially protected position. Because passengers board and leave the boat via the aftship this part has been fitted with particularly sturdy metal guards. Because these boats are undergoing very rough handling by their native crews the requirements with regard to their performance, sturdiness, and maintenance are extremely high. Thus, for example, the boats must be able to remain foilborne even when sudden full rudder is applied at full speed. Four boats of this special 29-ton type have been constructed at the Gusto Shipyard in Schiedam (Holland) for the Shell Petroleum Company in Maracaibo.

Continued successful and profitable operation with the PT 20 stirred up sufficient interest in a larger type of boat to be used in open waters farther away from the coast and suitable for interisland services. The prototype of the PT 50 was constructed early in 1958, again by the Rodriquez shipyard in Messina (Fig. 15).

In this 60-ton boat, passengers are placed below the main deck. Thus that deck contributes considerably to the strength of a hull, allowing structural weight savings. The machinery consists of two of the same type of Diesel engines tried out with great success during a period of over 4 years in the PT 20 boats. Shafting is simplified as compared with the smaller craft by eliminating the V-drive. Both rear and forward foil are rigidly attached to the hull, but the lift of the forward foil can be modified by hydraulically operated flaps.

Fig. 15. The PT 50 hydrofoil boat

Figure 16 shows the general arrangement. The passenger room is divided into two compartments which are separated from each other by the engine room. The forward cabin contains a bar, and a little saloon is provided on the upper deck, aft of which there are baggage compartments. Two PT 50 vessels which have been delivered to Venezuela are fitted with air-conditioning installations.

Figure 13 also shows the power curve $N_{e/2}$ of the PT 50 for comparison with the PT 20. It reveals that the power is somewhat higher, especially at increased speeds, which must be attributed to the twin shaft and twin rudder arrangement and to the not very favorable location of the propeller chosen in order to give better protection.

Technical Data for the two types are as follows:

	PT 20		PT 50	
Length overall	68	feet	89	feet
Displacement fully loaded	28	tons	60	tons
Payload	6.8	tons	15.0	tons
Number of passengers	75		140	
Max. power	1350	hp	2700	hp
Max. speed	42	knots	40	knots
Cruising speed	38	knots	36	knots
Power at cruising speed	920	hp	1000	hp
Range	300	naut mi	300	naut mi
Power/ton	48.2	hp/ton	45	hp/ton
Power at cruising/Payload	135	hp/ton	134	hp/ton
Power at cruising/Passengers	12.3	hp/pass.	14.3	hp/pass.

The Supramar company is working on the design of some larger and faster types of hydrofoil boats intended for use under heavier, open-sea conditions and over longer distances. A 110 multiple-purpose type with a carrying capacity of at least 200 passengers will be provided alternatively for Diesel and gas turbine propulsion. With two Mercedes-Benz engines of 3000 hp each, a speed of 47 knots is expected, which will be
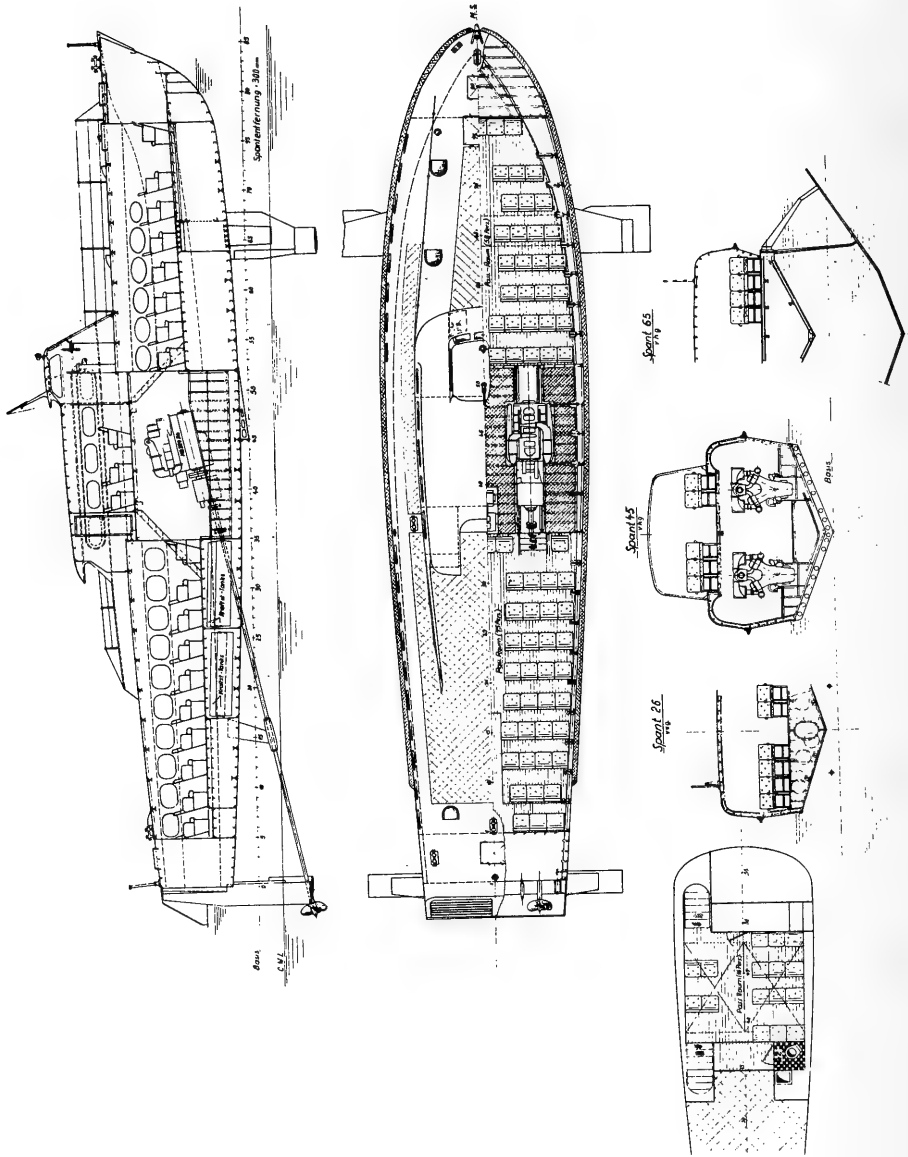
Fig. 16. The PT 50 hydrofoil boat

increased to 53 knots if the Diesel engines are replaced by two 4200-hp Bristol-Proteus turbines.

The next larger type was originally planned with a displacement of 120 tons but this was later increased to 160 tons. With accomodations for 400 passengers over short distances or 320 baggage-carrying passengers and four motor cars, a top speed is expected of 50 to 60 knots, depending on the type of turbine.

The project of a 300-ton boat with supercavitating foils to carry about 550 passengers will be discussed in a subsequent section with regard to its economical and attainable speed and to the limits of its application. It is proposed to power this craft with two Bristol Siddeley-Olympus turbines with a continuous output of 17,500 hp each. The cruising speed is estimated to be 70 knots, thus reaching the technically possible limit, as we shall see later on, but still representing from the commercial point of view a very profitable speed under favorable conditions.

Depending on the area of application either the surface-piercing foil or the new type of fully-submerged foil, now in development, will be employed in these future craft.

DEVELOPMENT OF COMMERCIAL PASSENGER SERVICE WITH HYDROFOIL BOATS

For the introduction of hydrofoil boats in public service, Supramar in 1952 constructed a 9-ton boat (PT10) with a seating capacity of 28 passengers and powered by a 500-hp Mercedes-Benz Diesel engine located in the stern. Soon after her first demonstration on Lake Lucerne, Italian and Swiss navigation companies chartered this boat for passenger services between the Swiss and Italian part of Lago Maggiore under the technical management of Supramar. Thus the first scheduled hydrofoil boat service in the history of shipping was inaugurated on May 16, 1953 (on the same lake, incidentally, on which Forlanini succeeded in getting his hydrofoil test-boat "foilborne" for the first time 55 years ago).

Interest in the new "flying boat" became widespread and in many cases took on enthusiastic proportions. In a surprisingly short time travellers became accustomed to this rather strange means of transportation. With 27,000 nautical miles covered during this testing period, valuable experience was gained on the technical as well as on the commercial side of the business. By the middle of 1956 the first 28-ton boat (PT20) had completed several demonstration runs along the Italian coast and a round trip of 1600 nautical miles from Italy to Greece. It had proved its seaworthiness on many occasions and in waves up to 13 feet high. On the initiative of Mr. Rodriquez a shipping company named Aliscafi was established in Sicily and the first scheduled sea service inaugurated between Sicily and the Italian mainland in August 1956. Cutting the port-to-port time from Messina to Reggio di Calabria down to one-quarter of that of the conventional ferryboat and making 22 daily trips the boat thus set an example for the operation of other hydrofoil services. The results of this service after four years of operation are noteworthy: With a seating capacity of 75 passengers one boat alone has carried a record number of some 31,000 people in a single month. The average daily number of passengers is today between 800 and 900. To date the boat has carried a total number of approximately 1,000,000 passengers. The boats operating around Sicily have covered a combined distance of approximately 465,000 nautical miles, which is more than the round-trip distance to the moon.

After the establishment of the Messina-Reggio line other services have been organized between the following localities:

1957	Messina-Taormina		PT 20
1957	Messina-Liparian Islands-Palermo		PT 20
1959	Venice-Trieste		PT 20
1958	Lake Garda		PT 20
1960	Naples-Capri-Ischia		PT 50
1959	Maracaibo-Cabimas (Venezuela)	3	PT 20
1960	Stavanger-Bergen (Norway)		PT 50
1960	Stockholm-Mariehamn (Sweden-Finland)		PT 50
—	Buenos Aires-Montevideo	2	PT 50

The most prosperous services exist between Maracaibo and Cabimas and between Naples and Capri. On the first mentioned line two PT 20 boats carry an average of nearly 1700 passengers daily and over 600,000 per year over a distance of approximately 20 miles. The shipping company was able to amortize the two vessels within one year. On the Naples-Capri line, operated with a PT 50, passenger fees had to be raised on account of an excess of passengers. A second PT 50 has been ordered and two PT 20s have been sent to Naples in the meantime to assist in operations during the season. A second PT 50 was also requested for the Stavanger-Bergen line only two months after its inauguration.

On many occasions Supramar boats had the opportunity to demonstrate their seariding qualities under very severe weather conditions. Soon after establishment of the PT 50 line at Naples a heavy storm caused the 500-ton ferryboats to discontinue their trips between Naples and Capri. The PT 50, however, maintained its service in an overloaded condition carrying 170 passengers instead of the regular number of 140. On another occasion a PT 20, passing through the Straits of Otranto was forced down by waves of an estimated height of 13 feet but short length. It was still possible to maintain an average speed of 15 knots. In the Caribbean Sea another PT 20 got caught in the fringe of a hurricane and was able to continue her journey in half-foilborne condition in long waves averaging 16 feet in height.

As regards maintenance, inspections are undertaken at regular intervals of about 2 to 3 months, including cleaning of hull, bottom, and foils. In a tropical climate, where intensified growth of barnacles affects the drag of the foils, more frequent inspection and cleaning is indicated. If the foils are not retractable, this work is usually carried out by aqualung divers. Disregarding major machinery overhaul, which is normally due after 5000 operating hours, the maintenance of the foils requires about 25 percent of the maintenance work of the entire boat.

Strength and reliability of the foil system was several times demonstrated when boats ran aground and were still able to continue operation. A boat colliding with a pier caused considerable damage to the latter while suffering only minor deformations of the plating around the foil suspension point that did not interrupt service.

PROBLEMS OF ECONOMY IN COMMERCIAL HYDROFOIL OPERATION

Six years of experience in public passenger service with hydrofoil boats proved that the commercial application of this type of craft is very profitable in areas with an adequate passenger frequency. Similar to air transportation the comparatively high speed of hydrofoil boats in relation to other waterborne craft results in a high earning power. Since the present foilborne craft usually operate at speeds up to 3 times that of other boats, their potential carrying capacity is up to 3 times greater. In other words, a hydrofoil boat can be considered to be equal in capacity to a ship up to 3 times its size.

Figure 17 presents an analysis of actual commercial experience for the type PT 20 (assuming 2 boats in service) based on prevailing European conditions and a price of 6 cts/kg for Diesel oil and 53 cts/kg for lubricating oil. The graph indicates the yearly net return to be expected over ticket price (cents per nautical mile) multiplied by the load factor (number of passengers per available seats). As a function of three parameters the graph thus enables anticipation of whether commercial application of hydrofoil boats would be profitable under given local conditions. Assuming a fare of 8 cents per nautical mile, a load factor of 0.5, and 1500 operating hours per year the graph shows a yearly net profit of slightly more than 30 percent of the invested capital.
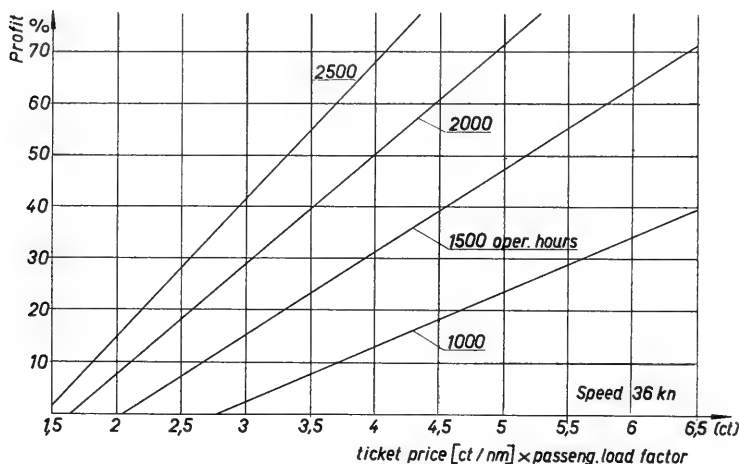
Fig. 17. Commercial experience for the PT 20

The diagram is based on a cruising speed of 36 knots. In order to determine the influence of speed on profits and also the economical speed of the vessel at which the most favorable relation between costs and revenues is obtained the curve depicted in Fig. 17 was computed under the following suppositions:

Load factor:	60 percent	
Fare:	8 cts/naut mi	
Diesel engine	specific weight:	4.3 kg/hp
	specific fuel consumption:	166 g/hp/hr
	price of engine:	$26/hp
Turbine	specific weight:	1.3 kg/hp
	specific fuel consumption:	320 g/hp/hr
	price of engine:	$44/hp.

The engine weights include gears and all auxiliaries as well as ducts, pipings, etc. The highest profit is obtained with either Diesel or turbine propulsion at a cruising speed of 40 knots. Although the engine output at that speed is nearly 60 percent higher than at 30 knots the remarkable profit is obtained by 33 percent higher revenues in accordance with the equal increase in passenger-miles. On account of the higher price of the engine and its higher

fuel consumption the interest on the invested capital earned with a turbine-driven boat is
only 85 percent of that of a Diesel-powered vessel. However, the fact that the modest
space requirements for turbines permit the accomodation of additional passengers has not
been taken into consideration. The conditions will be changed if prices and consumption
figures for turbines can be further reduced in the future.

We shall now consider the field of application for the commercial hydrofoil boat within
the framework of modern transportation and with regard to any competing craft. We will also
investigate its limitations as far as technical practicability, speed, and economy is
concerned.

Table 1 presents the principal data as they affect the economy of the hydrofoil boat
and its three competitors: the conventional displacement boat, the airplane, and the heli-
copter. The data are based on an assumed distance of 100 nautical miles. For an estimate

Table 1
Comparison of Prices and Operating Costs

	Type	Block-speed V (knots)	No. of seats	Price ton ($)	Price seat ($)	Price seat V_r* ($)	Operat. costs passeng. mi (¢)
Passenger Boat	26.5 tons	12	92	3,600	700	700	1.4
Hydrofoil	PT 20	36	75	9,300	2,800	900	1.6
Airplane	Convair	150	44	43,000	18,000	1,500	3.4
Helicopter	Sikorsky S-55	72	10	~130,000	~40,000	6,700	12.0

* $V_r = V/V_{pass. boat}$.

of economy the two last columns are the most interesting. They indicate price per seat
divided by block-speed (port-to-port speed) and the direct operating costs per passenger
mile (expenditures less cost of ground organization). It appears that the foilborne craft is
very economical compared with the other means of transportation and under the assumed
conditions. In spite of the slightly lower "initial capital expenditure per passenger mile"
and operation costs of the displacement boat, the attainable revenues within a certain
operation period are higher for the hydrofoil boat because it travels three times as fast. It
must also be taken into consideration that the public is generally willing to pay higher
fares for faster transportation. The comparison with the commercial airplane reveals that
its initial costs are higher and its total operation costs very much higher if the expenditures
for the ground organization are taken into regard. With total operating expenses estimated
to be at least 7 times those of the hydrofoil craft, the helicopter cannot be considered to
represent an economical instrument of transportation at present.

In order to find the speed ranges within which the hydrofoil boat and its competitors
can be successfully employed we have already shown in Fig. 1 the power coefficient for
the craft in question over speed. First of all the earning power for a hydrofoil boat with

550 passengers was calculated as a function of speed in order to determine the limit from a commercial point of view. In doing this the following conditions were assumed:

Load factor:	60 percent (330 passengers)
Ticket price per nautical mile (in correspondence with the average economy class fares for airplanes):	7 cts
Operating hours per year:	2000
Range:	500 nautical miles
Total weight of turbine including gear and accessories:	1.55 pounds/hp
Specific fuel consumption:	0.6 pounds/hp
Purchasing price of turbine including gear and accessories:	$42/hp.

For the fixed costs the same assumptions as in Figs. 2 and 17 were made. The specific power requirements shown are based on measurements in various boats of the Schertel-Sachsenberg system. It turned out that the power coefficient $N_e/\Delta^{7/6}$ given on a logarithmic scale over the Froude number $V/\sqrt{\ell}$ (ℓ = foil distance) lies on a nearly straight line for all hydrofoil boats constructed, so that reliable figures are available. Values of a much lower order given in other theoretical treatises, which neglect the fact that after a relatively short operating time the foils are no longer hydraulically smooth, are not realistic.

In Fig. 3 the curves of profitableness and of the boat's power in consideration of the increasing displacement (turbine and fuel weight) are plotted against speed. The number of turbines to be installed was based on the Bristol Siddeley Olympus turbine with 22,700 hp maximum and 17,500 hp continuous output. Under the assumptions made, the best profit is obtained at about 50 knots. With increasing speed earning power reduces and one may consider 85 knots as the utmost limit at which the boat can still render a profit under otherwise favorable conditions. The limit of technical practicability, however, can probably be expected at 75 knots at the present stage of the art when observing the requirements of the classification committees and the regulations of the London Ship Safety Convention, especially with reference to electrical installations, auxiliaries, and safety installations. Apart from the fact that a larger engine plant can hardly be properly installed, the amount of fuel necessary for greater speeds increases at such a rate that the number of passengers necessary for obtaining a profit can no longer be maintained.

Figure 1 shows that 38 knots was chosen as the lower limit of application of the commercial hydrofoil boat of the given size (160 feet) and 80 knots as the upper limit. Exceeding this limit under economically acceptable conditions, for the case in question, seems possible only if hydrofoil boats with better lift/drag ratios or lighter engines with less fuel consumption are developed in future. In the speed range beyond 80 knots the superiority of the airplane — as far as power requirement is concerned — increases continuously with the speed.

The diagram also contains the dotted curve of the "flown" values of ground effect machines (hovercraft) which operate at an altitude of about 5 percent of the craft's diameter. Because only scant results are available, this curve does not pretend to be correct. Data of projects which have not yet been completed or power figures at altitudes of less than 0.05 diameter are not represented. A comparison between the hydrofoil boat and the hovercraft is justified only if the flight altitude of the latter would be great enough that both types can manage the same height of waves. However, it can be assumed that the respective curve will be considerably improved in the course of development.

The length of a route between two points which can still be operated advantageously in competition with an airline is also dependent on the economic maximum speed of the hydrofoil boat. Preference obviously will be given to the airplane if it requires much less time for the trip and if both the airplane and the hydrofoil company charge the same prices. Assuming a maximum speed for the hydrofoil boat of 75 knots and for the medium-distance airplane a block speed of 360 knots, it can be safely predicted that for all distances beyond 300 nautical miles, for which the hydrofoil boat needs more than four hours, travellers will prefer the airplane with its 50 minutes of flying time, even counting the time lost getting to and from the airports.

It can be expected that under the existing circumstances the longest economically favorable distance for the hydrofoil boat lies between 300 and 400 nautical miles. Although quite a lot of publicity has been given to the idea of a future Atlantic hydrofoil service it appears very improbable, if not impossible, that hydrofoil boats will ever be suitable for this task which can be much better accomplished and with better economic results by modern airplanes.

NOTATIONS USED

a = vertical acceleration
b = span of hydrofoil
c = chord of hydrofoil
h = submergence below water surface
ℓ = foil distance
w = weight
v = speed in ft/sec or in knots
q = $0.51\rho v^2$ = dynamic pressure
A = b^2/S = aspect ratio
B = fuel consumption
C_D = D/qS = drag coefficient
C_L = L/qS = lift coefficient
D = drag of hydrofoil
L = lift of hydrofoil
L_W = wavelength
F = Froude number
H = wave height
N = motor power
S = projected foil area
W = orbital sensitiveness
Z = wing characteristic
Δ = displacement
a = angle of incidence
γ = weight density of water
ϑ = dihedral angle
δ = wave slope
ρ = γ/q = mass density

DISCUSSION

Christofer Hook (Atlantic Hydrofin Corportation, Villeneuve le Roi (S&O), France.

Baron von Schertel gave the example of phase shift in the case of following waves for the surface-piercing system but he neglected to point out that the main advantage of the submerged foil is the opportunity it provides for correcting this out-of-phase effect by application of an advance or prediction signal to the incidence changes. Ideally, this would lead us to a telescopic sensing device whose advance position with respect to the controlled foil would be adjusted to suit different ratios of hull to wavelength. In practice, a simplified compromise in the form of a fixed advance length is perfectly satisfactory since only relatively short waves are significant.

It is also feasible to incorporate into such a sensing device a wave-height measuring system, coupled to powerful damping, so that all waves up to a given maximum (corresponding roughly to the height clearance) may be filtered out, resulting in practically level flight over waves up to this size. For larger waves the aforementioned size may be subtracted as a constant so that, for example, a wave 6 feet high may be dealt with as if it were only 3 feet high.

It is too often assumed that a given hydrofoil system must be restricted to a given severity of sea and that beyond this some disaster must follow. The impression given is not improved by the fact that the details of the type of disaster are left to our imagination! This is, however, somewhat unfair since a similar restriction should also be placed on normal boats, which should then also be sold with a "sea severity tag" attached — which is not done. A good hydrofoil can perform in seas well beyond the capacity of a crash boat to follow, as has been shown in U.S. Navy reports, and when failure to follow is eventually arrived at it is not followed by any kind of disaster but merely by a sitdown, and the ship can always continue in a half-foilborne condition; in fact, pitching is so severely damped by foil action that a light hull fitted with foils will survive where the same hull with foils removed will break up. The matter of wave filtering becomes so important at sea that fine comparisons of relative lift/drag ratios of the two methods becomes pointless.

Finally, I think that the purely mechanical method cannot be lightly dismissed as bulky and vulnerable since its reliability is unquestionable. Since an increase of C_L is obtained by incidence instead of by carrying reserve foil area we can offset the gain in weight consequent in the elimination of this weight against the added hardware required to manipulate the prediction method and we fill find that there is no added weight. On the basis of cost, if I may be excused, I may perhaps point out that for a sport boat or 4-passenger size the cost of the hardware does not exceed $100. I think that all hydrofoil men here today should realize that we are very much riding on the wave created 25 years ago by the Schertel-Sachsenberg group and that, had it not been for the commercial successes of this group, hydrofoils would never have got going again after the fizzle out that followed the Bell experiments in about 1920.

H. Von Schertel

Mr. Hook is right when he points out that the description of phase shift for a hydrofoil boat travelling in a following sea, given in the paper, refers to the surface-piercing foil

system, and that the behavior of a boat fitted with fully-submerged foils controlled by a
predicting sensor would be different. I tried to give the advantages of fully-submerged
foils as far as I could in a paper of the present length.

L. S. Snell (The De Havilland Engine Company Limited)

Baron Von Schertel makes certain assumptions in Fig. 17 when comparing the perform-
ance of the Diesel engine and gas turbine. He goes on to say that "conditions will be
changed if prices and consumption figures for turbines can be further reduced in the future."

It must be remembered that though the specific fuel consumption (S.F.C.) of the Diesel
engine can be taken as generally constant at about 0.4 lb/b.h.p.-hr, a wide variety of gas
turbines with equally widely differing performances can be produced. The S.F.C. quoted in
the paper has already been improved upon, though unfortunately at the expense of cost and
bulk. Figure D1 shows schematically three engine types recently evaluated for a small
high-performance craft. That on the right utilizes a simple open cycle and its design owed
much to aero engine practice. The efficiency of this simple cycle can be improved by rais-
ing the turbine inlet temperature and increasing the compression ratio, if this can be
associated with an increase in compressor efficiency. Modification to this cycle is desir-
able if good economy is the main aim. The center illustration shows the addition of a heat
exchanger which recovers some of the exhaust heat previously lost, while the remaining
diagram depicts a quite sophisticated arrangement using three stages of compression with
inter-coolers and exhaust heat regeneration.

Figure D2 shows the performance expected from each of these arrangements compared
with that obtained from the conventional Diesel engine. The component efficiencies and
maximum cycle temperatures used in these calculations are quite modest and are those
liable to be encountered in a marine engine rather than an aero engine. Examination of
these curves indicates a most significant point, that is whereas the Diesel engine has a
consistently good specific fuel consumption over a very wide load range, the simpler gas
turbines markedly worsen as the throttle is closed.

The author said that after using practically full power to get on the hydrofoils, cruise
then takes place at about 55 percent maximum power. Cruise economy at this point is,
therefore, the main consideration in the choice of prime mover. Unfortunately the choice of
a simple open cycle working on high compression ratios and high turbine inlet temperatures
can be most misleading as, although the S.F.C. is considerably improved at near 100 per-
cent full power, at 55 percent the S.F.C. is not materially better. This state of affairs
might well be more of a problem for the present generation of hydrofoil craft as it would
appear that as cruising speeds increase so the cruise power will proportionately increase.

A near ideal solution would be to evolve a variable-mass-flow engine fitted with an
exhaust heat regenerator. With decreasing throttle, mass flow would similarly decrease, and
if a near-constant pressure ratio and turbine inlet temperature was employed, the thermal
ratio of the heat exchanger would be markedly improved and, coupled with reduced ducting
losses, would give an increasingly better S.F.C. with closure of the throttle.

During the course of the analysis previously referred to, account was taken of the
additional space available not only for the gas turbine compared with the Diesel engine but
for the varying amounts of space which could be saved with the different gas turbine con-
figurations and their associated fuel tanks. Surprisingly enough, the higher fuel consumption

SIMPLE CYCLE

C.
C.C.
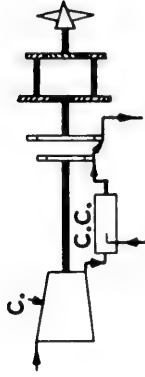
C.   Compressor
C.C.   Combustion Chamber

EXHAUST HEAT
EXCHANGER CYCLE
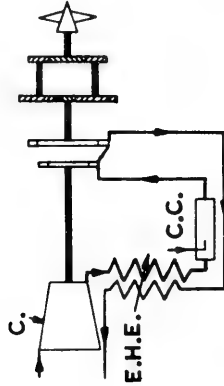
C.
C.C.
E.H.E.

C.   Compressor
C.C.   Combustion Chamber
E.H.E. Exhaust Heat Exchanger

INTERCOOLED, EXHAUST HEAT
EXCHANGER CYCLE

H.P.C.
I.P.C.
I.C.
C.C.
E.H.E.
I.C.
L.P.C.
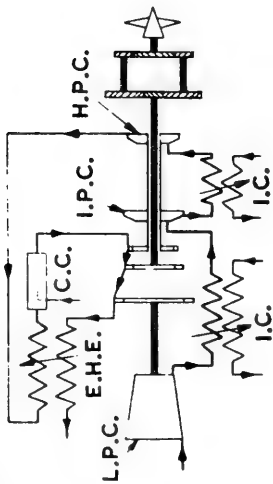
C.C.   Combustion Chamber
E.H.E. Exhaust Heat Exchanger
I.C.   Intercooler
L.P.C. Low Pressure Compressor
I.P.C. Intermediate Pressure Compressor
H.P.C. High Pressure Compressor

Air ———

Fuel ———   Burnt gases ———   Sea water ———

Fig. D1. Air-breathing gas turbine cycles
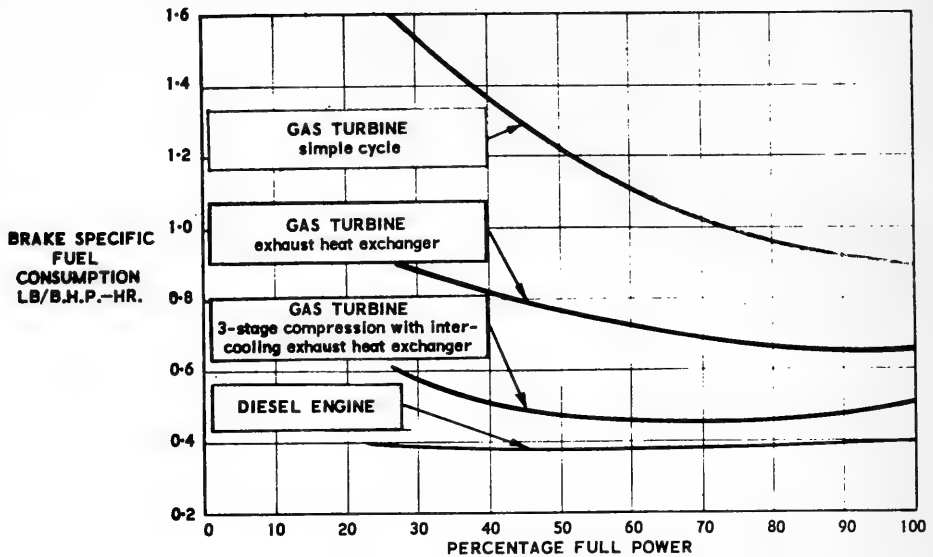
Fig. D2. Surface performance of air-breathing engines

of the simpler cycles was just about offset by the engine room volume and weight saved, so that for ranges of up to 1000 nautical miles there was little to choose between the installations; above this figure the more sophisticated units showed to advantage. However, in this design evaluation the installational size of the Diesel engine concerned cut the payload so much that its use could not be considered.

This raises a further point, very much to the forefront of the engine designer's mind, that above a certain size, Diesel engine specifics — both weightwise and volumewise — greatly increase as high duty materials and associated workshop practices can no longer be employed. One British engine, for instance, uses 36 pistons and 3 crankshafts in order to get the largest engine size which can be made from the better class materials and precision methods of manufacture. It would, therefore, seem that apart from small, highly specialized or experimental craft, the gas turbine should really come into its own at shaft horsepowers of, say, 4000 and above for the type of craft the author discussed.

Speaking very personally, I feel that no real progress will come with the adoption of the gas turbine for high-speed marine craft until units are designed expressly for this purpose, not merely rehashes of aero engines. The knowledge and facilities exist for designing and developing these units; the engineer should be given the opportunity of doing this at the earliest possible date.

R. N. Newton (Admiralty Experiment Works)

I would like to refer to two specific points arising from Baron Von Schertel's excellent paper which bear directly upon the general comments I made concerning hydrofoil craft and GEMs in the discussion of Mr. Oakley's paper on high-performance ships.

Near the end of the section titled "Present Types of Commercial Passenger Boats" Baron Von Schertel listed particulars of the PT 20 and PT 50 Supramar craft. While the figures quoted leave no doubt as to the economical performance of such craft in calm weather, i.e., their relatively low horsepower for a given speed, it should be noted that the maximum speeds quoted are not really high in comparison with modern planing forms and the range, in particular, is very limited.

Now there can be little doubt, I think, that higher speeds will be achieved with the larger craft which the Supramar Company are contemplating, but one is left to wonder whether they will have the range for open sea voyages as claimed, or the ability to operate in heavy sea conditions.

After listing the existing services the paper states that the craft have demonstrated their sea-riding qualities and then goes on to quote three occasions upon which a craft was forced down by the waves. In other words it is at least admitted that this type of craft is limited by the sea condition. Unfortunately the paper does not say at what speed the craft were able to proceed in waves, nor is there any proof of the heights of waves quoted – as much as 16 feet in one case. One of the most difficult quantities to estimate, without the use of apparatus only now coming into use, is the height and length of waves. I venture to suggest that the heights quoted in the paper are heavily exaggerated.

To emphasize the point I would like to quote an extract from a recent report of David P. Brown, President of the Board of Managers of the American Bureau of Shipping:

"After months of study of plans and design criteria as well as inspection during construction, the first of several hydrofoil passenger craft is about to be submitted to the committee for classification. Requests to class this type of craft were considered favorably by the technical committee last autumn, subject to appropriate limitations as to the area of operation and indication in the classification symbols that the craft is of special design and not comparable to a normal vessel in respect of scantlings and certain machinery details. Hydrofoil launches are now being built for use in Lake Maracaibo and in the Caribbean."

In conclusion may I repeat the plea I made in the discussion on Mr. Oakley's paper for more research into the seaworthiness of this type of craft.

H. Von Schertel

Mr. Newton expressed the view that hydrofoil boats can get into sea conditions in which they have to come down onto the sea. The behavior of hydrofoil boats in a seaway depends, of course, on the length of the waves, and on the direction of travel of the craft relative to the waves. Our experience over more than 10 years shows that the hydrofoil craft can run in almost any sea condition, occasionally, of course, with reduced speed (as is the case with any type of boat) and in a half-foilborne condition. Also I would like to add that in this condition hydrofoil boats have proved to have superior sea-riding qualities over planing boats, owing to the damping action of the foils. This fact has also been stressed by Mr. Hook. Concerning speed in waves, comparison runs which have been made between our commercial boats and several Navy craft showed that the higher the waves encountered the more the difference in speed was in favor of the hydrofoil boat.

Mr. Newton emphasized that the range of 300 miles given in the paper for our hydrofoil boats does not bear any comparison with fast planing craft. May I draw the attention Mr. Newton to the fact that the paper only deals with rather short-distance commercial boats with a high passenger load. In the case of a planing boat and a hydrofoil boat of equal speed and displacement, the range of the hydrofoil craft will be considerably higher on account of the much lower motor power and the associated low fuel consumption.

A. Hadjidakis (Aquavion Holland N.V.)

There are many things wherein I fully agree with Baron Von Schertel, for instance: that the efficient speed for a hydrofoil craft lies between 40 and 50 knots; that the required engine power per ton displacement is about 40 b.h.p.; and that seaworthiness increases with size (it would be terrible if we disagreed on this point). Our thinking was very much in the same direction. Compare for instance Baron Von Schertel's Fig. 7 with Fig. 7 in my paper.

However, there are some points where we differ. In the first place, I wonder why the foil incidence of your hydrofoils is such that a lift coefficient of only 0.22 is obtained. Is this so chosen to prevent cavitation at full speed or perhaps to get better takeoff characteristics, or is there some other reason? We use lift coefficients of up to 0.45 at top speed. In the second place, it surprised me that a gas turbine engine gives a lower profit if used in the PT 20 type, as is indicated in your Fig. 2. In my opinion it should be contrary. Let the specific weights be 4.3 kg/hp for the Diesel engine and 1.3 kg/hp for the gas turbine, which gives a difference of 3 kg/hp, or for 1375 hp a weight decrease of say 4 tons. Because of double fuel consumption, fuel weight will increase say 1.5 tons. But there is still 2.5 tons left, which means at least some 25 extra passengers; that is to say an increase of income of one third, as the PT 20 carries 75 passengers normally. Furthermore, only a small engine room would be required, so there would be more space left for other things.

H. Von Schertel

The lift coefficient in the example given is only 0.22 because a speed of 45 knots was assumed, so that the lift coefficient must be kept rather low to minimize or avoid ventilation and cavitation. A certain margin must be left between the lift coefficient at which ventilation occurs and the C_L value actually used in order to allow for the orbital motion in the waves.

As to the question of operational economics with turbine propulsion for the type PT 20, it has to be taken into consideration that the number of passengers is limited by the available space in the boat. The turbine-driven boat will be lighter and require a smaller engine power, which however does not compensate for the high initial cost and consumption of turbines. In my paper I remarked that economy would improve with the turbine boat if passenger space could be gained by reducing the engine room size.

E. V. Telfer (Institute for Shipbuilding, Trondheim)

As a simple naval architect listening to your deliberations I have been a little puzzled as to how to present your thoughts nondimensionally so far as these exciting craft are

concerned. At the moment it appears to me that you prefer to think entirely dimensionally round each particular problem and in so doing do not necessarily see the picture as a whole.

For example, in Mr. Wennagel's paper there is one very interesting diagram (here Fig. D3B) given in dimensional form which can with advantage be re-presented in nondimensional form. Normally in ship work we use a resistance coefficient based on a speed-squared relation associated with a relative speed. One such combination is the Froude $\textcircled{C}$ and $\textcircled{K}$ presentation; and so long as resistance does vary approximately as speed squared, the corresponding $\textcircled{C}$ value is substantially constant. When the performance of a fast vessel is so presented, however, we see (Fig. D3A) that the speed-squared relation required for non-dimensionality is no indication at all of the power of the speed with which the resistance is actually varying. Actually, for speeds beyond the maximum $\textcircled{C}$, the resistance is more nearly varying directly as the speed. In this case it is better to use a nondimensional presentation which respects this fact, and this is easily obtained by plotting values of
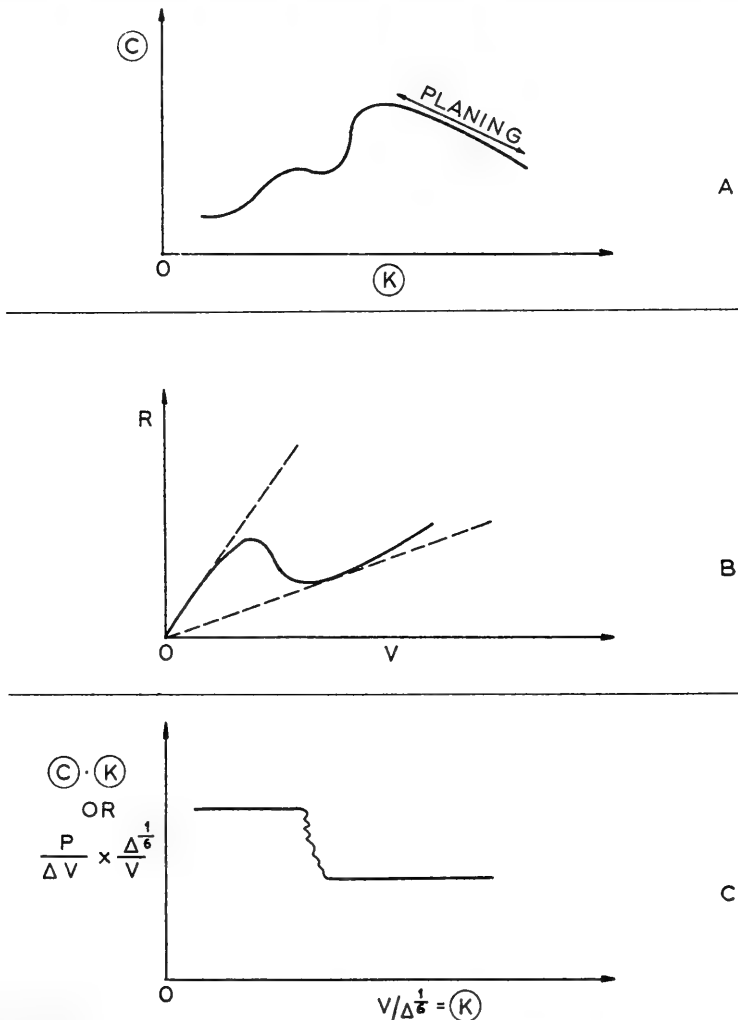
Fig. D3. Comparisons of dimensional and nondimensional presentations

ⒸㆍⓀ against Ⓚ. This would convert Mr. Wennagel's diagram from B to C. From the latter we see most clearly that the conditions imply two regimes of broadly constant but different ⒸㆍⓀ values. What is the significance of these two regimes? Incidentally the ⒸㆍⓀ product reduces to $(P/\Delta V)/$ Ⓚ. The term in parentheses, i.e., power per ton-knot, is the transport coefficient and is a direct commercial measure of the design efficiency.

Our discussions include many references to Froude number, i.e., Froude speed-length number. I doubt, however, so far as hydrofoil craft are concerned, whether we have a truly representative length to use in the Froude number. I suggest therefore, since for these craft displacement or weight is constant, that the Froude displacement-speed factor, i.e.,
$K = 0.5834 \ V/\Delta^{1/6}$, should always be used for their performance nondimensional presentation.

H. Von Schertel

The Froude number is based on the distance between the fore and aft hulls.

Douglas Hill (Grumman Aircraft Engineering Corporation)

We continue to be indebted to Baron Von Schertel for his reporting of the operating experience of the craft of his design, as well as for his pioneering work in the development of hydrofoils and their introduction into commercial service. Those of us interested in the development of hydrofoils look to the experience with these craft as a milestone on the road leading to the large-scale introduction of hydrofoils for commercial and naval use.

There can be little quarrel with Baron Von Schertel's evaluation of the potential of commercial hydrofoils on the basis of the evidence he presents and the scope of his presentation. In the publicity which has attended the growing awareness of the potentialities of hydrofoil craft, it is perhaps true that the feasibility of future vessels — a transatlantic passenger liner, for example — has been overemphasized by the standards of today's commercial realities. Assuming that hydrofoil craft are better suited to coach than to stateroom accommodations, we can draw on the experience of other modes of coach transport to substantiate Baron Von Schertel's observations on the practical operating range of passenger-carrying hydrofoils. A comparison of the length of journeys of travelers by air, railroad coach, and intercity bus in the United States reveals that, while the average distance travelled varies substantially between the modes of transport, the average duration of the journey is remarkably consistent:

Conveyance	Average Length of Journey (statute miles)	Average Speed (mph)	Average Time (hr)
Airplane	577	220	2.6
Railroad Coach	110	40	2.7
Intercity Bus	79	30 (est.)	2.6

It would seem reasonable to expect that the widespread use of hydrofoils for coach transportation would likewise result in an average trip duration of about 2.6 hours.

Most journeys would be shorter than the average, some perhaps much longer. The peak trip length can therefore be expected to be shorter than the length of the average trip. On domestic United States airlines, for example, the most common trip length is of the order of

200 miles, corresponding to a flight of about 55 minutes. It is not surprising to find, therefore, that the hydrofoil routes described as the most prosperous are also the shortest, requiring runs of less than an hour. A journey of 300 to 400 miles, requiring 6 to 8 hours of travel at 50 knots, would seem to be approaching the limit of coach-passenger endurance, and we must agree with Baron Von Schertel that longer trips do not promise commercial success.

If indeed the time required for a trip is the factor limiting the number of passengers which may be attracted, it follows that faster boats will draw more passengers for a given route. In the example of Fig. 3, it is indicated that the most profitable speed of the boat under consideration is 50 knots, assuming a constant load factor. If the load factor itself increases with velocity, however, the most profitable speed will be greater than 50 knots.

This only serves to point out that the best speed of a hydrofoil craft from a commercial standpoint is influenced by market considerations as well as by hydrodynamic performance and operating costs. To arrive at general conclusions as to the characteristics of a commercial craft which will be most profitable, a more comprehensive analysis than the one presented is required. We shall have to examine the entire range of feasible speeds, sizes, route lengths, power plants, types of foil, and possible payloads. We shall have to examine not only how variations in these basic parameters affect hydrodynamic performance but how they may affect the operating costs and the value of the craft as transportation equipment. And all of these must be examined in the context of the environment—physical and economic—in which the hydrofoil is expected to operate.

Such an analysis is not made in this paper, and we must read it with this caution. It may appear to be more than it claims to be; it may seem to present conclusions where it provides illustrations. We have no reason to doubt, for example, that under the conditions assumed the most profitable speed for the PT 300 is 50 knots, or that a Diesel-powered PT 20 is more profitable than one which is powered by a gas turbine. We should not necessarily infer, however, that 50 knots is thus the optimum speed for hydrofoil craft nor that Diesel engines are generally more profitable than gas turbines.

The promise of hydrofoils would seem to justify a more searching evaluation: first, of their economic characteristics and, second, of where these characteristics may pay off. The Von Schertel boats have demonstrated that the hydrofoil may successfully perform the role of a waterborne bus. Why isn't consideration being given to the analogous—and potentially larger—role of ocean-going truck?

At present, the vast majority of waterborne commerce moves at speeds of 15 knots or less. As Baron Von Schertel points out, no other waterborne vehicle has been developed to provide higher speed service, as the motor vehicle and railroad do on land. The need for express cargo transport by water has been clearly demonstrated. Twenty-knot Mariner class ships have been able to draw traffic away from slower ships. Shippers pay premium rates to ship by fast passenger liner, at speeds of less than 30 knots. And at the far end of the speed spectrum, transoceanic air cargo has been growing at the rate of 10 to 15 percent per year.

In a great many respects, the hydrofoil craft seems to qualify as an "answer" to the cargo aircraft for steamship lines:

1. Its speed range is more than double that of displacement ships of comparable size.

2. Practical vessels can be built in much smaller sizes than displacement ships without sacrificing sea-keeping capability. Smaller ships permit faster turnaround in port and more frequent service. Delivery times of a day or two, rather than a week or two, are possible.

3. As Baron Von Schertel points out, the hydrofoil can operate from existing facilities and does not require extensive shore installations as airplanes do. It can provide a self-contained express link in the transportation networks which now exist around the ports of the world.

4. Economically, the hydrofoil is at its best at the shorter ranges where the aircraft — present and projected — is at its poorest.

Within foreseeable advances in the state of the art, the ranges for economical operation of hydrofoils will be substantially lower than those of aircraft. Carrying cargo instead of passengers will not, of course, repeal these limits but it will enable the hydrofoil to service routes where its own endurance, rather that that of its passengers, is the limiting factor. While the hydrofoil cannot now be expected to provide economical transatlantic service, there are major trade areas within its range capabilities. These include the Caribbean area, for example, and, it would seem, the seas adjacent to Europe. Furthermore, there are indications that the maritime industry, at least in the United States, is ripe for the introduction of a high-performance, high-productivity vessel. Long a labor-intensive industry, the merchant marine shows increasing signs of a transition to high-productivity capital equipment. Containerized cargo handling operations are now a reality and specially designed containerships are now in service. Attention is being given to the automation of ship operation. The trend toward faster displacement ships continues.

The possible role of the hydrofoil in cargo transport is indicated by the nature of the cargo it might carry. Cargo aircraft are generally considered to be taking the "cream" of the freight market — the highest valued commodities which can best afford the premium freight charges. Of the commodities valued in excess of \$40 per pound which are imported to the U.S., for example, it is not uncommon for the entire amount to be shipped by air. On the other hand, virtually no commodities valued at less than \$1 per pound are imported by air.

Hydrofoil cargo transports are not likely to recapture the very high valued cargo nor will they be suitable for the low valued bulk cargoes. There is a middle ground, however, consisting of general cargo — manufactured goods such as machinery, motor vehicles and parts, electrical equipment, and textile manufactures — which constitute a substantial portion of ocean-going commerce and for which the hydrofoil may be a suitable transport.

The use of high-speed hydrofoil ocean transports would require that they be recognized as an expensive, but valuable, piece of capital equipment. Their high cost would have to be matched by high utilization to realize their productivity potential. New concepts in ocean shipping would be required, as well as the traditional ship operating virtues: minimum crews which debark at the end of a run to be replaced by another crew in the manner of airline practice; turnaround times measured in hours or minutes rather than days; rapid engine replacement in port so that major maintenance does not tie up the ship.

The history of air transport is primarily the development of the passenger market. The passenger and his baggage have offered the highest revenues, and today's airline passengers are the heirs of the early travelers who paid premium fares for the novelty as well as

the speed of air travel. Only now are the airlines turning to large scale freight transport for its own sake.

The initial commercial uses of hydrofoil craft have understandably followed the pattern of early commercial aircraft. The virtues of the hydrofoil, however, are not those of the airplane. As Baron Von Schertel points out, it will be well to recognize the pre-eminence of the airplane for passenger transport beyond the range of a few hundred miles. If commercial hydrofoils are to amount to more than a novelty, we shall have to look beyond the operating experience of today's boats. It will be necessary to recognize the unique characteristics of hydrofoils, to acknowledge their limitations, and to exploit their potentialities with vigor and imagination.

*   *   *

GROUND EFFECT MACHINE RESEARCH AND DEVELOPMENT IN THE UNITED STATES

Harvey R. Chaplin
David Taylor Model Basin

Ground effect machine (GEM) investigations in the United States have grown at an astonishing rate since early 1957. At present they involve some 40 commercial firms, laboratories, etc., and represent an increasingly significant investment of capital and engineering manpower. These investigations are thus far largely exploratory in nature. They represent a considerable variety of approaches, both as to types of ground cushion phenomena employed, and vehicle applications envisioned. The various ground cushion concepts are reviewed, in terms of elementary principles of fluid mechanics. All of the concepts are shown to give direct relationships between vehicle performance and vehicle size/height ratio. GEM developments are therefore expected to tend ultimately toward large ocean-going vehicles operating very close to the surface. Some of the outstanding advantages and problems of the various ground cushion concepts are discussed, but present knowledge does not support strong opinions as to which of the concepts will prevail.

SYMBOLS

S	Base area in square feet
h	Height above surface in feet
C	Perimeter of the base in feet
l	Vehicle length in feet
b	Vehicle beam in feet
G	Nozzle width in feet
θ	Normal jet discharge angle in degrees (see Figs. 1 and 3)
β	Tangential jet deflection angle in degrees (see Fig. 3)
Δp	Effective cushion (base) pressure in pounds per square foot gage
ρ	Mass density of air in slugs per cubic foot
ρ_w	Mass density of water in slugs per cubic foot
V_j	Average jet velocity at discharge feet per second
V_e	Full-expansion velocity, in feet per second, of cushion air (velocity cushion air would attain if allowed to expand to atmospheric pressure)

V_0 — Free-stream velocity in feet per second

q_0 — Free-stream dynamic pressure in pounds per square foot $\left(q_0 = \frac{1}{2}\rho V_0^2\right)$

L — Total lift in pounds

L_0 — Aerodynamic lift in pounds (lift contributed by pressure distribution associated with external flow field)

D_{ram} — Ram drag (momentum drag) in pounds

D_f — Parasite drag in pounds

T_j — Thrust component of jet reaction

D — Net drag in pounds $(D = D_{ram} + D_f - T_j)$

C_{L0} — Aerodynamic lift coefficient $(C_{L0} = L_0/qS)$

C_{Df} — Parasite drag coefficient $(C_{Df} = D_f/q_0 S)$

P_c — Cushion-system power in pound-feet per second

P_p — Propulsion-system power in pound-feet per second

P — Total power $(P = P_c + P_p)$

M — Figure of merit $\quad M = \left(\dfrac{1}{2\sqrt{\rho}}\dfrac{L}{P}\sqrt{\dfrac{L}{S}}\right)$

$\mho$ — Nondimensional velocity parameter $\left(\mho = \dfrac{V_0}{\sqrt{L/(\rho S)}}\right)$

$M_w, \mho_w$ — Same as M, $\mho$, but with ρ_w substituted for ρ

η_A — Augmentation efficiency

η_d — Duct efficiency

η_p — Compressor efficiency

η_{int} — Internal efficiency

η_F — Propulsive efficiency

D_c — Discharge coefficient

E — Energy ratio (ratio of maximum kinetic energy flux in system to power dissipation)

k_p — Effective pressure recovery factor $\left(k_p = \dfrac{\Delta\rho}{\frac{1}{2}\rho V_e^2}\right)$

D_e — Equivalent diameter $D_e = 4\,\dfrac{S}{C}$

INTRODUCTION

Just over three years ago, in early 1957, a report [1] by the NACA of experiments with a ground effect phenomenon sparked one of the most unique engineering and technical movements of modern U.S. history, a movement which appears to be still gathering momentum. A recent article in the technical press reported some forty firms now actively engaged in some form of ground effect machine (GEM) investigations, financed by government support nearing the ten-million-dollar mark plus an even larger investment of private funds.

Numerous economic and psychological reasons have been advanced to account for this remarkable growth of GEM activity. Certainly a major factor is the fascinating simplicity of the basic ground cushion concepts. The most casual technical training affords qualitative understanding of the basic ground cushion principles, and innumerable arrangements of readily available mechanical components which can produce a ground cushion come easily to mind. It is not really surprising that so many individuals should have felt the urge to put something together and putter around with it a bit. Even so, it may take something more to explain the scope and vigor of GEM activity — and the financial investment which it represents — at a time when the GEM's place in the transportation field is still highly uncertain.

This same simplicity of the ground cushion concept occasioned many a remark of surprise, in those early days of 1957, that "someone hadn't thought of it before." Of course, it turned out that someone had, notably, Kaario of Finland, Weiland of Switzerland, Cockerell of England, and Frost of Canada. Even in the U.S., a rather astonishing number of GEM models and vehicles of various types were soon found to be already in existence in widely scattered back yards, basements, and garages. Nevertheless, nearly all of the many GEM programs now in progress in the U.S. can be traced to the NACA report of 1957 and to the subsequent government activity which it inspired.

Equally as interesting as the volume of GEM work now in progress is its diversity. At least seven different ground cushion concepts, with almost countless combinations and variations, are under serious study. Sizable independent programs are being devoted to studies of engines, compressors, ducting problems, and structural design considerations. While in itself one of the most interesting aspects of the U.S. GEM picture, this diversity makes a comprehensive review of GEM research and development impractical. The present paper will be confined to a review of seven of the more significant vehicle concepts, in terms of simple fluid mechanics principles, with sketchy indications of the present stage of development and prospects of each. Sources of more detailed information will be given wherever possible.

THE GROUND CUSHION CONCEPTS

Seven ground cushion concepts have been chosen as representing, either directly or in combination, most of the basic ideas under active consideration in the U.S. Several of these concepts are at a rather primitive stage of development. In the analyses which follow, an attempt is made to reduce the various concepts to their lowest common denominator, in order that their similarities and distinctions will be readily apparent. To this end, the analyses follow what is termed, throughout this paper, "simplified ideal theory." This entails assumptions of inviscid, incompressible flow, liberal application of the one-dimensional flow approximations, and neglect of aerodynamic pressures and forces induced by the external flow field. It might be argued with some justice that these analyses should be termed "oversimplified ideal theory." Certainly, there is a deplorable lack of rigor, and the results are obviously not directly applicable to engineering problems. Nevertheless, it is believed that the essential features of the basic principles involved are retained in the results; and that the useful purposes of providing clear understanding and meaningful comparisons are served. In the case of the most highly developed concept, the air curtain, an engineering analysis (still highly simplified) will also be given, and compared to experimental results, to illustrate the relation between the simplified ideal theory and physical reality.

SIMPLE AIR CURTAIN

The air curtain (or "annular jet" or "peripheral jet") concepts have received by far the most attention and serious study. They are correspondingly the furthest advanced, in terms of practical understanding and engineering data. The simple air curtain is illustrated in Fig. 1. As in all the ground cushion concepts, the major source of lift force is the ground

Simplified Ideal Theory:

Hovering		Cruise	
$L = \Delta p S$	(1-1)	$D_{ram} = \rho V_j G C V_0$	(1-6)
$\Delta p h = \rho V_j^2 \, G \, (1 - \sin \theta)$	(1-2)	$P_p = D_{ram} V_0$	(1-7)
$P_c = V_j G C \, (\tfrac{1}{2} \rho V_j^2 + \tfrac{1}{2} \Delta p)$	(1-3)	$P_c = V_j G C \, (\tfrac{1}{2} \rho V_j^2 + \tfrac{1}{2} \Delta p - q_0)$	(1-8)
$M \equiv \dfrac{1}{2\sqrt{\rho}} \dfrac{L}{P_c} \sqrt{\dfrac{L}{S}}$	(1-4)	$\mathcal{v} \equiv V_0 \Big/ \sqrt{\dfrac{L}{\rho S}} = \sqrt{\dfrac{2}{C_L}}$	(1-9)
$M_{opt} = \dfrac{S}{h C}$	(1-5)	$\left(\dfrac{L V_0}{P}\right)_{opt} = 2 \, \dfrac{S}{h C} \, \dfrac{\mathcal{v}}{\sqrt{1 + \mathcal{v}^2}}$	(1-10)

Fig. 1. Simple air curtain

cushion itself, a region of positive gage pressure trapped between the vehicle and the ground. With the air curtain types, this ground cushion is generated and contained by a jet of air exhausted downward and inward from a nozzle at the periphery of the base. With the simple air curtain, the resultant jet reaction force is vertical, and propulsion must be provided by a separate device (shown schematically in Fig. 1 as a propeller).

Hovering

The jet reaction force contributes to the lift, but this contribution is small compared to the cushion lift, so long as the vehicle is near the ground. The lift is approximated by the product of cushion pressure times base area:

$$L = \Delta p S \; . \tag{1-1}$$

The cushion pressure also reacts against the air curtain with a force which must balance the momentum change within the curtain. This relationship is approximated by

$$\Delta p h = \rho V_j^2 \, G \, (1 - \sin \theta) \tag{1-2}$$

where the jet discharge angle θ is taken, by convention, to be negative for the inward-inclined jet sketched in Fig. 1.

The power required is the product of jet volume flow rate times compressor pressure rise, approximated by

$$P_c = V_j G\, C\left(\frac{1}{2}\rho V_j^2 + \frac{1}{2}\Delta p\right) \tag{1-3}$$

where the compressor pressure rise equals the jet total pressure and is the sum of mean dynamic pressure (approximated by $(1/2)\rho V_j^2$) and mean static pressure (approximated by $(1/2)\Delta p$).

Hovering performance is expressed by the dimensionless figure of merit,

$$M = \frac{1}{2\sqrt{\rho}}\frac{L}{P}\sqrt{\frac{L}{S}} \tag{1-4}$$

which provides a direct indication of the important lift/power ratio L/P, and a direct comparison with the ideal shrouded propeller or helicopter (with fixed figures of merit, outside ground effect, of 1.0 and $\sqrt{1/2}$, respectively). Combining Eqs. (1-1) through (1-4), gives

$$M = (1 - \sin\theta)\frac{\sqrt{\frac{G}{h}(1 - \sin\theta)}}{1 + \frac{G}{h}(1 - \sin\theta)} \cdot \frac{S}{hC}$$

which has a maximum value (when $G/h = 1/2$, $\theta = -90°$) of

$$M_{opt} = \frac{S}{hC}. \tag{1-5}$$

A more thorough analysis (see Ref. 3, for example) gives slightly different values for optimum nozzle width ratio G/h and jet angle θ, but almost exactly the same result for optimum figure of merit M_{opt}. Practical design limitations, internal losses, etc., will limit actual vehicles to about $M = 0.6\, S/hC$.

The ratio S/hC is called the size/height ratio. The initiate to the GEM field will find that a few minutes devoted to firmly fixing the size/height ratio and its geometric meaning in his mind will be well spent. This ratio is of predominant importance in virtually all considerations of all types of ground effect machines. The size/height ratio may be thought of as an area ratio, between the "cushion area" S of the vehicle base and the "curtain area" hC of an imaginary peripheral screen sealing in the ground cushion. Or, it may be thought of as a length ratio. Noting that, for a circular plan form, the quantity S/C is equivalent to one-fourth the diameter, $S/hC = D_e/4h$, where D_e is the "equivalent diameter" of the plan form.

Cruise

When the simple air curtain vehicle moves horizontally in forward flight, two modifications to the hovering equations occur. First, a "ram" drag D_{ram} equal to the air mass flow rate through the peripheral nozzle times the forward velocity, is experienced by the vehicle;

and the propulsion system must expend energy at the rate $P_p = D_{ram} V_0$ to overcome this drag (Fig. 1, Eqs. (1-6), (1-7). Second, while the cushion power P_c is still the product of air volume flow rate times compressor pressure rise, the required pressure rise is now reduced by the amount q_0 of the free-stream dynamic pressure recovered by the inlet (Eq. (1-8), Fig. 1).

The cruise performance is expressed by the dimensionless "equivalent lift/drag ratio" LV_0/P (Both the range of the GEM and its direct operating cost per ton-mile are directly proportional to the equivalent lift/drag ratio.). Combining Eqs. (1-7) and (1-8) with (1-1) and (1-2) and solving again for optimum G/h ($= 1/2 (1 + U^2)$) and θ ($= -90°$) gives

$$\left(\frac{LV_0}{P}\right)_{opt} = 2 \frac{S}{hC} \frac{U}{\sqrt{1 + U^2}} \tag{1-10}$$

where U is the dimensionless velocity parameter $V_0/ \sqrt{L/(\rho S)}$.

Since optimum nozzle width ratio G/h decreases with increasing forward velocity, Eq. (1-10) represents an envelope curve for possible designs (or possible settings of an adjustable-nozzle design).

Equation (1-10) describes a curve which rises asymptotically to the value $2 S/hC$ as the forward velocity increases without limit. Consideration of the parasite drag will, of course, cause the equivalent lift/drag ratio to fall below this simplified ideal solution and to peak out at some value of U corresponding to the "optimum cruise speed." This, and other practical considerations, will be discussed further when a simplified engineering analysis of the air curtain vehicle is presented in a later section of this paper. It may be said here that actual vehicles of the simple air curtain type will probably be limited to equivalent lift/drag ratios of about 0.7 S/hC, at optimum cruise speeds corresponding roughly to $U = 1.0$.

More detailed information on the simple air curtain is found in Refs. 2 to 5.

AIR CURTAIN WITH SKEGS

If the GEM is to operate exclusively over water, and at moderate speeds, a substantial power saving is effected by the use of side plates, or skegs, which extend into the water as sketched in Fig. 2. The equations are exactly the same as for the simple air curtain except that the air curtain is furnished to only the portion $2b$ of the total perimeter $2b + 2l$. Both the figure of merit and the equivalent lift/drag ratio are hence improved in proportion to the factor $1 + l/b$ (Fig. 2, Eqs. (2-1), (2-2)).

In practice, of course, the drag on the submerged portion of the skeg becomes very significant at high speeds. The exact breakeven point between the simple air curtain and the air curtain with skegs depends on the roughness of the water surface (which determines the minimum skeg submersion necessary to effect a seal). It is generally felt, however, that the application of submerged skegs is confined to speeds below 50 knots.

A compromise between the simple air curtain and the air curtain with skegs is also being studied wherein side plates extend below the base part way to the water, with air curtains issuing from nozzles at the lower extremities of the side plates. The total curtain
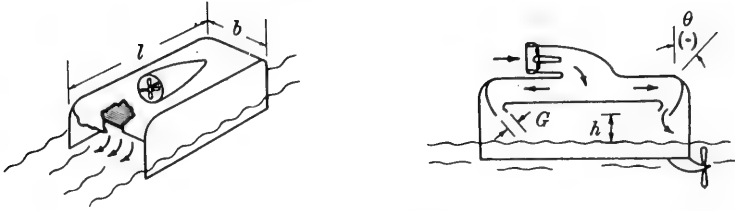
Simplified Ideal Theory:

Equations same as for air curtain, except that power is
furnished to only the portion $(2\,b)$ of the perimeter $(2\,l + 2\,b)$

Hover		Cruise	
$M \equiv \dfrac{1}{2\sqrt{\rho}}\,\dfrac{L}{P}\sqrt{\dfrac{L}{S}}$			
$M_{opt} = \dfrac{S}{hC}\left(1 + \dfrac{l}{b}\right)$	(2-1)	$\left(\dfrac{LV_0}{P}\right)_{opt} = 2\,\dfrac{S}{hC}\,\dfrac{\upsilon}{\sqrt{1 + \upsilon^2}}\left(1 + \dfrac{l}{b}\right)$	(2-2)

Fig. 2. Air curtain with skegs

area is $2\,bh + 2\,lh'$ (where h' is the clearance of the side plates above the water) as compared to $hC = 2\,bh + 2\,lh$ for the simple air curtain. The simplified ideal theory performance is hence

$$M_{opt} = \frac{S}{hC}\;\frac{1 + \dfrac{l}{b}}{1 + \dfrac{l}{b}\cdot\dfrac{h'}{h}}$$

$$\left(\frac{LV_0}{P}\right)_{opt} = 2\,\frac{S}{hC}\cdot\frac{\upsilon}{\sqrt{1 + \upsilon^2}}\cdot\frac{1 + \dfrac{l}{b}}{1 + \dfrac{l}{b}\cdot\dfrac{h'}{h}}\,.$$

The proponents of this compromise believe that the side plates, because of their low frontal area, can be designed to survive occasional high-speed impacts with higher-than-average waves.

More detailed information on the air curtain with skegs is found in Refs. 6 and 7.

INTEGRATED AIR CURTAIN

The integrated air curtain provides for propulsion by directing the peripheral jet at a rearward-inclined angle, so that the net resultant jet reaction force is inclined forward from vertical. This system is illustrated in Fig. 3. Vanes in the peripheral nozzle deflect the jet exhaust rearward through the tangential jet deflection angle β. If the vehicle has a
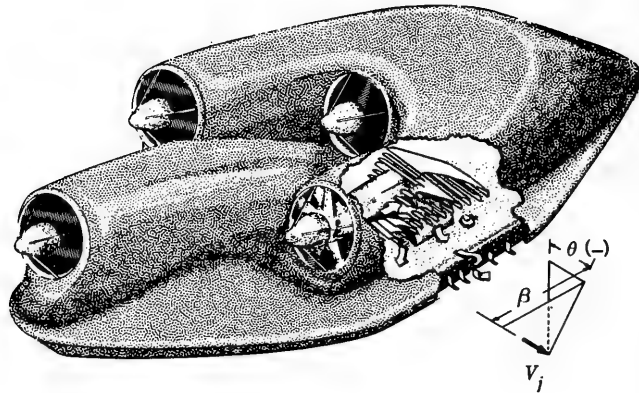
Simplified Ideal Theory:

Cruise
$V_0 = V_j \sin \beta$ (ram drag = thrust) $\hspace{2cm}$ (3-1)
$L = \Delta p \, S$ $\hspace{2cm}$ (3-2)
$\Delta p h = \rho V_j^2 G (1 - \sin \theta) \cos^2 \beta$ $\hspace{2cm}$ (3-3)
$P = P_c = V_j GC \cos \beta \left(\frac{1}{2} \rho V_j^2 + \frac{\Delta p}{2} - q_0 \right)$ $\hspace{0.5cm}$ (3-4)
$\mathcal{V} \equiv \dfrac{V_0}{\sqrt{L/(\rho S)}} = \dfrac{\tan \beta}{\sqrt{\dfrac{G}{h}} (1 - \sin \theta)}$ $\hspace{1cm}$ (3-5)
$\boxed{\left(\dfrac{L V_0}{P} \right)_{opt} = 2 \, \dfrac{S}{h C} \mathcal{V}}$ $\hspace{2cm}$ (3-6)

Fig. 3. Integrated air curtain

slender plan form, with pointed bow and stern, so that the entire peripheral nozzle lies nearly parallel to the direction of flight, then the rearward velocity component produced by tangential deflection is, at all points along the nozzle exit, nearly equal to $V_j \sin \beta$. The thrust component of jet reaction is hence mass flow times $V_j \sin \beta$, and equals the ram drag (mass flow times V_0) when

$$V_0 = V_j \sin \beta . \tag{3-1}$$

The base pressure and jet momentum relationship is modified from the simple air curtain case (Eq. (1-2)) as follows: The effective nozzle area per unit nozzle length is reduced in proportion to $\cos \beta$, and only the fraction $\cos \beta$ of the jet momentum enters into reaction against the ground cushion (since the tangential component of jet momentum is unchanged as the jet curves outward). The equivalent relationship for the integrated air curtain is therefore

$$\Delta ph = \rho V_j^2 G (1 - \sin \theta) \cos^2 \beta . \tag{3-3}$$

The cushion power expression is the same for the simple air curtain (Eq. (1-8)) except for the modified effective nozzle area:

$$P_c = V_j G C \cos \beta \left(\frac{1}{2} \rho V_j^2 + \frac{1}{2} \Delta p - q_0 \right) . \tag{3-4}$$

Combining, and solving for optimum nozzle width ratio G/h ($= 1/2$) and jet angle θ ($= -90°$) gives for the equivalent lift/drag ratio

$$\left(\frac{LV_0}{P}\right)_{opt} = 2 \frac{S}{hC} \mathrm{U} . \tag{3-6}$$

Comparison of this equation with Eq. (1-10) for the simple air curtain shows that the results are equivalent at very low speeds, but the integrated air curtain becomes vastly superior at high speeds. Close examination of the integrated air curtain equations (Fig. 3) will reveal that the power required, compressor pressure rise, internal air mass-flow rate, and optimum nozzle width are all independent of speed. In practice, all of these advantages are somewhat diluted (but not negated) by the effects of parasite drag and internal losses. The best design practice might be to provide sufficient tangential jet deflection to counter-act the ram drag, plus a separate propulsion system to counteract the parasite drag. This and other practical considerations are discussed further in the simplified engineering analy-sis of air cushion performance presented in a later section of this paper. It may be said here that actual air cushion vehicles will probably be limited to equivalent lift/drag ratios of the order of 0.9 S/hC, at optimum cruise speeds corresponding roughly to $\mathrm{U} = 1.0$.

More detailed information on the integrated air curtain is found in Refs. 4 and 5.

WATER CURTAIN

In principle, a ground cushion can be contained by a peripheral jet of water in just the same manner as by a jet of air. This concept is represented schematically in Fig. 4. Air is pumped to the base of the vehicle until the ground cushion is established, at which point equilibrium is reached between the change of momentum within the water curtain and the

Simplified Ideal Theory:

Equations same as for air curtain (neglecting gravity) except
that water density appears instead of air density.

Hovering	Cruise
Simple Water Curtain	

$$M_w \equiv \frac{1}{2\sqrt{\rho_w}} \; \frac{1}{P_c} \sqrt{\frac{L}{S}} \qquad (4\text{-}1)$$

$$\boxed{M_{w,\text{opt}} = \frac{S}{hC}} \qquad (4\text{-}2)$$

$$M_{\text{opt}} \doteq 29 \; \frac{S}{hC} \qquad (4\text{-}3)$$

$$\boxed{\left(\frac{LV_0}{P}\right)_{\text{opt}} = 2 \; \frac{S}{hC} \; \frac{v_w}{\sqrt{1+v_w^2}}} \qquad (4\text{-}4)$$

$$\left(\frac{LV_0}{P}\right)_{\text{opt}} \doteq 2 \; \frac{S}{hC} \; \frac{v}{\sqrt{0.0012+v^2}} \qquad (4\text{-}5)$$

Integrated Water Curtain

$$\boxed{\left(\frac{LV_0}{P}\right)_{\text{opt}} = 2 \; \frac{S}{hC} \; v_w} \qquad (4\text{-}6)$$

$$\left(\frac{LV_0}{P}\right)_{\text{opt}} \doteq 58 \; \frac{S}{hC} \; v \qquad (4\text{-}7)$$

Note remarks in text!!

Fig. 4. Water curtain

reaction of the cushion pressure against the curtain. Gravity has a favorable effect on the
water curtain in that the jet gains momentum as it falls from the nozzle to the surface; and
it has an unfavorable effect on the pumping power, in that the water must be raised from the
surface to the level of the nozzle. The problem is greatly simplified, and the essential
character of the result is unchanged, if these effects are neglected. The equations for the
water curtain then become identical with those for the air curtain (Figs. 1 through 3), except
that water density ρ_w is substituted for air density ρ. The results, in terms of dimensionless
parameters referred to water density (Fig. 4, Eqs. (4-2), (4-4), (4-6)), are exactly analogous
to the air curtain results. However, when the parameters are referred to air density, it is
apparent that, in principle, the water curtain enjoys a tremendous advantage. In the hover-
ing case, and in the case of the integrated water curtain at cruise, the results (Eqs. (4-3)
and (4-7)) show the water curtain doing the same job as the air curtain with 1/29 as much
power required.

The trouble with this rosy picture becomes apparent when it is recalled that the opti-
mum nozzle width G on which these results are based, is half the operating height h. A
piping system large enough to supply such a nozzle, and filled with water, would weigh a

staggering amount. It is obviously necessary to compromise in favor of a much, much thinner nozzle. In both of the cases cited, simplified ideal theory gives the power as proportional to the quantity

$$\left(\frac{1}{\sqrt{2\dfrac{G}{h}}} + \sqrt{2\dfrac{G}{h}} \right) .$$

The compromise to thinner nozzles thus destroys much of the theoretical advantage. (For example, if $G/h = 1/200$ instead of $1/2$, the power required is increased by a factor of five, leaving the water curtain with roughly a 6:1 theoretical advantage over the air curtain compared to the original 29:1 advantage.) Furthermore, experiments show that a thin water curtain provides an imperfect seal, so that air must be pumped into the cushion at a quite substantial rate to maintain the cushion pressure. This makes further serious inroads into the theoretical advantage. Just how much advantage is left, if any, is not quite clear at present. Certainly, the water curtain concept should not be discounted without careful study, and a vigorous study program is, in fact, underway.

More detailed information on the water curtain concept is found in Ref. 8.

PLENUM

The plenum is by far the simplest of the ground cushion concepts, both in principle and in physical embodiment. The plenum concept is represented schematically in Fig. 5. The vehicle has a recessed base. Air is simply pumped into the recess and allowed to leak out along the ground.

Hover

Neglecting internal velocities in comparison to the full-expansion velocity, V_e, gives

$$\text{Lift} \qquad\qquad L = \Delta p S \qquad\qquad\qquad (5\text{-}1)$$

$$\text{Cushion pressure} \qquad \Delta p = \frac{1}{2}\rho\, V_e^2 \qquad\qquad (5\text{-}2)$$

$$\text{Cushion power} \qquad P_c = V_c\, D_c\, h\, C\, \Delta p \qquad (5\text{-}3)$$

$$\text{Figure of merit} \qquad M = \sqrt{\frac{1}{2}}\; \frac{1}{2D_c}\; \frac{S}{hC} \qquad (5\text{-}4)$$

where D_c is the discharge coefficient of the leakage flow, $D_c\, hC$ being the flow area at full expansion. Using a typical value of 0.61 for D_c gives

$$M = 0.58\; \frac{S}{hC} . \qquad\qquad\qquad (5\text{-}5)$$
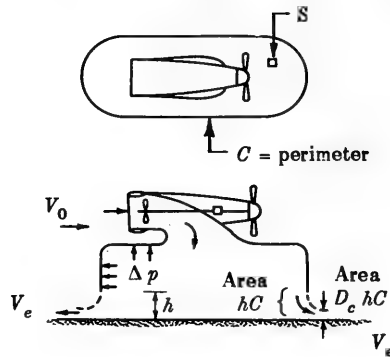
Simplified Ideal Theory:

Hovering		Cruise	
$L = \Delta p S$	(5-1)	$D_{ram} = \rho V_e D_c h C V_0$	(5-6)
$\Delta p = \frac{1}{2} \rho V_e^2$	(5-2)	$P_p = D_{ram} V_0$	(5-7)
$P_c = V_e D_c h C \Delta p$	(5-3)	$P_c = V_e D_c h C (\Delta p - q_0)$	(5-8)
$M \equiv \dfrac{1}{2\sqrt{\rho}} \dfrac{L}{P_c} \sqrt{\dfrac{L}{S}}$		$\upsilon \equiv V_0 \Big/ \sqrt{\dfrac{L}{\rho S}} = \sqrt{2}\,\dfrac{V_0}{V_e}$	(5-9)
$= \dfrac{0.353}{D_c} \dfrac{S}{hC}$	(5-4)	$\left(\dfrac{L V_0}{P}\right)_{opt} \doteq 1.16\,\dfrac{S}{hC}\,\dfrac{\upsilon}{1 + \frac{1}{2}\upsilon^2}$	(5-10)
$M \doteq 0.58\,\dfrac{S}{hC}$	(5-5)		

Fig. 5. Plenum

Cruise

The ram drag (mass flow times flight velocity), propulsive power, and cushion power (same as in hovering, except for effect of ram pressure recovery in inlet) are given by

$$D_{ram} = \rho V_e D_c h C V_0 \tag{5-6}$$

$$P_p = D_{ram} V_0 \tag{5-7}$$

$$P_c = V_e D_c h C (\Delta p - q_0). \tag{5-8}$$

Introducing the dimensionless velocity parameter

$$\upsilon \equiv V_0 \Big/ \sqrt{\frac{L}{\rho S}} = \sqrt{2}\,\frac{V_0}{V_e} \tag{5-9}$$

and again using the value 0.61 for D_c gives

$$\frac{L\,V_0}{P} \doteq 1.16\, \frac{S}{hC} \cdot \frac{\upsilon}{1 + \frac{1}{2}\upsilon^2} \cdot \tag{5-10}$$

Compared with the corresponding air curtain results, the plenum concept falls considerably short, both as to figure of merit and (especially) equivalent lift/drag ratio. Nevertheless, it has its supporters among GEM investigators, because of its extreme simplicity. Of the GEM concepts, the plenum is the most compatible with cheap, lightweight, rugged construction.

More detailed information on the plenum concept is found in Refs. 9 and 10.

RAM WING

The ram wing is believed to be the oldest of the ground cushion concepts, having been introduced in Finland by Kaario as early as 1935. The ram wing concept is represented schematically in Fig. 6. The vehicle takes the form of a box with the bottom and front side removed. The basic ram wing has no hovering capability, but if it moves forward very close to the ground (so that velocities within the ground cushion are negligible), the ram pressure $\rho V_0^2/2$ builds up beneath the base, giving a lift force

$$L = \frac{1}{2}\rho V_0^2 S \ . \tag{6-1}$$

Simplified Ideal Theory:

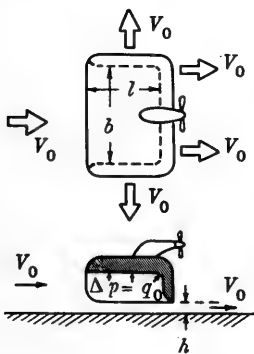| Cruise	
$L \ = \ \tfrac{1}{2}\,\rho\,V_0^2\ lb$	(6-1)
$D_{ram} = \rho V_0\,(2\,lhD_c)\,V_0$	(6-2)
$P \ = D_{ram}\,V_0$	(6-3)
$\left(\dfrac{L\,V_0}{P}\right)_{opt} \doteq 1.64\ \dfrac{S}{h\,C}\ \dfrac{1 + b/l}{2}$	(6-4)
$\upsilon \ \equiv \ \dfrac{V_0}{\sqrt{L/(\rho\,S)}} = \ \sqrt{2}$	(6-5)

Fig. 6. Ram wing

Only the air which leaks out at the tips contributes to the ram drag, since the air leaked out the rear recovers it original rearward momentum. Assuming the discharge coefficient D_c to be 0.61,

$$D_{ram} = \rho V_0\,(2l\,hD_c)\,V_0 \tag{6-2}$$

$$P = D_{\text{ram}} V_0 \qquad\qquad\qquad (6\text{-}3)$$

$$\frac{LV_0}{P} = 1.64 \; \frac{S}{hC} \; \frac{1 + \dfrac{b}{l}}{2} \; . \qquad\qquad (6\text{-}4)$$

This elementary solution gives equilibrium flight at only one speed, corresponding to

$$\mathcal{U} \equiv \frac{V_0}{\sqrt{L \; / \; (\rho S)}} = \sqrt{2} \; . \qquad\qquad (6\text{-}5)$$

In practice, one of the other ground cushion concepts must be combined with the ram wing to maintain the ground cushion during acceleration to and deceleration from this equilibrium speed. For equilibrium at speeds higher than given by (6-5), the height h must increase until the cushion pressure falls to something less than the full ram pressure. Even at $\mathcal{U} = 2$, the lift contributed by suction pressure induced on the upper surface of the wing (neglected by the simplified ideal theory) is significant, but it does not dominate the problem. At higher speeds this suction-pressure lift does begin to predominate, and the simplified ideal theory must be abandoned in favor of approaches along the line of conventional wing theory.

It is interesting to note, from Eq. (6-4), that the ram wing, like the conventional aircraft wing, gives much better performance with high aspect ratio, b/l.

There has been practically no development effort devoted to the ram wing in the U.S. However, several U.S. groups have recently begun study programs, and a rapid expansion of activity in this area is not unlikely.

Kaario's discussion of the ram wing concept is found in Ref. 11.

DIFFUSER-RECIRCULATION SYSTEM

From an academic point of view, the diffuser-recirculation system is perhaps the most interesting of all the ground cushion concepts. It is the only one which can, in principle, sustain a vehicle at a finite height above the ground without dissipating any power.

The diffuser-recirculation system is represented schematically in Fig. 7. A recirculating flow, rather like a standing ring vortex, is maintained within and under the vehicle. At the periphery of the base, the flow passes through a nozzle G, and is then exposed to atmospheric pressure until it passes through the gap h between the underside of the base and the rim. The static pressure at the gap h is thus essentially atmospheric. The geometry of the base and internal passages is so arranged that the highest velocity (and thus the lowest pressure) of the flow occurs at the periphery, where the flow is exposed to atmospheric pressure. The average static pressure under the vehicle is therefore higher than atmospheric, giving a net lift force on the vehicle. Under the assumption of inviscid flow, this is a closed system with no energy dissipation. Simplified ideal theory thus gives

$$M_{\text{opt}} \equiv \frac{1}{2\sqrt{\rho}} \frac{L}{P} \sqrt{\frac{L}{S}} = \infty$$

$$\left(\frac{L\,V_0}{P}\right)_{opt} = \infty \; .$$

Nozzle G

Gap h

Diffuser-Recirculation
Vehicle

Test
Section

Open-Jet
Wind Tunnel
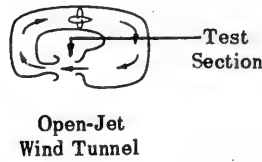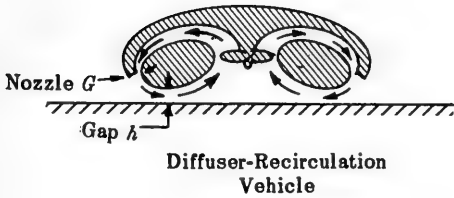
Simplified Ideal Theory:

Hover: $M \equiv \dfrac{1}{2\sqrt{\rho}} \dfrac{L}{P} \sqrt{\dfrac{L}{S}} = \infty$

Cruise: $\dfrac{L\,V_0}{P} = \infty$

Wind Tunnel Analogy:

Hover: $M = \dfrac{E\,K_p^{3/2}}{2\sqrt{2}} \dfrac{S}{h\,C}$

Cruise: $\dfrac{L\,V_0}{P} = \dfrac{E\,K_p^{3/2}}{\sqrt{2}} \dfrac{S}{h\,C} \, \psi$

Fig. 7. Diffuser-recirculation system

Most of the research and development effort in the diffuser-recirculation area is concerned with modifications and variations of the basic system described. The practical outlook for the basic diffuser-recirculation system is not encouraging, primarily because of the following considerations:

1. The geometric relationship between the nozzle G and gap h is rather critical. This relationship can be established properly only for a single operating height; and variations in h from wind and surface disturbances cannot be avoided. Particularly disconcerting is the occurrence of an unstable condition, wherein lift force decreases with decreasing height, at heights below the optimum.

2. In practice, as in theory, the performance is totally dependent upon efficient diffusion (deceleration and static pressure recovery) of the flow as it moves inward between the vehicle base and the ground. Irregularities in the surface over which the vehicle moves would make efficient diffusion impossible.

An interesting analogy can be drawn between the diffuser-recirculation vehicle and the open-jet wind tunnel, also sketched in Fig. 7. The wind tunnel is also a closed system in which the maximum velocity occurs at a section (the test section) where the flow is exposed to the atmosphere. The power dissipation of the wind tunnel would be zero with inviscid flow; and, like the vehicle, its actual performance depends upon an efficient diffusion process. Tunnel performance is often expressed by the "energy ratio" E, defined as the ratio of the kinetic energy flux through the test section to the power dissipation. Applying this terminology to the vehicle, taking the gap area hC as analogous to the test section area, gives

$$P_c = \frac{1}{2} \rho V_e^3 h \frac{C}{E}$$

$$L = \Delta p S = k_p \frac{1}{2} \rho V_e^2 S$$

where k_p is the effective pressure recovery factor. This gives

$$M \equiv \frac{1}{2\sqrt{\rho}} \frac{L}{P} \sqrt{\frac{L}{S}} = \left(\frac{k_p}{2}\right)^{3/2} \frac{S}{hC} \; .$$

Open-jet wind tunnels typically have energy ratios around 3.0. Using this value, and assigning (arbitrarily, and probably optimistically) the value of 0.7 to k_p would give

$$M \doteq 0.6 \frac{S}{hC}$$

as a rough estimate of actual hovering performance, under favorable conditions. This is the same as the estimated actual hovering performance of well-designed air curtain vehicles.

This numerical result is questionable, due to the assumptions employed. Of greater significance is the demonstration that, for the diffuser-recirculation concept, just as for all of the other ground cushion concepts, the performance is directly dependent on the size/ height ratio, S/hC.

More detailed information on the diffuser-recirculation concept is found in Ref. 12.

SIMPLIFIED ENGINEERING ANALYSIS OF THE AIR CURTAIN VEHICLE

The foregoing "simplified ideal theory" analyses serve only to give mathematical expression to the basic ideas involved in the various ground cushion concepts. Comparisons between the various concepts on this basis are still only comparisons of ideas. Realistic comparisons of engineering merit will require not only more complete analysis, but a considerable background of systematic empirical information. Such comparisons are not possible at the present state of the art. More complete analyses of several of the concepts will be found in the references, but only in the case of the air curtain concepts is there a sufficient body of systematic experimental data to support a realistic assessment of the practical performance.

It would be superfluous to repeat here any detailed analysis of air curtain vehicle performance. It may be useful, however, to follow a simplified development, along the lines of the simplified ideal theory, but accounting, in an elementary way, for the most significant of the effects previously neglected. These are:

1. Internal losses, accounted for by a duct efficiency η_d, compressor efficiency η_p, and internal efficiency $\eta_{int} = \eta_p \eta_d$.

2. Base pressure loss, accounted for by an augmentation efficiency η_A.

3. Aerodynamic lift coefficient C_{L_0}, and parasite drag coefficient C_{Df}, produced by the external flow field.

4. Propulsion system losses, accounted for by the propulsive efficiency η_F.

Both tangential jet deflection β (Fig. 3) and separate-propulsion-system power will be accounted for. This is appropriate to a semi-integrated air curtain concept, wherein part, but not all, of the thrust is derived from the air curtain itself. The resulting equations will be reducible to the simple or integrated air curtain cases simply by setting β equal to zero, or setting air-curtain thrust equal to net drag, respectively.

The lift is approximated by

$$L = \Delta p S \left[+ C_{L_0} \; q_0 \; S \right] \tag{8-1}$$

(The box will be used to indicate modifications to the simplified ideal theory.)

The base pressure is approximated by

$$\Delta p = \rho \, V_j^2 \, \frac{G}{h} \, (1 - \sin \theta) \, \cos^2 \beta \, \left[\eta_A \right] . \tag{8-2}$$

The cushion power is approximated by

$$P_c = \left[\frac{1}{\eta_{int}} \right] V_j \cdot G \cdot C \, \cos \, \beta (\frac{1}{2} \rho \, V_j^2 + \frac{1}{2} \Delta p - \left[\eta_d \right] \cdot q_0) . \tag{8-3}$$

The ram drag, parasite drag, and air curtain thrust are given by

$$D_{ram} = \rho \, V_j \, G \, C \, \cos \, \beta \, V_0 \tag{8-4}$$

$$D_f = \left[C_{Df} \; q_0 \; S \right] \tag{8-5}$$

$$T_j = \rho \, V_j^2 \, G \, C \, \cos \, \beta \, \sin \, \beta \, \left[\frac{2l}{C} \right] \tag{8-6}$$

where the factor $2l/C$ accounts for the fact that the tangential force component of each element of the air curtain lies tangential to the local periphery, not, in general, precisely parallel to the direction of flight.

The propulsion power is net drag times flight velocity, corrected for propulsive efficiency:

$$P_p = \frac{(D_{ram} + \left[D_f \right] - T_j) \, V_0}{\left[\eta_F \right]} . \tag{8-7}$$

Combining, and forming dimensionless ratios:

$$\frac{P_c}{L^{3/2}/\sqrt{\rho S}} = \frac{1}{\eta_{int}} \frac{\sqrt{(1 - \sin\theta)\frac{G}{h}\eta_A}}{2(1 - \sin\theta)\frac{S}{hC}\eta_A} \left[\left(\frac{1}{(1 - \sin\theta)\frac{G}{h}\eta_A \cos^2\beta} + 1\right)\right.$$

$$\left. \cdot \left(1 - \frac{C_{L_0}}{2}\mathcal{V}^2\right)^{3/2} - \eta_d\mathcal{V}^2\left(1 - \frac{C_{L_0}}{2}\mathcal{V}^2\right)^{\frac{1}{2}}\right] \tag{8-8}$$

$$\frac{P_p}{L^{3/2}/\sqrt{\rho S}} = \frac{1}{\eta_F} \frac{D}{L} \mathcal{V} \tag{8-9}$$

$$\frac{D}{L} = \frac{\sqrt{(1 - \sin\theta)\frac{G}{h}\eta_A}}{(1 - \sin\theta)\frac{S}{hC}\eta_A} \sqrt{1 - \frac{C_{L_0}}{2}\mathcal{V}^2} \; \mathcal{V} + \frac{C_{Df}}{2}\mathcal{V}^2$$

$$- \frac{\tan\beta}{(1 - \sin\theta)\frac{S}{hC}\eta_A}\left(1 - \frac{C_{L_0}}{2}\mathcal{V}^2\right)\frac{2l}{C} \tag{8-10}$$

$$\frac{LV_0}{P} = \mathcal{V} \bigg/ \left(\frac{P_c + P_p}{L^{3/2}/\sqrt{\rho S}}\right). \tag{8-11}$$

These last four equations form a system from which realistic estimates of air curtain performance (whether simple, integrated, or semi-integrated air curtain) can be made — if estimates of the parameters η_A, C_{L_0}, and C_{Df} can be obtained. The problem of providing a reliable basis for estimating these three parameters occupies much of the systematic GEM research now underway in the U.S. (The internal-, duct-, and propulsive-efficiency problems are, of course, age-old problems, not peculiar to GEM's, and highly developed techniques for dealing with them are available in the literature.) Some progress has been reported in the references. A good deal of additional progress can be expected in the immediate future.

It will suit our present purposes to side-step the question of how these estimates can be made, and to use, for our discussion, a source of data for which the necessary parameters have been evaluated to some reasonable degree of accuracy, experimentally. Such a source is Ref. 5, which presents data from wind-tunnel tests of the David Taylor Model Basin's Gem Model 448. This model represents the nearest approach to a realistic, practical GEM configuration for which laboratory-controlled performance test data are presently available.

Photographs of the model are presented in Fig. 8. The sketch in Fig. 3, used to illustrate the integrated air curtain concept, is also representative of the geometric arrangement
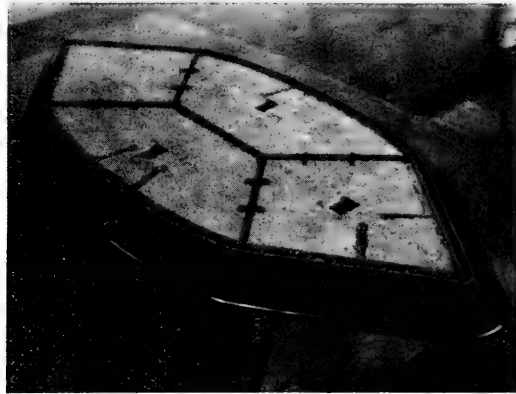
Fig. 8. DTMB GEM Model 448

and airflow path of Model 448. The four compressor nacelles are powered by calibrated electric motors. Several interchangeable sets of nozzle control vanes were employed to produce various tangential deflection angles β (see Fig. 3). The model is not equipped with an actual propulsion system, but propulsive power was accounted for in the test data reduction by arbitrarily assuming it to equal $1.25\,DV_0$ (i.e., $\eta_F = 0.8$). (It should be noted that, as explained in Ref. 3, the assumption $P_p = 1.25\,DV_0$ becomes unrealistic at low forward speeds. Nevertheless, it provides a convenient and reasonable basis for quick examination of the overall performance characteristics.) The performance parameters necessary for evaluation of Eqs. (8-8) through (8-11) vary slightly with changing test conditions, but it will suffice for our purposes to use the fixed set:

$$\eta_{\text{int}} = 0.57 \qquad \eta_A = 0.73$$

$$\eta_d \doteq 0.70 \qquad C_{L_0} = 0.42$$

$$\eta_F = 0.80 \qquad C_{Df} = 0.074.$$

(These performance parameters reflect design features dictated by scale and by research
utility considerations. A highly developed vehicle should have substantially improved
internal and duct efficiency and parasite drag coefficient, perhaps 0.8, 0.9, and 0.04,
respectively.) The pertinent geometric data for the model are:

$$S = 20.50 \text{ square feet}$$
$$C = 18.85 \text{ feet}$$
$$l = 8.45 \text{ feet}$$
$$G = 0.058 \text{ foot}$$
$$\theta = -45°.$$

Performance calculations from Eqs. (8-8) through (8-11) are compared with experimental
results in Fig. 9. The consistent agreement, over wide ranges of test conditions, strongly
suggests that the very elementary considerations employed in the simplified engineering
analysis correctly represent the major physical phenomena involved.

(It is not our purpose here to consider the detailed performance of the air curtain GEM.
However, in passing, one should note: (a) the strong, almost linear dependence of the
equivalent lift/drag ratio, LV_0/P, on size-height ratio, S/hC, shown in Fig. 9a, (b) the
significant performance advantage indicated in Fig. 9b for the vehicle with controlled tan-
gential deflection β of the air curtain, and (c) the further advantage indicated for such a
vehicle, in Fig. 9c, in terms of the power-required distribution between cushion power and
propulsive power. The total installed power required, if separate power sources are used for
the cushion system and propulsion system, will be the sum of the maximum cushion power
required and the maximum propulsion power required. This sum, especially for the simple
air curtain ($\beta = 0$) is very much larger than the maximum total power required at any given
instant.)

Having confirmed that the simplified engineering analysis gives a reasonable represen-
tation of the actual facts, we are in a position to examine the relationship between the
simplified ideal theory and physical reality. It will be easiest to consider the simple air
curtain ($\beta = 0$) for this purpose. For direct comparison, the appropriate form of simplified
ideal theory is obtained from Eqs. (8-8) through (8-11) by setting

$$\eta_{int} = \eta_d = \eta_F = \eta_A = 1.0$$

$$C_{L_0} = C_{Df} = 0 .$$

The most important information one may hope to obtain from simplified ideal theory is a
qualitative prediction of equivalent lift/drag ratio. The calculation of optimum equivalent
lift/drag ratios from Eqs. (8-8) through (8-11) is rather laborious. However, as suggested by
Ref. 4, and confirmed by Fig. 9, an excellent indication of effects on optimum performance
is obtained by considering performance at $\mathcal{V} = 1$. Figure 10 gives the result of such a cal-
culation, starting with simplified ideal theory, and with successive curves which result from
setting the performance parameters, in steps, to the values appropriate to Model 448. Each
of the "real" effects gives a successively less optimistic performance prediction compared
to the simplified ideal theory. At the end, the actual equivalent lift/drag ratio of Model 448
is very much lower than predicted by simplified ideal theory (about one-half), but the essen-
tial conclusion of the simplified ideal theory as to the nearly linear relationship between
equivalent lift/drag ratio and size/height ratio is borne out.
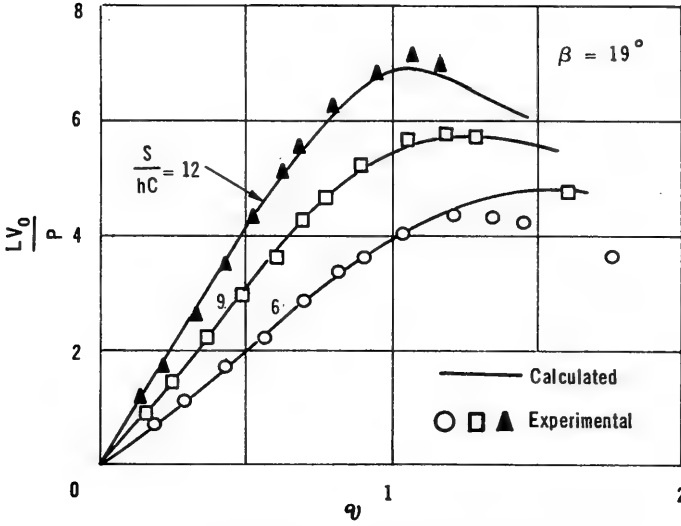
(a) Equivalent lift/drag versus speed
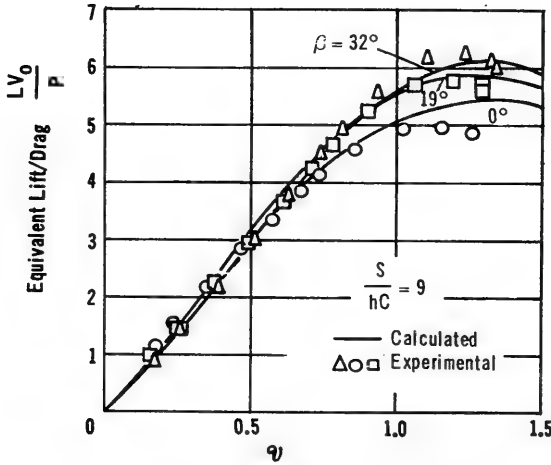
(b) Effect of β on equivalent lift/drag

Fig. 9. Comparison of "simplified engineering analysis" calculations with experiment
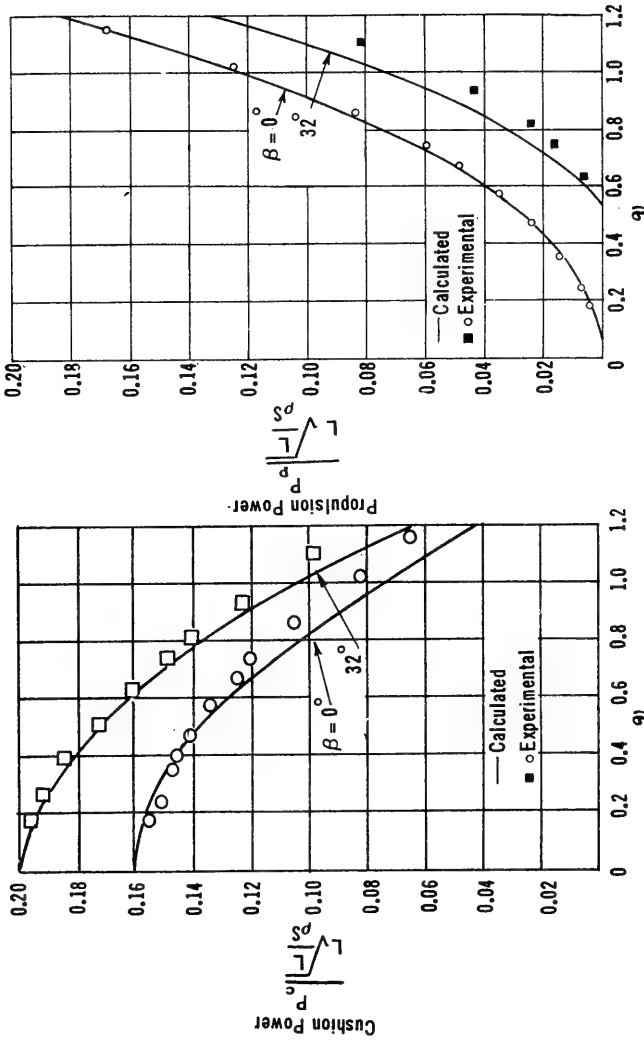
(c) Distribution of power between cushion and propulsion systems, $S/hC = 9$

Fig. 9. Comparison of "simplified engineering analysis" calculations with experiment (Cont'd)
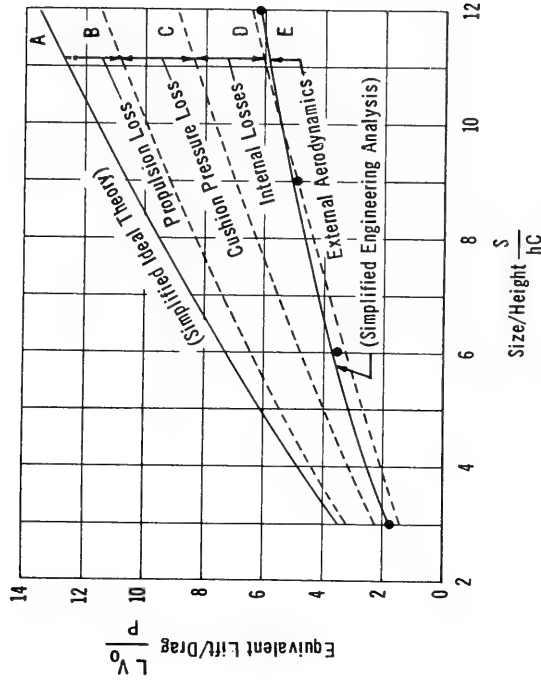
Curve	η_F	η_A	η_{Int}	η_d	C_{L_0}	C_{D_f}
A	1.0	1.0	1.0	1.0	0	0
B	0.8	1.0	1.0	1.0	0	0
C	0.8	0.733	1.0	1.0	0	0
D	0.8	0.733	0.57	0.70	0	0
E	0.8	0.733	0.57	0.70	0.42	0.074

Legend

$\beta = 0$ $\mathcal{V} = 1$

Calculated ⎱
(Equations [8-8] ⎰
through [8-11])

Experiment
(Reference 5)

Fig. 10. Influence of "real" effects neglected by the simplified ideal theory

Similar demonstrations have been or could be made, from data available in the references, that the hovering performance (figure of merit) is also, experimentally, almost directly proportional to the size/height ratio in the cases of all the air curtain types, the water curtain type, and the plenum type. The hovering performance is less significant, in terms of vehicle usefulness; but this lends additional support to the essential conclusions of the simplified ideal theory.

RESUME

The simplified ideal analyses furnish valuable insight into the fundamental ideas of the air cushion concepts. They furnish, further, the invaluable information that all of the air cushion concepts have in common the property of rapidly improving performance with increasing size/height ratio. Unfortunately, they leave unresolved — as does also experience to date — the essential question: Which concept is best for which application?

The following remarks are in large part merely the author's opinions:

Air Curtain — Most thoroughly studied, and correspondingly best understood of the air cushion concepts; most logical choice for early applications.

Plenum — Simplest and cheapest to build but ranks low in performance; very poor prospects for favorable high-speed performance unless combined with another concept, such as ram wing.

Ram Wing — Interesting only in combination with some other concept to provide low-speed flight capability; requires much additional research to evaluate practical problems and merits; appears to have great potential, if stability and control problems prove tractable.

Diffuser-Recirculation System — Intriguing idea, but unlikely to prove practical.

Water Curtain — Falls far short of theoretical expectations, but may eventually prove advantageous for moderate-speed over-water applications; not amphibious

Skegs — (Previously considered in combination with air curtain, but equally suitable for combination with any of the other concepts.) Likely to prove advantageous for moderate-speed over-water applications; not amphibious.

THE GEM'S PLACE IN TRANSPORTATION

In every one of the ground cushion concepts considered, elementary analysis indicates a direct dependence of the performance on the size/height ratio. Except for the air cushion types, the available experimental evidence is rather limited; but every bit of data which is available tends to confirm this direct dependence. This alone is enough to identify the natural form and habitat of ground effect machines: very large vehicles operating very close to the earth's surface. Since land areas are, in general, topographically unsuitable for the operation of large, high-speed vehicles at low heights, this means ocean-going GEM's. A more specific idea of the sizes and heights involved is afforded by Fig. 11. For a GEM with $LV_0/P = 0.9\ S/hC$ (appropriate to a highly developed air curtain vehicle) the equivalent lift/drag ratio is plotted in comparison with existing aircraft, and the size is given for each of several operating heights. The argument implied in Fig. 11 is, of course, somewhat superficial. There is the possibility that one of the other ground cushion concepts will
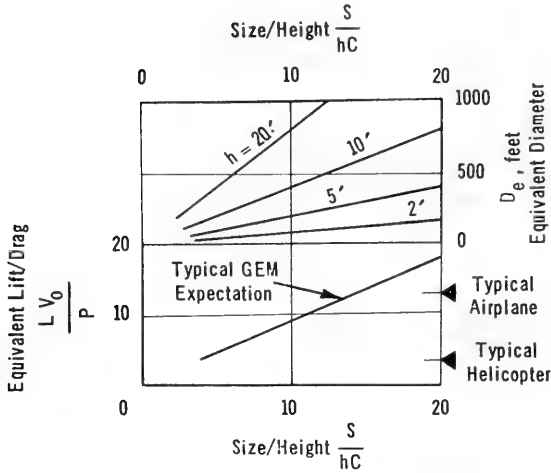
Fig. 11. The relationship between performance
and size for a GEM

provide better performance than the air cushion. There is the possibility that a GEM can compete successfully, even with somewhat inferior lift/drag ratio, because of its more flexible load-handling abilities and terminal facility requirements. And there is the possibility that the GEM's apparent compatibility with nuclear power will, in future years, loom larger than the lift/drag consideration. Nevertheless, it would be necessary to stretch any or all of these possibilities rather far to avoid the conclusion that ocean-going GEM's will be very large vehicles indeed. As such, their development represents a very imposing economic undertaking, and, while a great deal of current GEM research and study is directed toward the ocean-going machine, it may be assumed that serious development efforts will await clarification of the present confused state of knowledge.

In the meantime, GEM applications will be made in "fringe" areas where special circumstances or special requirements make moderate-size GEM's attractive. The two main categories of such fringe areas are:

1. The limited application possibilities over flat inland areas and protected waters, where extremely low operating heights afford good performance for moderate-size vehicles. These include passenger and cargo ferries, emergency craft, sport craft, and swamp buggies.

2. Limited military application possibilities where requirements for speed, amphibious capability, and load-carrying ability outweigh the conventional economic performance criteria.

Early applications are likely to center around the air curtain concepts. Only in this area is the state of the art sufficiently advanced to permit rational design. Where the future will lead is anybody's guess.

Whatever form the GEM of the future takes, this much is certain: If energetic and enthusiastic activity count for much, the GEM's future in the U.S. should be very bright indeed.

REFERENCES

Air Curtain

[1] Von Glahn, U.H., "Exploratory Study of Ground Proximity Effects on Thrust of Annular and Circular Nozzles," Washington, National Advisory Committee for Aeronautics TN 3982, Apr. 1957

[2] Chaplin, H.R., "Theory of the Annular Nozzle in Proximity to the Ground," David Taylor Model Basin Aero Report 923, July 1957

[3] Crewe, P.R., and Eggington, W.J., "The Hovercraft — A New Concept in Maritime Transport," London, The Royal Institution of Naval Architects, Nov. 1959

[4] Chaplin, H.R., "Ground Cushion Research at the David Taylor Model Basin — A Brief Summary of Progress to Date," Presented at Princeton Univ. Symposium on Ground Effect Phenomena, Oct. 21-23, 1959

[5] Johnson, A.E., "Wind Tunnel Investigation of DTMB GEM Model 448," David Taylor Model Basin (In preparation)

[6] Cathers, D., Hirsch, A.A., and Walker, W., "Air Pressure Levitation," Paper presented at the Feb. 1960 meeting of the Chesapeake Section of the Society of Naval Architects and Marine Engineers, Washington, 1960

[7] Hirsch, A.A., "The Hovering Performance of a Two-Dimensional Ground Effect Machine Over Water," Presented at Princeton Univ. Symposium on Ground Effect Phenomena, Oct. 21-23, 1959

Water Curtain

[8] DeVault, R.T., "Introduction to the Hughes Hydrostreak Concept," Culver City, Calif., Hughes Aircraft Co. Report X-424, Nov. 1959

Plenum

[9] Dobson, F.A., "The Airlifter," Dobson Aircraft Corp., Whittier Calif., Dec. 1957

[10] Wright, E., "The Effect of Configuration on the Lift of a Two-Dimensional Open Plenum Ground Effect Machine," Princeton Univ. Report 516, May 1960

Ram Wing

[11] Kaario, T.J., "The Principles of Ground Effect Vehicles," Presented at Princeton Univ. Symposium on Ground Effect Phenomena, Oct. 21-23, 1959

Diffuser-Recirculation

[12] Gates, M.F., and Sargent, E.R., "Development of a Unique GEM Concept With Potential for Achieving Efficient Forward Flight," Presented at Princeton Univ. Symposium on Ground Effect Phenomena, Oct. 21-23, 1959

BIBLIOGRAPHY

Liberatore, E.K., "GEM Activities and Bibliography," Buffalo, Bell Aerosystems Co., Mar. 1960

ADDENDUM

ILLUSTRATIVE COMPARISON OF THE GROUND CUSHION CONCEPTS

Direct comparisons between the various ground cushion concepts are very risky at the present state of the art. The simplified theory presented in the body of this paper neglects many factors, which may affect one concept more than another, and the degree of experimental understanding is by no means the same for all of the concepts. For this reason it was originally decided to avoid direct comparisons.

However, in retrospect it became apparent that direct comparisons would go far toward clarifying many of the points made. It was decided to present the comparisons shown in Fig. 12 after all. The reader is implored to accept Fig. 12 as merely illustrative of some of the distinctive characteristics of the different concepts, and to use it cautiously or not at all as a criterion of their relative practical usefulness.
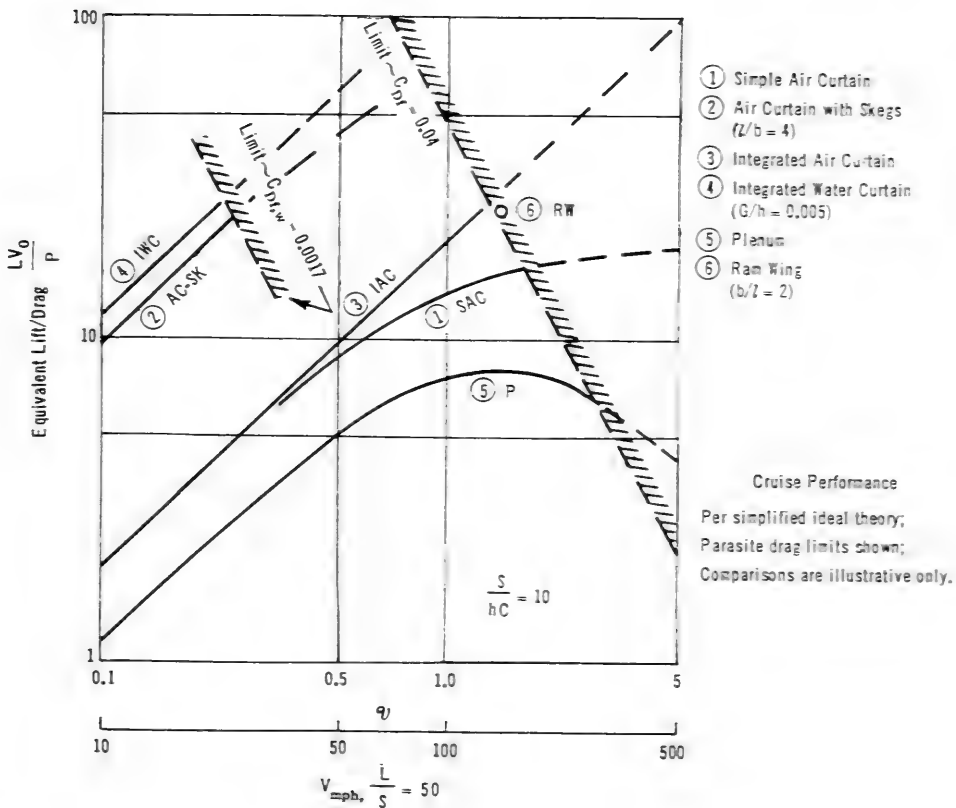
The cruise performance curves for the six concepts shown are plotted directly from the simplified ideal theory. Special assumptions, such as length/beam ratio of 4 for the air curtain with skegs, and nozzle-width/operating-height ratio of 0.005 for the water curtain, are noted in the legend. The seventh concept, the diffuser-recirculation system, is omitted, since the dearth of practical experience makes it impractical to plot a curve of even illustrative value.

Also shown in Fig. 12 are performance limits imposed by parasite drag, under assumed parasite drag coefficients:

$$C_{Df} = \frac{D_f}{\frac{1}{2} \rho V_0^2 S}$$

$$C_{Df, w} = \frac{D_f}{\frac{1}{2} \rho_w V_0^2 S} .$$

The "simplified ideal theory" curves account for cushion power and momentum drag but ignore parasite drag. The "limit" curves account for parasite drag but ignore all other power requirements, as follows:

$$P_{limit} = D_f V_0$$

$$L \equiv \frac{\rho S V_0^2}{\mathsf{U}^2}$$

$$\left(\frac{LV_0}{P}\right)_{limit} = \frac{2}{C_{Df}\mathsf{U}^2} = \frac{2}{C_{Df, w}\mathsf{U}^2} \cdot \frac{\rho}{\rho_w} .$$

The concepts which do not involve contact with the water (curves 1, 3, 5, 6) are assumed, for illustrative comparison purposes, to have parasite drag coefficients of $C_{Df} = 0.04$; the concepts which do involve water contact are assumed to have $C_{Df, w} = 0.0017$. (A calculation which included cushion power, momentum drag, and parasite drag would give a curve which followed closely below the "simplified ideal" curve at low speed, then peaked over and followed closely below the "limit" curve at high speed.)

The relative performance picture afforded by Fig. 12 should be interpreted as follows:

1. Within the no-water-contact family, the relationship between curves 1, 3, and 5 is probably in reasonable qualitative harmony with the facts. If lower S/hC or lower C_{Df} were assumed, the integrated air curtain would appear slightly better, compared to the simple air curtain; the plenum, slightly poorer. Curve 6, for the ram wing, is only a single point, since under the approximations used in theory, equilibrium flight occurs at only one speed coefficient, $\mathsf{U} = \sqrt{2}$. If lower S/hC or lower C_{Df} were assumed, the ram wing could be made to appear superior to the other members of the no-water-contact family, by assigning it a higher aspect ratio b/l.

2. Within the water-contact family, the positions of curves 2 and 4 relative to each other are not meaningful, since they can be substantially changed or reversed by assigning a different nozzle-width ratio G/h to the water curtain and/or a different length/beam ratio l/b to the air curtain with skegs.

3. Between the two families, absolute performance comparisons are meaningless for the same reasons. However, the significant and valid point that the water-contact concepts are superior at low speeds, while the no-water-contact concepts are superior at high speeds, is very well illustrated. The exact degree of superiority, and speed range to which it applies, depends very heavily on the respective parasite drag coefficients. The values of C_{Df} and $C_{Df, w}$ used in Fig. 12 were selected arbitrarily, for illustrative purposes only.

DISCUSSION

R. L. Weigel (University of California)

I do not want this to be construed as a criticism of Mr. Chaplin's paper: the subject he was given was extremely broad to cover. However, there is one important aspect that he did not touch upon and that is the wave resistance of this type of vehicle moving over the water surface. I have chosen this one aspect because I think it of general interest to naval architects and furthermore, as this meeting is dedicated to Sir Thomas Havelock, I think it is interesting that the technique used in predicting the wave resistance is due to Sir Thomas Havelock. Rather than considering a true ship, he considered a pressure disturbance moving over the surface of the water, and this is precisely the problem of the ground effect machine. Sir Thomas Havelock's main advance is that he considered a pressure area rather than a pressure point, and he formulated his problem in such a manner that numerical results could be calculated from the equations rather than just looking at the integrals and so forth. Furthermore, he even went so far as to calculate the resistance in almost the exact form that is needed to obtain the information for designing a ground effect machine. Sir Thomas Havelock considered a pressure disturbance something like that shown in Fig. D1 where pressure is measured vertically and the radius of the disturbance is measured along the abscissa, with axial symmetry assumed. Now, he chose one particular shape; however, tests that we have made have indicated that we can have quite irregular shapes such as a double hump shape and the resistance is practically the same as one obtains from this shape that Havelock assumed.[*]

Havelock's[†] numerical results are shown in Fig. D2. Very often in naval architecture we are dealing with the deep-water aspects and a Froude number based upon the length of the ship. If we deal in inland waterways we talk about a Froude number based upon the water depth. It turns out for ground effect machines we must consider both of these simultaneously. So we have a parameter which is the diameter of the pressure disturbance divided by the water depth. This is a dimensionless resistance which is a specific weight of water (ρg) times the resistance, and this is the wave resistance (R) divided by 2π times the diameter of the ground effect machine times the maximum pressure squared (that exists

* R.L. Wiegel, C.M. Snyder, and J.B. Williams, "Water Gravity Waves Generated by a Moving Low Pressure Area," Trans. Amer. Geophys. Union 39 (No. 2):224-236 (Apr. 1958).
† T.H. Havelock, "The Effect of Shallow Water on Wave Resistance," Proc. Roy. Soc. (London) A100 (No. A705):409-505 (Feb. 1, 1922).
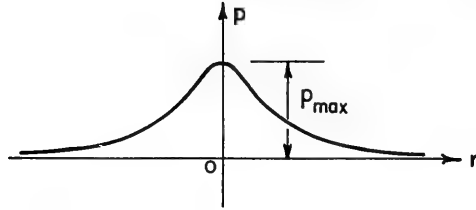
D = Effective diameter of pressure area, feet.

d = Water depth, feet.

ρ = Mass density of water, slugs/ft.^{2}

g = Gravity, ft./sec.^{3}

R = Wave resistance, pounds.

P_{max} = Maximum pressure of pressure area, lbs/ft.^{2}

Fig. D1. A pressure disturbance on the water surface
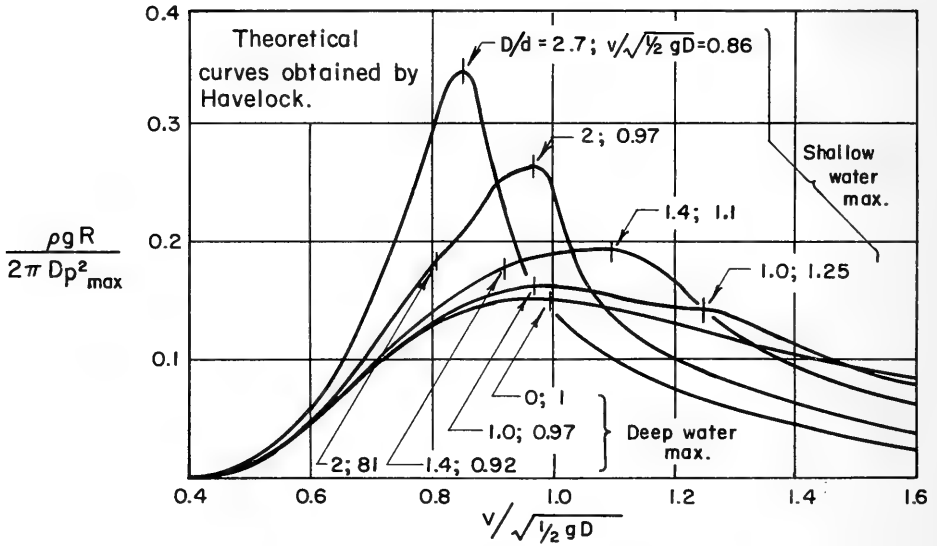
Fig. D2. Theoretical curves obtained by Havelock

in the base cavity). Then, for various values of the ratio of the diameter of the disturbance to the water depth we can get a series of curves as shown (Fig. D2); where the diameter is great compared with the water depth we have a shallow water resistance peak, where the diameter is small compared with the water depth we have the typical deep-water peak, and where we have intermediate values we have double peaks, the deep-water and the shallow-water peak, or shoulders. I think the thing of primary interest is just how great is the wave resistance due to a high-speed vessel of this sort. Using the results of Havelock I made several calculations just briefly to give you an idea. If we choose a craft that is large, that's the type the Navy is considering, the type that Mr. Chaplin mentioned, with the diameter of 300 feet, flying over the ocean at some relatively high speed (I have had to choose a

speed of only 65 knots, which is low, but if I chose higher it would have been off these curves) the resistance will be lower than what I show here. If it is moving over water deep enough so that $D/d \approx 0$ (where d is the water depth), then $V/\sqrt{gD/2} = 1.6$, and $\rho g R/2\pi D p^2_{max}$ = 0.085. In very deep water it turns out that the horsepower that is utilized in wave resistance is only 12-1/2 hp, for a base pressure of 5 pounds per square foot, which is practically negligible, as we are talking about a craft with a 40,000- to 50,000-hp motor. It is almost unbelievable. The horsepower loss is dependent upon the square of the base pressure, so if you get up to the more modern concepts, which have a higher base pressure loading, and you go up to say 30 pounds per square foot the horsepower goes up to 440, and even this is only of the order of 1 percent. It is becoming appreciable but is still relatively small. In operating the GEM, it will move from deep water into shallow water as it is coming ashore and here is where we have to be careful. We can hit some of these "hump" speeds and for one combination which I picked at semirandom (I chose a water depth of 100 feet and a forward speed of 55 knots) the wave resistance can rise to over 1500 to 1600 hp. In general when we are operating over deep water at high speeds, the wave resistance will be negligible. The only time it will tend to become important is when one is bringing it in over relatively shallow water. The stopping of one of these vehicles is a major problem. Consequently this high resistance that one gets as one comes into shallow water probably will turn out to be very useful because I think that maybe for slowing a GEM we can make use of this shallow wave resistance.

In practice the peak pressure will be higher than the average base pressure on a GEM, and the power necessary to overcome wave resistance will be higher than the values mentioned, perhaps by a factor of almost two.

L. W. Rosenthal (Folland Aircraft Limited)

I would like to thank Mr. Chaplin for the very pleasant paper he presented, but I am going to be so ungracious as to suggest that it had the wrong title! I think perhaps it might well have been called "A Simplified Method of Comparing the Performance of Ground Effect Machines." During the whole of the Symposium, I have hoped that the hydrodynamicists would have discussed the position of the ground effect machine in the light of the conclusions that Mr. Chaplin had arrived at. When Mr. Oakley spoke, he did in fact suggest that attention had been given to the position of the ground effect machine, with the limitations that we know, in the marine transport pattern. Unfortunately, he did not develop this point. Mr. Van Manen, discussing the Crewe Eggington hypothetical project, quietly but firmly took it to pieces on the structure weight grounds, but he gave no constructive comment on what he would suggest instead. Mr. Newton followed this up by saying that the structural problem concerned with a large ground effect machine in a seaway needed investigation, but here again he gave no lead at all. Mr. Chaplin broadly touches on the place of the ground effect machine but his comments are based on a general parameter and not necessarily on the specialized uses to which we might be able to put the vehicle at the moment.

What I would like to suggest, if this is not ungracious again, is that possibly the hydrodynamicist and the naval architect are dragging their feet on this particular problem, or is it that no conclusions have yet been reached and we are looking for something or some information which does not yet exist.

Another point to which Mr. Chaplin made no reference in his assessment of the small machines, and this could hardly have been considered a secondary one, is the means of obtaining pitch and roll stability and the penalties associated therewith. I would like to

ask if Mr. Chaplin would like to discuss these points in the light of the title of his paper "Research and Development of Ground Effect Machines in the United States."

J. L. Wosser (ONR, Washington)

After listening to all the papers on hydrofoils and associated subjects that have been delivered to date at this meeting, let me state that I am very impressed with the level of the work that has been done. There has been just this one paper presented in the area of ground effect machines (GEMs). Most of this was Mr. Chaplin's original work. It included a brief summary of some of the other things that have been done, but very brief. I would like to point out that as far as we in the United States are concerned, we consider the GEM state of the art stands about where that of the airplane did in 1904, or where you gentlemen with the hydrofoil boat were in 1930. We are just getting started in this field, research wise. However, there is a considerable research effort underway.

Within the Office of Naval Research we are supporting some 16 research tasks, all coordinated into an overall GEM research program. Our objectives in this area are not the far-out aims that Mr. Chaplin mentioned at the conclusion of his paper: the 600-foot trans-oceanic GEM. In order to get this type of research effort underway, we have more immediate aims. We are looking for the areas where the GEM's unique capabilities to travel over all types of surfaces (water, land, ice, snow, and mud) with equal facility can be utilized for military purposes. Now, this military approach is not the direction of the effort that is going on in England, and I am sure that Mr. Shaw will tell you about their commercial interests in a moment.

In addition to the work of the Office of Naval Research, extensive programs are being sponsored by Bureau of Naval Weapons, Bureau of Ships, and the Army Transportation Corps — all looking at their own areas of interest where the GEM has unique capabilities. The Army is particularly interested in overland vehicles that can travel over ice fields, mud flats, river deltas, etc., to open up these areas for future exploration or military operations. To give you a complete outline of the work that is being done would take too long. A thumbnail sketch would show that we have programs underway that will utilize more sophisticated approaches to some of the simplified theories you have heard presented today: viscous analyses of flow inside and external to the machines, propulsion and structural loads analyses, stability and control criteria, and ditching and flotation tests at the Seakeeping Basin here at Wageningen.

In conclusion, let me tell you a few of the things that have been achieved in the GEM area to date. During his talk Mr. Chaplin showed you some of the machines now in existence. Remember that we consider this thing to be in the period 1904 aircraft wise, or just starting out hydrofoil wise. In England, they have flown a GEM at 60 mph over the water on the Solent and successfully operated in eight-foot waves. In Switzerland, we watched a demonstration of a 30×30 foot-machine move over the water at 51 knots. The Curtiss-Wright Aircar has been officially clocked at 65 mph. At the present time, Mr. Carl Weiland, now working for the Reynold's Metals Company, is building a 90-mph machine at Louisville, Kentucky. This is supposed to be flying by Christmas (1960).

Yesterday I received a letter which I have already shown to Mr. Chaplin, so this will not come as any surprise. About two years ago at an Institute of the Aeronautical Sciences meeting in New York I met a Dr. Bertelsen. We discussed theoretical aerodynamics and GEMs for an hour and a half before I found out that he was an M.D., an obstetrician from

Illinois. He delivers babies and dabbles in aerodynamics on the side. So, with that as a background, these are abstracts from the letter I received from him yesterday: "Since I saw you in January 1960 at the IAS meeting, considerable work on Ground Effect Machines has obviously been done all over the world. We too have been busy. We now have what we consider to be the world's best Ground Effect Machine from the standpoint of control, hill climbing, stability and all around utility. We have a 200-hp, four-passenger flying machine in the chassis stage and have gotten well along in testing it. We get 12-inch altitude at 1600 lbs. gross weight, climb a 10-degree slope and go 50 mph over land or water. I feel that with all the theory and experimentation, we lead the world and challenge all comers in this category of small personal Ground Effect Vehicles."

R. A. Shaw (Ministry of Aviation, London)

It seems to me that you are mostly ship men here and therefore at a disadvantage in assessing the possibilities of what we call hovercraft in England and what you call ground effect machines in America. (What you call them on the continent, I have not yet discovered.) You are at a disadvantage because you look at them and you think, Reynolds' number, Froude's number — must explain it all this way.. It isn't really very helpful in working out an understanding of hovercraft or ground effect machines because, perhaps fortunately for everyone, the Froude number is not very important as far as ground effect machines are concerned, at least you soon get out of the regime in which it is important. Perhaps the particular case in which it will continue to be important is when your machine enters shallow water and does the transition from water to land. Apart from this, as ship people I feel that you are at a disadvantage because the problems of ground effect machines are largely the problems which have been studied by the aircraft industry in the past. Hovercraft certainly stand astride the two fields but a proper appreciation of ground effect machines and their future, I think, is easier for the aircraft people who rather rub their hands and say "jolly good, this is easy stuff," by comparison with the ship people who say "what a troublesome problem." It isn't really easy stuff because there are a lot of very curious things in it. What I wanted to bring home to you was that you couldn't assess it simply by ship standards. There are many subtleties in ground effect machines, and to give you an example, in a machine like the SRN-1, the British hovercraft, there was more power lost between the fan and the ducts than was used in the lifting and propulsion of the machine. This is just part of the problem of design, how to use your power effectively and efficiently in a novel way. People haven't got habits of thinking about hovercraft so they don't naturally choose a good solution. We have got to go through that process of finding good solutions and that's why people like Dr. Bertleson, who are following the example of the Wright Brothers and starting at the beginning, are just as likely at this stage to hit on a good solution as well-informed gentlemen at national establishments. In fact, we are in the pioneering stage and have to assess our progress in terms of that stage; it is 1904 as Col. Wosser said. But despite the fact that it is only 1904, or perhaps to be precise 1905, we are in England at the moment, building a 25-ton hovercraft capable of cruising at about 70 knots and carrying about 50 or 60 people several hundred miles. This is being achieved within a few years of the concept taking hold and within a year or 18 months of our first demonstration. By contrast, in the hydrofoil business, hydrofoils have been talked about for a generation and although they are now at the 80-ton stage, it has taken a generation to get there. With a background of aircraft experience it does look possible to get into the ground effect business in a matter of five years. I want to redress any influence which Mr. Chaplin's final statement might have on this audience in thinking that unless you got into the 600-foot or 10,000-ton class, ground effect machines have no place, by reinforcing what Col. Wosser said and that is you must not consider them in relation to conventional forms of transport on conventional routes.

You have got to think of the places you can't get to any other way, the marshes, the bogs, the ice flows, the out of the way places where you can't land an aeroplane. These are the places where I believe the hovercraft will really take root and where we shall gain the experience we need to allow us ultimately to build big ocean craft.

L. Landweber (Iowa Institute of Hydraulic Research)

The following comments were written before the contents of the present paper were known. That can be justified, however, by noting that these comments will serve as a bulwark to the title of Mr. Chaplin's presentation which they supplement by describing the work in this field that is being done at the Iowa Institute of Hydraulic Research. These comments were written by Lawrence R. Mack and Joachim Malsy:

Increasing interest in the possibilities of ground effect machines has led many organizations in several countries to undertake basic studies of ground effect phenomena or studies of the means of practical utilization of these phenomena or both. During the past two years the Iowa Institute of Hydraulic Research, with the financial support of the Office of Naval Research, Contract Nonr 1509(03), has conducted both analytical and experimental investigations of the behavior of an annular-jet nozzle in proximity to solid and liquid surfaces. The results of the first year's work were presented at the Princeton Symposium on Ground Effect Phenomena in October 1959.[*] Since then a thesis describing an experimental study of an annular jet moving over water has been completed;[†] the results of this study, together with certain results for a stationary jet over land obtained preparatory to the over water experiments, are contained in a forthcoming report to the Office of Naval Research.[‡] It is the intent of this discussion to summarize briefly these results.

A rigidly supported 7-inch-diameter annular nozzle discharging air vertically at different rates through a 1/8-inch gap was towed at different altitudes and speeds (including zero velocity) over initially quiescent water. Chosen combinations of these three variables led to 18 runs, for each of which the configuration of the water surface in the vicinity of the nozzle and the pressure distribution on the base of the nozzle were determined and plotted in the form of contour drawings.

The measurements of water-surface configuration were obtained by means of a capacitance wire and a point gage and were supplemented by stereo photographs as an aid in preparing contour maps. All stationary cases show a deep annular depression, caused by the impinging jet sheet, about 1.2 nozzle radii from the center line of the jet. The water surface under the nozzle base was considerably higher than what would, under the assumption of hydrostatic pressure distribution in the water, correspond to the pressure within the base cavity, a ridge at about 0.7 nozzle radius actually projecting above the still water surface. Forward speeds produced a considerable change in surface configuration from that of the static case. A forward ridge, or bow wave, was clearly discernible in all runs. With higher jet momenta and especially with higher speed, this bow wave seemed to split into two separate ridges, each situated in front of the nozzle about 45 degrees from the direction of

[*] Lawrence R. Mack and Ben-Chie Yen, "Theoretical and Experimental Research on Annular Jets over Land and Water," Proc. Symposium on Ground Effect Phenomena, Princeton, Oct. 1959, pp. 263-284. Also available as Reprint No. 164, State University of Iowa Reprints in Engineering.

[†] Joachim K. Malsy, "Experimental Investigation of an Annular Jet Traveling over Water," M.S. Thesis, State University of Iowa, Aug. 1960.

[‡] Lawrence R. Mack and Joachim Malsy, "Experimental Studies of an Annular Jet," Iowa Institute of Hydraulic Research Report to the Office of Naval Research, Sept. 1960.

forward motion. At low velocities a half-moon-shaped depression, concave rearward, was beneath the front part of the base plate, the deepest parts being situated on either side of the nozzle center. This deep, very clearly visible depression moved to the rear with increasing speed and decreasing jet momentum. A high wave directly to the rear, which at times almost touched the nozzle, behaved similarly. In general, it can be said that all observed surface phenomena moved to the rear and became less pronounced in magnitude with increasing forward speed and decreasing jet momentum.

Base-plate pressures were measured at 14 piezometer holes, the number of locations being tripled for some runs by making two 45-degree rotations of the base plate, and isopiestic lines were drawn. In the stationary cases, especially for the higher altitude, a dip in pressure was noticed at about 0.7 nozzle radius, the same location as an elevation in the water surface. For all cases of forward speed the pressures were larger in the rear than in front, pressures at the center and extreme rear tending to be the highest. A roughly circular pressure valley at about 0.7 nozzle radius was clearly discernible, culminating in a saddle point between the two peak pressures. The high pressures to the rear and low pressures to the front combined to give nose-down pitching moments *acting on the base plate* for all cases of forward motion.

The total base-plate lift, and hence the lift-augmentation factor, for each run was obtained by integration of the pressure distribution. As expected, the augmentation factor was found to increase with decreasing altitude for all conditions. For the stationary runs the augmentation increased with decreasing jet momentum for a given altitude, in qualitative agreement with the theoretical predictions of Mack and Yen (first footnote) even though the surface-configuration data did not support certain of their assumptions. The numerical magnitudes of augmentation, however, were less than their idealized predictions. For constant altitude and jet momentum, forward speed, within the experimental range, improved the augmentation initially, then caused a decrease at still higher speed. This feature, particularly the increase of augmentation with increasing speed at low speeds, was more pronounced for the lower altitude tested. It thus appears that there is an optimum forward speed for each combination of altitude and jet momentum.

The same basic 7-inch annular nozzle, but with interchangeable mouthpieces, was also tested statically over a ground board. Discharge angles of 0, 15, and 30 degrees inward with a 1/8-inch annulus width were used, as were 0- and 15-degree angles with gaps of 5/16 and 1/2 inch. As expected, the 30-degree discharge angle gave the highest augmentation; no significant distinction in augmentation was noted, however, between the 0- and 15-degree angles. It was found that, within the gap range tested, the augmentation factor and the radial uniformity of pressure both increased with increasing gap width. This behavior of the former is in qualitative agreement with the theoretical prediction of Mack and Yen (first footnote, Fig. 1) within its range of validity (altitude less than the nozzle radius).

The results summarized herein of tests conducted at the Iowa Institute of Hydraulic Research on annular jets moving over water and stationary over land are described more fully in the report to the Office of Naval Research already referred to.

E. C. Tupper (Admiralty Experiment Works)

Mr. Chaplin did a very good job in condensing this research work into such a relatively short paper and I hate to suggest more work for him, but I would like to make two points.

First of all, I should like to emphasize how important it is that we should not progress too far with detailed experimental and theoretical work into the optimum form for resistance and propulsion alone. It may well be that many of the configurations so studied will prove quite unacceptable from the point of view of stability or seaworthiness. In my opinion, a broad, less detailed, study is first required into all aspects of design to determine the ranges of the principal dimensions which are likely to prove suitable for a balanced design.

Second, I would like to support Mr. Rosenthal's plea for some comments upon stability for the various configurations which have been discussed. This obviously is of prime importance in operation over waves as well as over calm water, and I would like the author's comments on whether passive stability may be adequate in some cases, or whether active stabilizing will always be necessary.

Harvey R. Chaplin

I will not reply at great length to the various comments, but will touch just a couple of the specific questions. About the optimum plan form for waves, certainly we don't have the answers on this yet but there is a program at the Netherlands Ship Model Basin underway now which will give answers having some bearing on this question and other programs within the United States too which are touching on this question. The plan form on which most of the recent air curtain research has been concentrated has been the plan form of the model which the photograph has shown, which is not too far distant from the ship forms and may not be totally unsuitable from the standpoint of possible wave impact. The stability question of course, is a very important question and it would be inexcusable not to cover the stability if we knew what to say about it. Again on the air curtain, a good bit is known about the stability; we know how to stabilize the machine, how to give it some natural stability, and we are close to knowing an answer to the question of whether it will be possible to have inherent stability or whether it will be necessary to have artificial stability. I personally feel that for the air cushion at speeds up to 100 knots it will be possible to have inherent stability without the black box. Beyond those two specific points, if I may abstract other comments en mass, they would add up to the fact that I have left an awful lot out and this is certainly true. I am afraid I cannot undertake to fill in very many of the gaps in the limited time that we have. Fortunately, some of the gaps were filled in by the commenters themselves and I thank them for that. Certainly the one thing that I shouldn't have left out is what was pointed out by Professor Wiegel, and this is the wave drag problem which bears on the person to whom the Symposium is dedicated. I certainly owe him gratitude for pointing out this inexcusable oversight. As to the title of the paper, I have to take my excuse from the fact that, as you know, in the scheme of things, the title and abstract of the paper were submitted some months in advance of the paper itself and as is often the case, the paper at the time it was submitted was quite a bit different from the way it was envisioned at the time the title was submitted.

*   *   *

HYDRODYNAMIC ASPECTS OF A DEEP-DIVING OCEANOGRAPHIC SUBMARINE

P. Mandel
Massachusetts Institute of Technology

INTRODUCTION

There is little question that the major problems that arise in the design of very deep diving submarines are in the field of structures and not in the field of hydrodynamics. However, several hydrodynamic problems exist that are peculiar to the very deep diving oceanographic submarines that are of little or no importance in the design of the most advanced military submarines. These problems arise in connection with: (a) the ballast systems needed for operation at great depths, (b) the oscillations that may be excited by vortex shedding during vertical ascent or descent, (c) the effects on depth and trim angle control of the compressibility of the submarine hull and of sea water, (d) the precise control in both the horizontal and vertical planes needed to perform the mission of the boat, and (e) directional stability when under tow on the surface. This paper will concern itself largely with these five questions plus some introductory discussion of how the configuration of a deep-diving submarine compares to military submarines and bodies of revolution of elementary shape.

This paper will draw on experience gained during the design of the oceanographic submarine Aluminaut which is described in Ref. 1. The design of this unique vehicle was based on general concepts initiated by Dr. Edward Wenk, formerly of Southwest Research Institute, San Antonio, Texas. The design was developed to its current state under a project initiated by Mr. J. Louis Reynolds, Vice President, Reynolds Metals Company. Negotiations for construction of the boat are currently nearing completion.

The Aluminaut differs in basic concept from the previous generation of deep-diving vehicles marked by the bathyscaphes FRNS and Trieste which were developed by Auguste Piccard. It will be recalled that it was the Trieste which made the record-breaking dive on January 22, 1960, to a depth of 37,800 feet. These vehicles depend on a buoyant liquid, gasoline, to support about 90 percent of their total weight while their small pressure hulls support only about 5 percent of their total weight. The remainder of their weight is supported by the buoyancy of structure. In contrast the buoyancy of the pressure hull of the Aluminaut supports over 80 percent of its total weight. The marked effect of this change of concept can be seen by study of Table 1. With a total submerged displacement of slightly more than half of the Trieste, the Aluminaut has about 9-1/2 times the useful volume and possesses mobility and endurance that are vastly superior to the Trieste. It is these deficiencies of the Trieste plus the difficulties in handling large quantities of volatile gasoline that prevent full appreciation in oceanographic research work of her superlative depth capability. Even the retrogress of the Aluminaut from the remarkable depth capability of the Trieste is more apparent than real since only about 40 percent of the world's ocean area is greater than 15,000 feet deep. Thus, the Aluminaut has great potentiality as an oceanographic research vehicle.

Table 1
Comparison of Characteristics of the Trieste and the Aluminaut

Category	Items	Trieste	Aluminaut
Dimensions	Length overall, ft	49.5	50.7
	Max. Beam, ft	11.5	10
	Draft, before dive, ft	17.5	11.5
	Inside diameter of pressure hull, ft	6.56	7.0
	Inside length of pressure hull, ft	6.56	39
	Thickness of pressure hull material, inches	3.54	6
Volumes (cu ft)	Total submerged volume at depth	3,940	2,280
	Internal volume of pressure hull	148	1,405
	Buoyant volume of pressure hull	191	1,860
Weights (lb)	Pressure hull structural weight	21,520	89,030
	Other structural weight	33,600	7,500
	Ballast, permanent and jettisonable	24,620	21,200
	Propulsion, batteries, pumps, controls	?	12,400
	Flotation fluid	157,000	12,650
	Scientific payload	~500	~4,000
	Total submerged displacement	252,000	149,000
Materials	Pressure hull material	Steel	Aluminum
	Flotation fluid	Gasoline	Silicone
Performance Characteristics	Operating depth, ft	37,800	15,000
	Test	?	17,000
	Collapse depth, ft	?	21,000
	Max. horizontal speed, knots	1/4	4.7
	Horizontal endurance, miles	4	96
	Endurance, hours	8*	36 normal
			72 emergency
	Vertical speed, fps	3	3 normal
			11 max
	Power available for instruments, kwh	2-1/2	64
	Crew Number	2	3

*1/2-4 hours at depth depending on time for vertical traverse.

THE ALUMINAUT CONFIGURATION

The configuration of a deep-diving submarine is largely determined on the basis of structural and arrangement requirements. For the Aluminaut a cylindrical pressure hull with hemispherical ends was selected as a good compromise between an optimum structural configuration and a configuration most suitable for housing people and equipment. The forward pressure hull hemisphere and the cylindrical portion of the hull form the basic external hull of the submarine since these are not entirely unsuitable from a hydrodynamic point of view. For hydrodynamic reasons, however, the aft pressure hemisphere is enclosed within a non-pressureproof, almost conical, stern capsule that provides some hydrodynamic fairing and also serves to house the electric propulsion motor and control mechanism. This obviates the need for large mechanical penetrations of the pressure hull. This capsule is filled with a buoyant silicon fluid (specific gravity—0.76) that provides a suitable environment for the motor in addition to providing a modest amount of buoyancy (~13 percent). The stern

capsule is pressure equalized to the open sea at all times so that it may be constructed of relatively light structure. Figures 1 and 2 show the general configuration of the submarine.

The configuration, thus determined, has somewhat different proportions than the usual military submarine. The length/diameter, L/D, ratio is lower and the prismatic coefficient, C_p, (ratio of volume of submarine to volume of circumscribing cylinder) is higher than the corresponding proportions of military submarines. These properties of the Aluminaut are conducive to minimizing wetted surface and hence frictional drag at the expense of an increase in separation and form drag. The differences in wetted surface between the Aluminaut and military submarines and the wetted surfaces of elementary body of revolution shapes similar to submarines are shown in Fig. 3. The ordinate of this figure is the wetted surface of solids of unit volume. (For example, a cubic prism of unit volume has a wetted surface of 6.) To compute the wetted surface of geometrically similar volumes, it is only necessary to multiply the value of the ordinates in Fig. 3 by the volume raised to the 2/3 power. It is seen that not only does the Aluminaut have substantially less wetted surface than military submarines because of her low L/D and high C_p, but with those proportions her hemispherical nose and essentially conical stern offer almost as low wetted surface per unit volume as the less hydrodynamically satisfactory combination of conical nose and stern. The comparison is as follows at the Aluminaut L/D and C_p:

Configuration	Wetted Surface for Unit Volume
Hemi-nose; conical tail	6.90
Conical nose; conical tail	6.89

The additional useful information shown in Fig. 3, computed on the basis of information given in Appendix A and taken from Fig. 7 of Ref. 2, is in the nature of a postscript to the main purpose of this paper. Primarily, the figure shows the large penalty in wetted surface associated with high length/diameter ratios, which is well known, and the variation of wetted surface with prismatic coefficient and end shape, which is not so well known. Within the range of L/D's suitable for streamlined bodies ($L/D > 3$) and at low values of C_p, the bodies with conically shaped nose as well as tail, have the least wetted surface, the bodies with hemispherical noses and conical tails have the next greatest, while bodies with sub-marinelike noses and tails have the most wetted surface. This latter fact is consistent with the frequent observation that achieving reasonable form drag usually involves increased wetted surface and frictional drag. At high prismatic coefficients the effect of end shape on wetted surface is not nearly as decisive as at low values of C_p. It might also be observed that to achieve the complete continuity at the intersections of the parallel middle body and the end shapes that is needed to minimize form drag, and that is so obviously missing with pure conical or even hemispherical ends, much higher prismatic coefficients are associated with a fixed percentage of parallel middle body L_x' for the submarinelike bodies than for the simpler shapes. All in all it is evident from Fig. 3 that the L/D ratio is the most important parameter influencing wetted surface and that prismatic coefficients in the practical range from 0.50 to 0.90 are also conducive to minimizing wetted surface for any fixed L/D ratio. For a more thorough discussion of this particular question, the reader is referred to Section 3 of Ref. 2.

Figures 1 and 2 indicate that the Aluminaut is encumbered with many appendages. Most of these are needed to house equipment or ballasting functions (described subsequently) that are advantageously mounted external to the main pressure hull. As shown in Fig. 2, and also subsequently in Fig. 6, some of these appendages are not suitably faired, but this problem is fully appreciated by all concerned and it has been decided that the building plans will incorporate suitable fairings. Even faired, it is estimated that the appendages will more than double the bare hull-drag of the submarine in horizontal motion. Drag estimates will be shown in Fig. 13.
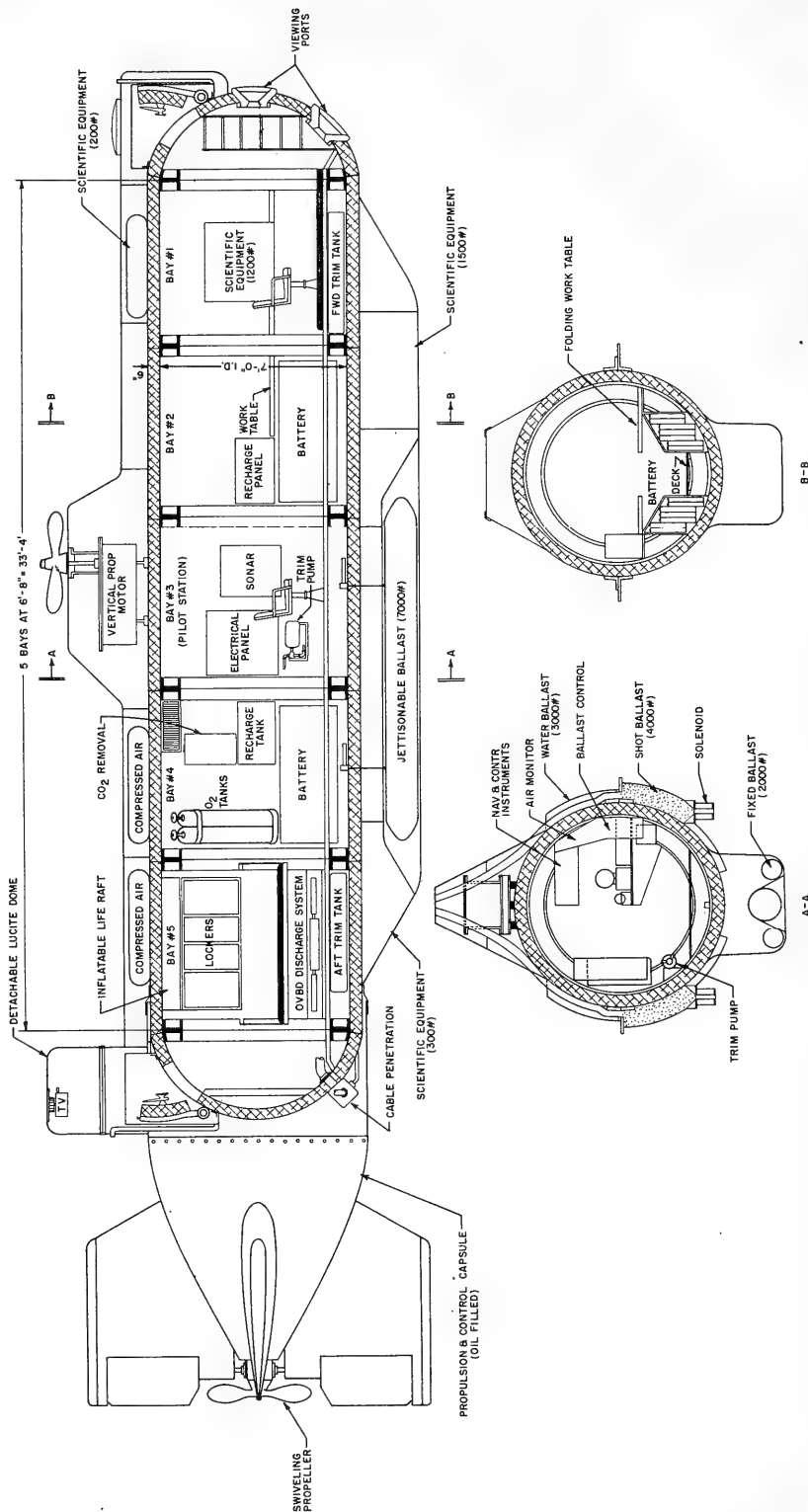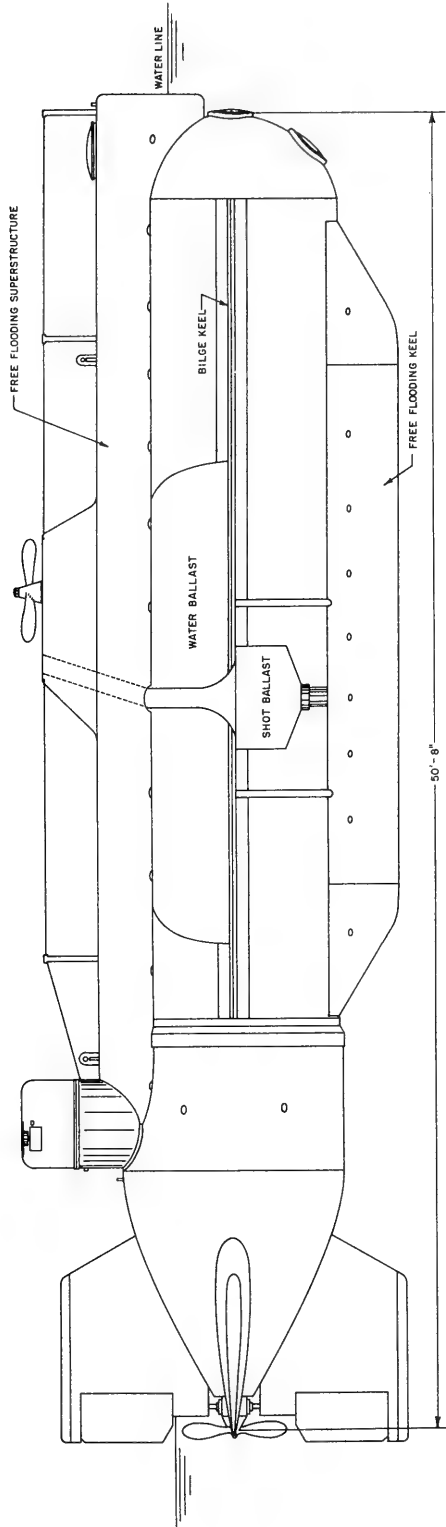
Fig. 1. Aluminaut inboard profile and sections

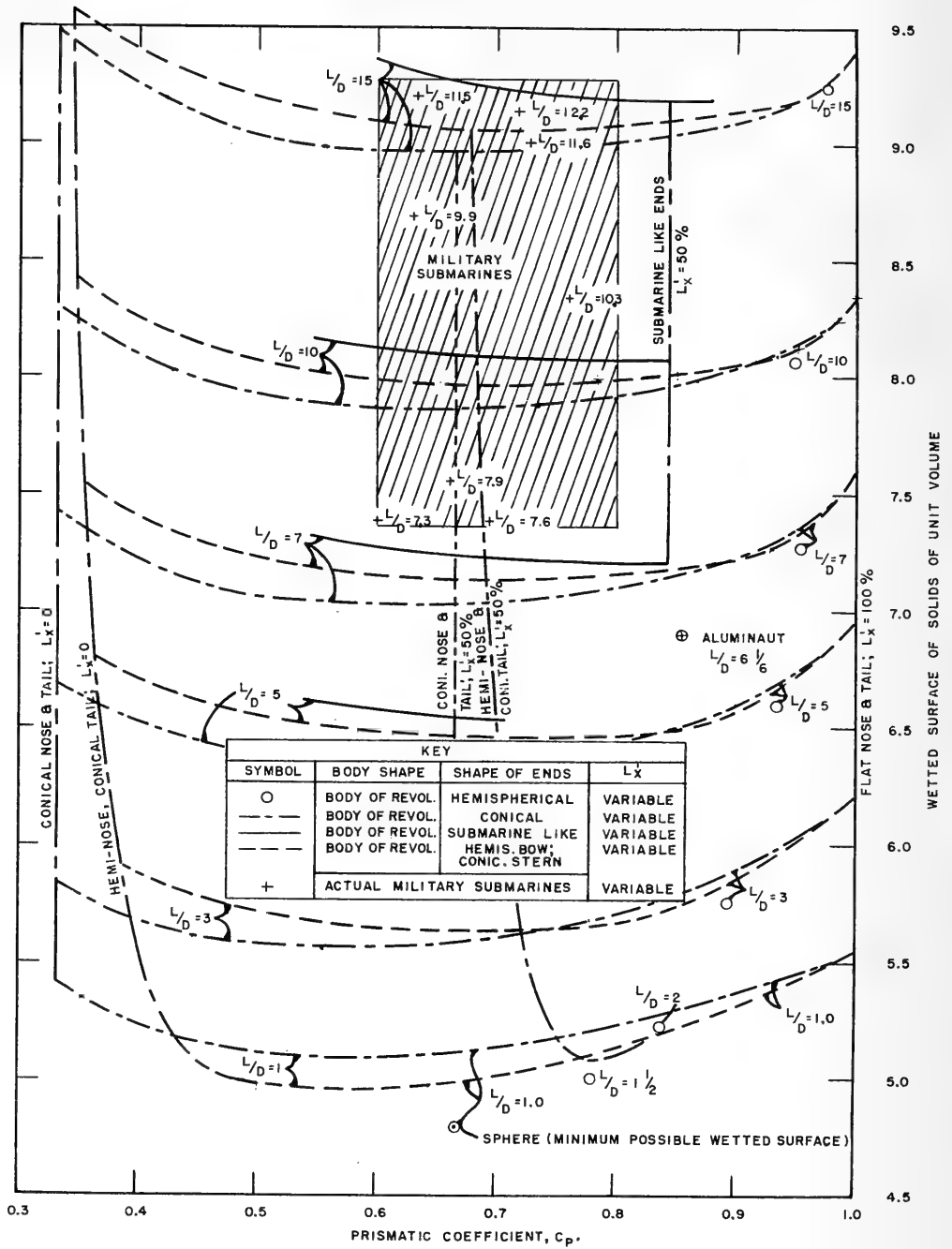Fig. 2. Aluminaut outboard profile

Fig. 3. Wetted surface of bodies of revolution as a function of length/diameter ratio, prismatic coefficient, and end shape

BALLAST SYSTEMS

Although water is ordinarily employed for variable ballast on submarines, the energy and pump weights required to eject water at great depths render almost essential the use of alternate ballast systems at such depths. Actually four ballast systems are employed on the Aluminaut, three of which are variable and one of which is fixed:

1. The ballast intended for routine ascent at great depths is 4,000 pounds of iron shot, contained in two amidship external saddle tanks shown in Figs. 1 and 2. These tanks are loaded through filling tubes in the superstructure when the boat is on the surface and emptied as desired through hollow solonoids at the bottom of both tanks. When energized (they draw only 36 watts each) the solonoids magnetically solidify the shot so as to plug the shot-tank aperture. When current to the solonoids is cut, either deliberately or by accident, gravity will cause the shot to flow out at any depth of operation. Thus, this system which was devised by Piccard for the bathyscaphes is relatively fail safe. To prevent electrolytic action with the iron shot, the aluminum saddle tanks are lined and the filling tubes molded of plastic. Special measures such as the prevention of exposure of wet shot to the air must also be taken to prevent the iron shot from corroding and consolidating. The iron shot described here has been successfully used with the bathyscaphes.

2. To augment the preceding system and also to permit the submergence of the boat from the surface to be under the complete control of the pilot within the boat a conventional water-ballast system is also provided. The tanks of this system which are also external to the pressure hull have a capacity of 3,000 pounds of sea water and are always open to the sea. Like conventional submarines, water is excluded from these tanks by means of a closed air valve; it can be admitted by opening the air valve and can be ejected from these tanks by compressed air stored in flasks located above the pressure hull as shown in Fig. 1. Because these flasks are initially charged for practical reasons to a pressure of only 2,200 psi, the water tanks can only be blown at depths less than about 4,800 feet. It is this fact that necessitates the provision of the iron shot system for use at greater depths.

3. For faster (and more reliable in the event of inadvertent flooding) emergency ascent, provision is made for jettisoning a 7,000-pound chunk of aluminum-wrapped lead stored in the lower keel structure. This ballast can be quickly released by the pilot by a simple mechanism that cuts two 1/4-inch-diameter supporting cables. The penetrations for these cables are the only mechanical penetrations of the pressure hull.

4. The remaining ballast is fixed and is divided between nonwastable ballast needed for stability purposes and wastable ballast margin available for design, construction, or future growth. Two thousand pounds of nonwastable ballast for stability purposes is located very low in the boat in the free-flooding keel in the form of solid aluminum bars. Five thousand pounds of wastable growth margin (on paper until the boat is completed) is allowed for at the location of the center of gravity of the entire boat. Upon completion of the boat, the remnant of this margin would actually have to be installed as ballast in the keel with the nonwastable ballast where it would further improve stability. The distinction between these two kinds of fixed ballast is further clarified in Section 5 of Ref. 2.

The three variable ballast systems permit the submarine to be operated at a great variety of equilibrium and nonequilibrium conditions. The more important of these conditions for the Aluminaut are tabulated in Table 2, which also shows the freeboard to the deck for the surface conditions and the metacentric heights for all conditions. Some of the same information is illustrated in Fig. 4.

Table 2
Weight, Buoyancy, Stability, and Freeboard

| Condition No.	Operation	Solid	Shot	Water	Weight (lb.)	Buoyancy (lb.)	Net Buoyancy (lb.)	Free-Board to Deck (ft.)	Meta-centric Height (in.)
1	Surface - light condition	No	No	No	135,140	135,140	0	2.05	2.65
2	Surface - normal condition	Yes	No	No	142,140	142,140	0	1.66	5.44
3	Surface - prepare to dive	Yes	Yes	No	146,140	146,140	0	1.10	5.76
4	Normal descent	Yes	Yes	Yes	149,140	148,640	-500	-	5.22
5	Operation at scheduled depth	Yes	Yes	Yes	149,140	149,140	0	-	5.22
6	Normal ascent - deep	Yes	No	Yes	145,140	148,620	3,480	-	4.99
7	Normal ascent - shallow	Yes	No	No	142,140	148,120	5,980	-	5.53
7A	Normal ascent - shallow (optional)	Yes	Yes	No	146,140	148,640	2,500	-	5.81
8	Panic ascent - deep	No	No	Yes	138,140	147,700	9,560	-	2.56
9	Panic ascent - shallow	No	No	No	135,140	147,200	12,060	-	3.08
10	Surface - special condition	Yes	No	Yes	145,140	145,140	0	1.20	4.92
11	Surface from panic ascent (optional)	No	No	Yes	138,140	138,140	0	1.78	2.11
12	Gradual ascent (optional)	Yes	1/2	Yes	147,140	148,890	1,750	-	5.10
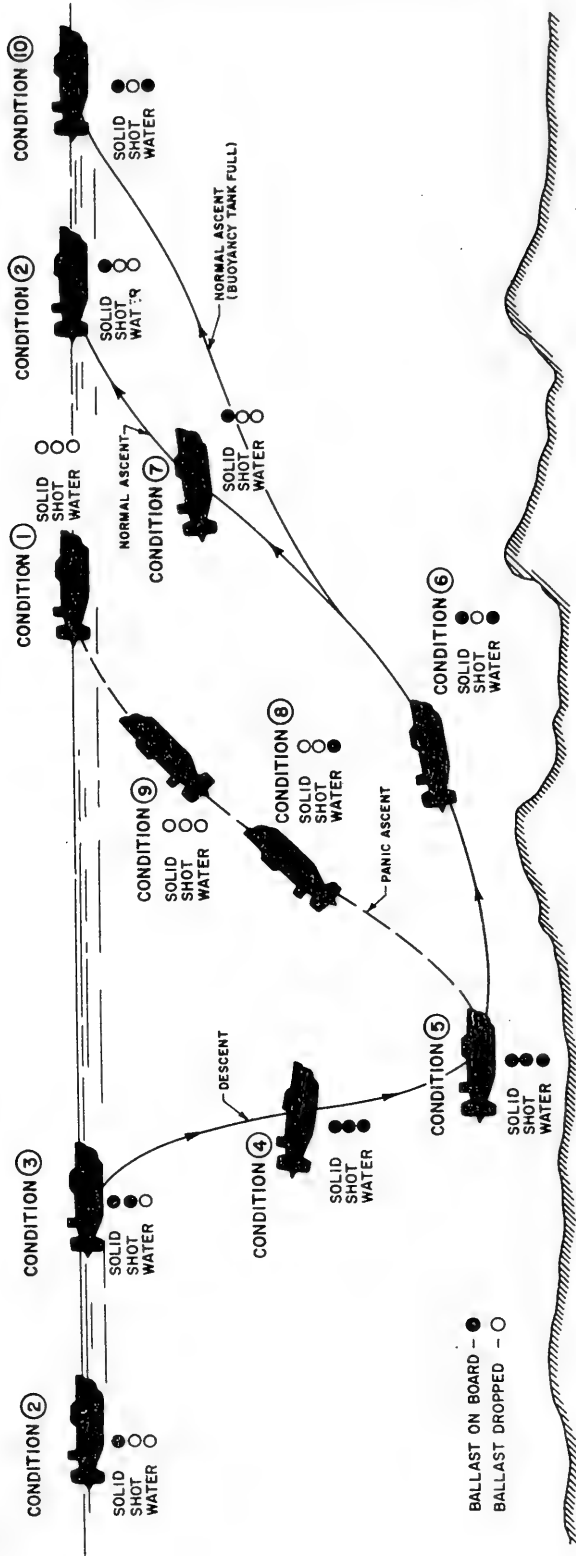
Fig. 4. Aluminaut ballast conditions

Normal diving and ascending procedures will be able to be carried out as follows on the Aluminaut. Condition 2 (see Table 2 and Fig. 4) would obtain when the Aluminaut is alongside an auxiliary vessel preparing for a dive. All solid variable as well as fixed ballast is on board, but it may be considered that the iron shot and water ballast had been jettisoned on a previous dive. When the boat has been made ready for submergence in all other respects, iron shot would be added from the mother ship to produce condition 3. In this condition the water tanks are still empty so that the boat is still afloat with over a foot of freeboard to the deck. The final submergence of the boat is now under the complete control of the pilot and when he is ready, he can flood the ballast tank, bringing the boat to condition 4 with a negative buoyancy of about 500 pounds. In all probability, the pilot would choose at this point to speed his descent by propelling the boat to the desired depth of operation. It would take roughly 50 minutes to reach 15,000 feet with a 30-degree down angle utilizing full power on the main propeller (40 minutes with the vertical propeller working also). Otherwise, it would take about 4-1/2 hours.

With no further change in ballasting the boat would be at neutral equilibrium at 15,000 feet since due to compressibility effects (which will be discussed subsequently) the initial 500 pounds of negative buoyancy would disappear at that depth. This corresponds to condition 5.

Ascent can be achieved by any of the ballast arrangements shown in Table 2 and Fig. 4. The fastest panic condition ascent, which involves jettisoning the solid lead ballast and iron shot at 15,000-foot depth and the ballast water at 4,800 feet, utilizing full power on both the horizontal and vertical propellers, and a 30-degree up angle would take 22 minutes from 15,000 feet with no leakage. With no power available (and no leakage) the panic ascent would consume about 44 minutes. Consideration was given earlier in the design to provision of an overboard discharge pump capable of handling a very modest amount of leakage at 15,000 feet. It was concluded that the weight saved by not installing the pump was greater than the weight of water which the pump could eject during an ascent.

MOTION CHARACTERISTICS DURING VERTICAL ASCENT—PRELIMINARY CONSIDERATIONS

Piccard reported in Ref. 3 that on several occasions the bathyscaphes experienced rather violent oscillations while rising freely under the influence of positive buoyancy. Since it was known that the Aluminaut would possess substantially less metacentric stability than the Trieste, which would tend to permit larger oscillations, it was decided to study this problem thoroughly during the feasibility and design study of the Aluminaut.

Bodies which are streamlined in planes through their longitudinal axis of symmetry, are usually very blunt in planes normal to their axis of symmetry. It is well known that such blunt bodies will shed Karman vortices. For cylindrical bodies moving normal to their axis, which corresponds fairly closely to the case of submarines rising vertically, it can be shown that the dependence of the period of the vortex shedding upon the various characteristics of the flow is expressed by a single curve of the Strouhal number $D/T_e V$ against the Reynolds number VD/ν, where T_e is the period of the vortex shedding (period of excitation), D is the diameter of the cylinder, V is the velocity, and ν is the kinematic viscosity of the fluid. This curve was obtained experimentally in Ref. 4 for Reynolds numbers up to about 10^6 and plotted in such forms in Ref. 5 that extrapolation to slightly higher Reynolds was not too difficult. It is shown in Fig. 5 for Reynolds numbers up to about 4×10^6. Also shown in Fig. 5 is cylinder-drag data as a function of Reynolds number taken from

Ref. 6. It will be noted that the critical Reynolds number reflecting an abrupt change in the flow regime takes place between the model- and full-scale range. These data were used to compute both the vertical velocities of ascent as well as the approximate periods of excitations that could cause oscillations of the Aluminaut during a rapid ascent.

If the excitation periods computed in the preceding correspond to the natural period of oscillation of the submarine during any particular ascent, severe oscillations would
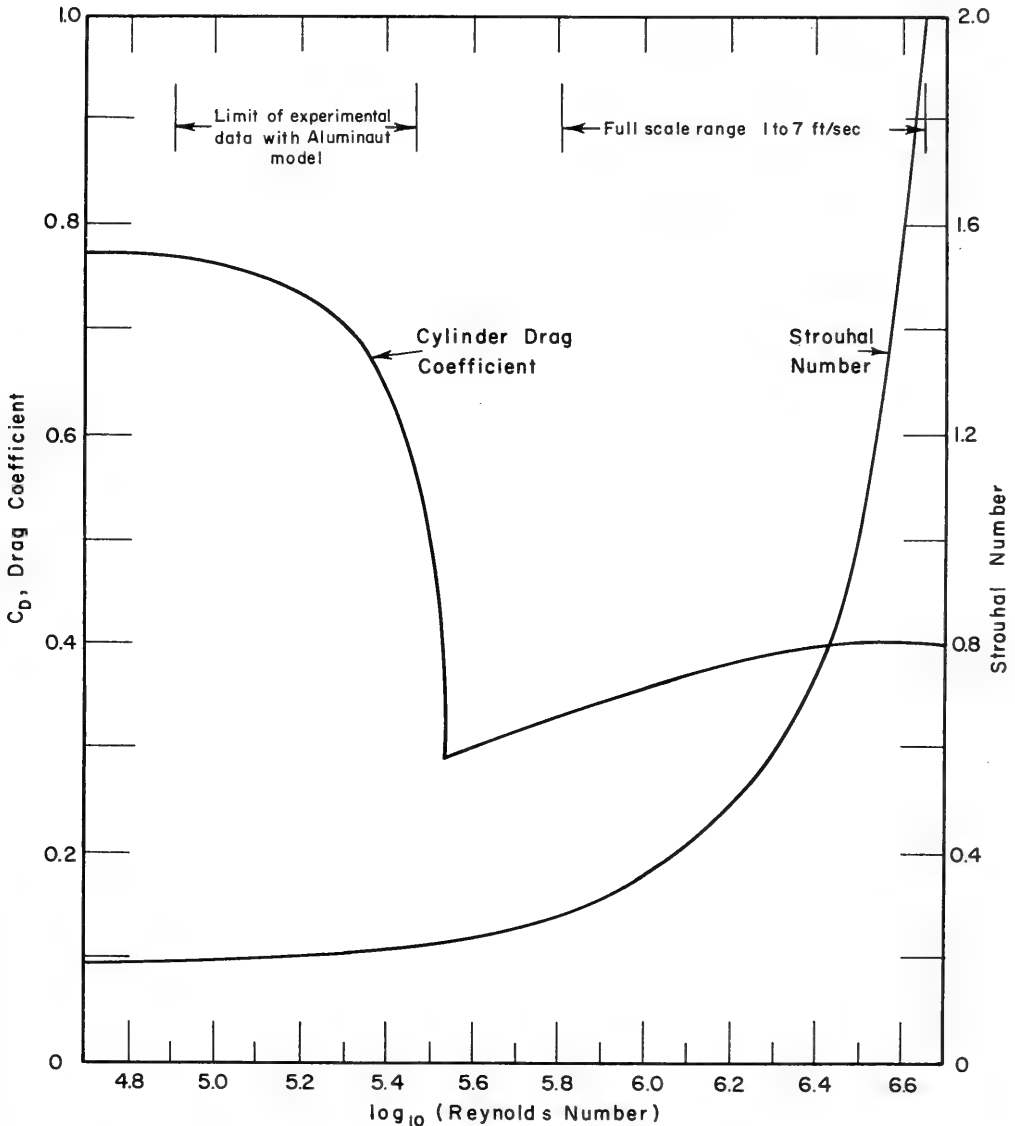

Fig. 5. Effect of the Reynolds number on the vortex shedding frequency and the drag of cylinders

doubtlessly ensue. The natural rolling period of a submerged submarine is conveniently expressed as follows:

$$T_n = 2\pi k_x / \sqrt{gBG}$$

where T_n = the natural roll period

k_x = radius of gyration of weight about the longitudinal axis of symmetry (varies from about 3.3 feet for condition 9 in Table 2 to 3.6 feet for conditions 4 and 5)

g = the acceleration due to gravity

BG = the metacentric height (tabulated in Table 2).

Utilizing all of the preceding information, it would be possible to predict which of the nonequilibrium conditions shown in Table 2 was likely to result in severe oscillations. However, this information would be insufficient to permit an estimate of the amplitude of oscillation. Furthermore, a freely rising submarine could obviously partake of coupled motions that might render the elementary analysis discussed up to this point inadequate. For these reasons the decision was made to conduct an experimental model study of the ascent of the Aluminaut.

MODEL STUDY

The Model and Facility

On the basis of a model-scale study conducted by the author, Southwest Research Institute constructed the 1/12-scale, 49-inch-long hollow aluminum model shown in Figs. 6 and 7. The unfairnesses evident in Fig. 6 were ameliorated by the use of modeling clay, and as
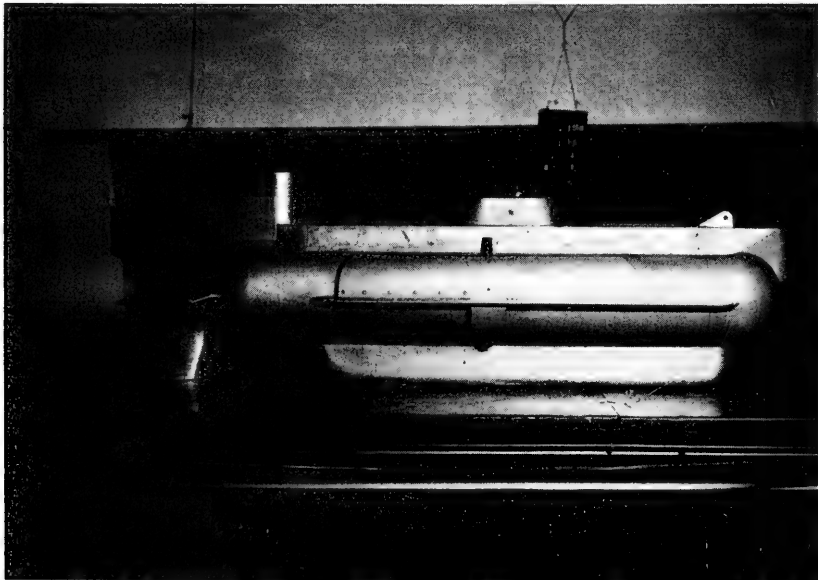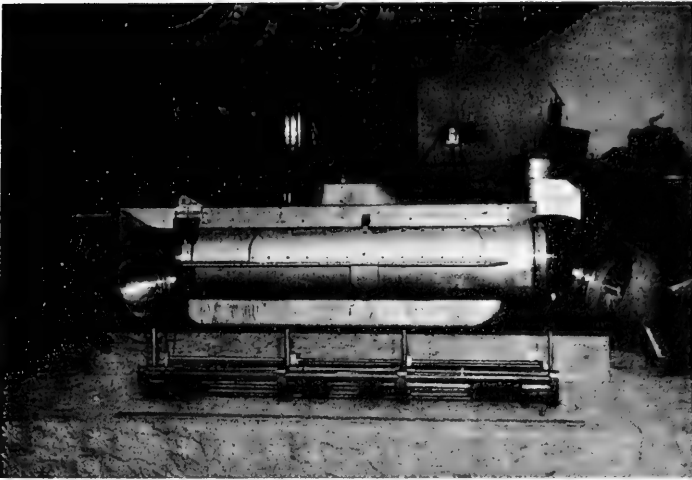

Fig. 6. Assembled aluminaut model

Fig. 7. Internals removed from aluminaut model, showing adjustable
weights for vertical ascent tests

indicated earlier these changes will presumably be incorporated into the full-scale. The
internal weight arrangement evident in Fig. 7 permitted considerable adjustment not only of
the net buoyancy of the model (by means of adding or subtracting weights), but also of its
natural period of roll for any fixed net buoyancy (by means of altering the vertical position
of the weights as well as the radius of gyration). The amplitude of these adjustments is
evident from Table 3 which describes the conditions that apply to each vertical ascent test
conducted with the model.

Table 3
Vertical Ascent Tests; Model Variables Tested

Test No.	Date of Test	Weight of Model (lb.)‡	Net Buoy-ancy (lb.)	Meta-centric Height (in.)‡	Roll Gyra-dius (in.)‡	Free Roll Period (sec.)‡	Bilge Keels§	Stern Fins§
i	6/10-12/59*	64.2	33.2	0.79	4.33	1.57	Narrow	Small
ii	6/10-12/59	64.2	33.2	0.79	4.33	1.57	Narrow	Small
iii	6/10-12/59	82.5	14.9	1.09	4.02	1.23	Narrow	Small
iv	6/10-12/59	86.1	11.3	1.14	3.97	1.20	Narrow	Small
v	6/10-12/59	89.6	7.8	1.19	3.92	1.15	Narrow	Small
vi	6/10-12/59	79.4	18.0	1.05	4.07	1.27	Narrow	Small
vii	6/10-12/59	70.3	27.1	0.90	4.23	1.41	Narrow	Small
viii	6/10-12/59	82.5	14.9	1.09	4.02	1.23	Wide	Small
ix	6/10-12/59	86.1	11.3	1.14	3.97	1.20	Wide	Small
x	6/10-12/59	79.4	18.0	1.05	4.07	1.27	Wide	Small

*Net buoyancies of the 6/10-12/59 tests were computed on the basis of 97.4 pounds total buoyancy.
‡Weights, metacentric heights, and gyradii do not include the effects of inadvertent flooding water.
§See Table 4.

Table 3 (Continued)
Vertical Ascent Tests; Model Variables Tested

Test No.	Date of Test	Weight of Model (lb.)‡	Net Buoy-ancy (lb.)	Meta-centric Height (in.)‡	Roll Gyra-dius (in.)‡	Free Roll Period (sec.)‡	Bilge Keels§	Stern Fins§
xi	6/10-12/59*	70.3	27.1	0.90	4.23	1.41	Wide	Small
1	7/27-29/59†	97.9	4.1	1.30	3.83	1.08	Narrow	Large
2	7/27-29/59	95.1	6.9	1.26	3.86	1.10	Narrow	Large
3	7/27-29/59	95.1	6.9	0.95	3.75	1.32	Narrow	Large
4	7/27-29/59	95.1	6.9	0.58	3.65	1.54	Narrow	Large
5	7/27-29/59	93.3	8.7	1.24	3.88	1.12	Narrow	Large
7	7/27-29/59	93.3	8.7	0.59	3.67	1.54	Narrow	Large
8	7/27-29/59	91.5	10.5	1.22	3.90	1.15	Narrow	Large
10	7/27-29/59	91.5	10.5	0.59	3.70	1.55	Narrow	Large
11	7/27-29/59	89.7	12.3	1.19	3.93	1.16	Narrow	Large
13	7/27-29/59	89.7	12.3	0.59	3.73	1.55	Narrow	Large
14	7/27-29/59	87.9	14.1	1.17	3.95	1.18	Narrow	Large
16	7/27-29/59	87.9	14.1	0.59	3.77	1.55	Narrow	Large
17	7/27-29/59	82.9	19.1	1.10	4.02	1.23	Narrow	Large
18	7/27-29/59	77.9	24.1	1.03	4.09	1.30	Narrow	Large
18A	7/27-29/59	75.6	26.4	0.99	4.13	1.33	Narrow	Large
19	7/27-29/59	72.6	29.4	0.94	4.19	1.37	Narrow	Large
27-7	7/27-29/59	93.3	8.7	0.59	3.67	1.54	Wide	Large
27-10	7/27-29/59	91.5	10.5	0.59	3.70	1.55	Wide	Large
27-8	7/27-29/59	91.5	10.5	1.22	3.90	1.15	Wide	Large
27-8	7/27-29/59	91.5	10.5	1.22	3.90	1.15	Wide	Large
27-8	7/27-29/59	91.5	10.5	1.22	3.90	1.15	Wide	Large
27-8	7/27-29/59	91.5	10.5	1.22	3.90	1.15	Wide	Large

*Net buoyancies of the 6/10-12/59 tests were computed on the basis of 97.4 pounds total buoyancy.
†Net buoyancies of the 7/27-29/59 tests computed on the basis of 102.0 pounds total buoyancy.
‡Weights, metacentric heights, and gyradii do not include the effects of inadvertent flooding water.
§See Table 4.

Since it was known that the shape and size of external appendages would strongly influence the damping of any oscillations, two different sets of bilge keels and stern fins were made to be fitted to the model. These are described in Table 4 and identified in Table 3.

Table 4

Item	Model Dimensions	Proj. Area (sq ft)	Approx. Drag Coef. (Ref. 7)
Narrow Bilge Keels	29 x 3/4 in. x $\overline{2}$	0.402	2.0
Wide Bilge Keels	29 x 1-1/2 in. x $\overline{2}$	0.805	2.0
Small Stern Planes	2.6 x 3.7 in. x $\overline{2}$	0.133	1.16
Large Stern Planes	5.8 x 3.5 in. x $\overline{2}$	0.282	1.16

The vertical ascent tests were conducted at the Underwater Weapons Tank Facility of the Naval Ordnance Laboratory at White Oak, Maryland. This facility proved to be well suited to the purposes of the tests. Figure 8 shows the facility setup schematically. The fact that the launching platform could be freely raised and lowered permitted great flexibility in conducting the tests. Moving pictures of the vertical ascent tests were obtained by underwater photographers from the staff of the U.S. Naval Underwater Photographic Unit in Washington.

U.S. Naval Underwater Photographic Unit in Washington.

The instrumentation used to measure the results obtained in this facility was, however, quite crude. The speeds of ascent were measured with stop watches while the roll oscillations
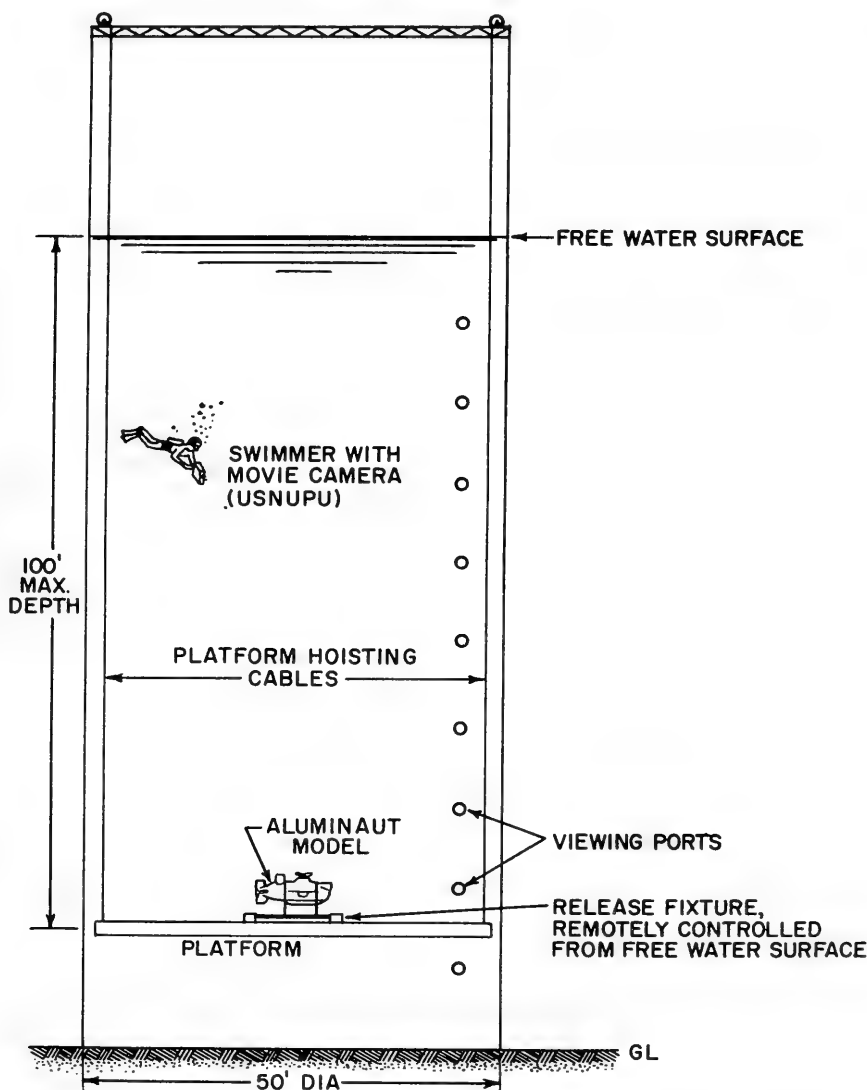

Fig. 8. Vertical ascent test setup at NOL Underwater Weapons Tank Facility

had to be based on visual observations through the viewing ports in the sides of the tank.
It might be noted, however, that in spite of the limitations imposed by both the crudity of
the measurements and inadvertent leakage of the model, the tests provided important guid-
ance to the design of the Aluminaut.

Model Drag

Results showing the relationship between ascent velocity and the net buoyancy and
drag for the model conditions and configurations tabulated in Table 3 are shown in Fig. 9.
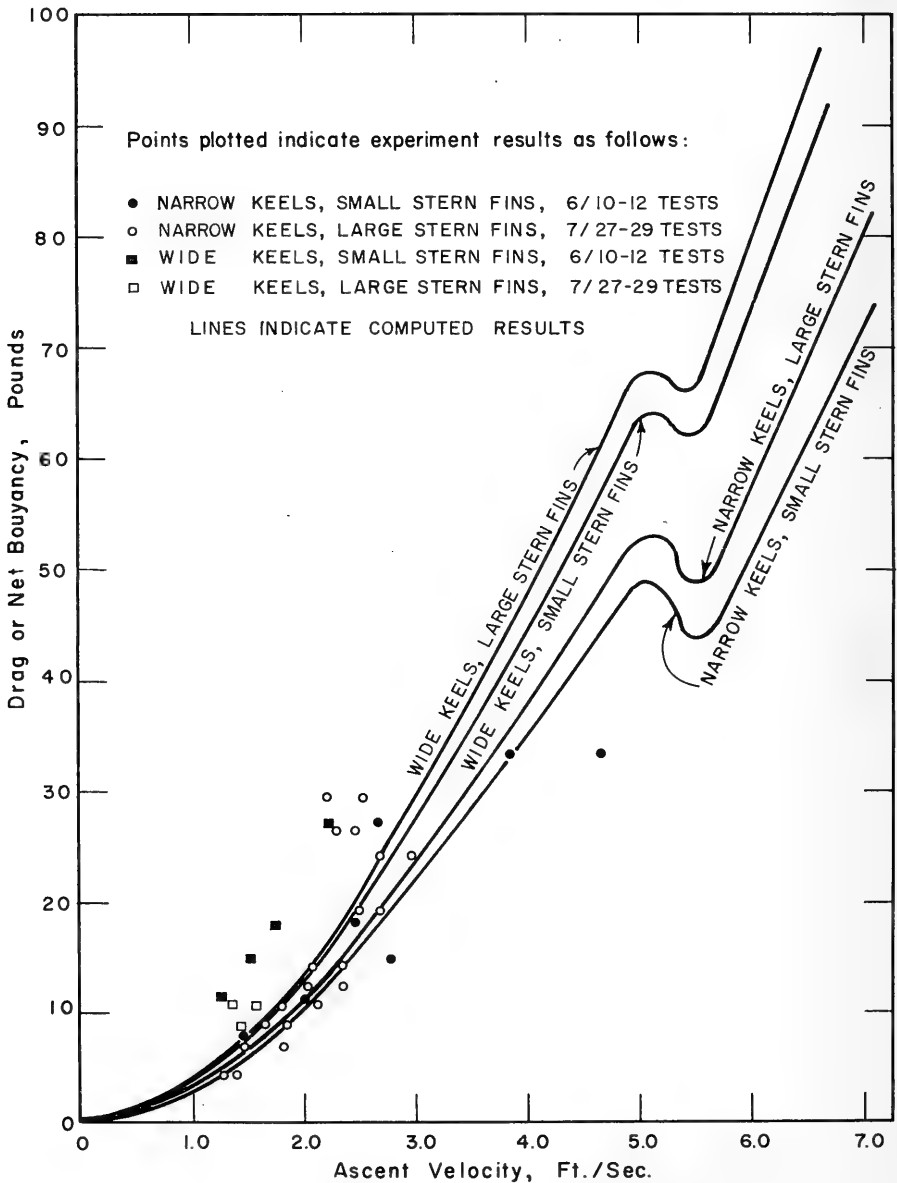

Fig. 9. Model vertical-drag data, experimental and computed

Also shown are computed data for the same configurations utilizing data given in Fig. 5 and Table 4. The scatter of experimental results is large, but considering the uncertainty introduced by the presence of an unaccountable amount of flooding water during some of the tests, the experimental results were considered as roughly confirming the computed data. In particular, the wide keel tests of 6/10-12/59 showed consistent serious deviation from the computed data. It will be noted that in none of the tests did the velocities approach those associated with the sharp discontinuity in the drag curve.

Model Oscillations

Test results of roll oscillation are plotted in Fig. 10 as a function of both ascent velocity, determined experimentally, and natural roll period, as tabulated in Table 3. Maximum double amplitude rolls observed during each test are shown symbolically for each point plotted. Also shown in Fig. 10 are the approximate periods of the roll excitation caused by the periodic vortex shedding computed on the basis of the Strouhal number curve shown in Fig. 5. With the introduction of bilge keels located at the maximum beam of the model, the maximum width to be used in the computation of the excitation period could be either 8 inches, the diameter of the cylinder, or 9-1/2 inches, the maximum tip to tip beam. This accounts for the range of values of excitation period shown in Fig. 10.

In general, as would be expected, the closer the correspondence between the natural roll period and the period of excitation, the larger the roll amplitude that resulted. It might be noted that it is very likely that the actual natural roll periods of the model during some of these tests were longer than the computed periods because of leakage. A moderate increase in the natural roll periods of some of the test spots would have improved the correlation between maximum roll amplitude and resonance.

While the proximity to resonance explains several of the large observed roll amplitudes in Fig. 10, in most instances the test conditions with low metacentric heights (large natural periods) showed larger roll amplitudes than conditions with large metacentric heights (small natural period). Although not directly apparent from Fig. 10, the preceding statement applies at constant tuning factor (ratio of natural period to excitation period). For example, the comparison of results of test 14 to tests 10 and 7 or test 11 to test 4 shows this tendency. The only exception to this pattern are tests 13 and 17. This effect of metacentric height is consistent with vibration theory (e.g., Ref. 8).

Only data for the narrow bilge keel tests of July 27-29 are shown in Fig. 10 since none of the wide keel tests showed strong oscillations and, in fact, most of those tests showed no oscillations at all. Therefore, it may be concluded that a substantial reduction in roll amplitude can be achieved with wider bilge keels. However, this is achieved at the expense of a considerable increase in vertical drag (see Fig. 11), particularly in the range of full-scale Reynolds number where the bare cylinder drag is a much smaller fraction of the total than it is in the model range.

In addition to quantitative data on roll amplitude and vertical velocity, the free ascent tests revealed strong cross-coupling between vertical forces and horizontal motion. As a result, the model usually achieved some ahead velocity while solely under the influence of a vertical force. This cross-coupling is probably enhanced by the strong fore and aft asymmetry introduced by the presence of large stern fins. Usually, only a slight pitch or yaw developed during the tests. However, during test 16 a strong pitch developed. Nevertheless, in no case was there evidence that the coupled motions prevented the predicted occurrence of roll oscillations.
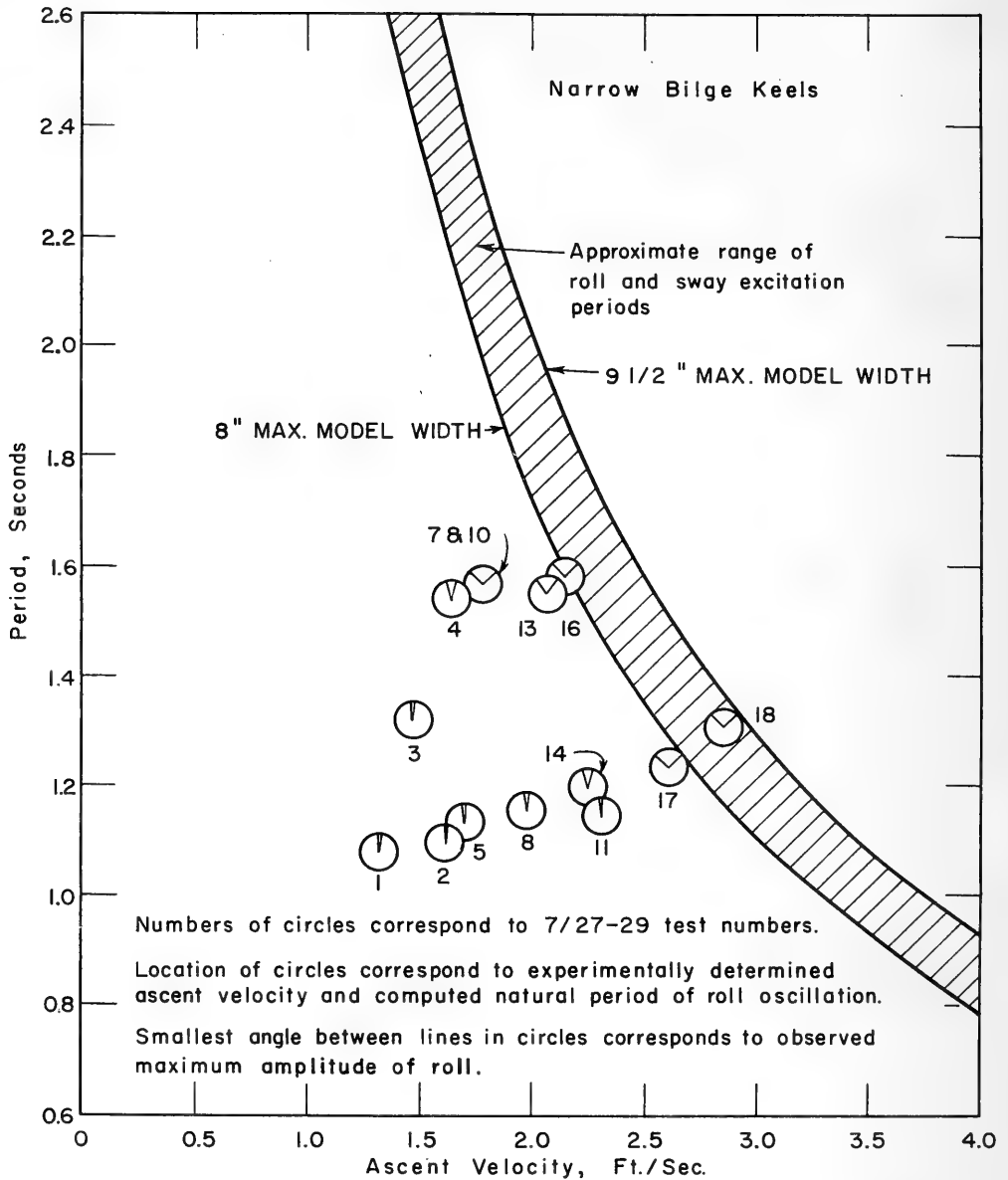
Fig. 10. Model oscillation data, experimental and computed

PREDICTION OF FULL-SCALE DATA

While the model results are of great importance in confirming design philosophy, they cannot be applied directly to predicting full-scale performance. Examination of Fig. 5 shows that both the nondimensional drag and roll excitation period change radically between the model range and the full scale. However, with the assumption that the limited experimental data modestly confirm design calculations within the model range, one can utilize the full-scale data in Fig. 5 with more confidence.

Full-Scale Drag

Full-scale drag vs ascent velocity curves are shown in Fig. 11. The uppermost curve corresponds to the Aluminaut design, as it is contemplated at this time with 12-inch bilge keels and large stern fins. It is seen that this condition results in more than double the bare cylinder drag. Also shown in Fig. 11 are the intercepts corresponding to actual buoyancy conditions of the Aluminaut shown in Table 2. Comments have already been made concerning the speed of descent in condition 4 and the speed of ascent in the panic conditions 8 and 9. In the normal ascent if all of the shot ballast were dropped and water ballast
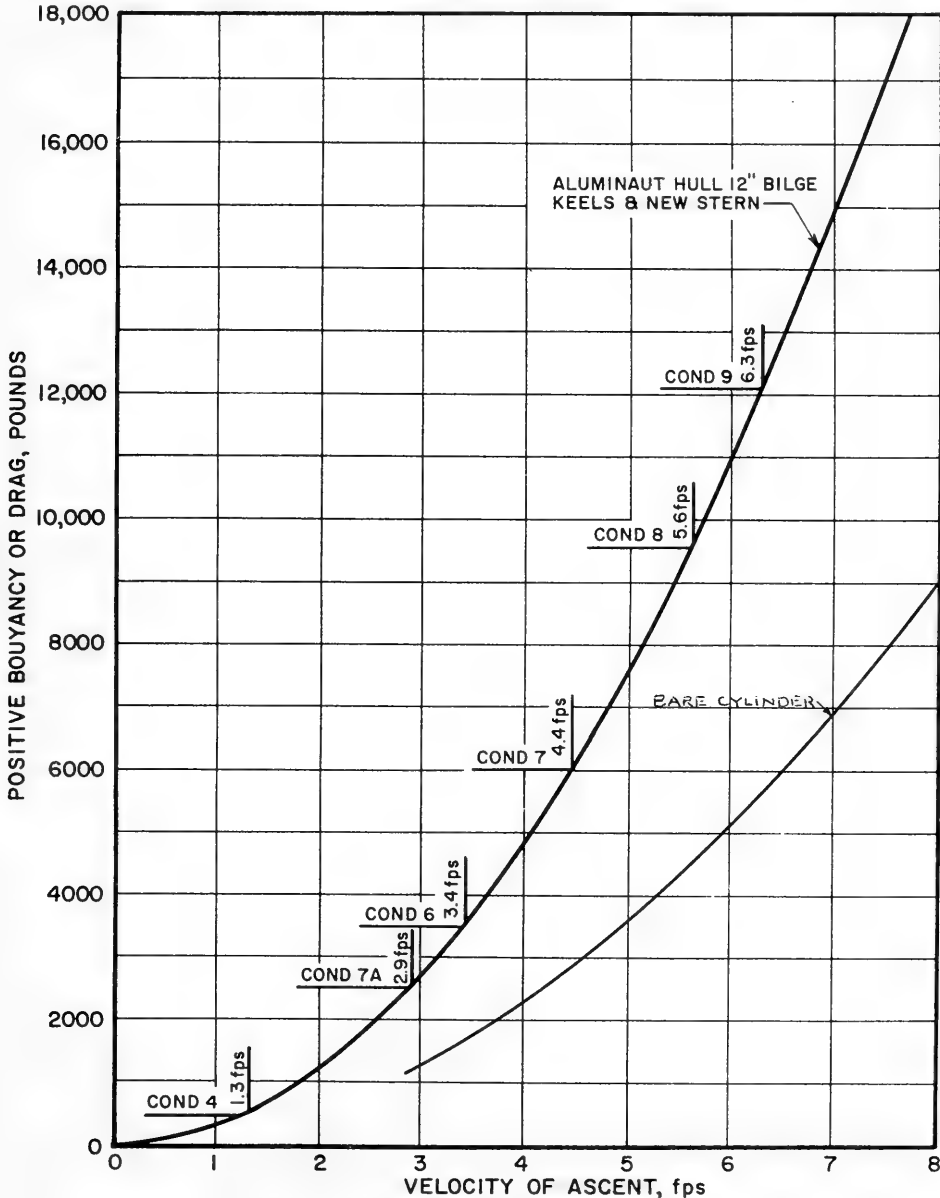

Fig. 11. Full-scale computed vertical-drag data

pumped out at moderately shallow depths (condition 7), it would take approximately 62.5 minutes to reach the surface. In fact, better time would be made if no ballast were dropped, but full power were preserved and utilized for the ascent using a 30-degree up angle. With this assumption it would take only 49 minutes to reach the surface. It appears very likely that this method of ascending will be preferred in the normal situation to dropping and losing expensive shot ballast.

Full-Scale Oscillation

Predicted excitation and oscillation periods for the full-scale Aluminaut are shown in Fig. 12. Bearing in mind the results of the model tests, it might be surmised that normal ascent conditions 6 and 7A might suffer the most severe oscillations of any of the conditions. This conclusion is tempered by the fact that, as noted in the previous section, it is very likely that propulsion would be used to speed the ascent in these conditions. With the boat driven to the surface with, say, a 30-degree up angle, it is not likely that severe oscillations would ensue even if the shot ballast was also dropped.

While it is likely that propulsion will be utilized for normal ascents, in the panic conditions, 8 and 9, propulsion may not be available. Therefore, it is of particular significance that these two conditions are, in fact, very far removed from resonance (tuning factor = 5 and 6 respectively). Therefore, in spite of their low metacentric heights, these conditions should not suffer large roll amplitudes.

Although not noted in Fig. 12, the range of predicted excitation periods on that figure is bounded by two different water temperatures. For the full scale, the influence of the range of possible values of water kinematic viscosity on ascent velocity and frequency of excitation is much more pronounced than the influence of assumed maximum body width. Since water temperatures between 40° and 80°F might be encountered, kinematic viscosities associated with these temperatures were used to form the boundary conditions.

CONCLUSIONS FROM VERTICAL ASCENT TESTS AND COMPUTATIONS

1. Despite large scatter, the experimental drag and oscillation data reasonably conform to analytically predicted results.

2. At resonance a substantial reduction in roll amplitudes can be achieved with wide bilge keels at the expense of a considerable increase in drag.

3. Strong cross-coupling caused the model to attain some ahead velocity. Pitch and yaw also were evident during many of the tests. These did not appear to interfere with the predicted roll oscillations.

4. For the normal ascent, the vertical velocity achievable by dropping ballast is so low that power preserved and utilized for propulsion would provide larger ascent velocities.

5. The only two buoyancy conditions liable to experience large roll oscillations are the normal ascent conditions 6 and 7A. This situation is vitiated by the fact that in actual operation it will probably be preferable to utilize propulsion for the normal ascent rather than drop ballast.

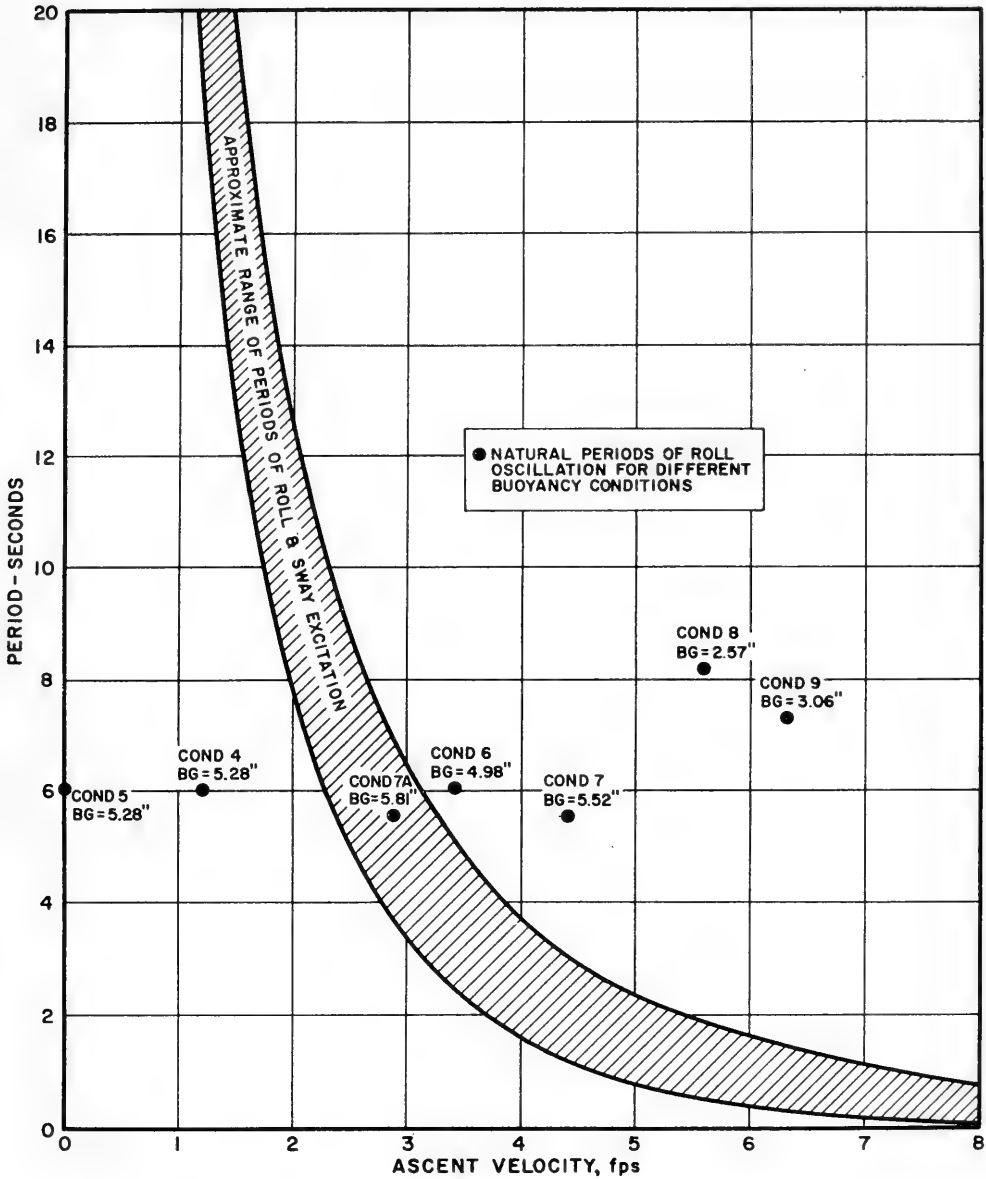Fig. 12. Full-scale computed excitation and oscillation periods

6. The two panic ascent conditions, 8 and 9, are so far removed from resonance that strong oscillations are extremely unlikely.

EFFECTS OF COMPRESSIBILITY

Pressure hulls of either shallow- or deep-diving submarines deform elastically under the external pressure of submergence. The associated loss in volume is usually small and

is to some extent compensated for by the compressibility of water. In relatively-thin-hulled shallow-depth submarines, however, the loss in volume represents a hull compressibility which is greater than the compressibility of the surrounding sea water. As a consequence the hull becomes less buoyant as it dives, which is an inherently unstable condition. Thus, a thin-hulled submarine that is neutrally buoyant near the surface must by some means discharge ballast at deeper depth in order to attain neutral buoyancy again at that depth.

Contrary to this situation, the thick hull of the Aluminaut is less compressible than water. As a result the boat becomes lighter as it sinks. Thus theoretically it should be possible when it is desired to dive the Aluminaut to its operating depth to take in a precise amount of excess ballast so that the Aluminaut has negative buoyancy near the surface. Without further intake or discharge of ballast the boat should then sink slowly to its operating depth where it will be in perfect equilibrium if the proper amount of excess ballast was initially taken aboard.

Particulars are shown in Table 5. The density of water at 15,000-foot submergence is about 2 percent greater than its density near the surface. Thus an incompressible hull would gain about 2 percent of its near surface buoyancy at a depth of 15,000 feet. On the other hand, if a thin-hulled submarine such as are now designed for shallow depths could be designed somehow to accept 15,000-foot submergence, it would lose about 5-1/2 percent of its near surface volume at that submergence and thus lose about 3-1/2 percent of its near surface buoyancy. The Aluminaut pressure hull is closer to the incompressible hull in this respect and loses only about 0.5 percent of its near surface volume at 15,000-foot submergence. Thus, it gains 1-1/2 percent of its near surface buoyancy at 15,000 feet. However, the overall compressibility of the entire Aluminaut configuration is considerably greater than 0.5 percent, primarily because the pressure-equalized silicone fluid in the stern capsule is itself much more compressible than water. It is estimated that the compressibility of the entire Aluminaut configuration is about 1-1/2 percent; thus it gains only about 0.5 percent of its near surface buoyancy at 15,000 feet. However, this calculation is believed to be too sensitive to subtle influence to be entirely depended upon, and must be carefully checked during the initial dive of the boat itself.

Table 5
Effects of Compressibility

Compressibility of Hull	Depth of Submergence, (ft)	Ratio of Water Density at Depth and Water Density at Surface	Ratio of Hull Volume at Depth and Hull Volume at Surface	Gain or loss Buoyancy
Incompressible hull	7,500	1.01	1.00	1% gain
Incompressible hull	15,000	1.02	1.00	2% gain
Hull as compressible as water	7,500	1.01	0.990	0
Hull as compressible as water	15,000	1.02	0.981	0
Thin hull submarine	7,500	1.01	0.975	1.5% loss
Thin hull submarine	15,000	1.02	0.945	3.5% loss
Aluminaut, pressure hull only	15,000	1.02	0.995	1.5% gain
Aluminaut, entire configuration	15,000	1.02	0.985	0.5% gain

The statements that have been made concerning the compressibility of thin-hull submarines apply with equal verity to vehicles like the bathyscaphes that use light-density fluids for flotation. Although the pressure hull of the Trieste may also be less compressible than sea water, the fact that the Trieste derives 90 percent of its buoyancy from light-density gasoline makes its overall compressibility almost as large as that of gasoline. Since gasoline compresses at a rate about twice that of water, the bathyscaphes, like the thin-hulled shallow-depth submarines, are unstable in depth.

There is yet another effect of compressibility with the Aluminaut hull in addition to the effect on net buoyancy at depth. The compressibility of the silicone fluid in the stern capsule of the Aluminaut introduces a significant shift forward in the longitudinal position of the center of buoyancy between near surface operation and operation at depth. This fact in conjunction with personnel movements on board was used to help determine the capacity of the trim tanks that are installed inside the pressure hull.

Because of the contraction of the pressure hull with depth, allowance has had to be made with attachment of all internal and external mountings to make sure that neither they are damaged nor the hull is locally restrained. Calculations indicate that at the test depth of 17,000, the radial displacement of the Aluminaut pressure hull is about 0.172 inch.

MANEUVERING IN BOTH PLANES

Most of the oceanographers who would be the potential users of the Aluminaut emphasized to the designers the necessity for precise control in both the horizontal and vertical planes. Because of the low speed of the Aluminaut, it was apparent that the desired degree of control could not be achieved by control surfaces alone as it is with higher speed submarines. For that reason two techniques are employed that are not usually used with submarines in addition to several other more conventional techniques. One is a propeller to provide thrust in the vertical direction and the other is a swiveling main propulsion propeller to permit directing the thrust in the horizontal plane. These are described in the subsequent sections.

Control in the Vertical Plane

To permit positive control in the vertical plane at all speeds a four-foot-diameter propeller driven by a 5-horsepower motor is mounted on top of a small superstructure about 15 percent of the length forward of amidship as shown in Figs. 1 and 2. This superstructure, which is also oil-filled, houses the motor, which is reversible and has a stepped speed control. With 5 horsepower the propeller can develop about 400 pounds of thrust as shown subsequently in Fig. 13. This thrust can be directed either upward or downward by reversing the motor. Since the magnitude of the thrust is not dependent on the speed of advance of the boat as it would be if it were developed by control surfaces, it should provide positive vertical depth control at any speed of advance.

In addition to the vertical propeller, two additional systems are provided for control in the vertical plane. The most effective of these, particularly in the speed range of the Aluminaut, is a conventional hydrostatic trim system that can be used to control pitch angle. The system as presently designed employs a pump driven by a 1-1/2-horsepower motor that can transfer 1,000 pounds of water between the two trim tanks shown in Fig. 1 in a period of two minutes. The moment produced of 26,500 foot-pounds is sufficient to trim the

submerged Aluminaut about 20 degrees against her metacentric stability. As mentioned earlier, the trim system is currently sized primarily to accommodate the trim unbalance imposed by the loss of buoyancy in the stern capsule at depth and the movement of personnel within the boat. However this system could be readily enlarged after completion of the boat if it is evident that additional capacity is needed to augment pitch angle control.

Stern control surfaces are also employed partially to improve directional stability in the vertical plane, but also to serve as trim tabs to assist in maintaining horizontal flight without constant use of the vertical propeller. It is possible that they may not be able to fulfill even the latter limited mission in the event that the critical speed (see Section 7 of Ref. 2) falls within the operating speeds of the Aluminaut. At this speed no combination of hull pitch angle and stern plane angle can simultaneously balance out both the hydrodynamic forces and the combination of hydrodynamic and hydrostatic moments that act on any submarine. However, at speeds just slightly removed from the critical value the stern planes will be effective as trim tabs even though they may have to be used in a sense opposite to that which intuition would dictate.

Even with the preceding systems for controlling pitch angle and depth, difficulty may be encountered in maneuvering along an irregular bottom. For this purpose use of a trail rope such as is used by balloonists for maintaining constant distance above an irregular land terrain may be helpful. However, there has been little or no experience with this device with submarines and the forces involved may be too small to be effective. In the event that difficulties are experienced after the boat is in operation, the alternatives remain of refining the controls of the vertical propeller or increasing the capacity and refining the controls of the hydrostatic trim system.

Main Propulsion and Control in the Horizontal Plane

A 15-horsepower dc motor located in the stern capsule and connected via bevel gears to a four-foot-diameter propeller is used for main propulsion. This motor (as well as the topside motor for the vertical propeller) has hydrodynamic problems of its own since it must operate in an environment of very high pressure oil. To improve motor efficiency, both the rotating as well as the fixed elements must be especially streamlined to minimize hydrodynamic drag. Even with these measures a motor efficiency of only about 50 percent is assumed. It is expected, however, that the motor can be substantially overloaded because of the excellent heat dissipation into the surrounding medium. As shown in Fig. 13, a maximum horizontal speed of about 4.7 knots is expected with 15 horsepower.

Stability and control in the horizontal plane is effected by large fixed fins, balanced rudders (each 6 square feet in area) and provision to swivel the main propulsion propeller through a total arc of 120 degrees. Both the rudders and propeller pivot on a common vertical shaft as indicated in Figs. 1 and 2. The swiveling propeller by itself should assure excellent control at any speed in the horizontal plane.

DIRECTIONAL STABILITY IN TOW TESTS

Full-scale operations with the Aluminaut doubtlessly will at some time require that she be towed on the surface to the scene of diving operations. Experience in the past with vessels of similar shape to the Aluminaut has revealed that in some conditions, the behavior

NOTE: CURVES OF CONSTANT SHP ARE
DISCONTINUOUS BETWEEN HORIZONTAL
AND VERTICAL MOTION, BECAUSE OF
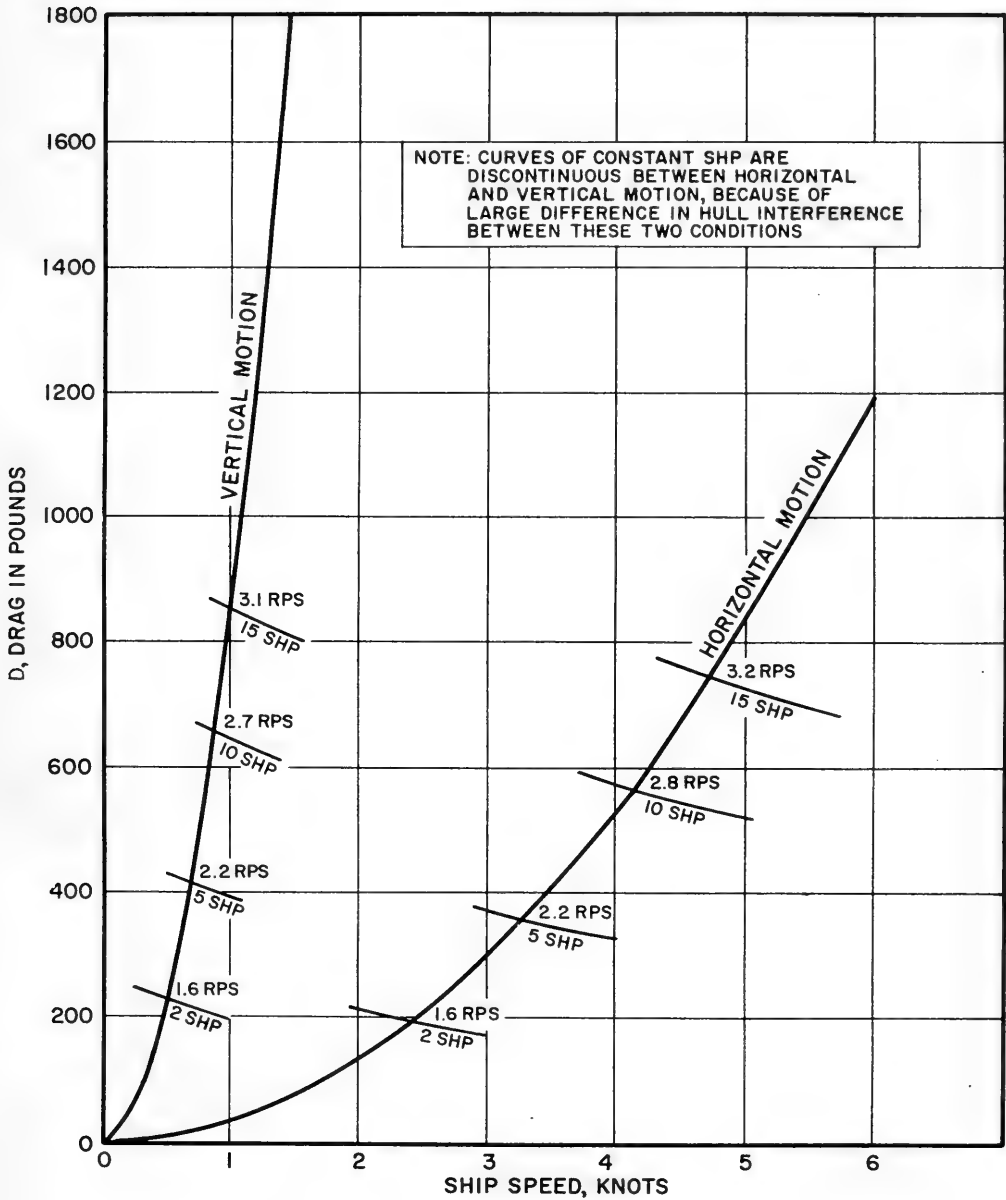LARGE DIFFERENCE IN HULL INTERFERENCE
BETWEEN THESE TWO CONDITIONS

Fig. 13. Resistance and power, ship and shaft

of the towed vessel is so erratic that towing becomes difficult and hazardous. It was for these reasons that tests were carried out with the 1/12-scale Aluminaut model in order to observe its behavior while being towed on the surface.

Test Arrangements

The Aluminaut model was towed about two model lengths behind a model of an Oceanographic Research ship at the M.I.T. Ship Model Towing Tank. The research ship model was in turn towed by the ordinary gravity towing arrangement employed at the M.I.T. tank. Thus, the towing vessel was restrained to straight-ahead motion while the towed vessel was unrestrained except for the tension on the towing line.

Several towing arrangements were employed:

(a) Ahead tow - single tow line attached to a bracket on the centerline of the forward deck of the Aluminaut.

(b) Ahead tow - bridle tow lines attached to the extremeties of a one-foot-wide spanner fixed to the forward deck of the Aluminaut.

(c) Ahead tow - bridle tow line attached to the leading edges of the Aluminaut bilge keels.

(d) Astern tow - single tow line attached to upper rudder of the Aluminaut.

Tests were conducted with both the small and the large stern planes and rudder described in Table 4. During all tests the model was equipped with the wide bilge keels. Limited tests were also conducted with the stern fins removed.

Test Results

Distinct differences in the behavior of the towed Aluminaut model were observed with the different towing arrangements. The Aluminaut model was initially set directly behind and in line with the towing model. Upon release and movement of the towing model, the following situations could be observed:

Description of Behavior	Characterization of Behavior
1. The Aluminaut model would veer off course and collide with nearest tank wall.	Unsatisfactory
2. The model would initially veer off course, but return and cross its initial position and collide with the opposite tank wall.	Unsatisfactory
3. The model would initially veer off slightly to one side, but within the length and width of the tank, it would tend to return to a stable equilibrium position.	Satisfactory

Description of Behavior	Characterization of Behavior
4. The model would remain in a stable equilibrium position throughout the run.	Satisfactory

Tests with the small stern fins yielded the following results:

Towing Arrangement	Characterization of Behavior	Comments
(a)	Unsatisfactory	
(b)	Satisfactory	Equilibrium position slightly to port of initial position
(c)	Satisfactory	Equilibrium position slightly to port of initial position
(d)	Satisfactory	

Similar results were obtained with the large stern fin tests except that with towing arrangements (b) and (c) the model veered more to port and the equilibrium position was further to port. In order to help ascertain the cause of this distinct bias, configurations (b) and (c) were tried with the model set initially heading to starboard. The model still turned to port and established a stable equilibrium position on the port side of its initial position. Subsequently, the model was also tested with the stern fins removed entirely. In this condition, towing arrangements (b) and (c) became unstable, although no bias either to port or starboard was evident. It was concluded from these tests that both the original and enlarged rudders were not set exactly parallel to the center line of the model, and that the bias to port which was even more evident with the enlarged rudders was due to the inaccurate initial setting of the rudders.

Application to Full-Scale Towing

The model results indicate that towing arrangements (b) and (c), or (d), would be satisfactory for the full scale. From a practical point of view, (c) or (d) appear preferable to (b) which involves the fitting of a large spanner subjected to very heavy cantilevered loads. The bias that the model possessed for the port side is considered of little consequence since the zero position of the full-scale rudders can be easily adjusted. It was concluded from the tests that satisfactory towing of the Aluminaut on the surface could be accomplished with at least two simple towing arrangements.

SUMMARY OF PAPER

The contrasts between the Aluminaut and both the previous generations of deep-diving vehicles and conventional military submarines are emphasized in this paper. In the field of hydrodynamics, special problems arise with deep-diving submarines that require different ballasting systems as well as different devices for effecting superior control at low speeds.

In addition, the oscillations arising from rapid vertical ascent or descent and the effects of compressibility become nonnegligible for deep-diving submarines. It is believed that the compromises made in the design of the Aluminaut effect reasonable solutions to each of these problems.

In particular, the use of iron shot as ballast appears to be a satisfactory substitute for water ballast and pumps at very deep depths. The possibility still exists, nevertheless, that the iron shot may prove to be redundant for normal ascents and it may prove feasible to abandon its use. In that event its equivalent weight would be incorporated in solid ballast for use in emergency ascents.

Model tests have reasonably confirmed theoretical predictions of the measures needed to avoid large oscillations in vertical ascents. In particular, the tried and true measures of avoiding resonance and incorporating damping devices such as bilge keels promise to yield satisfactory solutions. It has been demonstrated that in the panic ascents where it would be particularly desirable to avoid large amplitudes of roll the tuning factors are in fact far removed from resonance.

The fact that the overall configuration of the Aluminaut is somewhat less compressible than sea water yields the desirable characteristic of stability in depth. This is in contrast to thin-hull submarines and earlier bathyscaphes that must drop ballast to achieve neutral buoyancy at any depth below the surface.

The use of a vertical propeller augmented by a hydrostatic trimming system as well as stern planes is expected to provide satisfactory depth and pitch angle control at all speeds. The possibility of using a trail rope for navigating over the bottom remains to be explored. Excellent control in the horizontal plane should be achieved by the ability of the main propulsion propeller in conjunction with the rudders to swivel through an arc of 120 degrees.

Model tests indicated that satisfactory towing of the Aluminaut on the surface could probably be accomplished either by towing it stern first or by towing it bow first with a bridle arrangement attached to the leading edges of the bilge keels.

Taken as a whole, the Aluminaut promises to open a new era in ocean exploration and ocean utilization. While the primary problems associated with its development lie in the field of structures, this paper shows that careful consideration has also been given to its potential hydrodynamic problems.

But, it is to Dr. Edward Wenk, Jr., formerly of Southwest Research Institute, that the author is principally indebted. Dr. Wenk enlisted his work on this project and it is largely his enthusiasm, initiative, and drive that have carried the project through the difficult formative stages.

REFERENCES

[1] Wenk, Dehart, Kissinger, and Mandel, "An Oceanographic Research Submarine of Aluminum for Operation to 15,000 feet," Royal Institute of Naval Architects, Mar. 23, 1960

[2] Arentzen, E.S., and Mandel, P., "Naval Architectural Aspects of Submarine Design," Trans. Soc. Naval Architects Marine Engrs., Vol. 68, 1960

[3] Piccard, A., "Earth, Sky, and Sea," New York: Oxford University Press, 1956

[4] Relf, E.F., and Simmons, L.F.G., "The Frequency of Eddies Generated by the Motion of Circular Cylinders through a Fluid," British Advisory Committee for Aeronautics, R. and M. 917, 1924

[5] Landweber, L., "Flow About a Pair of Adjacent Parallel Cylinders Normal to a Stream," David Taylor Model Basin Report 485, July 1942

[6] Marks, L.S., "Mechanical Engineers Handbook," 6th edition, New York: McGraw-Hill, 1958, pp. 11-84, Fig. 21

[7] Hoerner, S.F., "Aerodynamic Drag," Midland Park, N.J., 1951, pp. 21-25 (The 2nd edition, published in 1958, is titled "Fluid-dynamic Drag")

[8] McGoldrick, R.T., "A Vibration Manual for Engineers," 2nd edition, David Taylor Model Basin Report 189, Dec. 1957 (obtainable from Office of Technical Services, Dept of Commerce, PB131785)

APPENDIX

The data plotted in Fig. 3 for the elementary body of revolution shapes are based upon the expressions for the dimensional and nondimensional volume and wetted surface of simple cylinders, cones, and hemispheres as follows:

	Cylinder	Hemisphere	Cone
Dimensional Volume, ∇	$\frac{\pi}{4}D^2 L_x$	$\frac{\pi}{12}D^3$	$\frac{\pi}{12}D^2 L_t$
Nondimensional Volume, C_p	1.0	2/3	1/3
Dimensional Wetted Surface*, S	πDL	$\frac{\pi}{2}D^2$	$\frac{\pi}{4}DL_t\sqrt{\dfrac{D^2}{L_t^2}+4}$
Nondimensional Wetted Surface, C_s	1.0	1.0	$\frac{1}{4}\sqrt{\dfrac{D^2}{L_t^2}+4}$

*Excluding area of flat ends in these cases.

Where:
L = length
L_x = length of cylinder (parallel middle body)
L_t = length of single conical end
D = diameter of cylinder, hemisphere, or base of cone
∇ = volume
C_p = prismatic coefficient $= \dfrac{\nabla}{\dfrac{\pi}{4}D^2L}$

S = wetted surface
C_s = wetted surface coefficient $= \dfrac{S}{\pi DL}$.

When these basic shapes are combined together with either the cones or the hemispheres forming the ends, the sums of the wetted areas as expressed above form the total wetted surface including that of the ends. The total Length L is then the sum of L_x plus the length of both ends. It then becomes convenient to introduce the nondimensional expressions $L_x' = L_x/L$ and $L_t' = L_t/L$. With these definitions the following relationships apply:

Hemispherical Ends:

$$L_x = L - D ; \quad L_x' = 1 - \frac{D}{L}$$

$$C_p = \frac{\frac{\pi}{4}D^2L_x + \frac{\pi}{6}D^3}{\frac{\pi}{4}D^2L} = 1 - \frac{1}{3}\frac{D}{L}$$

$$C_s = \frac{\pi DL_x + \pi D^2}{\pi DL} = 1.0$$

Conical Ends:

$$L_x = L - 2L_t ; \quad L_x' = 1 - 2L_t'$$

$$C_p = \frac{\frac{\pi}{4}D^2L_x + \frac{\pi}{6}D^2L_t}{\frac{\pi}{4}D^2L} = 1 - \frac{4}{3}L_t'$$

$$C_s = \frac{\pi DL_x + \frac{\pi}{2}DL_t\sqrt{\frac{D^2}{L_t^2}+4}}{\pi DL} = 1 - 2L_t' + \frac{1}{2}\sqrt{\frac{D^2}{L^2}+4L_t'^2}$$

Hemispherical nose, Conical Tail:

$$L_x = L - L_t - \frac{D}{2} ; \quad L_x' = 1 - L_t' - \frac{1}{2}\frac{D}{L}$$

$$C_p = \frac{\frac{\pi}{4}D^2L_x + \frac{\pi}{12}D^3 + \frac{\pi}{12}D^2L_t'}{\frac{\pi}{4}D^2L} = 1 - 2/3L_t' - \frac{1}{6}\frac{D}{L}$$

$$C_s = \frac{\pi DL_x + \frac{\pi}{2}D^2 + \frac{\pi}{4}DL_t\sqrt{\frac{D^2}{L_t^2}+4}}{\pi DL} = 1 - L_t' + \sqrt{\frac{D^2}{L^2}+4L_t'^2}$$

Flat Ends: $\qquad$ $L_x = L \; ; \; L_x' = 1.0 \; ; \; C_p = 1.0$

$$C_s = \frac{\pi DL_x + \frac{\pi}{2}D^2}{\pi DL} = 1 + \frac{1}{2}\frac{D}{L} \; .$$

For all configurations the wetted surface can be expressed in terms of the volume ∇, C_p, C_s, L/D as follows:

$$S = C_s \left(16\pi\frac{L}{D}\right)^{1/3}\left(\frac{\nabla}{C_p}\right)^{2/3} \; .$$

Cursory inspection of all of the preceding relationships will indicate the wisdom of leaving them in the parametric form in which they are expressed. Since both C_p and C_s are expressed in terms of L_t', it could be eliminated as a parameter and the wetted surface could then be expressed directly as a function of C_p and L/D for any given volume. The resulting expressions would, however, be extremely ponderous.

DISCUSSION

E. C. Tupper (Admiralty Experiment Works)

My remarks are not so much a question directed to the author, but rather a request to him that he might study certain problems associated with the control of this submarine when it is in operation. I think it is desirable to go a little into the background of the problem to bring out the points I wish to make. There are two points of great interest in the control of an underwater body in the vertical plane. So as not to become involved in any problems of nomenclature, I will call these points A and B.

Point A is a fixed point in the submarine which would typically be about a third or a quarter of the length from the bow. Ignoring transient effects, a vertical force applied at point A would cause the submarine to rise or dive while still maintaining level trim. Point B moves with changing speed; at very high speed it is almost coincident with point A, but, with decreasing speed, it moves aft until, at zero speed, it is infinitely aft of the submarine. Again, ignoring transient effects, a force applied at point B will cause a submarine to change trim but not to change depth. The author did mention that the action of these after hydroplanes might be reversed at low speed. This will occur at the speed at which point B coincides with the position of the after hydroplanes. At that speed, the after hydroplanes can only change the trim and not depth. A downward force applied ahead of point B would cause an increase in depth and a downward force applied after point B would cause a decrease in depth so that, in passing through the speed at which point B coincides with these after hydroplanes, there will be a reversal in the effect on depth of using the planes.

I would like to suggest to the author that it would be interesting to study, when he has the submarine in operation, whether the vertical propeller, which would seem to be almost at point A, does in fact control depth without significant effect upon trim, and also to study the actual speed, which may well be about 2-1/2 knots, at which the reversal of the after hydroplanes' influence on depth occurs.

Serge G. Bindel (Bassin d'Essais des Carenes, Paris)

I was very interested in the results given by Prof. Mandel, and particularly in those concerning the rolling oscillation during vertical ascent; they confirm the results obtained in the Paris Model Tank when studying the bathyscaph of the French Navy.

I should like, however, to make one remark regarding the dynamic stability of such a ship during vertical motion. There is a problem for ascent, but there is generally no problem when diving. This fact may be due to the presence of the bridge fairwater, which plays a nonsymmetrical role in the two directions of the motion, even if, as in the present case, its height is not too large. The effect of the fairwater is, in some manner, like this of a longitudinal fin on the stability on straight course for a surface ship; when diving, the fairwater is aft and its effect is favorable; in the contrary, when ascending, the fairwater is fore and its effect is unfavorable. The problem is, of course, more complicated than for a surface ship, because of the existence of a static positive stability. Therefore, if Karman's vortices are responsible for the excitation, my opinion is that it is necessary to take into account the dynamic stability of the motion and, when designing such a submarine, to avoid, if possible, a too developed bridge fairwater.

Owen H. Oakley (U.S. Bureau of Ships)

I couldn't resist commenting on Mr. Mandel's excellent paper because he and I were involved together in the business of submarine design for a number of years. I would like to make only one comment and that with respect to the comparison of the Aluminaut with the Trieste. Mr. Mandel noted a ratio of one to ten in the internal volumes of the two craft in favor of the Aluminaut, but that is really not quite fair. One thing should have been emphasized more, and that is that the Aluminaut is good for about 15,000 feet of submergence, where the Trieste is good for some 37,000 feet. The problem of density of structure required for the deeper submergence comes into the matter very strongly, as does the basic difference in the means of providing buoyancy. Mr. Tupper covered a point very nicely that I wanted to touch upon, namely, what is the critical speed, and I would like to inquire whether an attempt was made to estimate this.

P. Mandel

Mr. Oakley has pointed out an oversight in the oral presentation of the paper. The fact that the Trieste is capable of diving to more than twice the depth of the Aluminaut places some very severe constraints on her design that are not nearly as limiting for the Aluminaut. I have more amply covered this point in the written text of the paper.

I have not attempted to predict the critical speed for the Aluminaut. The critical speed is extremely sensitive to the magnitude of the hydrodynamic vertical force and moment due to asymmetry, designated Z^* and M^* in Ref. 2. There is no known method of analytically predicting this force and moment and attempts to rationalize experimental values have been unsuccessful. In any event there is little necessity for accurately predicting the critical speed in the case of the Aluminaut since it is intended to place primary reliance on the vertical propeller and on the hydrostatic trim system for control in the vertical plane.

With respect to the oscillations in dive as well as in ascent, the Aluminaut can only descend by means of overweight at a very modest speed. As shown in Table 2, the

Aluminaut can only be ballasted to be some 500 pounds overweight and with that overweight its descent to 15,000 feet would take some four and one-half hours. Therefore, the vertical descent shown in Fig. 12 corresponds to a very modest speed where oscillations do not occur, and where the conditions are well removed from resonance. This is why we were primarily concerned with the ascent condition in the investigation.

*   *   *

SUBMARINE CARGO SHIPS AND TANKERS

F. H. Todd
National Physical Laboratory

INTRODUCTION

The naval architect has always had to battle with the twin elements of wind and water, and these have provided very powerful barriers to any great increase in the speed of ships. Because a ship is floating at the boundary between two elements of very different densities, it creates waves on the surface as it moves and any increase beyond a certain speed leads to an excessive increase in the wavemaking resistance and consequently to an uneconomic rise in costs of construction and operation. This situation may be thought of in some respects as being analogous to the "sonic barrier" in aircraft design. Much research has been carried out into the reduction of wavemaking resistance, both by experiment and theory, and this has led to the adoption of very fine waterlines forward, U shaped sections and bulbous bows, which has enabled the speed of surface ships to be raised appreciably in the course of the years.

The effect of the wind is not only to increase the drag of the ship by its direct effect, but by creating rough seas or storm conditions forces the ship to slow down to avoid the excessive pitching and heaving motions and the damage to the structure which would eventually ensue. Such slowing down means loss of time or subsequent expenditure of extra power to make up schedules, since in general no owner wishes to do other than make full use of a very expensive investment. Again, research has done much to help the naval architect combat such conditions. The adoption of fine entrances, high freeboards, and good flare above water have, for example, enabled designers to improve the seagoing qualities of trawlers almost beyond recognition, while the perfecting of antirolling fins has reduced this motion to almost negligible amount in those ships fitted with them. There remains the problem of reducing pitching by similar means, and the bulbous bow does present some advantages in this way also.

The naval architect may well have envied his aeronautical colleague who, faced with similar weather problems, has taken the modern aircraft to very high altitudes where atmospheric conditions are calm and stable. He has long been aware of the possibilities of lifting a ship above the water surface on foils to reduce its own wavemaking and avoid the surface wind-generated waves, and of the advantages of taking a ship below the surface to escape both rough weather and wavemaking resistance.

The perfecting of the internal combustion engine, which enabled the aeronautical engineer to achieve his desires by giving him a source of power having a high power/weight ratio and a relatively high efficiency, also allowed the naval designer to build hydrofoil boats which can attain the same speed as a high-speed conventional motor boat for about half the power. These are not new in conception, for the first such hydrofoil craft "flew" in Italy as long ago as 1906, attaining a speed of some 38 knots [1]. Of recent years the interest in hydrofoil boats has greatly increased, many new foil configurations have been evolved,

and passenger-carrying hydrofoil craft are now in use in a number of sheltered waters. It is natural that efforts should be made to extend this principle to larger ships, but the difficulties in the way are considerable — the foils and their supports become more massive and heavy, detracting from the deadweight carrying capacity, they are a source of trouble due to the large draft they cause when the boat is on the surface coming into port, and since they are essentially high speed craft the large powers necessary must be transmitted from the hull to propellers a long way below the hull. Studies of such designs are going on, and we shall doubtless see much larger craft of this type built for specialised services, but their use for carrying the bulk cargoes of the world seems unlikely. Moreover, such boats still have to contend with the ocean waves on the surface of the sea, and therefore for any given size have limitations as to the sea state in which they can operate. By going below the surface, both wavemaking resistance and bad weather can be avoided altogether, and with the advent of nuclear propulsion the naval architect for the first time is in a position to seriously contemplate such a procedure. The use of nuclear reactors as a source of heat has freed the ship from dependence on the atmosphere and made possible the true submersible, which would spend all its seagoing time deeply submerged and only surface near the ends of its voyages. The hull can therefore be shaped for minimum resistance under deep-submerged conditions, with little concern as to its surface performance. The benefits to be gained are, of course, the elimination of surface wavemaking resistance, the reduction of form resistance to a minimum by streamlining the hull, and escape from the effects of bad weather.

The availability of nuclear propulsion for ships, as in the case of other new inventions, has led to a search for useful and practical applications. So far as the navies of the world are concerned, there is no doubt as to the value of nuclear propulsion in submarines to enable them to remain submerged almost indefinitely and in other ships in order to maintain fleets at sea for long periods without refueling. Nuclear-propelled submarines, apart from their military use, could be of extreme value for the delivery of fuel and supplies to combatant ships or to beleaguered islands or ports. From the national safety point of view, also, submarine tankers and cargo ships would be of inestimable value because of their relative immunity from enemy attack. A considerable number of military nuclear-propelled submarines are now in commission and it may well be that the first nuclear-propelled submarine supply ship will also be built by one of the navies of the world. The Russians, because of their particular geographical problems, have made the first application of nuclear propulsion to a surface ice-breaker which can, as a result, stay at sea for long periods to keep the lanes open throughout the winter.

The spectacular voyages of the USS NAUTILUS and SKATE under the North Pole in 1958 have also shown that submarines can be navigated for long distances under water without having to surface for sights of the sun or stars. This fact has led to much speculation regarding the possible use of such ships on routes which are closed by ice for part or all of the year.

As we shall see later, the submarine ship must operate at fairly high speeds to show material advantages over the surface ship, perhaps 30 knots or above. This fact may have some attraction to passengers who suffer from travel sickness but enjoy the restful atmosphere of a ship, and limited passenger accommodation may become a feature of such vessels. True, the passengers would not see the sea, but neither do many travellers today, who divide their time between dining saloon, bar, and cabin, and there is certainly no less to see than in the upper atmosphere!

When we come to consider such ships for commercial use, however, a number of operating problems are introduced, and it is the purpose of this paper to review these and, it is

hoped, to stimulate discussion and draw forth new ideas. One of the main advantages of nuclear-propelled ships is the saving in space no longer required for bunkers, and the consequent increase in carrying capacity. The weight of the shielding around the reactors cancels out much of the saving in weight by the elimination of fuel, and this would suggest that such machinery is most suitable for long-haul voyages. The average dry-cargo ships have been developed largely along the requirements of certain trades, and these are not likely to alter materially in type. Moreover, the oil fuel is very often carried in the double bottom, and such space is not of use for additional cargo. These considerations lead to the general conclusion that the ships most suited to nuclear propulsion are those carrying bulk cargoes such as ore, grain, and oil. In the case of the latter, with a liquid cargo the ease of handling is such that the ships could just as easily be submarines as surface ships, and it is this aspect of nuclear propulsion which seems to have caught the public imagination.

Economic nuclear propulsion in the strictly commercial sense is as yet some time away, but if it is eventually to be applied to submarine cargo ships, then there are without doubt many difficult problems to solve, and it is certainly not too early to begin research into them if we are to be ready to design and build such ships.

HYDRODYNAMIC ADVANTAGES OF SUBMARINE SHIPS

Although this symposium is supposed to deal with the field of naval hydrodynamics, it would not be realistic to treat this particular problem purely from that standpoint. There are so many practical limitations which would come into the design of a submarine cargo ship or tanker that they must be given consideration, as only in this way can we give due weight to all the conflicting claims. In this section the question of powering will be considered and estimates made for both surface and submarine ships. These will be used later in the paper as a basis for discussion when we come to deal with the problems of operating and maintaining such craft.

From the hydrodynamic point of view, the two greatest savings that we can expect by going under water are the elimination of the wavemaking resistance and the escape from the effects of rough weather. Owing to the good hull form which one can design for a real submersible, it is reasonable to expect that the form resistance would also be reduced.

The wavemaking resistance is a relatively small part of the total resistance for surface ships at low speeds, and therefore one would not expect any great savings in power by its elimination at low speeds of operation. Indeed, the submarine under such conditions begins with a considerable handicap in that the wetted surface will be considerably greater than that of the equivalent surface ship and therefore the skin-friction resistance of the submarine will be considerably higher. Only if this can be offset by a corresponding reduction in form resistance will the submarine be able to break even with her surface counterpart. At higher speeds the wavemaking resistance of the surface ship begins to increase very rapidly (in the order of V^6) and to attain these higher speeds a continual fining of the hull is necessary together with an increase in ship dimensions in order to carry a given amount of deadweight. Eventually we reach a speed at which it is no longer economic to drive the surface ship, and it is here that the submarine would show a very real advantage in terms of power. We can thus conclude on purely general grounds that the elimination of wavemaking resistance by using a submarine ship will only begin to give substantial returns when used at comparatively high speeds.

In order to have some actual figures on which to base a discussion, calculations have been made of the horsepower required for both surface and submarine ships of displacements from 25,000 tons up to 150,000 tons. From these figures estimates have been made of the powers required for surface and submarine ships of the same deadweight, as this is the only fair way of assessing their respective merits. This particular range of displacement was chosen because the lowest figure represents the smallest ship for which marine nuclear installations at present envisaged would be suitable and the highest figure is comparable with the largest tankers at present being built and having deadweights in the neighbourhood of 100,000 tons.

For the surface ships the results have been taken from the David Taylor Model Basin Series 60 [2]. For a number of displacements within the above range the EHP has been calculated for Series 60 models having block coefficients of 0.60, 0.70, and 0.80. The ships all have a length to beam ratio of 6.5 and a beam to draft ratio of 3.0. The ship powers have been estimated from the model results using the A.T.T.C. 1947 line with a correlation allowance ΔC_F of +0.0004. In designing ships of different speeds, it would be natural to use a finer block coefficient for the higher speeds, and the comparisons have therefore been made at a speed appropriate to each fulness. These speeds have been determined from the modified Alexander formula

$$V/\sqrt{L} = 2\ (1.06 - C_B).$$

In order to convert these EHP values into DHP at the propeller, it is necessary to make certain assumptions regarding the propulsive efficiency and appendage allowances. In the first place, it has been assumed that where the DHP is less than 40,000, the ship will be propelled by a single screw, where it is between 40,000 and 80,000, it will have twin screws, and above this higher figure, will have four propellers. For the single screw ships a quasi-propulsive coefficient of 0.72 has been used, in accordance with the experiments with Series 60, and no allowance has been made for appendages. It is assumed, in effect, that with modern large ships of all-welded construction, the allowance of $\Delta C_F = +0.0004$ will be sufficient to take account of any ordinary appendage resistance as well as any hull roughness effects. In such cases, therefore, the DHP has been taken as equal to the EHP divided by the QPC. For the twin and quadruple screw ships, the QPC has been taken as 0.68 and an appendage allowance of 10 percent and 20 percent respectively has been added to take account of the bossings or shafts and A-brackets in these arrangements.

For the submarines, estimates have been made for two different prismatic coefficients, namely 0.60 and 0.65, using various published works by Weinblum, Amtsberg, Crago, etc. These apply to streamlined bodies of revolution having their maximum diameter at a point 40 percent from the nose. Again, the skin-friction resistance of the ship has been estimated by using the A.T.T.C. 1947 line and including an allowance of $\Delta C_F = +0.0004$. The length/diameter ratio has been taken as 7.0, which is approximately the optimum for vessels of this form having the appropriate tail surfaces to give adequate directional stability.

The dimensions of the surface ships and submarines for the displacement ranges covered are shown in Tables 1 and 2 and Fig. 1, and charts of EHP/V^3 in Figs. 2 through 6. The EHP values for submarines of different displacements are also listed in Table 3, and those for surface tankers in Table 4. This latter table also includes estimates from NPL data, which show close agreement with those made from the Series 60. As will be seen in making the comparison for vessels of equal deadweight, the use of a circular submarine form leads to very unrealistic dimensions as regards draft. In order to be able to assess the

Table 1
Dimensions of Surface Tankers
$L/B = 6.5; \; B/d = 3.0; \; V/\sqrt{L_{BP}} = 2(1.06 - C_B)$

Δ (tons)	L_{BP} (ft)	B (ft)	d (ft)	WS (sq ft)	$V/\sqrt{L_{BP}}$	$V/\sqrt{L_{WL}}$	V (knots)	EHP including $+0.0004$
$C_B = 0.60; \; \Delta/(L/100)^3 = 135.3; \; L = 100 \sqrt[3]{\Delta}/5.14$								
25,000	569	87.5	29.2	58,000	0.92	0.912	21.93	17,800
50,000	716	110.2	36.7	92,000	0.92	0.912	24.60	39,200
75,000	820	126.2	42.1	120,600	0.92	0.912	26.30	62,200
100,000	903	139	46.3	146,200	0.92	0.912	27.65	87,150
125,000	962	148	49.3	166,000	0.92	0.912	28.50	110,000
$C_B = 0.70; \; \Delta/(L/100)^3 = 160; \; L = 100 \sqrt[3]{\Delta}/5.43$								
25,000	538	82.8	27.6	57,300	0.72	0.715	16.73	7,230
50,000	678	104.4	34.8	91,000	0.72	0.715	18.78	15,870
75,000	777	119.6	39.9	119,500	0.72	0.715	20.10	25,250
100,000	855	131.5	43.8	144,800	0.72	0.715	21.10	35,000
125,000	921	141.7	47.2	168,000	0.72	0.715	21.90	45,300
$C_B = 0.80; \; \Delta/(L/100)^3 = 180.4; \; L = 100 \sqrt[3]{\Delta}/5.65$								
25,000	518	79.7	26.6	57,500	0.52	0.516	11.83	2,430
50,000	652	100.2	33.4	91,200	0.52	0.516	13.30	5,340
75,000	747	115	38.3	120,000	0.52	0.516	14.22	8,500
100,000	821	126.3	42.1	144,800	0.52	0.516	14.90	11,660
125,000	885	136	45.3	168,000	0.52	0.516	15.50	15,180

Table 2
Dimensions of Submarines with Circular Cross Section

Δ (tons)	L (ft)	D (ft)	Wetted Surface (sq ft)
$C_p = 0.60$; $L/D = 7.0$; $L = 15.37\,\Delta^{1/3}$			
25,000	450	64.3	65,200
50,000	567	81.0	104,000
75,000	649	92.7	136,000
100,000	714	102	164,600
125,000	770	110	191,200
150,000	817	116.7	216,000
$C_p = 0.65$; $L/D = 7.0$; $L = 14.98\,\Delta^{1/3}$			
25,000	438	62.5	65,400
50,000	552	78.9	104,000
75,000	632	90.3	136,200
100,000	695	99.3	164,800
125,000	750	107.1	192,100
150,000	796	113.7	216,000
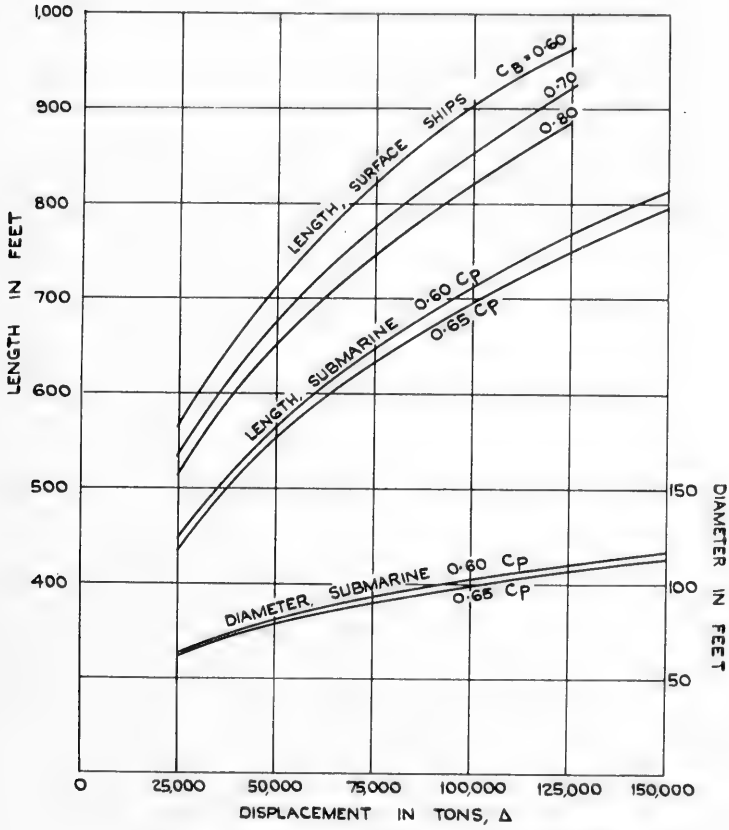
Fig. 1. Dimensions of surface ships and submarines
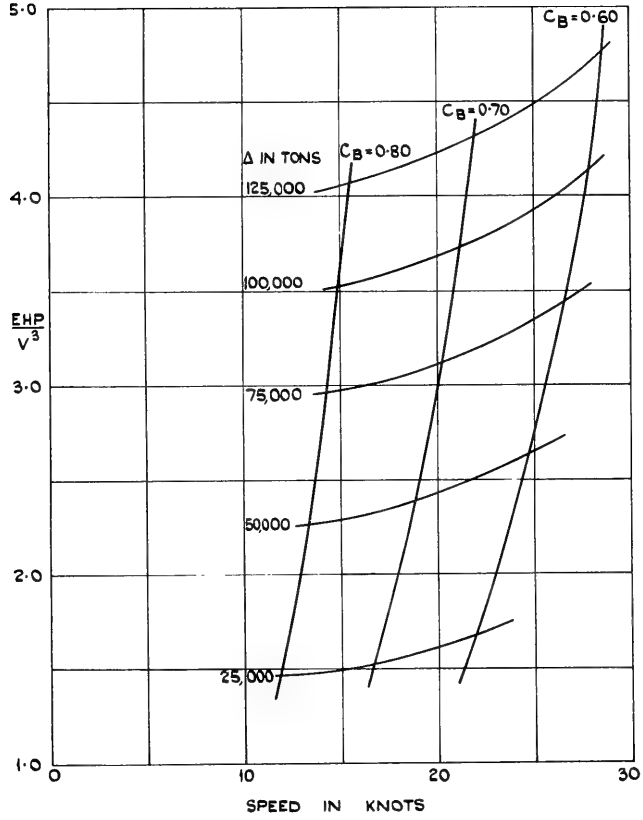
Fig. 2. EHP values for surface ships relative to speed

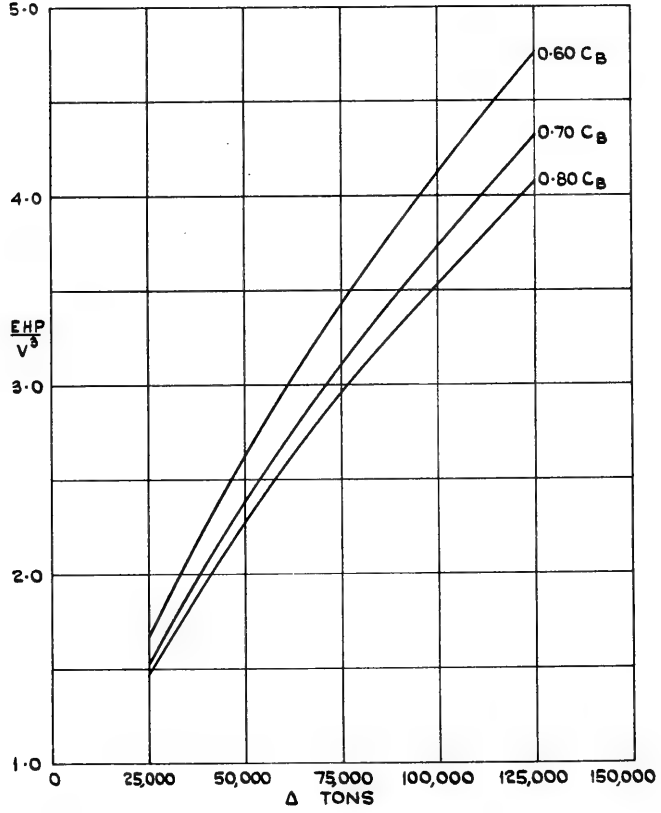Fig. 3. EHP values for submarines relative to speed

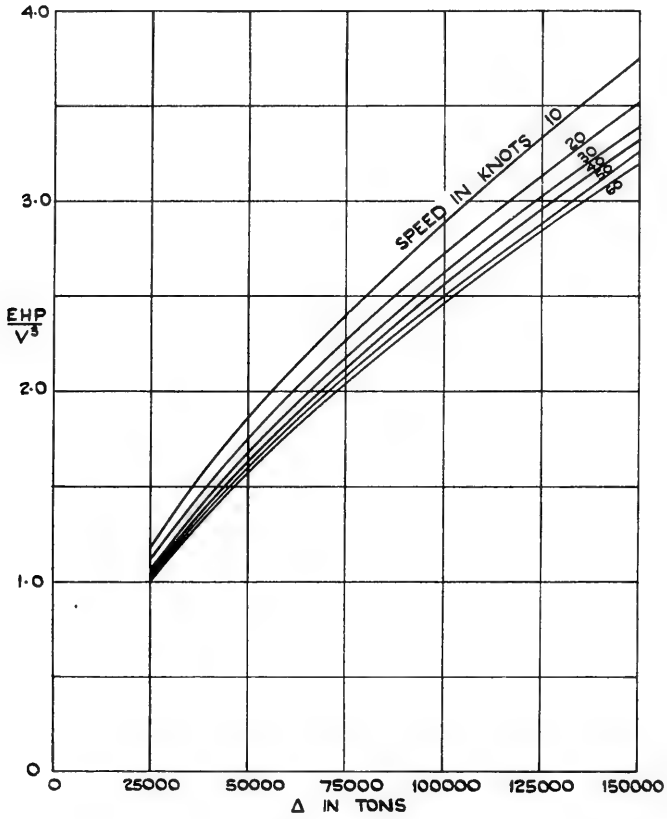Fig. 4. EHP values for surface ships relative to displacement
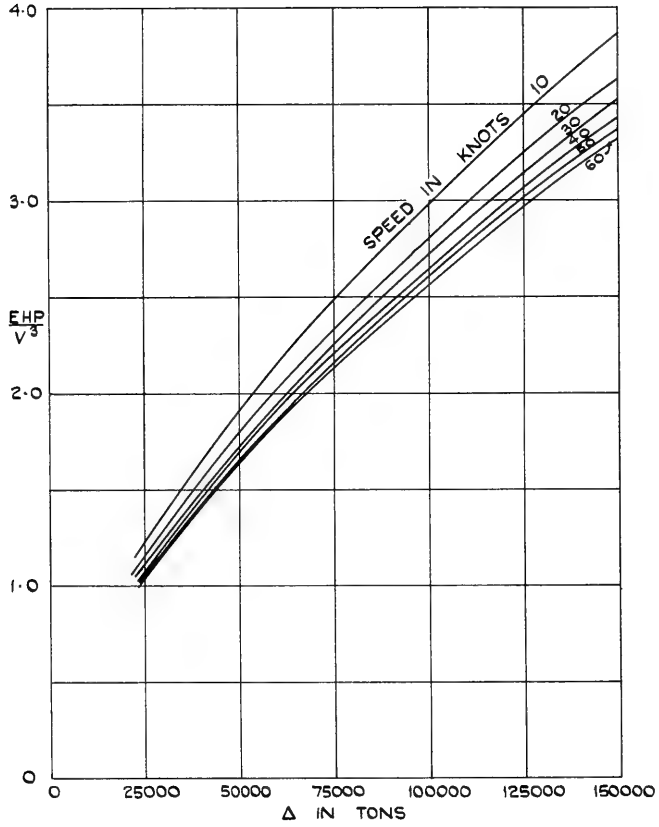
Fig. 5. EHP values for 0.60 C_p submarine

Fig. 6. EHP values for 0.65 C_p submarine

Table 3

EHP Values for Submarines with Circular Cross Section

(based on A.T.T.C. 1947 line + 0.0004)

V (knots)	EHP (for displacement in tons)*					
	25,000	50,000	75,000	100,000	125,000	150,000
$C_p = 0.60$						
10	1,194	1,870	2,407	2,885	3,335	3,748
20	8,960	14,000	18,120	21,700	25,080	28,180
30	29,040	45,500	58,920	70,530	81,480	91,540
40	67,400	105,100	135,900	163,500	188,900	212,200
50	128,800	201,800	261,500	312,200	360,500	407,300
60	220,100	342,800	443,200	533,246	615,800	691,600
$C_p = 0.65$						
10	1,236	1,920	2,498	2,985	3,450	3,865
20	9,260	14,430	18,750	22,400	26,000	29,130
30	30,200	47,000	61,000	73,300	85,000	95,120
40	69,800	109,000	141,500	169,000	196,000	219,500
50	134,000	208,700	271,000	325,000	377,000	422,000
60	227,600	356,500	462,000	552,000	640,500	717,000

* Figures below lines require DHP of more than 200,000.

Table 4
Comparison Between EHP Values for Surface Ships
Derived from NPL Data and Series 60

Δ (tons)	L_{BP} (ft)	B (ft)	d (ft)	C_B	$\dfrac{V}{\sqrt{L_{BP}}}$	V (knots)	EHP	
							NPL*	Series 60†
25,000	569	87.5	29.2	0.60	0.92	21.93	17,820	17,800
50,000	716	110.2	36.7			24.6	39,360	39,200
75,000	820	126.2	42.1			26.3	62,500	62,200
100,000	903	139.0	46.3			27.65	87,440	87,150
125,000	962	148.0	49.3			28.5	110,710	110,000
25,000	538	82.8	27.6	0.70	0.72	16.73	7,170	7,230
50,000	678	104.4	34.8			18.78	15,830	15,870
75,000	777	119.6	39.9			20.10	25,190	25,250
100,000	855	131.5	43.8			21.10	35,110	35,000
125,000	921	141.7	47.2			21.9	45,310	45,300
25,000	518	79.7	26.6	0.80	0.52	11.83	2,343	2,430
50,000	652	100.2	33.4			11.83	5,196	5,340
75,000	747	115.0	38.3			13.30	8.226	8.500
100,000	821	126.3	42.1			14.90	11,400	11,660
125,000	885	136.0	45.3			15.50	14,800	15,180

*Model results extrapolated by Froude frictional coefficients, no allowance.
† Model results extrapolated by A.T.T.C. 1947 line with an allowance $\Delta C_F = +0.0004$.

effects of this, estimates have also been made for submarines having elliptical cross sec-
tions in which the maximum beam was four times the maximum draft. For a circular-section
submarine the draft could also be decreased by an increase in the length/diameter ratio, but
this would involve a progressively greater increase in drag and also a considerable penalty
in the form of extra hull weight.

In order to convert the EHP values for the submarines to DHP, the same assumption as
for surface ships has been made regarding the range of powers for one-, two-, and four-screw
arrangements. The QPC has been assumed to be 0.80 for the single-screw designs and 0.67
for the twin- and quadruple-screw. The propulsive efficiency for the single-screw arrange-
ment has been taken somewhat higher than that for the corresponding surface ship because
of the better wake conditions attained behind the body of revolution form. For appendage
resistance, 20 percent has been allowed for the conning tower, rudders, stern and bow diving
planes, flooding holes, and similar items not present on a surface ship, a further 10 percent
for bossings or shaft brackets on the twin-screw ships, and 20 percent for the quadruple-
screw ships. These figures give total allowances of 20 percent, 30 percent, and 40 percent
for the one-, two-, and four-screw arrangements respectively.

The above figures for the submarine are based on the assumption that it is sufficiently
deeply immersed below the surface that there is no residual wavemaking. This means as a
rough guide that it is immersed to a depth of at least half its length or some 4 or 5 diam-
eters. The effects of depth of submersion have been investigated by model experiments in
the Saunders-Roe tank. Models representing an 80,000-ton-displacement submarine were
run at various depths below the surface from 100 to 300 feet and over a corresponding ship
speed range of 20 to 50 knots [3]. The values of the resistance for a length/diameter ratio
of 7 are shown in Table 5 and plotted in Fig. 7. There is certainly some depth effect still
in evidence at the deepest depth of submersion, namely 300 feet, as is shown by the in-
crease in resistance with speed at that depth. As the depth is decreased it is seen that the
increase in resistance for the lower speeds does not increase very rapidly until the depth
reaches something approaching 100 feet. For the higher speeds, however, the increase is
much more rapid and for 50 knots, for example, the increase between 300- and 100-foot sub-
mersion is no less than 200 percent. It is therefore evident that if we are to obtain the full
benefit from the elimination of wavemaking resistance any large submarine of this type must

Table 5

Effect of Depth of Submersion on Resistance
for a Submarine of 80,000-Ton Displacement, $L/D = 7$, and Maximum
Section 40 percent L from Nose (from Ref. 3)

Depth of Submersion (ft)	Speed (knots)						
	20	25	30	35	40	45	50
	Values* of $R/V^2 \times 10^{-4}$						
100	0.100	0.160	0.233	0.338	0.437	0.451	0.445
150	0.062	0.104	0.144	0.187	0.244	0.262	0.272
200	0.062	0.080	0.111	0.122	0.150	0.183	0.192
300	0.075	0.096	0.100	0.098	0.113	0.134	0.144

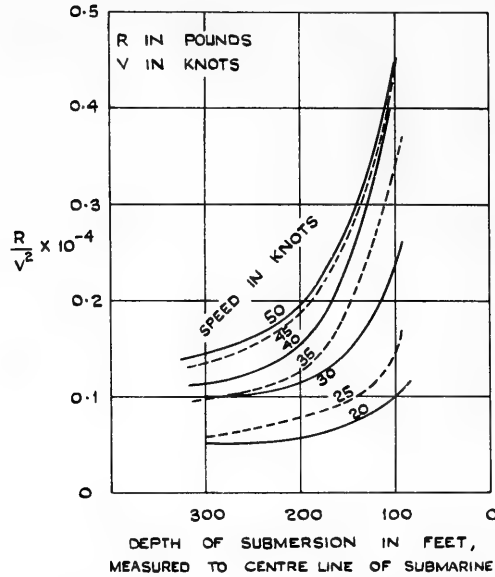*R = resistance in pounds; V = speed in knots.

Fig. 7. Effect of depth of submergence on a
submarine of 80,000-ton displacement, L/D
= 7.0 (from Ref. 3)

run at a considerable depth below the surface. From these same model experiments Mr. Crago
has shown that if the submarine is running in shallow water there can be a serious bottom
effect also. For the same submarine of 80,000-ton displacement, for example, at 50 knots in
water 300 feet deep, the resistance is some four times as great as in deep water when deeply
immersed. For a ship of this size this figure is somewhat academic, as no one could ever
contemplate driving such a ship at 50 knots in such a depth of water! But the results serve
to indicate the problems that are likely to be met with when a large submarine is approaching
shallow water on the continental shelf or when coming into estuaries. In fact, for a vessel of
this size we must revise our ideas of what we mean by shallow water.

Before leaving this question of resistance, it is worth while pointing out that in a sub-
marine of this type the resistance would be almost wholly frictional, and to obtain the full
benefit in power reduction it would be essential to keep the hull clean at all times, since
any penalty due to roughness and fouling would be considerably greater than in the corre-
sponding surface ship. This points to the need for frequent dockings, and as we shall see
when discussing the operation of such a ship, this poses considerable problems. For a ves-
sel of this type running deeply submerged in the comparatively calm conditions a long way
below the surface of the sea, it is interesting to consider the possibility of maintaining
laminar flow over the hull to a greater or lesser extent. The benefits to be derived from
such a possibility are, of course, great. For a submarine 650 feet in length with a dis-
placement of 75,000 tons running at a speed of 20 knots, the corresponding Reynolds number
is 1.7×10^9. The values of C_F for turbulent and laminar flow are 0.00144 and 0.00010
respectively, and if we assume that the laminar flow hull is *perfectly* smooth and omit the $\triangle C_F$
allowance of +0.0004 in this case, but add 20 percent in each for conning tower, etc., then
the ratio of total resistance for laminar and turbulent flow is 0.25. This is an ideal condi-
tion, of course, for a number of reasons. To encourage laminar flow over the hull, the shape

would have to be modified, in particular by moving the maximum diameter further aft, and this would increase the form drag. The hull would have to have certain fittings like conning tower, bow planes, flooding holes, anchors, etc., and no matter how these might be housed in recesses with covering doors, etc., they would inevitably act to some extent as turbulence stimulators, and the actual resistance would in fact be much nearer to the turbulent figure. While the idea of maintaining laminar flow is therefore extremely attractive, the practical difficulties of maintaining the requisite smoothness over the whole surface of a steel structure of this kind immersed in salt water and subject to all the effects of corrosion and fouling present almost insuperable difficulties. Of recent months other devices to maintain laminar flow have been suggested, such as the use of a soft skin of rubber with liquid backing which would damp out the onset of turbulence and so prevent transition. Not enough is yet known of these ideas to be able to express any real opinion about them but they would certainly be expensive both to fit and to maintain and, unless they were immune to surface deterioration and fouling, it seems would soon lose their efficiency.

COMPARISON OF SURFACE AND SUBMARINE SHIPS OF THE SAME DEADWEIGHT

A considerable number of papers has been written giving comparisons between conventionally propelled and nuclear propelled surface tankers. These have shown in general that the nuclear propelled tanker cannot yet compete economically with one having conventional machinery unless the capital cost of the nuclear plant and the cost of nuclear fuel become considerably less than their present values. This paper is not concerned with the relative merits of conventional and nuclear machinery, but since the submarine cargo ship or tanker can only be contemplated on the basis of nuclear propulsion, any comparisons made are on the basis of nuclear machinery for both ships. In this way the weight of the machinery will be comparable in both cases and will therefore affect the deadweight available equally in each case.

Several authors have given values of the deadweight/displacement ratio for nuclear propelled surface and submarine tankers, and values of this ratio are shown in Figure 8. Although there is considerable scatter in this diagram, it is considered that if we take a
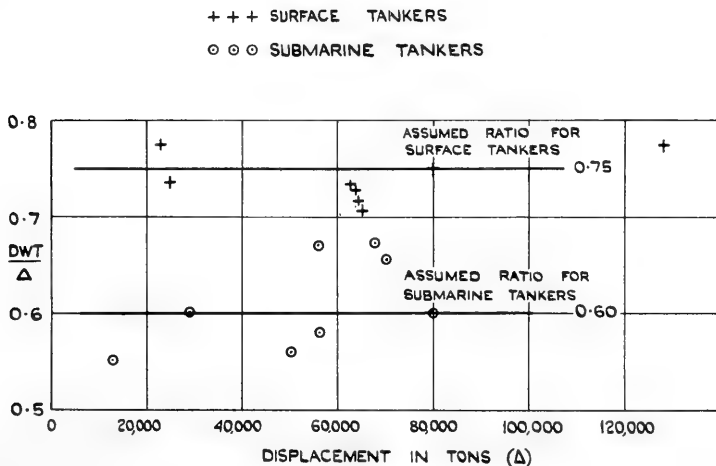

Fig. 8. Deadweight/displacement ratios

value of deadweight to displacement ratio equal to 0.60 for submarine tankers and 0.75 for surface tankers, a fair comparison between the two types would be obtained. A comparison between surface and submarine tankers is shown in Table 6 for ships having deadweights of 18,750, 56,250, and 93,750 tons. Using the appropriate deadweight/displacement coefficients from Fig. 8, the displacements have been calculated and the ship dimensions, EHPs, and DHPs have been taken from the curves obtained as described in the preceding section. The results for three of these cases are shown in Figs. 9, 10, and 11, where curves are given of DHP to a base of speed in knots for a surface tanker and two submarine tankers having respectively circular and elliptical sections. The submarine tanker throughout has a prismatic coefficient of 0.60. On the other hand, the block coefficient of the surface tanker has been varied to suit the speed/length ratio, being 0.80 at the lower end of the speed range and 0.60 at the top end. The figures for the surface tanker do not include any allowance for the effect of rough weather, and the following remarks therefore apply to smooth water conditions for the surface ships, and are favourable to them in this respect. Making the comparison in this way, however, enables certain other points to be brought out.

Looking first at the results for the circular section submarine and the surface tanker, we see that at the lowest speeds in question, namely 10 to 15 knots, there is practically no difference in the power requirements between these two types of ship. Since there is very little wavemaking in the case of the surface ship at these speeds we can infer from this that the reduction in form drag for the streamlined submarine as compared with that for the surface ship is sufficient to compensate for the increased frictional resistance of the submarine due to its augmented wetted surface. At higher speeds the circular section submarine tanker always requires less power. For vessels having a deadweight of 18,750 tons the difference in power is some 5000 on 25,000, and this is about the smallest ship for which a nuclear propulsion plant could be designed at present. For the largest ship having a deadweight of 93,750, which is comparable with the largest tankers built today, the power for the surface ship at 27 knots is some 190,000 and this is reduced to about 140,000 in the case of the circular submarine. It is also worth noting that there is no appreciable difference in power for these two designs up to a speed of 23 knots and to get the benefit from the submarine design one needs to go to higher speeds; however, at 27 knots the figures just quoted show that we are faced with a power plant comparable with those of the "Queens," and this of course would involve many problems regarding the housing of nuclear reactors, heat exchangers, etc., within reasonably sized containers for fitting in a submarine. When allowance is made for the effects of weather, the comparison would be much more favourable to the submarine, either from the point of view of the greater power and fuel consumption to maintain speed on the surface ship or from the loss in speed of the surface ship at the same power. Opinions as to the weather allowances necessary on different trade routes vary, but the tables and curves given here will enable anyone interested in this problem to make his own estimates in these matters for any desired weather conditions.

Curves are also shown in these three figures for a submarine of the same deadweight but having a beam equal to four times the draft. The only factor which has been taken into account in making the estimates for these elliptical section ships is the increase in wetted surface necessary to obtain the same volume within the elliptical section. Doubtless in such a design the displacement would have to be increased to a considerable extent to allow for the effect of the different shape of hull upon steel weight, and it is probable that the residuary resistance coefficient would also be considerably increased as compared with that for the circular section. For both these reasons, therefore, the power curves shown are likely to be an underestimate.

Teasdale has published similar curves for surface and submarine tankers, both nuclear propelled, having a deadweight of 45,600 tons including the weight of the reactor [4].

Table 6
Comparison of Tankers of Constant Deadweight*

Type of Tanker	Δ (tons)	C_B or C_p	L_{BP} or L (ft)	B (ft)	d (ft)	V (knots)	EHP§	No. of Screws	DHP
Deadweight = 18,750 tons									
Surface	25,000	0.60	569	87.5	29.2	21.93	17,800	1	24,730
Surface	25,000	0.70	538	82.8	27.6	16.73	7,230	1	10,050
Surface	25,000	0.80	518	79.7	26.6	11.83	2,430	1	3,380
Submarine									
Circular†	31,250	0.60	484	69.1	69.1	11.83	2,238	1	3,345
Circular	31,250	0.60	484	69.1	69.1	16.73	6,190	1	9,260
Circular	31,250	0.60	484	69.1	69.1	21.93	13,400	1	20,100
Elliptical‡	31,250	0.60	484	138.2	34.55	11.83	3,260	1	4,880
Elliptical	31,250	0.60	484	138.2	34.55	16.73	9,025	1	13,510
Elliptical	31,250	0.60	484	138.2	34.55	21.93	19,550	1	29,320
Circular†	31,250	0.65	472	67.4	67.4	11.83	2,288	1	3,420
Circular	31,250	0.65	472	67.4	67.4	16.73	6,315	1	9,530
Circular	31,250	0.65	472	67.4	67.4	21.93	13,900	1	20,860
Elliptical‡	31,250	0.65	472	134.8	33.7	11.83	3,336	1	4,990
Elliptical	31,250	0.65	472	134.8	33.7	16.73	9,300	1	13,900
Elliptical	31,250	0.65	472	134.8	33.7	21.93	20,280	1	30,400
Deadweight = 56,250 tons									
Surface	75,000	0.60	820	126.2	42.1	26.3	62,200	4	109,900
Surface	75,000	0.70	777	119.6	39.9	20.1	25,250	1	35,060
Surface	75,000	0.80	747	115.0	38.3	14.22	8,500	1	11,800
Submarine									
Circular†	93,750	0.60	698	99.7	99.7	14.22	7,765	1	11,650
Circular	93,750	0.60	698	99.7	99.7	20.1	21,200	1	31,800
Circular	93,750	0.60	698	99.7	99.7	26.3	46,200	4	96,600
Elliptical‡	93,750	0.60	698	199.4	49.85	14.22	11,300	1	17,000
Elliptical	93,750	0.60	698	199.4	49.85	20.1	30,950	2	60,000
Elliptical	93,750	0.60	698	199.4	49.85	26.3	67,500	4	141,000
Circular†	93,750	0.65	680	97.1	97.1	14.22	8,050	1	12,080
Circular	93,750	0.65	680	97.1	97.1	20.1	21,930	1	32,950
Circular	93,750	0.65	680	97.1	97.1	26.3	47,850	4	100,000
Elliptical‡	93,750	0.65	680	194.2	48.55	14.22	11,750	1	17,620
Elliptical	93,750	0.65	680	194.2	48.55	20.1	32,000	2	62,000
Elliptical	93,750	0.65	680	194.2	48.55	26.3	69,800	4	145,800
Deadweight = 93,750 tons									
Surface	125,000	0.60	962	148	49.3	28.5	110,000	4	194,000
Surface	125,000	0.70	921	141.7	47.2	21.9	45,300	2	73,300
Surface	125,000	0.80	885	136.0	45.3	15.5	15,180	1	21,080
Submarine									
Circular†	156,250	0.60	828	118.3	118.3	15.5	13,780	1	20,680
Circular	156,250	0.60	828	118.3	118.3	21.9	37,800	2	73,400
Circular	156,250	0.60	828	118.3	118.3	28.5	81,050	4	169,300
Elliptical‡	156,250	0.60	828	236.6	59.15	15.5	20,100	1	30,200
Elliptical	156,250	0.60	828	236.6	59.15	21.9	55,150	4	115,300
Elliptical	156,250	0.60	828	236.6	59.15	28.5	118,100	4	247,200
Circular†	156,250	0.65	807	115.3	115.3	15.5	14,230	1	21,380
Circular	156,250	0.65	807	115.3	115.3	21.9	38,900	2	75,500
Circular	156,250	0.65	807	115.3	115.3	28.5	83,600	4	175,000
Elliptical‡	156,250	0.65	807	230.6	57.65	15.5	20,800	1	31,200
Elliptical	156,250	0.65	807	230.6	57.65	21.9	56,800	4	118,700
Elliptical	156,250	0.65	807	230.6	57.65	28.5	122,000	4	255,200

* Deadweight/displacement ratio taken as 0.75 for surface tankers and 0.60 for submarine tankers.
† Streamlined body of revolution, circular sections, $L/D = 7.0$.
‡ Streamlined body, elliptical sections, $B/d = 4.0$.
§ EHP based on A.T.T.C. 1947 line plus 0.0004.
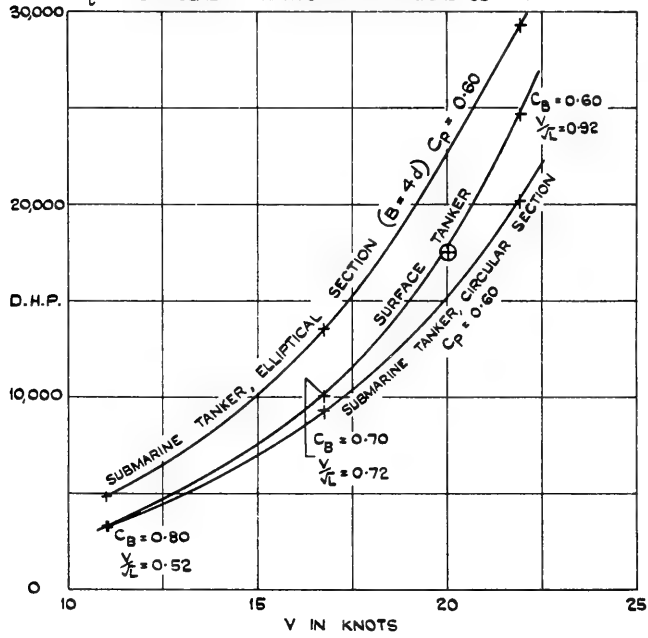
Fig. 9. Comparison of surface and submarine tankers of 18,750
tons deadweight

Fig. 10. Comparison of surface and submarine tankers of 56,250
tons deadweight
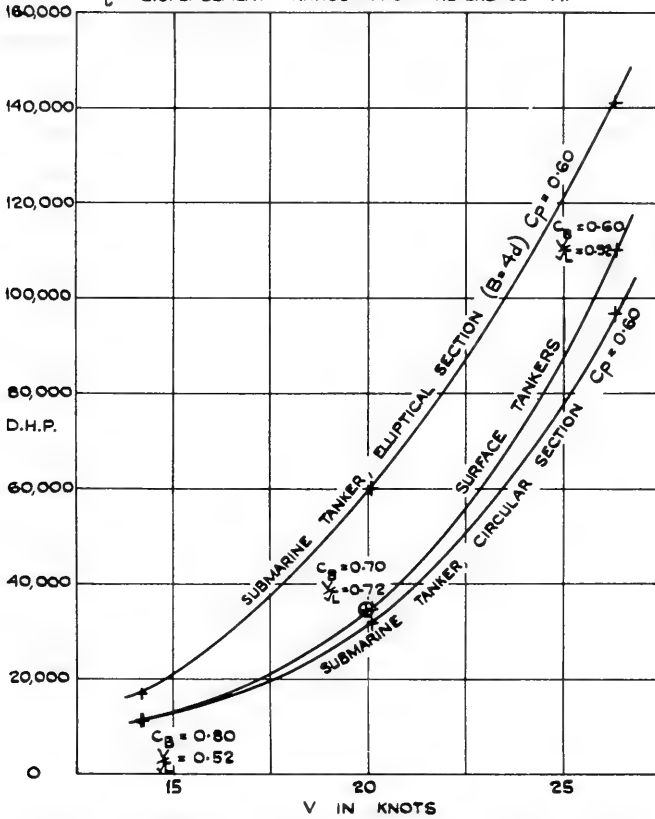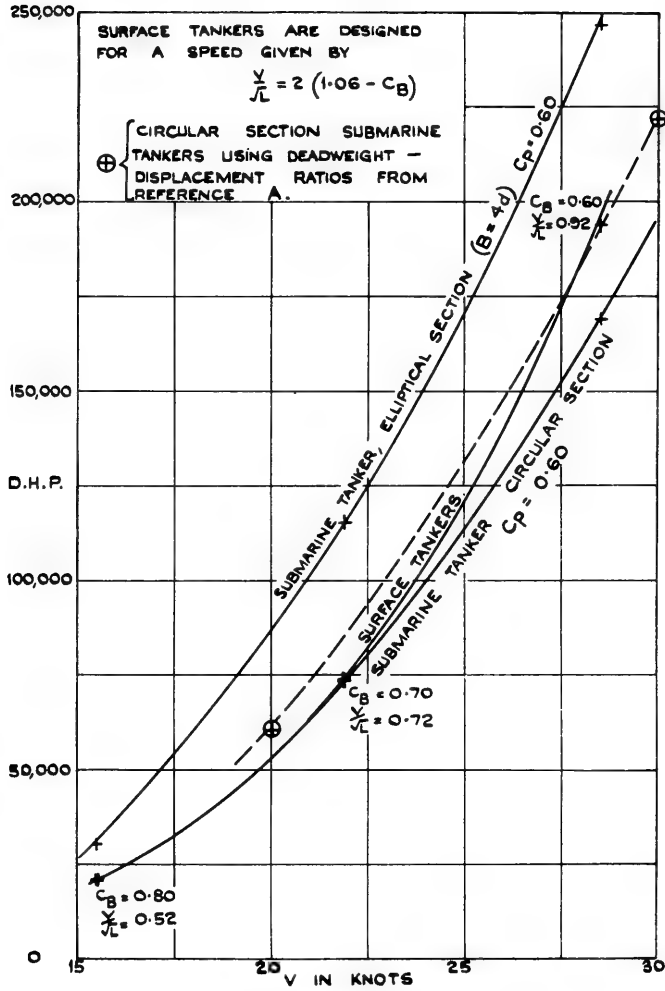
Fig. 11. Comparison of surface and submarine tankers of 93,750
tons deadweight

His power curves are reproduced in Fig. 12 and show the same general relationship between the circular and elliptical section submarines although the estimates are based on quite independent data. The principal difference between his curves and those shown in the present paper is that the power curve for the surface ship is considerably higher and much nearer to the elliptical submarine than to the circular one. This difference can be accounted for by the fact that Teasdale included a "normal" allowance for service conditions, in other words, for the effect of wind and rough seas.
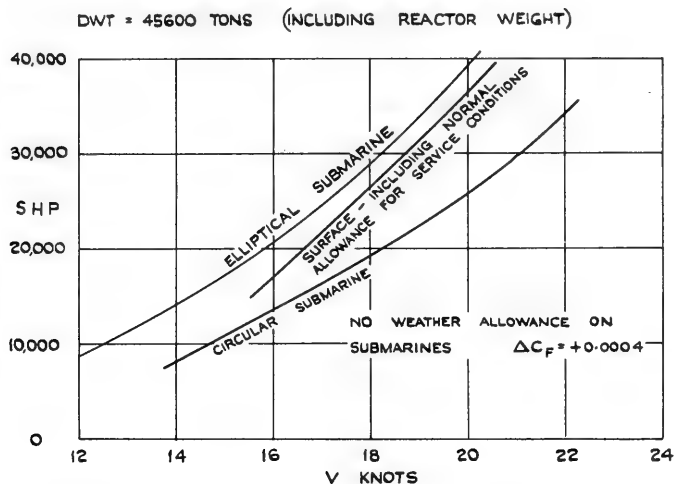
TYPE	SURFACE				SUBMARINES	
SHP	16,000	22,000	30,000	40,000	UP TO 40,000	
SHAPE	HULL FINED TO SUIT HIGHER SPEEDS				CIRCULAR	ELLIPTICAL
L FT	710	743	761	785	538	800
B FT	102·5	103·5	104·3	108·1	108	160
d FT SURFACED SUBMERGED	38·0	38·0	38·0	38·0	90 108	45 50
LOADED Δ TONS SURFACED SUBMERGED	62300	62950	63650	64490	67860 74650	69860 76860
WS SQ FT	110,000 AVERAGE				125070	204120
C_B	0·785	0·754	0·738	0·700		

Fig. 12. Comparison of nuclear propelled surface and submarine tankers (from Ref. 4)

OPERATING PROBLEMS

The strength of submarine cargo ships and problems of manoeuvrability are both extremely important factors in the design of such ships. The first is not strictly "hydrodynamic" and the second is to be discussed in another paper, so the present remarks will be confined to very general aspects of these two problems.

It has been said that in the case of submarine tankers carrying liquid cargoes of one sort or another, they need only have a central pressure hull containing the machinery,

living spaces, and buoyancy tanks, the external cargo spaces being of very light construc-
tion since the liquid pressures inside and outside could be equalised. It has been claimed
in fact in a study conducted in Japan that this could result in an actual reduction in steel
weight. But can we indeed accept this conception? There is always the possibility of a
power failure or other mishap which would force the ship to surface at sea and possibly in
bad weather, and it would seem that under these conditions the submarine would need to
possess longitudinal strength comparable with that of any surface ship. This would seem a
hazard particularly to be catered for in any pioneer submarine tankers, because in these
early ships there will doubtless be many precautions taken to ensure a shutdown of the
reactor in the event of any unforeseen or unacceptable faults in the equipment. It may even
be that a shutdown could follow a mere fault in the controlling instrumentation. Moreover,
with the very large draft of such a vessel, she may in many cases have to load or unload at
a deep water terminal in a relatively exposed position where the conditions of the sea may
be quite rough as compared with those normally existing in harbour. Also in approaching
port when the water depth becomes less than some 400 or 500 feet such a submarine would
undoubtedly have to surface and do the last part of the journey as a surface ship and
therefore subject to the effects of rough weather. Taking all these possibilities into
account, it seems extremely doubtful whether the conception of a very light structural hull
for submarine tankers would be acceptable, at least until considerable experience had been
gained in their operation. For a cargo ship there is no question but that a pressure hull
would be necessary throughout. The Mitchell Engineering Company have carried out an
investigation into such a cargo submarine and have come to the conclusion that the hull
would need to be made of mild steel up to 3 1/2 inches in thickness amidships in way of
the machinery and compensating tanks, and vary down to 1 inch in thickness toward the
end. On this basis they estimated the deadweight/displacement ratio to be 0.56 for an
ore-carrying submarine of 50,000-ton displacement [5]. There are many other problems
involved in the construction of a hull of such dimensions. As has already been pointed out
when discussing the resistance qualities of different designs, the circular hull submarine
leads to very large drafts such as could not be catered for by any existing docks or terminal
ports. On the other hand, the circular hull is the only economical one from a structural
point of view and any departure from exact circularity will mean the provision of extra stiff-
ness and greater thickness of plating [6]. Although liquid cargoes could be handled very
easily from a submarine, other types of cargo could be very awkward in their demands for
large hatches which would have to be pressure resisting and which would, in fact, form
another weakness in the strength qualities of the hull. It is probable from a strength point
of view that the only reasonable cargoes would be bulk ones such as iron ore or similar
high-density materials.

Two of the most important qualities in such a ship would be its directional stability
and controllability. If we consider a submarine some 800 feet in length travelling at an
immersion of 400 feet and built to resist pressures up to twice this depth, we are asking
the crew virtually to fly the vessel in an atmosphere whose depth is only equal to the
length of the submarine. This would probably give any air pilot nightmares! Since in
order to compete commercially on a power basis with the surface ship the submarine would
also have to travel at some 30 knots or more, it is easy to see how by the accidental
occurrence of even a moderate trim by the bow the ship could very soon exceed her safe
diving depth. The question of providing adequate directional stability and controllability
is therefore a paramount one in the whole design.

In order to obtain adequate transverse and longitudinal stability, it will be necessary
for the submarine to carry permanent ballast, as is done in military craft. It is also impera-
tive to have some surplus buoyancy when on the surface, and in any commercially operated
craft the amount of such reserve buoyancy would almost certainly be controlled by

legislation. It is probable that these two items together would amount to not less than 25 percent of the displacement. Although such a vessel would not have to carry bunkers, there would be little if any saving of weight in this respect since the shielding for the reactor would be of the same order of magnitude. All these considerations add up to the fact that a submarine cargo ship or tanker would require considerably greater displacement than a surface ship to carry the same deadweight.

Any nuclear propelled ship will call for a much greater skill in the engine room crew than does a conventionally powered ship. If in addition the nuclear propelled ship is also a submarine, then the navigating crew must also be very highly skilled and undergo long periods of training comparable with those of similar navy crews. The additional cost of this skill could be considerable and may be an important factor in the overall comparison.

At least in the single-screw designs it will be necessary to have some means of auxiliary propulsion such as motors and batteries or diesel engines for use on the surface in an emergency. If a single-screw submarine were designed for use under ice, it would seem almost essential to have electrical auxiliary propulsion since in these circumstances it would be impossible to bring the ship to the surface until she was clear of the ice. In the case of a twin-screw ship with two entirely separate propulsion plants, auxiliary propulsion could probably be dispensed with.

Considering in more detail the operation of the circular and elliptical submarines and the surface ships for which the estimates of power are shown in Figs. 9, 10, and 11, we see that the circular section submarine requires a lower power than either the surface ship or the elliptical submarine. However, we see that the advantage is not large unless we contemplate speeds of 25 or 30 knots and it is a question of the economics of the oil industry whether it is justifiable to carry a commodity such as oil or indeed any other nonperishable bulk cargo at such high speeds. It is not proposed here to enter into these economic questions, but it may be sufficient to point out that these will vary from time to time, as witnessed by the fact that during the Suez crisis the cost of transporting oil via the Cape rose to £19 per ton as compared with the normal freight rate of £2 per ton via Suez. In addition, it has been estimated that the capital cost of a submarine tanker would be of the order of twice that of the equivalent surface ship [7,8]. It would appear, therefore, that the advantages from a commercial point of view would not be large enough at commercial speeds to counteract the increased capital cost of the submarine and the increased costs of maintenance, crew, insurance, and the large expenditure which would be necessary for research and development before such a ship could be built. Beyond these operational problems is the further one that a circular hull submarine large enough to justify nuclear propulsion and competition with similar surface ships would have a very large draft and would require new building facilities, new dry-docking facilities, and new terminals. It would also be very limited in respect of the world ports in which it could be accommodated and would certainly not be able to pass through the Suez or Panama Canals for many years to come. If such a ship to carry oil from the Middle East to Europe had to go via the Cape, then this would far outweigh any advantages it might have in regard to lower power requirements.

If we restrict the draft of the submarine to a figure comparable with that of the equivalent surface tanker, then we are forced into accepting a submarine having elliptical sections. As an extreme case the figures have been calculated for such submarines of different deadweights having a beam/draft ratio of 4:1 and the power curves for these have been given in Figs. 9, 10, and 11. It is at once seen that from a power point of view, even after making some weather allowance for the surface ship, there is no longer any overall benefit to be derived on the basis of power. If the thesis is accepted that for a submarine tanker the structure carrying the oil can be of light scantlings, then there would not be a very great

penalty on weight in going to the elliptical section. However, in a cargo-carrying submarine
or a tanker in which the whole hull was built to resist pressure, then there would be a very
substantial penalty in weight through such a change in shape. The comparison between the
submarine and the surface ship is therefore seen to be more unfavourable to the submarine
when we consider a hull with elliptical sections.

The outcome of this whole discussion points to the fact that from a commercial point of
view there is little attraction in submarine cargo ships or tankers so long as we restrict our
thoughts to speeds within the limits for which economic surface vessels can be designed.
However, if we wish to go beyond these speeds, then the submarine would be the only
answer for the carriage of bulk cargoes. For lighter specialised cargoes, it may well be that
the answer is to go the other way and use hydrofoil craft. If submarine ships were justified
by a sufficient demand for the transport of bulk cargoes at such high speeds, the figures that
have been given for the powers required, even when we are not compelled to make provision
for surface wavemaking and rough weather, still mount rapidly and very soon attain astro-
nomical proportions. In Table 3 a line has been drawn showing where the power required
exceeds 200,000 DHP, which means a propelling installation of the same order of magnitude
as that of the QUEEN ELIZABETH, and of course to house any such nuclear plant in a sub-
marine would be quite a task. The containing vessel for the 20,000-shaft-horsepower nuclear
plant for the American cargo ship SAVANNAH is 50 feet long and 35 feet in diameter, and
one can imagine that with 200,000 horsepower together with the space required for perma-
nent ballast, trimming tanks, buoyancy tanks, living quarters, and so on, the deadweight/
displacement ratio would be rather small.

From time to time it has been suggested that a smaller tanker of the nuclear propelled
submarine type might be competitive with a much larger surface tanker. Such a comparison
has been made by Teasdale [4] between a 47,000-ton-deadweight surface tanker and a
26,000-ton-deadweight submarine tanker of circular cross section and having dimensions
which do not exceed those of the surface ship. He estimated that if the submarine were
travelling at a high enough speed to deliver the same quantity of oil per year as the surface
tanker, the fuel consumption would be about four times as great. From his analysis he
doubted whether the capital cost of the submarine would be sufficiently less than that of
the surface ship to offset such a penalty.

TERMINAL PROBLEMS

The draft of water in many ports and harbours today does not exceed 35 feet and in
very few does it exceed 50 feet. This would impose many problems on the building and sub-
sequent dry-docking of submarines of the size we have been discussing. The draft problem
could be overcome by going to an elliptical section shape for the hull, but this would give a
submarine of excessive beam for most dry docks and would also bring in the other problems
which we have mentioned in the previous section. For the ordinary routine loading and
unloading processes, it would be necessary to build offshore loading terminals or use feeder
services to bring the oil in to the refineries. This would mean that the ship might be sub-
ject to rough weather and therefore would have to be designed with normal longitudinal
strength and not be able to have a light scantling outer structure. Another point of some
interest for such large ships approaching the shore is the fact that once the depth of water
was reduced much below 600 feet they would have to surface and do the last part of their
journey as surface ships. To achieve the high efficiency of underwater propulsion which
has been the aim of all these designs it is necessary to go to a streamlined body of revolu-
tion with the very minimum of appendages. However, when such a vessel has to come to

the surface it has about the worst possible shape for good performance. The maximum speed under these conditions would probably be quite low, and if the approach to the terminal ports runs for long distances over a continental shelf or similar shallow water, this could add appreciably to the time of passage and so offset to some extent the better submerged performance. Such a large craft would be exceedingly difficult to manoeuvre in shallow water, and would be quite unwieldy at the terminals, and especially if made of light scantlings would be liable to serious damage and during berthing operations would need the assistance of tugs. In common with nuclear propelled surface ships, it would also be necessary for the port authorities to monitor continually for radioactivity and to maintain the equivalent of a fire-fighting service to give warning and to cope with any such accident. Even voyages under ice can be fraught with considerable dangers other than those of navigation. According to information resulting from the voyage of the NAUTILUS, the ice over the North Pole is some 9 to 13 feet in thickness but with occasional ridges penetrating some 100 feet below this. In addition, from time to time icebergs were met with which were imprisoned in the surface ice and reached no less than 1000 feet below the surface. The use of a polar route into the Pacific is also subject to the limitation that water in the Bering Straits is only some 150 feet in depth. It is obvious that extremely careful navigation would be called for to cope with such hazards.

CONCLUSIONS

The general conclusion which can be drawn from all the above evidence is that submarine cargo ships and tankers of circular cross section could be designed to compete with surface ships of the same deadweight as regards their power requirements, especially when one takes into consideration the effects of rough weather, from which the submarine would be immune. Such submarine ships would have excessive drafts, however, and if this is avoided by using elliptical sections, then the submarine's superiority soon disappears. However, up to such speeds as those for which an economical surface ship can be designed, say of the order of 25 to 30 knots, the capital cost of the submarine, of the necessary docking facilities, and of the provision of offshore terminals could not at present be justified on economic grounds. At the very least it would be necessary for a consortium of owners to combine in the building of terminals and dry docks for common use before a fleet of such submarines was put into service. At higher speeds, above 30 knots, the submarine begins to have very appreciable advantages as regards power, but of course at these high speeds the price to be paid in terms of fuel consumption is also high and the propelling machinery would begin to take up more and more of the volume of the ship, thus reducing her deadweight. Whether such ships would be a good financial proposition or not would depend on the interplay of capital cost, insurance, maintenance, fuel and operating costs, the freight rate obtainable for oil or other bulk cargoes, and the route on which the ship is employed. If this were between the Middle East and the United Kingdom, for example, a submarine tanker of circular section of anything greater than about 25,000 tons deadweight would be unable to use the Suez Canal in its present form. The economic advantages of large size in the carriage of bulk cargoes could therefore only be realised in this trade so far as submarine tankers are concerned by routing them around the Cape, with all the attendant disadvantages. These would not, of course, enter into other routes, such as Venezuela to Europe. The first marine nuclear propulsion plants will certainly be expensive, but the ingenuity of the engineer will undoubtedly reduce these as time goes on. Nuclear fuel costs, which at present are perhaps twice those of conventional fuels will also come down in the course of time and with the more widespread use of atomic energy in other fields.

So far we have restricted ourselves to a comparison between nuclear propelled surface and submarine ships. The case for the submarine would be even less favourable at this time if we were to compare it with a conventionally propelled surface tanker. The British Shipbuilding Research Association has compared surface tankers having respectively conventional and nuclear propulsion plants and has shown that even on the assumption of economic parity between capital and fuel costs there is no commercial attraction in installing in a surface tanker a nuclear plant of higher power than the conventional ones being installed at present [9]. It has also been shown, in the case of a tanker of 65,000 tons deadweight with 25,000 shaft horsepower employed on the Middle East-United Kingdom route, that while the cost per ton of transporting oil via the nuclear ship might be within 15 percent of that for the conventional ship, the cost for the nuclear ship begins to rise again at speeds above 17 knots [10]. This means that from the point of view of economy there is really no inducement to fit higher powers in nuclear ships than are at present fitted in conventional ships. The greatest commercial incentive for submarine ships at the moment would appear to be their use on special routes where surface ships cannot be used and on which there might be the attraction of making special profits. One such route which has been mentioned on many occasions is that from Canadian ports carrying out ore in winter underneath the ice, and another has been the suggestion put forward in the London Times that by going under the polar ice it is possible to halve the distance between London and Tokyo [8].

Leaving aside economic questions, there is no doubt as to the extreme advantage of having such craft for military use and for the transport of valuable cargoes in wartime. It may well be that some government will build a craft of this type very soon, both for its military potential and national prestige, and to gain experience in the operation of such ships. Something of the magnitude of the tasks facing the designer of such submarine cargo carriers as we have been discussing may be realised when it is recalled that the largest submarine built to date is the USS TRITON, which has a length of 447 feet, a displacement of 5900 tons, and two nuclear reactors. This is the longest and most powerful submarine yet built and it is a very long way to go from this to tankers of the order of 60,000 or 80,000 tons. Although the tasks are formidable, there is no doubt as to the challenge they present and the extreme interest which they engender in the mind of the designer. Using a completely submerged hull of ideal form, the propeller designer is presented with wonderful opportunities of realising his ideal propeller — a circumferentially uniform wake, the chance to apply impeller theory to marine problems, and the knowledge that at such deep depths cavitation will no longer be a paramount inhibitor always looking over his shoulder. To the hull designer, the challenge will be to eliminate all possible sources of parasite drag by attention to hull form, appendages, and smoothness of surface and to ensure adequate directional stability and control, while tantalisingly in the offing will be the lure of someday, somehow, achieving laminar flow over some of the hull surface. Inevitably progress will be made only by small steps, and the development of a successful submarine cargo ship or tanker will involve many years of research and development and much money. From the scientific and technical point of view, such a vessel presents a great challenge to the naval architect and marine engineer, who will doubtless continue to dream of the possible solutions until the day comes when they are given the opportunity to translate their ideas into reality.

ACKNOWLEDGMENTS

REFERENCES

[1] Crewe, P.R., "The Hydrofoil Boat; Its History and Future Prospects," Instn. Naval Architects Trans. 100:329 (1958)

[2] Todd, F.H., Stuntz, G.R., and Pien, P.C., "Series 60 – The Effect upon Resistance and Power of Variation in Ship Proportions," Soc. Naval Architects Marine Engrs. Trans. 65:445 (1957)

[3] Crago, W.A., "Test Results on Submarine Tankers," Impulse, No. 4, Mar. 1958

[4] Teasdale, J.A., "Characteristics and Performance of Nuclear-Powered Submarine Cargo Vessels," North East Coast Instn. of Engrs. and Shipbldrs. 57:461 (1958-59)

[5] Mitchell Engineering Co., "Nuclear-Powered Submarine 'Moby Dick'," 1960

[6] McKee, A.I., "Recent Submarine Design Practices and Problems," Soc. Naval Architects Marine Engrs., paper 11 for meeting Nov. 12-13, 1959

[7] Article on submarine tankers, Journal of Commerce, Jan. 17, 1957

[8] Shipping Correspondent, "Undersea Voyages," The London Times, Aug. 13, 1958

[9] Smith, S.L., and Richards, J.E., "Nuclear Power for the Propulsion of Merchant Ships," Instn. Engrs. Shipbldrs. in Scotland 100(pt7):698 (1957)

[10] Norton, E., "Future Trends in Marine Engineering," Shipbuilding and Shipping Record, International Design and Equipment Number, 1958

DISCUSSION

R. N. Newton (Admiralty Experiment Works)

We should all be grateful to Dr. Todd for presenting what seems to me to constitute the most comprehensive review of this popular topic, to date. He has dealt with almost every aspect of the general problem and I would like merely to place more emphasis on some of the points which he has made and which militate against the opinion, frequently expressed, that submarine tankers offer great advantages in the commercial field.

In that part of his paper which compares the two types of tanker on the basis of the same deadweight, Dr. Todd assumes, from data provided by other authors, a ratio of dead-weight to displacement in a nuclear propelled submarine of 0.6 (see Fig. 8). With this value of 0.6 the DHP curves of the circular sectioned submarine tanker in Figs. 9, 10, and 11 lie below those of the surface tanker at all speeds worth considering. The crossover points beyond which the submarine tanker has the advantage over the surface tanker are 11, 14, and 22 knots for equal deadweights of 18,750, 56,250, and 93,750 tons respectively. This paints a rather rosy picture for the submarine, but if the ratio of deadweight to dis-placement for the submarine tanker is less than 0.6, a very different picture would be obtained. It is not clear from the paper how the authors concerned arrived at their figures for this ratio, but it is significant to remark that the values indicated in Fig. 8 show a much wider scatter than those for surface tankers. Immediately I notice that Dr. Van Manen gave in his paper a figure of 0.41 for a 100,000-ton tanker and 0.50 for a 43,000-ton tanker. There is only one way to arrive at a realistic figure, viz., by carrying out a detailed design, and, speaking with some experience in the design of military submarines, I venture to suggest that a more realistic figure would be nearer to 0.5 than 0.6, for several reasons. The most important of these is the inherently unsuitable shape of the pressure hull to accommodate machinery and equipment with a degree of compactness consistent with good maintenance such as is possible in a surface ship. Others include the weight and space necessary for additional ship services such as trimming and compensating systems, special air-condition-ing apparatus, three sets of control gear (two hydroplane gears and one rudder gear), addi-tional navigational and operational aids, and the fact that many of the ship services must be designed to much greater pressures than in the case of a surface ship. The effect of a lower deadweight/displacement ratio would be to raise the submarine curves in Figs. 9, 10, and 11 and to greatly increase the speeds at which the submarine gains the advantage over the surface tanker to such values as to raise grave doubts as to whether the machinery to drive the vessel at such speeds could be accommodated. In the case of the 56,250-ton tanker in Fig. 10, for instance, if a deadweight/displacement ratio of 0.5 were used the crossover point would rise to the region of 27 knots and the DHP required to 118,000.

Immediately the question arises "could the machinery and propellers to provide this power be accommodated in any reasonable size of pressure hull to suit other requirements?" I am strongly of the opinion that it could not. If this opinion is correct, it follows that, if for any reason a submerged tanker of such size became necessary, then with the present means of propulsion and types of fuel it would be necessary to accept a very heavy loss in dead-weight ratio compared with a surface tanker.

Against this, however, must be weighed the distinct advantage of being able to operate with impunity in any weather except when approaching the terminal points of the voyage, as pointed out by Dr. Todd.

In the section of the paper dealing with operating problems, Dr. Todd has called briefly, but very effectively, to the need to take account of dynamic stability and control when submerged. Even with the comparatively small military submarines now being built, the problems involved are both complex and numerous. Compared with the submarines of the last war, underwater speeds have doubled and trebled. The speed beyond which the submerged tanker begins to gain over the surface ship is in this region. Consequently the time available to the commanding officer, and to whatever control apparatus with which the submarine is equipped, to take corrective action is very much shorter — not more than one-third of that in an orthodox submarine of the last war.

Fortunately much has been learned regarding the dynamic stability and control of normal sized submarines. By the application of theory and model experiments correlated to

the results of full scale trials, it is now possible to determine stability criteria and to design and use automatic control systems to suit the stability and the response of the submarine. For such large submerged tankers as those under discussion similar investigations would have to be carried out and would, in fact, be vital since the margin of safety involved in terms of time and the depth range is obviously much smaller.

On the question of structural design it is fair to state that the unpressurized structure which may contain liquid cargo offers no insuperable design or constructional difficulties, but, as Dr. Todd points out, it is indeed a grave assumption that it could be of light scantling. On the other hand the problem of designing the pressure hull and the consequences which could result from the application of incorrect principles are much more serious. Sudden collapse of the hull can arise from elastic failure of the structure or plastic failure of the material, so that the problem involves not only the theory to avoid one or both of these but also the development of special steels. This development work becomes more and more difficult as the thickness of the steel increases, i.e., as the size of the pressure hull increases. Construction of the pressure hull is a highly specialized technique. Not only must the hull be built to a small degree of ovality, or "out of circularity," but it is necessary to employ highly specialized welding techniques. Local weaknesses brought about by poor design or bad workmanship introduce a danger factor since they could lead to early local failure and sudden collapse of the hull.

Merely to emphasize the vital nature of these two problems of stability and strength let us take Dr. Todd's example of a submerged tanker 800 feet long with a pressure hull say 600 feet long and a collapse depth 800 feet. Let us also suppose, as he does, that the tanker is proceeding at about 30 knots at 400 feet depth in order to gain the advantage of not generating waves, and then let us suppose that for some unforeseen reason it takes on a bow-down angle of 10 degrees for just 40 seconds. In that short space of time the fore end of the pressure hull would have exceeded the collapse depth and complete disaster would follow. It is as well to stress that this is by no means a hypothetical case but a real possibility.

It is for such reasons as those which I have attempted to emphasize, and many others which Dr. Todd has mentioned, that I incline to the opinion that, although the possibilities of submarine tankers as cargo vessels for commercial use present a great challenge to the naval architect and marine engineer, there are many equally challenging and important aspects of surface ship propulsion which require our immediate and undivided attention in the near future. Not the least of these is the design and construction of hull forms capable of maintaining higher speeds in rough weather.

F. H. Todd

Mr. Newton rightly points out that the relative merits of the surface and submarine tankers in the matter of power depend very greatly upon the values assumed for the ratio of deadweight to displacement, and stresses that only detailed design calculations can give reliable guidance on this point. At the time of writing this paper, no such data appeared to be extant, but recently the results of such detailed weight estimates have been published in the U.S. by Russo, Turner, and Wood.* Detailed designs have been made for a number of submarine tankers with nuclear machinery having streamlined, body-of-revolution hulls, with

---

* Vito L. Russo, H. Turner, and Frank W. Wood, "Submarine Tankers," Society of Naval Architects and Marine Engineers, New York, Nov. 1960.

and without parallel body, and rectangular hulls having rounded corners. The deadweight/displacement ratios depend upon the size of the ship and its speed, and some representative figures taken from the reference are given in Table D1, as they are of general interest.

Table D1
Deadweight/Displacement Ratios (from Russo, Turner, and Wood)

Speed (knots)	Section	Parallel (%)	Length (ft)	Beam (ft)	Depth (ft)	Dwt. to Surf. Displ.	SHP	Power Increase for Rect. Section (%)
Deadweight = 20,000 tons								
20	Circle	0	525	75.5	75.5	0.546	16,900	—
20	Rect.	59.5	555	80	40	0.527	27,400	62
30	Circle	0	560	79.0	79.0	0.467	68,600	—
30	Rect.	58	570	90	40	0.460	95,400	40
Deadweight = 30,000 tons								
20	Circle	0	600	85.5	85.5	0.559	22,100	—
20	Rect.	60.8	650	100	40	0.536	38,900	76
30	Circle	0	625	89.5	89.5	0.490	87,200	—
30	Rect.	55.5	625	120	40	0.478	128,000	47
Deadweight = 40,000 tons								
20	Circle	0	660	93.5	93.5	0.566	26,800	—
20	Rect.	60.6	710	120	40	0.546	48,400	80
30	Circle	0	680	98.0	98.0	0.500	104,400	—
30	Rect.	64.1	780	120	40	0.489	152,000	45

For the tankers having circular sections the ratio at 20 knots varies from 0.546 at 20,000 tons deadweight to 0.566 for 40,000 tons. At 30 knots the corresponding figures are 0.467 and 0.500. These ratios are referred to surface displacement. If we convert them to submerged displacement, which is the one used in my paper, the values become 0.496, 0.515, 0.425, and 0.455 respectively. These values are all appreciably less than the figure of 0.60 used in the original power estimates. The latter have therefore been revised, using the new deadweight/displacement figures as derived above, but otherwise they are upon exactly the same basis as the earlier estimates. The calculated powers are shown in Table D2 and the appropriate spots have been added to Figs. 9, 10, and 11. For the smallest tanker, of 18,750 tons deadweight, the circular-hulled submarine now requires exactly the same power as the surface tanker at 20 knots, so that the crossover point (for smooth water operation) has been raised from about 11 knots to 20 knots. The same applies to the intermediate 56,250-ton-deadweight tanker, the crossover rising from 14 knots to 20 knots. For the largest ship, of 93,750-ton deadweight, the submarine tanker does not become less resistful than the surface ship (in smooth water) until the speed is some 28 knots.

These figures substantially agree with those suggested by Mr. Newton. I was aware at the time of writing the paper that the assumed value of 0.6 for the deadweight/displacement ratio was probably high, especially as many of the examples originated from the protagonists

of the submarine cargo ship. Indeed, in an earlier paper* I had used a value of 0.5, but felt it necessary to err on the side of optimism rather than to run the risk of being charged with pessimism and lack of foresight! This comparison is for circular-hulled submarines, which, of course, suffer from the extreme drafts noted in the paper. In the American paper referred to, power requirements are also given for rectangular section submarines, some of which are shown in Table D1. While this type of section enables the draft to be kept within reasonable bounds (not greater than 40 feet for 40,000 tons deadweight) the price to be paid in power is very considerable, varying from 60 to 80 percent increase at 20 knots and 40 to 50 percent at 30 knots. These powers are higher than those given in my paper for elliptical sections, but, of course, they have the advantage of less beam. With limitations on beam, draft, or both, forcing us to adopt elliptical or rectangular sections, it is obvious that the commercial merits of the submarine tanker as compared with those of her surface sister will be hard to find, even when allowance is made for rough sea effects upon the surface ship, as long as there is no demand for the high speed (and therefore high cost) transport of bulk cargoes across the oceans.

In view of Mr. Newton's experience in submarine design problems, his remarks on the difficulties inherent in providing adequate strength in such large submarines will be of great value to all interested in this subject, and we are indebted to him for his penetrating analysis of the problem.

Table D2
Power Calculations for Submarine Tankers
(Body of Revolution Hull, No Parallel Body, C_p = 0.60, L/D = 7.0)

Deadweight (tons)	18,750		56,250		93,750	
Speed (knots)	20	30	20	30	20	30
Dwt./Submerged $\triangle$	0.50	0.425	0.515	0.455	0.530	0.485
Submerged $\triangle$ (tons)	37,500	44,100	109,500	124,000	177,000	193,500
Length (feet)	513	543	735	766	862	887
Diameter (feet)	73.3	77.6	105.0	109.4	123.1	126.7
E.H.P., naked	11,680	41,580	23,040	81,000	31,040	106,110
Number of propellers	1	2	1	4	2	4
Appendage allowance	20%	30%	20%	40%	30%	40%
Q.P.C.	0.80	0.67	0.80	0.67	0.67	0.67
DHP at propeller	17,520	80,500	34,500	169,200	60,200	222,000

H. Lackenby (British Shipbuilding Research Association)

I should like to make a few general remarks on the strength of the author's conclusions, especially as I have since ascertained that they have a bearing on remarks I made on Dr. van Manen's paper on Monday which touched on the same subject. As I said at that time,

---

*F. H. Todd, "Submarine Tankers," Shipbuilding and Shipping Record, Aug. 21, 1958.

when comparing the performance of surface and submarine vessels one has to be careful about the basis of comparison. Although for a given deadweight of say 25,000 tons the break-even point as regards power for certain designs may be as high as 25 or 30 knots, one has to bear in mind that a surface tanker of 25 knots would not be really economical compared with a commercial tanker which would have a speed of about 15 or 16 knots. As I said before, I am speaking here of economy on the basis of cost per ton-mile of cargo carried under present conditions. This was one of the findings arising from freighting calculations carried out by the British Shipbuilding Research Association in conjunction with ship-owners in connection with extensive nuclear energy studies, reference to which the author has made in the paper. This point is really covered by the second paragraph of the author's conclusions with which I certainly agree. Incidentally it might be of interest to mention that I understand that freighting calculations have also shown that, if anything, the speed of some recently built conventional tankers is perhaps a little on the high side as far as economic running is concerned. From the military point of view, of course, the situation could be quite different as the author has clearly explained.

What I am really saying here is that in my remarks on Dr. van Manen's paper on Monday I anticipated these particular aspects of the author's conclusions, although I was not aware of this at the time.

I should also like to say that I agree with the author's conclusions generally, in addition to those to which I have referred already. There is just one point of detail I should like to raise, namely, the limit of power for a single screw surface ship which the author has taken as 40,000 SHP. Some years ago we looked into this at BSRA in connection with the nuclear studies for tankers referred to earlier and we were advised that for a number of reasons and in particular the possible incidence of excessive cavitation erosion, 20,000 to 25,000 SHP was about the practical limit at the time. Perhaps the author may care to comment on this point.

F. H. Todd

The British Shipbuilding Research Association has carried out a great deal of research into the subject of nuclear propulsion, and it is therefore gratifying to know that Mr. Lackenby is in general agreement with my conclusions as to the commercial merits of its application to submarine cargo ships and tankers. With reference to the use of an upper limit of 40,000 horsepower for a single-screw ship, such power absorption is, of course, fairly common on multi-screw ships. In single-screw surface ships the wake variation conditions are considerably more onerous, and as Mr. Lackenby has said this introduces the danger of cavitation erosion. In the submarine this is not nearly such a serious problem since the circumferential variation can be kept quite small by paying good attention to the shape and location of appendages. Moreover, we are here talking of the future, and with the advance in knowledge about propeller-excited vibration and the necessary stern shapes and clearances to reduce the forces to a minimum, we may look forward to a steady increase in the maximum power we can put through a single screw.

J. M. Ferguson (John Brown and Co., Limited, Glasgow)

I do not wish to discuss at all the technical side of Dr. Todd's paper but I wish to express a thought which has caused a great amount of discussion between my colleagues and myself, mainly during lunch periods. We have been discussing the possibilities of

these submarine tankers because at the moment at Clydebank we have been building such a number of present day modern large tankers. Now, as you are all aware, in these present-day tankers a great deal of attention is being paid to the amenities for the crew. The very rapid turn round of these tankers, both at their loading port and at their delivery port means that the crew generally get very few advantages of leave or of getting home and the conditions on board the tankers are made all the more pleasant and congenial for these men. When you come to the submarine tanker, I would like you to think of the psychological aspect of the environmental conditions. These people are to be living in artificial conditions, with no daylight for days and weeks at a time, and the financial cost of making these conditions congenial and tolerable would add very considerably to the economic aspect of running these ships. In the case of the American submarine NAUTILUS, which did that epoch-making trip under the ice in the Polar regions, the crew, when you read the description of the voyage, had quite extensive arrangements made for their entertainment and to keep them happy; but they were doing a special job, they were being filled with a feeling of prestige attached to the job. To maintain, as would you call it, an equally high standard of "esprit de crew," then, quite a lot of money is involved. I would like that thought to be kept in mind because I do feel that when such craft do come along that aspect of it which apparently has not been considered so far will require quite an amount of attention.

.

F. H. Todd

Mr. Ferguson has called attention to a very important point in the operating of submarine cargo ships and tankers — the maintenance of the health and happiness of the crews. This would without question involve owners in a considerable increase in running costs. As mentioned in the paper, the operation of such craft will call for very highly skilled personnel, both for navigational and engineering purposes, and this also will add still further to the costs, and these two factors together may be of importance in the overall economic comparison.

M. F. Gunning (Netherlands United Shipbuilding Bureau)

We have made some fairly detailed investigations into a 20,000-ton tanker with a moderate eccentricity of the ellipse of the midship section with proper diving depth, reasonable strength of outer hull, etc., and we find that we come well above 0.6, closer to 0.65, deadweight ratio. Here, I am sorry, I am very much at loggerheads with my very good friend Mr. Newton.

F. H. Todd

The question of deadweight/displacement ratio has been discussed at length, and Mr. Gunning's figure of 0.65 seems to be very much higher than those quoted by people with experience in the design of naval submarines and those given as the result of a very thorough study of commercial submarines by the Maritime Administration in the U.S., which I have referred to. Mr. Gunning is himself a submarine designer, and I can only leave this point to the experts in this field to sort out!

J. A. Teasdale (Furness Shipbuilding Company, Limited, Billingham)

The largest known military submarine has a displacement of only one-fifth that of the smallest vessel considered in this comprehensive paper and so far no fully commercial submarine has been in service. The author, therefore, is to be congratulated upon his approach to the comparison between surface and submarine merchant vessels and the interesting presentation of the results of his work.

In order to properly compare these results with other works on the same subject a little more information is required on the data used in the study. Firstly, is the displacement referred to in Tables 2, 3, and 6 and Fig. 8 one of surface or submerged condition? Secondly, what form drag allowance has been assumed for the submarines? Various sources put this allowance as high as 15 percent of the skin friction value. Thirdly, the method of determining the deadweight of the submarines seems to be very approximate and perhaps misleading. The deadweight/displacement ratio is unlikely to be constant for a range of displacement of over 100,000 tons and a range of horsepower of more than 200,000 DHP.

Since these designs of submarine tanker are intended to be of relatively high speed compared with conventional submarines and accurate depth control at low speeds is not so important, there should be no necessity for bow diving planes. Even without these it is doubtful whether the appendage allowance would be less than 25 percent of the EHP of the bare hull.

The author states, "If we restrict the draught of the submarine to a figure comparable with that of the equivalent surface tanker, then we are forced into accepting a submarine having elliptical sections." The writer would venture to suggest that if ever a submarine tanker project becomes fact, then the practical design is likely to have a substantial parallel body of rectangular section with radiused corners. The ends, of course, would be as streamlined as possible.

R. Brard (Bassin d'Essais des Carènes, Paris)

Undoubtedly, the question that Dr. Todd has chosen for this Symposium is an interesting one. Numerous papers have already been written on this subject, that is, a consequence of the promises of atomic propulsion. But the problem of submarines, cargo ships, and tankers is quite different from that of navy ships and there is no evidence that the excellent navy solution is excellent for merchant marines. Dr. Todd made a very acute analysis of the various parts of the problem. He examined them not only from a hydrodynamical point of view, but also from others that are to be considered, and particularly those of the operating problems, terminal problems, and economical problems. I think that the values of the main parameters on which Dr. Todd grounds his analysis, should not give rise to discussion, but in a final synthesis, the weights of each aspect could be somewhat subjective. The conclusion of Dr. Todd seems, however, prudent and full of sense. Many studies are necessary before submarine cargo ships and tankers become practical, but those concerned with this question will find in Dr. Todd's reflections many very useful materials.

F. H. Todd

I am grateful to Admiral Brard for his remarks, and agree completely with his opinion that military and commercial submarines are two quite different propositions. It was my

principal aim to give sufficient hydrodynamic data covering a variety of sizes of submarines for anyone studying the subject to make his own power estimates and draw his own conclusions. As power is only one of many factors, however, I did endeavour to call attention to other features in such ships, and, as Admiral Brard says, the relative importance of each of these will vary from ship to ship according to the purpose it is to serve.

In conclusion, I would like to make a few remarks on the philosophy of the theme of this symposium — high performance ships. I have tried to show in the paper that the naval architect and naval scientist have long been aware of the possibilities — and problems — of using submarines for commercial purposes, and how they have to a large extent been waiting for a propulsion plant independent of atmospheric air. From time to time — and indeed in the introductory proceedings of this conference — comments are directed against us to the effect that we have only increased the speed of ships twofold in a hundred years, whereas our aerodynamic friends have done it tenfold in fifty years. I would like to suggest, nevertheless, that we have made some progress in that time — from the old SAVANNAH to the new SAVANNAH in a hundred years seems quite a step, as does that from the old Cunard BRITANNIA of 1840 to the QUEEN ELIZABETH of 1940. As a naval architect and scientist, I feel that we have not altogether failed in developing our science.

One of the great problems from which we have always suffered, and which I have tried to bring out in the paper, is the continual insistence in our particular art or science, whichever you like to call it, that ships must always pay for themselves in the economic sense. This, I think, is where our aeronautical friends have had a terrific advantage. We have striven for years to get just one research ship of our own on which to carry out the many full-scale experiments necessary for the progress of our science, but to no avail. The aeronautical engineer designs an aircraft, and builds one, two, three, or more prototypes for development testing, and is undeterred if some of these, and many millions of pounds, go up in smoke in the process. I believe that if we were given similar opportunities in the way of government support for research and development, and if our steps were not continually dogged by this attitude that every ship built must be a commercial success, we would make a great deal faster progress.

*   *   *

EXPERIMENTAL TECHNIQUES AND METHODS OF ANALYSIS
USED IN SUBMERGED BODY RESEARCH

Alex Goodman
David Taylor Model Basin

This paper deals with the various experimental techniques and methods of analysis which are either presently being used or are contemplated in the near future at the David Taylor Model Basin in the field of dynamic stability and control of submerged bodies. The advantages and disadvantages of the various techniques are discussed. Primary emphasis is placed on the principles and operation of the DTMB Planar-Motion-Mechanism System, since this device is unique and is being used extensively to provide stability and control data for submerged bodies in six degrees of freedom. Emphasis is also placed on the concepts, techniques, and philosophies used in simulator studies and motion analyses. A brief description of the new rotating arm facility, and the free-running model technique are also presented.

NOTATION

The nomenclature defined in DTMB Report 1319 is used herein where applicable. The positive direction of axes, angles, forces, moments, and velocities are shown in the accompanying sketch. The coefficients and symbols are defined as follows:*

Symbol	Dimensionless Form	Definition
A_b	$A_b{}' = \dfrac{A_b}{l^2}$	Projected area of bow planes
A_r	$A_r{}' = \dfrac{A_r}{l^2}$	Projected area of rudders
A_s	$A_s{}' = \dfrac{A_s}{l^2}$	Projected area of stern planes
AP		After perpendicular
AR		Aspect ratio

---

*All derivatives with respect to angular quantities are given as "per radian."
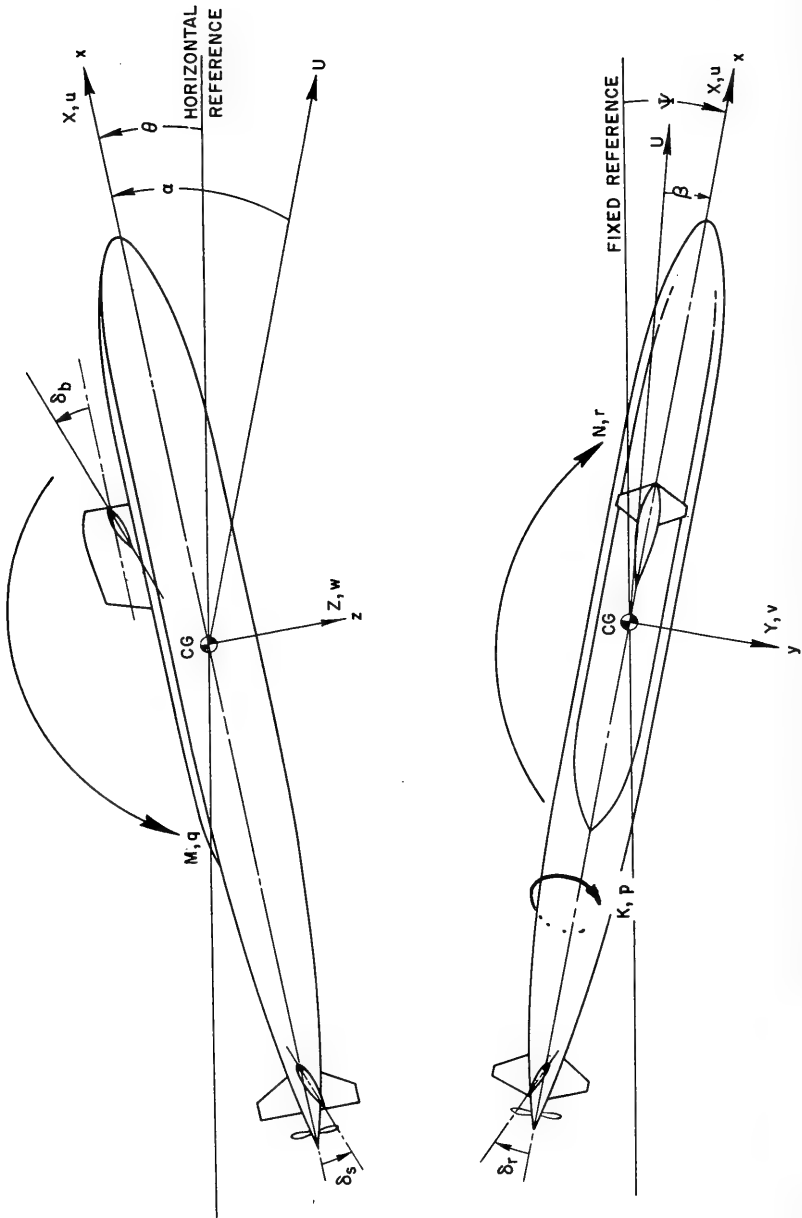
Symbol	Dimensionless Form	Definition
B	$B' = \dfrac{B}{\frac{1}{2}\rho l^2 U^2}$	Buoyancy force
CB		Center of buoyancy of submarine
CG		Center of mass of submarine
c		Damping constant
c_c		Critical damping constant
d	$d' = \dfrac{d}{l}$	Diameter of body
FP		Forward perpendicular
h		Depth of submergence to center of mass
I_x, I_y, I_z	$I_x' = \dfrac{I_x}{\frac{1}{2}\rho l^5}$	Moment of inertia of the body about x-, y-, z-axis
K	$K' = \dfrac{K}{\frac{1}{2}\rho l^3 U^2}$	Hydrodynamic moment about x-axis through center of gravity
K_p	$K_p' = \dfrac{K_p}{\frac{1}{2}\rho l^4 U}$	Derivative of moment component with respect to angular velocity component p
$K_{\dot p}$	$K_{\dot p}' = \dfrac{K_{\dot p}}{\frac{1}{2}\rho l^5}$	Derivative of moment component with respect to angular acceleration component $\dot p$
K_r	$K_r' = \dfrac{K_r}{\frac{1}{2}\rho l^4 U}$	Derivative of moment component with respect to angular velocity component r
$K_{\dot r}$	$K_{\dot r}' = \dfrac{K_{\dot r}}{\frac{1}{2}\rho l^5}$	Derivative of moment component with respect to angular acceleration component $\dot r$
K_v	$K_v' = \dfrac{K_v}{\frac{1}{2}\rho l^3 U}$	Derivative of moment component with respect to velocity component v

Symbol	Dimensionless Form	Definition
$K_{\dot{v}}$	$K_{\dot{v}}' = \dfrac{K_{\dot{v}}}{\frac{1}{2}\rho l^4}$	Derivative of moment component with respect to acceleration component $\dot{v}$
K_{δ_r}	$K_{\delta_r}' = \dfrac{K_{\delta_r}}{\frac{1}{2}\rho l^3 U^2}$	Derivative of moment component with respect to rudder angle component δ_r
k_y	$k_y' = \dfrac{k_y}{l}$	Radius of gyration of ship and added mass of ship about y-axis
l	$l' = 1$	Characteristic length of submarine
M	$M' = \dfrac{M}{\frac{1}{2}\rho l^3 U^2}$	Hydrodynamic moment about y-axis through center of gravity
M_q	$M_q' = \dfrac{M_q}{\frac{1}{2}\rho l^4 U}$	Derivative of moment component with respect to angular velocity component q
$M_{\dot{q}}$	$M_{\dot{q}}' = \dfrac{M_{\dot{q}}}{\frac{1}{2}\rho l^5}$	Derivative of moment component with respect to angular acceleration component $\dot{q}$
M_w	$M_w' = \dfrac{M_w}{\frac{1}{2}\rho l^3 U}$	Derivative of moment component with respect to velocity component w
$M_{\dot{w}}$	$M_{\dot{w}}' = \dfrac{M_{\dot{w}}}{\frac{1}{2}\rho l^4}$	Derivative of moment component with respect to acceleration component $\dot{w}$
M_δ, N_δ	$M_\delta' = \dfrac{M_\delta}{\frac{1}{2}\rho l^3 U^2}$	Derivative of moment component with respect to control surface angle component δ
M_{δ_b}	$M_{\delta_b}' = \dfrac{M_{\delta_b}}{\frac{1}{2}\rho l^3 U^2}$	Derivative of moment component with respect to bow plane angle component δ_b
M_{δ_s}	$M_{\delta_s}' = \dfrac{M_{\delta_s}}{\frac{1}{2}\rho l^3 U^2}$	Derivative of moment component with respect to stern plane angle component δ_s

Symbol	Dimensionless Form	Definition
M_θ	$M_\theta' = \dfrac{M_\theta}{\frac{1}{2}\rho l^3 U^2}$	Derivative of moment component with respect to pitch angle component θ
M_*	$M_*' = \dfrac{M_*}{\frac{1}{2}\rho l^3 U^2}$	Hydrodynamic moment at zero angle of attack
m	$m' = \dfrac{m}{\frac{1}{2}\rho l^3}$	Mass of submarine, including water in free-flooding spaces
N	$N' = \dfrac{N}{\frac{1}{2}\rho l^3 U^2}$	Hydrodynamic moment about z-axis through center of gravity
N_r	$N_r' = \dfrac{N_r}{\frac{1}{2}\rho l^4 U}$	Derivative of moment component with respect to angular velocity component r
$N_{\dot r}$	$N_{\dot r}' = \dfrac{N_{\dot r}}{\frac{1}{2}\rho l^5}$	Derivative of moment component with respect to angular acceleration component $\dot r$
N_v	$N_v' = \dfrac{N_v}{\frac{1}{2}\rho l\ U}$	Derivative of moment component with respect to velocity component v
$N_{\dot v}$	$N_{\dot v}' = \dfrac{N_{\dot v}}{\frac{1}{2}\rho l^4}$	Derivative of moment component with respect to acceleration component $\dot v$
N_{δ_r}	$N_{\delta_r}' = \dfrac{N_{\delta_r}}{\frac{1}{2}\rho l^3 U^2}$	Derivative of moment with respect to rudder angle component δ_r
p	$p' = \dfrac{pl}{U}$	Angular velocity component relative to x-axis
$\dot p$	$\dot p' = \dfrac{\dot p l^2}{U^2}$	Angular acceleration component relative to x-axis
q	$q' = \dfrac{ql}{U}$	Angular velocity component relative to y-axis

Symbol	Dimensionless Form	Definition
$\dot{q}$	$\dot{q}' = \dfrac{\dot{q}l^2}{U^2}$	Angular acceleration component relative to y-axis
r	$r' = \dfrac{rl}{U}$	Angular velocity component relative to z-axis
$\dot{r}$	$\dot{r}' = \dfrac{\dot{r}l^2}{U^2}$	Angular acceleration component relative to z-axis
$t_{1/2}$		Time for oscillatory motion to damp to one-half initial amplitude
U	$U' = 1$	Velocity of origin of body axes relative to fluid in feet per second
V_k		Velocity of origin of body axes relative to fluid in knots
v	$v' = \dfrac{v}{U}$	Component along y-axis of velocity of origin of body relative to fluid
$\dot{v}$	$\dot{v}' = \dfrac{\dot{v}l}{U^2}$	Component along y-axis of acceleration of origin of body relative to fluid
w	$w' = \dfrac{w}{U}$	Component along z-axis of velocity of origin of body axes relative to fluid
$\dot{w}$	$\dot{w}' = \dfrac{\dot{w}l}{U^2}$	Component along z-axis of acceleration of origin of body axes relative to fluid
X	$X' = \dfrac{X}{\frac{1}{2}\rho l^2 U^2}$	Hydrodynamic longitudinal force, positive forward
x		The longitudinal axis, directed from the after to the forward end of the submarine with origin taken at the center of gravity
$x_B,\ z_B$	$x_B{}' = \dfrac{x_B}{l}$	Coordinates of center of buoyancy with respect to body axes
	$z_B{}' = \dfrac{z_B}{l}$	
x_{CG}	$x_{CG}{}' = \dfrac{x_{CG}}{l}$	Distance from reference point to center of gravity of model.

Symbol	Dimensionless Form	Definition
Y	$Y' = \dfrac{Y}{\frac{1}{2}\rho l^2 U^2}$	Hydrodynamic lateral force, positive to starboard
Y_r	$Y_r' = \dfrac{Y_r}{\frac{1}{2}\rho l^3 U}$	Derivative of lateral force component with respect to angular velocity component r
$Y_{\dot{r}}$	$Y_{\dot{r}}' = \dfrac{Y_{\dot{r}}}{\frac{1}{2}\rho l^4}$	Derivative of lateral force component with respect to angular acceleration component $\dot{r}$
Y_v	$Y_v' = \dfrac{Y_v}{\frac{1}{2}\rho l^2 U}$	Derivative of lateral force component with respect to velocity component v
$Y_{\dot{v}}$	$Y_{\dot{v}}' = \dfrac{Y_{\dot{v}}}{\frac{1}{2}\rho l^3}$	Derivative of lateral force component with respect to acceleration component $\dot{v}$
$Y_\delta,\ Z_\delta$	$Y_\delta' = \dfrac{Y_\delta}{\frac{1}{2}\rho l^2 U^2}$	Derivative of force component with respect to control surface angle component δ
Y_{δ_r}	$Y_{\delta_r}' = \dfrac{Y_{\delta_r}}{\frac{1}{2}\rho l^2 U^2}$	Derivative of lateral force component with respect to rudder angle component δ_r
y		Distance along the transverse axis, directed to starboard with origin taken at center of gravity
Z	$Z' = \dfrac{Z}{\frac{1}{2}\rho l^2 U^2}$	Hydrodynamic normal force, positive downward
Z_q	$Z_q' = \dfrac{Z_q}{\frac{1}{2}\rho l^3 U}$	Derivative of normal force component with respect to angular velocity component q
$Z_{\dot{q}}$	$Z_{\dot{q}}' = \dfrac{Z_{\dot{q}}}{\frac{1}{2}\rho l^4}$	Derivative of normal force component with respect to angular acceleration component $\dot{q}$
Z_w	$Z_w' = \dfrac{Z_w}{\frac{1}{2}\rho l^2 U}$	Derivative of normal force component with respect to velocity component w

Symbol	Dimensionless Form	Definition
$Z_{\dot{w}}$	$Z_{\dot{w}}' = \dfrac{Z_{\dot{w}}}{\frac{1}{2}\rho l^3}$	Derivative of normal force component with respect to acceleration component $\dot{w}$
Z_{δ_b}	$Z_{\delta_b}' = \dfrac{Z_{\delta_b}}{\frac{1}{2}\rho l^2 U^2}$	Derivative of normal force component with respect to bow plane angle δ_b
Z_{δ_s}	$Z_{\delta_s}' = \dfrac{Z_{\delta_s}}{\frac{1}{2}\rho l^2 U^2}$	Derivative of normal force component with respect to stern-plane angle component δ_s
Z_*	$Z_*' = \dfrac{Z_*}{\frac{1}{2}\rho l^2 U^2}$	Normal force at zero angle of attack
z		Distance along the normal axis, directed from top to bottom (deck to keel), with origin taken at center of gravity
α		The angle of attack; the angle to the longitudinal body axis from the projection into the principal plane of symmetry of the velocity of the origin of the body axes relative to the fluid, positive in positive sense of rotation about the y-axis
β		The drift or sideslip angle; the angle to the principal plane of symmetry from the velocity of the origin of the body axes relative to the fluid, positive in the positive sense of rotation about the z-axis
δ		Angular displacement of a control surface
δ_b		Angular displacement of bow planes, positive trailing edge down
δ_r		Angular displacement of rudders, positive trailing edge port
δ_s		Angular displacement of stern planes, positive trailing edge down
θ		The angle of pitch; the angle of elevation of the x-axis positive bow up
ρ	$\rho' = 1$	Mass density of water
σ_i	$\sigma_i' = \sigma_i \dfrac{l}{U}$	Roots of stability equation, $i = 1, 2, \ldots$

Symbol	Dimensionless Form	Definition
ψ		The angle of yaw
ω	$\omega' = \dfrac{\omega l}{U}$	Circular frequency of oscillation
ω_n	$\omega_n' = \dfrac{\omega_n l}{U}$	Natural frequency of undamped oscillation

Subscripts:

in	In-phase component of force or moment
out	Out-of-phase or quadrature component of force or moment
o	Maximum amplitude
1	Associated with forward strut
2	Associated with aft strut
m	Model.

INTRODUCTION

The problems associated with the dynamic behavior of the submarine and other submerged bodies, that is, stability, performance, and ease of handling, have become increasingly more and more important with each new increase in submerged speed. This has been particularly true for motions in the vertical plane since the submarine must be operated, strictly on instruments, within the confines of a layer of water usually no greater than a few boat lengths. Also, the increase in submerged speed has given rise to some serious dynamic problems for motions in the horizontal plane and made the problem of emergency recovery increasingly more acute.

In the early stages of development in the field of submarine stability and control the designer was faced with the problem of providing a combination of characteristics and means for controlling the submarine which would result in satisfactory dynamic behavior. A major difficulty in providing for this was the lack of sufficient information to guide him in the choice of a combination of physical characteristics which would result in adequate stability, performance, and ease of handling. Another major difficulty was the lack of straightforward design methods and experimental or theoretical techniques for obtaining a desired combination of characteristics. In those cases where the results of model tests in the form of the various hydrodynamic coefficients were available, the interpretations that could readily be made relating them to adequate dynamic behavior were rather limited. The designer was further handicapped in that he had no standards by which he could evaluate the dynamic behavior of the submarine.

The mission of the Stability and Control Division at the David Taylor Model Basin has been, therefore, to remedy this situation. This has been partially accomplished by the

development of a set of desirable handling qualities which could be used in optimizing the submerged body design [1], development of methods which give an objective evaluation of the submerged body's dynamic behavior, and improvements in, and development of, new prediction and experimental techniques which could be used by the designer to evaluate the submerged body performance.

This paper presents and describes the various experimental techniques and methods of analysis used at the David Taylor Model Basin in the field of dynamic stability and control of submerged bodies. The advantages and disadvantages of the various techniques are presented. Primary emphasis is placed on the principles and operation of the DTMB Planar-Motion-Mechanism System [2] as well as on the concepts, techniques, and philosophies used in simulator and motion analysis studies. Throughout the presentation, it will be noted that frequent references will be made to the use of the various techniques as applied to the submarine stability and control problem. Most of the data acquired by these techniques have been for submarines because of the urgency that submarine problems have assumed in recent years. It should be noted, however, that these techniques are also applicable to other types of marine vehicles.

COMPARISON OF EXPERIMENTAL TECHNIQUES

The various approaches to the solution of problems in the field of dynamic stability and control of a submerged body moving through a fluid, shown in Fig. 1, have been employed by naval architects and aerodynamicists for many years. Many investigators have used the free-running or flying-model techniques since a direct evaluation of the performance of the design is provided [3,4]. However, this method does not provide data which can be related to the physical characteristics of the design or to support the design changes required for improved performance. The full-scale technique suffers from the same shortcomings. However, this technique is used mainly for providing data for model-full-scale correlation.

In recent years, the development of general-purpose analog and high-speed digital computers has resulted in the extensive use of the mathematical-model technique. This technique, which is based on a thorough analysis of the differential equations which govern the motions, provides a solution and basic understanding of the dynamic stability and control problems of a submerged body. However, these differential equations of motion are comprised of numerous coefficients or derivatives which are of hydrodynamic origin.
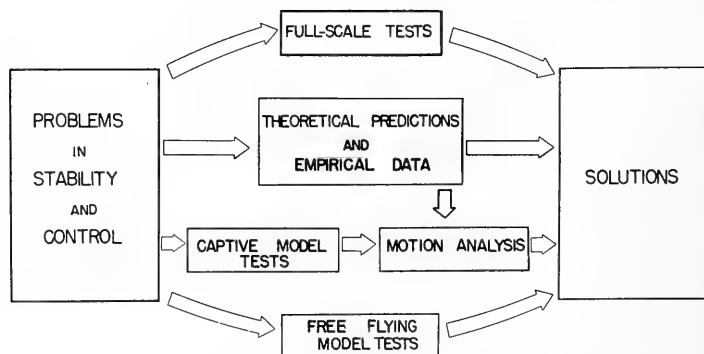
Fig. 1. Approaches to problems in stability and control

Consequently, to obtain solutions for any given configuration by means of this technique, it is necessary to know these coefficients with reasonable accuracy. Many attempts have been made in the past to fulfill this requirement by utilizing various experimental (captive model) and theoretical techniques, or combinations of both.

Among the various captive-model techniques used, fairly refined methods have been developed by model basins and wind tunnels for measuring forces and moments due to body orientation and control deflection; the so-called static stability and control coefficients. However, the various experimental methods used to determine forces and moments associated with variations in linear acceleration, angular velocity, and angular acceleration have been successful in only a limited number of cases. The techniques that have been tried in this respect have required the use of facilities such as the rotating arm, free oscillator, forced oscillator, curved-flow and rolling-flow tunnels, and curved models in a straight flow facility [3]. Each of these techniques has certain limitations and problems associated with either accuracy of instrumentation, model support, friction, accuracy of flow (curved and rolling flow) [5,6], and accuracy of model construction (curved model). Also, none of these techniques provide a direct measure of all the hydrodynamic coefficients required in the equations of motion for six degrees of freedom. The DTMB Planar-Motion-Mechanism System recently developed at the David Taylor Model Basin, however, incorporates in one device a means for experimentally determining all of the hydrodynamic-stability coefficients required in the equations of motion for a submerged body in six degrees of freedom.

A comparison of the main advantages and disadvantages of several of the basic experimental techniques that have been discussed is presented in Table 1. Based on this comparison, it can be seen that the mathematical model technique, in conjunction with accurately determined hydrodynamic coefficients, provides the most powerful and versatile design and research tool for the study and analysis of stability and control problems.

PLANAR-MOTION-MECHANISM SYSTEM

The DTMB Planar-Motion-Mechanism System incorporates in one device a means for experimentally determining all of the hydrodynamic-stability and control coefficients required in the equations of motion for a submerged body in six degrees of freedom. These include the static-stability and control, rotary-stability, and acceleration coefficients. The unique features of the system are the methods used to impart hydrodynamically pure pitching, heaving, and rolling motions to a given submerged body, as well as the dynamometry and data analysis equipment employed. These enable the explicit and accurate determination of individual derivatives without resort to the solution of simultaneous equations as is necessary when other types of oscillation devices are used. Although the system was designed primarily for submerged body research it can also be used to determine the hydrodynamic coefficients for other types of marine vehicles such as hydrofoil boats and ground effect machines.

General Considerations

The derivatives and composition of the equations of motion have formed the subject of numerous text books and papers [7-9]. For the purpose of this paper, therefore, only the general nature of these equations are considered. This is done to give some insight into the problems which must be faced in the design of experimental facilities for the evaluation of the equations.

Table 1
Comparison of Experimental Techniques

(a) Free-Running Model Technique	
Advantages	
1. Direct evaluation of performance of specific designs	3. Can be used to study extreme maneuvers which may be too complicated to handle by analytical or computer methods
2. Can be economical and expedient	
Disadvantages	
1. Does not provide data which can be directly related to the design of body and individual appendages	3. Froude or dynamic scaling necessary for mass, moment of inertia, and metacentric stability
2. Does not provide data to directly support design changes to effect improvements in performance	

(b) Mathematical Model Techniques	
Advantages	
1. Provides means of evaluating handling qualities or operational characteristics of proposed design well in advance of construction	4. Provides measures of capabilities of the design tempered by existence of human operator or automatic control device in control loop
2. Provides simple means of studying effects of practical variations of basic design which may be necessary to improve performance	5. Can be used in human engineering studies
	6. Can be used to study overall performance of various combined systems
3. Can be used to determine effects of various environmental conditions on performance	7. Can be used to train personnel
Disadvantages	
1. Requires an accurate set of hydrodynamic coefficients of the design for the equations of motion	2. Requires expensive facilities

(c) Captive Model Techniques	
Advantages	
1. Provides basic data on which to support design of individual body and appendages	4. Results can be utilized to study effects of proposed design changes without additional model tests
2. Provides basic data which can be used with the equations of motion in computer and simulator studies to evaluate inherent and closed-loop performance	5. Data are perpetuated so that further studies can be made at a later time without the need for additional model tests
3. Provides data which can be directly utilized in design of automatic control systems	6. Provides powerful tool for doing research or systematic series work on stability and control
	7. Dynamic scaling not necessary
Disadvantages	
1. Data are one step removed from directly indicating all the handling qualities	3. Requires expensive facilities
2. Method may become uneconomical for evaluating performance of one specific design	

The hydrodynamic forces and moments which enter into the equations of motion as coefficients are usually classified into three categories: static, rotary, and acceleration. The static coefficients are due to components of linear velocity of the body relative to the fluid, the rotary coefficients are due to angular velocity, and the acceleration coefficients are due to either linear or angular acceleration. Within limited ranges the coefficients are linear with respect to the appropriate variables and thus may be utilized as static, rotary, and acceleration derivatives in linearized equations of motion.

It may be concluded from the foregoing classification, that the experimental determination of the coefficients of the equations of motion requires facilities which will impart linear and angular velocities and accelerations to a given body with respect to a fluid. For example, the usual basin facilities have carriages designed to tow models in a straight line at constant speed. Such facilities can be equipped to orient models in either pitch or yaw to obtain the static coefficients. However, more specialized types of facilities, such as rotating arm or oscillator, are required to impart the angular velocities that are necessary to obtain rotary coefficients. The oscillator type of facility provides also linear and angular accelerations so that the acceleration coefficients may be determined experimentally.

The choice of a suitable facility for determining hydrodynamic coefficients involves many considerations pertaining to accuracy, expediency, and ease of data analysis. A detailed treatment of these problems is beyond the scope of this paper. However, of primary concern is the degree to which the experimental technique involves explicit relationships and avoids the need for solutions of matrices. Also techniques which involve extrapolations should be avoided. To illustrate, a carriage which tows a model at uniform velocity in straight-line pitched or yawed flight is a direct and explicit means of determining static coefficients. Similarly, a rotating arm which tows a model at uniform angular velocity and tangential to the circular path at each of several different radii is a means for determining rotary coefficient explicitly. On the other hand, the use of the rotating arm to obtain static coefficients should be considered as an indirect procedure since the data must be extrapolated to infinite radius. The usual oscillator techniques are even more indirect and, at best, require solutions of simultaneous equations to obtain rotary and acceleration derivatives.

Each of the techniques mentioned can be used most advantageously for obtaining one category of hydrodynamic coefficients. The straight-line towing carriage supplies only the static coefficients. The rotating arm supplies rotary coefficients directly and static coefficients indirectly. The oscillator supplies all three categories of coefficients, but all indirectly.

The foregoing considerations suggest the desirability of having a single system to determine explicitly all of the coefficients required in the equations of motion for six degrees of freedom. To accomplish this objective, it is necessary to develop a facility which can move a body through water with "hydrodynamically pure" linear velocities, angular velocities, linear accelerations, and angular accelerations in all degrees of freedom. This concept forms the basis of the DTMB Planar-Motion-Mechanism System.

Principles of Operation

The DTMB Planar-Motion-Mechanism System as it physically exists is described briefly in the next section. It is desirable, however, to consider first the principles underlying the operation of the mechanism so that the design concept can be generally understood. In the interest of simplicity the mode of operation applicable only to submerged bodies in the

vertical plane will be used to describe the principles of the system. The system of axes as well as the symbols and coefficients used in this section have been defined in the notation at the beginning of this paper.

The kind of motion for static coefficients is commonly used by wind tunnel and model basin facilities and, therefore, does not need to be explained in detail. Figure 2 schematically represents this type of motion. The components are given with respect to a body-axis system with the origin at the center of gravity, CG.
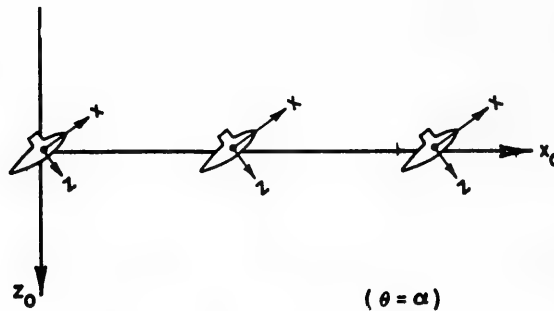
Fig. 2. Straight-line pitched motion for steady-state tests

The system produces this motion by using a towing carriage to tow the model in a straight path at constant velocity. Discrete pitch angles for each run are set by a tilt table which supports the model through a pair of twin struts. Control surface angles are also set discretely for each run. Forces are measured by internal balances at each of the two struts to obtain static forces and moments.

The unique feature of the DTMB Planar Motion Mechanism is the kinds of motions produced to enable the explicit determination of the rotary and acceleration coefficients. Sinusoidal motions are imparted to the model at the point of attachment of each of the two towing struts while the model is being towed through the water by the carriage. The motions are phased in such a manner as to produce the desired conditions of hydrodynamically "pure heaving" and "pure pitching." It is possible also, if required for any reason, to produce various combinations of pitching and heaving. Figure 3 illustrates various types of motions including (a) the type of motion usually associated with oscillators, (b) pure heaving, and (c) pure pitching. The latter two are the basic motions associated with the DTMB Planar Motion Mechanism. The pure rolling motion is not illustrated but consists simply of oscillations about the longitudinal body axis.

The oscillator motion depicted by Fig. 3a is actually a combination of pure pitching and heaving motions. Since the CG is constrained to move in a straight path while the model, which oscillates in a see-saw fashion, assumes sinusoidally varying angles of attack and pitch angles. As a result a mixture of static, rotary, and acceleration forces and moments is produced. It becomes necessary, therefore, to perform a similar oscillation about a second reference point. The two oscillation conditions together with the static tests provide data which can be used to separate the hydrodynamic coefficients. The solution of simultaneous equations involved in this process, however, could lead to errors because of the wide differences in magnitude between the various individual coefficients. The oscillator type of
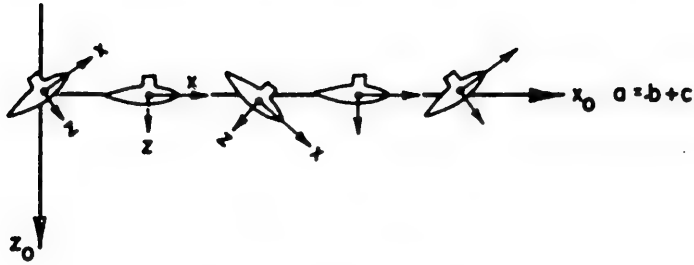
(a) Combined pitching and heaving
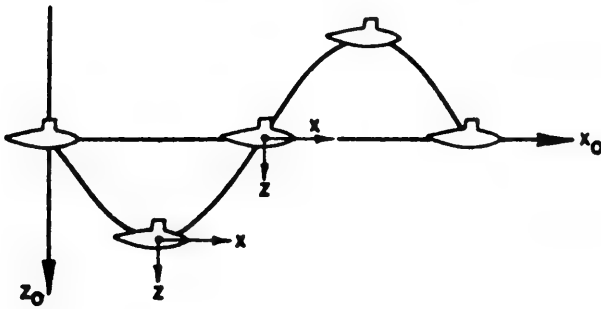
(b) Pure heaving
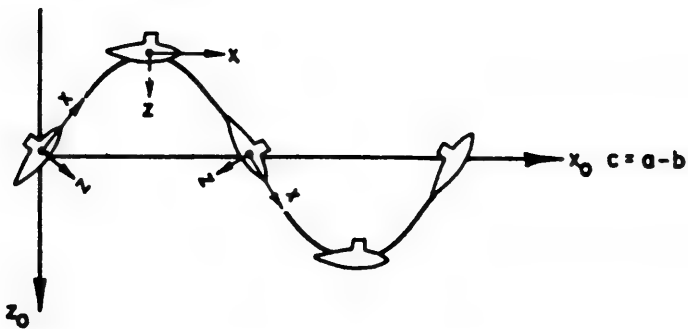
(c) Pure pitching

Fig. 3. Oscillation types of motion

motion is produced by the Planar Motion Mechanism when the two struts move sinusoidally 180 degrees out of phase with each other.

The pure heaving motion shown in Fig. 3b is obtained when both struts move sinusoidally in phase with each other. This results in a motion whereby the model CG moves in a sinusoidal path while the pitch angle θ is invariant with time.

The pure pitching motion shown in Fig. 3c is obtained by moving both struts out of phase with each other; the phase angle between struts, ϕ_s, is dependent upon frequency of oscillation, forward speed, and distance of each strut from the CG. This relationship can be expressed as

$$\cos \phi_s = \frac{1 - \left(\dfrac{\omega x}{U}\right)^2}{1 + \left(\dfrac{\omega x}{U}\right)^2}$$

and is derived as Eq. (A20) in Appendix A. The resulting motion is one in which the model CG moves in a sinusoidal path with the model axis always tangent to the path (angle of attack $\alpha = 0$).

The process for obtaining translatory acceleration derivatives from pure heaving tests is represented diagrammatically in Fig. 4. The diagrams across the top of the figure show the motions of the aft and forward struts with respect to each other. Corresponding positions of a component resolver (which has been replaced by a sine-cosine potentiometer in the new system), provided with the electrical system to rectify the sinusoidal signals from the force balances, are also shown. At the left is a column of graphs showing the resulting motions and forces at the CG. The right-hand column contains the mathematical relationships represented by each graph. Descending from the top of Fig. 4, there is the vertical displacement z curve, the associated velocity $\dot{z}$ curve, the associated acceleration $\ddot{z}$ curve, and the vertical force Z_R curve. It may be noted that the Z_R curve is displaced in point of time from the z curve by phase angle ϕ. Thus Z_R can be considered as being made up of two components, one in phase with the motion at the CG, Z_{in}, and the other in quadrature with the motion at the CG, Z_{out}. The shaded area per cycle under each curve represents the magnitudes of Z_{in} and Z_{out}, respectively.

The process for obtaining rotary and angular acceleration derivatives from pure pitching tests is represented diagrammatically in Fig. 5. The order followed is similar to that shown in Fig. 4. In this case, the pitch angle traces (θ, $\dot{\theta}$, and $\ddot{\theta}$) are of primary interest. The Z_R curve is displaced in point of time from the θ curve by phase angle ϕ. The procedure for resolving the resultant force into in-phase and quadrature components is similar to that for the pure heaving case. The shaded area per cycle under each curve represents the magnitudes of Z_{in} and Z_{out}, respectively.

In the pure heaving case the in-phase component of force is directly related to the linear acceleration and, therefore, can be used to compute explicitly the associated acceleration derivatives. Similarly, in the pure pitching case the in-phase component of force is directly related to the angular acceleration and the quadrature component is directly related to the angular acceleration and the quadrature component is directly related to the angular velocity. Thus both the angular acceleration and rotary derivatives can be computed explicitly. The relationships between the various rotary and acceleration derivatives and the respective

Pure Heaving

Aft   F'wd   Synchronous Switch

270°

180°   0° — $\omega t = 0$

90°

Normal

$x_1 = x_2$ $\phi_s = 0$

$x_1 + x_2 = b$

$z = a \sin \omega t$

$\dot{z} = w = \omega a \cos \omega t = w_0 \cos \omega t$

$\ddot{z} = \dot{w} = -\omega^2 a \sin \omega t = -\dot{w}_0 \sin \omega t$

$Z_R = Z_0 \sin(\omega t - \phi) = (Z_0 \cos \phi) \sin \omega t$

$-(Z_0 \sin \phi) \cos \omega t = Z_{in} \sin \omega t + Z_{out} \cos \omega t$

$$Z_{in} = \frac{\pi}{2} \cdot \frac{1}{2\pi} \left[\int_0^{\pi} Z_0 \sin(\omega t - \phi) \, d(\omega t) - \int_{\pi}^{2\pi} Z_0 \sin(\omega t - \phi) \, d(\omega t) \right] = Z_0 \cos \phi$$

$$Z_{out} = \frac{\pi}{2} \cdot \frac{1}{2\pi} \left[\int_0^{\pi/2} Z_0 \sin(\omega t - \phi) \, d(\omega t) - \int_{\pi/2}^{3/2\pi} Z_0 \sin(\omega t + \phi) \, d(\omega t) + \int_{3/2\pi}^{2\pi} Z_0 \sin(\omega t - \phi) \, d\omega t \right] = -Z_0 \sin \phi$$
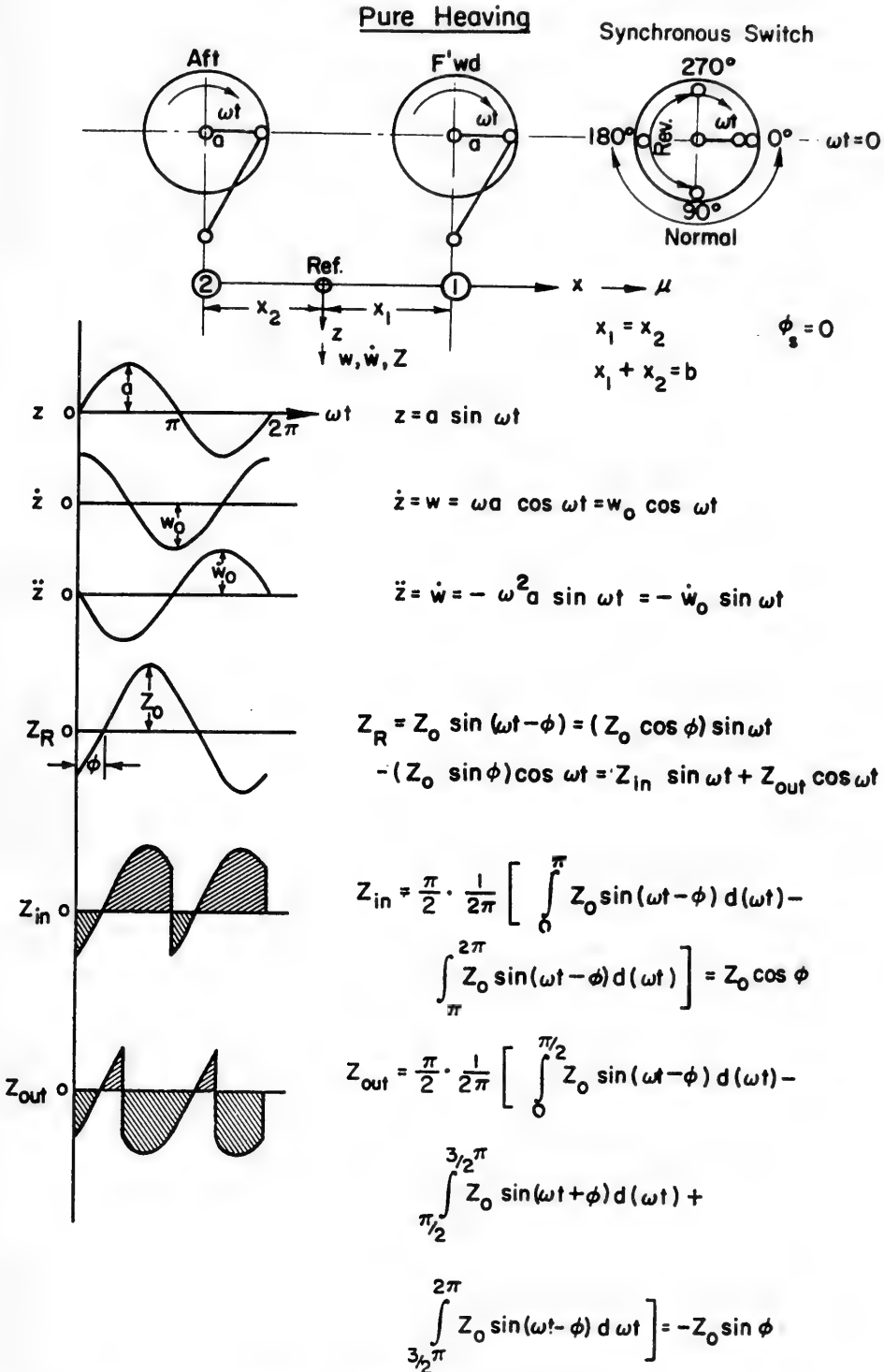
Fig. 4. Analysis of pure heaving motion

Pure Pitching

Aft   Fwd   Synchronous Switch
270°

ωt ωt $\omega t = 0$ 180° Rev 0° $(\omega t)_1$

a a ϕ_S 90°

$q, \dot{q}, M$ Ref.   Normal

② ⊕ ① ⟶ x ⟶ μ

$\leftarrow x_2 \rightarrow \downarrow z \leftarrow x_1 \rightarrow$ $x_1 = x_2$; $x_1 + x_2 = b$

$\downarrow w, \dot{w}, Z$

$\omega t = 0$ $(\omega t)_1 = \dfrac{\pi}{2} + \dfrac{\phi_S}{2}$

$z_1 = a \sin \omega t$

$z_2 = a \sin(\omega t - \phi_S)$

$\theta = \dfrac{z_2 - z_1}{b} = -\dfrac{2a}{b} \sin \dfrac{\phi_S}{2} \left[\cos(\omega t - \dfrac{\phi_S}{2}) \right]$

$= -\theta_0 \cos(\omega t - \dfrac{\phi_S}{2})$

$\dot{\theta} = q = \omega \theta_0 \sin(\omega t - \dfrac{\phi_S}{2})$

$\ddot{\theta} = \dot{q} = \omega^2 \theta_0 \cos(\omega t - \dfrac{\phi_S}{2})$

$Z_R = Z_0 \cos \left[(\omega t - \dfrac{\phi_S}{2}) - \phi \right]$

$= Z_0 \cos \phi \cos(\omega t - \dfrac{\phi_S}{2}) + Z_0 \sin \phi \sin(\omega t - \dfrac{\phi_S}{2})$

$Z_{in} = \dfrac{\pi}{2} \cdot \dfrac{1}{2\pi} \left[\int_{\frac{\pi}{2} + \frac{\phi_S}{2}}^{\frac{3}{2}\pi + \frac{\phi_S}{2}} Z_R \, d(\omega t) - \int_{\frac{\pi}{2} + \frac{\phi_S}{2}}^{\frac{3}{2}\pi + \frac{\phi_S}{2}} Z_R \, d(\omega t) \right] = -Z_0 \cos \phi$

$Z_{out} = \dfrac{\pi}{2} \cdot \dfrac{1}{2\pi} \left[\int_{\frac{\pi}{2} + \frac{\phi_S}{2}}^{\pi + \frac{\phi_S}{2}} Z_R \, d(\omega t) - \int_{\pi + \frac{\phi_S}{2}}^{2\pi + \frac{\phi_S}{2}} Z_R \, d(\omega t) + \int_{2\pi + \frac{\phi_S}{2}}^{\frac{\pi}{2} + \frac{\phi_S}{2}} Z_R \, d(\omega t) \right]$

$= Z_0 \sin \phi$
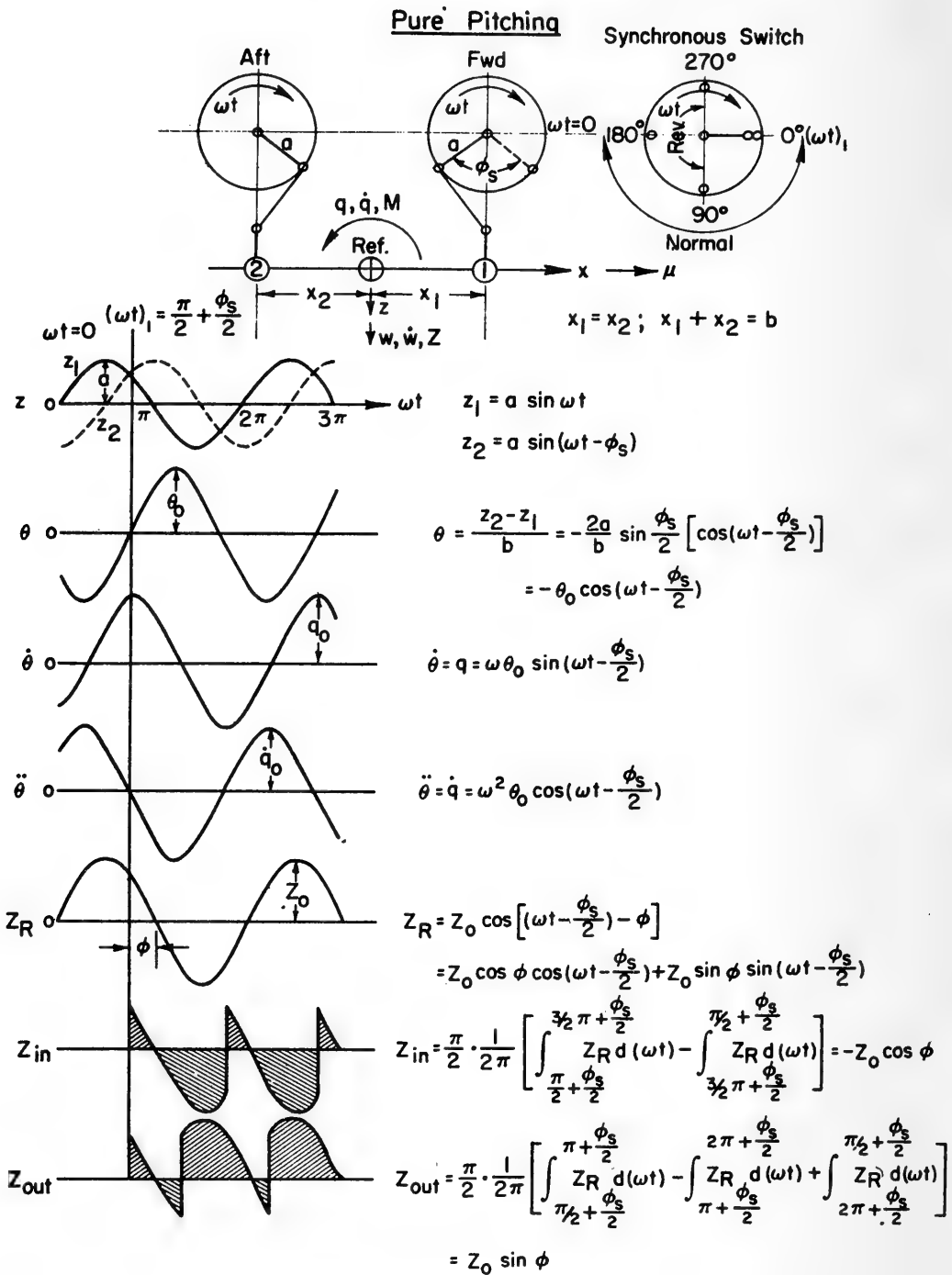
Fig. 5. Analysis of pure pitching motion

in-phase and quadrature components of force are presented in Table 2. The derivation of these reduction equations is presented in Appendix B.

Description of Facility

The DTMB Planar-Motion-Mechanism System is a complete system for obtaining hydrodynamic coefficients from model tests. It embraces all mechanical, electrical, and electronic components necessary to carry out all functions from the delivery of the model to finalized processing of data preparatory to analysis. This includes preparation of the model for testing, conduct of static and oscillation tests, sensing and recording of test data, and processing data digitally in tabulated form. The main features of the system such as model support and positioning equipment, forced-motion mechanism, dynamometry, and Instrumentation Penthouse containing recording and control equipment are shown in Figs. 6 to 23. A description of each of these components has been presented in great detail in Ref. 2. However, the roll-oscillation mechanism and new instrumentation system shown in Figures 15, 20, and 22 were developed and placed into operation after the publication of Ref. 2 and have not been described heretofore.

Roll-Oscillation System — Briefly, the roll-oscillation system produces an oscillation of the body about its longitudinal axes. Modifications and additions to the drive system and roll gage assembly, shown in Figs. 13 and 17, respectively, were required to incorporate this additional mode of motion.
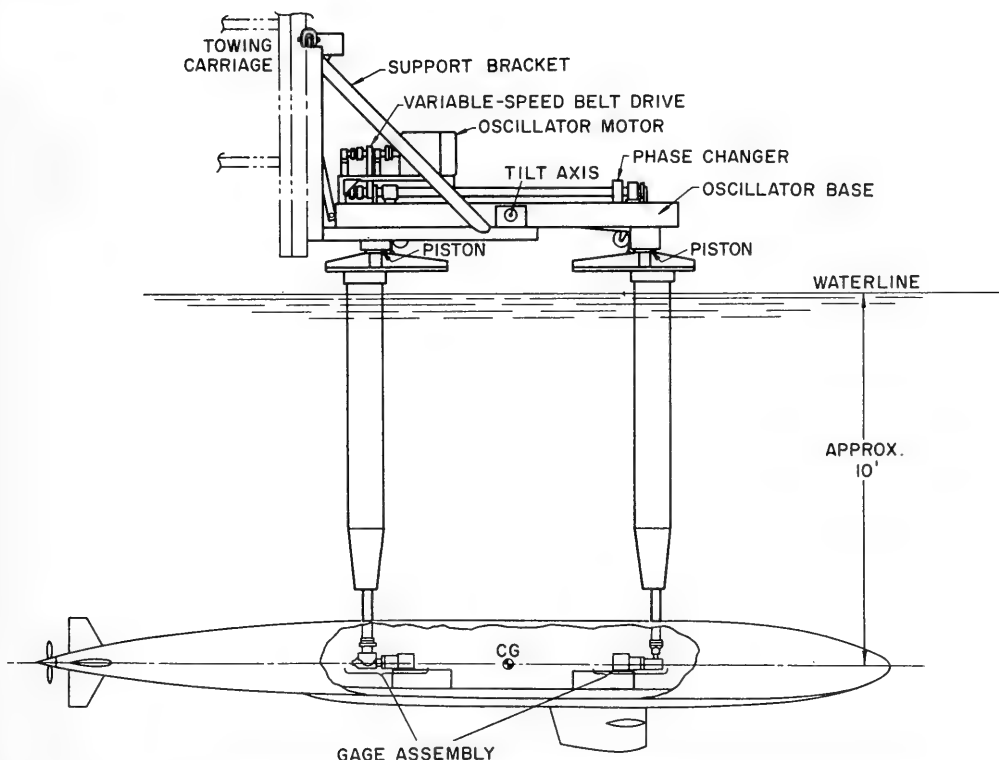
Fig. 6. Schematic arrangement of DTMB Planar Motion Mechanism with model attached

Table 2
Reduction Equations for Rotary and Acceleration Derivatives*

	Vertical Plane	
Derivative	Model Erect	Model Inverted
$Z_{\dot{w}}{}' - m_m{}'$	$-\dfrac{\partial[(Z_1{}')_{in} + (Z_2{}')_{in}]}{\partial \dot{w}_o{}'}$	$\dfrac{\partial[(Z_1{}')_{in} + (Z_2{}')_{in}]}{\partial \dot{w}_o{}'}$
$M_{\dot{w}}{}' + x_{CG}{}'m_m{}'$	$-\dfrac{x}{\ell}\dfrac{\partial[(Z_2{}')_{in} - (Z_1{}')_{in}]}{\partial \dot{w}_o{}'}$	$\dfrac{x}{\ell}\dfrac{\partial[(Z_2{}')_{in} - (Z_1{}')_{in}]}{\partial \dot{w}_o{}'}$
$Z_q{}' + m_m{}'$	$\dfrac{\partial[(Z_1{}')_{out} + (Z_2{}')_{out}]}{\partial q_o{}'}$	$-\dfrac{\partial[(Z_1{}')_{out} + (Z_2{}')_{out}]}{\partial q_o{}'}$
$M_q{}' - x_{CG}{}'m_m{}'$	$\dfrac{x}{\ell}\dfrac{\partial[(Z_2{}')_{out} - (Z_1{}')_{out}]}{\partial q_o{}'}$	$-\dfrac{x}{\ell}\dfrac{\partial[(Z_2{}')_{out} - (Z_1{}')_{out}]}{\partial q_o{}'}$
$Z_{\dot{q}}{}' + x_{CG}{}'m_m{}'$	$\dfrac{\partial[(Z_1{}')_{in} + (Z_2{}')_{in}]}{\partial \dot{q}_o{}'}$	$\dfrac{\partial[(Z_1{}')_{in} + (Z_2{}')_{in}]}{\partial \dot{q}_o{}'}$
$M_{\dot{q}}{}' - I_{y_m}{}'$	$\dfrac{x}{\ell}\dfrac{\partial[(Z_2{}')_{in} - (Z_1{}')_{in}]}{\partial \dot{q}_o{}'} + \dfrac{(M_\theta)_m}{\frac{1}{2}\rho\ell^5}\bigg/\omega^2$	$-\dfrac{x}{\ell}\dfrac{\partial[(Z_2{}')_{in} - (Z_1{}')_{in}]}{\partial \dot{q}_o{}'} + \dfrac{(M_\theta)_m}{\frac{1}{2}\rho\ell^5}\bigg/\omega^2$

	Horizontal Plane	
Derivative	Starboard Down	Port Down
$Y_{\dot{v}}{}' - m_m{}'$	$-\dfrac{\partial[(Y_1{}')_{in} + (Y_2{}')_{in}]}{\partial \dot{v}_o{}'}$	$\dfrac{\partial[(Y_1{}')_{in} + (Y_2{}')_{in}]}{\partial \dot{v}_o{}'}$
$N_{\dot{v}}{}' - x_{CG}{}'m_m{}'$	$\dfrac{x}{\ell}\dfrac{\partial[(Y_2{}')_{in} - (Y_1{}')_{in}]}{\partial \dot{v}_o{}'}$	$-\dfrac{x}{\ell}\dfrac{\partial[(Y_2{}')_{in} - (Y_1{}')_{in}]}{\partial \dot{v}_o{}'}$
$Y_r{}' - m_m{}'$	$-\dfrac{\partial[(Y_1{}')_{out} + (Y_2{}')_{out}]}{\partial r_o{}'}$	$+\dfrac{\partial[(Y_1{}')_{out} + (Y_2{}')_{out}]}{\partial r_o{}'}$
$N_r{}' - x_{CG}{}'m_m{}'$	$+\dfrac{x}{\ell}\dfrac{\partial[(Y_2{}')_{out} - (Y_1{}')_{out}]}{\partial r_o{}'}$	$-\dfrac{x}{\ell}\dfrac{\partial[(Y_2{}')_{out} - (Y_1{}')_{out}]}{\partial r_o{}'}$
$Y_{\dot{r}}{}' - x_{CG}{}'m_m{}'$	$-\dfrac{\partial[(Y_1{}')_{in} + (Y_2{}')_{in}]}{\partial \dot{r}_o{}'}$	$\dfrac{\partial[(Y_1{}')_{in} + (Y_2{}')_{in}]}{\partial \dot{r}_o{}'}$
$N_{\dot{r}}{}' - I_{z_m}{}'$	$\dfrac{x}{\ell}\dfrac{\partial[(Y_2{}')_{in} - (Y_1{}')_{in}]}{\partial \dot{r}_o{}'} + \dfrac{(N_\psi)_m}{\frac{1}{2}\rho\ell^5}\bigg/\omega^2$	$-\dfrac{x}{\ell}\dfrac{\partial[(Y_2{}')_{in} - (Y_1{}')_{in}]}{\partial \dot{r}_o{}'} + \dfrac{(N_\psi)_m}{\frac{1}{2}\rho\ell^5}\bigg/\omega^2$
$K_{\dot{v}}{}'$	$-\dfrac{\partial(K')_{in}}{\partial \dot{v}_o{}'}$	$\dfrac{\partial(K')_{in}}{\partial \dot{v}_m{}'}$
$K_r{}'$	$-\dfrac{\partial(K')_{out}}{\partial r_o{}'}$	$+\dfrac{\partial(K')_{out}}{\partial r_o{}'}$
$K_{\dot{r}}{}'$	$-\dfrac{\partial(K')_{in}}{\partial \dot{r}_o{}'}$	$\dfrac{\partial(K')_{in}}{\partial \dot{r}_m{}'}$
$K_p{}'$	$-\dfrac{\partial(K')_{out}}{\partial p_o{}'}$	$-\dfrac{\partial(K')_{out}}{\partial p_o{}'}$
$K_{\dot{p}}{}' - I_{x_m}{}'$	$-\dfrac{\partial(K')_{in}}{\partial \dot{p}_o{}'} + \dfrac{(K_\phi)_m}{\frac{1}{2}\rho\ell^5}\bigg/\omega^2$	$-\dfrac{\partial(K')_{in}}{\partial \dot{p}_o{}'} + \dfrac{(K_\phi)_m}{\frac{1}{2}\rho\ell^5}\bigg/\omega^2$
$\dot{w}_o{}' = \dfrac{a}{\ell}\dfrac{\omega^2\ell^2}{U^2}$	$\dot{v}_o{}' = \dfrac{a}{\ell}\dfrac{\omega^2\ell^2}{U^2}$	
$q_o{}' = \dfrac{\omega\ell}{U}\dfrac{2a}{b}\sin\dfrac{\phi_a}{2}$	$r_o{}' = \dfrac{\omega\ell}{U}\dfrac{2a}{b}\sin\dfrac{\phi_a}{2}$	$p_o{}' = \phi_o\dfrac{\omega\ell}{U}$
$\dot{q}_o{}' = \dfrac{\omega^2\ell^2}{U^2}\dfrac{2a}{b}\sin\dfrac{\phi_a}{2}$	$\dot{r}_o{}' = \dfrac{\omega^2\ell^2}{U^2}\dfrac{2a}{b}\sin\dfrac{\phi_a}{2}$	$\dot{p}_o = \phi_o\dfrac{\omega^2\ell^2}{U^2}$

* $m_m{}'$, $(M_\theta)_m$, $(N_\psi)_m$, and $(K_\phi)_m$ determined from standstill tests
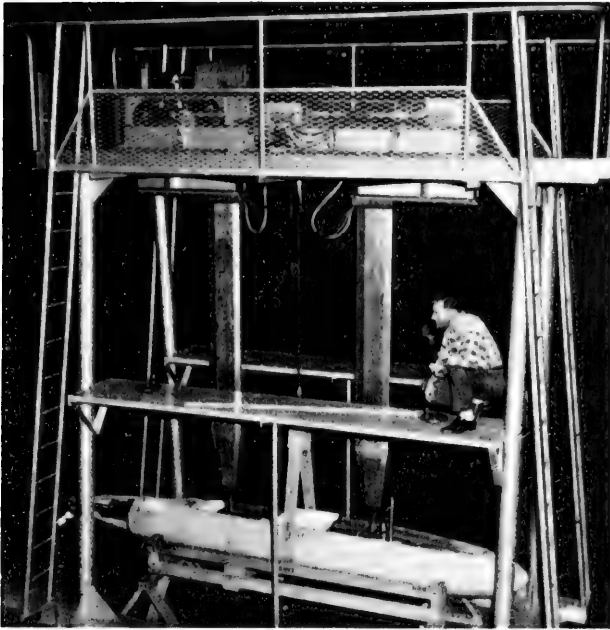
Fig. 7. Tilt table with model attached
mounted on storage stand
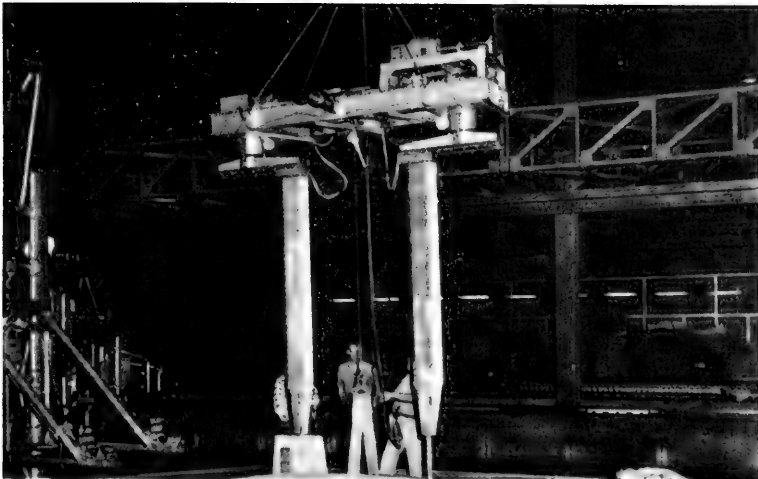
Fig. 8. Tilt table with model attached being moved
by overhead crane

Alex Goodman
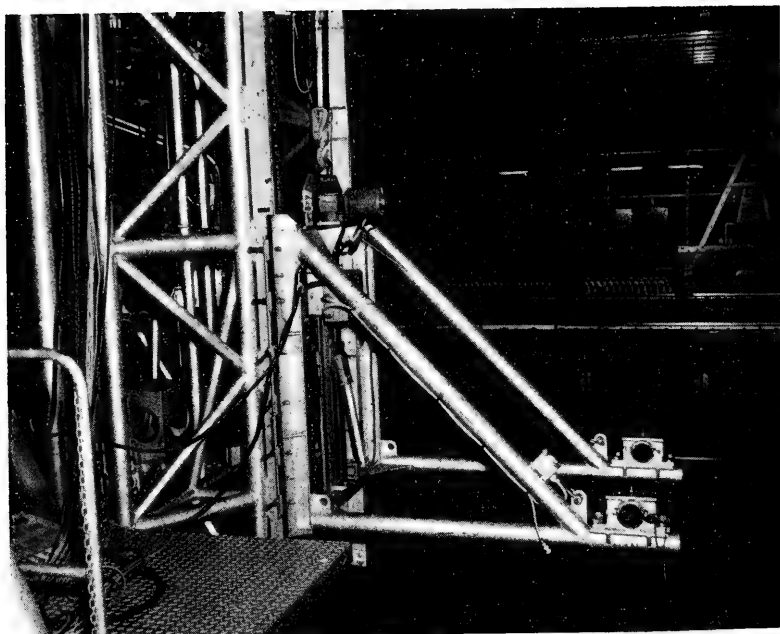
Fig. 9. Tilt table support bracket attached to towing carriage
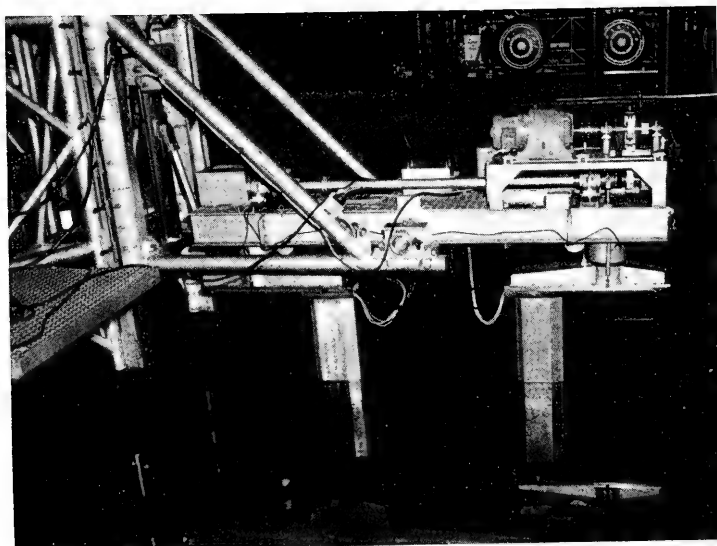
Fig. 10. Tilt table

Fig. 11. Tilting mechanism
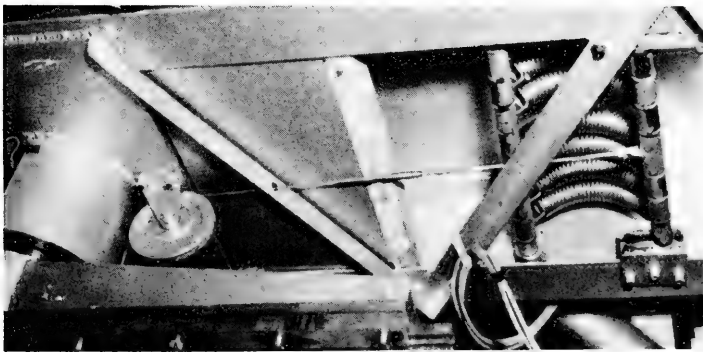
Fig. 12. Counterbalancing device

The lower pulley shaft of the drive system, shown in Fig. 13, was modified so that it would operate in two modes; as a power transmitting shaft for the pure heaving and pitching modes, and as a power transmitting shaft for the rolling mode. This is accomplished by mounting the lower set of Gilmore pulleys on a shaft which is support by ball bearings to an inner shaft which is directly coupled to the main drive shaft. For pitching and heaving, the outer and inner pulley shafts are connected by means of a tapered pin. For the rolling mode, the taper pin is removed, and the strut-pistons are locked. The pulley at the end of the idler shaft, shown in Fig. 15a, is connected by means of a Gilmore belt to a pulley-shaft system attached to the aft strut-piston. This pulley can be positioned along a keyed shaft so that a fixed relationship is maintained between the pulley and the aft strut. Power is transmitted to the slider crank mechanism attached to the aft strut, by means of another
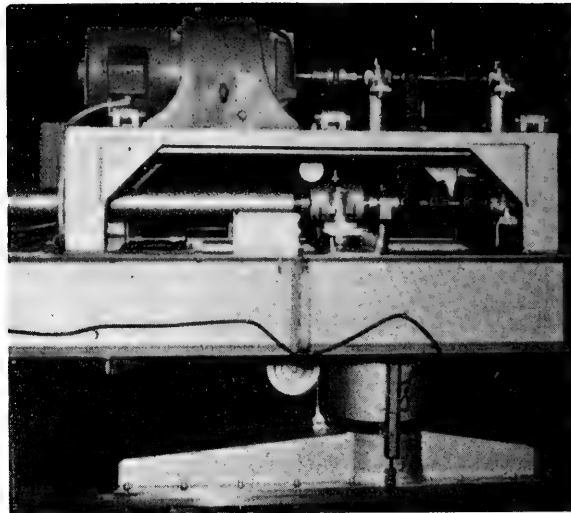
Fig. 13. Drive system for forced-motion mechanism
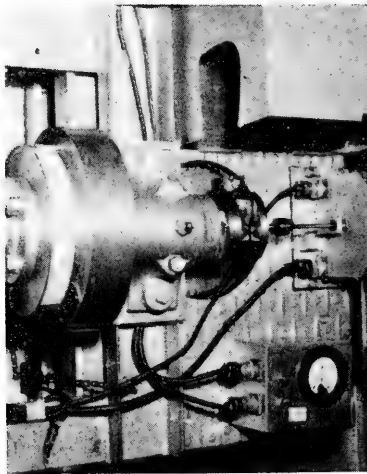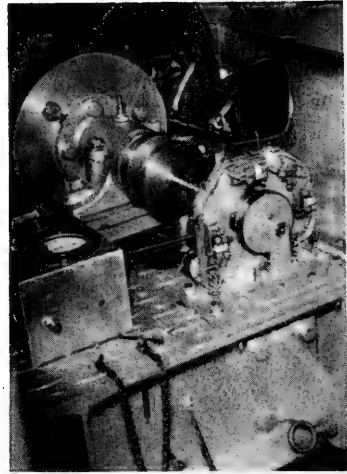
(a) Top view   (b) End view
Fig. 14. Phase-changer and synchronous switch

pulley-Gilmore belt system. The slider crank mechanism used in this case has an eccentricity of 0.125 inches and a connecting rod length of 5.000 inches; or a length of connecting rod to eccentricity of 40.0. The sinusoidal motion produced by the slider crank mechanism is transmitted to a 1.0-inch-diameter push-rod, shown in Fig. 15b, which is guided by linear bearings attached to the aft strut. The end of the push-rod is attached to the modified roll gage by means of the 3.000-inch crank arm assembly shown in Fig. 15c. The maximum amplitude of the roll oscillation is therefore, ±2.38 degrees

$$\left(\phi_0 = \tan^{-1} \frac{0.125}{3.000} \right)$$
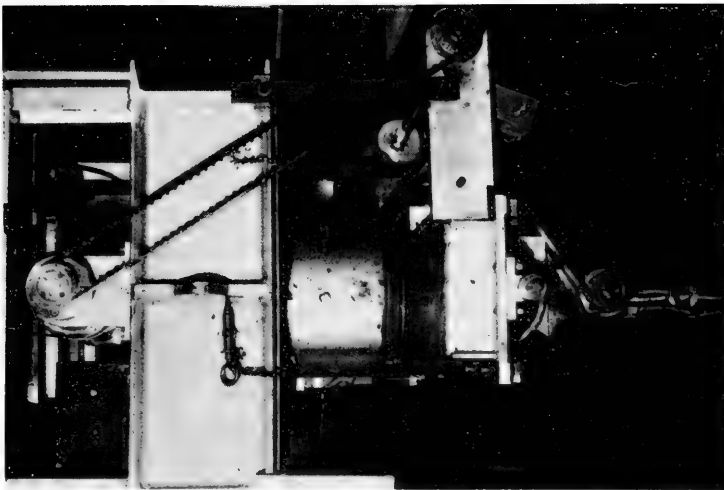
(a) Roll oscillation drive mechanism
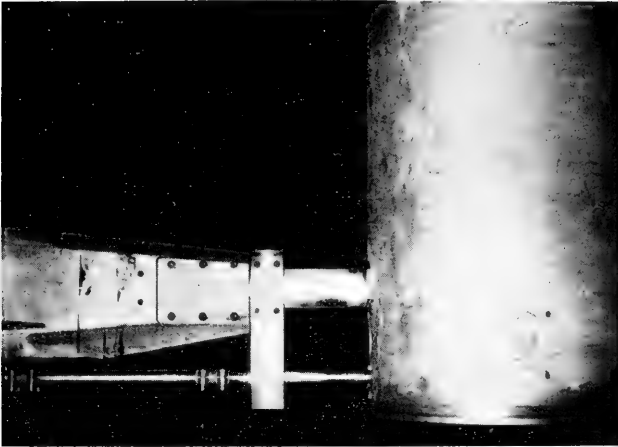
(b) Roll push rod
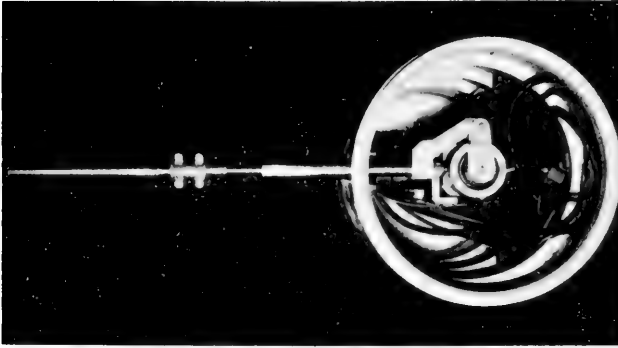
(c) Push-rod attachment to roll balance

Fig. 15. Roll oscillation mechanism
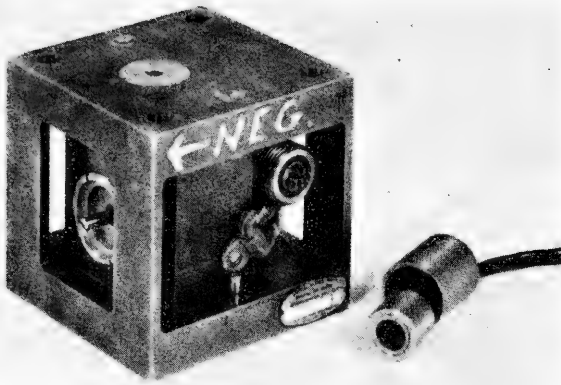
Fig. 16. Modular force gage

(a) Assembled with gimbal
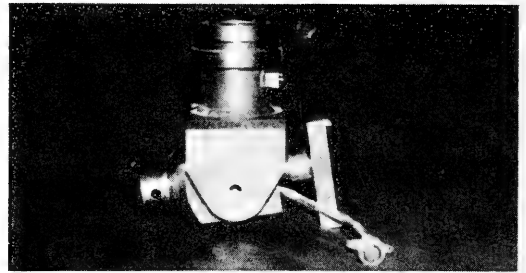
(b) Individual components

(c) Modified roll gage

GIMBAL BLOCK

PUSH-ROD ATTACHMENT

SHAFT
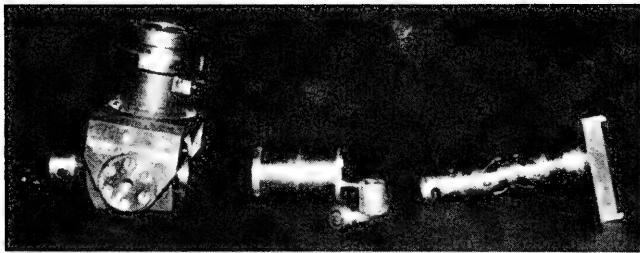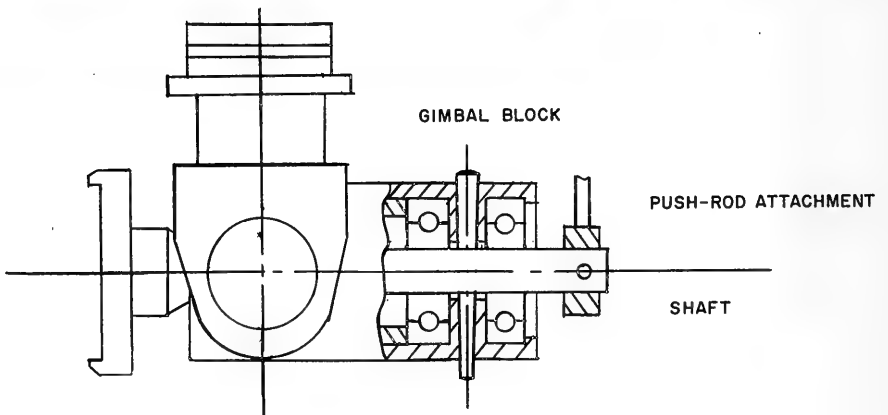
Fig. 17(a), (b), (c). Roll gage

(a) Top view
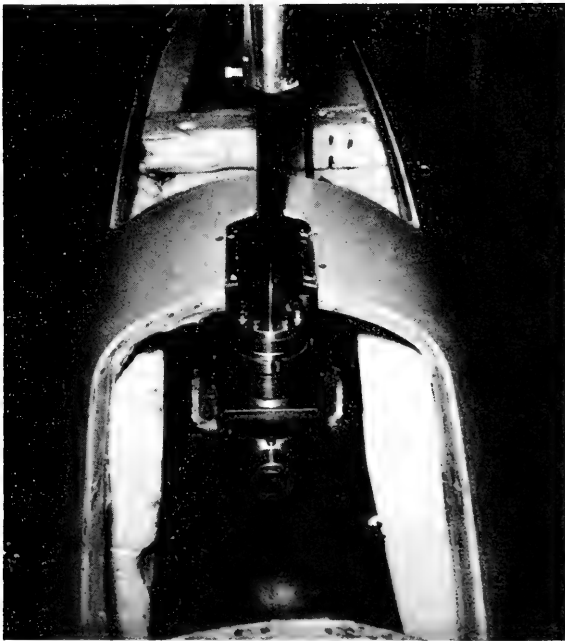
(b) Fore and aft view

Fig. 18. Gage assembly
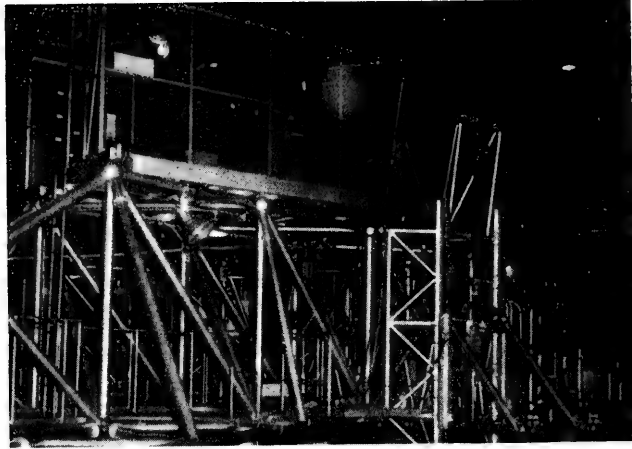
Fig. 19. Penthouse mounted on top of carriage
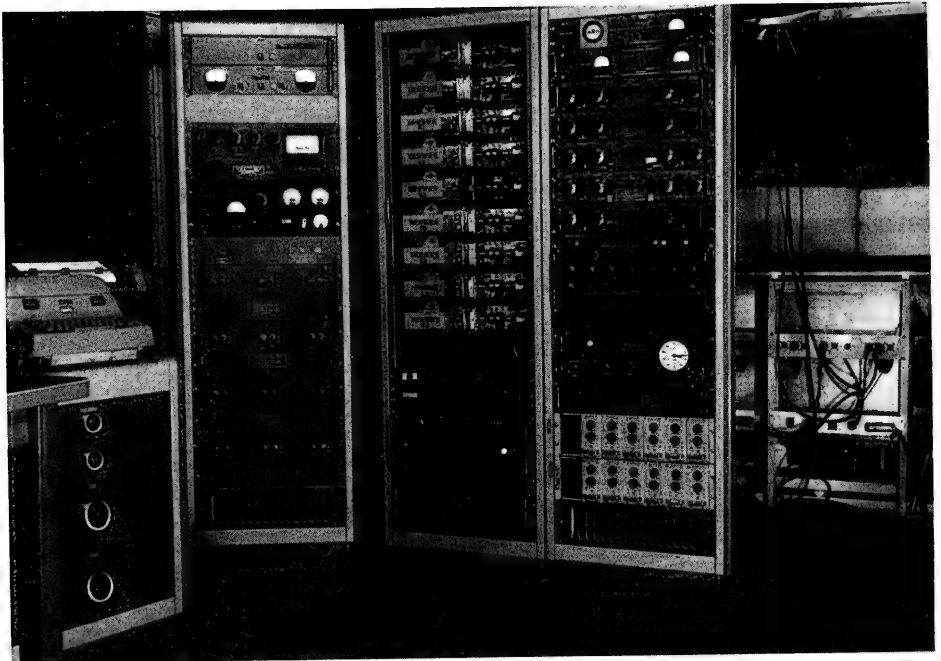
Fig. 20. Inside view of penthouse showing instrumentation
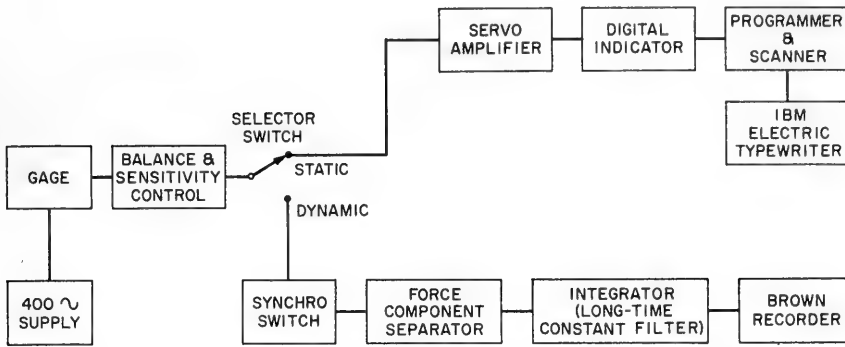
Fig. 21. Instrumentation system for Planar-Motion-Mechanism System
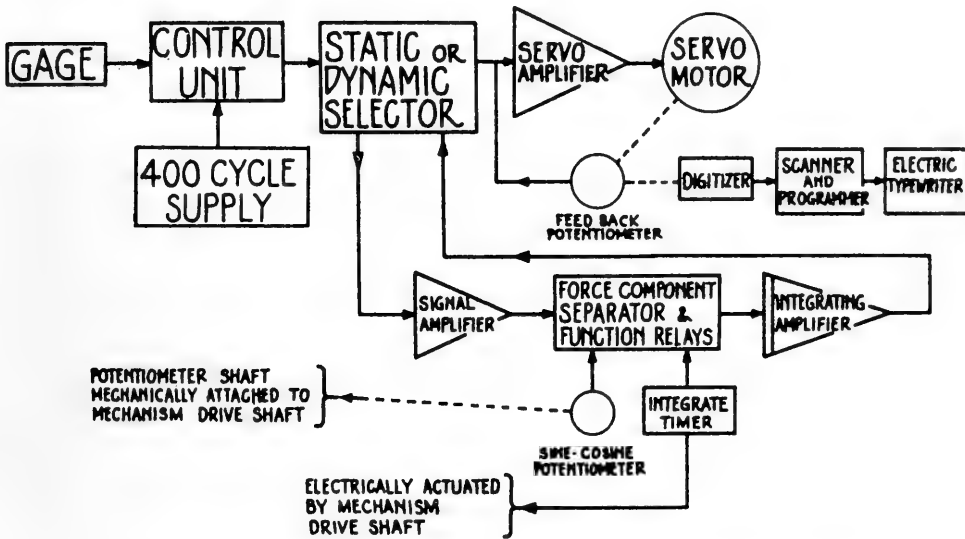
Fig. 22. New instrumentation system for static and dynamic stability tests

The roll gage assembly, shown in Figs. 17a and 17b, was modified as sketched in Fig. 17c. The longer shaft is now supported in the gimbal block by two ball bearings. For the static, heaving, and pitching tests, the shaft is attached to the gimbal block by a large taper pin. In this mode the balances and gimbal block assembly function as described in Ref. 2.

For the rolling tests, the taper pin is removed and the push-rod attachment is installed. The body can now be oscillated in roll through the roll gage located at the aft strut and the three-degree-of-freedom gimbal located at the forward strut.

The range of oscillation frequencies and frequency changing procedures for the rolling mode are the same as for the pitching and heaving modes [2].
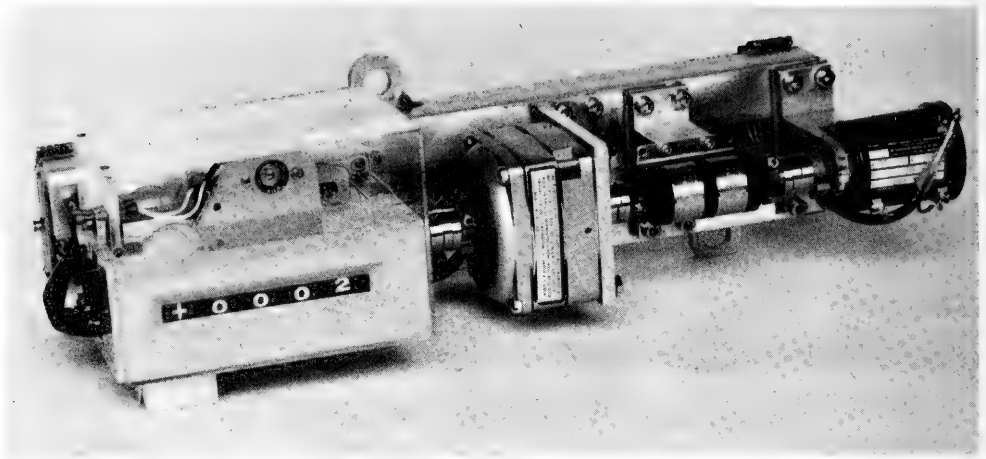
Fig. 23. Digital indicator

Instrumentation for Static and Dynamic Stability Tests — A comparison of the old and new measuring and recording systems, presented in Figs. 21 and 22, respectively, shows that both systems are essentially the same for the static stability tests. The major difference is in the method and equipment used in the dynamic tests. For completeness, however, the measuring and recording equipment used in the static and dynamic tests, shown by the block diagram in Fig. 22, will be described.

The recording equipment for the static stability tests is a digital system designed to display and read out the unique steady-state value of each force and moment sensed by the transducers for any given test condition. The system is made up of seven channels to conform to the number of gages in the model. Each channel is separate in all respects except for the power supply that it shares in common.

Briefly, each channel is essentially an automatic null-balancing system; the transducer in the gage and the digital indicator combine together in a servo system. The transducer output is balanced by a potentiometer. When a gage in the model is deflected, the resulting error signal from the transducer is amplified and drives a servo motor which positions a potentiometer to restore electrical balance, or null, to the system. The amount that the potentiometer is moved is then a measure of the force or moment applied at the gage. The various components and circuitry which constitute the recording systems are shown by the block diagram in Fig. 22.

The upper path of Fig. 22 applies to the digital system used for static stability tests. A Brown recorder could be used in place of the digital system. The term gage is used to denote the variable reluctance transducer whether it be the magnigage used with the modular force gages or the magnitorque used with the roll gages. The 400-cycle power source supplies a 4.5-volt carrier to the gage in such a manner that the current divides into two paths, one about each coil. If the core of the gage is electrically centered, the impedances of the gage halves are equal, and consequently the voltages are equal. As the core is displaced, the impedance of one gage half increases and that of the other decreases with corresponding voltage changes.

Alternating voltage from the gage passes to the balance and sensitivity control box, which contains a silicon diode bridge as well as other adjustments and refinements that are described in more detail later. The voltage is rectified by the diode bridge to produce full-wave rectified direct-current voltage. The total rectified voltage obtained across both coils is constant and is used as a reference voltage. Polarity is established by making one side of the line positive and the other negative. The voltage measured between each coil changes, however, when the gage core is displaced; the voltage across one coil increases while the other decreases an equal amount so that the reference voltage always remains constant. This is analogous to a three-wire system in which the voltage across the outside lines remains constant but the voltage from one side to the common is made variable. The feedback potentiometer, which is on the shaft of the digital indicator, is wired similarly; the voltage across the end terminals is the reference voltage and the common is attached to the potentiometer slider. When the gage core is at electrical center, the potentiometer slider is at midposition. When the gage core is displaced, an error signal results.

The error signal is fed through a mode selector switch (static or dynamic; digital or recorder) to a chopper servo-amplifier similar to that contained in the Brown recorder manufactured by Minneapolis-Honeywell Company. The chopper converts the direct-current error signal into 60-cycle alternating current. The resulting signal is amplified to drive a servo motor which in turn drives the potentiometer slider until the error signal is reduced to zero and a null-balance established.

The digital indicator, shown in Fig. 23, is the active part of the feedback loop. The assembly is made up largely of commercially obtainable components. Beginning from the left, it may be seen that there is a digitizer with a detent unit, servo motor, speed reducer, and potentiometer. The components are aligned axially and are connected together with Oldham couplings to minimize binding. The Metron speed reducer, is an antibacklash planetary gear box with a reduction of 21 to 1. It is inserted between the servo motor and 10-turn Heliopot (± 0.05 linearity) so that the range of the system is ± 5 turns on the potentiometer, with a little to spare. The digitizer is connected directly to the through-shaft of the servo motor. The digitizer is a unit manufactured by the Dayton Instrument Company. It is essentially a four-digit mechanical counter and plus-minus wheel, equipped with electrical contacts. Eleven wires are brought out of each decade, one for each unit and one common. These wires lead to the programmer and scanner and then to the readout equipment. The detent unit, which is integral with the digitizer, consists of a solenoid-operated star wheel. The star wheel is used to center the unit decade on a contact, when command for readout is given the solenoid is energized and the digit wheels are placed in contact with the electrical brushes.

The digital indicator operates in two modes: balancing and readout. In the balancing mode, it is part of the feedback loop, as explained earlier. In the readout mode, the servo motor is automatically stopped and the digitizer serves as a memory which stores the last reading obtained.

The scanner and programmer unit is the brain of the readout system. It serves two functions: first, introducing predetermined data such as run number, body angle, and control surface angle and secondly, scanning and sequencing the data actively obtained during the test. When a test run is made, the digital indicators are allowed to settle out at an approximately fixed reading. At command, the servo motors are automatically stopped and the scanner unit scans each channel, decomplimenting if necessary, and feeds the readings in correct sequence, one digit at a time, to the solenoid-operated IBM electric typewriter. The typewriter tabulates the data on a form specially prepared for the purpose, as shown by the reduced sample given in Fig. 24.

SUBMAP STABILITY AND CONTROL DATA SHEET
PRMC-TR. 13 (2-58)

SHEET NO. 23

MODEL 4737	ENGINEER(S) Young-Schwarting	NOTES Strip tests in top rudder and prop. off Sens 5:1 all gages except y's
X HORIZONTAL ☐ VERTICAL		
DAY 5-5-59 T 1515		

RUN NO	d	α	β	λ_r	λ_b	ν_s	x_1	x_2	y_1	y_2	z_1	z_2	κ	SPARE	DIR	Δt	SPEED	RPM #1	RPM #2
2023			00	002			0001	0000	0000	0000	0000	0000	0000		D	05	00180	00001	00002	0 0
2024			00	-000			0015	-0203	-0021	0016	-0070	0008	0000		0	05	10140	00002	00001	0 0
2025			02	-000			0042	-0212	0232	-0058	-0084	0044	0000		D	05	10144	00002	00001	0 0
2026			04	-000			0067	-0213	0482	-0120	-0088	0163	0000		D	05	10144	00001	00001	0 0
2027			-00	000			0022	-0207	-0012	0019	-0066	0015	0000		D	05	10157	00001	00002	0 0
2028			-02	000			0010	-0195	-0295	0110	-0056	0069	0000		0	05	10146	00001	00001	0 0
2029			-04	001			0027	-0187	-0536	0158	-0032	0190	0000		0	05	10145	00001	00001	0 0
2030			-06	001			0029	-0190	-0793	0173	-0008	0425	0000		D	05	10153	00002	00001	0 0
2031			-08	000			0032	-0188	-1041	0155	-0019	0738	00000		0	05	10153	00001	00001	0 0
2032			-12	000			0001	-0200	-1060*	0061	0062	1098*	-0001		D	05	10145	00001	00001	0 0
							* after n0 means hit limit												
2033			00	050			0020	-0212	-0060	0111	-0063	0011	-000		0	05	10145	00001	00001	0 0
2034			02	049			0042	-0216	0186	0045	-0075	0044	-0001		D	05	10141	00001	00002	0 0
2035			04	049			0066	-0218	0427	-0004	-0085	0157	-0001		D	05	10154	00001	00002	0 0
2036			-00	049			0021	-0214	-0057	0111	-0062	-0000	-0001		D	05	10138	00001	00001	0 0
2037			-02	050			0008	-0200	-0335	0193	-0041	0056	-0002		D	05	10149	00002	00001	0 0
2038			-04	049			0021	-0198	-0580	0243	-0014	0194	-0002		D	05	10143	00001	00002	0 0
2039			00	-046			0020	-0211	0014	-0061	-0066	0008	-0001		D	05	10137	00002	00002	0 0
2040			02	-044			0040	-0211	0268	-0139	-0073	0040	-0001		D	05	10141	00002	00002	0 0
2041			04	-045			0064	-0210	0520	-0196	-0075	0157	-0001		D	05	10143	00001	00001	0 0
2042			-00	-045			0016	-0206	0018	-0062	-0057	0005	-0001		D	05	10146	00002	00002	0 0
2043			-02	-045			0010	-0194	-0254	0016	-0050	0062	-0002		D	05	10142	00001	00001	0 0
2044			-04	-045			0027	-0188	-0499	0059	-0026	0191	-0002		D	05	10148	00001	00001	0 0

Fig. 24. Typical data sheet for static and dynamic tests

As mentioned earlier, the balance and sensitivity control box contains features that are provided for the purpose of maintaining accuracy and increasing versatility of the system. Among these features are the means of checking zero, adjusting and checking sensitivity, changing zero reference, and filtering to smooth out the data.

A zero-check switch is provided to separate any change of reading due to causes other than actual gage displacement. These changes could be due to causes such as changes in value of circuit resistors or diodes. When the switch is closed, the primaries of two input transformers of the control circuit are connected in parallel so that their voltages must be equal regardless of gage core position. If the zero-check reading differs from the original value, the difference is due to changes in the control unit circuitry rather than the gage. Thus, the reading obtained on the digital indicator may be corrected by this amount. If the gage is not balanced at the time of testing due to preload or core offset, it is desirable to balance it directly. This is accomplished by a "gage zero" potentiometer which is adjusted to make the impedances across the two gage halves equal.

The "pen position" adjustment is provided to set the initial reading of the digital indicator or recorder to any desired value while the model is at rest. The usual practice for steady-state tests is to adjust the digital indicator to read zero when there are no hydrodynamic loads on the system. The setting is periodically checked before each run or group of runs to maintain the zero. The advantages of this procedure are that it provides a means for

determining easily whether any changes other than hydrodynamic have occurred in the total system and it eliminates the need for subtracting arbitrary readings on each channel to obtain the net readings. The pen position adjustment is accomplished by a potentiometer which is connected in parallel with the feedback potentiometer.

A span or sensitivity adjustment is provided to establish the calibration of the digital indicator in terms of the load on the gage. The span control is a potentiometer which is placed in series with the part of the circuit that goes with the feedback potentiometer slider. Thus the unbalanced voltage resulting from displacement of the gage appears across the span potentiometer as well as any other resistors placed in series with it. The range of sensitivity varies from nearly zero to an amount somewhat in excess of that required to accommodate the maximum sensitivity of all the types of transducers used in the tests. The span potentiometer has a calibrated index and can be locked into place. However, since the control units and gages can be interchanged, the span potentiometer setting is not sufficiently accurate. Therefore a system for setting sensitivity which is independent of the transducer movement is provided. This "span check" is made by applying a step signal to simulate an actual transducer change. To do this, a precision resistor in the control box is shunted across one gage coil. The resulting span check reading on the digital corresponds to the given sensitivity and to the nominal setting on the span potentiometer.

Span control settings and span checks are usually established with the modular force gage or roll balance mounted on a calibration stand. Since all components of the measurement system are linear, the settings are determined on the basis of that required to give a reading of exactly 1000 counts on each channel for some predetermined load. As mentioned earlier, the usual sensitivity is 200 pounds for 1000 counts; however, sensitivities of twice or one-half of this amount are used from time to time, depending on the range of loads encountered in the test. The span checks for each calibration are recorded in a log book. These values have been found to hold true for any particular gage and control box combination over a period of years.

The signal coming from the gages is a fluctuating one even in steady-state tests. This is due largely to carriage vibrations which are transmitted to the model through the rigid attachment. A filter is provided in the control box to smooth this signal to obtain one steady value at the digital indicators. The filters are made up in steps so that only the amount needed for smoothing is used without needlessly sacrificing speed of response. The filter switch connects successive values of capacitance between the span potentiometer slider and one side of the feedback potentiometer. The polarity between these two points is always the same, so that electrolytic capacitors of reasonable size can be used. Since this capacitance is outside the servo feedback loop, it introduces no instability.

The recording and measuring equipment for the dynamic tests uses the same control unit, 400-cycle power supply, and digital readout or Brown recorder system. The distinguishing features are: the introduction of the signal amplifier, the force component separator, the integrating amplifier, the multiganged sine-cosine potentiometer, and the integrate timer and function relays. These components are shown by the lower leg of the block diagram of Fig. 22. They become part of the measuring and readout system when the selector switch is thrown from static to dynamic. The selector switch also selects the type of readout; that is, digital or Brown recorder. The digital system, however, is represented in Fig. 22.

The signal amplifier shown by the block diagram is a high-gain transistorized amplifier that provides accurate amplification of signals in millivoltages over the frequency range from direct current to 20 kilocycles. Some of the principle features of this amplifier are: high

input impedance, and therefore negligible loading effect on transducer initiating signals, drift of less than 2 microvolts per 10°F change in ambient temperature for the 0.1- to 30-millivolt input ranges, and for frequencies of 0 to 10 cycles per second, an equivalent input noise of about 4 microvolts peak to peak. This amplifier, the Accudata III, is manufactured by Minneapolis-Honeywell Company. Seven of these amplifiers are used in the system; one for each gage.

The multiganged sine-cosine potentiometer (eight potentiometers mounted on one shaft) is mechanically attached to the Planar Motion Mechanism driveshaft in the same manner as that used for synchronous switch, shown in Fig. 14, and rotates at the displacement frequency ω. Each sine-cosine potentiometer has a function conformity of ±0.25 percent from 0 to 360 degrees. These potentiometers are manufactured by the Beckman Heliopot Company.

The output of the signal amplifier is applied to the input of the sine-cosine potentiometer within the circuitry of the force component separator. The force component separator consists of seven channels, one for each gage. The major components of the force component separator unit are the function switch, normal-reverse switch, and function relays.

The function switch has four settings which are identified as quadrature, reset, in-phase, and calibrate. The quadrature position electrically multiplies the amplified signal from each signal amplifier with the cos ωt generated by a corresponding cosine wiper of the sine-cosine potentiometers. The in-phase position performs a similar multiplication with sin ωt. In the reset position, the feedback capacitor of the integrating amplifier is shorted out and the output voltage of the integrating amplifier is returned to its zero level. In the calibrate position, the sine-cosine wipers are disconnected and the signal is multiplied by unity instead of either sin ωt or cos ωt. The significance of this will be discussed later. The normal-reverse switch changes the polarity of the signal feeding into the sine-cosine potentiometer. This feature eliminates the requirement for knowing the static zero precisely; that is, it eliminates the need for having the transducer balanced exactly.

The product of the signal with either the sin ωt or cos ωt is fed into the integrating amplifier. This amplifier is another Accudata III operated in the open-loop mode and having a precision capacitor in the feedback loop. Again, one integrator is used for each gage in the system. The feedback capacitor has a value of 0.5 microfarad (accurate to within ±0.1 percent) and is manufactured by Arco Electronics Company. The output voltage of the integrating amplifier is fed through the contacts of the function relays; identified as "integrate" and "hold." These relays are controlled by a precision stepping switch located in the integrate timer unit. The operation of the stepping switch is controlled by a microswitch which is actuated by a sweeper mounted on the drive shaft. The number of pulses to be counted, corresponding to revolutions of the drive shaft, can be selected by a switch located on the integrate-timer unit. The home position of the stepping switch and function relays corresponds to the reset position mentioned previously. Upon being pulsed, the stepping switch operates the integrate and hold relays and then rotates an amount corresponding to the selected number of cycles. At this point the integrate relay is deenergized, opening the input to the integrating amplifier. At the same time the hold relay maintains the charge on the feedback capacitor of the integrator. The integral of the signal is therefore, the output voltage of the integrating amplifier divided by the selected time of integration. This voltage can be recorded and read out by either the digital servo system or Brown recorder.

The operation performed by this system is equivalent to determining the Fourier coefficients of the fundamental of the gage signal [10,11], as illustrated in Appendix C.

The validity of the force-component-separator and integrator system, shown in Fig. 22, has been established on the basis of controlled laboratory tests. A sinusoidal load of known amplitude and frequency (0.1 to 1.0 cycle per second) was applied to a gage. The phase angle between the gage signal and the sine-cosine potentiometer was varied known amounts over a range of ±90 degrees. The study demonstrated that the amplitude of any individual component is determined to an accuracy of better than 1 percent.

One of the main advantage of this system, over the one described in Ref. 2, is the reduction in test time for the dynamic mode (about 50 percent) and the use of the digital-readout system for recording purposes.

Typical Test Results Obtained with the System

All the hydrodynamic coefficients required in the equations of motion for submerged bodies in six degrees of freedom can be obtained with the DTMB Planar-Motion-Mechanism System. This is accomplished by appropriate orientation of the model and mode of operation of the system.

Both the linear and nonlinear coefficients associated with static stability and control are determined using the system. In the case of the rotary and acceleration derivatives, however, only the linear coefficients are determined.

The various static, rotary, and acceleration coefficients that can be evaluated using this system are presented in Appendix B and Table 2. It is believed to be pertinent, however, to include representative samples of test results obtained for each of the three classes of coefficients. Examination of these samples should provide insight not only into the nature of these coefficients but also the quality with which they can be determined by the system. Before proceeding, it is reemphasized that all of the coefficients are obtained from the explicit relationships given in Table 2.

Typical test results for coefficients of the "static" variety are shown in Figs. 25, 26, and 27. The variation of normal force and pitching moment with body angle is shown in Fig. 25 and the variation of normal force and pitching moment with stern plane angle is shown for various body angles in Figs. 26, and 27, respectively. The body-angle and plane-angle range covered in this case is only ±6 degrees. Data are, in general, obtained over a body-angle range of ±15 degrees and a control-surface angle range of ±20 to ±45 degrees, depending on the particular control surface being investigated. As indicated in the figures, the derivatives are obtained from the slopes of the appropriate curves faired through the data points. The slopes of the body-angle curves are taken through a body angle of zero and become the static stability derivatives. The slopes of the control-surface curves for zero body angle are taken through a control-surface angle of zero and become the control derivatives.

The kind of results obtained from pure heaving tests is shown in Fig. 28. The slopes of the separate in-phase force component curves are used with the formulas given to obtain the linear acceleration derivatives, the added mass $Z_{\dot{w}}$ and associated moment $M_{\dot{w}}$.

Typical results of pure pitching tests which are used to obtain (damping) force and moment derivatives are shown in Fig. 29. It may be noted that the quadrature components of force measured at each of the two struts are plotted separately. It has been found desirable to do so since the slopes of the two curves can then be substituted directly into the two formulas shown in the figure to obtain the damping force derivative Z_q and damping moment derivative M_q.
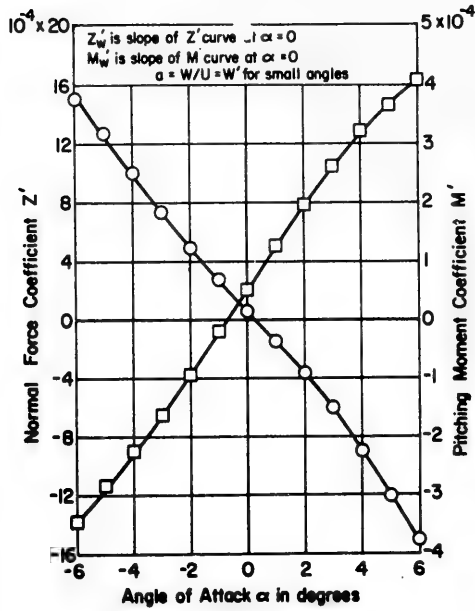
Fig. 25. Typical curves of static force and
moment versus body angle
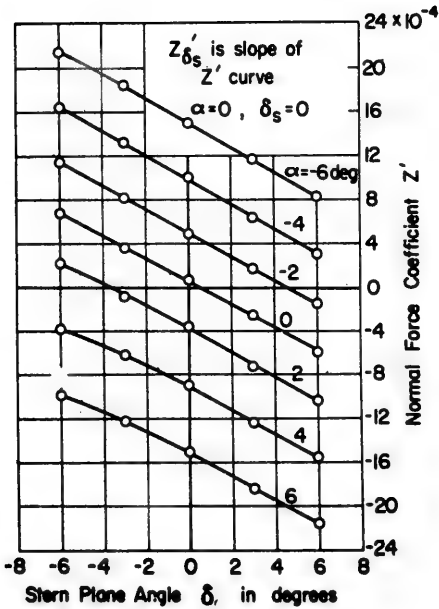
Fig. 26. Typical curves of static force ver-
sus control-surface angle for various body
angles.
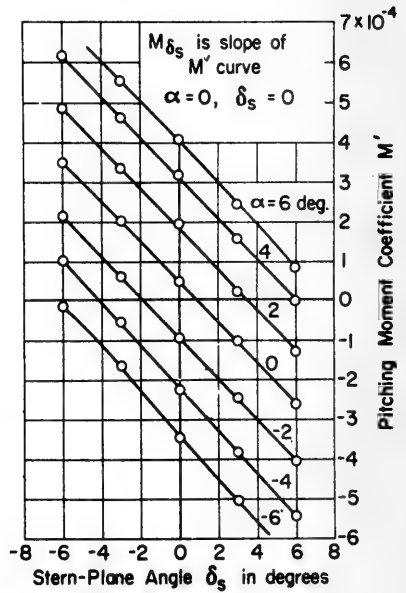
Fig. 27. Typical curves of static moment
versus control-surface angle for various
body angles
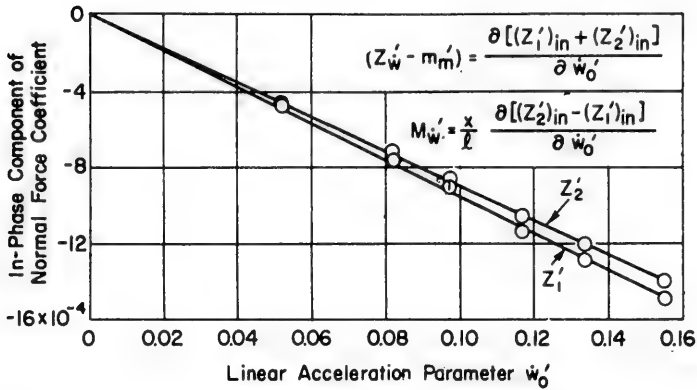
Fig. 28. Typical curves of forces versus linear acceleration amplitude from pure heaving tests used to obtain added mass (and associated moment)

Fig. 29. Typical curves of forces versus angular velocity amplitude from pure pitching tests used to obtain damping force and damping moment derivatives
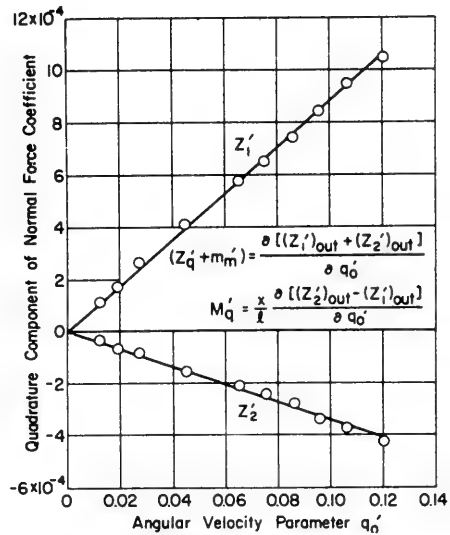
The curves of in-phase force components shown in Fig. 30 are also typical of the results obtained from pure pitching tests. Here again, the force components measured at each strut are plotted separately. The angular acceleration derivatives, the added moment of inertia $M_{\dot{q}}$ and associated force $Z_{\dot{q}}$, are obtained from the slopes of the curves using the formulas given in the figure.

Results are obtained in a similar manner for all the other hydrodynamic coefficients.

ROTATING ARM FACILITY

Another captive-model technique that has been used extensively in submerged body research, to determine explicitly the rotary coefficients for the differential equations of motion,
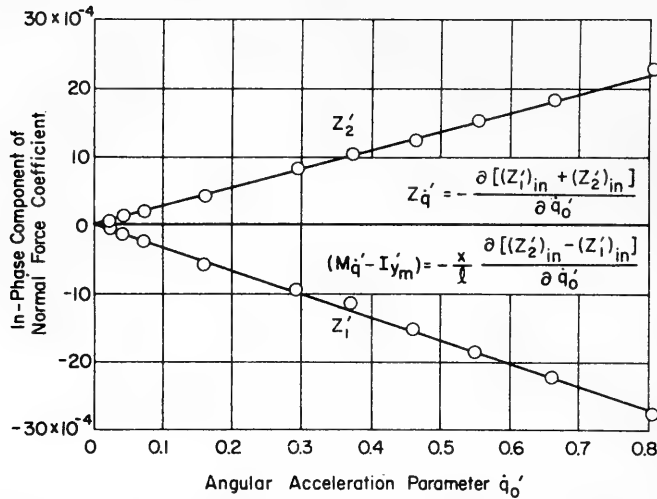
Fig. 30. Typical curves of forces versus angular acceleration amplitude from pure pitching tests used to obtain added moment of inertia (and associated force)

is the rotating arm technique [12]. In this case, the body is towed at uniform angular velocity in a circular path at different radii and the resultant forces and moments are determined for various body angles. The rotating arm technique has been used also to obtain the static-stability derivatives. In this case, the data for the various body angles are extrapolated to infinite radius and cross-plotted against the body angle. This is an indirect procedure and is generally not recommended.

The DTMB Planar-Motion-Mechanism System determines only the linear rotary derivatives. The DTMB rotating arm, using the same models, will supplement these results and provide a measure of the nonlinearities which are presently being estimated theoretically.

A detailed description of the DTMB rotating arm facility is presented in Ref. 13. For the purposes of the present paper a brief description of the main components, shown in Figs. 31 to 33, is presented herein.

The DTMB rotating arm basin is 260 feet in diameter and 21 feet deep. The arm pivots in the center on tapered roller bearings designed for centrifugal forces of 145,000 pounds. The drive system is located at the extreme end of the arm and consists of two 250-horsepower direct-current electric motors, directly coupled to two steel wheels which support the arm and run on an outer peripheral track. Each wheel is preloaded against the track by nested compression springs which provide a normal force of 61,000 pounds. A maximum steady-state speed of 30 knots can be achieved at the 120-foot radius for runs restricted to one turn. The arm, shown in Fig. 31, is a tabular aluminum structure weighing about 37,500 pounds and having natural frequencies in the vertical, horizontal, and torsional modes of greater than 3 cycles per second.

Submerged models are attached by a pair of towing struts to a model positioning apparatus, shown in Fig. 32. The positioning apparatus is attached to a carriage (Fig. 31) which can be remotely positioned along the arm to any radius from 12.5 feet to 120 feet from the
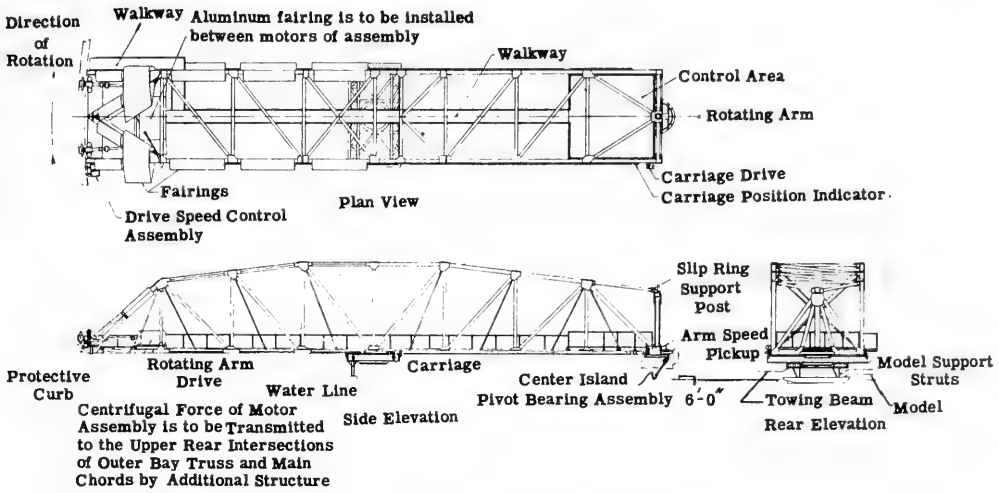
Fig. 31. Rotating arm general assembly
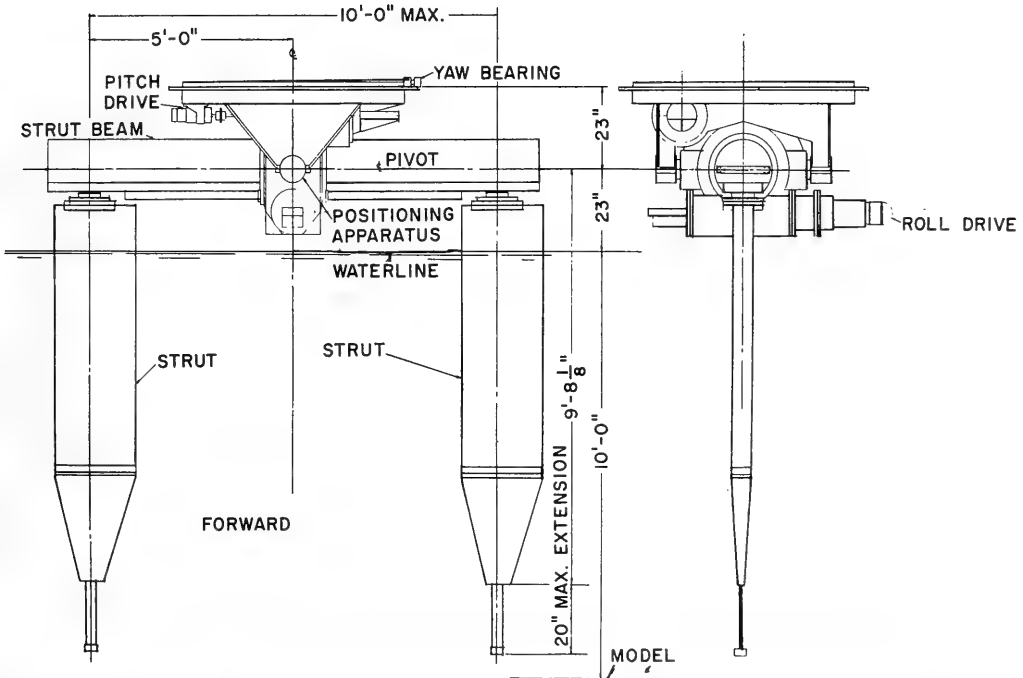
Fig. 32. Towing struts and model positioning arrangement for the rotating arm
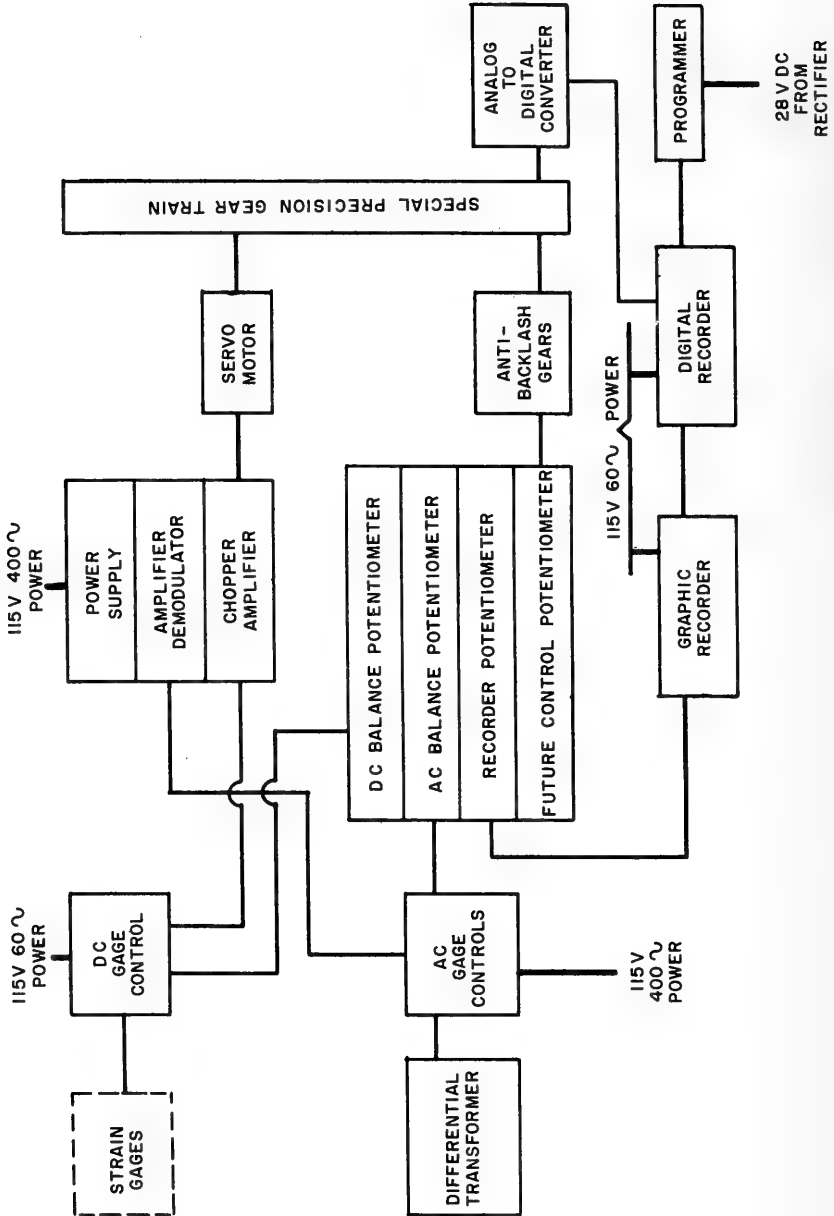
Fig. 33. Block diagram of measuring, indicating, and recording system for the rotating arm

center of the arm. The positioning apparatus is operated remotely and permits model attitudes of: yaw, plus or minus 30 degrees; pitch, plus or minus 15 degrees; and roll, 10-degree outboard, 40-degree inboard.

For yaw- and pitch-angle changes, the test location of the submerged body is unchanged. However, for roll angles, the center of roll positioning is high about the *CG* of the body, and an adjustment in radial position on the arm is necessary to maintain the proper location of the body. The positioning apparatus was made external to avoid large cutouts in the body with respect to the towing struts. Individual motor drives and position readouts are used to position the body at any attitude. Also, the support struts can be oriented with respect to the flow to minimize strut-body interference. The strut spacing is adjustable between 3.5 feet to 10 feet to accommodate various length bodies. The struts shown in Fig. 32 are similar to those used with the Planar-Motion-Mechanism System [2]. The main difference is that the upper end of the rotating arm strut has a larger chord (2.5 feet as compared to a 1.0-foot chord).

The internal balance system used with the rotating arm system is identical to that used with the Planar-Motion-Mechanism System. Likewise, the measuring, recording, and programming system, shown in Fig. 33, is essentially the same as the static-stability measuring system used with the Planar-Motion-Mechanism System.

Test runs are generally made within one turn of the rotating arm. The tangential velocity for submerged models is held constant for all radii at about 10 feet per second. For each of several discrete radii, the yaw angles (or pitch angles of a submarine model mounted on the side) is varied incrementally to investigate planar forces and moments.

MOTION ANALYSIS SIMULATOR AND FACILITY

The main purpose of any motion simulation facility is to represent, in the laboratory, the characteristics of proposed specific designs of surface ships, submarines, missiles, and other vehicles as well as the effects of the surrounding environment. Such a facility enables the designer to evaluate and improve the handling qualities or operational characteristics of a design, on the basis of established figures of merit, well in advance of construction. The facility may be used for parametric studies to investigate the importance of the various hydrodynamic coefficients and other parameters in the equations of motion. For simulating manned vehicles, the facility is used to study the responses of the human in the control loop as affected by indicators, displays, control linkage design, and environment. In addition, operating personnel can be trained well in advance of commissioning.

A simulation facility consists of a number of general-purpose electronic analog computers which are used to solve linear and nonlinear differential equations of motion such as presented in Appendix D. A general-purpose analog computer is an assembly of electronic and electromechanical units, which uses direct-current voltages as variables and can perform specific mathematical operations. When these units are connected together properly they can be used to solve mathematical equations. The independent variable is represented by time in the computer. The suitability of the computer for solving differential equations arises, therefore, from the ease with which an integration of voltage with respect to time can be achieved using a high gain direct-current amplifier having capacitance feedback [14,15]. The following basic mathematical operations, required to solve differential equations, are performed by an electronic analog computer: inversion, algebraic summation of a number of variables, multiplication by a constant, integration of a variable with respect to time,

multiplication or division of one variable by another, generation of trigonometrical functions, generation of nonlinear functions, and discontinuities.

The various components that comprise the DTMB Motion Analysis and Simulator Facility are presented in Figs. 34 to 39.

A typical computer circuit diagram for a submarine in six degrees of freedom is presented in Fig. 34. The various symbols used to represent the various computer components are presented in Fig. 34d. These components are interconnected by means of a plug-in patchboard. The patchboard, therefore, represents the "mathematical" model of the system. A computer is equipment with several patchboards, and therefore one mathematical model can be stored while another study is being conducted.

The DTMB analog computer, shown in Fig. 36, consists of four general purpose computers, manufactured by the Midcentury Instrumatic Corporation, and one analog computer manufactured by the Reeves Instrument Company. This facility presently consists of 168 operational amplifiers. (The number of operational amplifiers is usually used to express the size of a facility.) In addition, auxiliary equipment such as diode function generators, white-noise generators, X-Y plotting boards, two 8-channel Sanborn recorders, strip-chart recorders, and various instrument displays are available. The present facility will be expanded shortly to about 300 operational amplifiers when several new computers are procured. With this addition, the facility will be capable of handling, simultaneously, two six-degree-of-freedom submarine studies as well as other small problems.

Studies which involve the human operator as part of the closed loop are performed using the submarine simulator facility shown in Figs. 37 and 38. The simulator consists of cube-shaped cab (about 7 feet x 7 feet x 7 feet) capable of turning on a single axis equivalent to the pitch axis of a submarine. It is hoped that an additional degree of freedom, to simulate the rolling motion of the submarine, will be added in the near future. The cab contains two control stations, each equipped with an aircraft-type control stick (stick-wheel) and the necessary display instruments. The motion of the cab is governed by an electrohydraulic servo system receiving inputs from the analog computer. A block diagram of this circuit is presented in Figs. 34c and 39.

A comparison of the submarine control cycle with the simulator control cycle, presented in Fig. 35, shows that the cab constitutes one link in a complete submarine simulator control loop which involves the human operator. The equations of motion set up on the analog computer (mathematical model) constitute another link in the control loop. Movement of the control stick in the cab produces inputs to the computer which then calculates the resultant path of the submarine. The submarine attitude angle, depth, depth error, and plane angles are displayed by the instruments and the cab rotates to the computed pitch angle. Simultaneously, a graphical record of the submarine trajectory and other pertinent information is recorded by a multichannel recorder.

The Motion Analysis and Simulator Facility in combination with the concept of the definitive maneuver provides a powerful tool for studying the handling qualities of submarines. Several of the typical definitive maneuvers, shown in Figs. 40 to 43, are performed using this facility to provide numerical measures of the inherent characteristics of submarines.

The meander maneuver, shown in Fig. 40 provides numerical measures of the dynamic stability in the vertical plane; such as, time to damp to one-half amplitude $t_{1/2}$, damping ratio c/c_c, and damped period. The overshoot maneuver also shown in Fig. 40 provides
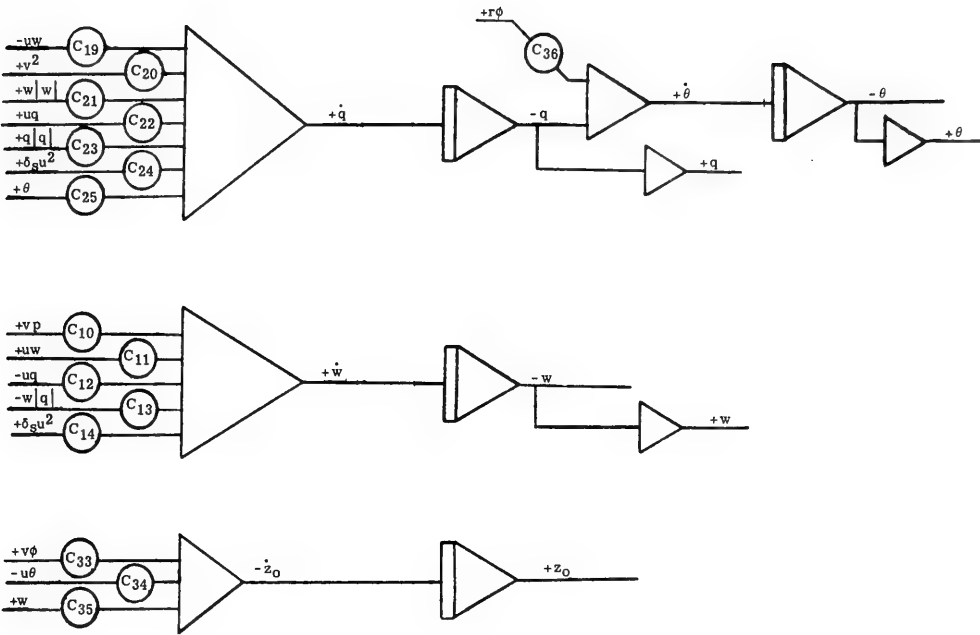
(a) Vertical Plane

(a) Vertical plane

Fig. 34 — Analog computer diagram of submarine equations

Alex Goodman
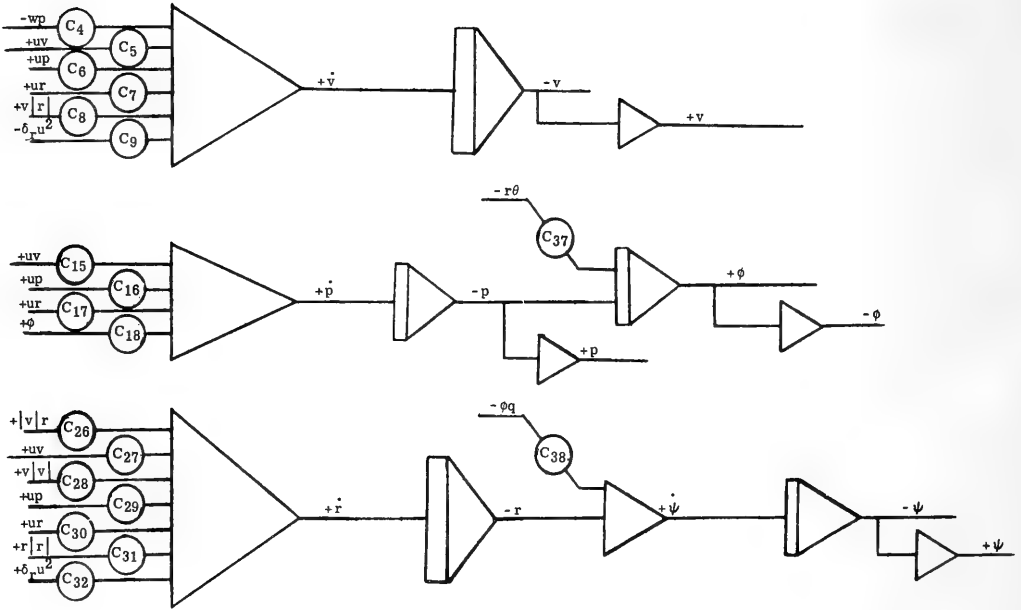
(b) Horizontal Plane

(b) Horizontal plane

Fig. 34 — Analog computer diagram of submarine equations (continued)

$$\delta_{pc} = \delta_{\not\!sc} + \delta_{rc}$$

$$\delta_{sc} = \delta_{\not\!sc} - \delta_{rc}$$

$$\delta_{\not\!s} = \frac{1}{2}\,(\delta_p + \delta_s)$$
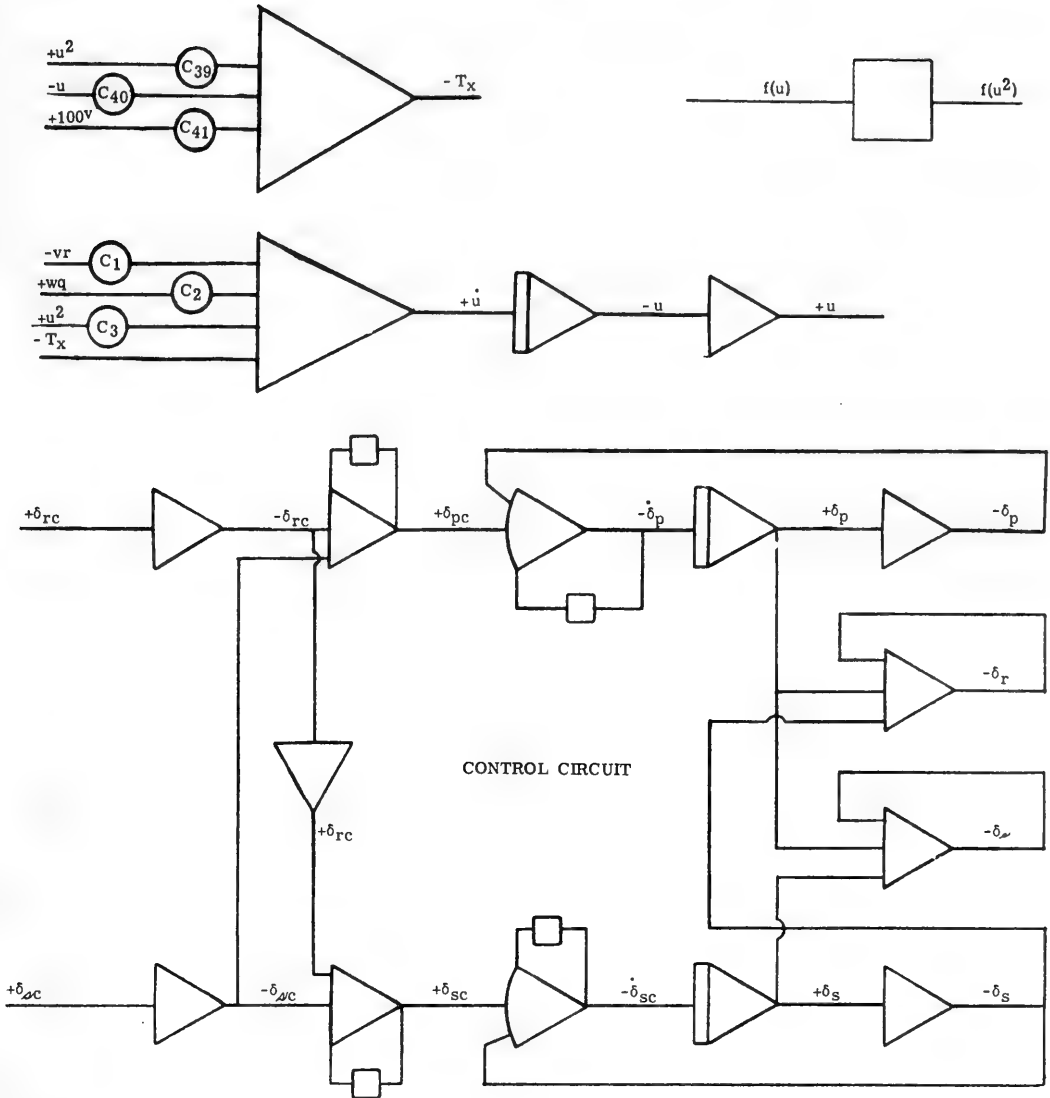
$$\delta_r = \frac{1}{2}\,(\delta_p - \delta_s)$$

where

$\delta_{\not\!sc}$, δ_{rc} are effective diving planes and rudder ordered angles

δ_{pc}, δ_{sc} are ordered angles to port and starboard shafts

δ_p , δ_s are actual angles of port and starboard shafts

$\delta_{\not\!s}$, δ_r are effective diving plane and rudder angles which would produce forces and moments equivalent to deflection angles of stocks

(c) Thrust representation, axial force and control circuit diagram

Fig. 34 — Analog computer diagram of submarine equations (continued)

SYMBOLS	DESCRIPTION	SCHEMATICS
	Summing Amplifier	
	Integrating Amplifier	
	Hi Gain Amplifier	
	Diode Limiter	
	Non-Linear Function Generator	
	Grounded Potentiometer	

(d) Description of symbols used in analog computer diagrams

Fig. 34—Analog computer diagram of submarine equations (continued)
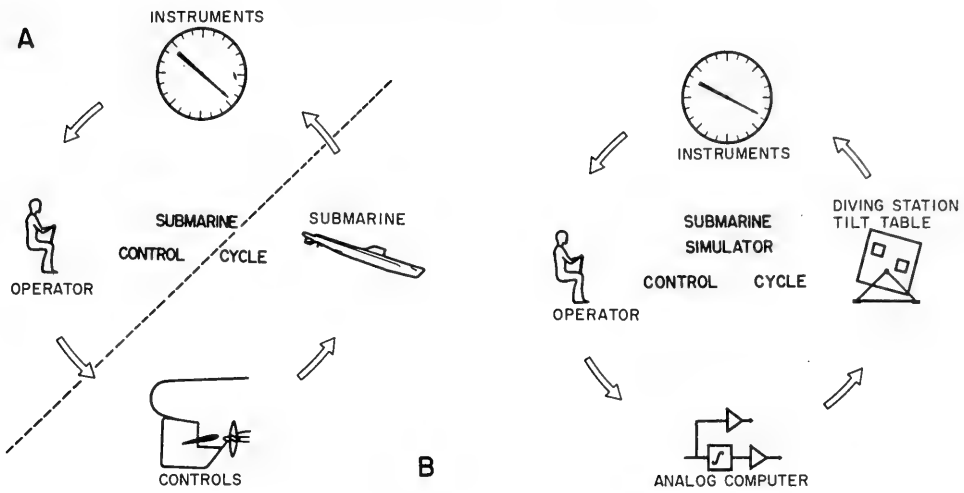
(a) Submarine control cycle   (b) Simulator control cycle

Fig. 35. Comparison between submarine control cycle and simulator control cycle
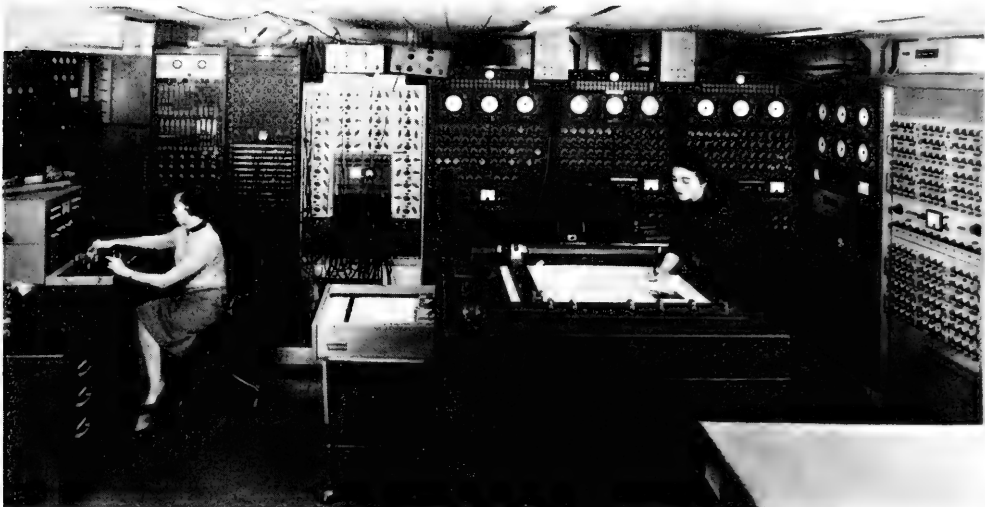
Fig. 36. DTMB analog computer facility

numerical measures of control effectiveness, such as time to reach execute, overshoot angle in the vertical plane, and overshoot depth in the vertical plane. A similar maneuver, such as shown in Fig. 42, can be used to define the ability to initiate and check a course change in the horizontal plane. The results of the Dieudonne spiral maneuver shown in Fig. 41 provides some measure of the inherent dynamic stability in the horizontal plane. These results are also indicative of the course-keeping characteristics of the submarine. Steady-turn studies such as shown in Fig. 43 provide numerical measures such as tactical diameter, advance, transfer, time to change heading 90 to 180 degrees, and loss of speed in the turn.
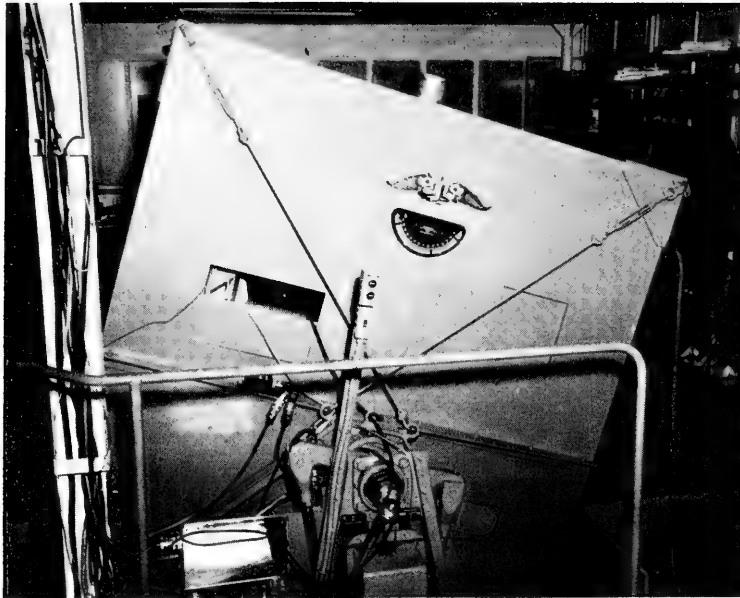
Fig. 37. DTMB submarine simulator facility

Definitive maneuvers which provide measures of the capabilities of the submarine tempered by the existence of a human operator or automatic control in the control loop can also be performed using the facility. Maneuvers such as depth-keeping and course-keeping, under various environmental conditions, provide numerical measures such as rms depth or course error, percent time on target, degrees traveled by control surfaces, and maximum values of these variables. Various other maneuvers such as limit-dives and emergency-recovery maneuvers also can be performed in the laboratory and evaluated before the submarine is built.

Instrumentation studies, which are in the nature of human engineering, can be carried out using the submarine simulator. The effect of various displays, indicators, lighting, and other devices on the performance of the submarine can be evaluated.

Thus, it can be seen that the DTMB Motion Analysis and Simulator Facility is a powerful and versatile design and research tool for the study and analysis of stability and control problems.

FREE-RUNNING MODEL TECHNIQUE

The free-running model technique has been used extensively in the past in studying the turning and maneuvering characteristics of surface ships [4]. With the emphasis that has been placed the performance of high-submerged-speed submarines, the necessity for turning data from submerged model tests has become more important. Early submerged maneuvering tests, in the vertical and horizontal planes, conducted at the David Taylor Model Basin employed a specially constructed 5-foot model provided by NACA. The model was powered electrically and controls were operated by compressed air through a flexible tubing which trailed astern of the model. Model trajectories were obtained, by photographing the movements of the model

(a) Starboard control stick and display
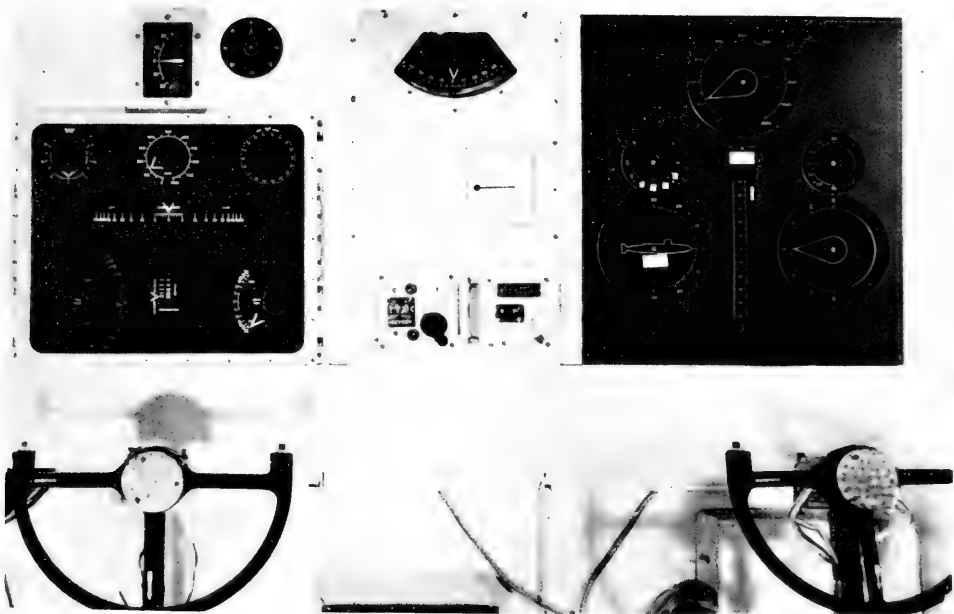
(b) Port and starboard control sticks and displays

Fig. 38. Interior views of the submarine simulator facility
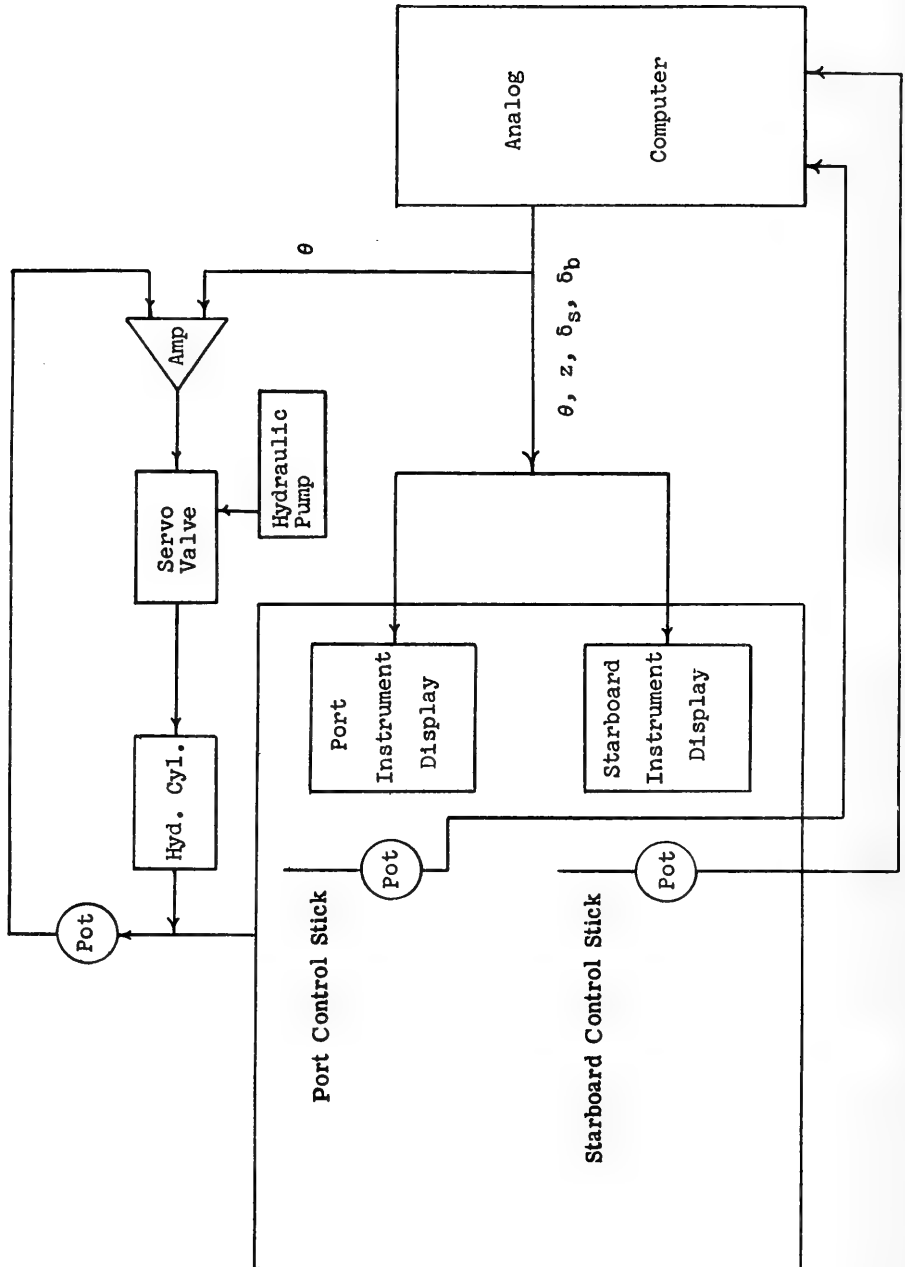
Fig. 39. Block diagram of the simulator circuit

Fig. 40. Typical meander and vertical overshoot maneuvers (definitive maneuvers)

(a) Stable ship

(b) Unstable ship
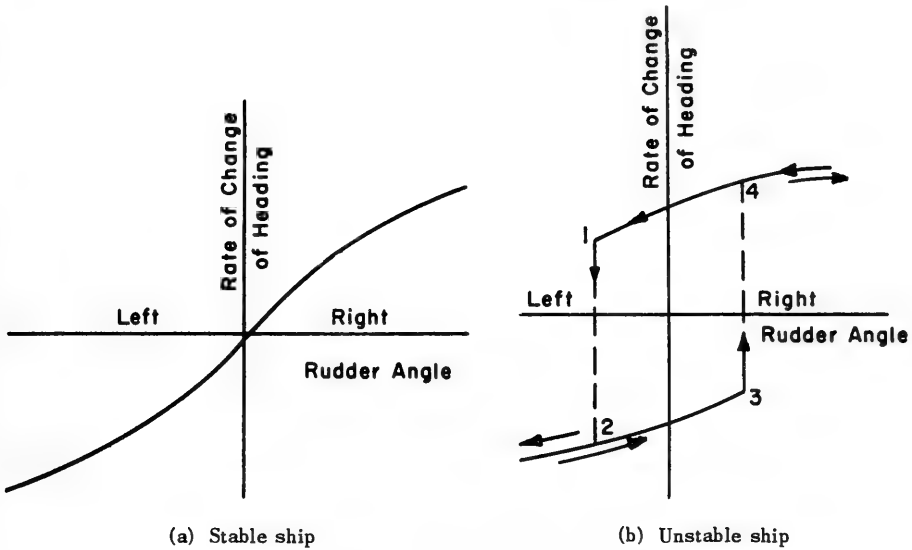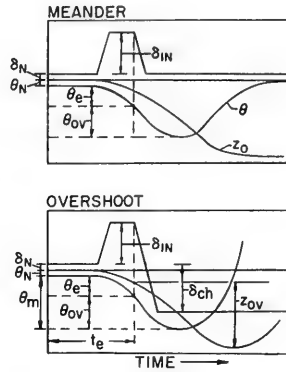
Fig. 41. Typical curves from spiral maneuvers

relative to a grid attached to the towing carriage, using cameras mounted inside the model. The main objections to this system are that it required an expensive model and that the excessive drag resistance of the tubing affected the maneuvering characteristics of the model.

With recent advances in electronic and electromechanical instrumentation, and waterproofing techniques, it became possible to perfect the free-running model technique using the standard 20-foot (nominal) submerged models used for both resistance and propulsion tests and stability and control tests.

The free-running submarine model tests are presently being performed in the J-basin at DTMB. Techniques have been developed so that these tests can be conducted in the new Maneuvering Basin using a model that is internally programmed and has internal recording equipment.
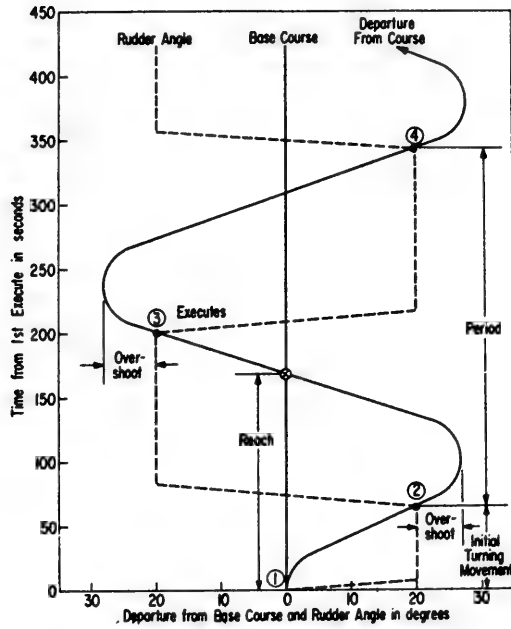
Fig. 42. Horizontal overshoot maneuver
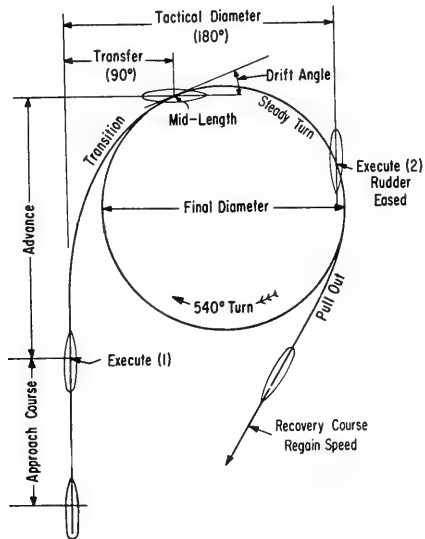
Fig. 43. Turning circle maneuvers

For the submerged tests in the J-basin, the model is provided with watertight equipment (propulsion motors, actuators, and gyros) and is ballasted so as to have only a slight reserve buoyancy. The final displacement and trim is achieved by means of the bow and stern ballast tanks. The power and control cables emerge from the model through a hollow faired tube and are supported by an overhead follower boom controlled from the carriage. The cable runs over a pulley and has a counterweight so arranged that the cable feeds out as the model submerges. A lightweight framework secured to the top of the faired tube supports flashing neon lights used in photographing (using overhead cameras) the turning path of the model. Portable control boxes are provided for both the rudder and stern plane so that the most desirable locations on the carriage could be used. The control boxes actuate waterproofed-rotary actuators, manufactured by Universal Match Corporation, which are mechanically linked to the rudders and stern planes. A trim angle indicator also is provided to simplify the work of the stern plane operator as it provides a faster and more sensitive indication then could be estimated visually. This information is obtained from a Minneapolis-Honeywell vertical gyro Type GG 33B-2 which is located in the model. The heading and rate of change of heading data are provided by a Humphrey Model FG01-0203 gyro and a Humphrey Model RG03-0117-1 gyro, respectively, and are of value to the operator of the rudder control in obtaining a straight approach course.

At the beginning of each run the model is floating with only the top of the bridge fairwater projecting out of the water. After the model has attained the desired test speed, it is maneuvered down to the test depth by means of the stern diving planes. The definitive maneuvers shown in Figs. 41 to 43, are then performed to evaluate the handling qualities of the submarine in the horizontal plane.

ACKNOWLEDGMENT

REFERENCES

[1] Gertler, M., and Gover, S.C., "Handling Quality Criteria for Surface Ships," paper presented at the Meeting of the Chesapeake Chapter of the Society of Naval Architects and Marine Engineers on May 2, 1959

[2] Gertler, M., "The DTMB Planar-Motion-Mechanism System," paper presented at the Symposium on the Towing Tank Facilities, Instrumentation and Measuring Technique on September 22-25, 1959

[3] Orlik-Ruckemann, "Methods of Measurement of Aircraft Dynamic Stability Derivatives,"
     National Research Council of Canada Aeronautical Report LR-254

[4] Gover, S.C., "Free-Running Model Techniques for the Evaluation of Ship-Handling
     Qualities," David Taylor Model Basin Report 1350, July 1959

[5] Bird, J.D., Jaquet, B.M., and Cowan, J.W., "Effect of Fuseage and Tail Surfaces and
     Low-Speed Yawing Characteristics of a Swept-Wing Model as Determined in the Curves-
     Flow Test Section of the Langley Stability Tunnel," NACA TN 2483, Oct. 1951

[6] MacLachlan, R. and Letko, W., "Correlation of Two Experimental Methods of Deter-
     mining the Rolling Characteristics of Unswept Wings," NACA TN 1309, May 1947

[7] Lamb, Sir Horace, "Hydrodynamics," Sixth Edition, Dover Publications

[8] Lopes, L.A., "Motion Equations for Torpedoes," NavOrd Report 2090, NOTS 827, U.S.
     Naval Ordnance Station, Inyokern, Feb. 1954

[9] Strumpf, A., "Equations of Motion of a Submerged Body with Varying Mass," Davidson
     Laboratory Report 771, May 1960

[10] Beam, B.A., "A Wind Tunnel Test Technique for Measuring the Dynamic Rotary Sta-
     bility Derivatives Including the Cross Derivatives at Subsonic and Supersonic Speeds,"
     NACA Report 1258, 1956

[11] Tuckerman, R.G., "A Phase-Component Measurement System," David Taylor Model
     Basin Report 1139, Apr. 1958

[12] Fried, W., "A Rotating Arm for Towing Models of Ships and Other Forms in Circular
     Paths," Experimental Towing Tank Report 299, Feb. 1946

[13] Brownell, W.F., "A Rotating Arm and Maneuvering Basin," David Taylor Model Basin
     Report 1053, July 1956

[14] Johnson, C.L., "Analog Computer Techniques," New York:McGraw-Hill, 1956

[15] Wass, C.A.A., "Introduction to Electronic Analogue Computers," New York:McGraw-
     Hill, 1956

APPENDIX A

Derivation of Phase Angle Required Between Struts for
Pure Pitching Motion

The condition that must be satisfied to obtain a pure pitching motion for a body moving
through a fluid is that the pitch angle varies with time while the angle of attack α, meas-
ured at the CG, is maintained equal to zero at all times. The motion is one in which the
body CG moves in a sinusoidal path, with the longitudinal body axis tangent to the path,
as shown in Fig. 3c. This motion in some respects is similar to that produced by a rotating
arm.

The system that will be analyzed uses a slider crank mechanism having a large ratio of length of connecting rod to eccentricity. There is no appreciable error introduced, therefore, by assuming that the motion is sinusoidal for purposes of analysis. Referring to the notation and schematic diagram shown in Fig. 5, the motion of the forward and aft struts (taken with respect to the midposition of the forward strut) can be expressed as follows:

$$z_1 = a_1 \sin \omega t \tag{A1}$$

$$z_2 = a_2 \sin (\omega t - \phi_s) \tag{A2}$$

where the crank arms a_1 and a_2 are assumed to be variables. The vertical displacement of the body CG is, therefore,

$$z_o = \frac{x_2 z_1 + x_1 z_2}{b} . \tag{A3}$$

Expanding Eq. (A3) results in

$$z_o = \frac{a_1 x_1}{b} \left[\left(\frac{x_2}{x_1} + \frac{a_2}{a_1} \cos \phi_s \right) \sin \omega t - \frac{a_2}{a_1} \sin \phi_s \cos \omega t \right] \tag{A4}$$

where the strut spacing with respect to the body CG, x_1, and x_2 are assumed also to be variables. The vertical velocity of the body CG can be obtained by differentiating Eq. (4) and expressed as

$$\dot{z}_o = \frac{a_1 x_1 \omega}{b} \left[\left(\frac{x_2}{x_1} + \frac{a_2}{a_1} \cos \phi_s \right) \cos \omega t + \frac{a_2}{a_1} \sin \phi_s \sin \omega t \right]. \tag{A5}$$

For the case of pure pitching the struts are out of phase with each other, and a body pitch angle results and can be expressed in terms of the motion of each strut as

$$\theta = \frac{z_2 - z_1}{b} \tag{A6}$$

or expanding:

$$\theta = - \frac{a_1}{b} \left[\left(1 - \frac{a_2}{a_1} \cos \phi_s \right) \sin \omega t + \frac{a_2}{a_1} \sin \phi_s \cos \omega t \right] . \tag{A7}$$

The vertical velocity of the CG with respect to the inertial axes can be written as

$$\dot{z}_o = w \cos \theta - u \sin \theta \tag{A8}$$

and for small angles, where $\cos \theta = 1$, $\sin \theta = \theta$, and $u = U$, can be simplified to

$$\dot{z}_o = w - U\theta. \tag{A9}$$

Also, since $w/U = \alpha$ (for small angles), Eq. (A9) can be restated as

$$\dot{z}_o = U(\alpha - \theta). \tag{A10}$$

As stated previously, the primary condition that must be satisfied for pure pitching motion is that $\alpha = 0$. Equation (A10), therefore, reduces to

$$\dot{z}_o = -U\theta. \tag{A11}$$

Substituting Eqs. (A5) and (A7) into Eq. (A11) results in

$$\frac{\omega x_1}{U} \left[\left(\frac{x_2}{x_1} + \frac{a_2}{a_1} \cos \phi_s \right) \cos \omega t + \frac{a_2}{a_1} \sin \phi_s \sin \omega t \right]$$

$$= \left[\left(1 - \frac{a_2}{a_1} \cos \phi_s \right) \sin \omega t + \frac{a_2}{a_1} \sin \phi_s \cos \omega t \right]. \tag{A12}$$

Equating sine and cosine terms results in

$$\frac{\omega x_1}{U} \cos \phi_s - \sin \phi_s = - \left(\frac{\omega x_1}{U} \right) \left(\frac{x_2}{x_1} \right) \left(\frac{a_1}{a_2} \right) \tag{A13}$$

$$\cos \phi_s + \left(\frac{\omega x_1}{U} \right) \sin \phi_s = \left(\frac{a_1}{a_2} \right). \tag{A14}$$

Solving Eqs. (A13) and (A14) for $\sin \phi_s$ and $\cos \phi_s$ results in the following relationships:

$$\sin \phi_s = \frac{\dfrac{\omega x_1}{U} \left(1 + \dfrac{x_2}{x_1} \right)}{\left(\dfrac{a_2}{a_1} \right) \left[1 + \left(\dfrac{\omega x_1}{U} \right)^2 \right]} \tag{A15}$$

$$\cos \phi_s = \frac{\dfrac{a_1}{a_2} - \dfrac{x_2}{x_1} \left(\dfrac{\omega x_1}{U} \right)^2}{1 + \left(\dfrac{\omega x_1}{U} \right)^2}. \tag{A16}$$

A boundary condition that must be satisfied is that $\sin \phi_s$ cannot be greater than one. Therefore,

$$\frac{\partial(\sin \phi_s)}{\partial \left(\frac{\omega x_1}{U}\right)} = 0 = \frac{\left(1 + \frac{x_2}{x_1}\right)\left[1 + \left(\frac{\omega x_1}{U}\right)^2 - 2\left(\frac{\omega x_1}{U}\right)^2\right]}{\left(\frac{a_2}{a_1}\right)\left[1 + \left(\frac{\omega x_1}{U}\right)^2\right]^2} \cdot \quad\text{(A17)}$$

The value of $\omega x_1/U$ which satisfies Eq. (A17) is $\omega x_1/U = 1$. This result can be used to determine the relationship between the crank-length ratio and the strut-spacing ratio by substituting $\omega x_1/U = 1$ in Eq. (A15) as follows:

$$\sin \phi_s = 1 = \frac{\left(1 + \frac{x_2}{x_1}\right)}{2\left(\frac{a_2}{a_1}\right)} \quad\text{(A18)}$$

or, restating Eq. (A18),

$$\frac{a_2}{a_1} = \frac{1}{2}\left(1 + \frac{x_2}{x_1}\right) \cdot \quad\text{(A19)}$$

The present Planar Motion Mechanism was designed having equal crank lengths. Therefore, in accordance with Eq. (A19), the strut spacing with respect to the body CG must be equal. For these conditions, the expression for the phase angle between struts for pure pitching motion reduces to

$$\cos \phi_s = \frac{1 - \left(\frac{\omega x}{U}\right)^2}{1 + \left(\frac{\omega x}{U}\right)^2} \quad\text{(A20)}$$

and the body pitch angle relation becomes

$$\theta = -\left(\frac{2a}{b} \sin \frac{\phi_s}{2}\right)\left[\cos \left(\omega t - \frac{\phi_s}{2}\right)\right] \quad\text{(A21)}$$

where

$$\left(\frac{2a}{b} \sin \frac{\phi_s}{2}\right)$$

is the maximum amplitude of the pitch angle θ_o.

As can be seen from Fig. 5, there is a given relationship between the point in the cycle when the pitch angle is zero and the zero point of the resolver (synchronous switch or

sine-cosine potentiometer). The pitch angle trajectory of the model is a direct function of the phase angle between struts as shown by Eq. (A21). Therefore, the zero-pitch-angle point $(\omega t)_1$ will vary with strut-phase angle. This requires that the resolver be repositioned and synchronized with the zero-pitch-angle point for each condition of pure pitching.

The relationship between the zero-pitch-angle point $(\omega t)_1$ and the strut-phase angle can be determined from Eq. (A5). At the point $(\omega t)_1$ in the cycle, $\phi = 0$, $z_1 = z_2$, and z_o is a maximum. Therefore for $x_2/x_1 = a_2/a_1 = 1$, Eq. (A5) reduces to

$$\dot{z}_o = 0 = (1 + \cos \phi_s) \cos \omega t + \sin \phi_s \sin \omega t \qquad (A22)$$

and

$$\tan \omega t = \frac{1 + \cos \phi_s}{\sin \phi_s} \qquad (A23)$$

or

$$(\omega t) = \tan^{-1} \left[\frac{1 + \cos \phi_s}{\sin \phi_s} \right] . \qquad (A24)$$

Differentiating with respect to ϕ_s yields

$$\frac{\partial (\omega t)}{\partial \phi_s} = \frac{1}{2} . \qquad (A25)$$

APPENDIX B

Derivation of Reduction Equations

The Planar Motion Mechanism separates the motions of a body moving through a fluid into the hydrodynamically pure pitching and pure heaving motions as defined in Fig. 3. The differential equations of motion referred to a moving body axis system are used to establish a direct and explicit relationship between the various rotary and acceleration derivatives and the measured quadrature and in-phase components of the forces and moments. The linear force and moment equations describing the body motions with respect to the initial equilibrium conditions can be written as:

Transverse Force:

$$Y = Y_{\dot{r}} \dot{r} + \left(\frac{1}{2} \rho \ell^3 Y_r' + m \right) rU + (Y_{\dot{v}} - m) \dot{v}$$

$$+ \left(\frac{1}{2} \rho \ell^2 U Y_v' \right) v + \left(\frac{1}{2} \rho \ell^3 Y_p' \right) p + Y_{\dot{p}} \dot{p} . \qquad (B1)$$

Normal Force:

$$Z = Z_{\dot{q}}\dot{q} + \left(\frac{1}{2}\rho\ell^3 Z_q' + m\right)qU + (Z_{\dot{w}} - m)\dot{w}$$

$$+ \left(\frac{1}{2}\rho\ell^2 UZ_w'\right)w + \left(\frac{1}{2}\rho\ell^2 UZ_v'\right)v + Z_* \ . \tag{B2}$$

Rolling Moment:

$$K = (K_{\dot{p}} - I_x)\dot{p} + \left(\frac{1}{2}\rho\ell^4 UK_p'\right)p + K_\phi + K_{\dot{r}}\dot{r}$$

$$+ \left(\frac{1}{2}\rho\ell^4 UK_r'\right)r + K_{\dot{v}}\dot{v} + \left(\frac{1}{2}\rho\ell^3 UK_v'\right)v \ . \tag{B3}$$

Pitching Moment:

$$M = (M_{\dot{q}} - I_y)\dot{q} + \left(\frac{1}{2}\rho\ell^4 UM_q'\right)q + M_\theta\theta + M_{\dot{w}}\dot{w}$$

$$+ \left(\frac{1}{2}\rho\ell^3 UM_w'\right)w + \left(\frac{1}{2}\rho\ell^3 UM_v'\right)v + M_* \ . \tag{B4}$$

Yawing Moment:

$$N = (N_{\dot{r}} - I_z)\dot{r} + \left(\frac{1}{2}\rho\ell^4 UN_r'\right)r + N_{\dot{v}}\dot{v}$$

$$+ \left(\frac{1}{2}\rho\ell^3 UN_v'\right)v + \left(\frac{1}{2}\rho\ell^4 UN_p'\right)p + N_{\dot{p}}\dot{p} \ . \tag{B5}$$

PURE HEAVING MOTION

The reduction equations for the pure heaving motion can be derived using Eqs. (A9), (B2), and (B4). For this motion, the pitch angle θ is zero at all times since the phase angle between the struts is zero.

As shown schematically in Figs. 3b and 4, the vertical displacement of the body CG can be expressed as

$$z_o = a \sin \omega t \ , \tag{B6}$$

the linear velocity as

$$\dot{z}_o = a\omega \cos \omega t \ , \tag{B7}$$

and the linear acceleration as

$$\ddot{z}_o = -a\omega^2 \sin \omega t \ . \tag{B8}$$

Since $\theta = q = \dot{q} = 0$, Eq. (A9) reduces to $\dot{z}_0 = w$. Therefore

$$w = a\omega \, \cos \, \omega t \tag{B9}$$

and

$$\dot{w} = -a\omega^2 \, \sin \, \omega t \, . \tag{B10}$$

Substituting Eqs. (B9) and (B10) in Eqs. (B2) and (B3), results in

$$Z = -a\omega^2(Z_{\dot{w}}' - m_m) \, \sin \, \omega t + a\omega \left(\frac{1}{2} \rho \ell^2 \, UZ_w'\right) \, \cos \, \omega t + Z_* \tag{B11}$$

and

$$M = -a\omega^2 M_{\dot{w}} \, \sin \, \omega t + a\omega \left(\frac{1}{2} \rho \ell^3 UM_w'\right) \, \cos \, \omega t + M_* \tag{B12}$$

where m_m is the model mass.

The component of force and moment in phase with the motion can be written as

$$Z_{in} = -a\omega^2(Z_{\dot{w}} - m) \tag{B13}$$

and

$$M_{in} = -a\omega^2 M_{\dot{w}} \, . \tag{B14}$$

The internal balance system, shown in Fig. 6, measures the components of force at two points spaced equidistant from the body CG. Therefore, Eqs. (B13) and (B14) can be rewritten as

$$(Z_1)_{in} + (Z_2)_{in} = -a\omega^2(Z_{\dot{w}} - m) \tag{B15}$$

and

$$x\left[(Z_2)_{in} - (Z_1)_{in}\right] = -a\omega^2 M_{\dot{w}} \, . \tag{B16}$$

The heaving acceleration derivatives, written in nondimensional form can be expressed as

$$(Z_{\dot{w}}' - m_m') = -\frac{\partial\left[(Z_1')_{in} + (Z_2')_{in}\right]}{\partial \dot{w}_o'} \tag{B17}$$

and

$$M_{\dot{w}}' = -\frac{x}{\ell} \frac{\partial\left[(Z_2')_{in} - (Z_1')_{in}\right]}{\partial \dot{w}_o'} \tag{B18}$$

where

$$\dot{w}_o{'} = \frac{a}{\ell} \frac{\omega^2 \ell^2}{U^2}$$

is the amplitude of the linear acceleration.

Similarly, the reduction equations for the case of pure sideslipping (lateral translatory motion), as presented in Table 2, can be derived.

PURE PITCHING MOTION

The condition for pure pitching, as studied in Appendix A, is satisfied when the angle of attack α, measured at the CG, is equal to zero at all times. For this condition, the resultant linear velocity w and linear acceleration $\dot{w}$ are zero. The pitch angle, pitching velocity, and pitching acceleration can be expressed as

$$\theta = \frac{z_2 - z_1}{b} = - \left(\frac{2a}{b} \sin \frac{\phi_s}{2}\right) \left[\cos \left(\omega t - \frac{\phi_s}{2}\right)\right], \qquad (B19)$$

the angular velocity as

$$\dot{\theta} = q = - \omega \left(\frac{2a}{b} \sin \frac{\phi_s}{2}\right) \left[- \sin \left(\omega t - \frac{\phi_s}{2}\right)\right], \qquad (B20)$$

and the angular acceleration as

$$\ddot{\theta} = \dot{q} = \omega^2 \left(\frac{2a}{b} \sin \frac{\phi_s}{2}\right) \left[\cos \left(\omega t - \frac{\phi_s}{2}\right)\right] \qquad (B21)$$

where

$$\left(\frac{2a}{b} \sin \frac{\phi_s}{2}\right)$$

is the maximum amplitude of the pitch angle θ_o.

Substituting Eqs. (B19), (B20), and (B21) in Eqs. (B2) and (B4) yields:

$$Z = \omega^2 \left(\frac{2a}{b} \sin \frac{\phi_s}{2}\right) Z_{\dot{q}} \cos \left(\omega t - \frac{\phi_s}{2}\right)$$

$$- \omega U \left(\frac{2a}{b} \sin \frac{\phi_s}{2}\right) \left(\frac{1}{2} \rho \ell^3 Z_q{'} + m_m\right) \left[- \sin \left(\omega t - \frac{\phi_s}{2}\right) + Z_* \right] \qquad (B22)$$

and

$$M = \omega^2 \left(\frac{2a}{b} \sin \frac{\phi_s}{2}\right) (M_{\dot{q}} - I_{ym}) \cos \left(\omega t - \frac{\phi_s}{2}\right)$$

$$- \omega U \left(\frac{2a}{b} \sin \frac{\phi_s}{2}\right) \left(\frac{1}{2} \rho \ell^4 M_q'\right) \left[- \sin \left(\omega t - \frac{\phi_s}{2}\right)\right]$$

$$- \left(\frac{2a}{b} \sin \frac{\phi_s}{2}\right) (M_\theta)_m \left[\cos \left(\omega t - \frac{\phi_s}{2}\right)\right] + M_* \qquad \text{(B23)}$$

where I_{ym} and $(M_\theta)_m$ refer to the model moment of inertia and metacentric stability, respectively.

As for the heaving case, in-phase and quadrature components of force and moment can be written as:

$$(Z_1)_{in} + (Z_2)_{in} = \omega^2 \left(\frac{2a}{b} \sin \frac{\phi_s}{2}\right) Z_{\dot{q}} \qquad \text{(B24)}$$

$$(Z_1)_{out} + (Z_2)_{out} = -\omega U \left(\frac{2a}{b} \sin \frac{\phi_s}{2}\right) \left(\frac{1}{2} \rho \ell^3 Z_q' + m_m\right) \qquad \text{(B25)}$$

$$x \left[(Z_2)_{in} - (Z_1)_{in}\right] = \omega^2 \left(\frac{2a}{b} \sin \frac{\phi_s}{2}\right) (M_{\dot{q}} - I_{ym}) - M_{\theta m} \left(\frac{2a}{b} \sin \frac{\phi_s}{2}\right) \qquad \text{(B26)}$$

$$x \left[(Z_2)_{out} - (Z_1)_{out}\right] = -\omega U \left(\frac{2a}{b} \sin \frac{\phi_s}{2}\right) \left(\frac{1}{2} \rho \ell^4 M_q'\right) \qquad \text{(B27)}$$

The pitching rotary and acceleration derivatives, written in nondimensional form, can be expressed as:

$$Z_{\dot{q}}' = \frac{\partial \left[(Z_1')_{in} + (Z_2')_{in}\right]}{\partial \dot{q}_o'} \qquad \text{(B28)}$$

$$(Z_q' + m_m') = - \frac{\partial \left[(Z_1')_{out} + (Z_2')_{out}\right]}{\partial q_o'} \qquad \text{(B29}$$

$$(M_q' - I_{ym}') = \frac{x}{\ell} \frac{\left[(Z_2')_{in} - (Z_1')_{in}\right]}{\partial \dot{q}_o'} + \frac{\frac{(M_\theta)_m}{\frac{1}{2} \rho \ell^2}}{\omega^2} \qquad \text{(B30)}$$

$$M_q' = -\frac{x}{\ell} \frac{\partial\left[(Z_2')_{out} - (Z_1')_{out}\right]}{\partial q_o'} \tag{B31}$$

where

$$q_o' = \left(\frac{2a}{b} \sin \frac{\phi_s}{2}\right) \frac{\omega \ell}{U} \tag{B32}$$

and

$$\dot{q}_o' = \left(\frac{2a}{b} \sin \frac{\phi_s}{2}\right) \frac{\omega^2 \ell^2}{U^2} \tag{B33}$$

are the maximum amplitudes of the angular velocity and acceleration, respectively.

The relationships for pure yawing and rolling, presented in Table 2, can be derived in a similar manner.

The model mass m_m and metacentric stability $(M_\theta)_m$ are evaluated experimentally by performing inclining tests (standstills). The model moment of inertia I_{ym} is determined from oscillation tests performed in air. For these tests, the model-ballast condition is the same as during the regular tests.

APPENDIX C

Mathematical Operations Performed by Instrumentation System

As indicated in the section entitled "Instrumentation for Static and Dynamic Stability Tests," the operation of the present electronic system differs from that described in Ref. 2 in that a true integration of the gage signal is performed.

To illustrate, assume a pure heaving condition which results in a gage signal of the form such as given in Fig. 4:

$$Z_R = Z_* + Z_o \sin (\omega t - \phi) \tag{C1}$$

which can be written as

$$Z_R = Z_* + Z_o (\cos \phi) \sin \omega t - Z_o (\sin \phi) \cos \omega t \tag{C2}$$

or

$$Z_R = Z_* + Z_{in} \sin \omega t - Z_{out} \cos \omega t. \tag{C3}$$

The in-phase and quadrature (out-of-phase) components can be obtained by operating on the gage signal in the following manner:

$$Z_{in} = \frac{1}{\pi} \int_0^{2\pi} Z_R \sin \omega t \ d(\omega t) \tag{C4}$$

and

$$Z_{out} = \frac{1}{\pi} \int_0^{2\pi} Z_R \cos \omega t \ d(\omega t). \tag{C5}$$

The operations indicated by Eqs. (C4) and (C5) are performed by the force-component separator, sine-cosine potentiometer, integrating amplifier, and timer diagrammed in Fig. 22.

The result of the integration is provided by the digital readout and is defined as

$$Z_{in} = Z_o \cos \phi \tag{C6}$$

and

$$Z_{out} = -Z_o \sin \phi. \tag{C7}$$

Likewise, for the pure pitching condition the resultant gage signal has the form (see Fig. 5)

$$Z_R = Z_* + Z_o \cos \left[\left(\omega t - \frac{\phi_s}{2} \right) - \phi \right] \tag{C8}$$

or

$$Z_R = Z_* + (Z_o \cos \phi) \cos \left(\omega t - \frac{\phi_s}{2} \right) + (Z_o \sin \phi) \sin \left(\omega t - \frac{\phi_s}{2} \right). \tag{C9}$$

The integration performed is as follows:

$$Z_{in} = \frac{1}{\pi} \int_{(\omega t)_1}^{(\omega t)_1 + 2\pi} Z_R \sin \left[\omega t - (\omega t)_1 \right] \ d(\omega t) \tag{C10}$$

and

$$Z_{out} = \frac{1}{\pi} \int_{(\omega t)_1}^{(\omega t)_1 + 2\pi} Z_R \cos \left[\omega t - (\omega t)_1 \right] \ d(\omega t) \tag{C11}$$

where

$$(\omega t)_1 = \frac{\pi}{2} + \frac{\phi_s}{2} .$$

Equations (C10) and (C11) reduce to

$$Z_{in} = -Z_o \cos \phi \qquad \text{(C12)}$$

and

$$Z_{out} = Z_o \sin \phi. \qquad \text{(C13)}$$

Thus, the operation performed by the electronic system is equivalent to determining the Fourier coefficients of the fundamental of the gage signal.

APPENDIX D

Equations of Motion for Submarines

The differential equations of motion in dimensional form, referred to a moving body axes system which is coincident with the principal axes of inertia and having the origin at the center of mass, can be written for the case when the submarine is initially in level flight and at a steady forward speed as:

Axial Force

$$m(\dot{u} - vr + wq) = \frac{\rho}{2}\ell^3 \left[X'_{\dot{u}}\dot{u} - Y'_{\dot{v}}vr + Z'_{\dot{w}}wq \right]$$

$$+ \frac{\rho}{2}\ell^2 \left[X'_{(uu)}u^2 + X'_{(vv)}v^2 + X'_{(ww)}w^2 \right]$$

$$+ \frac{\rho}{2}\ell^2 u^2 \left[X'_{(\delta r \delta r)}\delta_r^2 + X'_{(\delta s \delta s)}\delta_s^2 + X'_{(\delta b \delta b)}\delta_b^2 \right]$$

$$+ (F_x)_P.$$

Lateral Force

$$m(\dot{v} - wp + ur) = \frac{\rho}{2}\ell^3 \left[Y'_{\dot{v}}\dot{v} - Z'_{\dot{w}}wp \right]$$

$$+ \frac{\rho}{2}\ell^2 \left[Y'_* u^2 + Y'_v \dot{u}v + Y'_{(v|v|)}v|v| \right]$$

$$+ \frac{\rho}{2}\ell^3 \left[Y'_r ur + Y'_{(|r|\delta r)}u|r|\delta r + Y'_{(|v|r)}|v|r + Y'_p up \right]$$

$$+ \frac{\rho}{2}\ell^4 \left[Y'_{\dot{r}}\dot{r} + Y'_{\dot{p}}\dot{p} \right] + \frac{\rho}{2}\ell^2 u^2 Y'_{\delta r}\delta_r + (F_y)_s.$$

Normal Force

$$m(\dot{w} - uq + vp) = \frac{\rho}{2}\ell^3 \left[Z'_{\dot{w}}\dot{w} + Y'_{\dot{v}}vp \right]$$

$$+ \frac{\rho}{2}\ell^2 \left[Z'_{*}u^2 + Z'_{w}uw + Z'_{(w|w|)}w|w| \right]$$

$$+ \frac{\rho}{2}\ell^3 \left[Z'_{q}uq + Z'_{(|q|\delta s)}u|q|\delta s + Z'_{(|w|q)}|w|q \right]$$

$$+ \frac{\rho}{2}\ell^2 Z'_{(vv)}v^2 + \frac{\rho}{2}\ell^3 Z'_{(vr)}vr + \frac{\rho}{2}\ell^4 Z'_{(rr)}r^2$$

$$+ \frac{\rho}{2}\ell^2 u^2 \left[Z'_{\delta s}\delta_s + Z'_{\delta b}\delta_b \right] + \frac{\rho}{2}\ell^4 Z'_{\dot{q}}\dot{q} + (F_z)_s .$$

Rolling Moment

$$I_x\dot{p} + (I_z - I_y)qr = \frac{\rho}{2}\ell^5 \left[K'_{\dot{p}}\dot{p} + (N'_r - M'_{\dot{q}})qr + K'_{\dot{r}}\dot{r} + K_{(p|p|)}p|p| \right]$$

$$+ \frac{\rho}{2}\ell^3 \left[K'_{*}u^2 + K'_{v}uv + K'_{(v|v|)}v|v| \right]$$

$$+ \frac{\rho}{2}\ell^4 \left[K'_{p}up + K'_{r}ur + K'_{\dot{v}}\dot{v} \right]$$

$$+ \frac{\rho}{2}\ell^3 u^2 K'_{\delta r}\delta_r + Bz_B \sin \phi + (Q_x)_s .$$

Pitching Moment

$$I_y\dot{q} + (I_x - I_z)rp = \frac{\rho}{2}\ell^5 \left[M'_{\dot{q}}\dot{q} + (K'_p - N'_{\dot{r}})rp \right]$$

$$+ \frac{\rho}{2}\ell^3 \left[M'_{*}u^2 + M'_{w}uw + M'_{(w|w|)}w|w| \right]$$

$$+ \frac{\rho}{2}\ell^4 \left[M'_{q}uq + M'_{(|q|\delta s)}u|q|\delta s + M'_{(|w|q)}|w|q \right]$$

$$+ \frac{\rho}{2}\ell^3 M'_{(vv)}v^2 + \frac{\rho}{2}\ell^4 M'_{(vr)}vr$$

$$+ \frac{\rho}{2}\ell^5 M'_{(rr)}r^2 + \frac{\rho}{2}\ell^4 M'_{\dot{w}} + \frac{\rho}{2}\ell^3 u^2 \left[M'_{\delta s}\delta_s + M'_{\delta b}\delta_b \right]$$

$$+ Bz_B \sin \theta + (Q_y)_s$$

Yawing Moment

$$I_z \dot{r} + (I_y - I_x)pq = \frac{\rho}{2}\ell^5 \left[N'_{\dot{r}}\dot{r} + (M'_{\dot{q}} - K'_{\dot{p}})pq + N'_{\dot{p}}\dot{p} \right]$$

$$+ \frac{\rho}{2}\ell^3 \left[N'_*u^2 + N'_v uv + N'_{(v|v|)}v|v| \right]$$

$$+ \frac{\rho}{2}\ell^4 \left[N'_r ur + N'_{(|r|\delta r)}u|r|\delta r + N'_{(|v|r)}|v|r \right]$$

$$+ \frac{\rho}{2}\ell^4 \left[N'_p up + N'_{\dot{v}}v \right] + \frac{\rho}{2}\ell^3 u^2 N'_{\delta_r}\delta_r + (Q_z)_s.$$

Kinematic Relations

$$U^2 = u^2 + v^2 + w^2$$

$$\dot{z}_I = -u \sin \theta + v \cos \theta \sin \phi + w \cos \theta \cos \phi$$

$$\cong w - u\theta + v\phi$$

$$\dot{\phi} = p + \dot{\psi} \sin \theta$$

$$\cong p + r\theta$$

$$\dot{\theta} = \frac{q - \dot{\psi} \cos \theta \sin \phi}{\cos \phi}$$

$$\cong q - r\phi$$

$$\dot{\psi} = \frac{r + \dot{\theta} \sin \phi}{\cos \theta \cos \phi}$$

$$\cong r + q\phi.$$

Auxiliary Relations

$$(F_x)_P = a_1 u^2 + a_2 uU_c + a_3 U_c^2$$

or

$$= (1-t) aU_c^2 .$$

DISCUSSION

H. N. Abramson (Southwest Research Institute, San Antonio)

Submerged body technology shows two interesting trends; one is toward increasing fineness and the other is toward higher speed. These two together tend to introduce a new important factor and this is the elasticity of the structure. In short, hydroelastic considerations may become important for stability and control investigations of submerged bodies. I would very much like to have the author's comments on what considerations he and his colleagues have given to introducing hydroelastic effects into their theoretical and experimental studies.

E. C. Tupper (Admiralty Experiment Works)

The author mentioned in his paper the question of certain standards by which the performance of the submarine could be judged. I would like the author if he will, to state what these standards are in both the vertical and the horizontal plane. Only by studying in a computer, say, the way in which the performance of the submarine varies as regards these standards, can one judge the importance of various hydrodynamic derivatives. For instance, the author mentioned that we have what are commonly called the static, rotary, and acceleration derivatives. We feel, at the Admiralty Experiment Works, that the acceleration derivatives are not critical. There are basically four for the simple equations of motion in the vertical plane and we feel that two of these can be ignored and the other two can be calculated with sufficient accuracy and therefore do not need to be measured.

We have not studied the horizontal plane problem completely, but we feel that the most important point here is the nonlinearity introduced by the very large reductions in speed which can occur when maneuvering in the horizontal plane. I would like to make a plea, therefore, for some description of the standards which the author considers to be important.

It would be very interesting if the author could give us any information on comparisons between results with the oscillator technique which he has described and other methods of test, in particular the comparison with the rotary derivatives between the oscillator and rotating arm methods of testing.

S. T. Mathews (National Research Council, Ottawa)

I think we should congratulate Mr. Goodman and his colleagues at the David Taylor Model Basin for developing what I consider the most powerful method of considering this submarine stability and control problem, experimentally anyway. Surely these experimental results are most useful or even essential before we further develop the theoretical methods. I have a few points of detail. I would like to ask Mr. Goodman if the carrying out of static moment and force tests is not superfluous, because the same results are obtained by the oscillating heaving tests. I would be glad to have any comments he has on how the results obtained by the two methods compare. Mr. Tupper took one of my points. I was going to ask specifically if we could have any comparisons between results obtained for the rotary static moment and force derivations from the oscillating mechanism as compared with a rotating arm. It seems to me that no mention has been made of surface models; for linear seaworthiness considerations one could obtain much useful data using the oscillating mechanism technique, in pitch and heave, and also we could get results in yaw, I would think, certainly at low

Froude numbers. It would also seem that the technique could be extended to cover non-linearities if a different sort of recording technique were used.

J. P. Breslin (Davidson Laboratory, Stevens Institute of Technology)

I have a few questions I would like to put to the author and the first one is the question as to what the David Taylor Model Basin does about strut interference on the planar motion experiments.

The Davidson Laboratory has been operating a rotating arm now for about 16 years and has been greatly interested in refining and improving the techniques, particularly for the investigation of interferences, of coupling effects, and of nonlinear behavior of submarines and bodies of revolution with a mind to exploring the behavior of such vessels in radical maneuvers. In this regard, it is rather interesting that in the model regime the Navy has been able to get along without very much information in this area of large course deviations for this long period of time. We look forward with great interest to the developments which will come from the David Taylor rotating arm, not only for the comparisons for which Mr. Tupper asked, but also for the predictions of nonlinear coefficients which are necessary for modern-day treatment of evasive and radical maneuvers.

My second point has to do with the assertion that in regard to accuracy one ought to look somewhat askance at rotating arm methods for determining static derivatives. The Davidson Laboratory and the Model Basin have had a number of discussions on this matter and as a matter of fact the Model Basin has supported us in the very recent past in an experimental investigation in which we conducted experiments in the straight tank to measure static derivatives and repeated the experiments on the rotating arm, interpolating or extrapolating, depending upon how you interpret the procedure to obtain the derivatives at infinite radius. I am happy to say that these experiments,* as well as several that have been made in the past, always give very close agreement. Of course, general statements of a sweeping nature are all subject to exceptions and perhaps the class of bodies with very small damping is one in which close scrutiny should be made of the difference between the techniques.

Finally, I would like to call the attention of the participants to the great usefulness of the small model in such explorations to map out the gross effects of shape and control surface location so that modern concepts of optimizing maneuverability and controllability can be more readily achieved. The David Taylor Model Basin has certainly done an exceptional job in developing equipment which is suitable for proof testing of designs and this is a very important aspect of their part in the naval establishment, but it is urged that the use of the rotating arm at the Davidson Laboratory and other small facilities be continued for interesting exploratory research.

R. Brard (Bassin d'Essais des Carènes, Paris)

I would like to say how we appreciate the work done by the David Taylor Model Basin in order to study the maneuverability of the submarines and I would too address warm congratulations to the staff, and particularly Mr. Goodman, for their beautiful results, specially those concerning the maneuvering of the submarine under the polar ice cap.

*S. Tsakonas, "Effect of Appendage and Hull Form on Hydrodynamic Coefficients of Surface Ships," Davidson Laboratory Report 740, July 1959

I would ask him if he has given reflexion to the following point. If the motion of the ship is not steady, the hydrodynamic forces and moments on the ship depend, partly, at the instant t, on the motion of the ship before this instant t. Therefore, the equations of the motion of the ship are not exactly the same as in the case where the forces and moments would at each instant equal their values in steady motion. One study made in France shows that the condition of stability is not modified; but the trend to the steady motion is more accentuated. Thus, the transient motions are affected in such a manner that, furthermore, seems to be favorable.

Alex Goodman

Dr. Todd's paper raised a question pertaining to the stability and control requirements of a large submarine tanker. In my opinion, it would seem that such a vehicle would require a high degree of inherent stability as well as a properly designed autopilot. I noted a touch of pessimism in Mr. Newton's comment on Dr. Todd's paper which I cannot share. I think that with the techniques and means available today, solutions to the stability and control problems of such vehicles can be obtained without any difficulty.

I would like to thank the discussers for their comments. I will be brief with my replies to the various questions that have been asked. Dr. Abramson asked whether the effects of hydroelasticity on the stability and control of submarines have been considered. We have not considered such effects. However, prediction of full-scale performance based on rigid-body dynamics has been very good. Answers to several of Mr. Tupper's questions are in the written manuscript as well as in other Model Basin sources. Mr. Tupper questioned the need for the experimental determination of the acceleration derivatives by stating that theoretical techniques are available to estimate these derivatives. It is true that theoretical means are available for estimating the acceleration derivatives; however, in my opinion they are not accurate enough when it is required to determine the degree of stability. I can only say that by using the results obtained from tests using the Planar-Motion-Mechanism System we have been able to achieve excellent correlation with full scale performance. Correlations between this technique and the rotating arm technique are planned using the same model, essentially the same support system, and the same force-measuring-instrumentation system. I would like to thank Mr. Mathews for his compliments. As far as his question pertaining to the use of the Planar Motion Mechanism for the surface ship model testing, I can only say that some thought has been given to using this technique for such problems. However, I think we will first obtain some experience using the rotating-arm technique for the surface ship problem. Dr. Breslin raised a question regarding the effects of strut interference on the measurement. An extensive and detailed study of strut interference has been conducted at the Model Basin. The results of this study led to the strut design which has been incorporated in the Planar-Motion-Mechanism System, that is, small-chord struts in the vicinity of the model and angles of attack of the body being taken in the plane of the strut. As I mentioned in my presentation, this eliminates the mutual interference effects between the strut and the body. There are small blockage effects. However, by choosing the proper extension of the lower half of the strut the resistance of bodies can be measured as accurately as is done by other standard techniques. As to the required accuracy of static coefficients, I don't recall to which paper Dr. Breslin was referring, but the one I remember which shows the comparison between static coefficients, obtained from straight line tests and those obtained by the extrapolation technique differed by as much as 10 to 20 percent. This is not a small percentage when we are talking about performing accurate analyses of maneuvers. With regard to Dr. Breslin's comment as to the economy regarding small models compared to large models, this is an argumentative point. DTMB is at an advantage, since we feel that the large model is much cheaper to construct than a small specialized model. We use standard internal equipment

which can be used from model to model, thereby eliminating the need for special purpose equipment for each model. There are other advantages associated with size. DTMB is not only in the business of checking specific designs; extensive systematic studies are also conducted at DTMB and the Planar-Motion-Mechanism System is very amenable to such studies and relatively cheap to operate. For example, it takes approximately one week of testing to completely define all the hydrodynamic characteristics for a specific submarine design.

*   *   *

A THEORY OF THE STABILITY OF LAMINAR FLOW
ALONG COMPLIANT PLATES

F. W. Boggs and N. Tokita
Research Center, U.S. Rubber Company,
Wayne, New Jersey

1. INTRODUCTION

A great deal of theoretical work has been done in recent years on viscous flow in the neighborhood of a rigid wall. This has made it possible to explain the initiation of turbulence through the development of flow instability. Laminar flow has been shown by the theory to be stable under conditions when it is actually observed, and it has been shown to be theoretically unstable under conditions when turbulent flow is known to prevail. These results developed by Tollmien, Schlichting, Lin, and many others [1-7] have been verified by Schubauer [8] at the National Bureau of Standards. Today the controversy which existed for many years over the nature of turbulent flow and its relationship to laminar flow seems to be settled.

The recent work of Kramer [9-11] showing the effect of a flexible boundary wall on fluid flow has emphasized the need to extend the boundary-layer theory to include this interesting and important case. This present paper undertakes the development of a theory which will predict the stability conditions of the boundary layer in contact with a flexible wall under the same general assumptions regarding the flow that were made by previous authors for the rigid wall and to the same degree of approximation. The result should, therefore, have the same kind of validity.

In this treatment the properties of the flexible wall are expressed in terms of its acoustical compliances.

One of the significant conclusions which follows from this work is that the conditions of stabilizing a flow are fairly critical and that all coatings which are flexible do not necessarily have a favorable effect on the flow conditions.

In subsequent papers we will attempt to extend this theory to some of the special cases of practical importance, but here we will confine ourselves to some very general conclusions.

The theories of boundary-layer stabilization are based on the supposition that the Navier-Stokes equations hold at all times and that transition from laminar to turbulent flow results when the laminar flow is unstable for some arbitrarily small perturbation. Stable laminar flow exists only if the flow is stable for every possible infinitesimal perturbation. It assumes but does not really prove that when a laminar flow fulfills these conditions, it will be the dominant flow pattern and that the drag coefficient calculated from such a laminar flow is the one applicable.

The question of the lower limit of turbulent flow is not considered by the Schlichting theory nor do we consider it here. Certainly, before the picture of flexible walls can be complete, a consideration of their influence on the fully turbulent boundary layer should be made.

The theory of boundary-layer stability starts by solving the Navier-Stokes equations and the equation of continuity for a steady state. An arbitrary perturbation developable in a Fourier series is added to this solution, and the conditions are studied under which this arbitrary perturbation will either increase or decrease as time proceeds. If no possible perturbation can increase, then the flow is assumed stable. Instability will exist if any perturbation exists capable of increasing in magnitude without external excitation. Between these stable and unstable conditions there exists a boundary at which a perturbation neither increases nor decreases in magnitude. This is known as neutral stability, and it separates the stable from the unstable conditions. The values of the parameters of the system which lie on the boundary separating the regions of stable and unstable flow are known as conditions of neutral stability. The plotting of these conditions makes it possible to separate the regions of stable and unstable flow, and on this basis to predict when instability will occur. The principal aim of this paper is to express the changes in the curves of neutral stability which are brought about by the presence of a flexible wall, the properties of this wall being expressed in terms of its compliances. These compliances may not only be calculated from the nature of the walls, but they may also be measured.

2. PERTURBATION OF TWO DIMENSIONAL PARALLEL FLOW

If we have a flow exclusively in the x direction which, however, depends on y, then we may examine the effect of a small perturbation on this flow. Suppose that $\overline{V}_x$ satisfies the Navier-Stokes equation and the equation of continuity and that it vanishes along rectilinear boundaries extending in the x direction. It has been shown that if the perturbation has the form

$$v_x = \int_{-\infty}^{+\infty} \frac{\partial \Phi(\overline{\alpha}, y)}{\partial y} \, e^{i(\overline{\alpha}x - \beta t)} \, d\overline{\alpha} \tag{2.1}$$

$$v_y = -\int_{-\infty}^{+\infty} i\overline{\alpha}\Phi(\overline{\alpha}, y) \, e^{i(\overline{\alpha}x - \beta t)} \, d\overline{\alpha} \tag{2.2}$$

then the function $\Phi(\overline{\alpha}, y)$ satisfies the Orr-Summerfeld equation

$$\left(\overline{V}_x(y) - \frac{\beta}{\overline{\alpha}}\right)\left(\frac{d^2\Phi}{dy^2} - \overline{\alpha}^2\Phi\right) - \frac{d^2\overline{V}_x}{dy^2}\Phi = -\frac{i\nu}{\overline{\alpha}}\left(\frac{d^4\Phi}{dy^4} - 2\overline{\alpha}^2\frac{d^2\Phi}{dy^2} + \overline{\alpha}^4\Phi\right). \tag{2.3}$$

It is usual to express the solution of Eq. (2.3) in terms of dimensionless variables appropriate to the system. Let us choose a characteristic length which may be the distance between the edges in Couette and plane Poiseuille flows or the thickness of a boundary layer in a boundary-layer problem. Let us express the velocity of flow in terms of the maximum

velocity $\bar{U}_m$. We will take $Y = y/\delta$ as an independent variable and introduce the following parameters:

$$R = \frac{\delta \bar{U}_m}{\nu}, \qquad \alpha = \bar{\alpha}\,\delta, \qquad C = \frac{\beta}{\bar{\alpha}\,\bar{U}_m}, \qquad g = \frac{\bar{V}_x}{\bar{U}_m}. \qquad (2.4)$$

Equation (2.3) then becomes

$$(g - c)\,(\Phi'' - \alpha^2\Phi) - g''\Phi = -\frac{i}{\alpha R}\,(\Phi'''' - 2\alpha^2\Phi'' + \alpha^4\Phi). \qquad (2.5)$$

The solution of Eq. (2.5) has been extensively discussed in the literature. It has been found that it may be expressed in terms of solutions of the left-hand side of Eq. (2.5) set equal to zero (proper attention being paid to the behavior at the branch point) and in terms of solutions of

$$\eta\,\frac{d^2\psi}{d\eta^2} + i\,\frac{d^4\psi}{d\eta^4} = 0 \qquad (2.6)$$

where $\eta = (a_1\alpha R)^{1/3}\,(Y - Y_\kappa)$, Y_κ is the value of y for which $g(y) = C$ and a_1 is the derivative of g at the point $y = Y_\kappa$. All previous solutions to these equations have assumed that v_x and v_y vanished on all boundaries and at infinity if the flow was not confined. In the case of the boundary layer with which we will primarily be concerned, the conditions are $v_x = v_y = 0$ for $y = 0$ and $y = \infty$. This requires four boundary conditions. If we choose an appropriate solution ϕ of the left-hand side of Eq. (2.5) which vanishes with its first derivative for large values of y and a similar solution of ψ of Eq. (2.6), then it can be shown that for the familiar solution of the stable equation, we obtain

$$\begin{vmatrix} \phi & \psi \\ \phi' & (a_1\alpha R)^{1/3}\psi' \end{vmatrix} = 0. \qquad (2.7)$$

This determinant is a complex function of the three variables α, R, and C. If for all real values of α and R the imaginary part of C is negative, then the flow will be stable. If we choose C real, we can plot any one of these variables (α, R, and C) as a function of one of the others for the condition that satisfies Eq. (2.7). The curves so obtained are known as curves of neutral stability and establish the boundary of stable flow conditions. Diagrams of this type permit one to predict not only whether the flow will be stable but the wavelengths which occur in the unstable regions of the diagrams. Our objective in this paper is to examine how these curves of neutral stability will be influenced by the compliant surfaces. This paper, however, contains only the basic principles which will need to be developed somewhat more fully.

3. BOUNDARY CONDITIONS FOR COMPLIANT SURFACES

The velocity of flow of a viscous liquid must be identical with the velocity of the wall at every point of contact. Suppose that $\vec{r}$ is the position of a point on the undeformed wall and that the deformation caused by forces in the flow is designated by the vector $\vec{\xi}(r)$. The

rate of deformation of the wall at the point $\vec{r} + \vec{\xi}(r)$ will be given by $\dot{\vec{\xi}}(r)$. This must be identical with the flow velocity at the position $\vec{r} + \vec{\xi}$. Hence, we will have

$$\dot{\vec{\xi}}(r) = \vec{v}(r + \xi) = \vec{v}(r) + \nabla\vec{v} \cdot \vec{\xi} + \cdots . \tag{3.1}$$

Since we are considering only small perturbations, we can neglect the effect of $\vec{\xi}$ on $\vec{v}$ and identify the rate of deformation of the surface with the velocity of flow at every point along the boundary. This will lead to the approximate relationship

$$\dot{\vec{\xi}}(r) = \vec{v}(r). \tag{3.2}$$

If the motion of the wall is due exclusively to the forces in the fluid boundary layer, we must express the surface deformation in terms of these forces. To completely establish the boundary conditions, we must, therefore, express the surface forces in terms of the flow. When this has been done Eq. (3.2) will become a differential expression in the stream function which must be satisfied on the boundary.

If the response of the surface to external forces is linear, we can always express both the forces and the corresponding response of the surface in terms of progressive waves, just as we did in the case of perturbation of the flow velocity. If ξ_x and ξ_y are the amplitude of a wave of wave number $\bar{\alpha}$ and frequency β traveling along the surface and if $P(\bar{\alpha}, \beta)$ and $T(\bar{\alpha}, \beta)$ are the corresponding expressions for the amplitude of the wave of pressure and tangential force, we can define a set of compliances such that the following equations are satisfied:

$$\begin{aligned}
\dot{\vec{\xi}}_x &= Y_{11}T + Y_{12}P \\
\dot{\vec{\xi}}_y &= Y_{21}T + Y_{22}P.
\end{aligned} \tag{3.3}$$

The constants Y_{ij} are dependent on the parameters $\bar{\alpha}$ and β and are determined by the specific nature of the wall. At a later date we hope to present detailed treatments in which these constants are calculated from the structure of the coating. In this paper we will confine ourselves to their general properties.

To complete the calculation of the boundary conditions, we must express the surface forces T and P in terms of the stream function. From the perturbation of the steady-state solution of the Navier-Stokes equation, we obtain

$$\frac{\partial v_x}{\partial t} + \bar{V}_x \frac{\partial v_x}{\partial x} + v_y \frac{d\bar{V}_x}{dy} + \frac{1}{\rho} \frac{\partial P}{\partial x} = \nu\nabla^2 v_x . \tag{3.4}$$

We assume that $\bar{V}_x$ vanishes on the boundary and that its derivative at this point is given by a constant depending on the nature of the boundary layer profile. In the case of Blasius profile this is equal to $\gamma U_m/\delta$ where γ is a dimensionless constant and the same for all boundary layers of this type. If we express v_x and v_y as was done in Eqs. (2.1) and (2.2) and if we use the dimensionless variable defined in the previous section as the independent variable and if we use the same dimensionless parameters, it is readily shown that the pressure assumes the form

$$P = \frac{\bar{U}_m \rho}{\delta} \left[\frac{1}{i\alpha R} \Phi'''(y) + \left(C + \frac{i\alpha}{R} \right) \Phi'(y) + \gamma \Phi(y) \right].$$

(3.5)

The tangential force will be given in turn by

$$T = \frac{\nu \rho}{\delta^2} \Phi'' = \frac{\bar{U}_m \rho}{\delta} \frac{\Phi''}{R}.$$

(3.6)

If we substitute Eqs. (3.5) and (3.6) into Eq. (3.3) which expresses the deformation of the surface in terms of the surface forces, we will obtain a relationship between the velocity on the boundary and its derivatives along the wall. Every term in this new expression will depend upon the stream function or on its derivatives and on the parameters of the system. These two equations, therefore, replace as boundary conditions the vanishing of the components of velocity on the surface of the body. The conditions at infinity will not be changed by the flexible wall and will, therefore, remain $v_x = v_y = 0$ as in the classical equation.

It was pointed out previously that the stream function Φ could be expressed as a linear sum of two functions ϕ and ψ. This will still be true since the differential equation is unchanged by the flexible wall. Consequently, these two functions obey the boundary conditions at infinity both for the flexible and for the inflexible wall and can be used in linear combination to develop the solution of the equation of the flow in the presence of a flexible wall. If we substitute into Eq. (3.3) a linear sum of these two functions, multiplying by arbitrary coefficients, we will obtain a set of two equations in the two arbitrary coefficients which much be satisfied. The condition of existence of solutions to these equations is the vanishing of a determinant which is related to the determinant obtained for the rigid wall. The set of linear equations which must be satisfied are given in

$$A \left\{ \phi'(y) - \bar{U}_m \rho \, Y_{12} \left[\frac{\Phi'''}{i\alpha R} + \left(C + \frac{i\alpha}{R} \right) \phi' + \gamma \phi \right] - \frac{\bar{U}_m \rho}{R} Y_{11} \phi'' \right\}$$

$$+ B \left\{ (a_1 \alpha R)^{1/3} \psi'(y) - \bar{U}_m \rho \, Y_{12} \left[\frac{a_1}{i} \psi''' + \left(C + \frac{i\alpha}{R} \right) (a_1 \alpha R)^{1/3} \psi' + \gamma \psi \right] \right.$$

$$\left. - \frac{\bar{U}_m \rho}{R} (a_1 \alpha R)^{1/3} Y_{11} \psi'' \right\} = 0$$

(3.7)

$$A \left\{ -i\alpha \phi - \bar{U}_m \rho \, Y_{22} \left[\frac{\phi'''}{i\alpha R} + \left(C + \frac{i\alpha}{R} \right) \phi' + \gamma \phi \right] - \frac{\bar{U}_m \rho}{R} Y_{21} \phi'' \right\}$$

$$+ B \left\{ -i\alpha \psi - \bar{U}_m \rho \, Y_{22} \left[\frac{a_1}{i} \psi''' + \left(C + \frac{i\alpha}{R} \right) (a_1 \alpha R)^{1/3} \psi' + \gamma \psi \right] \right.$$

$$\left. - \frac{\bar{U}_m \rho}{R} (a_1 \alpha R)^{1/3} Y_{21} \psi'' \right\} = 0.$$

Retaining only the terms in $(a_1 \alpha R)^{1/3}$ and those independent of this quantity, in other words neglecting the negative powers of αR, we will obtain the set of equations

$$A \left[\phi' - \bar{U}_m \rho \, Y_{12} (C\phi' + \gamma\phi) \right]$$

$$+ B \left\{ (a_1 \alpha R)^{1/3} \psi' - \bar{U}_m \rho Y_{12} \left[-ia_1 \psi''' + C(a_1 \alpha R)^{1/3} \psi' + \gamma\psi \right] \right\} = 0 \tag{3.8}$$

$$A \left[-i\alpha\phi - \bar{U}_m \rho \, Y_{22} (C\phi' + \gamma\phi) \right]$$

$$+ B \left\{ -i\alpha\psi - \bar{U}_m \rho Y_{22} \left[-ia_1 \psi''' + C(a_1 \alpha R)^{1/3} \psi' + \gamma\psi \right] \right\} = 0.$$

We make the substitution

$$e_1 = \bar{U}_m \rho \, Y_{22}$$
$$e_2 = \bar{U}_m \rho \, Y_{12} \tag{3.9}$$

and rearrange terms, and we obtain

$$A \left[(1 - e_2 C)\phi' - e_2 \gamma\phi \right]$$

$$+ B \left[(a_1 \alpha R)^{1/3} (1 - e_2 C) \psi' - e_2 \gamma\psi + ie_2 a_1 \psi''' \right] = 0 \tag{3.10}$$

$$A \left[-e_1 C\phi' - (i\alpha + e_1 \gamma)\phi \right]$$

$$+ B \left[-e_1 C(a_1 \alpha R)^{1/3} \psi' - (i\alpha + e_2 \gamma)\psi + ie_2 a_1 \psi''' \right] = 0.$$

The condition of existence of solutions in this set of equations is the setting equal to zero of the determinant of the coefficients of A and B. Again we will note that when e_1 and e_2 are equal to zero this condition will reduce to the one obtained for a rigid plate. This is as it should be since e_1 and e_2 vanishing means zero compliance; the plate cannot be deformed.

It may be readily seen that the matrix of the coefficients of A and B in Eq. (3.10) is given by

$$\begin{pmatrix} 1 - e_2 C & -e_2 \gamma \\ -e_1 C & -(i\alpha + e_1 \gamma) \end{pmatrix} \begin{pmatrix} \phi' & (a_1 \alpha R)^{1/3} \, \psi' \\ \phi & \psi \end{pmatrix} + \begin{pmatrix} 0 & ie_2 a_1 \psi''' \\ 0 & ie_1 a_1 \psi''' \end{pmatrix} . \tag{3.11}$$

To obtain the eigenvalues of the differential equation, we must set the determinant of this matrix equal to zero.

Since the second matrix in Eq. (3.11) is singular, we cannot divide through by it, but if the prefactor on the first term is not singular, we may multiply through by its inverse so that Eq. (3.11) is transformed to

$$
\begin{pmatrix} \phi' & (a_1\alpha R)^{1/3}\,\psi' \\ \\ \phi & \psi \end{pmatrix} + \frac{1}{\Delta}\begin{pmatrix} -(i\alpha + e_1\gamma) & e_2\gamma \\ \\ e_1 C & (1 - e_2 C) \end{pmatrix}\begin{pmatrix} 0 & ie_2 a_1\psi''' \\ \\ 0 & ie_1 a_1\psi''' \end{pmatrix}. \quad (3.12)
$$

This step requires examination. If the matrix has no inverse, if the operation cannot be carried out, then we have a special problem. In general, the boundary layer will be unstable if the zeros of the determinant (3.13) have positive real parts:

$$
\Delta = \begin{vmatrix} 1 - e_2 C & -e_2\gamma \\ \\ -e_1 C & -(i\alpha + e_1\gamma) \end{vmatrix} = -i\alpha + i\alpha e_2 C - e_1\gamma
$$

$$
= -i\alpha + i\alpha C \bar{U}_m \rho\, Y_{12} - \gamma \bar{U}_m \rho\, Y_{22}. \quad (3.13)
$$

Since we assume the compliances are passive, this will generally not be the case, so that we will be able actually to divide through by the matrix and obtain (3.12). Our stability conditions are then given in

$$
\begin{vmatrix} \phi' & (a_1\alpha R)^{1/3}\,\psi' \\ \\ \phi & \psi \end{vmatrix} + \begin{vmatrix} \phi' & \alpha e_2 \\ \\ \phi & ie_1 \end{vmatrix}\frac{a_1\psi'''}{\Delta} = 0. \quad (3.14)
$$

As can be seen the first term is the expression which must be set equal to zero in the case of the rigid boundary. The second term contains the added conditions imposed by the flexibility. Developing this determinant, we finally obtain the following equation for the conditions of the boundary:

$$
\frac{\psi}{Y_x(a_1\alpha R)^{1/3}\,\psi'} - \frac{\phi}{Y_x\phi'} + \left(\frac{ie_1}{\Delta} - \frac{\alpha e_2\,\phi}{\Delta\phi'}\right)\frac{a_1\psi'''}{Y_x(a_1\alpha R)^{1/3}\,\psi'} = 0. \quad (3.15)
$$

We will note that this boundary condition is expressed in terms of three functions depending upon the hydrodynamic conditions and on the two compliances. Two of the three functions which are involved are identical with the ones which appeared in the solution for the rigid body as developed by previous authors. We may rewrite in the form

$$
F(\zeta) - G(\alpha, C) = -\left[ie_1 - \alpha e_2 Y_x G(\alpha, C)\right]a_1 H(\zeta)/\Delta
$$

$$
F(\zeta) = \frac{\psi(\zeta)}{\zeta\psi'(\zeta)}, \qquad G(\alpha, C) = \frac{\phi}{Y_x\phi'} \qquad\qquad \begin{matrix} (3.16) \\ (\text{Cont.}) \end{matrix}
$$

$$H(\zeta) = \frac{\psi'''(\zeta)}{\zeta \psi'(\zeta)}$$

$$\zeta = -(a_1 \alpha R)^{1/3} Y_{\varkappa}$$

$$\frac{F(\zeta) - G(\alpha, C)}{a_1 H(\zeta)} = - \frac{Y_{22} + i\alpha Y_{\varkappa} G(\alpha, C) Y_{12}}{i\gamma Y_{22} + \alpha C Y_{12} - \dfrac{\alpha}{\overline{U}_m \rho}} .$$

(3.16)

4. SOME GENERAL PROPERTIES OF A SURFACE COMPLIANCE

Rayleigh was the first to show that solid bodies are subject to waves propagating over their surface. Such waves will exist in the case of a turbulent boundary layer in contact with a flexible surface and will play an important part in the nature of the compliance. Basically, there are two factors to be considered; the deformation which occurs at the point where the pressure is applied and the way this deformation propagates along the surface. We will consider the effect of both of these reactions of the surface. Let us suppose that we have a pressure of the type mentioned previously, and for the sake of simplicity, let us suppose that it varies periodically with the time so that it may be represented by the product of a complex exponential in the time and a function of x. In this case we may represent the pressure by an expression similar to

$$e^{-i\beta t} P(x) = \frac{1}{\sqrt{2\pi}} \int_{-\infty}^{+\infty} P(\overline{\alpha}) e^{i\overline{\alpha}x} d\overline{\alpha} e^{-i\beta t} .$$

(4.1)

This will cause periodic displacements of the surface velocity in the x and y direction which may be represented by

$$v_y = -i\beta e^{-i\beta t} \xi_y(x) = \int_{-\infty}^{+\infty} Y_{22}(\overline{\alpha}, \beta) P(\overline{\alpha}) e^{i\overline{\alpha}x} d\overline{\alpha} e^{-i\beta t}$$

(4.2)

$$v_x = -i\beta e^{-i\beta t} \xi_x(x) = \int_{-\infty}^{+\infty} Y_{21}(\overline{\alpha}, \beta) P(\overline{\alpha}) e^{i\overline{\alpha}x} d\overline{\alpha} e^{-i\beta t} .$$

In Eq. (4.2) the Y's are the surface compliances for a wave having a wave number $\overline{\alpha}$. If we use the Fourier inversion theorem for Eq. (4.1) and Eq. (4.2), we will obtain

$$P(\overline{\alpha}) = \frac{1}{\sqrt{2\pi}} \int_{-\infty}^{+\infty} P(x) e^{-i\overline{\alpha}x} dx$$

$$Y_{22}(\overline{\alpha}, \beta) P(\overline{\alpha}) = -\frac{i\beta}{2\pi} \int_{-\infty}^{+\infty} \xi_y(x) e^{-i\overline{\alpha}x} dx$$

(4.3)

$$Y_{21}(\bar{\alpha},\beta) \; P(\bar{\alpha}) \;\; = \;\; - \; \frac{i\beta}{2\pi} \int_{-\infty}^{+\infty} \xi_x(x) \; e^{-i\bar{\alpha}x} \; dx. \tag{4.4}$$

Combining these equations we obtain for the surface compliances

$$Y_{22}(\bar{\alpha},\beta) \;\; = \frac{\dfrac{-i\beta}{\sqrt{2\pi}} \displaystyle\int_{-\infty}^{+\infty} \xi_y(x) \; e^{-i\bar{\alpha}x} \; dx}{\displaystyle\int_{-\infty}^{+\infty} P(x) \; e^{-i\bar{\alpha}x} \; dx} \tag{4.5}$$

$$Y_{21}(\bar{\alpha},\beta) \;\; = \frac{\dfrac{-i\beta}{\sqrt{2\pi}} \displaystyle\int_{-\infty}^{+\infty} \xi_x(x) \; e^{-i\bar{\alpha}x} \; dx}{\displaystyle\int_{-\infty}^{+\infty} P(x) \; e^{-i\bar{\alpha}x} \; dx}. \tag{4.6}$$

So far these are purely formal relationships which, for example, would allow us to determine the surface compliance experimentally from the reaction of the surface to a pressure. This is useful in that equipment can be designed and has been designed to use this relation for the determination of the surface compliance of arbitrary surfaces. However, we must put it in more manageable shape for the determination of experimental quantities, and we will show how it can be used to relate the surface compliance to the propagation constant of Rayleigh waves at a given frequency. Let us suppose that the pressure is applied over a very small length which is allowed then to go to zero. Experimentally, this could be achieved by the use of a very narrow knife edge as a driving unit. We will have for the pressure

$$P(x) \;\; = \;\; \frac{F}{2\varepsilon} \qquad \text{when} \quad -\varepsilon < x < \varepsilon$$

$$P(x) \;\; = \;\; 0 \qquad \text{when} \quad x < -\varepsilon \;\; \text{or} \;\; x > \varepsilon. \tag{4.7}$$

Using these in Eq. (4.4) to obtain the Fourier integral of the pressure, we have

$$P(\bar{\alpha},\beta) \;\; = \;\; \frac{1}{\sqrt{2\pi}} \; F \; \frac{\sin \bar{\alpha}\varepsilon}{\bar{\alpha}\varepsilon} \; . \tag{4.8}$$

Taking the limit as $\varepsilon \to 0$ we finally obtain

$$P(\bar{\alpha},\beta) \;\; = \;\; \frac{1}{\sqrt{2\pi}} F \; \lim_{\varepsilon \to 0} \frac{\sin \bar{\alpha}\varepsilon}{\bar{\alpha}\varepsilon} \;\; = \;\; \frac{1}{\sqrt{2\pi}} F. \tag{4.9}$$

The compliances of the surface will be given respectively by

$$Y_{22} = -\frac{i\beta}{\sqrt{2\pi}\,F} \int_{-\infty}^{+\infty} \xi_y(x)\; e^{-i\bar{\alpha}x}\; dx \qquad (4.10)$$

$$Y_{21} = -\frac{i\beta}{\sqrt{2\pi}\,F} \int_{-\infty}^{+\infty} \xi_x(x)\; e^{-i\bar{\alpha}x}\; dx. \qquad (4.11)$$

The Fourier transforms in this case are carried out from minus infinity to plus infinity in the complex plane. It is convenient to use a real notation, in which case the integrals will go from zero to infinity. It is worth noting, however, that the normal displacement will be an even function of x, whereas the tangential displacement will be an odd function of x. As a consequence only the cosine transformation from zero to infinity will be important in the first instance, and the sine transform will be important in the second instance.

This gives us for the surface compliance

$$Y_{22}(\bar{\alpha},\beta) = -\frac{2i\beta}{\sqrt{2\pi}\,F} \int_0^{\infty} \xi_y(x)\; \cos\; \bar{\alpha}x\; dx \qquad (4.12)$$

$$Y_{21}(\bar{\alpha},\beta) = -\frac{2i\beta}{\sqrt{2\pi}\,F} \int_0^{\infty} \xi_x(x)\; \sin\; \bar{\alpha}x\; dx. \qquad (4.13)$$

Let us now suppose that the vertical vibration imparted by the knife edge gives rise to propagating waves having the propagating constant Γ. The compliances which apply to the normal and tangential components will be respectively given by

$$Y_{22}(\bar{\alpha},\beta) = -\frac{2i\beta\; f_o(\beta)}{\sqrt{2\pi}\,F} \int_0^{\infty} e^{i\Gamma x}\; \cos\; \bar{\alpha}x\; dx \qquad (4.14)$$

$$Y_{21}(\bar{\alpha},\beta) = -\frac{2i\beta\; g_o(\beta)}{\sqrt{2\pi}\,F} \int_0^{\infty} e^{i\Gamma x}\; \sin\; \bar{\alpha}x\; dx \qquad (4.15)$$

where $f_o(\beta)$ and $g_o(\beta)$ are functions of the frequency.

Carrying out the integral we obtain

$$Y_{22}(\bar{\alpha},\beta) = \frac{2\beta \; f_o(\beta)}{\sqrt{2\pi} \; \bar{\alpha} \; F} \frac{\left(\dfrac{\Gamma}{\bar{\alpha}}\right)}{\left(\dfrac{\Gamma}{\bar{\alpha}}\right)^2 - 1} \qquad (4.16)$$

$$Y_{21}(\bar{\alpha},\beta) = \frac{2\beta \; g_o(\beta)}{\sqrt{2\pi} \; \bar{\alpha} \; F} \frac{1}{\left(\dfrac{\Gamma}{\bar{\alpha}}\right)^2 - 1} \; . \qquad (4.17)$$

The quantity $\Gamma/\bar{\alpha}$ is the ratio of the wavelength of the disturbance in the boundary layer to the wavelength in the coating. One of the points of interest will be to consider the effect of a large difference between these two wavelengths and also what the behavior will be when these two wavelengths are close together.

If we calculate the corresponding dimensionless compliances, we obtain

$$e_1 = \rho \bar{U}_m Y_{22} = \frac{2}{\sqrt{2\pi}} \frac{\beta}{\bar{\alpha}} \frac{f_o(\beta)}{F} \left[\frac{\left(\dfrac{\Gamma}{\bar{\alpha}}\right)}{\left(\dfrac{\Gamma}{\bar{\alpha}}\right)^2 - 1} \right] \rho \bar{U}_m$$

$$= \frac{2}{\sqrt{2\pi}} C \frac{f_o(\beta)}{F} \rho \bar{U}_m^2 \left[\frac{\left(\dfrac{\Gamma}{\bar{\alpha}}\right)}{\left(\dfrac{\Gamma}{\bar{\alpha}}\right)^2 - 1} \right] = \frac{2}{\sqrt{2\pi}} C \frac{f_o(\beta)}{F} \rho \bar{U}_m^2 \left[\frac{\left(\dfrac{C}{v}\right)}{\left(\dfrac{C}{v}\right)^2 - 1} \right]$$

$$\simeq \frac{2}{\sqrt{2\pi}} \frac{\beta}{\Gamma} \frac{f_o(\beta)}{F} \rho \bar{U}_m^2 = \frac{2}{\sqrt{2\pi}} v \frac{f_o(\beta)}{F} \rho \bar{U}_m^2 \; , \qquad \text{for } \frac{\Gamma}{\bar{\alpha}} \gg 1$$

$$\simeq - \frac{2}{\sqrt{2\pi}} \frac{\beta\Gamma}{\bar{\alpha}^2} \frac{f_o(\beta)}{F} \rho \bar{U}_m^2 = - \frac{2}{\sqrt{2\pi}} \frac{C^2}{v} \frac{f_o(\beta)}{F} \rho \bar{U}_m^2, \quad \text{for } \frac{\Gamma}{\bar{\alpha}} \ll 1$$

$$\qquad (4.18)$$

$$e_2 = \rho \bar{U}_m Y_{21} = \frac{2}{\sqrt{2\pi}} \frac{\beta}{\bar{\alpha}} \frac{g_o(\beta)}{F} \left[\frac{1}{\left(\dfrac{\Gamma}{\bar{\alpha}}\right)^2 - 1} \right] \rho \bar{U}_m$$

$$= \frac{2}{\sqrt{2\pi}} C \frac{g_o(\beta)}{F} \left[\frac{1}{\left(\dfrac{\Gamma}{\bar{\alpha}}\right)^2 - 1} \right] \rho \bar{U}_m^2 = \frac{2}{\sqrt{2\pi}} C \frac{g_o(\beta)}{F} \rho \bar{U}_m^2 \left[\frac{1}{\left(\dfrac{C}{v}\right)^2 - 1} \right]$$

$$\simeq \frac{2}{\sqrt{2\pi}} \frac{\beta\bar{\alpha}}{\Gamma^2} \frac{g_o(\beta)}{F} \rho \bar{U}_m^2 = \frac{2}{\sqrt{2\pi}} \frac{v^2}{C} \frac{g_o(\beta)}{F} \rho \bar{U}_m^2 \; , \quad \text{for } \frac{\Gamma}{\bar{\alpha}} \gg 1$$

$$\simeq - \frac{2}{\sqrt{2\pi}} \frac{\beta}{\bar{\alpha}} \frac{g_o(\beta)}{F} \rho \bar{U}_m^2 = - \frac{2}{\sqrt{2\pi}} C \frac{g_o(\beta)}{F} \rho \bar{U}_m^2, \quad \text{for } \frac{\Gamma}{\bar{\alpha}} \ll 1. \; (4.19)$$

It is apparent that e_1 and e_2 both pass through the origin when β is equal to zero. It follows that they will both pass through the origin when C vanishes. Furthermore, when $\bar{\alpha}$ is small e_2 will be negligible and e_1 will be a function of β only. These two characteristics will have some important practical consequences which we will consider in the next section of this paper. It can also be seen by substituting that similar conditions will be obtained when the propagation constant of waves over the surface is proportional to the velocity of flow.

5. CURVE OF NEUTRAL STABILITY FOR A FLEXIBLE WALL

If Eq. (3.16) is rewritten in terms of e_1 and e_2, we obtain

$$\frac{F(\zeta) - G(\alpha, C)}{a_1 H(\zeta)} = -\frac{e_1 + i\alpha e_2 Y_x G(\alpha, C)}{C\alpha e_2 + i\gamma e_1 - \alpha} = \frac{-\dfrac{e_1}{\alpha} - iY_x G(\alpha, C) \, e_2}{Ce_2 + i\gamma \dfrac{e_1}{\alpha} - 1} . \qquad (5.1)$$

The left-hand side depends on the Reynolds number only through its dependence on ζ, whereas the right-hand side depends on the Reynolds number through the frequency β and wave number $\bar{\alpha}$, which depend on both the velocity and the Reynolds number. The curve of neutral stability can be obtained by identifying the real and imaginary parts of both sides of Eq. (5.1) and eliminating either α or C. For each value of $\bar{U}_m$ there will be a different curve of neutral stability and a corresponding critical Reynolds number which, if it exists, will depend on $\bar{U}_m$. The procedure outlined above represents a formidable amount of work which, even with the aid of calculators, would be forbidding. Can we find a procedure for obtaining bounds for the Reynolds number which will simplify the general discussion?

For a given velocity the right hand-side of Eq. (5.1) will be a function of two variables only, α and β. Furthermore, as we saw in Section 4 all the curves will pass through the origin and be tangential to each other when α and β are small.

If we hold α constant we can plot the right-hand side of Eq. (5.1) as a function of C treating R as a parameter. For a given value of α the right-hand side of Eq. (5.1) will be a single curve passing through the origin while the left-hand side will give a family of curves, one for each Reynolds number. The intersection of the curve corresponding to the right-hand side of (5.1) with each one of the family of curves for the left-hand side will correspond to a value of α and of R on the curve of neutral stability. If the family of curves representing the left has an envelope through the elimination of R, the value of the frequency corresponding to the intersection of this envelops with the right plotted for α and $\bar{U}_m$ constant will be an extreme value for C. The corresponding value of the frequency for each value of α will form a boundary separating areas of stability and instability. The value of the frequency along this boundary will be a function of the velocity and of α, and its value will be given by an equation of the form

$$\beta(\bar{U}_m, \alpha) = \frac{\bar{U}_m^2 \alpha C}{\nu \sqrt{R}} . \qquad (5.2)$$

In addition, we must specify that we are on the envelope. This will give a relationship between α and C. These two relations together will, therefore, lead to a relationship between the Reynolds number and the velocity, from which a family of curves of critical Reynolds numbers can be constructed.

A delineation of the family formed of the envelopes obtained by the elimination of the Reynolds numbers through the construction of the envelope requires a more detailed analysis of the way the right-hand side of Eq. (5.1) is formed. If we consider the function given to the left of Eq. (5.1), it is not difficult formally to construct the envelope.

The analytic expressions for the functions F, G, and H are inconvenient. We have used an approximate expression for the denominator and have constructed the envelope graphically. The value of the function in the numerator for a given set of values of α and C is obtained by simple graphical subtraction. Holding α constant and varying C, we obtain a family of curves with the general appearance given in Fig. 1. This family of curves has an envelope which is formed by the tangent to the common apices of the curves. There will be one such envelope for each value of α. This family of envelopes is given in Fig. 2, which was constructed from existing data. Each member of this family of envelopes separates the plane into two domains. Any point in the lower domain will have two members of the family of which it is an envelope passing through it, a point on the envelope will have only one, and finally a point above the envelope will have none. The locus of the points of intersection between the family of envelopes on the one hand and the compliances on the other will form the boundary between areas of stability and instability. Points corresponding to the compliance which are above the envelope cannot lead to unstable solutions.

In the discussion that follows we will consider the special case when e_2 vanishes. For small values of β and $\bar{\alpha}$, e.g., moderate speeds and large Reynolds numbers, this will be the most important case.

$\alpha = 0.5$
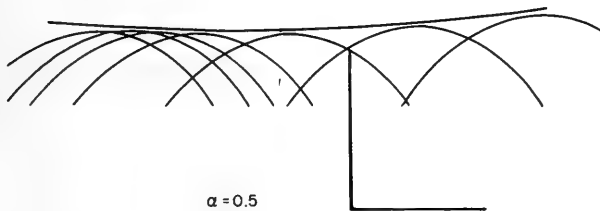
Fig. 1. Family of curves from Eq. (5.1) for constant α and a set of values of C
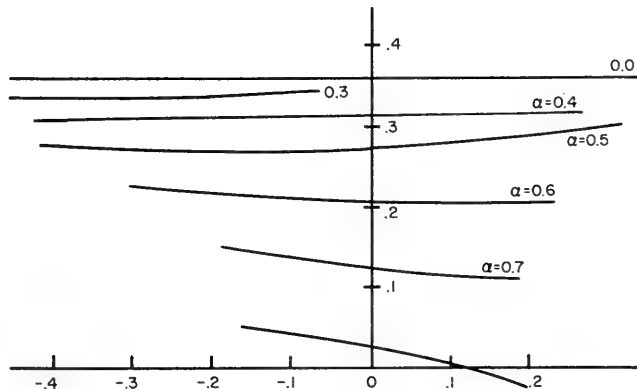
Fig. 2. Envelopes obtained as shown in Fig. 1

We can solve Eq. (5.1) for $e_1/i\alpha$, giving us

$$\frac{F - G}{a_1 H} = \frac{-\dfrac{e_1}{\alpha}}{i\gamma\,\dfrac{e_1}{\alpha} - 1}, \qquad \frac{\gamma e_1}{i\alpha} = \frac{-(F - G)}{(F - G) - iH},$$

$$\frac{\gamma e_1}{i\alpha} = \frac{-(F - G)}{(F - G) - 1}, \quad \text{for large } \zeta \qquad\qquad (5.3)$$

$$\frac{F - G}{(F - G) - 1} = Y \quad \text{or} \quad \frac{1}{Y} = 1 - \frac{1}{F - G}; \quad \text{here} \quad Y = i\gamma\,\frac{e_1}{\alpha}.$$

The family of curves given in Fig. 2 can be transformed graphically by a succession of projective transformations to give the family of curves given in Fig. 3. This is the appropriate form to use for Eq. (5.3). It should be noted that there is one member of this family corresponding to C equals 0, which is a boundary for all members of the family. The value of C for which the family of curves passes through the origin corresponds to a minimum value of C compatible with complete stability for a rigid flat plate. The study of this envelope is in fact a convenient way of visualizing the stability problem for a rigid wall as well as for a nonrigid one and leads to essentially the same results in the former case as the procedure employed by Schlichting.

Let us now proceed to a consideration of the general effect that e_1 will have on the stability of the flow. e_1 will be represented by a family of curves of the two variables

$$\beta = \frac{\bar{U}_m^2 \alpha C}{\nu \sqrt{R}}$$
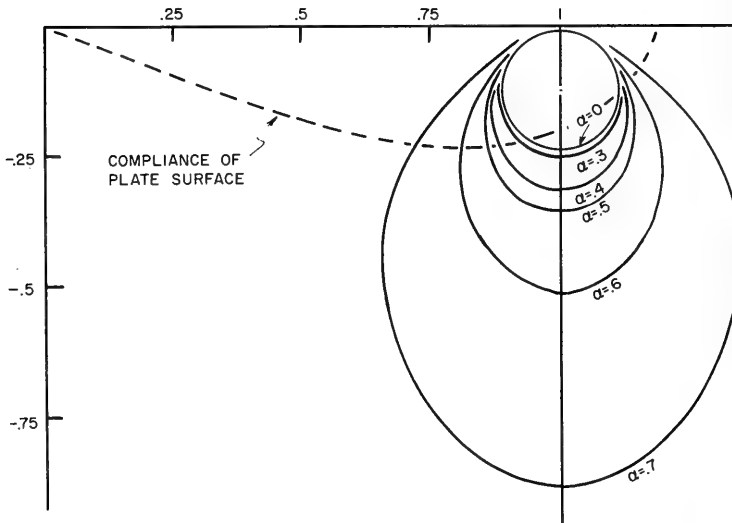
Fig. 3. Family of contours in the compliance, obtained by
transformation from Fig. 2

and

$$\bar{\alpha} = \frac{\bar{U}_m \alpha}{\nu\sqrt{R}} \quad,$$

which we know must be mutually tangent and pass through the origin for small values of both variables. If now for a fixed value of α we describe one of the families of curves, its intersection or intersections with the member of the envelope for a corresponding value of α will give points on the boundary line separating stable conditions from unstable conditions. In general, there will be two such intersections and usually the stable conditions will be those sections between the points of intersection. If the members of the family of curves of the compliance do not intersect the corresponding member of the family of envelopes, then either the system will always be stable or will always be unstable. Since the envelopes corresponding to unstable conditions for a rigid wall always enclose the origin and since the compliances must pass through the origin, it follows that there will be at all times at least one intersection with the compliance unless the compliance is so small as to be completely enclosed by the envelope. Since, however, in this family of curves the portion closest to the origin represents unstable conditions, it follows also that in the case where there is no intersection between the compliance and the envelope that the boundary layer will always be unstable. Consequently, in the case of interest there will always be at least one intersection corresponding to low frequencies between the members of the envelope and the family of compliances. These curves considered as a function of R, β, and the velocity of flow will form a family from which the extreme values of the Reynolds number can be deduced.

SUMMARY

We have given a very brief discussion of the principles on which an analysis of the effect of a flexible surface on fluid flow is based. It shows that through the introduction of the concept of surface compliance, the conditions of stability of laminar flow may be analyzed. A more detailed presentation would allow us to give conditions which will be fulfilled for a stable flow. In general, we show that the flow will be stable when certain contours in the complex plane exclude the origin. The presence of the flexible wall replaces the origin by a curve and the points of instability are the intersection of this curve with the contours.

APPENDIX

Reference 4 gives the relation

$$F(\zeta) = \frac{\psi(\zeta)}{\zeta\psi'(\zeta)} = \frac{\displaystyle\int_{+\infty}^{-\zeta}\int_{+\infty}^{\xi} \rho^{1/2}\, H'_{1/3}\left[\frac{2}{3}\,(i\rho)^{3/2}\right]\,d\rho\,d\xi}{-\displaystyle\int_{+\infty}^{-\zeta} \rho^{1/2}\, H'_{1/3}\left[\frac{2}{3}\,(i\rho)^{3/2}\right]\,d\rho}. \tag{A1}$$

For large values of ζ it is shown that

$$F(\zeta) = \zeta^{-3/2} e^{i\pi/4} \tag{A2}$$

We wish to calculate $\psi'''/\zeta\psi'$ in terms of F and its derivatives. Let

$$h = \frac{\psi'}{\psi} = \frac{1}{\zeta F(\zeta)} . \tag{A3}$$

In terms of h we obtain

$$\frac{\psi'''}{\zeta\psi'} = \frac{1}{\zeta}\left(h^2 + 3h' + \frac{h''}{h}\right) . \tag{A4}$$

For large values of ζ we obtain by combination of (A2) and (A4)

$$\frac{\psi'''}{\zeta\psi'} = \frac{1}{\zeta}\left[\zeta e^{-i\pi/2} + \frac{3e^{-i\pi/4}}{2\zeta^{1/2}} - \frac{1}{4\zeta^2}\right] \simeq e^{-i\pi/2} . \tag{A5}$$

ACKNOWLEDGMENTS

REFERENCES

[1] Tollmein, W., "Göttinger Monographie uber Grenzchichten," Pt B 3, 1956

[2] Schlichting, H., "Zur Entstchung des Turbulentz bei der Plallenstromung," Nachr. Ges. Wiss. Göttinger, Math. Phys. Klasse 182, 1933

[3] Schlichting, H., "Boundary Layer Theory," New York:McGraw-Hill, 1955

[4] Lin, C.C., "On the Stability of Two-Dimensional Parallel Flow," Quarterly of Appl. Math., Vol. III, pp. 117, 218, and 277

[5] Lin, C.C., "The Theory of Hydrodynamic Stability," Cambridge:The University Press, 1955

[6] Squire, H.B., "On the Stability of Three Dimensional Disturbances of Viscous Fluid Between Parallel Walls," Proc. Roy. Soc. A-142 (1933)

[7] Schlichting, H., and Ulrich, A., "Zur Berechnung des Umschlungs Laminar-Turbulent," Jahrbuch d. dt Luftfahrtforshung 18, 1942

[8] Schubauer, G.B., and Shramstad, H.K., "Laminar Boundary Layer Oscillations and Stability of Laminar Flow," National Bureau of Standards Research Paper 1772

[9] Max O. Kramer, Communication Jour. Aero-Space Sciences, June 1957

[10] Max O. Kramer, Communication Jour. Aero-Space Sciences, May 1959

[11] Max O. Kramer, "Boundary Layer Stabilization by Distributed Damping," Jour. Amer. Soc. of Naval Engineers 72:25 (1960)

DISCUSSION

T. G. Lang (U.S. Naval Ordnance Test Station)

I would like to mention that I have observed Dr. Kramer's experiments on models utilizing compliant surfaces in Long Beach Harbor in California and consider his test apparatus to be well designed and his reported results to be accurate. When the theory of distributed damping using compliant surfaces was first proposed by Dr. Kramer, it was mentioned that sea mammals such as porpoises and whales utilize this phenomena to reduce their drag. Reports by many observers of fish and sea mammals indicate high performance. I would like to describe a study which was recently conducted by the U.S. Naval Ordnance Test Station (NOTS) on the performance characteristics of a live porpoise. These results which I shall present are still preliminary since additional analysis is planned.

The performance tests were conducted by a group of NOTS personnel in the towing tank at Convair, San Diego. This tank is 315 feet long, 12 feet wide, and 6-1/2 feet deep. It was filled to a depth of 4-1/2 feet on June 3, 4, and 5 and to 6 feet on June 15 with sea water. This water was continuously filtered except during tests, and chemicals were added to prevent growth of plankton and bacteria. The tests were composed of two types. One type was a peak-effort run down the tank, and the other was a motionless glide through a series of large underwater hoops. The porpoise was tested both in its natural condition and with a ring, whose thickness varies from 1/16 to 1 inch, placed around its head section. The purpose of the thinnest ring was to induce turbulence on the body. The thicker rings were used to significantly increase the drag of the porpoise by a fixed amount and thereby aid in determining its horsepower output when the top speed with each ring is known.

Figure D1 shows a porpoise with such a ring placed around its head section. This is a porpoise similar to the one used in these tests, except it was trained to support itself in the position shown in the figure for several seconds. Figure D2 shows the dimensions of the porpoise (Pacific white-sided dolphin) which was tested in this program. It is 6.7 feet long, has a maximum diameter of 1.2 feet, and weighs 200 pounds. The distance versus time data were primarily measured by overhead cameras. Two cameras were mounted at the beginning of the runs behind underwater windows, but much of their data was lost due to camera malfunction.

Figure D3 shows that portion of the horsepower which was required on the peak effort runs to produce the recorded acceleration. It is noted that horsepowers up to 1.8 were
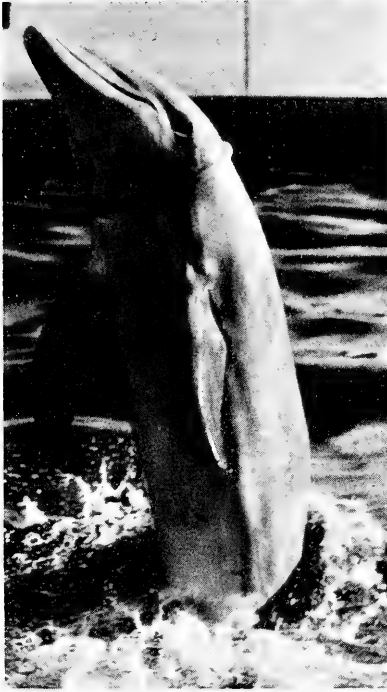
Fig. D1. Placement of ring on the porpoise head section

DIMENSIONS IN INCHES
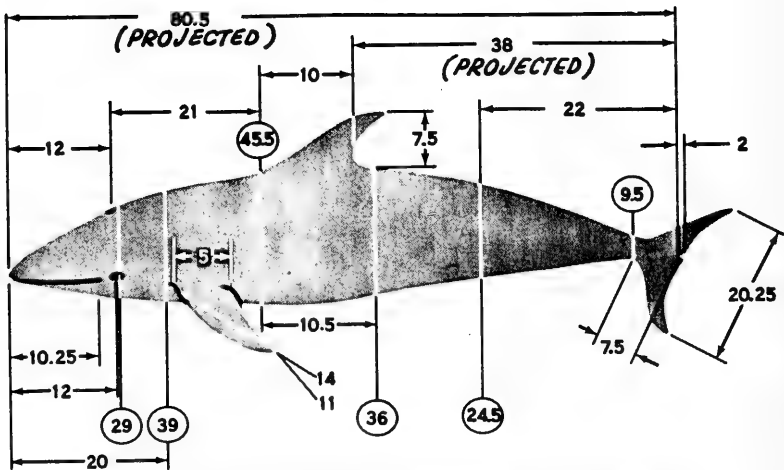
WEIGHT OF PORPOISE-200 LB

MEASUREMENTS ARE ALONG BODY UNLESS NOTED OTHERWISE. CIRCLED NUMBERS ARE GIRTH MEASUREMENTS.

Fig. D2. Dimensions of the porpoise tested
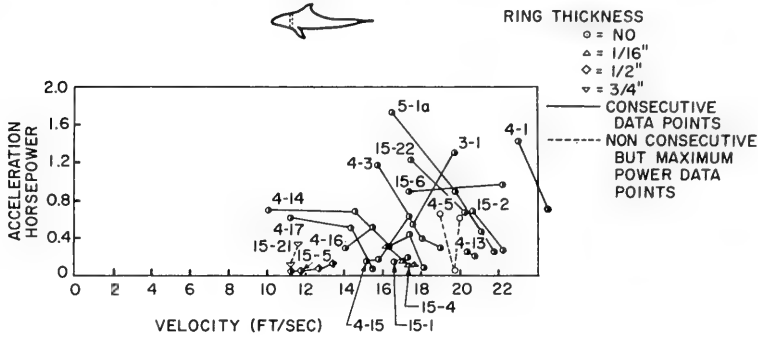
Fig. D3. Acceleration horsepower versus velocity

measured, and this does not include the horsepower expended in overcoming drag. This value of power is in agreement with that which humans can exert for the same time period. The lack of acceleration data at low speeds is due to the previously mentioned camera malfunction.

Figure D4 shows the results of the glide runs wherein the drag was calculated from the deceleration rate as the porpoise glided through underwater hoops. The data are plotted as drag area versus glide velocity, wherein the effects of virtual mass are included. This drag area is the drag divided by $1/2 \, \rho V^2$. The scatter of points for any one configuration is believed due to movement of the porpoise while gliding. For numerous reasons, the maxima of these points are considered to approach the correct drag value of a motionless gliding porpoise. Figure D5 is a plot of this same data against ring thickness. The solid lines are the estimated drag area at various glide speeds. The dotted line is a curve faired through the maximum drag area data points and is believed to represent the minimum value of the experimental drag area of the porpoise. The wave drag has not been subtracted from this data, but it has been calculated to be small at the higher glide speeds.
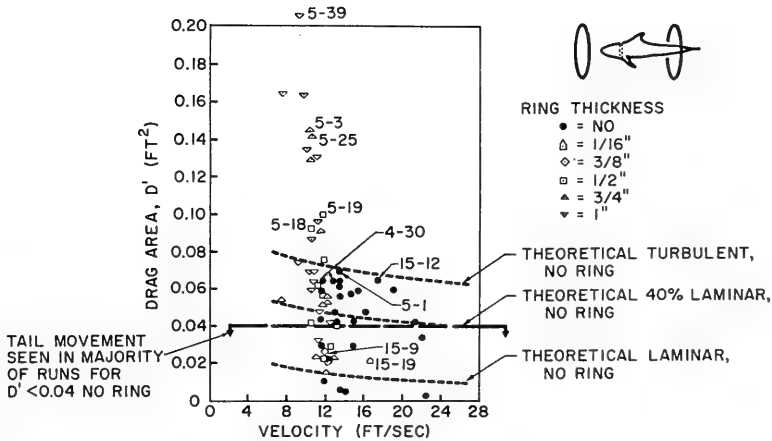
Fig. D4. Drag area versus velocity

$$D' = \frac{2m_L}{\rho X\Delta} \ln\left(\frac{\Delta t_2}{\Delta t_1}\right)$$
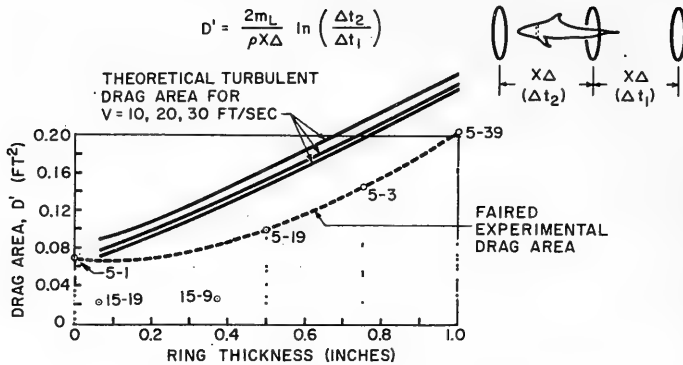
Fig. D5. Drag area versus ring thickness

Figure D6 shows the maximum recorded speed versus ring thickness. With no ring, the maximum speed was 25 ft/sec, which is only 15 knots. It is noted that the water depth has no effect on top speed, since it was 4-1/2 feet for the runs on June 3, 4, and 5, and 6 feet for the June 15 runs. Figure D7 shows the drag horsepower versus ring thickness. The drag horsepower was not measured but was calculated using the dotted-line experimental drag area of Fig. D5 and the top speed from Fig. D6. Of primary interest is the fact that the 2.0-horsepower maximum, recorded for the no-ring condition, agrees well with the recorded maximum acceleration horsepower. These results tend to indicate that the effective drag while swimming is essentially the same as that while gliding, and that the boundary layer in each case is effectively turbulent. It is noted, however, that the horsepower for the runs with rings is only 0.8 rather than 2.0. This fact would tend to indicate either that the rings had a large effect on the boundary layer while swimming, that they caused the porpoise to exert less effort due to irritation or some other cause, or else that the experimental ring drag values are low. The time during which the porpoise traveled at top speed was several seconds longer when a ring was carried than when it was not, so the expended horsepower with rings would have been expected to be around 1.3 to 1.6 rather than 2.0.

Figure D8 shows the porpoise body movement during a typical cycle while accelerating. The nose stations are aligned and the body position is sketched from different film frames
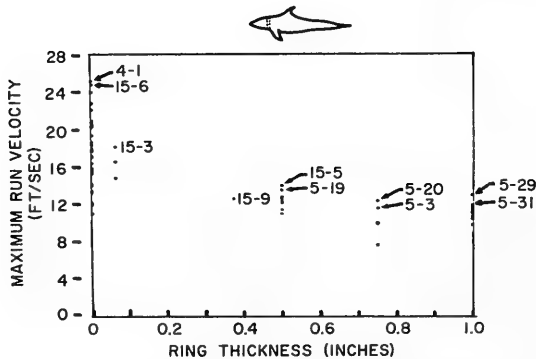
Fig. D6. Maximum velocity versus ring size
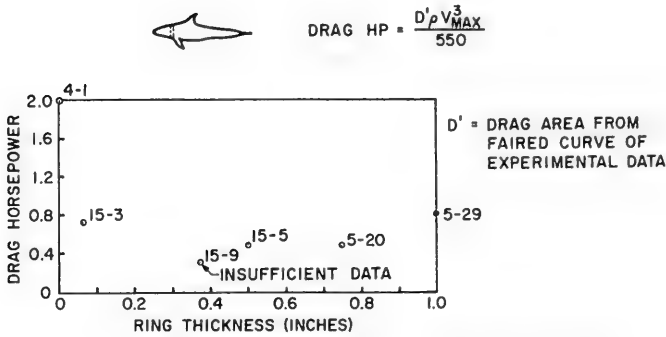
Fig. D7. Maximum drag horsepower versus ring thickness
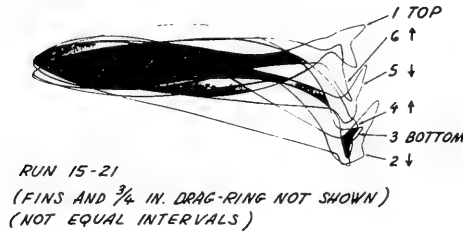
Fig. D8. Porpoise movements during
acceleration, nose sections aligned

to show body and tail movement. The fins have been removed from the sketches to improve clarity.

In conclusion, it can be stated that no unusual physical or hydrodynamic phenomena were apparent in this porpoise study. These tests, however, have not proved that unusual characteristics do not exist. It is possible that: (a) turbulence in the tank water or the added chemicals affected the ability of the porpoise to control its boundary layer, (b) the porpoise did not exert maximum effort, or (c) that unknown factors affected the results due to the unnatural environment. A report is in process which contains more detailed information on the study.

M. Landahl (Massachusetts Institute of Technology)

I want to comment on an error in the boundary condition, but first I want to point out that the present author here is not the only one who happened to fall in that trap because it is very easy to do it. The reason for it is as follows: When you have a wall, of course, you know that the steady boundary layer is such that whatever waves you may have superimposed on top of this layer, all components of velocity must vanish at the wall. But when you have a flexible wall you have to consider that you must satisfy the boundary condition on the wall itself and not on the mean position and this gives an extra term due to the finer slope of the profile which accounts for this extra term. This problem is really quite intriguing in a way; when you straighten things like this out it turns out that this problem mathematically is very

simple and, as a matter of fact, is simpler than the classical problem. The reason for this I will point out in a minute, I will first mention that other investigations in this area have been published and are on the way to being published. There is a forthcoming paper in the Journal of Fluid Mechanics by Dr. Bannerman of Cambridge and I think that his paper is by far the most comprehensive and has very interesting physical discussion on it. I said that the mathematical problem is really quite simple, however, the difficulties are in the physical interpretation of the results which are, I must say, extremely difficult. First of all, the reason why the mathematical problem is so simple is that you can state this problem as a direct problem instead of as an indirect problem. In this particular case you can, instead of asking, what is the stability for a particular layer, ask what kind of wall admittance should one choose to maintain neutrally stable oscillations for waves of a particular wavelength and wave number. This is quite straightforward and as a matter of fact if you straighten out all these initial difficulties the results come out to be extremely simple. The results show that in order to take care of the instability completely you have to supply energy into the boundary layer and consequently a passive wall layer will never do the trick. However, it turns out that a pure compliance of the surface, a pure spring compliance, that is, a very flexible wall, will push the minimum Reynolds number up quite a bit. You can push it up, as Dr. Boggs pointed out, as far as possible, but there is one particular thing here I must say I don't quite understand completely yet. It looks as if you say to the boundary layer, I take 5 percent of the energy out of you, and then the boundary layer says, all right, I give you 10 percent. The more energy you take out of it the more energy the boundary layer supplies, and this is a very peculiar thing, which I think has to be understood more completely before you can really design these layers with good knowledge.

F. S. Burt (Admiralty Research Laboratory)

At ARL we also discussed this problem of the use of damping in the skin to stabilize the laminar boundary layer and came to a similar conclusion, that in the normal instability case one might have to put energy into the layer rather than take it out. The only other thing I would like to ask Mr. Boggs is if he can give us some figures for the critical Reynolds number, both maximum and minimum that he was referring to in his figure, preferably in terms of length to the transition point, which is the more normal Reynolds number used for transition.

F. W. Boggs

To the question of the energy, I would like to point out one thing. We have found, as a practical matter, that when the mechanical loss in the rubber that we use in the coating becomes large, the coating becomes substantially ineffective, maybe even detrimental. As to how energy might be transferred I wonder whether it wouldn't be through the propagation; our feeling is, and my impression is also, from an examination of our data that it is only when you have propagation that you will have stabilization. If you have propagation of the Schlichting wave which differs from the propagation of the wave in the coating (let's suppose, just to make things simple, that there is a factor of 2), then if they are in phase at one spot, half a wavelength ahead they will be out of phase. So whereas in one case you would be transferring the energy into the boundary, a wavelength or half a wavelength away the energy transfer would be taking place in the other direction. I would think that this is the type of mechanism that might explain it. As to Mr. Lang's comments, we have discussed this and we have seen reports on porpoises that travel at very high speeds, but I don't know, every time you talk to somebody he gives you something higher. The Scientific American, where we all get our information now in the United States, had an article on this subject and

they quoted reliably something of the order of 25 knots, if I recall correctly. Two horse-power is about what the biologists will tell us the porpoise should deliver. I am quite interested that this is the figure that is gotten because this is just about right on the basis of the body weight and the amount of muscle and what we know about the muscle efficiency. The only question is, does the porpoise go 25 knots? The 2-horsepower figure cannot explain the 25 knots, even though it can explain the 15, so I think this is the question, are the speeds of the porpoises that we have just heard proverbial fish stories or are they the truth? I think that Mr. Burt's question perhaps I have answered already, except for the Reynolds number. We have rough calculations. The limits, I am sorry, I don't know in length; I haven't made the calculation, but they lie somewhere (and these calculations are uncorrected by Mr. Landahl's remarks so they are subject to some doubt) within the area of maybe between 10^7 and 10^9, about 45 miles an hour (excuse my nonnautical language) for the coatings which have given us the best results. This is fairly consistent with our experimental data. The calculations are rough and could easily be off by a factor of two and they might be off by a lot more, but we do not get 10^{20} or anything like that. These are modest figures.

*   *   *

THE FRENCH BATHYSCAPH PROGRAM

Pierre H. Willm
Ingénieur en chef du Génie Maritime, French Navy

INTRODUCTION

The purpose of the third symposium on naval hydrodynamics is to study the latest technical developments concerning the means of navigation available to all men. Therefore it seemed reasonable to include, among other topics, the survey of a very new achievement which enables man to reach the greatest depths actually known, namely, the bathyscaph. But it was perhaps less logical to ask France to deal with this subject, since the diving record is now held by the U.S. Navy with the bathyscaph TRIESTE, manned by CDR Don Walsh and Mr. Jacques Piccard, who reached 11,000 metres in January 1960. I wish to express my thanks to the organizers of this symposium who asked me to read this paper, thus emphasizing the part taken by France in the development of this system of underwater navigation.

In the short historical account with which I shall begin this paper, I intend to give more details about this French participation, and to sum up the different types of bathyscaphs actually known.

In the second part, I will recall the principles involved in this new kind of navigation as well as the operational sequence of bathyscaph diving.

In the third part, I will briefly describe the first French achievement, the FNRS-3, then, in the fourth part, the new type now under construction, the Bathyscaph 11,000.

I will conclude by mentioning a few scientific results obtained during the 80 dives made by the FNRS-3 since it was built.

I regret to have no exceptional announcement to disclose to this honorable assembly as regards hydrodynamics: the only new fact concerning propulsion is the essential part played by the weight and by the Archimedean principle of buoyancy in vertical movements of the craft. All movement in other directions is achieved by means of conventional propellers which are entirely satisfactory in every respect.

HISTORY

The first attempts at very deep diving were made by two Americans, Professors William Beebe and Otis Barton, who in 1934 succeeded in diving to 908 metres, a remarkable depth at that time. But the 1.45-metre diameter and 45-mm thick cast steel sphere in which they

were enclosed hung at the end of a steel cable. Far from being a safe device, this perma-
nent link with the surface was a source of real dangers; to say nothing of a possible
breaking of the cable, which would have resulted in the total loss of the sphere (which was
heavier than the upward pressure exerted on it), the motion of the surface ship, in a heavy
swell, was amplified by the cable, so that the Bathysphere (as its designers called it) was
very uncomfortable, and it was quite impossible to approach the bottom.

The inventor of the first self-contained deep-diving craft was Professor Auguste Piccard,
a Swiss scientist. He applied to underwater navigation the operating principles of the free
balloon. The observation sphere, which was much heavier than the volume of water which it
displaced, was attached under a thin sheet-metal tank, filled with petrol lighter than sea
water. This petrol was directly exposed to external pressure. Vertical movement was
effected by jettisoning ballast: steel shot for rising and petrol for sinking. Professor
Piccard, of the University of Brussels, submitted his design to the Belgian "Fonds National
de la Recherche Scientifique" (FNRS) which eventually granted the necessary funds (1939).
The construction, delayed by war, was resumed in 1945 under the joint direction of Profes-
sors Piccard and Cosyns.

The craft had been called FNRS-2 (FNRS-1 had been Piccard's and Cosyns stratopheric
balloon) and it was shipped in September 1948 to Dakar, where the first trials took place
with the assistance of the French Navy. Unfortunately, many defects in this first construc-
tion were revealed during these trials. However, the FNRS-2 succeeded in reaching a depth
of 1380 metres without passengers, but all hope of performing this feat a second time had to
be given up.

However, this semifailure had established the soundness of the general principles, and
it was decided to undertake the construction of a new craft on the same lines. The job was
entrusted to the French Navy by the Belgian "Recherche Scientifique." An agreement was
signed in October 1950 between the Belgian FNRS, the French CNRS, and the French Navy
concerning the design and construction of the new craft. Ingénieur Principal du Génie
Maritime Gempp , who was in charge of this work, retained only the sphere of the first bathy-
scaph and succeeded in building a vehicle capable of being towed in a moderate sea and
accessible to a crew when afloat, which was not the case with the FNRS-2, where the pas-
sengers had to shut themselves in the sphere before the bathyscaph was lowered and the
float was filled with petrol, so that the prediving operations were so complicated as to be
unacceptable.

Professor Auguste Piccard remained technical adviser to the French Navy for this work.
He paid several visits to Toulon to join in discussions of the project. But in the beginning
of 1952, he ceased to collaborate, in order to have another bathyscaph built in Italy, the
TRIESTE. This Italian bathyscaph was constructed at Castellamare di Stabia, near Naples,
and in August 1953, it dived to 3000 metres, manned by the famous Professor and his son,
Jacques.

Meanwhile, the FNRS-3, as the French bathyscaph was called in tribute to the Belgian
scientists who financed part of its construction, was planned and laid down in July 1952 by
Toulon Naval Dockyard. It was launched on June 3, 1953 and made its first dives to 2000
metres off Toulon in August 1953. It was then taken to Dakar (French West Africa) and
successfully achieved its first two dives to the maximum depth for which it had been
designed, reaching 4200 metres on January 31, 1954, without passengers, and 4050
metres on February 15,1954 with passengers. I took part in this record dive as the engineer
responsible for the construction, together with Capitaine de Corvette Houot, appointed com-
manding officer of the bathyscaph.

During this last dive, the bathyscaph descended to the greatest depth ever reached by man until the beginning of 1960, when the deepest sea floors known to this day (about 11,000 metres off the Philippines) were reached by the TRIESTE bought by the United States of America.

The U.S. Navy had acquired the TRIESTE with a view to using this powerful underwater research tool for oceanographic purposes. After the apparatus had undergone important changes: lengthening of the float, replacing the original sphere by a new one, forged by Krupp steelworks, in Germany, and enlarging the shot silos, it was an American bathyscaph which landed for the first time on the bottom of the Pacific Ocean, at the depth of 11,000 metres.

So, there are now two bathyscaphs in operation: one, the FNRS-3, is French, and the other, the TRIESTE, is American. Their research programs are quite similar: physical and biological oceanography, study of the propagation of supersonics and of electromagnetic radiations in sea water, and the geology of ocean bottoms. A second French bathyscaph is under construction in the Toulon Naval Dockyard; I shall mention it briefly at the end of this paper.

As to the existence of other deep-water oceanographic vessels, we can only guess, as these would be Russian. The USSR has stated several times that it was building bathyscaphs, but we have no information on this subject.

PRINCIPLES

To descend to great depths beneath the sea, man must enclose himself in a pressure hull that is watertight and capable of withstanding the pressure exerted upon it. To withstand a uniform external pressure, the best shape is a sphere; that is why the hulls of bathyscaphs have, up to now, taken the form of a sphere. Allowing for the safety factor selected and for the inside diameter necessary to meet the accommodation requirements, this sphere must have a certain thickness, which is determined by the strength calculation of materials. Owing to this thickness, the sphere is much heavier than the volume of water which it displaces. It would immediately sink to the bottom if it were not suspended underneath a float filled with extra-light petrol, which gives it the necessary buoyancy.

This is the main difference between a submarine and the bathyscaph: in the case of a submarine, the weight of the pressure hull plus the weight of all the hull fittings and inside equipment must be equal to the displacement. We shall apply the term bathyscaph to the machine for which the weight of the pressure hull, including that of internal and external fittings, is greater than its displacement. Therefore, the float is necessary to ensure the trim.

Vertical movement is effected by increasing or decreasing the machine's weight. The increase in weight is produced by jettisoning petrol (which is replaced by sea water); the dischargeable petrol is contained in a special tank, which is isolated from the float itself whose buoyancy must not be impaired; this attitude is absolutely necessary to the lift of the craft. The decrease of weight is produced by shedding ballast; this consists of small steel shot contained in vertical silos in the center of the float. This shot is held in at the base of the silos by the electromagnetic field of an electromagnet called an electrochute, which lets the shot fall when the current is cut. In addition, there is a safety device, called an electrorapid-release, which enables the opening of the silo to be freed completely

if the electrochute is blocked. In any case, the ballast is automatically released in the event of a power failure.

External pressure acts freely on the petrol through a stabilizing hole, in the bottom of the float. Unfortunately, this petrol has an important drawback: it is very compressible. When the bathyscaph sinks, the petrol is compressed and sea water enters the float.

The resulting increase in weight is markedly greater than the apparent decrease in weight due only to the increasing density of sea water. Therefore, once the bathyscaph has started to sink, it descends quicker and quicker. It is necessary to discharge shot during the descent, in order to slow down this movement and to avoid sinking into the soft muddy bottom from which it would perhaps be difficult to break loose. On the other hand, once the bathyscaph starts going up, its speed increases progressively and it is impossible to stop it. The maximum speed under such conditions is approximately 1 metre per second.

Sphere and float are joined by a metal frame. The float is surmounted by a narrow deck running from stem to stern, with a conning tower in the center, in order to protect from heavy seas, during the towing of the bathyscaph to the diving site, the various external fittings that have to be placed there and the upper hatch of the entry shaft to the sphere. This entry shaft runs vertically through the float and enables passengers to enter or leave the sphere while the bathyscaph is afloat. It also acts as the submersible's water-ballast; that is to say, being normally empty on the surface, it fills with water during diving. The increase in weight when it is flooded with water is enough to make the machine submerge.

Added to this, there are also devices enabling one to tow the bathyscaph on the surface, to fill the entry shaft (by a flooding valve in the bottom) and to empty it (by means of compressed air), to land on the bottom with the aid of a guide chain, and to drive it horizontally while under water. There is exterior lighting, for detection of the sea floor and of obstacles ahead, and means of communication with the outside world while under water or on the surface, various measuring instruments, and so on. I shall give a fuller description of these accessories in the next section concerning the FNRS-3.

THE BATHYSCAPH FNRS-3

The sphere of the FNRS-3 is made of cast steel containing nickel, chromium, and molybdenum, with a yield point of 95 kg/mm^2 after heat treatment. It was built by the Emile Henricot steel works, at Court St Etienne, in Belgium. Its inside diameter is 2 metres, and its thickness 9 centimetres, reinforced to 15 centimetres around the hatch and porthole. It is composed of two hemispheres separated by the equatorial plane normal to the porthole-hatch axis. The joint consists of the two metal faces bearing one upon the other. The hemispherical parts are held together, with an initial force of 24 tons, by 400 steel clamps gripping two flanges machined on both sides of the joint.

Water tightness at low depth is ensured by a synthetic rubber ring which is fitted on the sphere before setting up the clamps. The viewing portholes, made of Plexiglas, 150 millimetres thick, are shaped in a frustum of a cone, with two parallel planes and forming an angle of 90 degrees at the apex. The internal and external planes have a diameter of 100 and 400 millimetres, respectively. At great depths, the watertightness of the joint between porthole and sphere is ensured by the plasticity of the Plexiglas. The hatch is made up of a steel frustum of a cone with two parallel planes and an angle of 45 degrees at the apex. At the center, it has a porthole which is similar to the viewing port. This hatch, weighing about 140 kilograms, is hinged about an axis and balanced in all positions, like a

submarine hatch, so that it is comparatively easy to handle. Around the porthole ten transit holes have been made in the sphere to link the inside with the outside, as follows: electric cables (Pyrotenax cables with copper sheathing and insulated with pressure injected magnesia) and pipes for hydraulic fluid and compressed air.

The float which contains the lifting petrol is made of steel plating 4 to 6 millimetres thick. It is divided into a certain number of tanks which only communicate at the bottom (to limit the loss of petrol in case of damage). The shot silos and the entry shaft to the sphere run vertically through the float. This float has a length of 16 metres and a width of 3.35 metres. The center part is cylindrical and the ends are in the shape of a truncated cone; two stabilizing keels are fitted on each side of the float to improve the dynamic stability during vertical movements and in particular in the course of an overrapid ascent. Trials on models, undertaken at the trial tank of the Service Technique des Constructions et Armes Navales had revealed the existence of oscillations in the course of ascents in a state of slightly excessive positive buoyancy (all ballast jettisoned), which might have been dangerous to the equipment and uncomfortable for the crew.

To conclude this description of the FNRS-3, it is necessary to mention the outside storage batteries housed in two baths filled with oil and exposed to external pressure. These batteries are used to run the propelling motors and the searchlights and supply about 1000 ampere-hours at 28 volts. The two motors are one-horsepower each. They drive two horizontal shaft propellers which enable the bathyscaph to be steered and moved horizontally over an approximate range of 50 metres. There are six searchlights of 1000-watt each. The incandescent bulbs which equip them are enclosed in steel cylinders which are designed to withstand external pressure.

All the remote controls of this external equipment are housed inside the sphere. Contact is maintained with the surface by an ultrasonic transmitting-receiving set, during the diving (radio transmission only works while the bathyscaph is on the surface). An echo sounder gives the distance from the bottom, a log the vertical speed, and a compass indicates the bearing of the craft during the descent. Moreover, an air-regeneration plant enables two men to live for 48 hours in this confined space; the carbon dioxide is absorbed by soda lime; the oxygen consumed is replaced by a fresh supply contained in cylinders of compressed oxygen.

THE BATHYSCAPH 11,000

The Bathyscaph 11,000 is the name we have temporarily given to the new French craft under construction, to indicate the maximum depth for which it has been designed, that is to say, eleven-thousand metres.

The sphere of the Bathyscaph 11,000 is made of forged steel, alloyed with nickel, chrome, and molybdenum, with a yield point of 105 kg/mm^2 after heat treatment. It was built by the Compagnie des Ateliers et Forges de la Loire in its works of St. Chamond and St. Etienne (France).

Its internal diameter is 2.10 metres (2 metres in the case of the FNRS-3) and its thickness is 15 centimetres (9 centimetres in the case of the FNRS-3).

The hatch, in the shape of a truncated cone, has an opening diameter of 45 centimetres and is located at the upper part, to facilitate the inner arrangement of the sphere. Three

viewing portholes are provided; one looks forward and the other two are side portholes disposed in vertical planes forming an angle of 50 degrees with the fore and aft symmetry planes of the bathyscaph. The axes of the three portholes point downward forming an angle of 20 degrees with the horizontal plane.

To avoid all change in thickness which would impair the aplexism of the sphere, no stiffening has been provided in the area of the hatch and portholes. Each of these is equipped with an optical system mounted in a 21-millimetre-diameter hole, which is plugged by Plexiglas shaped in a frustrum of a cone, forming an angle of 90 degrees at the apex, and only 45 millimetres thick.

The watertight lead-throughs into the sphere for cables and pipes have been designed similarly to those of the FNRS-3.

The float is approximately twice the size of the former. It has been designed to reduce to a minimum the power required for towing and to increase the towing speeds. That is why the sphere is no longer suspended below the float but it is now integrated to it, and the only area which is now visible is that of the three portholes. It will be 21 metres long and 5 metres high and its extreme width will be 4 metres.

As in the case of the FNRS-3, the new bathyscaph will have steel shot in silos running vertically through the float and held in by electromagnets placed at the base.

The outside batteries will be much more powerful than those of the FNRS-3. They will be located on the after-part of the float and will be accessible, when the bathyscaph is afloat, through an after-shaft similar to the forward one leading to the sphere. These batteries will supply the necessary power to a 30-horsepower propulsion motor driving a propeller with a horizontal shaft lying in the fore and aft symmetry plane of the bathyscaph. In addition, a steering propeller with an axis normal to the fore and aft symmetry plane and a lifting propeller with a vertical axis will each be driven by a 5-horsepower motor.

The 1000-watt pressure-resisting searchlights are still under design. All the measuring, navigational, and communicating equipment now existing on the FNRS-3 will of course be fitted on the new bathyscaph. The construction of this craft is financed by the French "Centre National de la Recherche Scientifique." It was begun in 1959 and will be completed during 1961. After trial dives to the maximum designed depths, the Bathyscaph 11,000 will, like its predecessor, be placed at the disposal of the Recherche Scientifique.

CONCLUSION

Although the main purpose of this Symposium is to investigate the characteristics of high-performance ships, I think it may be of interest to conclude this paper with the scientific results obtained during the first five years of the FNRS-3's operational activities.

During this period, the French bathyscaph made more than 80 dives, in the course of which it was possible for scientists interested in various scientific activities to undertake their respective researches. Thus, biologists have had the opportunity of studying the behaviour of abyssal fauna and the distribution of plankton versus depth and physical characteristics of sea water. Geologists and sedimentologists have been able to observe the various aspects of the sea bottom, to confirm or refute certain of their hypotheses concerning the formation of underwater canyons in particular. Physicists have installed on the bathyscaph precision recorders for measuring temperature, pressure, the pH value, the

speed of ultrasonics and their absorption, and so on. The physicist oceanographers also intend to measure the speed of deep underwater currents, the existence of which was not even suspected before the first dives.

I feel that now is the time to state that it is definitely out of the question to carry out oceanographic research from oceanographic surface ships. Man must penetrate into the medium he wants to investigate, since he now has the means of doing so. The oceanographic ship of the future will have to be submersible and in order to dive below one-thousand metres, which is the actual limit for conventional submarines, it will also have to be a bathyscaph. But, on the other hand, the study of the sea will only prove a poor investment if each country works on its own, without close cooperation with its neighbor. Oceanography is an international science calling for an international organization. The recent International Geophysical Year has already pooled the efforts of a great number of nations towards this specific purpose. This effort must be pursued in the future. I sincerely wish that the present and future bathyscaphs be designed and operated jointly by all the research workers who are interested in oceanography. As a matter of fact this symposium is striking proof that any real progress in the matter should spring from international cooperation. That is why I wish to thank once more the organizers of this symposium for inviting France to present her program concerning bathyscaph.

DISCUSSION

M. St. Denis (Institute for Defense Analysis, Washington)

Man will always try to excel himself and, having gone high, he will try to go higher, or, having gone deep, he will try to go deeper; but fortunately in this case there is a bottom to things. This idea of breaking records may be sufficient justification for building a bathyscaph, but if one tries to give a scientific reason for going deep, one must ask himself what he is to gain thereby. When man goes deep, all he can do at great depths is to look and to collect, and it would seem to me that he can see and collect with a lot less complication than a bathyscaph by using instruments remotely controlled from the surface. But be that as it may, and accepting the author's viewpoint that it is advantageous to have a bathyscaph to go deep to do certain things, it becomes evident that a manned vehicle is going to grow in size because one will want to carry more and more instruments or more and more people. And with a growth in size of the bathyscaph there follows a growth in size of the float and eventually the vehicle is going to become bigger and bigger and costlier and costlier. So one must ask oneself if this trend in size and in cost cannot be reversed or at least retarded. It seems that this can, to a large extent, be done, and it can be done by the proper choice of materials. Steel, even high-tensile steel, has not the same strength-to-weight ratio of, say, aluminum which is slightly superior to it; and titanium is superior to aluminum in this respect and fiberglass is superior to both. I have just a simple question and that is this: In constructing the bathyscaph, was any thought given to the use of these alternate materials, and if so, why were they discarded?

*   *   *

A METHOD FOR A MORE PRECISE COMPUTATION OF HEAVING AND PITCHING MOTIONS BOTH IN SMOOTH WATER AND IN WAVES

O. Grim
Hamburg Model Basin (HSVA)

BACKGROUND

In the Symposium "On the Behaviour of Ships in a Seaway," in Wageningen, 1957, a paper "Durch Wellen an einem Schiffskörper erregte Kräfte" was read by the author, which will now be continued. In part II of that paper ideas were deduced which may be considered an improvement of the well-known strip method. At that time some simple numerical results were given on the basis of this improved strip method although the method was not entirely completed.

In the meantime, some progress has been made and, in addition, numerical work could be done to a much greater extent since an electronic computor is now available. This paper gives the results obtained starting from a complete summary of the method which is deemed useful since the representation given in 1957 is no longer considered satisfactory.

The methods which have been applied to the theoretical treatment of the problems of the ship waves may be crudely subdivided into two groups, viz., (a) methods of singularities and (b) strip methods. The methods mentioned under (a) have as a basis a representation of the ship body by periodical singularities [3,4,5]. They enable us in an elegant manner to consider certain important parameters within an expression for the velocity potential and then to examine the influence of these parameters. The weak point of these methods consists in the loose connection between the motion and the shape of the ship on the one hand and the distribution of the singularities on the other hand. As a consequence the condition on the surface of the body is hardly sufficiently satisfied. Therefore, these methods can only be expected to give qualitative information as to the influence of the main parameters and not quantitative results as to the influence of the shape of the ship.

The methods mentioned under (b), viz., strip methods [6], assume solutions to be known for corresponding problems on two-dimensional bodies of which the sections coincide with the sections of the ship body. The results for the three-dimensional body will then be obtained by adding those obtained from the two-dimensional bodies. It must be considered an advantage of these methods that one can start from relatively accurate results and that the influence of the shape of the sections can be allowed for. The well-known strip method, however, has several disadvantages, e.g., that the influence of the three-dimensional flow can scarcely be taken into account and that the influence of the speed of the ship cannot be established exactly.

In the method proposed by the author the advantages of the two methods shall be combined and their disadvantages shall, if possible, be avoided. A strip method will be applied for the distribution of the singularities; i.e., for each section of the ship the singularity will first be chosen to satisfy the condition on the surface of a two-dimensional body of the section in question. The distribution of singularities so obtained is not yet accurate, however, even if an accurate representation of the two-dimensional cases is taken as a basis, because the representation of the three-dimensional ship body requires a somewhat different distribution of singularities. An improved distribution will be obtained with the help of an integral equation.

The method will be described here for the speed $V = 0$ only. For $V \neq 0$ it is necessary to complete the formulae for the flow potential and, in addition, to allow for the speed in the boundary condition. These extensions have been worked out; since, however, numerical results are not yet available, this extension of the method will not be discussed here.

The following problems will be treated: the heaving motion, the pitching motion, and the forces generated in a vertical direction by waves. An ideal fluid free from friction will be assumed and, further, the problem will be linearized. It should be mentioned that the boundary condition at the body cannot be satisfied exactly. These approximations as well as additional simplications will be discussed in the course of the paper.

I. TWO-DIMENSIONAL PROBLEMS

Introduction

Since the treatment of the complete three-dimensional problem requires solutions of two-dimensional problems to be known, it is necessary to briefly discuss the latter. The method used is the same, in principle, as deduced by the author in 1953 [10] on the basis of which later published results were computed [12]. As now an electronic computor is available it was possible to carry out the computations both more precisely and for a sufficient large number of transverse section contours.

Computations have been made for three problems, viz.,

(a) for the periodical heaving motion of the body in smooth water,

(b) for the vertical force generated on the restrained body by a transverse surface wave, and

(c) for the hypothetical case of a two-dimensional body in a "longitudinal wave" which cannot be realized physically. For this case which is important relative to the method described under II results have been given by Abels [9].

Description of the Method

The system of coordinates is fixed in space. Its origin lies in the plane of the waterline when at rest and in the midst of the contour, the y-axis being horizontal, the z-axis being vertical. The computations have been carried out for transverse profiles which can be represented by the transformation formula of Lewis. On the basis of this formula the coordinates of the profile can be expressed by means of the parameters a and b and of the coordinate θ running from 0 to $-\pi$.
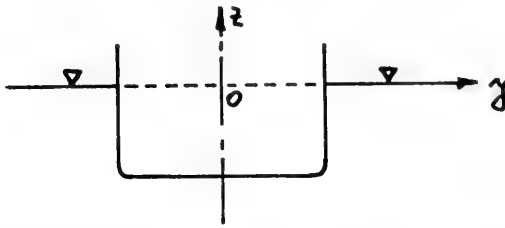
The formula for the boundary of the contour is expressed in nondimensional form as follows:

$$(y + iz) = e^{i\theta} + a e^{-i\theta} + b e^{-i3\theta}. \tag{1}$$

The following formulae for the potential and for the stream function caused by a heaving motion are applied:

$$\Phi = U \left[A_o \lim_{\mu \to 0} \int_0^\infty \frac{e^{Kz} \cos (Ky)}{K - \nu + i\mu} \, dK \right.$$

$$\left. + \sum_{n=1}^\infty A_n \int_0^\infty K^{2(n-1)} (K + \nu) \, e^{Kz} \cos (Ky) \, dK \right] \tag{2}$$

$$\psi = U \left[A_o \lim_{\mu \to 0} \int_0^\infty \frac{e^{Kz} \sin (Ky)}{K - \nu + i\mu} \, dK \right.$$

$$\left. + \sum_{n=1}^\infty A_n \int_0^\infty K^{2(n-1)} (K + \nu) \, e^{Kz} \sin (Ky) \, dK \right]$$

The time factor $e^{i\omega t}$ has been omitted. U describes the amplitude of the oscillatory velocity of the body. Both the condition of continuity and the condition on the free surface are satisfied. The problem is now to define the coefficients a such that the condition on the boundary of the contour is also satisfied. This requires a sufficient number of terms in the rows to be considered.

The condition on the boundary of the contour for the heaving motion is

$$\psi = Uy. \tag{3}$$

In case (b) — the restrained body in transverse waves — a surface wave with the orbital velocity 1 is assumed so that

$$\Phi_w = \frac{e^{\nu z}}{\nu} \cos (Ky)$$

$$\psi_w = \frac{e^{\nu z}}{\nu} \sin (\nu y). \tag{4}$$

The whole potential or the stream function, respectively, consists of the potential of the wave (4) and the potential (2) by which the deformation of the wave caused by the body is described. In Eq. (2) the factor U will then be omitted. For instance:

$$\psi = \frac{e^{\nu z}}{\nu} \sin (\nu y) + A_o \lim_{\mu \to 0} \int_0^\infty \frac{e^{Kz} \sin (Ky)}{K - \nu + i\mu} \, dK$$

$$+ \sum_{n=1}^\infty A_n \int_0^\infty K^{2(n-1)} (K + \nu) \, e^{Kz} \sin (Ky) \, dK. \tag{5}$$

Of course, the coefficients A have different values in this case as for the heaving motion.

In case (b) the condition at the boundary of the contour is

$$\psi = 0. \tag{6}$$

In the hypothetical case (c) the basis is a representation of a transverse section of the three-dimensional ship in a longitudinal wave. The potential of the nondeformed wave with the orbital velocity 1 is

$$\Phi_w = \frac{e^{\nu z}}{\nu} \cos (\nu x). \tag{7}$$

From this it follows that the velocity of the water particles in a vertical direction amounts to

$$e^{\nu z} \cos (\nu x) \tag{8}$$

and the hydrodynamic pressure to

$$-i\rho\omega \frac{e^{\nu z}}{\nu} \cos (\nu x). \tag{9}$$

The value of $\cos (\nu x)$ may be understood as the phase shift for the following and may be omitted in Eqs. (8) and (9).

The following question may be asked: Which two-dimensional potential $\Phi(y, z)$ describes such a velocity on the contour of the section of a two-dimensional body that the boundary

condition will be satisfied by this velocity together with Eq. (8)? This potential, for which Eq. (2) will be applied putting $U = 1$, can be defined as a transverse deformation of the longitudinal wave. At the boundary of the contour the following condition will be used:

$$d\psi = e^{\nu z} \, dy. \tag{10}$$

The boundary conditions (3), (6), and (10) cannot be satisfied exactly (except for $\omega = 0$ or $\omega = \infty$). It has been proved that the following procedure is well converging.

Into the boundary conditions (3), (6), or (10), Eqs. (2), (5), or (2), respectively, will be introduced. Within these equations the coordinates of the boundary of the contour can be replaced by Eq. (1). Then only <u>one</u> coordinate appears, viz., θ. The equations are written as follows:

$$B_o \left(\frac{\pi}{2} + \theta \right) + \sum_{n=1}^{\infty} B_n \sin (2n \, \theta) = 0, \quad \text{for} \quad -\pi \leq \theta \leq 0. \tag{11}$$

Of course, the coefficients A are linearly included in the coefficients B.

The boundary condition is satisfied if all coefficients B vanish in Eq. (11). In Eqs. (2) or (5) the series are cut off after N terms so that N unknown coefficients A are included. Then Eq. (11) is also cut off after N terms and N linearized equations are obtained:

$$B_o = 0; \qquad B_n = 0. \tag{12}$$

By Eq. (12) $2N$ equations are represented since the coefficients A or B, respectively, are complex numbers. Solving these equations the potential is found. The boundary condition is nearly satisfied. An error remains which changes sign on the contour several times and this more frequently the larger the N that is chosen.

Having computed the unknown coefficients A the problem is now to determine the hydrodynamic force. To obtain the force in a vertical direction the following integration around the contour is required:

$$\int \Phi \, dy . \tag{13}$$

In case (a) this integration yields only the hydrodynamic force. It is possible to add both the hydrostatic and the inertial force of the body and then to deal with the total force which is responsible for the heaving motion.

In case (b) only a hydrodynamic force exists. Therefore the integration yields immediately the force in a vertical direction which is caused from the wave on the restrained body.

In case (c) the force which follows from the pressure in the undisturbed wave is added to the force from (13). This is necessary since (13) yields only the force which arises from the deformation of the wave.

Representation of the Results: Figs. 1 to 24

More convenient than the parameters a and b of the transformation formula are the parameters H and β for the designation of the section contours:

$H = B/2T$ denotes the ratio of the half breadth of the profile in the waterline to the depth of the profile

β = (area of the section)$/BT$ denotes the fullness of the section profile.

Together with the transformation formula (1) the two parameters suffice to exactly define the sections.

The following results of the computations are represented in Figs. 1-24:

For the heaving motion: R, $A_o\pi/B$, C, and $\bar{A}$:

$R = R_r + iR_i$ represents the total force required to produce the heaving motion (real and imaginary part). R is made nondimensional by the amplitude of motion and by δB.
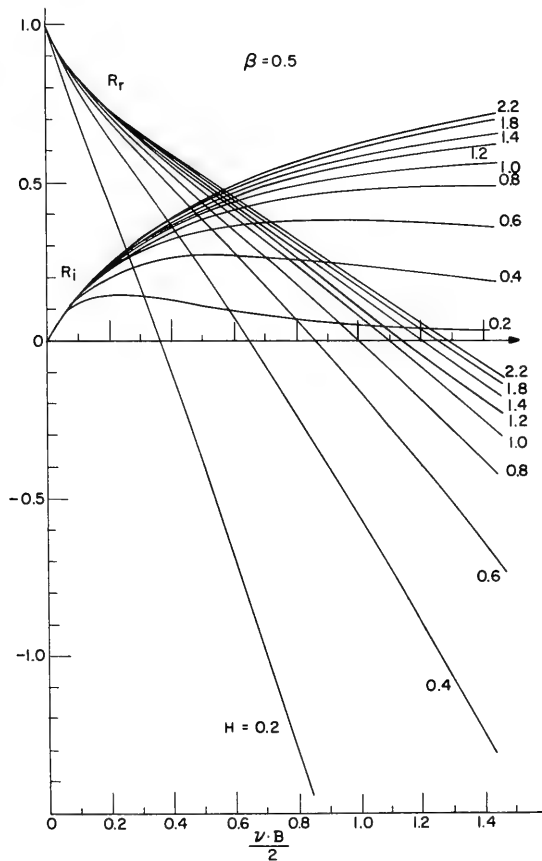
Fig. 1. Heaving motion; plot of force R for $\beta = 0.5$
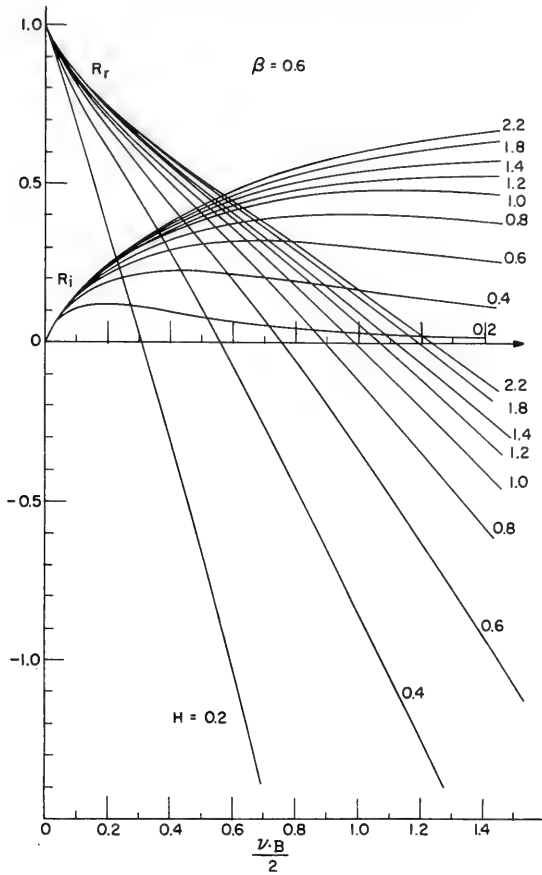
Fig. 2. Heaving motion; plot of force R for $\beta = 0.6$

Therefore, in the statical case, i.e., $\omega = 0$, R equals 1. For a periodical heaving motion, viz.,

$$z_o = \overline{Z}_o \, e^{i\omega t} \tag{14}$$

the force which is required to generate the heaving motion is

$$R \, \delta \, B \, \overline{Z}_o \, e^{i\omega t} . \tag{15}$$

This force is identical with

$$(m + m'') \, (\ddot{z}_o + N) \, \dot{z}_o + B z_o . \tag{16}$$

This form is known to be the one side of the equation of motion. It contains: the hydrodynamic force $m'' \ddot{z}_o + N \dot{z}_o$, the hydrostatic force $\delta B z_o$, and the inertial force $m \ddot{z}_o$.

$A_o \pi / B$ is the coefficient of the first term in (2) in nondimensional representation
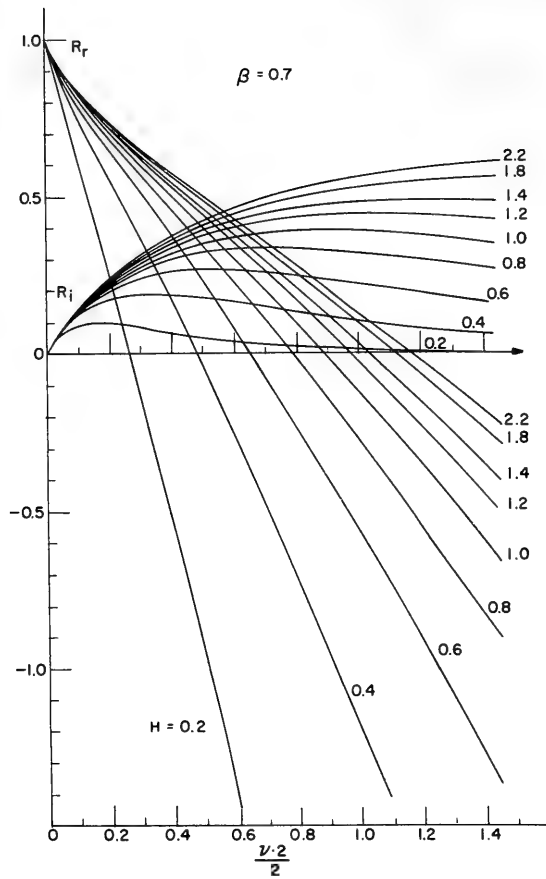
Fig. 3. Heaving motion; plot of force R for $\beta = 0.7$

C represents the hydrodynamic mass in nondimensional form, i.e.,

$$C = \frac{m''}{\rho \frac{\pi}{8} B^2} .$$
(17)

$\overline{A}$ represents the ratio of the amplitudes, i.e., the ratio of the amplitude of the surface waves drifting away from the body to the amplitude of the heaving motion. Between $\overline{A}$ and R_i the relation

$$R_i = \frac{g}{\omega^2 B} \overline{A^2}$$
(18)

holds because the work done by the force in unit time equals the energy dissipated by the waves.

For cases (b) and (c), viz, the restrained body in transverse or longitudinal waves, respectively, the following results are represented:
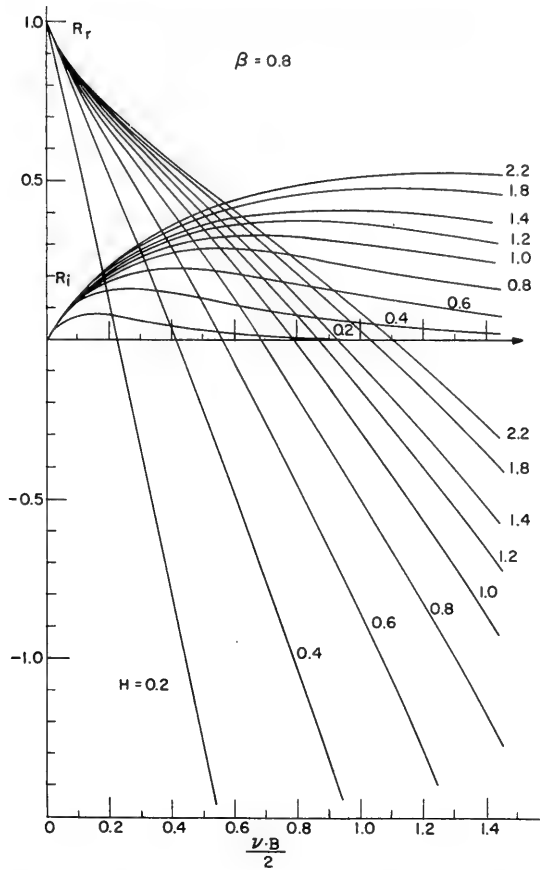
Fig. 4. Heaving motion; plot of force R for $\beta = 0.8$

$E = E_r + E_i$ which is the force in the vertical direction generated on the body by a sur-
face wave of amplitude 1. This force is made nondimensional by δB. In the case of a
very long wave ($\omega \to 0$) E necessarily equals 1. For this case the force can be looked
at as the hydrostatic buoyancy which corresponds to the additionally displaced volume.
This force has first of all a physical meaning only for the case (b).

For case (c) there is also plotted

$A_o \pi / B$ which is the coefficient of the first term in the formula for the potential in a non-
dimensional representation. (The diagrams for case (c) are not given here since they
are published in Ref. 9.)

All results are plotted against a frequency parameter which includes the beam B, viz.,

$$\frac{\nu B}{2} = \frac{\omega^2 B}{2g} .$$ (19)

In cases (b) and (c) this frequency parameter can also be expressed by the wavelength
λ:
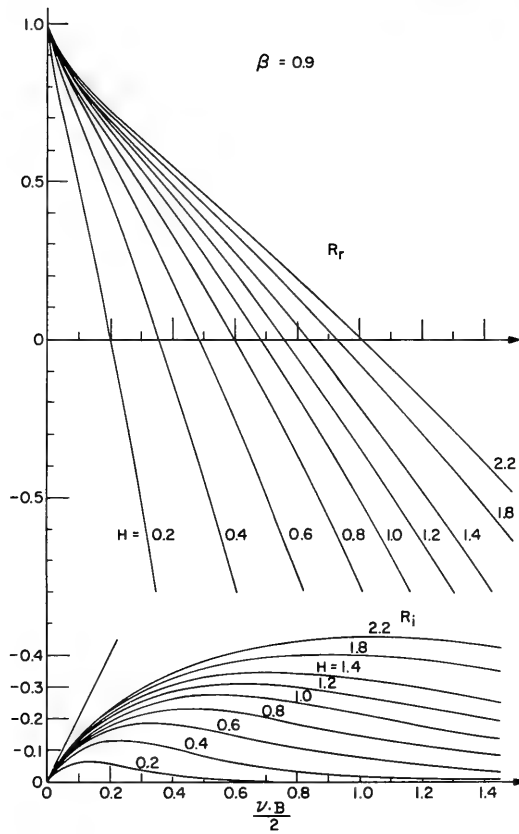
Fig. 5. Heaving motion; plot of force R for $\beta = 0.9$

$$\frac{\omega^2 B}{2g} = \pi \frac{B}{\lambda} . \tag{20}$$

With the help of these results the heaving motion of the free body generated by transverse surface waves may be determined. If the radius of the orbital circle of the surface wave is denoted $\bar{h}$ and the heaving motion produced by the surface wave z_o, the following equation must be satisfied:

$$z_o R = \bar{h} E . \tag{21}$$

From this the heaving motion of the free body can be computed both in magnitude and phase.

Convergence of the Method

To prove the convergence, first four terms in the series for the potential and then five terms were taken into account. The difference of the results is not significant. It, therefore, can be expected that both the convergence and the accuracy of the method are sufficient.
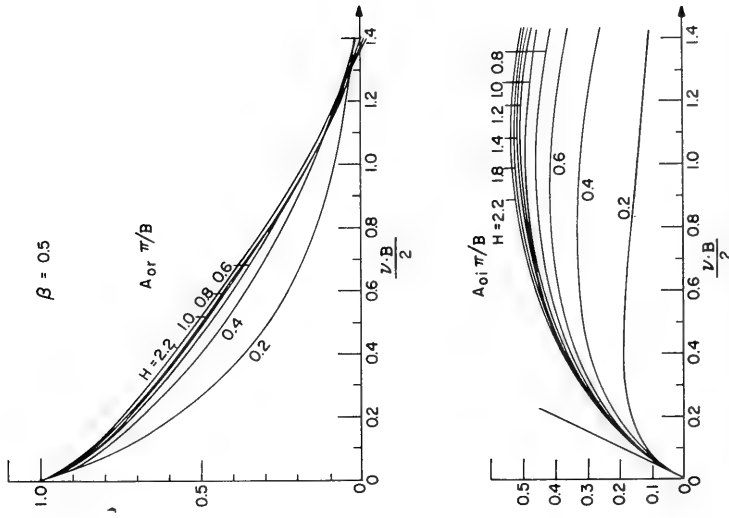
Fig. 7. Heaving motion; plot of singularity distribution $A_o \pi/B$ for $\beta = 0.5$

Fig. 6. Heaving motion; plot of force R for $\beta = 1.0$

Fig. 8. Heaving motion; plot of singularity
distribution $A_o\pi/B$ for $\beta = 0.6$
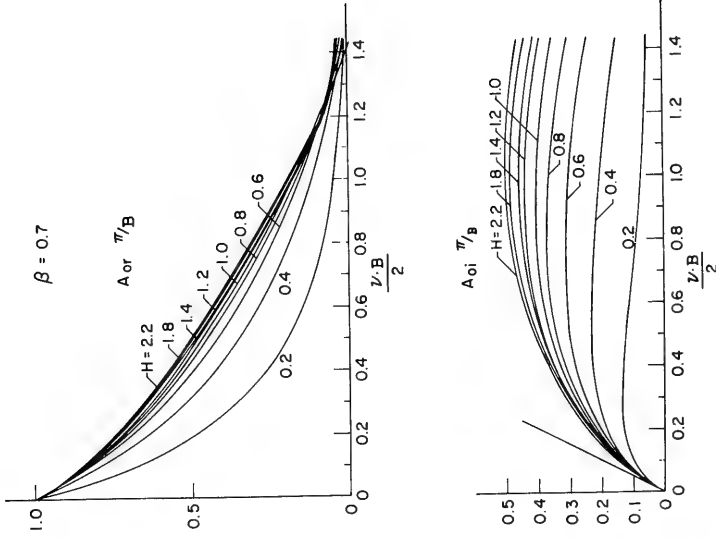
Fig. 9. Heaving motion; plot of singularity
distribution $A_o\pi/B$ for $\beta = 0.7$

Fig. 10. Heaving motion; plot of singularity
distribution $A_o\pi/B$ for $\beta = 0.8$
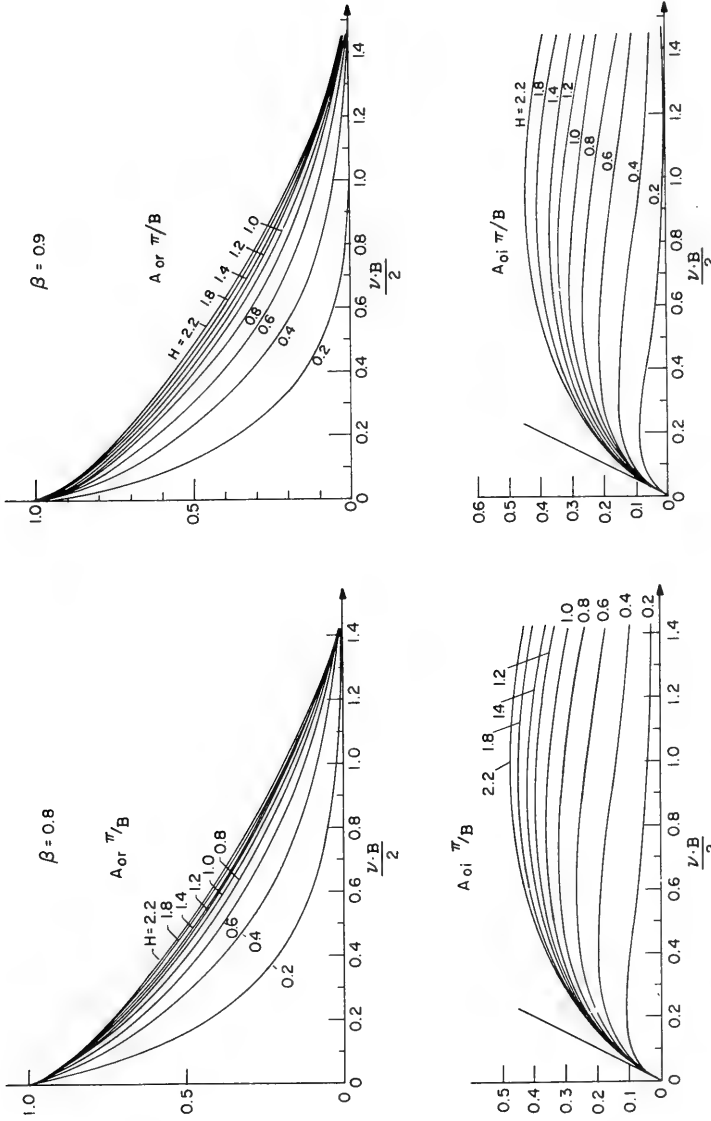
Fig. 11. Heaving motion; plot of singularity
distribution $A_o\pi/B$ for $\beta = 0.9$

Fig. 12. Heaving motion; plot of singularity
distribution $A_o \pi / B$ for $\beta = 1,0$

Fig. 13. Heaving motion; plots of C and of $\overline{A}$
for $\beta = 0.5$
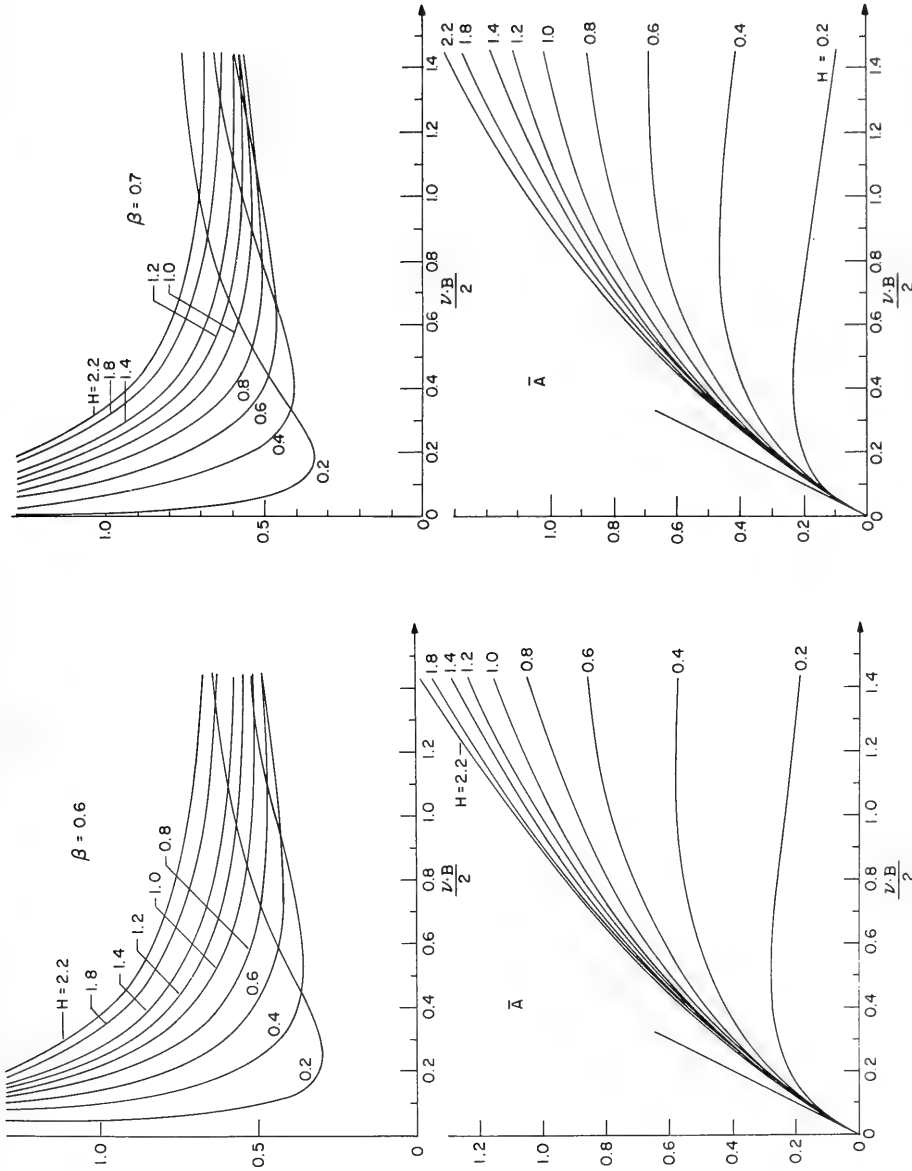
Fig. 14. Heaving motion; plots of C and of $\bar{A}$ for $\beta = 0.6$

Fig. 15. Heaving motion; plots of C and of $\bar{A}$ for $\beta = 0.7$

O. Grim
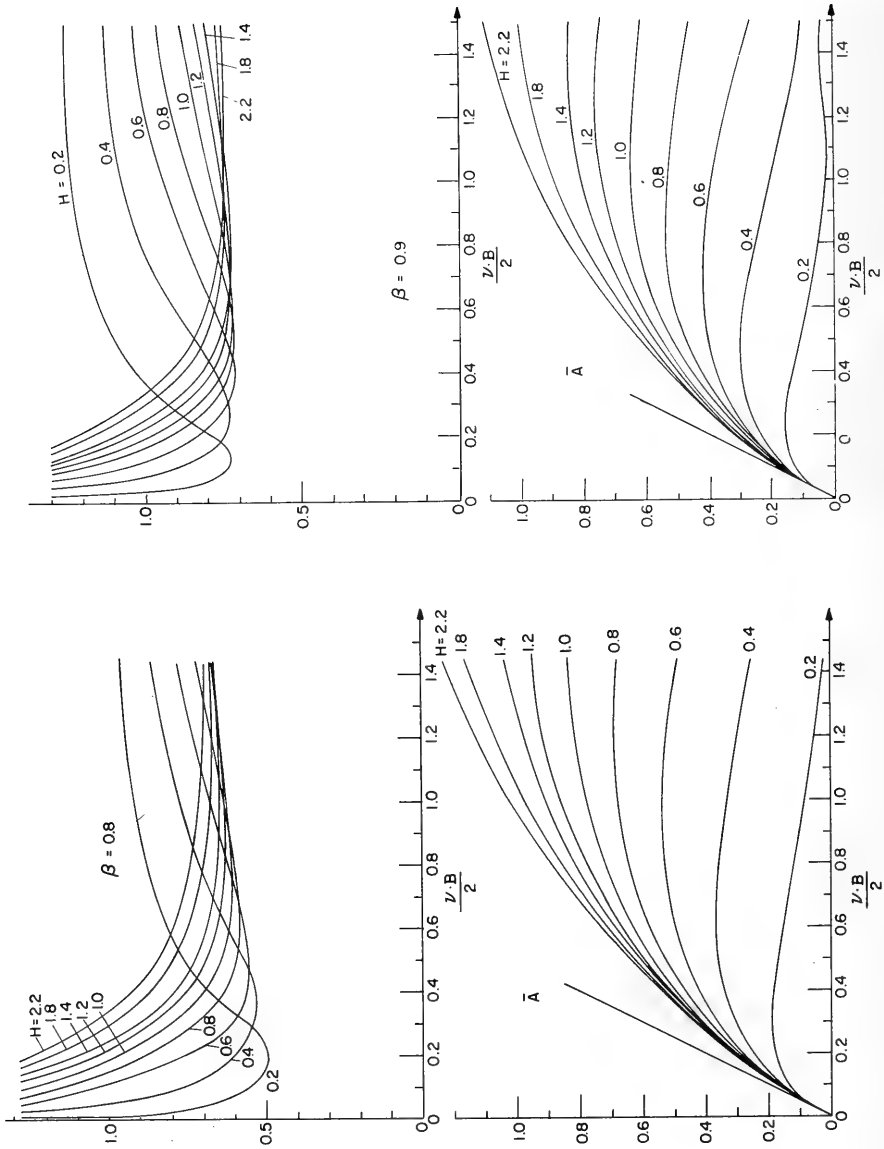
Fig. 17. Heaving motion; plots of C and of $\overline{A}$
for $\beta = 0.9$

Fig. 16. Heaving motion; plots of C and of $\overline{A}$
for $\beta = 0.8$

Fig. 19. Transverse wave; plot of force E
for $\beta = 0.5$

Fig. 18. Heaving motion; plots of C and of $\bar{A}$
for $\beta = 1.0$
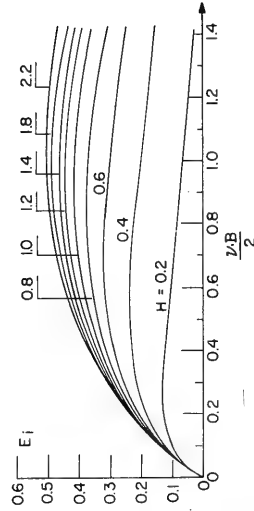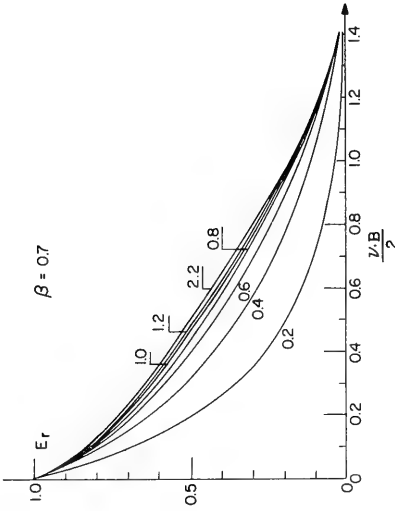
Fig. 21. Transverse wave; plot of force E
for $\beta = 0.7$
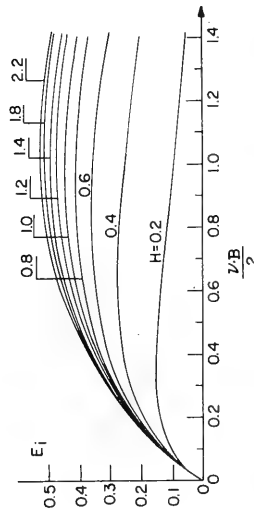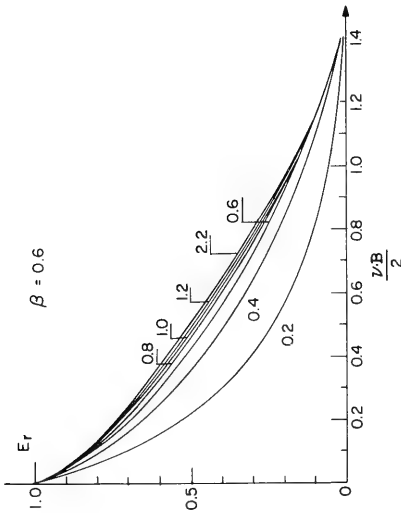
Fig. 20. Transverse wave; plot of force E.
for $\beta = 0.6$

Fig. 22. Transverse wave; plot of force E
for $\beta = 0.8$

Fig. 23. Transverse wave; plot of force E
for $\beta = 0.9$
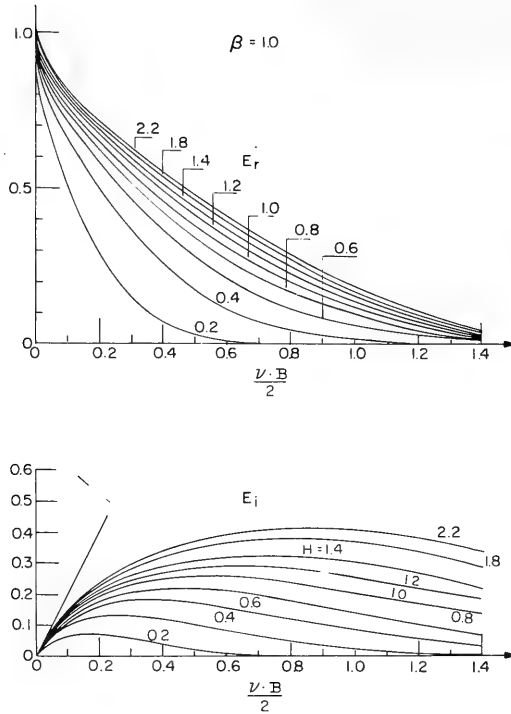
Fig. 24. Transverse wave; plot of force E
for $\beta = 1.0$

Summarizing Remarks to Part I

It is certain that sufficiently exact solutions are obtained in the way here described. Recently, a Japanese study by Tasai [7] has been published in which numerous numerical results are presented which agree closely with those given in this paper.

It should be mentioned that the method may be applied in the whole range of frequency from $\omega = 0$ to $\omega = \infty$. It appears necessary, however, that the sections are amenable to conformal mapping. In this respect difficulties may arise for sections of which the contour is not perpendicular to the waterline at their intersection.

The first term in Eq. (2) for the potential represents the potential of a periodical source in $y = 0$, $z = 0$. The coefficient A_o, therefore, represents a measure for the strength of the source. It is now extremely remarkable to learn from Figs. 7-12 that the coefficient A_o is complex and depends very strongly on both the shape of the section and the frequency. It is therefore a very crude and inaccurate approximation if only the shape of the waterline and the amplitude of the motion are considered for a method of singularities when choosing the singularities.

II. THREE-DIMENSIONAL PROBLEMS

Heaving and Pitching Motion in Smooth Water

The motion of the body is determined by the velocity $U_o(x)$ in a vertical direction. This velocity is constant and independent of x relative to the heaving motion. Relative to the pitching motion this velocity grows linearly when x increases. The time factor $e^{i\omega t}$ is omitted.

In Ref. 11 the formula

$$\Phi(x,y,z) \;=\; \frac{1}{2}\sum_{n=0}^{\infty}\int_{L} U_o(\xi)\;A_n(\xi)\;\varphi_n\Big[(x-\xi),y,z\Big]\;d\xi \qquad (22)$$

is chosen for the flow potential. The functions $\varphi_n[(x-\xi),y,z]$ within the integrals are denoted partial potentials and are expressed as follows:

$$\varphi_o\Big[(x-\xi),y,z\Big]$$

$$= \; \frac{2}{\pi}\int_{0}^{\infty}\cos\big[m(x-\xi)\big]\;dm\int_{0}^{\infty}\frac{e^{\sqrt{m^2+K^2}\,z}\;\cos\,(Ky)}{\sqrt{m^2+K^2}-\nu+i\mu}\;dK \qquad \text{for}\quad \mu\to 0$$

$$\varphi_n\Big[(x-\xi),y,z\Big]$$

(23)

$$= \; \frac{d^{2(n-1)}}{dz^{2(n-1)}}\left\{\frac{3z^2}{\big[(x-\xi)^2+y^2+z^2\big]^{5/2}}-\frac{1+\nu z}{\big[(x-\xi)^2+y^2+z^2\big]^{3/2}}\right\}.$$

This formula satisfies both the condition of continuity and the condition on the free water surface outside the ship body. When applied to the limit case of an infinitely long two-dimensional body this formula is identical with Eq. (2). The transition to the limit is performed as follows:

1. The distribution functions $A_n(x)$ become constants A_n which are placed before the integrals.

2. These coefficients A_n are chosen such that they are identical with those computed in part I.

3. The integrations are carried out from $-\infty$ to $+\infty$.

The formula furnishes a nearly exact solution in this limit case. Relative to a ship of finite length the distribution functions $A_n(x)$ are chosen identical at each section x with those distributions $A_n(x)$ which hold for the corresponding motion of the two-dimensional body. In Eq. (22) there are, therefore, no unknowns. It may also be expected that the

condition on the surface of the body is satisfied to a sufficient degree as long as the ship body is sufficiently slender, i.e., as long as L/B and L/T are great and the angle between the tangent on the waterlines and the plane of symmetry is small.

Relative to the methods of singularities an improvement is obtained because the relation between the singularities, the frequency and the contour parameters is satisfied to a higher degree.

To better recognize the improvement, Eq. (22) is transformed into the identical formula

$$\Phi(x,y,z) = \frac{1}{2} \sum_{n=0}^{\infty} U_o(x) \, A_n(x) \int_{-\infty}^{+\infty} \varphi_n \left[(x - \xi), y, z \right] \, d\xi$$

$$+ \int_{-\infty}^{+\infty} \left\{ \left[U_o(\xi) \, A_n(\xi) - U_o(x) \, A_n(x) \right] \, \varphi_n \left[(x - \xi), y, z \right] \, d\xi \right\} . \quad (24)$$

The first term represents the nearly two-dimensional flow around the section x because the integrals are independent of x. Only in consequence of the functions $A_n(x)$ a velocity component in x-direction arises. By this velocity component, however, the boundary condition is not considerably disturbed and it is nearly satisfied if the distribution functions are correspondingly chosen. Only the first term is taken into account for the common strip method. If the hydrodynamic pressure and the force in a vertical direction generated on a section are computed only from this term the same force as in part I is obtained. Applying the representation R used in part I one obtains

$$\frac{\delta}{\omega} \int_L U_o \, BR \, dx \qquad (25)$$

for the total force to generate the motion with velocity U_o or for the total moment

$$\frac{\delta}{\omega} \int_L x \, U_o \, BR \, dx . \qquad (26)$$

Here it is assumed for the computation of the moment that the weight of the body is distributed over the length in the same manner as the displacement. Of course, a different distribution of the weight can be taken into account.

The common strip method will be improved if the second term in Eq. (24) is also applied. This improvement is already included in Ref. 11. An additional improvement is discussed in the following considerations.

The second member in Eq. (24) may be explained physically as a flow generated at x by a distribution $[A_n(\xi) - A_n(x)]$ situated outside x. Since this distribution lies in $y = 0$, $z = 0$ and since the ship body is slender (i.e., the distribution does not change too rapidly with ξ, this additional flow at x will depend only a little on y inside the ship body, i.e., for

$|y| \leqq B/2$. Only a small error arises if in this second member of (24) $\varphi_n[(x-\xi),0,z]$ is written instead of $\varphi_n[(x-\xi),y,z]$. Since it is well-known that circular waves are generated by a periodical singularity of which the dependence on the coordinate z is described by the factor $e^{\nu z}$ (provided that the distance from the origin of the circular waves is not too small) it is suggested that the same dependence on the coordinate z holds for the second member of Eq. (24). For all singularities within this member have the same frequency and there are no singularities at x itself. It, therefore, may be permitted to further simplify the partial potentials in this second term, viz.:

$$\varphi_n\left[(x-\xi),y,z\right] \;\rightarrow\; e^{\nu z}\;\varphi_n\left[(x-\xi),0,0\right] \tag{27}$$

In this way the coordinates y and z are removed from the integrals. This term can then be described as a product of a function of x times the exponential function $e^{\nu z}$. This holds within the region of the ship body, i.e., for ordinates y which do not go far beyond $B/2$.

Since the condition on the surface of the body is well satisfied by the first member of Eq. (24) the second member causes a disturbance of this boundary condition. To reduce the error an additional velocity U as function of x will be introduced. U may be explained as the velocity of an additional deformation of the water surface (depending on x and z for $|y| \leqq B/2$) so that a certain section of the ship body has the velocity $(U_o + U)$ relative to the water surface. This deformation is called "additional" because a deformation (depending on y and z) takes place already in the two-dimensional case. The additional deformation diminishes when the depth increases following the function $e^{\nu z}$ because the influence of singularities with circular frequency ω lying far outside of x will be eliminated.

Therefore, the following formula instead of Eq. (22) will be chosen for the total potential:

$$\Phi(x,y,z) = \frac{1}{2} \sum_{n=0}^{\infty} \left\{ \int_L \left[U_o A_{na}(\xi) + U A_{nc}(\xi)\right]\; \varphi_n\left[(x-\xi),y,z\right]\; d\xi \right\}. \tag{28}$$

Two different distribution functions A_{na} and A_{nc} are introduced. The second indices of these functions denote the functions belonging to cases (a) and (c) treated in part I. Since the additional deformation U decreases when the depth increases, the distributions corresponding to the two-dimensional case (c) of the body "in longitudinal waves" will be chosen for this part since the motion of the water particles decreases with the same exponential function. This formula has been transformed in the same manner discussed previously into the identical formula:

$$\Phi(x,y,z) = \frac{1}{2} \sum_{n=0}^{\infty} \left\{ U_o(x)\, A_{na}(x) \int_{-\infty}^{+\infty} \varphi_n\left[(x-\xi),y,z\right]\; d\xi \right.$$

$$+ U(x)\, A_{nc}(x) \int_{-\infty}^{+\infty} \varphi_n\left[(x-\xi),y,z\right]\; d\xi + \int_{-\infty}^{+\infty} \left[U_o(\xi) A_{na}(\xi)\right.$$

$$\left. + U(\xi) A_{nc}(\xi) - U_o(x) A_{na}(x) - U(x) A_{nc}(x)\right] \varphi_n\,(x-\xi),y,z\; d\xi \right\}. \tag{29}$$

Again, as mentioned before, the common strip method results if only the first row is taken into account. The second row, again, represents essentially a plane flow around the sections.

To carry out the computations a further simplification, besides the one already mentioned, is applied for the third row. In this row only the member for $n = 0$ of the series over n members will be considered. The reason is that this member causes the greatest long-distance effect since the functions φ_n fade away at a greater distance from the origin of the disturbance more rapidly the greater n is. Besides, the potential of a periodical source is described by φ_o and only by this term circular waves, which transport energy, are described. Therefore, instead of the third row in Eq. (29),

$$\sim \frac{e^{\nu z}}{2} \int_{-\infty}^{+\infty} \left[U_o(\xi) \; A_{o\,a}(\xi) + U(\xi) \; A_{o\,c}(\xi) - U_o(x) \; A_{o\,a}(x) \right.$$

$$\left. - U(x) \; A_{o\,c}(x) \right] \; \varphi_n \left[(x - \xi), 0, 0 \right] \; d\xi \qquad (30)$$

is written and, the integral being a function of the coordinate x only, this row can be written

$$e^{\nu z} \; F(x) . \qquad (31)$$

The next problem is to determine U such that the condition on the surface of the body is satisfied to a sufficient extent. This means that the influence of the second member in (24) on the boundary condition is approximately eliminated.

A simplification is introduced relative to this boundary condition; viz., the velocity in longitudinal direction is neglected so that

$$\left[\frac{\partial \Phi}{\partial y} \; dz - \frac{\partial \Phi}{\partial z} \; dy \right]_S = U_o \; dy \qquad (32)$$

where S = the surface of the ship body.

The potential (29) is introduced into the left-hand side of this simplified boundary condition. This can be done without difficulty since solutions are known for the corresponding two-dimensional cases.

$$\left[- \frac{\partial \Phi}{\partial y} \; dz + \frac{\partial \Phi}{\partial z} \; dy \right]_S = U_o \, dy + U e^{\nu z} \; dy + \nu e^{\nu z} \; F(x) \; dy . \qquad (33)$$

The sum of these members equals $U_o \; dy$ from Eq. (32). The simplified boundary condition leads, therefore, to the following equation for the unknown function U:

$$U(x) + \nu F(x) = 0 . \qquad (34)$$

The application of the hypothetical two-dimensional case (c) is again confirmed by the appearance of the function $e^{\nu z}$ in the second and third row of Eq. (33).

In the equation for U, only the coordinate x appears. This equation is an integral equation.

Having determined U the task of determining the hydrodynamic forces remains.

Having satisfied Eq. (34), one may write for the potential instead of (29)

$$
\Phi = \frac{1}{2} U_o \sum_{n=0}^{\infty} A_{na}(x) \int_{-\infty}^{+\infty} \varphi_n \left[(x - \xi), y, z\right] d\xi
$$

$$
+ U - \frac{e^{\nu z}}{\nu} + \frac{1}{2} \sum_{n=0}^{\infty} A_{nc}(x) \int_{-\infty}^{+\infty} \varphi_n (x - \xi), y, z \ d\xi \quad . \tag{35}
$$

This expression does not satisfy the continuity condition any longer and is, therefore, not exact. However, the expression may be used for coordinates which correspond to the surface of the ship. For these coordinates this equation certainly represents a sufficient approximation. The computation of the hydrodynamic pressure and the integration of this pressure over the contour of the section in transverse direction to determine the force acting in a vertical direction has already been carried out in part I.

From the first member in Eq. (35) one obtains as in the common strip method:

$$
\delta \frac{\cdot B}{\omega} U_o R \ . \tag{36}
$$

From the second and third member in (35),

$$
\delta \frac{B}{\omega} U E_c \tag{37}
$$

for, the second member in (35) describes a "longitudinal wave" at x of orbital velocity U and the third member the additional two-dimensional potential computed for (c) in part I. E_c represents the nondimensional parameter of the force which is related to (c) of part I and which is generated by the "longitudinal wave."

The total force in a vertical direction on a section of a ship body amounts then to

$$
\delta \frac{B}{\omega} \left[U_o R + U E_c\right] \tag{38}
$$

The second member represents the correction to the common strip method. U, R, and E are complex functions.

The force and the moment for the whole ship body are obtained by corresponding integrations of Eq. (38) over x.

The Force Generated by Waves on the Ship Body

To compute the force it is assumed first that the ship body is restrained. The generating surface wave is supposed to run in longitudinal direction from fore to aft. The method can, however, also be applied for all running directions.

As compared to the Froude-Kryloff method an essential progress would be obtained if, instead of the quasi hydrostatic force computed from the nondeformed wave, the force E_c computed for case (c), viz., the ship in a "longitudinal wave" is introduced.

A different method is proposed in Ref. 11. Also this method could be improved.

The formula for the potential of the nondeformed surface wave of orbital velocity 1 is as follows, omitting the time factor $e^{i\omega t}$

$$\Phi_w = \frac{1}{\nu} e^{\nu(z+ix)}. \tag{39}$$

The following formula will be used for the total potential of the wave and deformation caused by the body:

$$\Phi(x,y,z) = \frac{e^{\nu(z+ix)}}{\nu} + \frac{1}{2} \sum_{n=0}^{\infty} \int_L e^{i\nu\xi} G(\xi) A_{nc}(\xi) \varphi_n\left[(x-\xi),y,z\right] d\xi. \tag{40}$$

This potential still exactly satisfies both the continuity equation and the condition on the free water surface. $G(x)$ represents a presently unknown complex function in a similar manner as $U(x)$.

Using the same simplifications as before, which are deemed permissible relative to points on the surface of the ship, Eq. (40) is simplified to

$$\Phi \sim e^{i\nu x}\left\{\frac{e^{\nu z}}{\nu} + \frac{1}{2} G(x) \sum_{n=0}^{\infty} A_{nc}(x) \int_{-\infty}^{+\infty} \varphi_n\left[(x-\xi),y,z\right] d\xi\right.$$

$$+ \frac{e^{\nu z}}{2} \int_{-\infty}^{+\infty} \left[e^{i\nu(\xi-x)} G(\xi) A_{oc}(\xi)\right.$$

$$\left.\left. - G(x) A_{oc}(x)\right] \varphi_o\left[(x-\xi),0,0\right] d\xi\right\}. \tag{41}$$

The last member in this equation can be written as follows:

$$e^{i\nu x} e^{\nu z} H(x) \tag{42}$$

since the integral in this row is a function of x only.

The following simplified condition on the surface of the ship body S will be used:

$$\left[-\frac{\partial \Phi}{\partial y}\, dz + \frac{\partial \Phi}{\partial z}\, dy \right]_S = 0. \tag{43}$$

The right-hand side of this boundary condition is zero since the body is assumed to be re-strained and since the whole potential will be introduced. The required computations have already been carried out or can easily be carried out. The boundary condition furnishes the relation

$$e^{\nu z}\, dy + G(x)\, e^{\nu z}\, dy + \nu H(x)\, e^{\nu z}\, dy = 0 \tag{44}$$

or the definition equation for the unknown function $G(x)$, viz.,

$$1 + G(x) + \nu H(x) = 0. \tag{45}$$

This is an integral equation for the unknown function $G(x)$.

After having determined this function G the next problem is to determine the exciting force.

Into the formula for the potential $H(x)$ will now be introduced

$$\Phi \sim e^{i\nu x}\, G(x) \left\{ -\frac{e^{\nu z}}{\nu} + \frac{1}{2} \sum_{n=0}^{\infty} A_{nc}(x) \int_{-\infty}^{+\infty} \varphi_n \left[(x - \xi), y, z \right]\, d\xi \right\}. \tag{46}$$

Although this formula does not yield an exact value for the potential, it gives a very close approximation for coordinates of points at the surface of the ship.

The hydrodynamic force per unit length in vertical direction has, for this expression, already been determined in part I under (c). This force amounts to

$$\delta \frac{B}{\omega}\, Ge^{i\nu x}\, E_c. \tag{47}$$

The result Eq. (46) may be conceived a two-fold deformation of the longitudinal wave caused by the ship body. The first member, viz.,

$$-\frac{G}{\nu}\, e^{\nu(z+ix)} \tag{48}$$

may be considered the potential of a longitudinal wave with variable effective wave ampli-tude of which the reduction factor relative to the oncoming wave amounts to $-G(x)$. This

member represents, therefore, a deformed wave which, in the region of the ship body, is independent of the coordinate y. The second member in (46), however, mainly represents a deformation of the wave which depends on the coordinate y. It may be convenient, although not quite exact, to denote $G(x)$ an effective wave amplitude.

Free Moving Ship Body in Longitudinal Waves

All hydrodynamic problems relative to the free moving ship body are already solved in the foregoing considerations since a linearized treatment is assumed.

Some hints will now be given how the motions are determined. All forces or moments, respectively, may be found by an integration of the forces per unit length over the length of the ship body. The exciting forces are found by an integration of Eq. (47), the restoring forces by an integration of Eq. (38). The results for the nondimensional heaving and pitching motions (made nondimensional by the wave amplitude or by the amplitude of the wave angle, respectively) are as follows:

$$z_o \int_L B(R + U_H E_c) \ dx + \psi \int_L xB(xR + U_P E_c) \ dx = \int_L BG \ e^{i\nu x} E_c \, dx \qquad (49)$$

and

$$z_o \int_L xB(R + U_H E_c) \ dx + \psi \int_L xB(xR + U_P E_c) \ dx = \int_L x \, BG \ e^{i\nu x} E_c \, dx. \qquad (50)$$

where E, G, R, and U are complex functions of x. The values of U are nondimensional values of the function $U(x)$ which follow from Eq. (34) for the case $U_{oH} = 1$ or $U_{oP} = x$, respectively. The indices H and P indicate that the equation for U is satisfied either for heaving or for pitching.

Using these values for the amplitudes of the motions two interesting functions* can be determined, viz., the resulting wave deformed in a longitudinal direction:

$$Ge^{i\nu x} - z_o U_H - \psi U_P \qquad (51)$$

referred to a space fixed zero-line or

$$Ge^{i\nu x} - z_o U_H - \psi U_P - z_o - \psi x \qquad (52)$$

referred to a zero-line moving with the ship.

The function (51) appears for the case of the free moving ship body instead of the function $Ge^{i\nu x}$ for the case of the restrained body. Taking the amplitude of the function (52) this function may be conceived as envelope of the wetted ship surface.

*Of physical significance.

Resistance

Since the deformation of the longitudinal wave has been determined one could try to compute the mean force generated by the wave in direction of the negative x-axis, i.e., the resistance W. However, it is necessary to simplify the distribution of the pressure for this purpose.

$$(52) = G e^{i\nu x} - z_o U_H - \gamma U_P - z_o - \gamma x$$

$$(51) = G e^{i\nu x} - z_o U_H - \gamma U_P$$
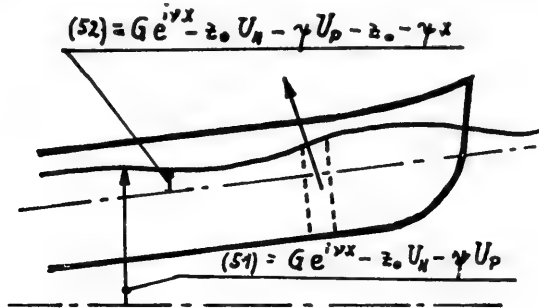
For the free moving ship body (see sketch) the contour of the surface of the wave is given by (51) relative to a line fixed in space and by (52) relative to a zero-line moving with the ship. An element of the ship body of length dx, bounded by two sections, displaces the volume:

$$V = \left[BT\beta + B(Ge^{i\nu x} - z_o U_H - \psi U_P - z_o - \psi x) \right] dx. \tag{53}$$

The simplifications now are introduced, when computing the resistance, that the magnitude of the buoyancy force equals δV and that its direction is perpendicular to the contour of the surface of the wave. These assumptions lead to the following formula for the force in the direction of the negative x-axis:

$$P = \delta \int_L \left[BT\beta + B(Ge^{i\nu x} - z_o U_H - \psi U_P - z_o - \psi x) \right] d(Ge^{i\nu x} - z_o U_H - \psi U_P). \tag{54}$$

Only the time mean value of this force is of interest, viz.,

$$W = \frac{\omega}{2\pi} \int_{\omega t = 0}^{\omega t = 2\pi} P \, dt. \tag{55}$$

The first member in (54), viz., βBT does not contribute to this mean value. The remainder may be written as the following sum:

$$W = W_1 + W_2$$

$$W_1 = \left[\delta \int_L B(Ge^{i\nu x} - z_o U_H - \psi U_P) \, d \; Ge^{i\nu x} - z_o U_H - \psi U_P) \right]_M$$

$$W_2 = \left[\delta \int_L B(- z_o - \psi x) \, d(Ge^{i\nu x} - z_o U_H - \psi U_P) \right]_M$$

$$\left. \right\} \tag{56}$$

The index M indicates that in both cases the mean value over the time is to be taken.

The first part can be looked at as caused by the reflexion of the wave on the ship body and the second part by the phase shift between the motions of the ship and the wave. This representation of the resistance is known [1,8] and it now appears possible to compute both parts of the resistance.

Example

The results for an example which have been computed from the method discussed before will now be given in detail. The ship body chosen is as follows:

$L/B = 6.4$; $B/T = 2.8$; T = constant for all sections; $\mathbb{B} = 0.9$, constant for all sections;

$$\frac{B_{section}}{B_{max}} \text{ (for 10 sections)} = 0.33, 0.70, 0.90, 0.99, 1.0, 1.0, 0.99, 0.90, 0.70, 0.33.$$

This ship body is symmetrical about $x = 0$. The 10 given sections lie in the midst of 10 equally long intervals.

Each integral equation (34) or (45), respectively, has been transformed into a system of linear equations and has then been solved. The 10 given sections were chosen as supporting points for this system of equations. Each system of equations contains, therefore, the 10 complex values U_H or U_P or G, respectively, of these sections as unknowns and, therefore, three times a system of 20 equations for 20 real unknowns had to be solved.

Figures 25-31 show the results in a nondimensional representation.

Figure 25 shows the deformation of the smooth water surface caused by the heaving and pitching motions. This deformation would not exist for an infinitely long body. The velocity of the deformation represented on the diagram is made nondimensional by the velocity U_o of the motion and the velocity of the bow is chosen for the pitching motion, i.e., U_o at $x = L/2$. Further λ/L is chosen a parameter. The ratio λ/L is defined by the relation

$$\frac{L\omega^2}{g} = 2\pi \frac{L}{\lambda}$$

since the wavelength λ has in this case no physical meaning.

Figure 26 gives the deformation at the point $x = 0$ which arises from the heaving motion, plotted against the frequency. This diagram is presented to show the course of U_H/U_o for $\omega \to 0$. From this course it follows that the virtual mass does not go to infinity for $\omega \to 0$, as it does with the common strip method. For the virtual mass, the virtual moment, the damping force, and the damping moment about the same values are obtained for $\omega \to 0$ as given in Ref. 11.

Figure 27 shows for the section $x = 0$ the coefficient C of the virtual mass and the hydrodynamic damping force both for the two-dimensional and for the three-dimensional case. The latter is computed on the basis of the former by means of the additional velocity.
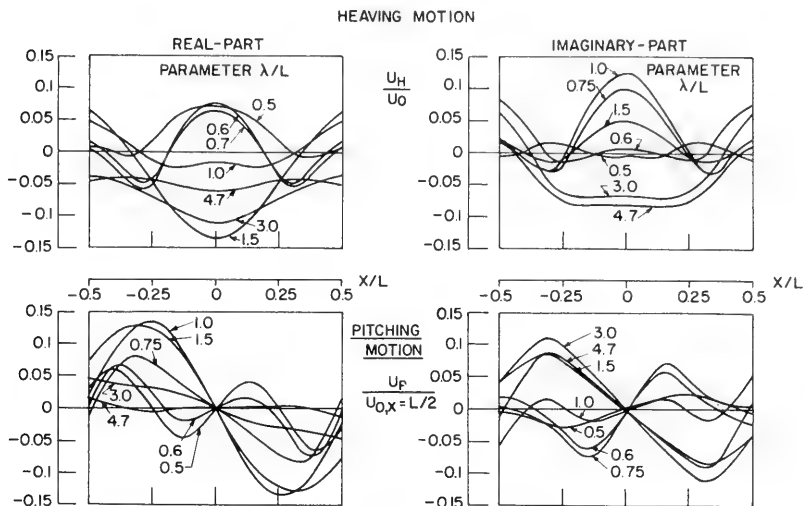
HEAVING MOTION

Fig. 25. Heaving motion and pitching motion

$$\left(\frac{U_H}{U_0}\right)_{x=0,\, \omega \to 0} \doteq \frac{\omega^2}{g} \cdot \frac{B}{\pi} \cdot \left[-\ln \cdot (1.783 \cdot \frac{\omega^2}{g} \cdot L) - i\pi\right] =$$
$$= 0.313 \cdot \frac{L}{\lambda} \cdot \left[-\ln \cdot (11.2 \cdot \frac{L}{\lambda}) - i\pi\right]$$
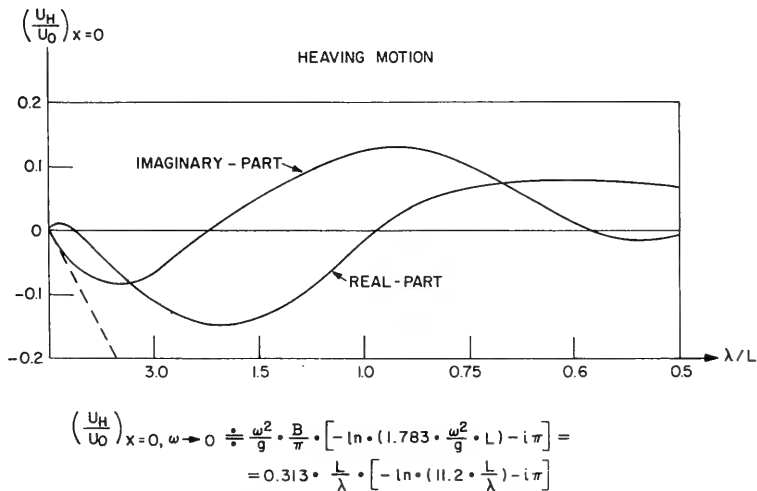
Fig. 26. Heaving motion

In Fig. 28 the amplitude of the motion of the sections of the ship body in vertical direction, viz., $z_o + \psi_x$ is plotted, made nondimensional by the wave amplitude $\bar{h}$.

In Fig. 29 the amplitude of the deformed wave is presented, made nondimensional by the wave amplitude. The upper diagram holds for the restrained body and the lower diagram for the free moving body. The amplitudes of the wave deformed in a longitudinal direction are, as is expected, less reduced relative to the undisturbed wave in the case of the free moving ship than of the restrained ship body. These differences are, again as is expected, smaller in the case of small wavelengths than of large ones. The enlargement of the wave amplitude for $\lambda/L = 1.0$ to 1.5 in the force part of the ship body in the case of the free moving ship is striking.
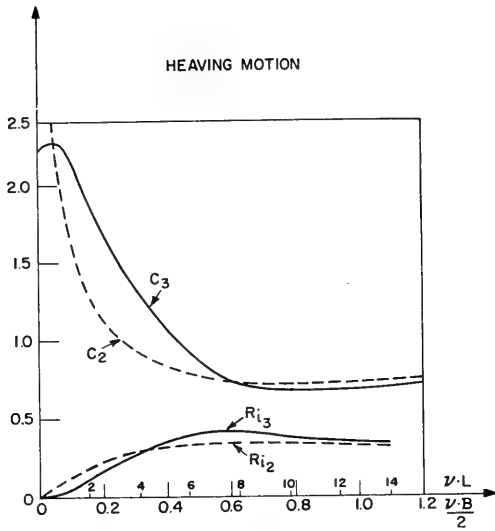
Fig. 27. Heaving motion; coefficient C and force R_i for the section $x = 0$, two- and three-dimensional
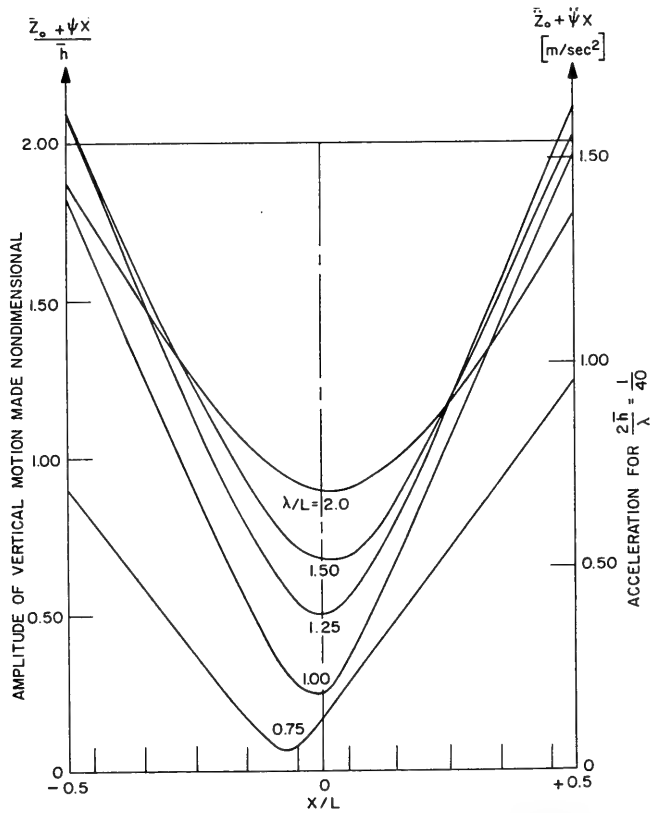
Fig. 28. Vertical motion of the sections of the ship

Fig. 30. Amplitude of the relative motion between the body and the wave surface made nondimensional by the length of the ship for waves of $2h/\lambda = 1/40$

Fig. 29. Amplitude of the deformed wave made nondimensional by the undeformed wave amplitude
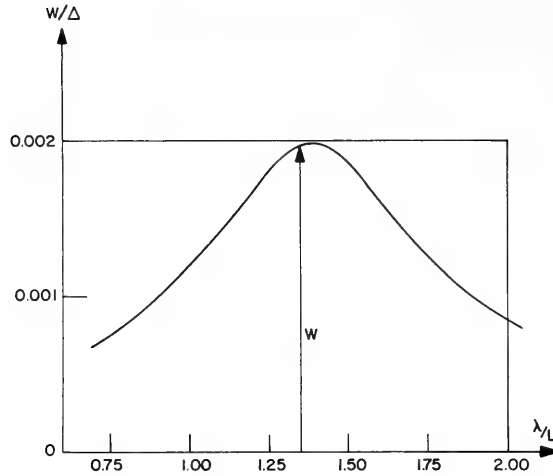
Fig. 31. Resistance arising from reflexion made
nondimensional by the weight of the ship for waves of
$2\bar{h}/\lambda = 1/40$

Figure 30 deals with the amplitude of the relative motion between the deformed wave and the ship body. This amplitude is not made nondimensional with the amplitude of the wave but with the length of the ship. The ratio of the wave height to the wavelength is taken 1/40. This representation has been selected because the envelope of the plotted curves shows to which maximal degree the water surface can move relative to the ship body for all waves of the ratio chosen.

Figure 31 shows the ratio of the resistance to the weight of the ship for a constant ratio of wave height to wavelength of 1/40. The first part of the resistance only arising from reflexion is represented.

Calculations for this example were previously carried out for a subdivision of the ship body in 8 sections and applying a quite different program for the computor. The results of both the computations closely coincide for both U and G, i.e., for the deformation of the free water surface in consequence of the heaving and pitching motion and for the deformation of the wave in the case of a restrained ship body. In the case of the heaving and particularly of the pitching motion somewhat greater values have been obtained with a subdivision into 10 sections. These deviations, as checking computations have shown, are mainly caused by the different subdivision of the ship body. It can be stated on the basis of this comparison that the accuracy of the calculation is sufficient.

ACKNOWLEDGMENT

NOMENCLATURE

x, y, z coordinates

ξ same coordinate as x (used only within integrals)

ω circular frequency

λ wavelength

$\bar{h}$ wave amplitude

$$\nu = \frac{\omega^2}{g} = \frac{2\pi}{\lambda}$$

δ density of water

ρ specific weight of the water

L, B, T length, beam and depth of the ship

B beam of a section (if used within integrals)

$$H = \frac{B}{2T}$$

$\mathcal{B}$ fullness of section

z_o heaving displacement

ψ angle of pitch

Φ velocity potential

φ_n partial potential

A_n coefficients of singularity distributions in the two-dimensional case and distribution functions in the three-dimensional case

U amplitude of the velocity

U_o velocity of a section in the three-dimensional case

U velocity of the water surface in the three-dimensional case which arises from the finite length of the body

G amplitude of the wave deformed by the restrained body

m mass per unit length

m'' virtual mass per unit length

N coefficient of the hydrodynamic damping force

R the total nondimensional force which is necessary to produce the heaving motion in the two-dimensional case

E nondimensional force excited by the wave in the two-dimensional case

C coefficient of the virtual mass

$\bar{A}$ ratio of amplitudes

REFERENCES

[1] Havelock, T.H., Trans. Inst. Naval Architects 86 (1945)

[2] Havelock, T.H., Trans. Inst. Naval Architects 97 (1956)

[3] Havelock, T.H., Trans. Inst. Naval Architects 99 (1958)

[4] Hanaoku, T.S., "Proceedings of the Symposium on the Behaviour of Ships in a Seaway," Wageningen, 1957

[5] Eggers, K., Ingenieur Archiv, 1960

[6] Korvin-Kroukovsky, B.V., and Jacobs, W.R., Soc. Nav. Arch. Marine Engrs., 1957

[7] Tasai, F., J. of Zosen Kiokai, July 1959

[8] Kreitner, H., Trans. Inst. Naval Architects 80 (1939)

[9] Abels, F., Jahrbuch der Schiffbautechnischen Gesellschaft 1959

[10] Grim, O., Jahrbuch der Schiffbautechnischen Gesellschaft 1953

[11] Grim, O., "Proceedings of the Symposium on the Behaviour of Ships in a Seaway," Wageningen, 1957

[12] Grim, O., Forschungshefte für Schiffstechnik 1957, S. 99

DISCUSSION

John V. Wehausen (University of California)

The following remarks are supplementary to that part of Dr. Grim's paper which deals with the heaving motion of two-dimensional bodies. However, they are also supplementary in an important sense to the whole paper, for they deal with the applicability of theory to experiment. The work described below was carried out by W. R. Porter as part of a doctoral dissertation at the University of California, Berkeley.

The aim of this work coincided in some respects with that of Dr. Grim in that we wished to obtain information for forms of shiplike section which could be used later in computations for three-dimensional bodies by a strip method or some modification. However, there was a further aim. Experimental evidence confirming the applicability of perfect-fluid theory with a linearized free-surface condition to oscillatory motion of a body in a real fluid with a free surface seemed to be very scarce, and we felt that more was needed. In order to make a comparison of theory and experiment, configurations were needed for which the theoretical calculations could be made with controllable accuracy and for which the corresponding experimental measurements could be carried out with available equipment. Two-dimensional shapes had several advantages for the experimental work. Furthermore, it was known how to generate by conformal mapping of a circle families of shiplike sections, the so-called Lewis forms, Landweber forms, Prohaska forms, etc. In addition, Ursell* had already carried through computations of added mass and damping coefficients for a circular cylinder by a method which seemed likely to lend itself to further generalization to include the forms mentioned above. This turned out to be the case. Further modification allowed the inclusion of a horizontal bottom.

In order to have a more sensitive test of the perfect fluid theory, it was decided to compute and measure the pressure distribution around the cylinders as well as the added mass and damping coefficients. The computations were programmed for and carried out on an IBM 704. We believe them to be accurate to within 0.5 percent.

At the time this work was carried out we did not know that Dr. Grim was also engaged in similar computations for infinite depth by the method which he had proposed much earlier in 1953. However, Tasai's paper in J. Zosen Kyokai 105:47 had come to our attention, after this work was well under way, and we recognized that the two approaches were identical.[†] However, since Tasai had not included the pressure distributions, in which we were especially interested, or finite depth, we decided to continue with the computations. Although Porter's computations show some small discrepancies with Tasai's, they confirm them generally, as well as those of Dr. Grim.

The experimental measurements have at this time been carried through only for a circular cylinder (10-inch radius). However, other shapes, especially U-shaped and bulbous sections, will be tested later. In carrying out the force and pressure measurements a retreat was necessary in one respect. Although, a phase resolver had been designed, constructed, and tested, it was not feasible during the first set of experiments to make use of it because of excessive noise in the signal, a difficulty we are confident of being able to overcome later. As a result, the experimental points shown in Figs. D1 and D2 are for the amplitudes of fluctuation of the total pressure and force. For these the agreement between theory and experiment seems to be very satisfactory. Although, extremely square U-sections may show greater deviations, it seems likely that perfect-fluid theory can be used to give adequately reliable predictions of the motion of stationary oscillating bodies.

A detailed description of this work may be found in the report of W. H. Porter, "Pressure Distributions, Added-Mass, and Damping Coefficients for Cylinders Oscillating in a Free Surface," Inst. of Engrg. Res., Univ. of Calif., Berkeley, Series No. 82, Issue No. 16 (July 1960).

---

*Quart. J. Mech. Appl. Math. 2:218 (1949).

[†] An English version of Tasai's paper (Rep. Res. Inst. Appl. Mech., Kyushu Univ., Fukuoka, Japan, 8(No. 26):131 (1959)) was later brought to our attention, and presumably renders our translation of the Japanese version (Inst. of Engrg. Res., Univ. of Calif., Berkeley, Series No. 82, Issue No. 15 (July 1960)) superfluous.
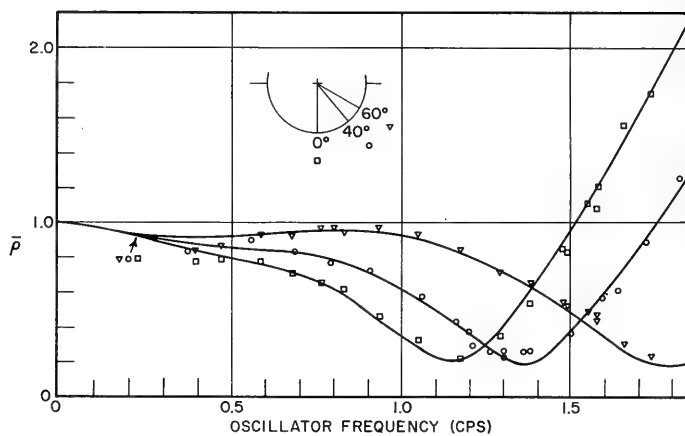
Fig. D1. The calculated and measured amplitude of
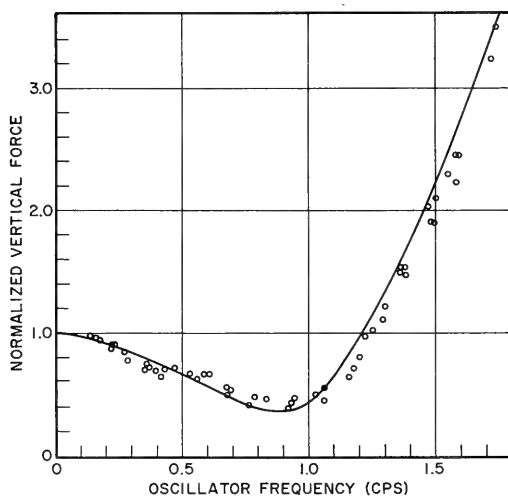total pressure fluctuation

Fig. D2. The calculated and measured
total vertical force

O. Grim

Prof. Wehausen's report about the work carried out at the University of California by
W. R. Porter must be welcomed. I have seen this work only recently and did not know about
it before the symposium. Indeed this work represents a helpful contribution to the problems
dealt with in my paper. It is important that the mentioned experiments will be continued be-
cause only a few experimental results with respect to the forces on oscillating two-dimen-
sional bodies are known. Such experimental results, however, are needed. Tasai, too, has
carried out such experimental work. Since no severe differences seem to exist between the
known theoretical and experimental results for the two-dimensional cases, we can be

encouraged to continue the theoretical work for the three-dimensional or any other more complicated cases. I am very pleased with this contribution.

P. Kaplan (Technical Research Group, Syosset, N.Y.)

We have received in this rendition by Dr. Grim, quite an outstanding piece of work in the sense that it covers many problems that have been considered in the past 10 years from the point of view of ship motion analysis. Dr. Grim, in the past, has provided the largest amount of available data for use in the predictions of motions of ships in waves. This latest work is an improvement in the sense that three dimensionality is rather important, since there are not many three-dimensional solutions for determining the coefficients and the resulting motions of ships in waves. One of the main points which I see here, from my point of view, leads me to a question which I would like to place before Dr. Grim. The very fine thing that you have found is a creation of a distortion in the wave pattern, even in the case of a ship which is restrained in waves. This means you have taken account of the influence of the free surface in computing the excitation. Now, this has never been done in all the latest work used for computing the motions of ships and also it has not been taken into account in determining the bending moments which act upon ship forms. Therefore, I would like to know if you can tell me if you have made a comparison of the magnitudes of the exciting forces on a restrained ship with your theory and compared it to the simple slender body theory which just replaces the effect of the interaction by a dipole and does not take into account the influence of the free surface. Secondly, I would also like to make a point here concerning Fig. 27 in the paper. I gather here that what has been found is an expression for the magnitude of the virtual mass coefficient and also the damping coefficient at the particular section. Two dimensionally, one finds the value at a section all the time, but now you have a three-dimensional effect which shows the inclusion of interactions. The point I would like to make is that the appearance of close values for the damping terms in both the two-dimensional and three-dimensional cases is not necessarily to be taken as saying that there appears to be only a small difference between two-dimensional and three-dimensional values when you look at a section. It happens to be so for this particular case. I can report, and will some time in the future, the fact that there are large differences in the local values of damping; that is, the distribution along the hull is quite different, yet the total values are about the same. So I think it important for this one case to see this closeness yet realize local values must be looked at with care. That, of course, is most true for bending analysis, which is of vital importance for the structure of ships.

O. Grim

Dr. Kaplan has put two questions: At first he asks how large the differences are between the normal strip method of computing the forces and the bending moments without any deformation of the wave and the other computations with the deformation of the wave. I have not made such a comparison, but I think the last figure in which the reduced wave amplitude is represented will enable us to make a judgment about this comparison. It may be that the forces and the bending moments will be reduced in about the same magnitude as the wave amplitudes. Dr. Kaplan's second question is whether the added mass and the damping force, mentioned in Fig. 27, are typical. I think that this is so and that the differences between the two-dimensional and the three-dimensional results for heaving and pitching motion are only important for the range where the frequency is near to zero, while in the other range these differences are not so important. More important are the differences for the ship in waves, and the reason for this is the following: For the ship which undergoes a heaving

motion with a large frequency, the forces exerted by the ship upon the water are in the same phase along the whole length of the ship. At each section of the ship an oscillatory force acts upon the water. The force at each section excites an elementary wave. If the ship makes a heaving motion with a large frequency, the resulting wave is small due to the phase relation between the elementary waves. However, for the ship in head seas the sum of all the elementary waves, which gives the deformation of the original head wave, is largely due to the phase relation between the elementary waves, which is different from the phase relation for heaving motion. This is the reason why the deformation is large for the ship in head seas and why the deformation of the surface of the water in the longitudinal direction is small for heaving motion with large frequencies.

J. B. Keller (New York University)

My comment is based on the following consideration. Dr. Grim's work begins with the solution of a certain two-dimensional problem and then he shows how to utilize a solution of the two-dimensional problem to solve the three-dimensional problem. I would like to point out another method of using two-dimensional problems to solve a three-dimensional problem. The method I have in mind is especially useful for short waves, i.e., waves that are short compared to the dimensions of a ship. The method is that of geometrical optics. I would like to suppose that Fig. D3 is the waterline of a ship which we are looking at from the top and I would like to consider the forces exerted on this ship by a wave coming in at some oblique direction. Then, according to the principals of geometrical optics, the wave can be thought to travel along rays and each ray will hit the waterline and be reflected according to the law of reflection and give rise to a reflected ray. The calculation of the reflection coefficient, that is the amplitude and phase of the reflected wave, is a local affair and depends only upon the geometry of the ship in the neighborhood of the point of reflection. Furthermore, since waves of short wavelength penetrate a very short distance into the water, it is only the geometry of the ship very near the surface at the point of reflection that determines the reflection coefficient. Since the geometry of a ship at a single point near the waterline can be described in terms of the radius of curvature of the vertical section and the slope of the ship at the waterline, and also, of course, the curvature of the waterline itself, those three quantities — the two radii of curvature and the slope — will determine completely the reflection properties for this particular ray. The radius of curvature of the waterline will be taken into account because neighboring rays get reflected in slightly different directions. The lateral divergence of the reflected rays will account for the curvature of the waterline. In order to compute the reflection coefficient for a given ray, it suffices to solve a two-dimensional problem, namely, reflection from a circular cylinder with the same curvature as the ship has in a vertical section at the waterline. The circular cylinder should cut the water with the same slope the ship has at that place. That is a two-dimensional problem that hasn't been solved, but never mind, I just promised to tell how to relate a two-dimensional problem to a three-dimensional one. If we could solve that two-dimensional problem for each position along the ship, then by such a geometrical construction we could calculate the reflected wave in the three-dimensional problem. The result for the two-dimensional problem might also be

Fig. D3. Geometric optics analogy

determined by measurement or by someone solving it. Thus, it is possible, by solving a relatively simple problem, to get results that should be useful for a relatively complicated one. I would like to conclude by saying that the same ideas can be applied to calculating the waves produced by the motion of the ship in pitching or heaving or other periodic motion. Again, in each case it is necessary to find the corresponding waves produced by the motion of a circular cylinder with the same radius of curvature and slope as the ship has at the point of interest and that problem hasn't been completely solved.

O. Grim

I can imagine that this is a good idea as a way to compute the wave propagation for any large frequency. However, for a prediction of the motions of a ship a more complete solution than only for the wave propagation is needed. It could be helpful to obtain by Prof. Keller's proposed simple method results which confirm those obtained from a more complete solution.

Owen H. Oakley (U.S. Bureau of Ships)

I am sure that if my colleagues, that is, my practical naval architectural-type colleagues, could see me standing here with the temerity to discuss Dr. Grim's paper they would be amazed, and I assure you I am too. I have two points to make, one trivial and one more on the serious side. First of all, in 1957 I was a shipmate of Dr. Grim on an icebreaker in the Sea of Bothnia. We were concerned with vertical movements of the ship, because, installed in the bow of this ship was an eccentric weight device known as the Stampflanage which, when properly tuned at the remote control station in the pilot house, created a pitching motion in the bow of the ship and thus helped to break ice. Dr. Grim was at the controls and occasionally he would turn the knobs the wrong way and a fore and aft surging motion would result which was a bit disturbing to say the least. I wonder whether Dr. Grim has considered the matter of surge in this present analysis; I should think it would be something he would be very much aware of. Now a more serious comment. As a general rule practical naval architects do not have occasion to give serious thought to this sort of theoretical work. However, occasionally one encounters problem where such mathematical assistance would be most welcome. Such an experience was the design of the escort research ship. We would have liked very much to have been able to calculate the response of this ship to waves, but since we could not, we had to build models and go to the trouble of testing them, finding where we were wrong, correcting it, and trying again. The theoretical and empirical development of this subject has been going on for a number of years; many excellent minds have worked on it and produced a prodigious quantity of papers on the various aspects of the problem. I hope that some day all of this work to which Dr. Grim has contributed so greatly will bear fruit and we will be able to sit down with pencil and paper or with computer or what have you and predict quantitatively the amplitudes of response of arbitrary shipforms. I am sure that the contribution which Dr. Grim has told us about today is another significant step in that direction.

O. Grim

I am glad to hear that Mr. Oakley likes to remember the time we spent together on the icebreaker in the Sea of Bothnia and I hope he forgives me for the wrong way in which I

twiddled the knobs of the pitching plant of the icebreaker. To the other point of Mr. Oakley's comments I have to say that I also am a naval architect and I too hope that the results of such complicated investigations can, in the future, be used by naval architects.

*   *   *

SEMISUBMERGED SHIPS FOR HIGH-SPEED
OPERATION IN ROUGH SEAS

Edward V. Lewis and John P. Breslin
Davidson Laboratory
Stevens Institute of Technology
Hoboken, New Jersey

To evaluate methods to obtain high speed at sea without large in-creases in ship size, several hull configurations were surveyed; in par-ticular semisubmerged craft designed to operate at or just below the sur-face. By increasing judiciously the amount of submerged hull-volume, both high-speed resistance and pitching motions in rough seas can be reduced.

The hull configurations that were surveyed included a craft that resem-bles a surfaced submarine, a slender ship with large bow and stern bulbs, and a craft (semisubmerged) that is similar to a shallow-running submarine with a permanent surface-piercing strut for air supply and ex-haust. The semisubmarine, potentially, can exceed submarine speeds because of its low resistance and good sea performance. In addition, the air-breathing power plant of the semisubmarine weighs less and requires less space than a nuclear power plant.

The study of the calm-water stability characteristics of the semisub-marine at intermediate and extreme speeds shows that depth and direc-tional stabilization can be achieved with tail fins of reasonable size, except at low and intermediate speeds, where stabilization by fin area alone is not attractive; however, active controls readily can provide op-eration at constant depth in calm water. Analog computer studies show a peculiar dependence upon the distribution of stabilizing surfaces and other parameters. Therefore, precise and extensive model tests are re-quired to explore the near-surface dynamics of this craft to fully develop its advantages.

INTRODUCTION

The successful development of the true submarine has resulted in a craft that can re-main submerged almost indefinitely and operate at high speeds in a three-dimensional realm of steadily increasing depth. When a submarine runs far below the surface, surface wave-making resistance is virtually eliminated; the remaining resistance is caused almost entirely by skin friction. Although a submarine can be made squat in comparison with a surface ship to minimize the ratio of wetted surface to volume, its surface area is greater than that of a comparable surface ship. This is a disadvantage at moderate speeds; however, at high speeds, this disadvantage is more than compensated for by the elimination of surface wave-making. Power is directly proportional to speed cubed, even at high speed; therefore, speed is limited only by the weight and size of the power plant.

The development of the submarine puts a new light on the problem of surface ship design. During World War II, the submarine and the destroyer were evenly matched. This is no longer true. Submarines have distinct advantages in speed and maneuverability, particularly when seas are rough. In addition, submarines have added advantages in evasiveness because they operate in a three-dimensional realm. To meet the challenge of the submarine, naval architects must develop high-performance surface ships. This problem has frequently been viewed with pessimism. It has been said that the only way to cope with the submarine is to go above the surface, as with a hydrofoil craft, or to go below it with another submarine. In this view, ships on the surface can only be fast if they are large, which increases cost.

There is another viewpoint, however, that suggests the need to give serious attention to the possibilities of more radical types of small surface craft that might be able to attain high speed even in rough seas.

POWER REQUIREMENTS

Figure 1 shows three directions for seeking higher ship speed than can be obtained with a conventional surface ship — for example, a destroyer. One direction is to go well below the surface to eliminate surface-wavemaking resistance. Another is to stay on the surface but to reduce surface-wavemaking resistance drastically with a longer and more slender hull. The third is to raise the hull above the surface with either a planing-type hull or hydrofoils.

In addition, Fig. 1 shows that there are a multitude of different possible types of craft, with successively larger submerged volumes, that can be designed to operate at the air-water interface. Other possibilities have been suggested by Boericke [1].

It is of interest to consider the comparative powering problems of these diverse waterborne craft. Because it is difficult to determine reliable figures for the propulsive coefficients, the comparison of the power required for these craft (Fig. 2) is based on effective horsepower (EHP). Displacement is a reasonably good index of size; therefore, EHP's have been estimated for the craft shown in Fig. 1. Each craft is assumed to have a displacement of 2844 tons, which corresponds to the displacement of a DD-692 class destroyer. This displacement was selected as the desirable maximum displacement for high-speed craft.

Figure 2 is a rough comparison of the calm-water resistances of these waterborne craft at speeds up to 70 knots. The craft that has the lowest resistance is an ideal, deep-running submarine with a minimum of appendages, optimum hull form, and an assumed length-to-diameter ratio of 7.0. Not only is a deeply submerged submarine the lowest in resistance of any type of craft, but even at 60 or 70 knots the EHP is far from astronomical.

For an ideal submarine form (H) running with its center 1-1/4 diameters below the surface (that is, the upper surface of the submarine is 3/4 diameter below the surface) there is a pronounced hump in resistance that corresponds to the maximum wavemaking speed. The submarine is close enough to the surface to produce a surface wave that causes this rise in EHP. As the speed of the submarine increases further, the wavemaking resistance becomes a decreasingly important part of the total resistance.

For an ideal submarine (about 210 feet long) with a strut (about 30 feet long) piercing the surface (G) there is a sizable increase of EHP, which rapidly goes up with speed. Information is still rather sketchy on the resistance of struts piercing the surface, but the plotted values are believed to be roughly correct. The disturbance of flow by the strut is not
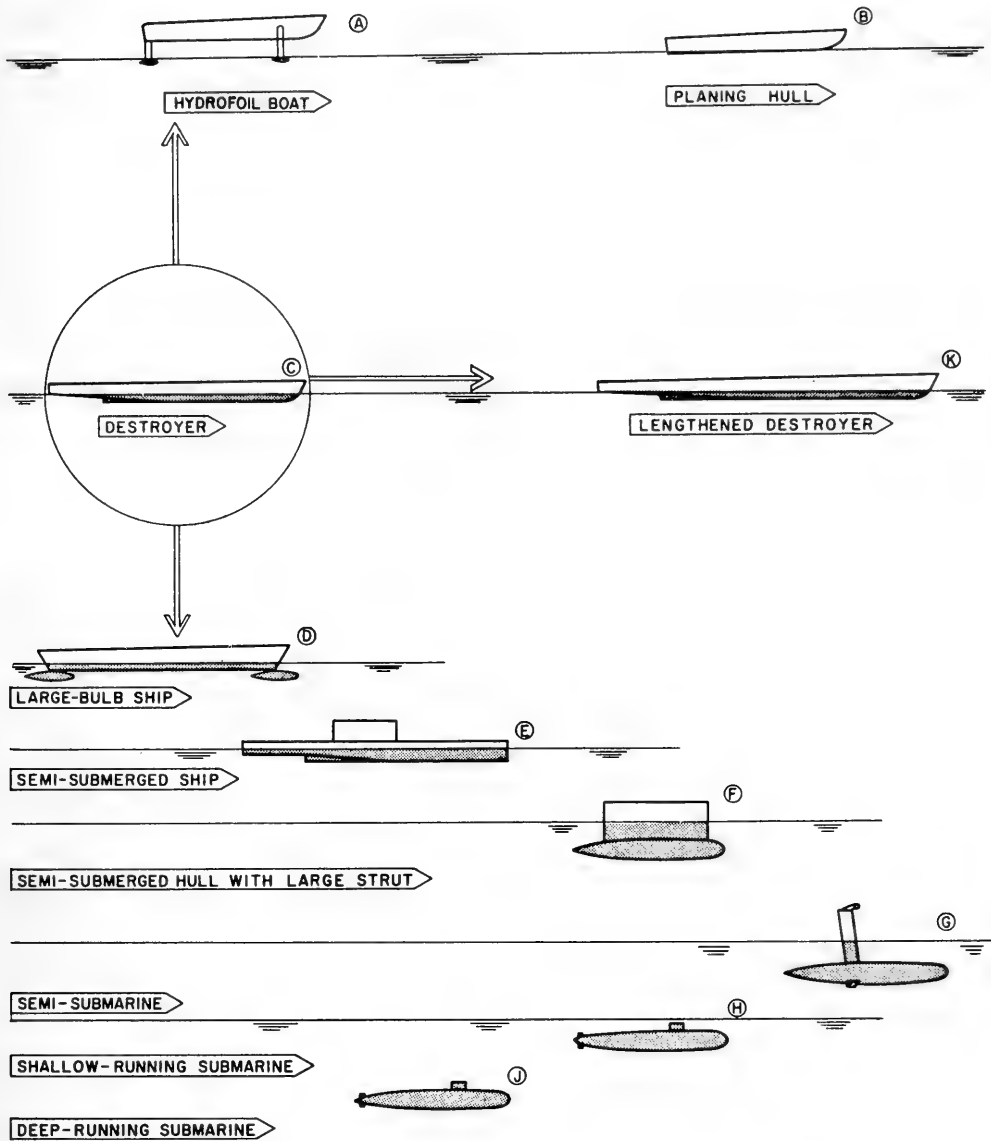
Fig. 1. Possible directions for seeking higher speeds at sea

wavemaking resistance in the usual sense (because the speed is very high for the length of the strut), but there is separation of flow, ventilation, and even cavitation that cause a very large increase in resistance, usually designated spray drag, which shows very emphatically the reason for trying to make the strut as small as possible.

For a typical destroyer (C), the EHP is considerably higher than for a submarine with a small strut, especially as speed goes up. In addition, this ship is slowed more than a submarine in rough water.

Figure 2 also shows that a surface ship could achieve very high speeds if it were designed to be much more slender than a destroyer (K). This would reduce the surface
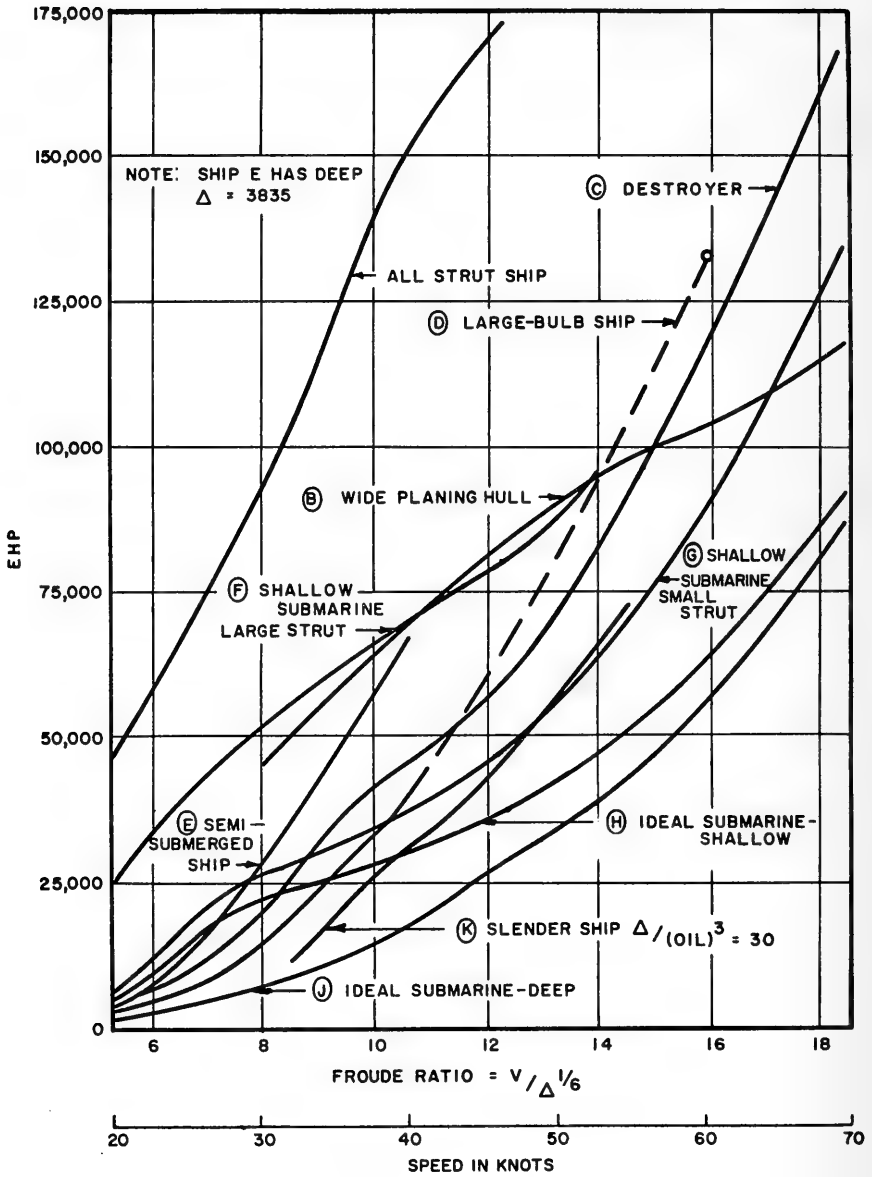
Fig. 2. Effective horsepower required versus speed
for a group of bodies with $\Delta = 2844$ tons

wavemaking resistance and thus compensate for increased frictional resistance. As the speed of this ship goes up, the EHP curve almost coincides with the curve for the shallow-running submarine with a small strut. This suggests the latter type of craft has no resistance advantage over a slender destroyer designed specifically to go at very high speed. However, the very slender destroyer would run into trouble at high speed in rough water, and the near-surface ship with strut may have advantages.

A submarine with a very large strut (F), as suggested by Boericke [1] and investigated by Mandel [2], shows comparatively high resistance, especially at high speeds. An all-strut ship — that is, a ship of the same displacement and about the same draft as the others but with its entire hull extending through the surface — has a very high EHP. Figure 2 also indicates that a large planing boat (B) of optimum-breadth would be better only at very high speeds (near the limit of this figure).

The semisubmerged hull form (E), reported by Lewis and Odenbrett [3], and the slender hull with large bow and stern bulbs (D) are capable of high-speed supercritical operation in rough seas with comparatively small pitching motions. The first of these ships, (E), shows rather poor calm-water EHP performance at deep rough-water draft, but the latter, (D), is remarkably good up to the limit of the speed range so far tested.

Therefore, a number of types of craft intermediate between conventional ships and submarines are feasible that promise remarkably low power requirements. However, the larger the proportion of the hull that is submerged, the more difficult the ship design problem becomes; available hull volume is curtailed and problems of transverse stability (static) become increasingly difficult with greater submergence. The cost of the craft can also be expected to increase correspondingly. Hence, it is desirable to consider and compare all types of craft thoroughly to determine the most satisfactory compromise for any particular need.

ROUGH-WATER PERFORMANCE

Of course, it is not enough for a surface or near-surface craft to show favorable calm-water resistance at high speed. If it is to compete with a deeply submerged submarine, the ship must be able to maintain good speed in rough-storm seas. This may be, in part, a powering problem. However, in high-speed craft, it is usually mainly a matter of avoiding or minimizing ship motions and indirect effects — such as wet decks, slamming, propeller racing, local high accelerations, etc. The ideal craft, therefore, is one that provides the best compromise between low-resistance characteristics and outstandingly good performance in rough water — capable of high speed in any sea condition.

(As background for the discussion of the problems of rough water performance, the balance of this section has been adapted from Ref. 4.)

Ship motions at sea are usually resolved into six components for study: the angular motions of roll, yaw, and pitch and the translatory motions of heave, surge, and sway. Some are more troublesome than others, but when one or two are reduced the others are apt to become more noticeable. Rolling has received particular attention ever since steam replaced sails and the steadying effect of canvas was lost. Because the forces involved in rolling are small, it has proved feasible to reduce these amplitudes drastically by various antirolling devices. The simplest device is the bilge keel, which has been generally accepted in shipbuilding for many years. Its effectiveness can be explained on the basis of the theory that irregular storm seas contain many regular component waves of a wide range of periods superimposed on one another. A ship will respond much more violently to one particular

band of wave periods (or frequencies) than to any others. This period is the natural rolling period of the ship. Consequently, the most serious rolling occurs in the natural period of the ship and, therefore, may be classed as synchronous rolling. In any oscillating system, simple damping is always effective in reducing synchronous oscillation. Therefore, by increasing the damping of roll, the bilge keel markedly reduces serious synchronous rolling.

Another damping device is the passive antirolling tank system, in which there has been a notable resurgence of interest recently. Such tanks installed in naval auxiliaries have proven to be remarkably effective. Important features are their low installation cost and equal effectiveness hove to and at forward speed. However, reduction rather than elimination of rolling is the best that can be expected.

For moderate and high-speed vessels, a much more effective method of reducing rolling appears to be controllable fins. These devices are so effective that the rolling problem appears to have been solved in principle, except for low-speed vessels for which an activated tank or gyroscope system is applicable. This does not mean that further research is not needed. There are problems of the interaction or coupling of other motions, particularly yaw, of obtaining increased effectiveness with reduced weight and cost, of avoiding structural failures of fin shafts, etc. Furthermore, the system for the control of roll must be coordinated with the system for the control of yaw, that is, the steering gear and gyro-pilot.

Heaving and pitching motions are the most difficult to overcome and present the most serious problems because they involve large vertical accelerations and cause shipping of water, slamming, and propeller racing. Furthermore, when other motions are controlled or reduced, they become even more noticeable. Consequently, attention will be focussed on these symmetrical modes of motion, assuming that methods are available for solving the other motion problems.

Model research in regular-head seas has brought three important facts into prominence [5]: (a) the amplitudes of motion are greatest in the vicinity of synchronism between the period of encounter and a ship's natural period of oscillation, (b) phase relationships leading to wet decks and slamming also are characteristic of synchronism, and (c) waves appreciably shorter than the length of a ship do not cause serious motions even at synchronism. On the basis of these general facts, there are two possible methods by which significant reduction of pitching and heaving amplitudes can be sought: avoiding synchronism with waves of ship length or longer, and reducing the magnification effect, which causes increased amplitudes near synchronism.

Although damping devices such as bow fins can reduce the magnification of motions somewhat, the most effective method of reducing motions is by avoiding synchronism. In a regular swell, this undesirable condition can be avoided by changing either course or speed. If the speed is changed, synchronism can be avoided by an increase or a decrease. If the speed for pitch synchronism is the critical speed, slowing brings the ship into the subcritical range; increasing speed brings the ship into the supercritical range. Figure 3 (from Ref. 5) shows the relationship between pitching period and speed for synchronism in head seas. For other headings, a simple cosine correction must be introduced. The curves that define the conditions for synchronous pitching show that (a) the longer the wavelength, the higher the critical period, and (b) in any particular wavelength, the lower the ratio of $T_p/\sqrt{L}$, the higher the critical speed.

When a ship encounters irregular storm seas, the situation does not remain so simple. Oceanographers have shown that storm seas can be considered as composed of a great many regular-wave trains of varying length and direction of travel, all superimposed on one
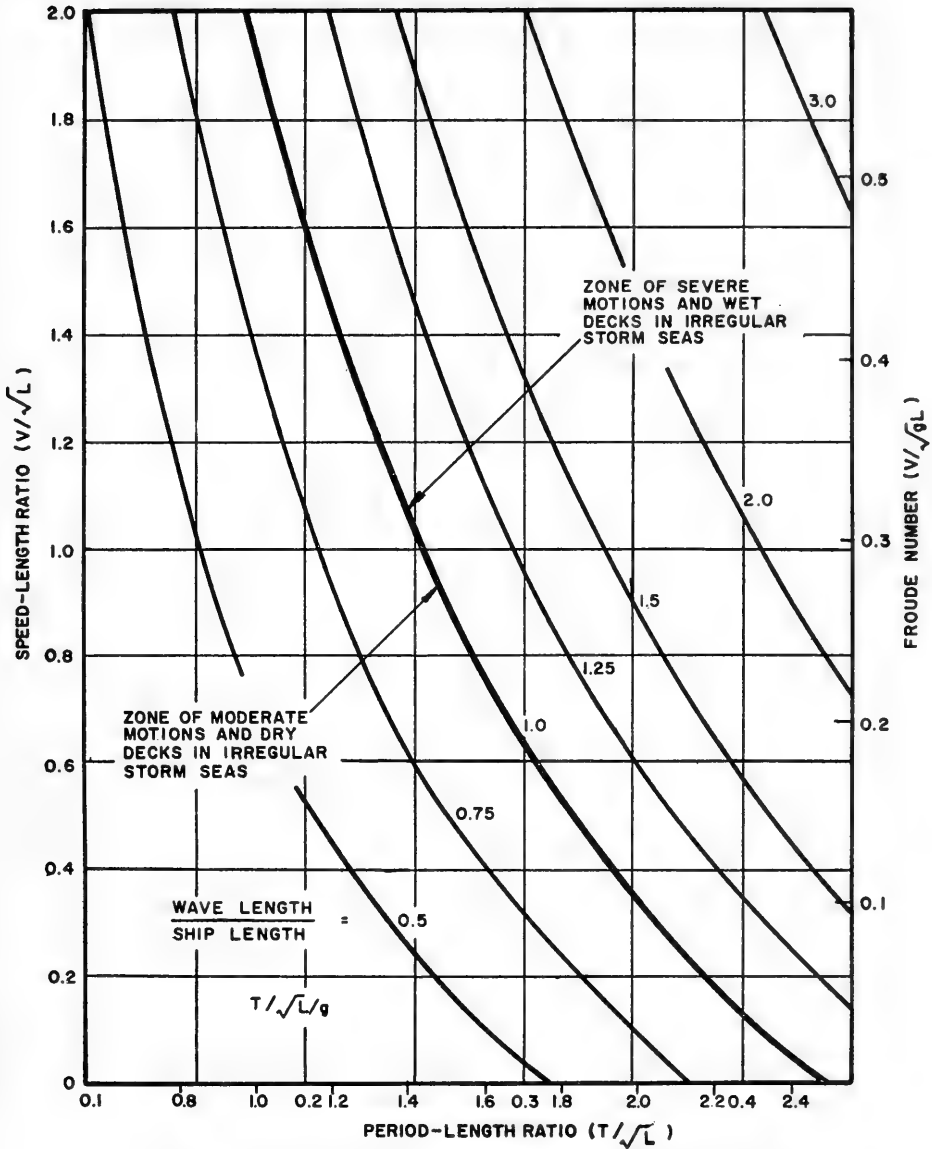
Fig. 3. Theoretical speed-length ratios for synchronous oscillation
in regular-head seas of different lengths (from Ref. 5)

another [6]. They also have confirmed the observations of seamen that shorter waves are formed first in a storm. As the wind continues to blow, longer components are formed without seriously affecting the smaller components. For a particular wind velocity, the sea reaches a limit when it attains its fully developed state. If the wind increases in strength, not only are the component waves believed to be higher, but — when the fully developed state is reached — longer components also will be present.

If a ship is able to attain a speed sufficiently high that its period of encounter with the longest important wave component is shorter than the natural pitching period, the ship will be in the supercritical condition for that particular storm. Most ships can attain this condition only in moderately heavy seas — that is, in light winds or in stronger winds of short duration. In general, whether or not a ship can attain the supercritical condition depends both on the sea state, indicated by wind velocity and duration, and on the ship's natural pitching period. Speeds for supercritical operation are shown for the case of head seas in Fig. 4, which is taken from Ref. 5. At other headings, the ship must reach even higher speeds to attain the supercritical condition.

Because short waves are present in both severe and moderate storm seas, it is impossible to avoid synchronism with all component waves by reducing speed. However, model tests have shown that waves appreciably shorter than the ship do not cause serious motions even at synchronism. Therefore, speeds that are low enough to avoid synchronism with waves of ship length and longer cause moderate motions. This condition may be termed the subcritical range. For head seas, it depends mainly on the ship length and the natural pitching period, that is, on the ratio $T_p/\sqrt{L}$, as shown in Fig. 3. At times, all ships must reduce speed in storm seas to attain the subcritical condition of moderate pitching.

In following seas, most ships steaming at ordinary speeds are always in the subcritical range. This explains the advantage of heaving to with wind and sea astern, provided that the ship can be kept under control. However, Mandel [7] has pointed out that unusual ship forms intended for supercritical operation in head seas may encounter critical conditions in following seas.

SUPERCRITICAL OPERATION IN ROUGH SEAS

It has been shown in Ref. 5 that for most ships the most promising method of reducing pitching and heaving motions is to use hull proportions that raise the critical-speed limit and permit higher subcritical speeds. This means increasing the length in relation to displacement, which results in a reduced period-length ratio, $T_p/\sqrt{L}$. A ship can then go at higher speed before synchronous response to waves of near ship length is experienced (Fig. 3).

Thus, in Ref. 8 a model 25 percent longer than a conventional DD-692 destroyer, but with the same displacement, had $T_p/\sqrt{L} = 0.20$ instead of 0.25. It was concluded that in a storm in which the conventional destroyer could attain a speed of 20 knots ($V/\sqrt{L} = 1.0$), the longer vessel could attain a speed of 30 knots or $V/\sqrt{L} = 1.4$ (Fig. 3). The longer destroyer was an abnormally slender ship, with $\Delta/(L/100)^3 = 30$. Tremendous problems of stability, structure, and hull arrangements would be encountered in the design of such a ship. It hardly seems feasible, therefore, to think of large increases of speed to 50 or 60 knots by going further in the direction of longer and thinner ships.

The most promising direction then to obtain really high speeds in head seas, where motions are most severe, is to aim at supercritical operation. At the same time, care must be
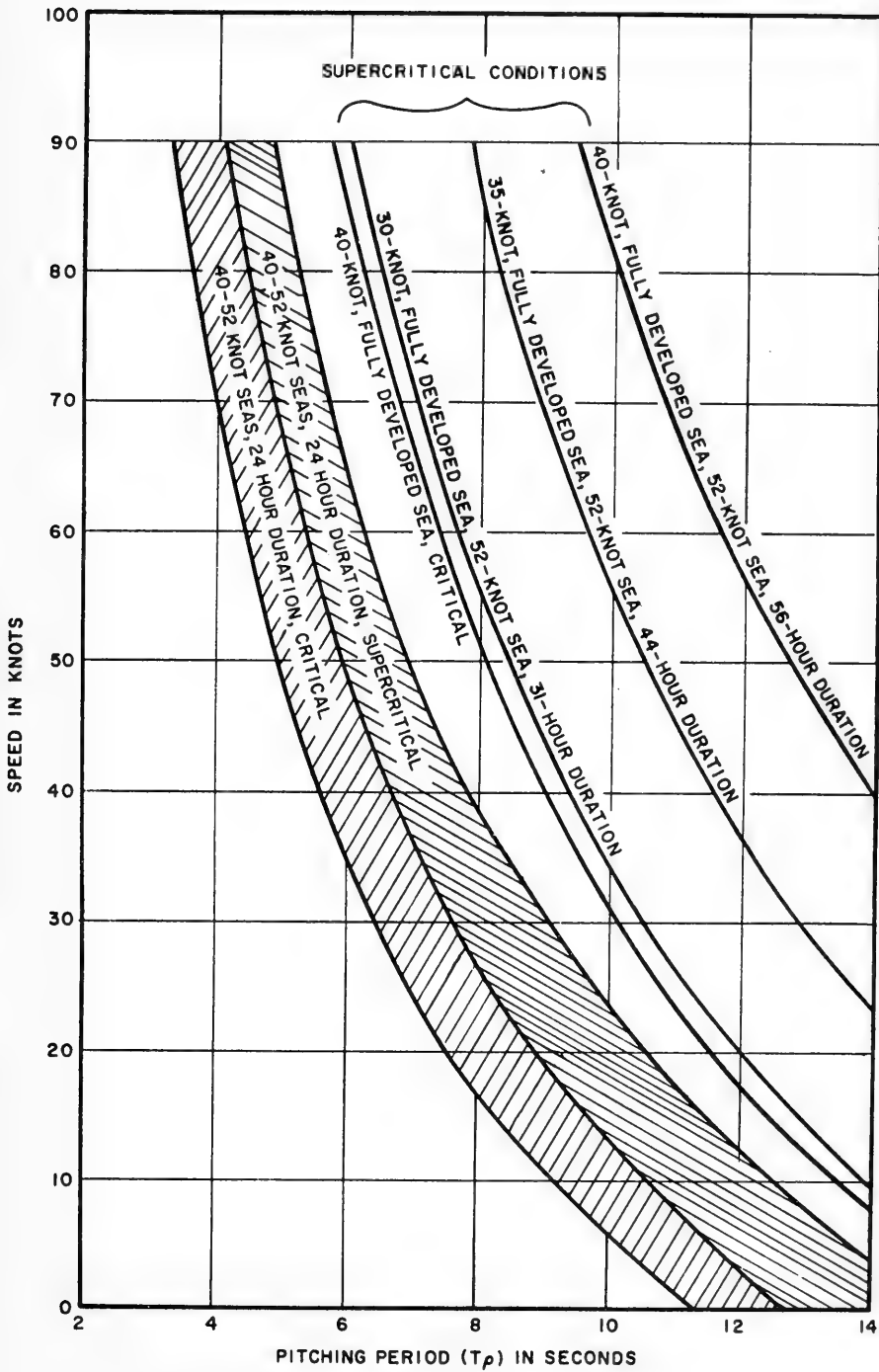
Fig. 4. Ship speeds for critical and supercritical operation,
based on a Neumann ideal spectra (from Ref. 5)

exercised to remain in the subcritical speed range in following seas. The basic idea is simply to attain high ship speed and a long, natural pitching period. The problem of high speed involves the question of reducing wavemaking resistance, which has already been discussed.

To consider all the possible means of increasing the natural pitching period (T_p) it is well to examine the equation given in Ref. 5:

$$T_p = 2\pi \sqrt{\frac{\nabla}{g\,B\,L}} \sqrt{\frac{C_k^2 + C_j^2 k_{yy}}{C_{IL}}} \qquad (1)$$

in which ∇ is displacement volume, g is acceleration of gravity, B is breadth, and L is length. The coefficient C_k is the inertia coefficient so that the longitudinal mass moment of inertia $J_L = \nabla e (C_k L)^2$, or $C_k = I/L \; J_L/\nabla e$; $(C_j^2 k_{yy})$ is an analogous coefficient of virtual inertia by which $\nabla \rho L^2$ must be multiplied to give the longitudinal mass moment of inertia of the entrained water. C_{IL} is the coefficient of longitudinal waterplane inertia defined by the relationship

$$BM_L = \frac{L^3 B}{\nabla} \, C_{IL}.$$

From Eq. (1) it can be seen that the following trends increase the natural pitching period:

1. Increase of displacement

2. Reduction of length or beam

3. Increase in virtual inertia $(C_j^2 k_{yy})$

4. Reduction in waterplane inertia (C_{IL})

5. Increase in mass moment of inertia (C_k).

Because a ship in supercritical operation tends to plunge through the waves rather than to ride over them, it is difficult to attempt to keep water off the foredeck. Accordingly, low freeboard and a heavily built deck is one way to cope with shipping of water, which at the same time permits a very narrow waterline. The body plan in Fig. 5 illustrates a possible design for a supercritical ship of this type, (E) of Fig. 1, a ship like a surfaced submarine, made longer and more slender to attain high surface speed. The normal waterline would be used for good weather operation; in bad weather, large peak ballast tanks would be filled to lengthen the pitching period by increasing the displacement, by increasing the radius of gyration, and by reducing the waterplane area (items 1, 4, and 5 above). Characteristics are compared with a typical destroyer in Table 1.

This semisubmerged model had $T_p/\sqrt{L} = 0.38$ in the deep-draft condition. Results of tests in regular- and irregular-head seas [3] confirmed theoretical expectations that a supercritical condition of moderate motions could be attained at speeds of 35 to 40 knots in moderately rough irregular-head seas (Fig. 6). Heaving motions were more pronounced than
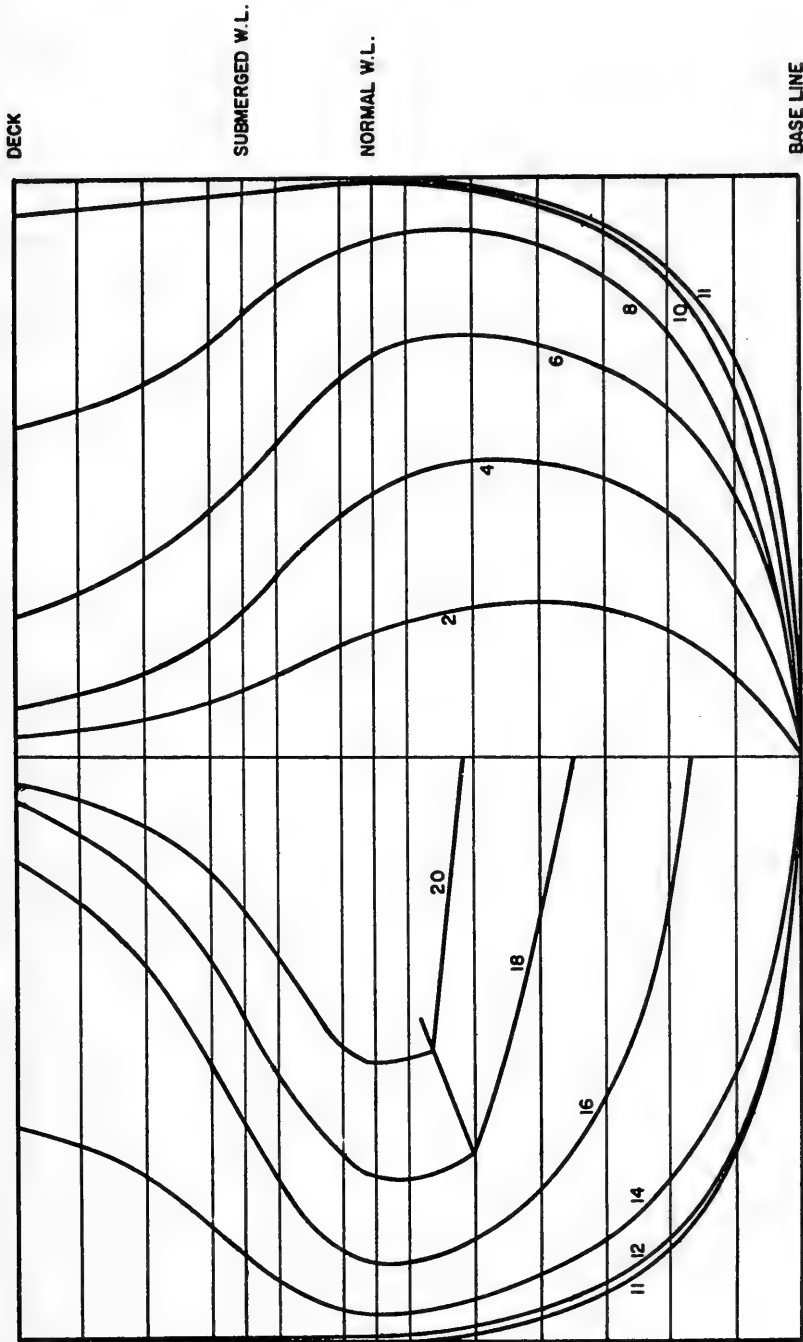
Fig. 5. Body plan of proposed semisubmerged ship for high speed supercritical operation (from Ref. 3)

Table 1
Characteristics of Unusual Ship Forms

Item	DD-692 Destroyer	Semisubmerged Ship	Large-Bulb Ship
Length overall (ft)	391	383.0	441
Length on WL (ft)	383.6	383.0	346
Length of each bulb (ft)			94.7
Beam (ft)	40.8	36.4	34.4
Draft (ft): hull, normal displ.	14.1	13.0	17.2
bottom of bulb, normal displ.			36
hull, deep displ.		17.0	
Displacement (long tons):			
hull, normal	3471	2770	2480
bulbs			991
total			3471
deep		3835	
$\Delta/(LWL/100)^3$	62	68*	84
Waterplane coefficient	0.77	0.57*	0.64
Longitudinal gyradius	0.24 L	0.27 L*	0.30 LWL
Natural pitching period, T_p (sec)	4.9	7.9*	8.9
Period-length ratio, $T_p/\sqrt{LWL}$	0.25	0.40*	0.48
Natural heave period (sec)	5.1	6.5*	6.3

*At deep draft.

pitching, but heaving accelerations were not unusually high in spite of the high average frequency of wave encounter. In irregular waves, the highest single value of heave acceleration was 0.45 g at 25 knots and 0.26 g at 40 knots. The reason for these moderate values was that the motion occurred primarily in the natural heaving period.

No following-sea tests were run, but the natural pitching period is such that subcritical operation is anticipated at speeds up to 45 knots. However, as previously noted, the power requirement at deep draft is exceedingly high, even in calm water, for practical considerations. Furthermore, wave impact on the superstructure would be a serious structural problem, and it might be necessary to raise the deckhouse up on columns to permit the waves to pass under it. Hence, though this type of craft looks interesting as a supercritical ship, there are serious problems to be solved to make it practicable.

Another type of supercritical craft is the slender hull with large bulbs mentioned earlier, (D) of Fig. 1. Available results of a model investigation of such a ship now under way at the Davidson Laboratory will be summarized. The objective here was to increase the natural pitching period by increasing the virtual mass moment of inertia of the hull, without incurring a resistance penalty in the process. That is, k_{yy} of Eq. (1) was greatly increased. The bulbs appear to be too deeply immersed to provide appreciable benefit in the form of damping of motions.

The hull form selected was the well-known ideal form developed by Wigley [9] for which the theoretical wavemaking resistance has been calculated. In this form, the underwater sections are parabolic, the waterlines are sinusoids, and the above water form is wall-sided. For the shape of the bulbs, a body of revolution was selected with length/depth = 5. Theoretical wave resistance of this type of body has also been calculated. The size of each
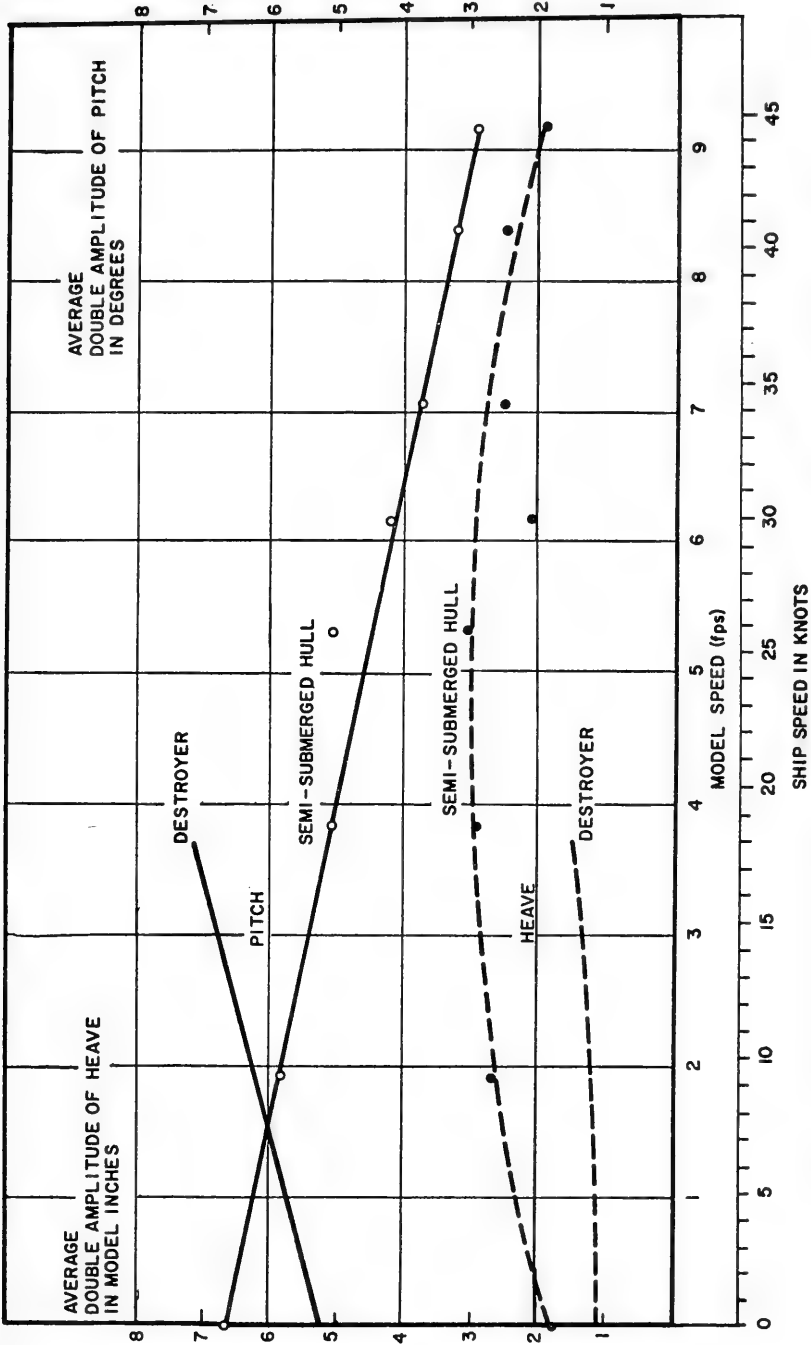
Fig. 6. Pitching and heaving motions in irregular waves with a significant height of 21.6 feet (from Ref. 3)

bulb was fixed at 20 percent of the volume of the hull alone. Thus, both bulbs represent 28.6 percent of the total displacement. The bulbs were attached to the hull in a manner that permitted their fore and aft location to be varied.

Figure 7 shows the model with 40 percent of the length of the forward bulb extending forward of the FP and 60 percent of the aft bulb extending aft of the AP. Full-scale characteristics of the large-bulb ship are given in Table 1, and compared with those of the typical destroyer and semisubmerged hull.
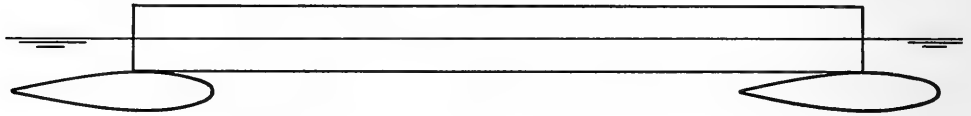
Fig. 7. Slender ship with large bow and stern bulbs

At present, neither the testing nor the analysis in this project has been completed. Results presented here are preliminary and subject to further evaluation when the testing program is completed. Because the forward position of the bow bulb showed the least resistance of the positions tested, it was selected for the regular $2.0L$ wave tests. Figure 8 compares the pitching motions of three types of ships. The worst pitching motions for the large-bulb model occur at about the speed for synchronous motions, 2.4 fps or 9.8 knots. At intermediate speeds, the motion of the large-bulb model was somewhat greater than the semisubmerged model, but at high speeds it was somewhat less.

Figure 9 shows one real shortcoming of the model. Worst heaving motions occur in the vicinity of 34 knots ship speed, where the amplitude approaches 2-1/2 times the amplitude of the wave. Synchronism for heave occurs at 6.8 fps or 28 knots ship speed. While the heaving was severe, maximum acceleration amidships accompanying the motion was 0.45 g in an $LWL/41$ wave, no worse than the semisubmerged model. However, the large heave amplitudes may actually cause the middle body of the ship to emerge from the water at speeds where maximum heaving motions occur. Nevertheless, this type of craft appears to offer real potentialities of high speed in rough water, and research is continuing on possible means of improving performance further. It has the advantage over the semisubmerged design in having less hull-volume limitations, and sufficient freeboard and flare can be provided forward to keep water off the foredeck.

SEMISUBMARINE

Characteristics

Finally, we may consider the possibility of larger proportions of submerged hull. Mandel has considered a hull with a surface-piercing fin almost as long as the hull ((F) of Fig. 1) with some success [2]. However, it is believed that the power requirements are excessive and that the only hope for success with this type of craft is to reduce the fin to the absolute minimum. Mr. E. Frankel stated at the Seminar on Ship Behavior at Sea, Stevens Institute of Technology, June 1960, that a model is now being investigated at M.I.T. in which the fin has been reduced to about 1/6 the length. Resistance and control problems for such a craft ((G) of Fig. 1) are now being investigated at Stevens.
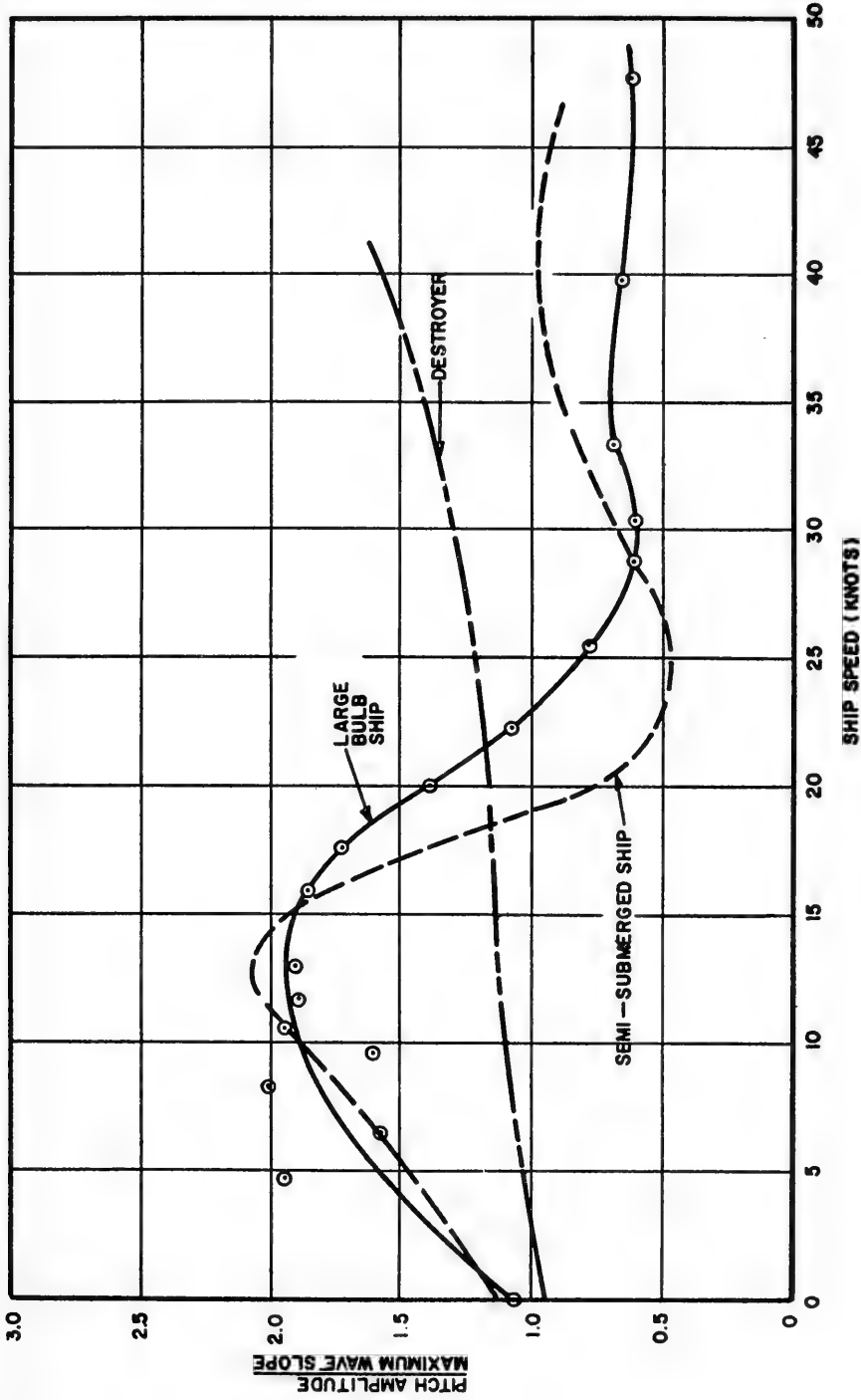
Fig. 8. Pitching motions in regular 2.0L waves
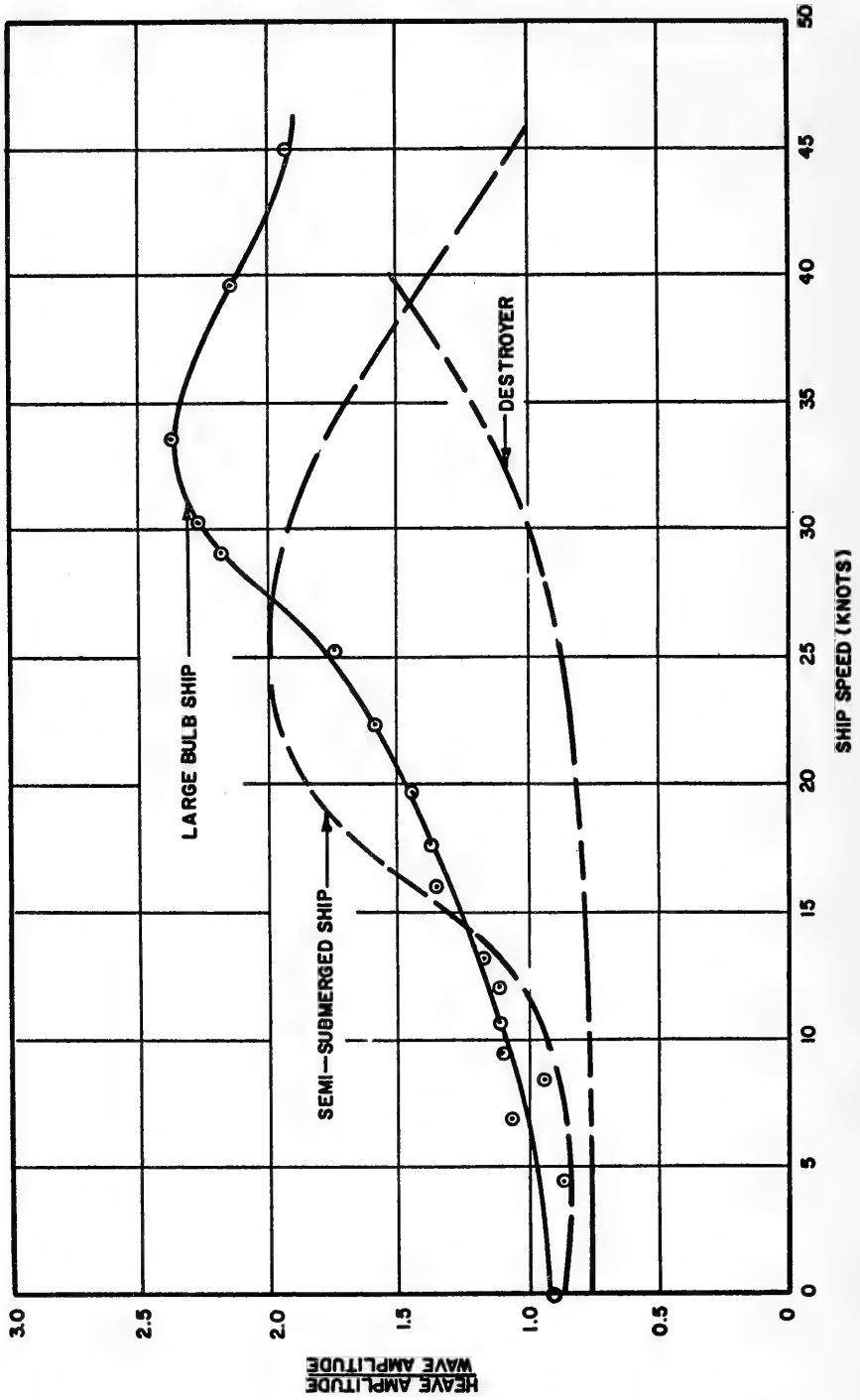
Fig. 9. Heaving motions in regular 2.0L waves

Before discussing control problems, it is important to consider in what way this craft would be better than a submarine. The question is, why should we take the trouble of having a strut piercing the surface, paying the penalty of additional resistance? In short, why not use a submarine? The answer is, for the moment at least, that there seems to be no doubt that the weight and size of nuclear power plants are greatly in excess of air-breathing plants of comparable power. In fact, the weight and space requirements of the present type of nuclear power plant seem to be two or three times as great as air-breathing plants. Furthermore, we have seen definite possibilities that the weight of air-breathing power plants can be further reduced. One of the most helpful developments here is the hydrofoil craft which, regardless of its own merits, is certainly stimulating the development of lightweight power plants that would make the air-breathing submarine even more advantageous.

Because the high-speed near-surface craft with surface-piercing strut (semisubmarine) has not been previously discussed in the literature and because of the many interesting technical problems associated with this type of ship, the balance of this paper will deal with this particular craft.

The appearance of the semisubmarine might be roughly as shown in Fig. 10. It would have a submarine-like hull, but not designed for high hydrostatic pressures. The strut would have to go high enough above the surface so that the crests of the waves would not cause difficulty. Its main function would be to take air down into the hull and carry exhaust gases out. It would be necessary to accept from the very outset the need for control devices, for we cannot expect it to run at a constant depth below the surface, even in calm water. The reason for this is, of course, that there are surface interaction effects. Any body moving at high speed, or even at moderate speed, below the surface experiences forces (which can be resolved into a moment and force) related to the wavemaking on the surface. These forces probably reach their maximum at the condition of maximum wavemaking resistance, but they are still present at very high speed. Fortunately, the effects at very high speeds appear tentatively to be generally favorable. To explore this problem at the Davidson Laboratory, simplified linear equations of motion have been set up and solved on an analog computer.
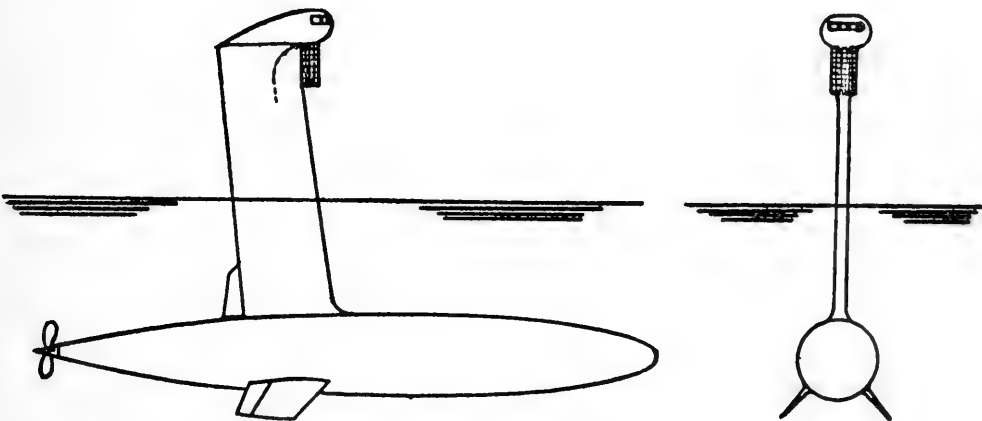
Fig. 10. High speed semisubmarine

Design Problems

It should be noted that the control of a semisubmarine involves more than a problem of stability in the usual sense. Suppose the heading of a stable ship is disturbed downward; if the craft is stable, it will steady down on a new course that will take it deeper and deeper. Similarly, if it is displaced upward, it will steady down on a new course upward so that it will eventually break surface. The ship should have a tendency to come back of its own accord to the original course and depth. This quality is here referred to as depth stability. It will be shown later that this can best be achieved by means of control surfaces with automatic control, which can keep the ship running level. This problem appears to be roughly the same difficulty as the control of completely submerged hydrofoils on a hydrofoil boat. It will be discussed in more detail in the next section.

If there is a large surface-piercing fin, or a smaller fin near each end of the craft, it may be expected that the increase or decrease of buoyancy associated with changes in immersion would assist in the depth control of the body. However, with a single minimum fin, the buoyancy effect appears to be small and reliance must be placed on dynamic control. A small amount of positive overall buoyancy would be desirable in the submerged condition for safety in case of power or control failure.

The next problem, after the consideration of maintaining a level course under a calm sea, is the behavior of the ship in a rough sea. Here we find that the head-sea case is no problem. The runs on the analog computer indicated that this particular design had a pitching period of about 20 seconds, or at least when it was disturbed it oscillated in a period of about 20 seconds, which is a sort of dynamic, natural pitching period. It signifies a very low response to outside disturbances, so that the high frequencies encountered in head seas will not cause motions of any consequence in the craft. However, in following seas we may expect that it will run into the critical zones of Fig. 1 of Ref. 7. The problem of providing vertical control so that the ship will run level or approximately so will be discussed further in the next section. In long waves it may be desirable for the ship to contour the surface, moving up and down, just as a hydrofoil craft must do.

Another problem to be investigated is that of lateral control and turning. A fore and aft location for the strut must be determined which, in combination with other fins, will provide satisfactory directional stability in a horizontal plane and at the same time will not lead to serious heeling in a turn. This problem can easily be investigated by the use of conventional model tests on a rotating arm. Recent work by Strumpf suggests that an arrangement of two fins as shown in Fig. 10 might be the most satisfactory solution in combination with the surface-piercing strut.

In addition to the purely hydrodynamic problems discussed, there are many other design problems to be solved, including the following:

1. Compact, lightweight air-breathing power plant,

2. Air supply and exhaust,

3. Structure of surface-piercing strut,

4. Static transverse stability,

5. Minimization of resistance by selection of optimum hull proportions and obtaining the best balance between depth and strut drag,

6. Automation of operation to minimize crew requirements.

Because of the high ship speeds and relatively low thrust loading considered, it does not appear difficult to obtain a conventional propeller of good efficiency. A single shaft should be used to obtain a high propulsive coefficient. There are virtually no limitations on propeller diameter (other than construction) and rpm may be selected to give a good efficiency along with low machinery weight. Submergence depth enters into the cavitation criterion to some degree, but there appears to be no difficulty in avoiding cavitation up to 45 or 50 knots. Cavitation is a problem for control surfaces, however.

The installation of a high-power propulsion plant dictates a minimum weight and space allowance. Gas-turbine main engines seem to satisfy these requirements. For naval purposes the ship must be able to achieve a high speed for short time intervals and must also be able to cruise at a considerably reduced speed for long time intervals. A single gas-turbine engine does not have the ability to operate efficiently over this considerable power range. Hence, to achieve high engine efficiency, multiple engines should be considered. At top speed all engines would be running. For this operation, engine life is a prime consideration. At low speed, fewer engines would be running and the idle ones could be disconnected from the reduction gear with a fluid coupling to facilitate maintenance and to eliminate windage losses.

The reduction gears to reduce the turbine shaft speed to a practical propeller speed involve very strict weight and, more important, space limitations. These considerations suggest an epicyclic gear train with high surface hardness and high K factor. This type of gear should have the ability to transmit power efficiently over a large range of powers. Even so, the gearing will undoubtedly be the largest single item of machinery weight.

Another possibility for reduced weight is to design a ducted type of propeller operating at very much higher rpm, perhaps in the supercavitating range. This would permit a drastic reduction of gear weight.

Air supply and turbine exhaust involve serious engineering problems to minimize pressure losses and yet keep the surface-piercing strut to minimum size. In any case, the ducting will certainly be a big item in machinery weight.

It is proposed that a compact control station be located at the top of the surface-piercing strut for good visibility. Permanent ballast of about 10 percent of displacement might be necessary to provide satisfactory static transverse stability.

Basic trends of semisubmarine characteristics have been studied in a preliminary way in connection with work of the Panel on Naval Vehicle Systems, Undersea Warfare Committee, National Academy of Sciences-National Research Council. Tentative design features of a series of craft of varying size were worked out on the basis of certain assumptions regarding technical potentialities [10]. These assumptions will be summarized before presenting the results.

Resistance

Resistance was estimated from model tests of simple bodies of revolution, with axes 1-1/4 diameters below the surface. An Ogive strut was selected, the size was established by the estimated engine air requirements. A length of 14 percent of ship length was used for the series. Strut resistance was calculated from Ref. 11, neglecting the elimination of tip losses by the attachment of the strut to a hull. The characteristics that were selected were not necessarily optimum.

The complication of a controllable pitch propeller was not considered necessary; however, for backing and for emergency propulsion, small auxiliary screws were assumed driven by medium-speed diesels. The speed that can be achieved with this propulsion will be around 5 or 6 knots.

For these tests the following characteristics were selected.

Hull-Form Coefficients — Length/beam ratio = $L/B = 7.0$; submergence beam ratio = $h/B = 1.25$ (to centerline); prismatic coefficient = $C_p = \nabla/(\pi/4)\,B^2 L = 0.650$; wetted surface coefficient = $K_s = W.S./\pi BL = 0.774$.

Ogive-Strut Coefficients — Thickness/chord ratio = $t/c = 0.167$; submergence/chord ratio = $h/c = 1.30$; $c/L = 0.139$.

Machinery — Main engines: GE converted aircraft engines, type MS240B, MS240A, 6000 rpm; reduction gears: double reduction, epicyclic type, small with low weight (estimated on the basis of Timmerman second reduction gears); overall fuel consumption: 0.55 /SHP-hr at $V = 45$ knots and 0.58 /SHP-hr at $V = 20$ knots.

Propulsion — For this study the top speed was chosen at 45 knots and the cruising speed at 20 knots. The propeller and propulsion characteristics chosen (not necessarily optimum) were as follows:

	$\Delta = 6000$	$\Delta = 3000$	$\Delta = 1500$	$\Delta = 750$
Propeller diameter	21.5 ft	16.8 ft	13.4 ft	10.0 ft
Shaft rpm	200	250	300	400
Propeller efficiency at 45 knots	74%	75%	76%	76%
Assumed hull efficiency	140%	120%	120%	120%

The appendage resistance allowance chosen was 10 percent in all four cases. All propellers were checked for avoidance of cavitation.

Weights

Assumed hull, machinery weights, and other data are shown in Table 2.

For any vehicle, whether for military or commercial service, the basic characteristics of interest are speed, range, and payload. Various types of plots can be prepared to show the relationship among these variables for different craft. However, for ASW purposes the particular need seems to be for a top speed between 45 and 50 knots and a cruising speed between 15 and 20 knots. Hence, in the present study fixed speeds have been assumed and trends have been determined of range versus payload for a family of vehicles of different sizes. The results are shown in Fig. 11.

The plot shows that for fixed speed and size, the payload available for weapons, detection gear, etc., varies inversely as range. And for any given range, the larger the ship the greater the payload must be. To be more specific, it appears that a 1500-ton craft for

Table 3
Weight Data for Semisubmarine Series [10]

Displacement (Δ) in tons	6000	3000	1500	750
Length (L) in feet	272	216	171.5	136
Beam (B) in feet	38.8	30.8	24.4	19.4
SHP	130,000	70,000	40,000	25,000
Weights in Tons				
Steel weight (0.35 Δ)	2100	1050	525	262
Outfit weight (0.10 Δ)	600	300	150	75
Salt-water ballast (0.05 Δ)	300	150	75	38
Lead ballast + margin (0.10 Δ)	600	300	150	75
Main propeller machinery	300	183	114	82
Crew and all stores	71	56	43	32
	3971	2039	1057	564
Deadweight = payload + fuel	2029	961	443	186
More Optimistic Design*				
Payload + fuel	2820	1360	655	299

*All weights reduced by 20 percent.

example, could perhaps carry a payload of about 100 tons over a range of 2500 to 4500 miles (including 10 hours at 45 knots). The larger ships could carry much more.

Even better results and higher speeds might be attained with high-rpm and supercavitating propellers. Although the design data given are only tentative, it is hoped that the suggested trends show the potentialities of unusual naval craft if the same level of technical effort is applied as in current hydrofoil boat designs.

CONTROL OF NEAR-SURFACE BODIES

The depth control of a body moving at high speed below, but close to, the water surface is an interesting problem. Therefore, it may be of value to summarize the theoretical work carried out so far for both the calm-water and following-wave cases. It is hoped that this will serve to clarify the problem and to specify areas that require research.

Dynamic Stability in Calm Water

The following analysis considers only small disturbances of equilibrium conditions, which the craft is assumed to have when proceeding at a constant speed (U) along a path
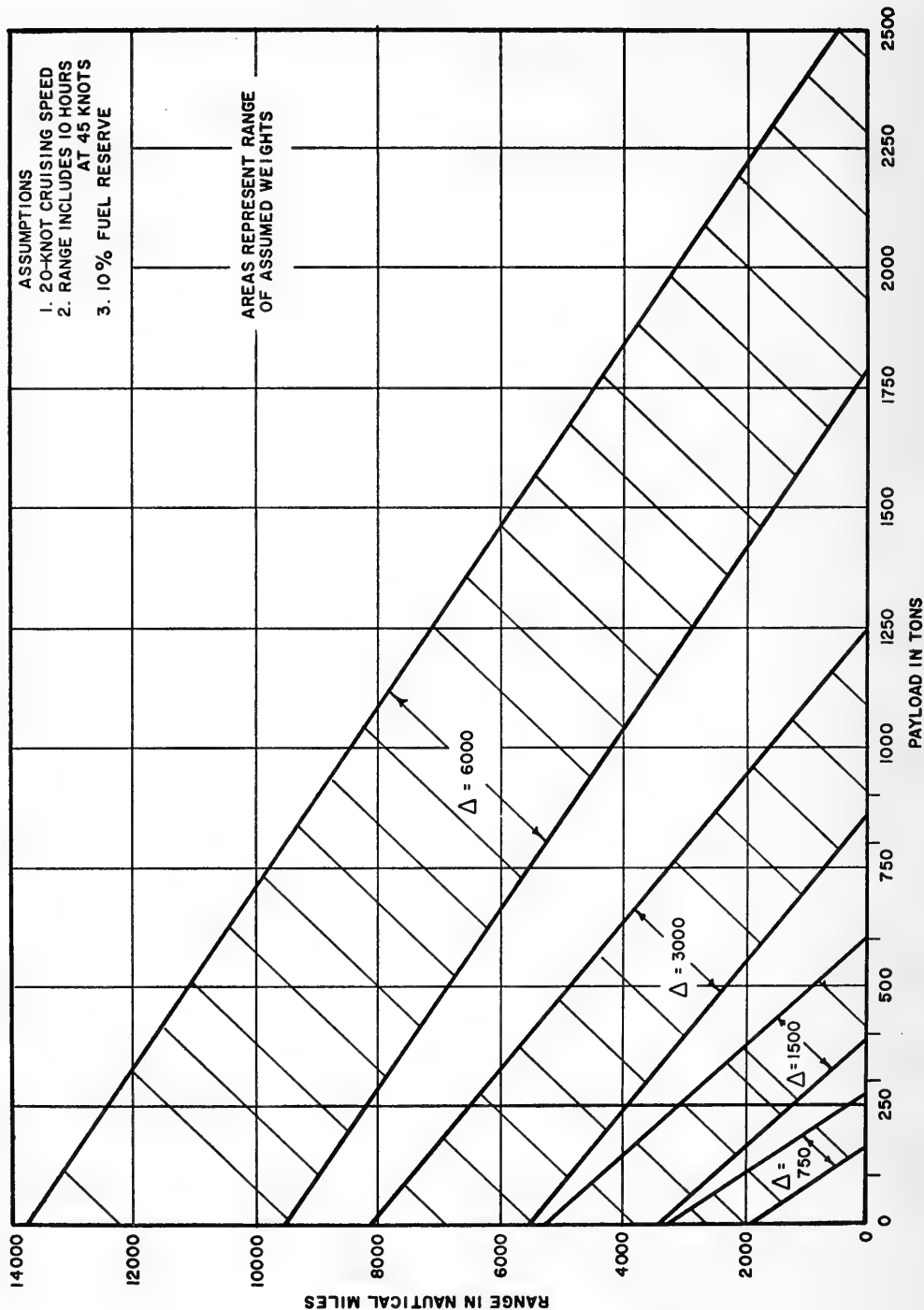
Fig. 11. Payload as related to range of a semisubmarine

$(z_o = h)$ parallel to the undisturbed free surface. For the heave and pitch analysis assume that there are no lateral excursions.

Stated briefly, the equations of motion for heave and pitch are

$$m'(\dot{w}' - q') = Z'(w', q', \dot{w}', \dot{q}', \dot{z}_o, \theta) \tag{2}$$

$$I'_y \dot{q}' = M'(w', q', \dot{w}', \dot{q}', z'_o, \theta) \tag{3}$$

where m' is the nondimensional mass of the craft $(2m/e\ell^3)$, w' is the vertical velocity of the center of gravity in fraction of speed (U, positive downward), q' is the nondimensional angular velocity about the transverse (y) axis, z'_o is the instantaneous distance from the free surface to the center of gravity in fraction of the length of the craft (ℓ, positive downward), θ is the pitch angle (positive nose-up), I'_y is the nondimensional mass moment of inertia about the y axis $(I'_y = I_y/(e/2)\ell^5)$, Z' is the nondimensional total vertical force (force $1/2e\ell^2 U^2$), M' is the nondimensional total pitching moment (about the y axis), and the dots above a symbol indicate differentiation with respect to nondimensional time $(s = Ut/\ell)$.

Motion near the free surface induces forces and moments that are dependent upon the distance (x_o) and possibly on the pitch angle (θ). These dependencies are, of course, not present when the ship is deeply submerged.

When the ship is near the free surface, the force and moment become dependent on z_o. There is also a possible dependence of the force and moment upon θ, which does not arise in the case of deeply submerged bodies. In view of the dependence on depth below the surface, it is advantageous to write the equations with respect to an axis system (x_o, y_o, z_o) that is fixed in the free surface, rather than with respect to a system (x, y, z) that is fixed in the body as is usually done. Expanding the right sides of Eqs. (2) and (3) in Taylor expansion and retaining only the linear terms yields:

$$(Z'_{\dot{w}} - m')\ddot{z}_o + Z'_w \dot{z}'_o + Z'_{z_o} z'_o + Z'_{\dot{q}}\ddot{\theta} + (Z'_q + Z'_{\dot{w}})\dot{\theta} + (Z'_w + Z'_\theta)\theta = 0 \tag{4}$$

$$M'_{\dot{w}}\ddot{Z}'_o + M'_w \dot{Z}'_o + M'_{z_o} Z'_o + (M'_{\dot{q}} - I'_y)\ddot{\theta} + (M'_{\dot{w}} + M'_q)\dot{\theta} + (M'_w + M'_\theta)2 = 0 \tag{5}$$

where all the coefficients are derivatives with respect to the indicated subscripts (except m and I_y). To obtain Eqs. (4) and (5), the kinematic relation between the motion referred to axes fixed in the craft and those fixed in the water surface has been used; therefore,

$$w = \dot{z}_o + \theta, \quad \text{and} \quad q = \dot{\theta}.$$

In principle, these equations can be solved analytically, but the results are somewhat unwieldy. They can also be solved on an analog computer. In our study we have attempted to glean some understanding from the analytical approach and have also used an analog for more rapid exploration of the influence of fin area and control on the response of the body when disturbed as it cruises at 30, 40, and 60 knots at a depth of 1.25 diameters (to the centerline). The following discussion will first reveal what has been learned from the hand-turned mathematics and will be followed by a recounting of the results of the analog studies.

Equations (4) and (5) represent a pair of linear coupled equations in z_o and θ of the form

$$L_1 z_o + L_2 \theta = 0$$
$$L_3 z_o + L_4 \theta = 0 \tag{6}$$

where $L_{1,\ldots,4}$ are the linear second-order operators displayed in Eqs. (4) and (5). The solution for either z_o or θ involves integration of single, fourth-order, linear differential equations of the following form:

$$(L_1 L_4 - L_2 L_3) \begin{Bmatrix} z_o \\ \theta \end{Bmatrix} = 0 \tag{7}$$

where (upon omission of the primes and the subscript o on z)

$$
\begin{aligned}
L_1 &= (Z_{\dot{w}} - m)D^2 + Z_w D + Z_z \\
L_2 &= Z_{\dot{q}} D^2 + (Z_q + Z_{\dot{w}})D + (Z_w + Z_\theta) \\
L_3 &= M_{\dot{w}} D^2 + M_w D + M_z \\
L_4 &= (M_{\dot{q}} - I_y)D^2 + (M_{\dot{w}} + M_q)D + (M_w + M_\theta)
\end{aligned}
\tag{8}
$$

and $D = d/ds$.

Thus, the equations for z and θ are in the form

$$(aD^4 + bD^3 + cD^2 + dD + e) \begin{Bmatrix} z \\ \theta \end{Bmatrix} = 0 \tag{9}$$

and the solutions are of the form

$$z = h + \sum_{i=1}^{4} z_i e^{\sigma_i s}; \qquad \theta = \sum_{i=1}^{4} \theta_i e^{\sigma_i s} \tag{10}$$

where h is the original depth and the σ_i's are the roots of the quartic equation

$$a\sigma^4 + b\sigma^3 + c\sigma^2 + d\sigma + e = 0. \tag{11}$$

For stability, or no exponential divergence, a, b, c, d, and e must each be greater than zero. In addition, for no oscillatory divergence

$$bcd - (ad^2 + b^2 e) > 0.$$

The last inequality is Routh's discriminant, which requires the real parts of all complex roots to be positive.

At this point we must note that stability as used here refers to directional and depth stability, that is, depth stability means that after an arbitrary excursion in either z or θ,

$$z \to h \quad \text{as} \quad t \quad \text{or} \quad s \to \infty$$

and directional stability means

$$\theta \to 0 \quad \text{as} \quad t \quad \text{or} \quad s \to \infty.$$

This is to be distinguished from the case of the deep-operating submarine, where the body is considered stable as long as it does not go into a diverging trajectory but settles on a new path that is straight but not in the same direction as that prior to the disturbance.

If we note that $M_{\dot{w}}$, $Z_{\dot{q}}$, M_θ are small and that $Z_\theta = 0$ (as may be proved for the doubly symmetric body under consideration) the coefficients of the characteristic equation take on the relatively simple form

$$a = 1$$

$$b = -\left(\frac{Z_w}{M_2} + \frac{M_q}{N_y} \right)$$

$$c = \frac{1}{M_2 N_y} \left[M_q Z_w - M_w \cdot (m + Z_q) \right] - \frac{Z_z}{M_2} \tag{12}$$

$$d = \frac{1}{M_2 N_y} \left(M_q Z_z - M_z Z_q \right)$$

$$e = \frac{1}{M_2 N_y} \left(M_w Z_z - M_z Z_w \right)$$

where $M_2 = m - Z_{\dot{w}}$, the virtual mass in direction z, and $N_y = I_y - M_{\dot{q}}$, the virtual mass moment of inertia.

It can be noted that a, b, and c are the same as will be found in the equation of motion for the deeply operating body, with the exception of the term $-Z_z/M_2$. The quantity d is seen to be an effective damping coefficient that is arrived at by coupling the damping force and moment derivatives with the free-surface force and moment derivatives, and e is an effective spring constant arrived at by a similar coupling of the static force and moment derivatives with Z_z and M_z. It is now necessary to say something about the characteristic of Z_z and M_z as functions of Froude number [12]. The force rates (Z_z and M_z) arise from the asymmetry of flow about the body when it is moving parallel to the water surface. At very low

Froude numbers, the surface acts as a rigid ceiling, which causes a suction or attractive force and virtually zero moment. This attractive force is considered negative because the positive direction is downward. Because this attractive force becomes less negative as z increases, Z_z is positive at low Froude numbers. At high Froude numbers, the reverse is true, that is, the force is one of repulsion and Z_z is negative. The force rate changes sign at a Froude number of $F = U\sqrt{g\ell} = 0.55$. Again, with increasing Froude number the moment changes from a small bow-up moment ($M_z < 0$) at low Froude numbers, to a bow-down moment ($M_z > 0$) for all Froude numbers greater than about 0.33.

Physically, the vertical attractive force at low Froude numbers tends to be destabilizing because any excursions toward the free surface will cause this force to increase. At high Froude numbers, the repelling effect is stabilizing. If we consider the effect of M_z in the absence of the force, then the moment is destabilizing at low Froude numbers and stabilizing at high Froude numbers in regard to simple exponential divergence. However, large values of M_z can lead to oscillatory divergence or instability.

The magnitudes of Z_z and M_z at 30 knots ($U/\sqrt{g\ell} = 0.62$) are significantly different from their values at 40 and 60 knots so that we may expect, and do find, a considerable difference in the stability or the fin area required for stability over this speed range. Although, other derivatives can be expected to be Froude-number dependent, such as M_w, M_θ, $M_{\dot{q}}$, Z_w, and $Z_{\dot{w}}$, they have very weak variations with Froude number at the submergence ratio and over the Froude numbers considered.

Exponential Instability

To establish stability criteria, consideration must be given to the requirement that each of the coefficients a, b, c, d, and e of the quartic equation in σ be positive. Equation (12) shows that a and b are positive; Z_w and M_q are both negative. Figure 12 is a graph of b as a function of tail area; note that b is large.

The coefficient c is composed of three terms; the last term is found to be small and, because the two remaining terms are composed of those derivatives which are considered to be independent of Froude number, the relation for stability arising from $c > 0$, that is,

$$M_q Z_w - M_w(m + Z_q) > 0 , \tag{13}$$

is exactly that required for the body when operating deeply submerged. Figure 13 is a graph of c as a function of fin area; a fin area of 220 ft^2 is the minimum required to prevent exponential divergence. In computing the changes in the various coefficients as a function of fin or tail area, a conservative lift rate of 2.0 was chosen to take into account the attrition expected from partial cavitation.

An inspection of the equation

$$d = \frac{1}{M_2 N_y} \left(M_q Z_z - M_z Z_q \right) \tag{14}$$

shows it to be positive for high Froude numbers but negative for those ranges of low Froude numbers where M_z is negative. Thus, this term can cause exponential divergence at low
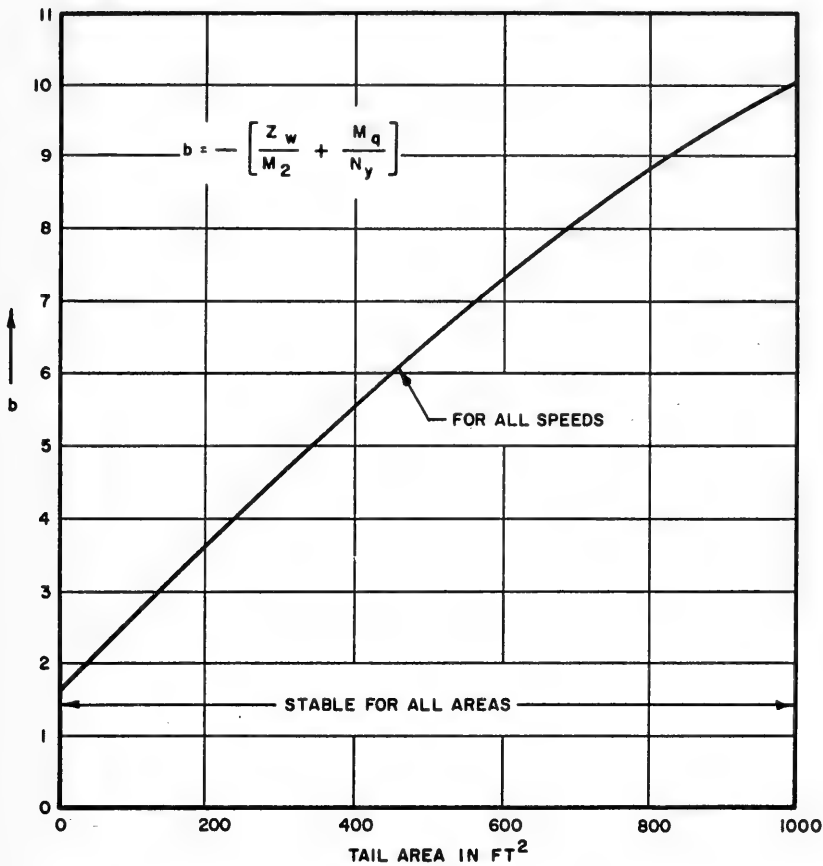
Fig. 12. Coefficient b versus tail fin area

Froude numbers but is not troublesome in regard to this type of instability at high Froude numbers. However, for Froude numbers where M_z is maximum, the attending increase in d can contribute to oscillatory instability. Figure 14 is a graph of d as a function of tail area.

The coefficient

$$e = \frac{1}{M_2 N_y}\left(M_w Z_z - M_z Z_w\right) \tag{15}$$

is negative for zero tail area. Figure 15 shows that the minimum tail area to prevent exponential divergence at 60 knots is 255 ft^2. Thus, the free-surface effects at high speed require a bit more tail area than the condition imposed by c for deep operation.

Oscillatory-Exponential Instability

If a pair of the roots of the quartic characteristic equation are complex, either damped or undamped sinusoidal oscillations will occur subsequent to an initial disturbance, depending
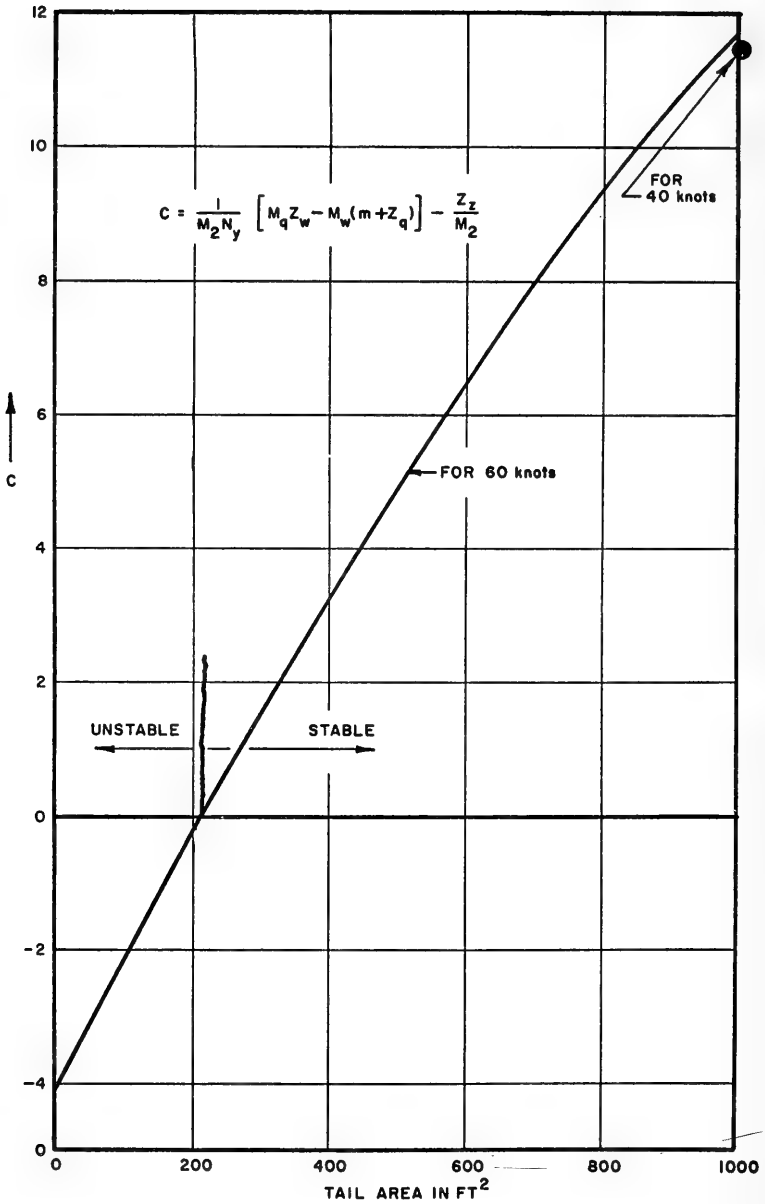
Fig. 13. Coefficient c versus tail fin area
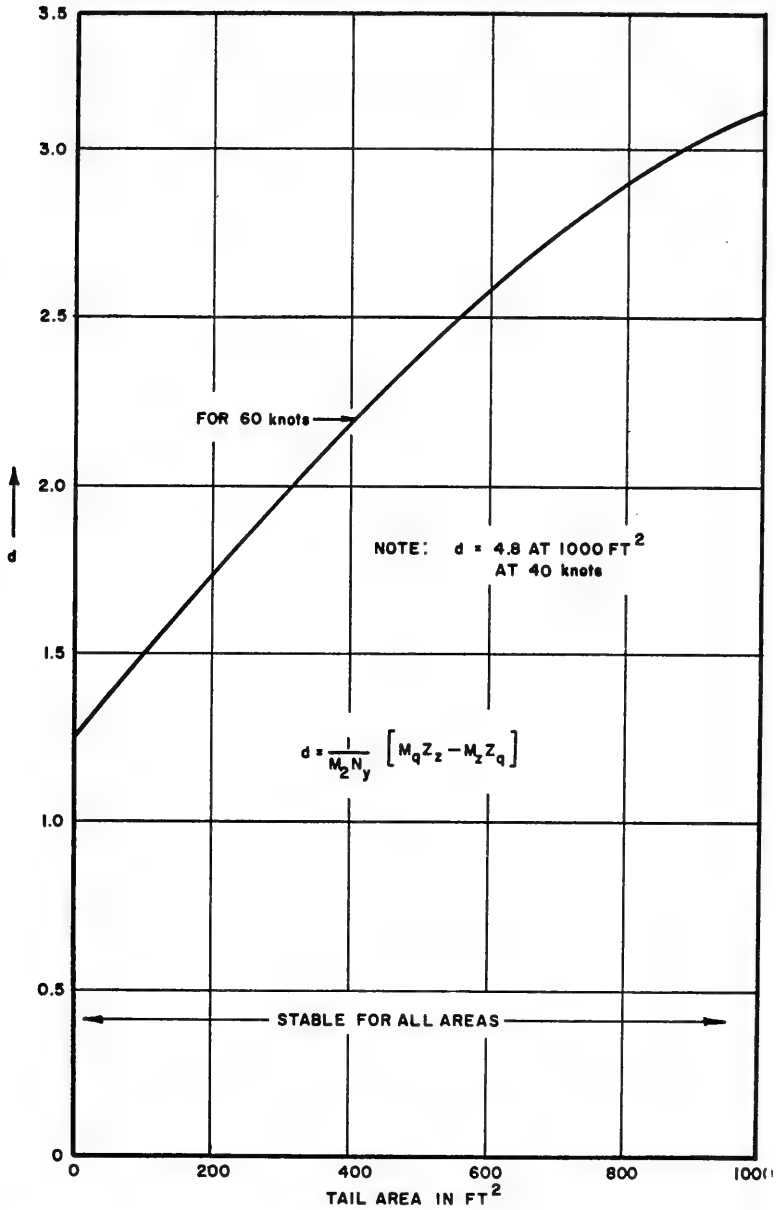
Fig. 14. Coefficient d versus tail fin area

The figure shows a graph with d on the vertical axis (ranging from 0 to 3.5) and TAIL AREA IN FT^2 on the horizontal axis (ranging from 0 to 1000).

FOR 60 knots

NOTE: $d = 4.8$ AT 1000 FT^2 AT 40 knots

$$d = \frac{1}{M_2 N_y} \left[M_q Z_z - M_z Z_q \right]$$

STABLE FOR ALL AREAS
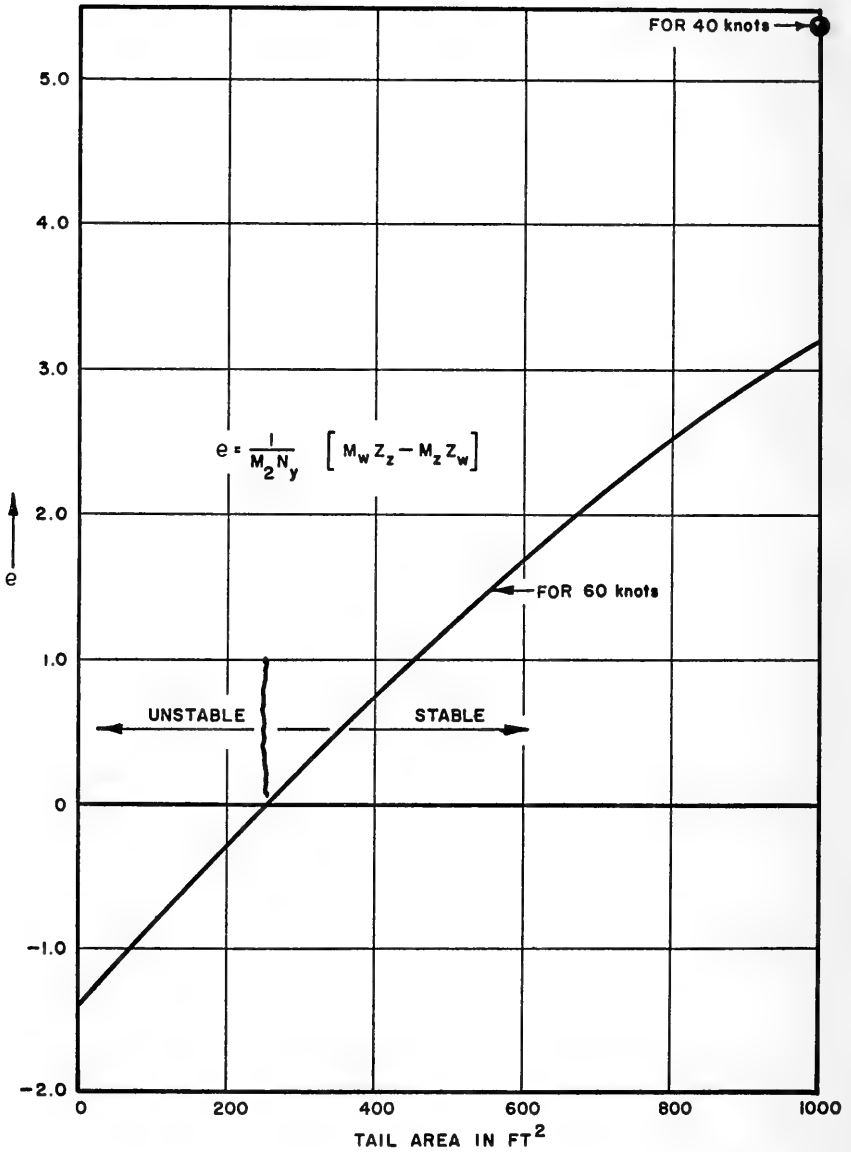
Fig. 15. Coefficient e versus tail fin area
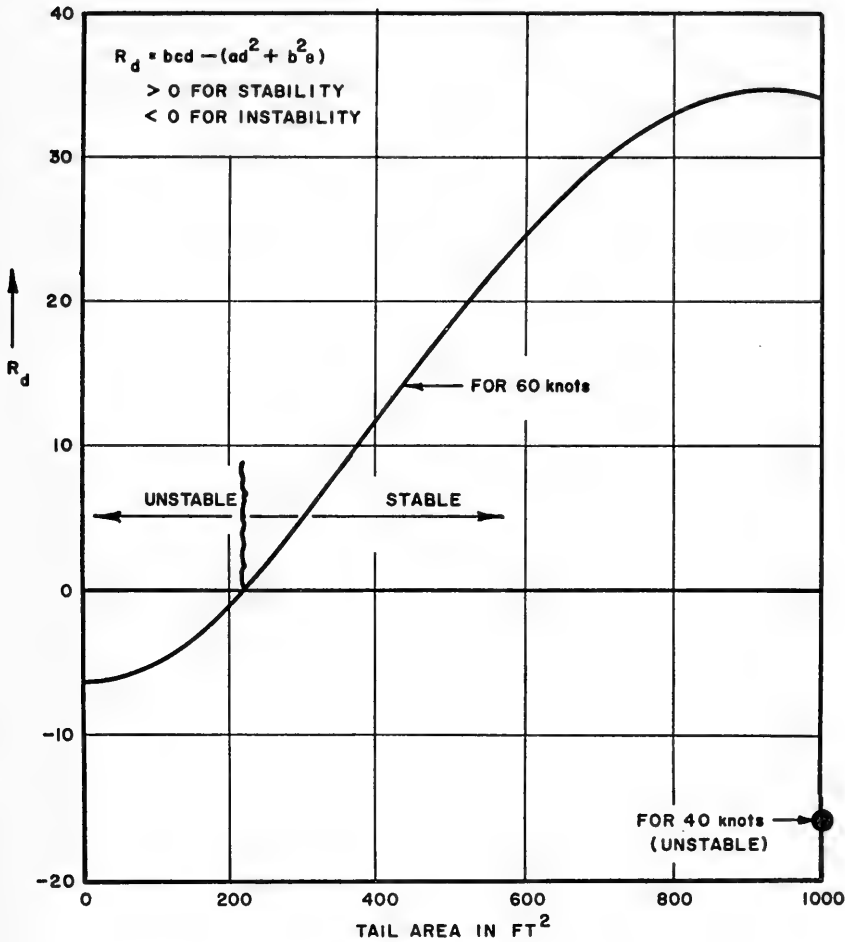
Fig. 16. Variation of the condition for oscillatory stability, R_d

upon whether the sign of the real part of this complex root is negative or positive. Routh's discriminant (R_d) provides the following relationship, which the coefficients must satisfy for stability.

$$R_d = bcd - (ad^2 + b^2e) > 0. \tag{16}$$

It can be seen that the quantities d and e, which represent coupling of the free surface effect with the body damping and static force rates must not become overly positive or the product bed will be overcome and oscillatory instability will result. Inspection of Fig. 16 shows that Routh's discriminant is positive at 60 knots for tail areas greater than 200 ft^2, but that even a tail area of 1000 ft^2 is insufficient at 40 knots. The loss of stability with decreasing speed is due mostly to the large change in M_z which, with some assistance from Z_z, produces a 12-fold change in the coefficient e, thus making it much more positive (even for a tail area of 300 ft^2) and resulting in a negative value for Routh's discriminant. It is also to be noted that increasing b, which is really the deep-water effective damping coefficient (depending on Z_w and M_q), will cause oscillatory divergence. This is also a

surprising result, which stems from the coupling of the body coefficients with the free sur-
face spring terms (M_z and Z_z). Thus, making the body overly stable for deep operation pro-
vides a very stiff effective spring coefficient (e), which appears to be most responsible for
divergent oscillatory oscillations.

Results of Analog Studies

Exploration of the influence of fin area, distribution of fin area, the sensitivity to cer-
tain coefficients, and the effectiveness of control can quickly be assessed by an analog com-
puter. The results of such studies are discussed in the following subsections.

Responses with Fixed Fin Areas — Results of the analog studies of responses with fixed
fin areas can be friefly summarized as in Table 3.

Table 3
Analog Computer Results for Fixed Fin Areas

Speed (knots)	All Fin Area Aft	3/4-Area Aft, 1/4-Area Forward	1/2-Area Aft, 1/2-Area Forward
Fin Area = 300 ft^2			
30	Divergent oscillations	—	—
40	Divergent oscillations	—	—
60	Damped oscillations	—	—
Fin Area = 1000 ft^2			
40	Slightly divergent oscillations	Damped oscillations	Divergent oscillations
60	Lightly damped oscillations	—	Heavily damped oscillations

Since the case of 300 ft^2 of fin area has been discussed, the following remarks will be
directed toward giving some rationalization of the curious result of very slight stability at
60 knots with 1000 ft^2 of fin area aft as compared with very marked stability when this area
is split into half forward and half aft. To begin with, this large area was selected as an
intuitive attempt to stabilize against the oscillatory instability at 30 knots without regard to
its implications on the stability of the deeply operating submarine. An inspection of the
criterion of stability for deep operation,

$$M_q Z_w - M_w(m + Z_q) > 0 ,$$

which is essentially the quantity c, shows that by adding too much tail fin, $m + Z_q$ can be
made negative (by making Z_q so negative that it overwhelms m) and, at the same time,

making M_w change from positive to negative so that the second product in the above inequality contests with the magnitude of the positive product $M_q Z_w$. Thus, it is possible to alter the stability in deep operation little beyond a certain maximum by a piling-on of fin area. At the same time, the quantity b increases enormously, and though b plays a minor role in determining stability in the deep operating case, in this case of coupled motion in the neighborhood of the free surface, it is very disadvantageous to make b large. This can be seen by again referring to Routh's discriminant

$$bcd - (ad^2 + b^2 e) > 0$$

which shows that the quadratic behavior of b can be overriding, provided the value of e is not too small.

As we take area from the stern and put it on the bow, c decreases only about 20 percent, b is large and does not change, and e decreases by a factor of 8 (d changes but is not decisive). Thus, the role of M_w (which has, with equal areas forward and aft, a destabilizing tendency with regard to deep operation) is to provide a much softer effective spring value e to this fourth-order system and thus permit quick decay of oscillations.

Control Effectiveness — The foregoing has shown that exponential instability will exist at Froude numbers below 0.3, that excessive tail area is not the answer at $F \approx 0.6$, and that reasonable tail area will only stabilize at $F \approx 1.2$ (which corresponds to an unlikely speed of 60 knots). This leads to the necessity of applying controls that obviously would be needed anyway for rough-water operation. A systematic study of the effectiveness of controls proportional to z, $\dot{z}$, θ, and $\dot{\theta}$ could and should be made to arrive at the best combination. In view of the shortness of time available for this study, computer runs were made only for a control function proportional to $\dot{\theta}$. An all movable control area of 300 ft^2 is considered to be actuated without time lag according to the equation

$$\text{Tail Angle} = \delta = k\dot{\theta}'.$$

When the gain factor k was varied to determine a suitable value, it was found that $k = 1.0$ is just enough at 30 knots to prevent divergent oscillations and that a value of $k = 2.0$ gives good control, requiring a tail angle of about twice the maximum pitch angle. Results of computer runs for this gain factor ($k = 2$) at different speeds are as follows, the values listed being the ratios of amplitudes of any cycle to that of the previous cycle:

Speed (knots)	$k = 1$	$k = 2$
30	0.92	0.35
40	0.30	critical damping
60	critical damping	critical damping

It therefore appears possible to control the craft in calm water over the speed range investigated by means that are quite reasonable. A more thorough analysis that involves the use of z, $\dot{z}$, and θ may well reveal a still more effective means to achieve controllability.

Sensitivity of the Analysis, and Recommendations Regarding Stability and Control — Runs were made on an analog computer to investigate the sensitivity of the response of the

stable system to variations in the virtual (or effective) mass and virtual mass moment of inertia. It was found that the rate of decay of stable oscillations is not sensitive to virtual mass nor to virtual moment of inertia, which is in contrast to studies on deeply submerged bodies. Also for the case of 60 knots with 300 ft^2 of tail area, the sensitivity of the response to variations of M_w' and Z_w' of ±20 percent was determined and found to be quite small. Because several of the stability characteristics of this craft are so profoundly different from those for which experience has been built up, it would seem worthwhile to conduct model tests to check the predictions made here and at the same time to widen the scope of the study. This might be done through the use of an ultrasensitive motion-following apparatus or with the use of freely operating models. Certainly, the stability in the horizontal plane will be very important, particularly in view of the excitation in roll and yaw that will be provided by the long strut. These programs should be backed up by rotating-arm experiments to determine static and rotary derivatives near the surface and also by oscillator tests to determine the influence of heave and pitch frequencies. Seaworthiness investigations must also be made, particularly for the case of following seas, where critical operation may be encountered.

CONCLUSIONS

The possibilities of small, fast ships operating on or near the surface appear excellent.

To permit the design and development of such craft, energetic research should be undertaken in the following hydrodynamic problems:

1. Propulsion by means of high-rpm machinery,

2. Drag of surface-piercing struts,

3. Forces and moments on high-speed bodies near the surface,

4. Depth control of near-surface bodies in following waves,

5. Optimization of control surface arrangements on submerged bodies,

6. Lateral control of a near-surface body with surface-piercing strut.

Parallel research and development should be carried on in other areas that affect the design of high-speed craft, particularly in the area of lightweight power plants.

The Navy should be encouraged to design and build experimental limited-purpose ships, not intended to undertake normal operational duties in the fleet. These ships would be of inestimable value in guiding future research, development, and design.

ACKNOWLEDGMENTS

REFERENCES

[1] Boericke, H., Jr., "Unusual Displacement Hull Forms for Higher Speeds," International Shipbuilding Progress, Volume 6, 1959

[2] Mandel, P., "The Potential of Semi-Submerged Ships in Rough Water Operation," New England Section Paper, Soc. Nav. Architects Marine Engrs., Mar. 1960

[3] Lewis, E.V., and Odenbrett, C., "Preliminary Evaluation of a Semi-Submerged Ship for High-Speed Operation in Rough Seas," Davidson Laboratory Report No. 736, Mar. 1959

[4] Lewis, E.V., "Possibilities for Reducing Ship Motions at Sea," J. Amer. Soc. Naval Engrs., Nov. 1958

[5] Lewis, E.V., "Ship Speeds in Irregular Seas," Trans. Soc. Nav. Architects Marine Engrs., 1955

[6] St. Denis, M., and Pierson, W.J., "On the Motions of Ships in Confused Seas," Trans. Soc. Nav. Architects Marine Engrs., 1953

[7] Mandel, P., "Subcritical and Supercritical Operation of Ships in Waves and the Coincidence of Maximum Damping," J. Ship Research, June 1950

[8] Numata, E., and Lewis, E. V., "An Experimental Study of the Effect of Extreme Variations in Proportions and Form on Ship Model Behavior in Waves," ETT Report 643, Dec. 1957

[9] Wigley, W.C.S., "Ship Wave Resistance, A Comparison of Mathematical Theory with Experimental Results," Trans. INA, 1926

[10] Lewis, E.V., and Garland, C., "A Preliminary Parametric Study of High-Speed Schnorkel Submarines," Davidson Laboratory Note 582

[11] Breslin, J.P., and Velleur, J.W., "The Hydrodynamic Characteristics of Several Surface Piercing Struts, Part I, Analysis of Drag at Zero Yaw," ETT Report 596, Jan. 1956

[12] Wigley, W.C.S., "Water Forces on Submerged Bodies in Motion," Trans. INA, 1953

DISCUSSION

H. N. Abramson (Southwest Research Institute, San Antonio)

The subject of this Symposium is, of course, devoted to problems of hydrodynamics of high performance ships. Thus far during the Symposium, however, I have heard a great number of discussions concerning economics and propulsion and even some structural topics, as well, and therefore I hope the organizers of the Symposium will not chastise me too greatly if I too digress, if only briefly. I hope that the authors will also forgive me if I give you a little story that is incidental, more or less, to the subject of the paper, but which, nevertheless, has some bearing. One final remark by way of introduction: The paper by Professor Mandel was on the hydrodynamics of a deep-diving submarine, which design was carried

through at my Institute. I hope that by my discussion, which is going to be very brief, you will not get the impression that our institute is concerned only with such very unusual types of vessels.

What I want to get to is the following consideration: The common yellow mineral known as sulphur exists in great abundance throughout the world, particularly along the gulf coast of the United States and Mexico, and in France and Italy. Sulphur is mined by the so-called Frasch process in which hot water is pumped down into the ground and the sulphur is forced out in molten form. This sulphur is then usually piled up in very large heaps in which it solidifies. Then one places a dynamite charge in the sulphur and blows off big chunks which are then loaded either on barges or on railroad cars and transported to other parts of the world. We began to think of a different means of transporting sulphur and for this we needed to know something about its structural properties, but we found out that even the largest sulphur producers in the world had little or no knowledge concerning the mechanical properties of sulphur. To make a long story short, sulphur is as strong as fairly high-grade Portland cement concrete: it has a very high compressive strength and a moderately good tensile strength. Our idea was, and we have investigated only certain of the economics involved here, to bring the sulphur up in molten form and to cast it in the form of a ship or boat and "sail" it to some other port or destination.

Because of its high compressive strength sulphur has some desirability for a semisubmerged boat. Unfortunately, its low tensile strength would require some reinforcing material, but since we had concrete barges during the war, why not a sulphur barge? To reduce wave impact forces and to improve operation in rough seas, why not a semisubmerged boat made of sulphur? It might be found rather than self-propelled, perhaps in train, and thus result in very large savings in transportation costs.

So, while I am not talking about particularly high performance ships of the semisubmerged type, and while I am talking about commercial aspects rather than military, I thought you might be amused by these speculations and considerations, bearing somewhat on the subject of semisubmerged ships, that we have been talking about. The stability studies and other considerations of the authors will certainly be of extreme interest to us if we pursue this subject further.

*   *   *

DESIGN DATA FOR HIGH SPEED DISPLACEMENT-TYPE HULLS AND A COMPARISON WITH HYDROFOIL CRAFT

W. J. Marwood and A. Silverleaf
National Physical Laboratory
Teddington

This paper is intended as a preliminary design guide and as a prelude to a more comprehensive research programme on high speed displacement-type hulls.

It includes a short survey of available NPL data on the resistance, propulsion, and running performance of this type of hull and a brief discussion on the shallow water effect.

The research programme planned at NPL is outlined and a description given of the first of a series of torsionmeters designed at NPL specially for use on trials of small high speed craft.

Finally some estimates are given of the power requirements of a suggested form of mixed craft in which the total weight is supported partly by the buoyancy of the hull and partly by fully submerged hydrofoils.

INTRODUCTION

Many small boats, such as patrol launches, work boats, and pleasure craft, operate at speed/length ratios of 1.2 to 3.5 (or Froude number F_n about 0.4 to 1.2). These boats traditionally have round-bilge displacement hulls, but there is very little published information about them to help their designers. While systematic series of model experiments have been made for most types of larger vessels, the relatively high cost of model tests has made it difficult to persuade owners and builders of small high speed boats to commission model experiments for new designs. Consequently there has long been a tendency to base hull designs for small boats on previous forms presumed to have been successful, without any proper basis for assessment of performance.

This paper is intended as a preliminary design guide and as a prelude to a more comprehensive research programme on this type of hull form which is being carried out at the Ship Hydrodynamics Laboratory of Ship Division, NPL; the large high-speed towing tank there will enable experiments to be made in better conditions than previously, including systematic measurements in head and following seas. The present paper is a short survey of available NPL data on the following aspects of the design of high speed displacement-type hulls:

1. Resistance of Round-Bilge Forms

   (a) Average results for models
   (b) Effect of beam/draft ratio and *LCB* position

       (c) Appendage resistance
       (d) Effect of changes in scale.

   2. Propulsion

       (a) Components of propulsive efficiency
       (b) Ship-model comparison.

   3. Running Performance

       (a) Effect of spray strips
       (b) Design of a round-bilge form for good seakeeping.

   4. Shallow Water Effects.

This account of the information available at present is followed by an outline of the programme of research now commencing at NPL, and by a description (in the Appendix) of the first torsionmeter specially designed at NPL for power measurements on small boats.

High speed hydrofoil boats are not uncommon, and are being actively developed at present. However, the use of hydrofoils to give partial lift to heavy displacement-type high speed boats operating at speeds less than the planing speed is not well-established. Some preliminary estimates of the value of such devices are given in this paper.

RESISTANCE OF ROUND-BILGE FORMS

Normal round-bilge hull forms designed to operate at speed/length ratios between 1.2 and 3.5 (F_n 0.4 to 1.2 approximately) have the following distinctive characteristics:

1. The afterbody has a flat or convex bottom having a dihedral angle (or rise of bottom) up to 45 degrees which runs smoothly into almost vertical sides with a rounded-bilge shape, not a sharp-angled chine.

2. The buttock lines are usually straight and almost parallel to the centre buttock line which usually runs aft at 10 to 15 degrees to the waterline.

3. The stern has a flat or rounded transom, except for low speed/length ratio forms which may have a cruiser-type stern.

4. The bow above water is designed for minimum interference with the bow wave. Any chine in the forebody is high in profile so as to reduce the breadth at the deck line, and will not extend as far aft as midships.

High speed round-bilge forms incorporate an unusually large number of design parameters. Besides such basic parameters as beam/draft and length/beam ratios, block and prismatic coefficients, features such as depth of transom and angle of rise of afterbuttocks may have considerable effects on resistance and propulsion characteristics.

Average Results for Models

In a first attempt to examine the effects of these design parameters, the measured model resistances for a varied group of about 30 round-bilge forms were plotted as in Figs. 1-11. The resistance coefficient $\textcircled{C}$ for a form of length $L = 100$ feet is throughout given in terms of the displacement/length ratio $\Delta / (0.01L)^3$ or, what is the same thing for $L = 100$ feet, the displacement Δ in tons. Figures 1-6 give the resistance coefficients for a series of speed/length ratios $V/\sqrt{L}$ from 1.7 to 4.0, with the specific value of the beam/draft ratio B/d shown for each form. These diagrams show no clear evidence of any systematic variation in resistance with B/d at any point in the speed range. In Figs. 8-11 the same results at $V/\sqrt{L} = 1.7$ are replotted, with the specific values of block coefficient, angle of entrance on waterline, position of LCB and length/beam ratio shown in turn. Again there is no clear evidence of any predominant form parameter.

If resistance data were available for a larger number of hull forms, say about 150, it should be possible to determine the influence of each of the principal form parameters by carrying out a multilinear regression analysis, using a high speed computer. With the limited data presently available this is not possible, and as a preliminary step mean lines have been drawn in each of Figs. 1-6. In addition, lines representing 5 and 10 percent deviation from these mean lines have been drawn. These show that most of the results lie within 5 percent of the mean lines. These mean lines are replotted in Fig. 7 to give, for ships of length 100 feet, average resistance coefficients for speed/length ratios from 1.4 to 3.5 for a range of displacements from 50 to 200 tons. It is suggested that for preliminary estimates these average values can be used with discretion to give the resistance generally within 5 percent for good standard hull forms.

Effect of Beam/Draft Ratio and LCB Position

The data in Figs. 1-11 indicate that it is probably unwise to assume the predominance of one parameter, say B/d, as has been done previously [1], and to ignore other form parameters. However, an attempt has been made to assess the effect of beam/draft ratio by comparing resistance coefficients for two models, each run at two displacements, which had different B/d values but were otherwise similar. The comparison is shown in Fig. 12 and Table 1, and suggests that at $V/\sqrt{L} = 2.5$ resistance varies approximately as the cube root of the beam/draft ratio but at $V/\sqrt{L} = 3.0$ the difference is much smaller. A similar comparison for two forms having a chine instead of a round bilge, and a fairly high chine line forward, given in Fig. 13, showed a much smaller variation with beam/draft ratio. Although these data are inadequate, they have been used to provide preliminary guidance on the effect of beam/draft ratio, as shown in Fig. 14.

Table 1

Comparison of Resistance Coefficients for Two 100-Foot Round-Bilge Models
with Different B/d Values

| Form	B/d	Δ (tons)	$\dfrac{V}{\sqrt{L}}$	$\textcircled{C}$ 100'		$(B{-}A)/A$ (percent)
				Form A	Form B	
A	2.92	100	2.5	1.70	1.88	+11
B	3.94		3.0	1.44	1.48	+3
$B{-}A$	1.02	80	2.5	1.55	1.72	+11
$(B{-}A)/A$	0.35		3.0	1.28	1.33	+4
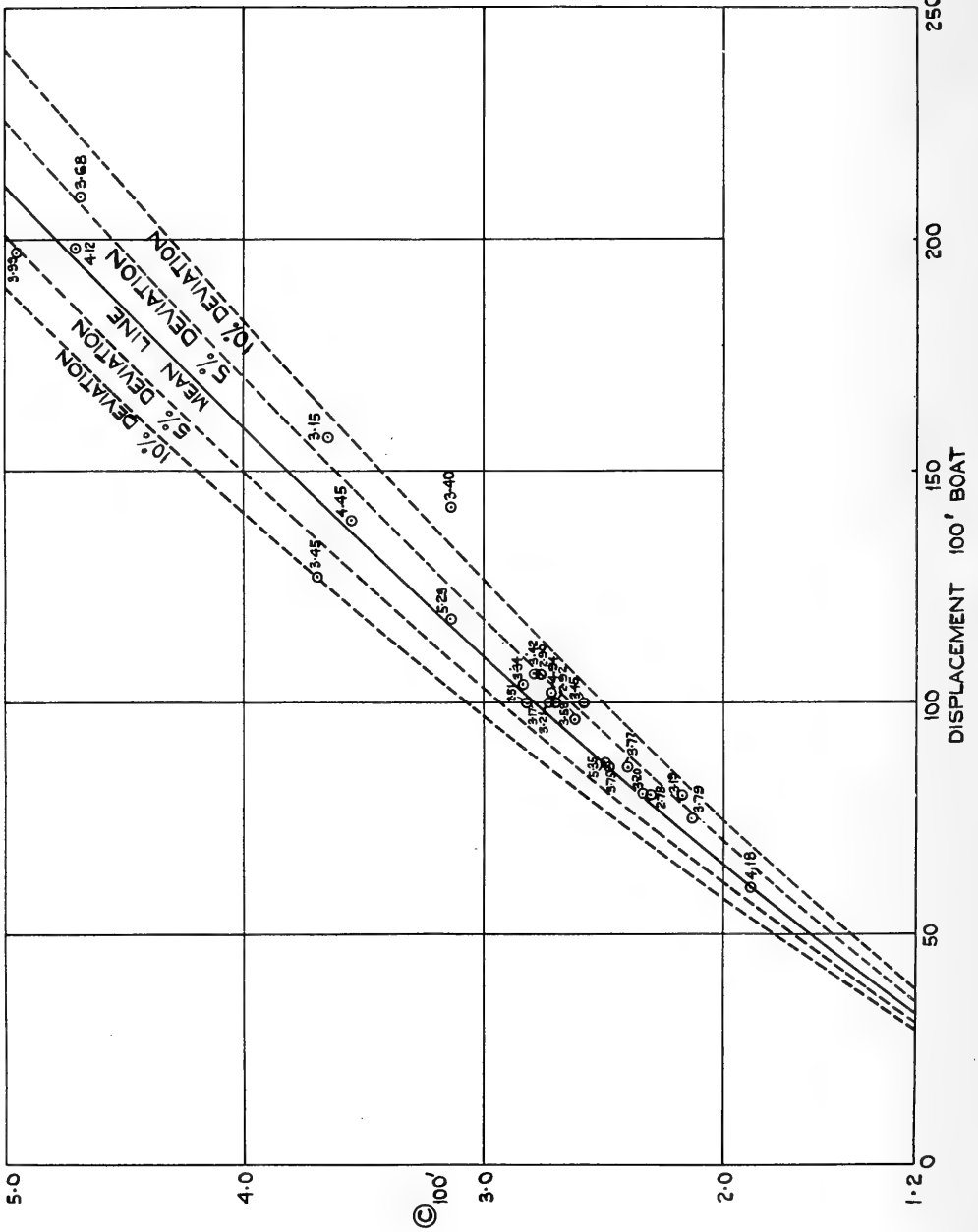
Fig. 1. Resistance coefficient Ⓒ for a 100-foot round-bilge boat versus displacement in tons; $V/\sqrt{L} = 1.70$; B/d values inserted
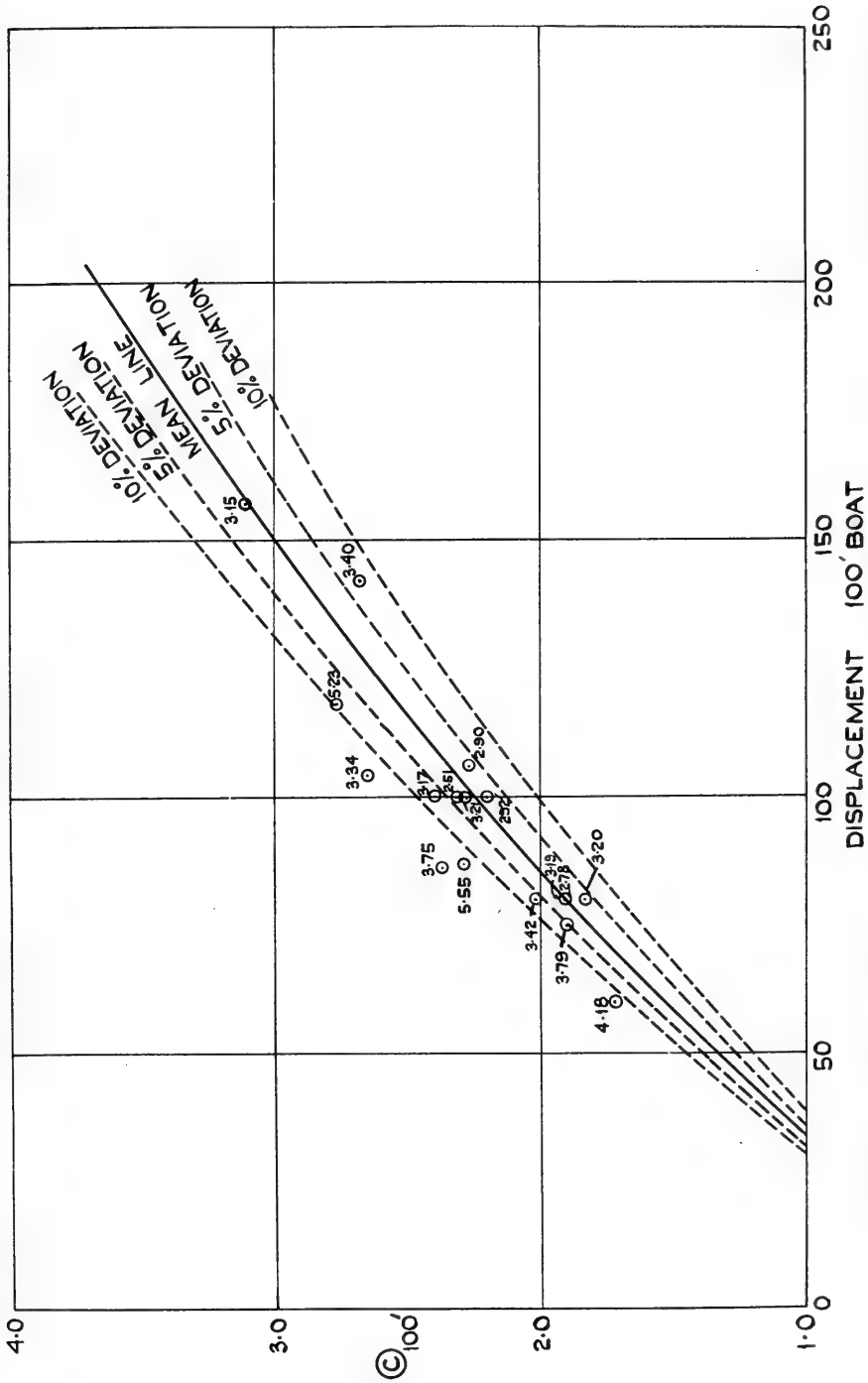
Fig. 2. Resistance coefficient Ⓒ for a 100-foot round-bilge boat versus displacement in tons; $V/\sqrt{L} = 2.10$; B/d values inserted
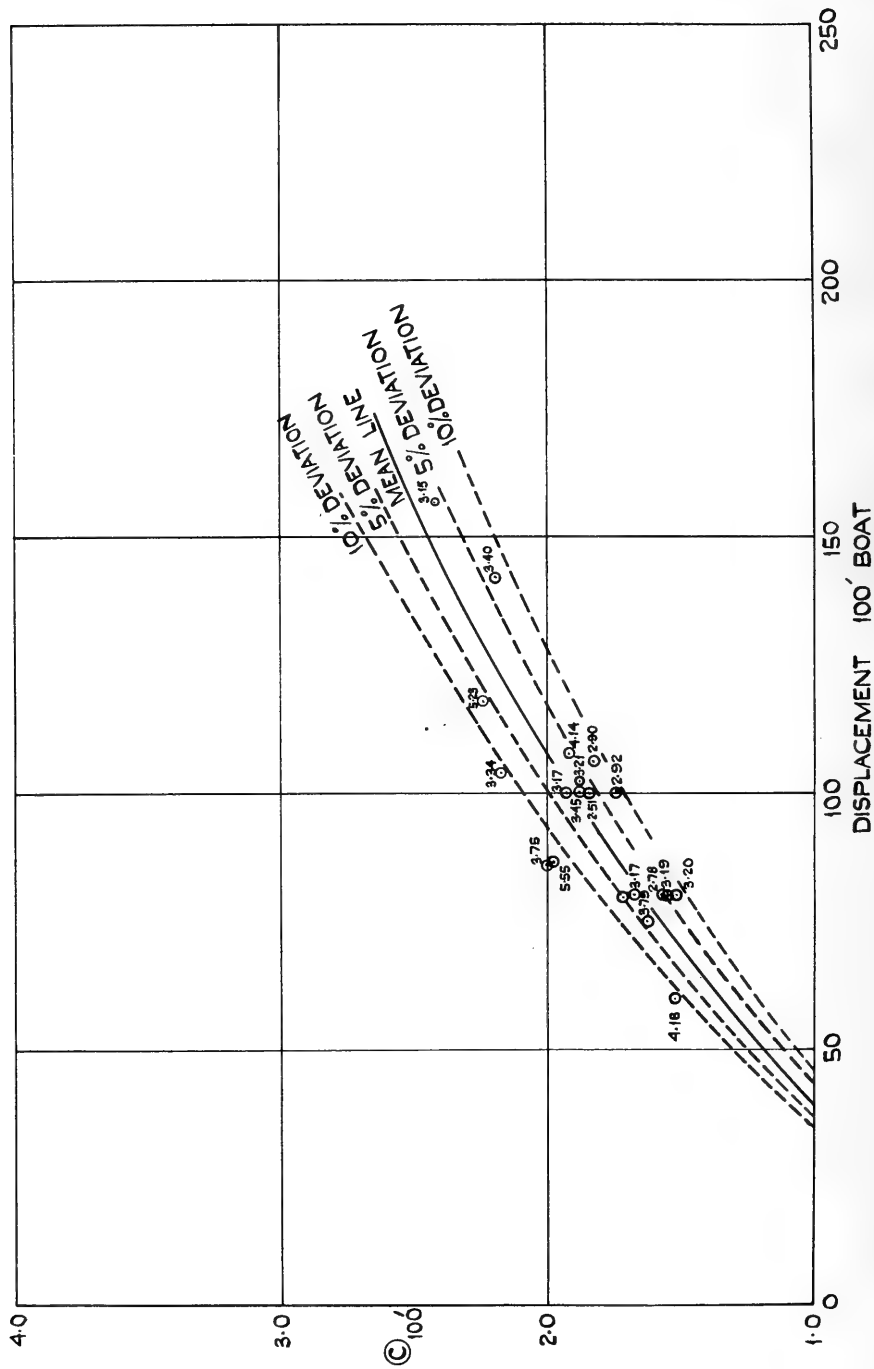
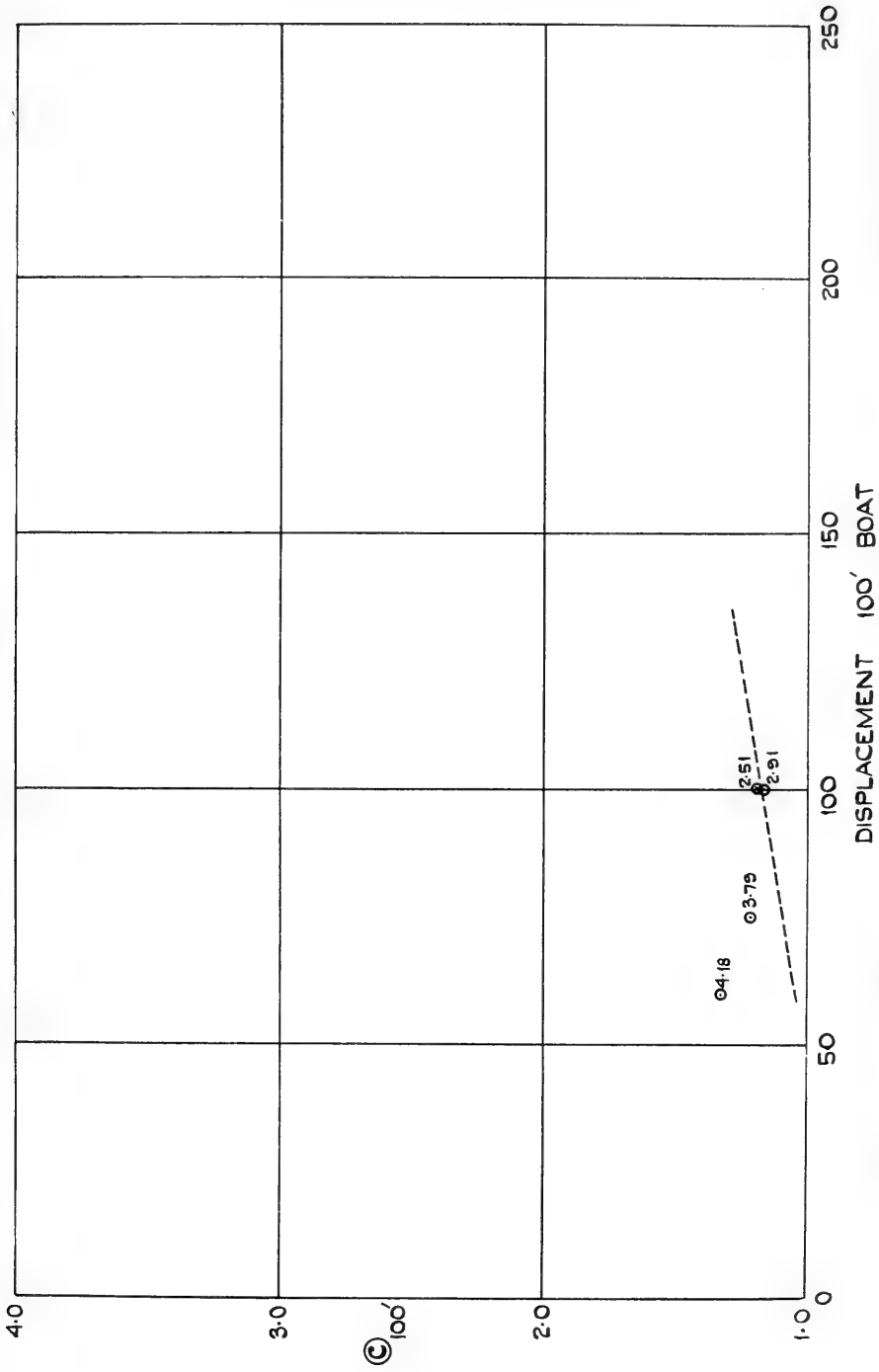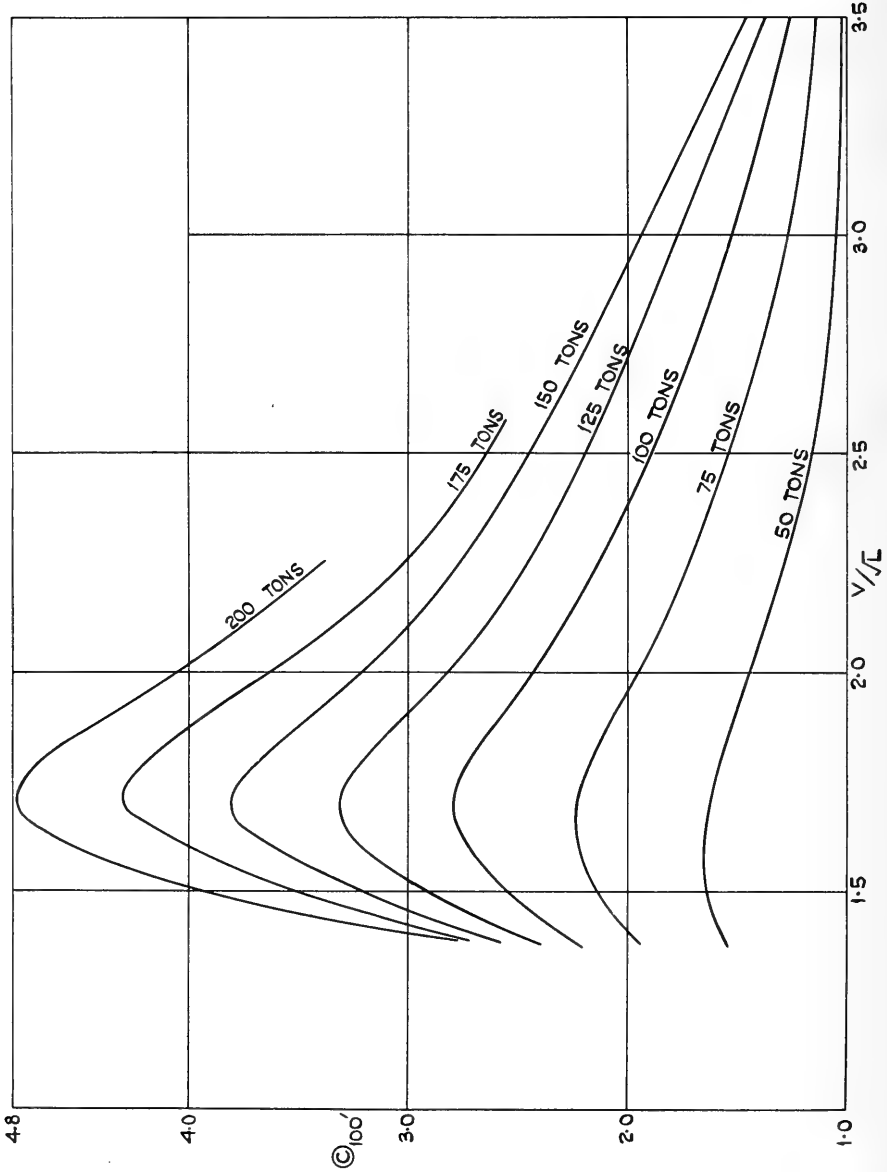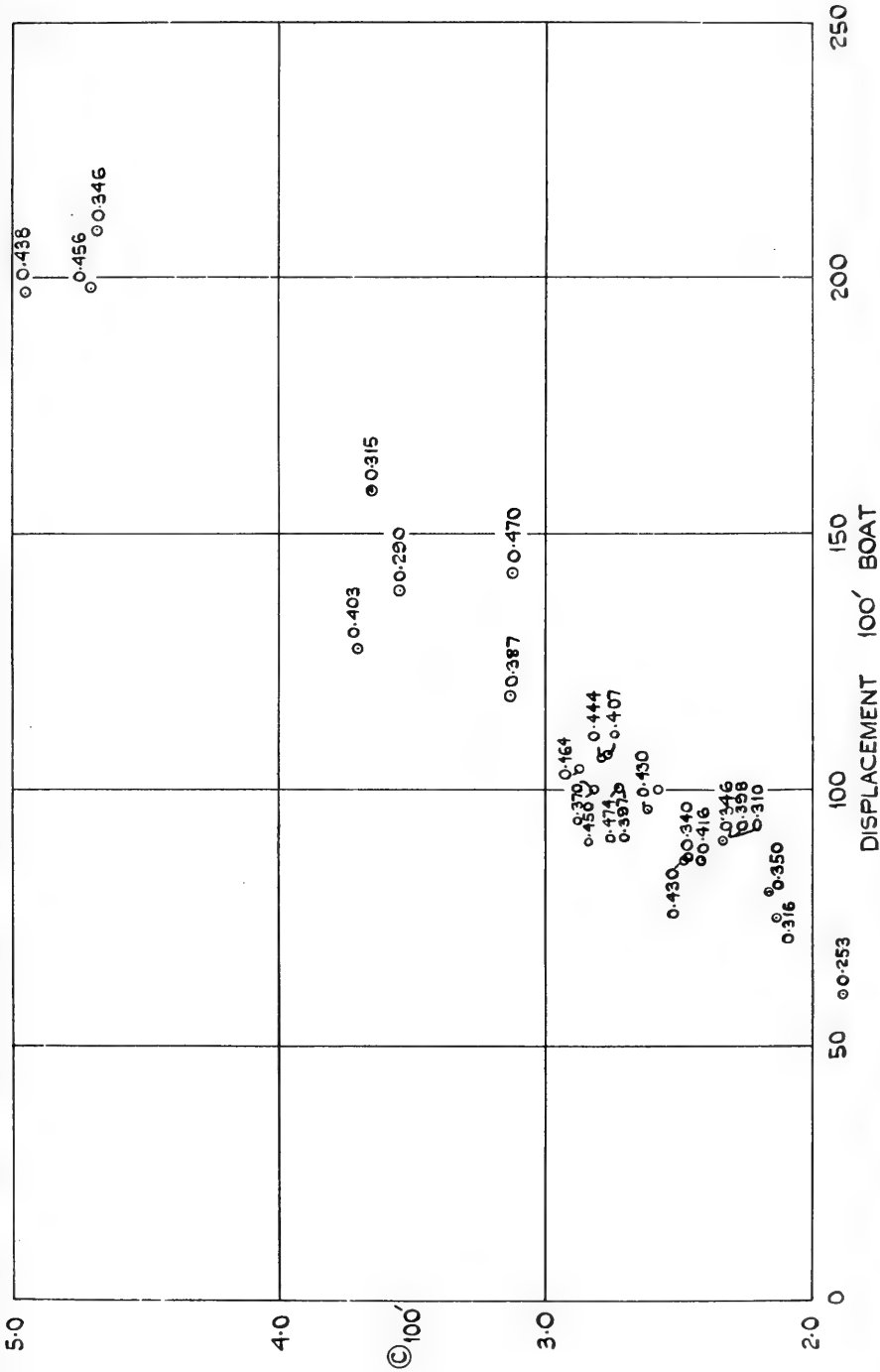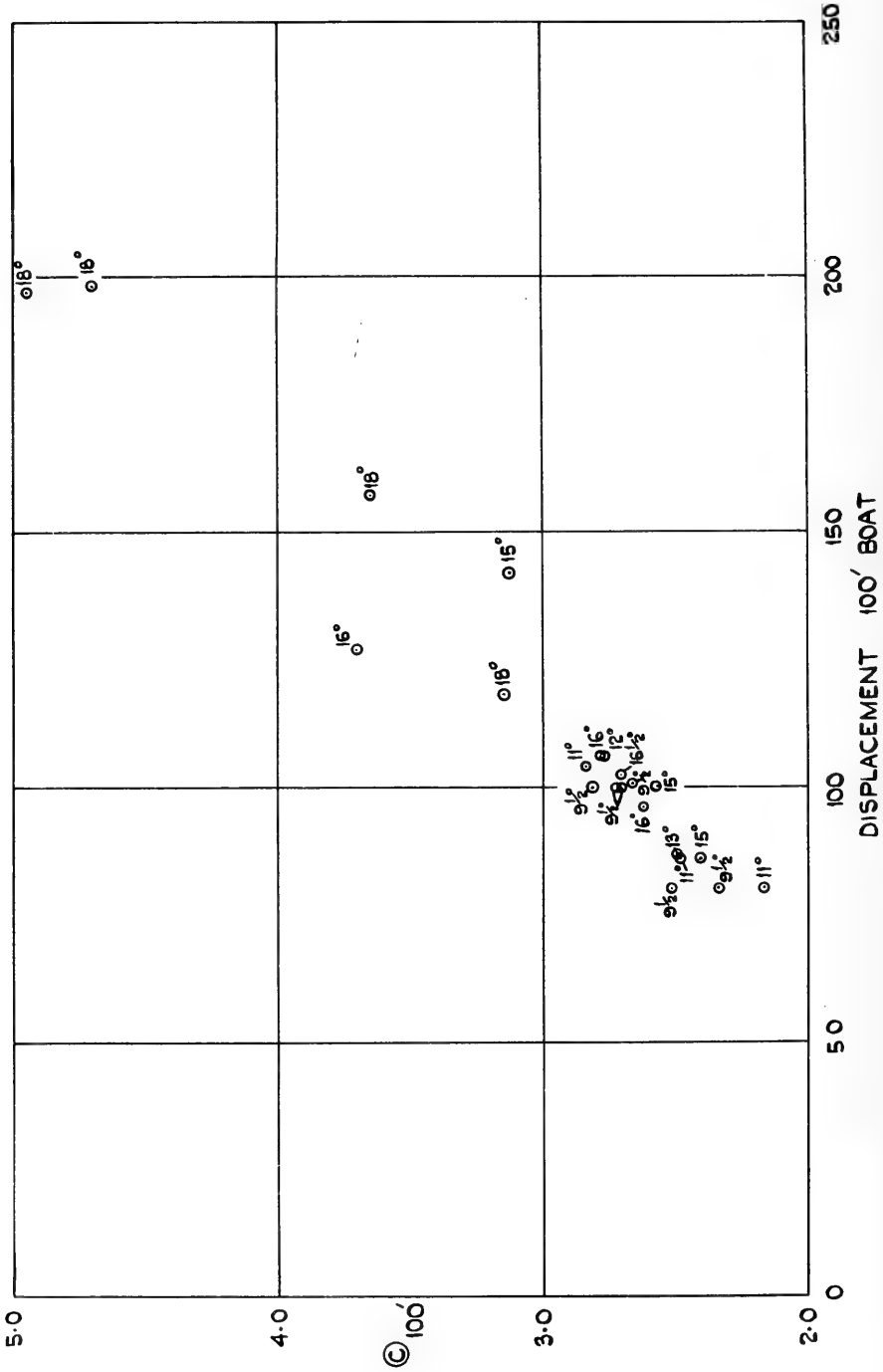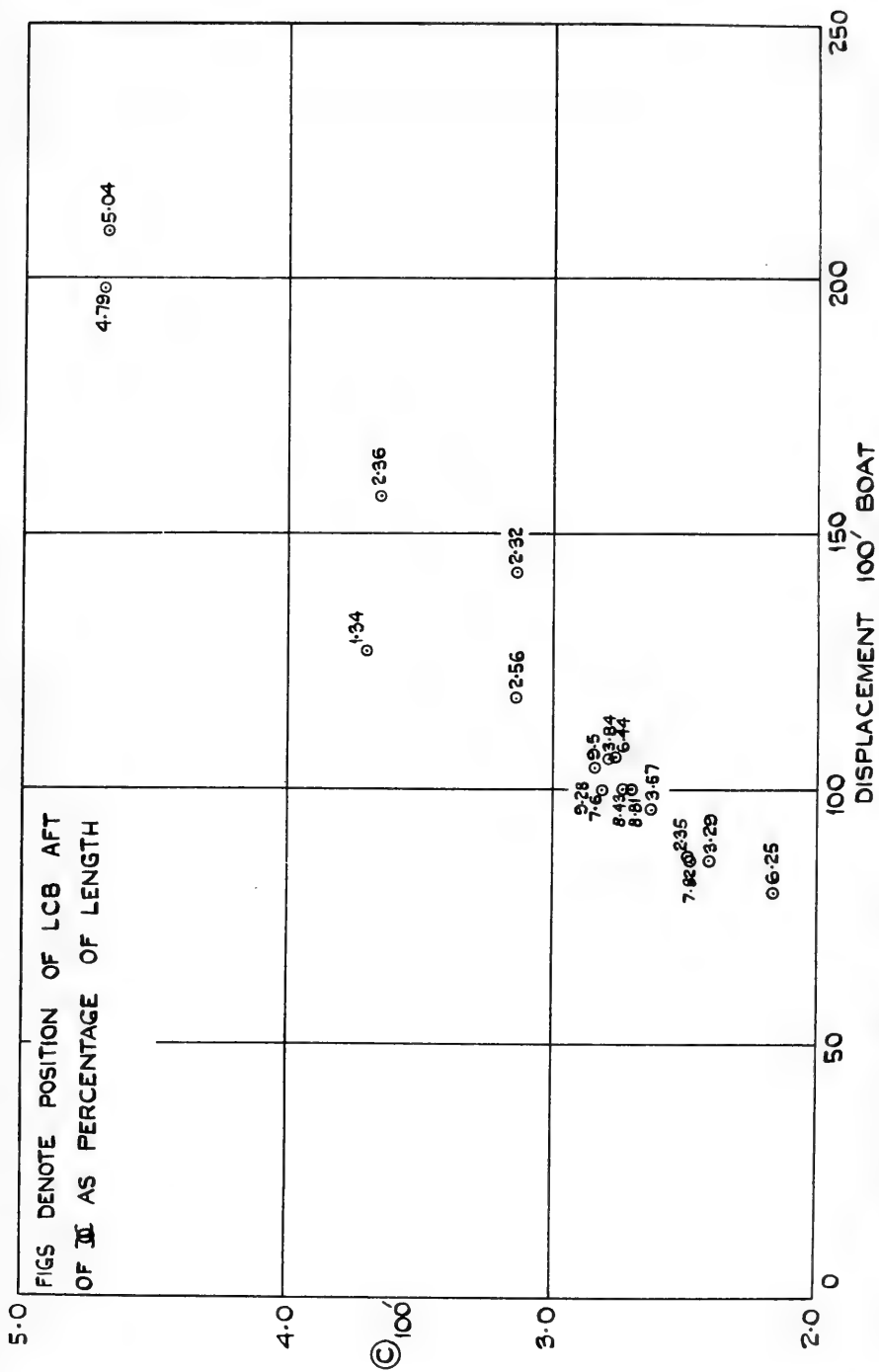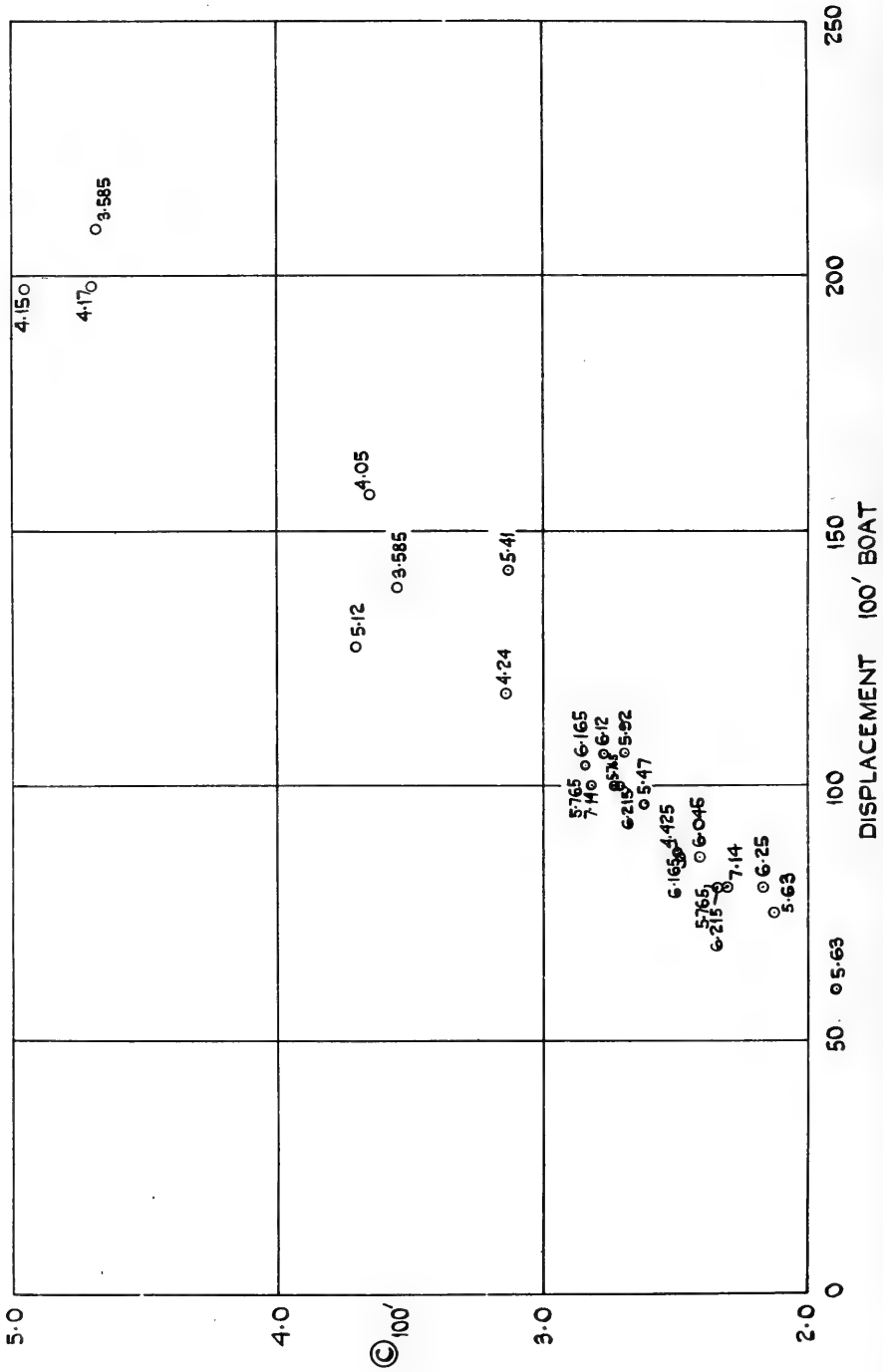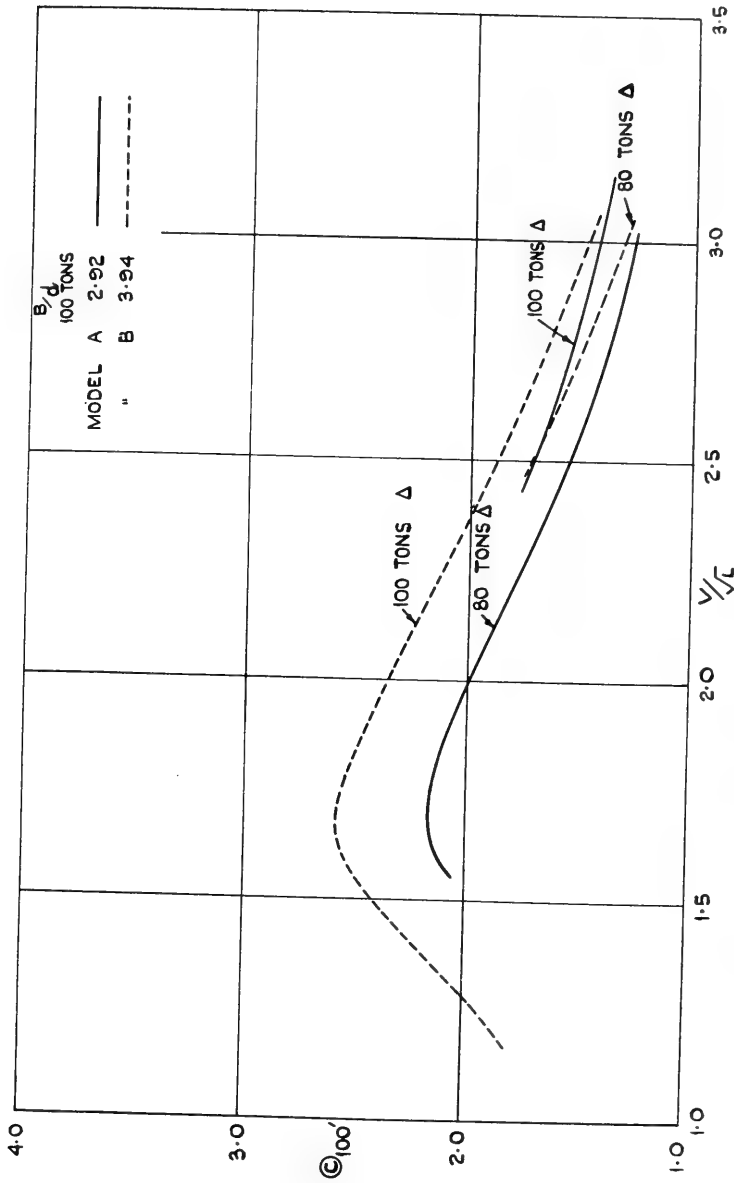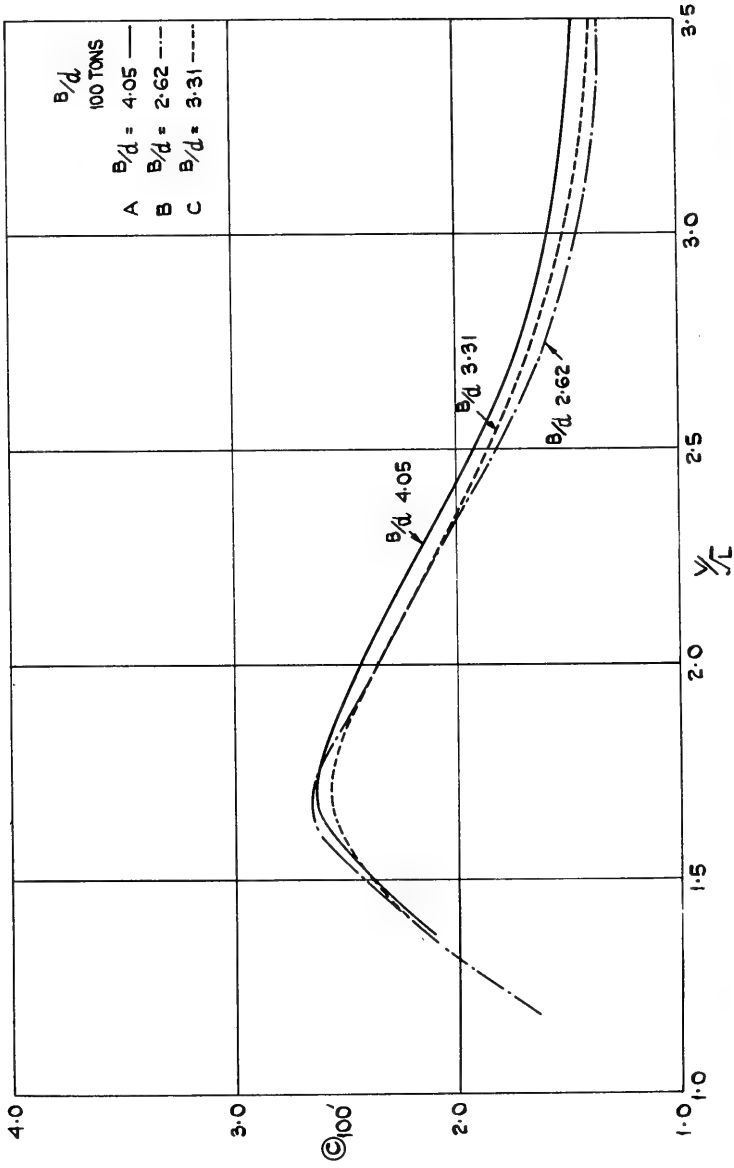Fig. 3. Resistance coefficient Ⓒ for a 100-foot round-bilge boat versus displacement in tons; $V/\sqrt{L} = 2.50$; B/d values inserted
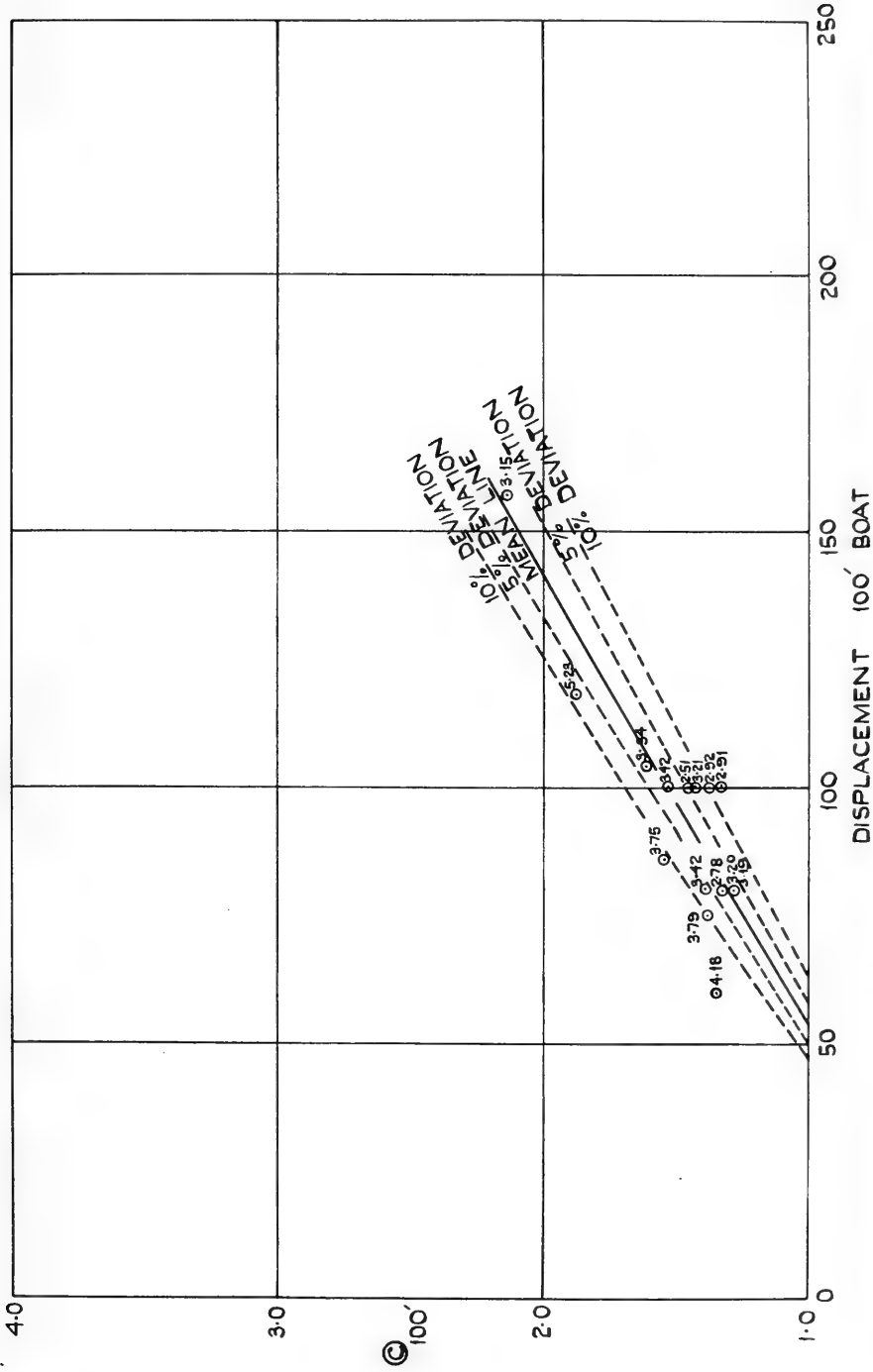
Fig. 4. Resistance coefficient Ⓒ for a 100-foot round-bilge boat versus displacement in tons; $V/\sqrt{L} = 3.0$; B/d values inserted
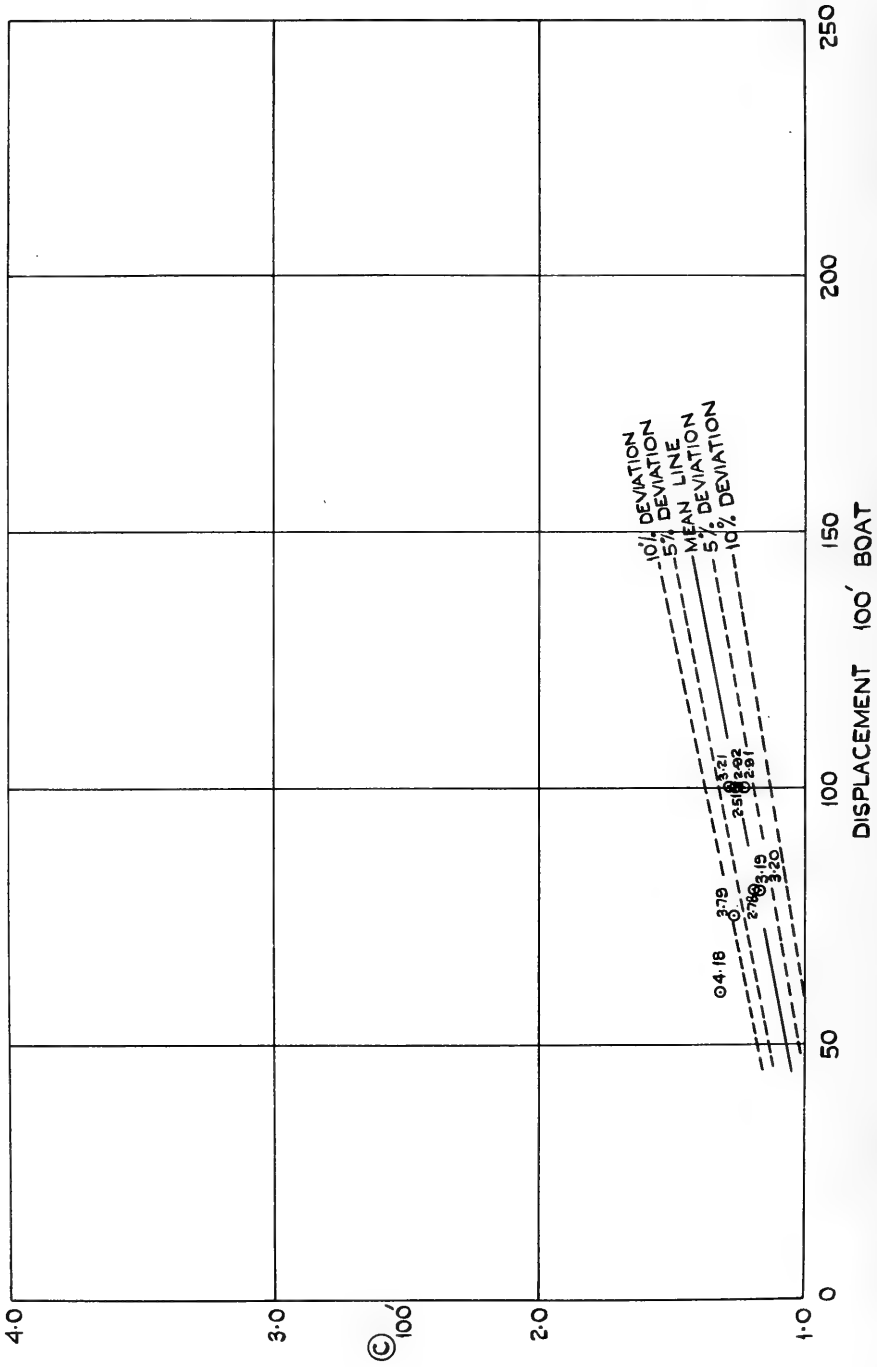
Fig. 5. Resistance coefficient Ⓒ for a 100-foot round-bilge boat versus displacement in tons; $V/\sqrt{L} = 3.50$; B/d values inserted

Fig. 6. Resistance coefficient Ⓒ for a 100-foot round-bilge boat versus displacement in tons; $V/\sqrt{L} = 4.0$; B/d values inserted

Fig. 7. Averaged values of the resistance coefficient Ⓒ for a 100-foot round-bilge boat versus $V/\sqrt{L}$; displacement values inserted

Fig. 8. Resistance coefficient ⓒ for a 100-foot round-bilge boat versus displacement in tons; $V/\sqrt{L}$ = 1.7; block coefficient values inserted

Fig. 9. Resistance coefficient Ⓒ for a 100-foot round-bilge boat versus displacement in tons; $V/\sqrt{L} = 1.7$; half angle of entrance values inserted

Fig. 10. Resistance coefficient ⓒ for a 100-foot round-bilge boat versus displacement in tons; $V/\sqrt{L} = 1.7$; longitudinal centre of buoyancy values inserted

Fig. 11. Resistance coefficient ⓒ for a 100-foot round-bilge boat versus displacement in tons; $V/\sqrt{L} = 1.7$; L/B values inserted

Fig. 12. Effect of B/d on the resistance coefficient for a 100-foot round-bilge boat

Fig. 13. Effect of B/d on the resistance coefficient for a 100-foot hard chine boat
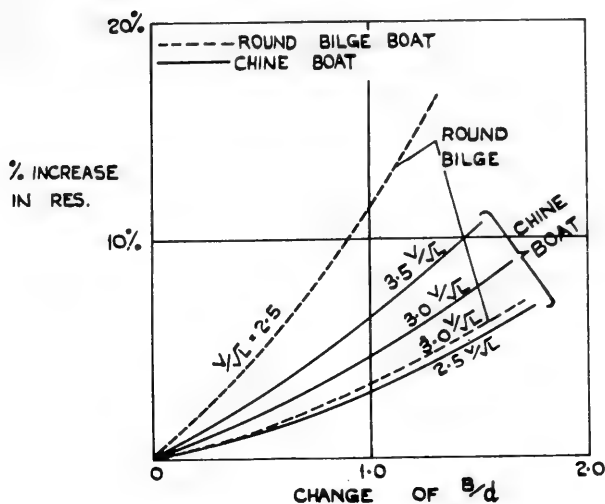
Fig. 14. Comparison of the effect of B/d on
round-bilge and hard chine boats

The available information does not permit any reliable estimate to be made of the effect of changing the position of the longitudinal centre of buoyancy (LCB), although this is generally considered to be an important parameter. As shown in Fig. 15 two forms, otherwise similar, with LCB positions 6.25 percent and 8.81 percent of the length aft of midships had almost identical resistance coefficients, possibly because the maximum advantage to be gained by moving the LCB aft had been achieved in the first of them. In both forms the forward waterlines were straight, and by moving the LCB further aft the half angle of entrance at the waterline, initially 11 degrees, was reduced to 9-1/2 degrees, probably the practical minimum. It is suggested that so long as the LCB is far enough aft to permit straight waterlines, there is little to be gained by further movement aft.

Appendage Resistance

Appendages for high speed displacement-type hulls generally comprise: shaft brackets, either A or I type, propeller shafts, usually angled to the flow, stub bossings at the hull, skegs, rudders, either single or twin, bilge keels, and bar keels.

The separate resistances of these appendages were measured in one case at NPL by removing each one in turn from a fully fitted model. The measured model resistances, expressed as percentages of the naked hull resistance, were: twin *"A"* brackets, 7.5%; shafts and stub bossings, not measurable; twin rudders (large), 10.5%; bilge keels (large) 4.0%; bar keels, 5.0%; for a total of 27.0%.

In accordance with current NPL practice for such appendages, this total was halved in estimating the additional full-scale resistance. At the design speed/length ratio 1.35, this gave an additional resistance coefficient δ Ⓒ of 0.27. For two other models the full-scale addition δ Ⓒ was 0.21; one of these had a single rudder and the other twin rudders, though neither had bilge keels, which are not usually fitted to launches and similar vessels. In all three cases the appendage resistance coefficient showed little variation with change
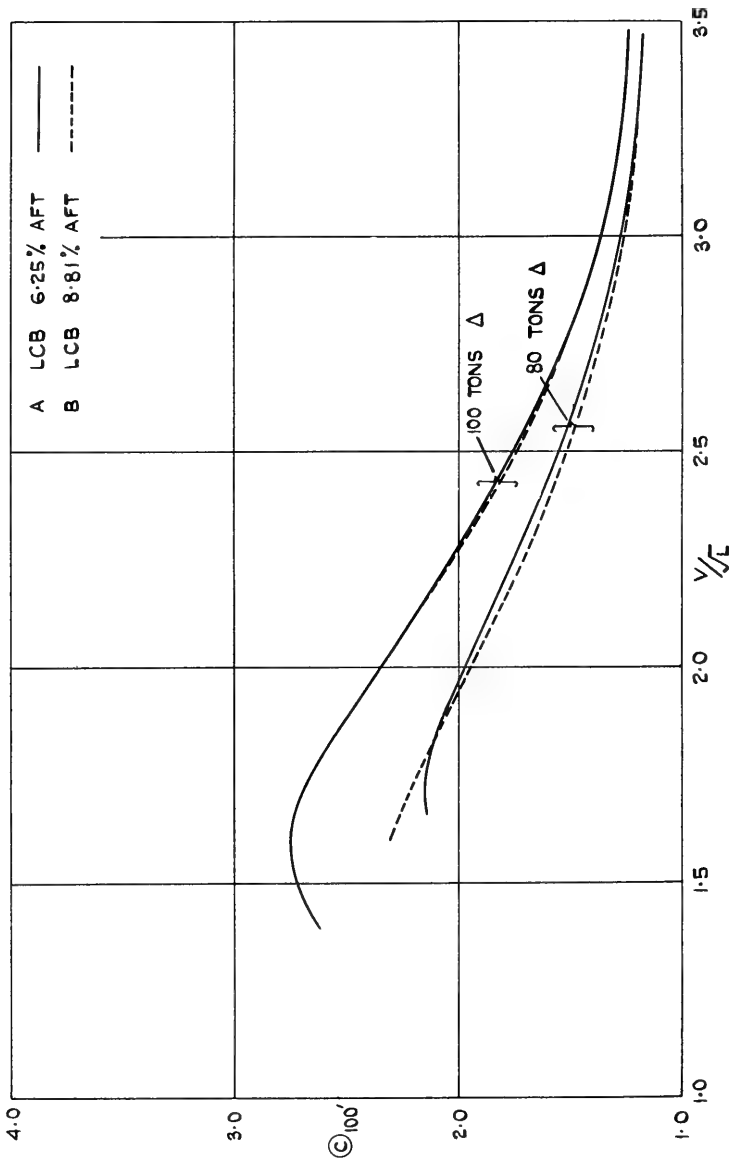
Fig. 15. Effect of the longitudinal centre of buoyancy on the resistance coefficient for a 100-foot round-bilge boat

of speed. These measurements suggest that the total resistance for typical appendage arrangements is more closely estimated by a constant δ ⓒ rather than by a constant proportion of the naked hull resistance. A tentative value for the resistance coefficient of normal stern arrangements, excluding bilge keels, is thus δ ⓒ = 0.20.

Effect of Changes in Scale

The average resistance coefficients ⓒ in Fig. 7 apply directly only to vessels of length $L = 100$ feet; for vessels of other lengths a skin friction correction must be applied. The conventional relation for this is

$$ⓒ_{100'} - ⓒ_L = (0_{100'} - 0_L) \, ⓈⒹ^{-0.175}$$

where the subscripts 100′ and L refer to vessels of length 100 feet and L feet respectively, "0" is Froude's friction coefficient, and Ⓢ and Ⓓ are Froude's circular wetted-surface and speed/length constants respectively. This does not hold for high speed displacement-type forms, but a modified relation does give friction corrections with practical accuracy. This modified relation is

$$ⓒ_{100'} - ⓒ_L = k(0_{100} - 0_L) \, ⓈⒹ^{-0.175}$$

where the factor k may be taken as a function of displacement/length ratios $\Delta / (0.01L)^3$ alone with sufficient accuracy for preliminary design purposes. Values of k and of Froude's "0" are shown in Fig. 16. It should be noted that the wetted surface area of a round-bilge displacement-type form does not vary sufficiently with speed to cause appreciable errors in using a fixed value of wetted area. For preliminary design purposes it is generally adequate to estimate the wetted area S from a simple formula such as the Denny-Munford relation

$$S = L(1.7d + BC_B)$$

where C_B is the block coefficient and the other symbols are as previously defined.

PROPULSION

Components of Propulsive Efficiency

Components of propulsive efficiency have been derived from the results of propulsion experiments made with eight different models. In these experiments the thrust was measured in the direction of the propeller shafting, and corrected to eliminate the effect of the weight of the propeller. The resistance was measured as the horizontal force in the direction of motion, but no attempt was made to compute the fore and aft component of the thrust. Open water experiments with propellers alone were made with the shaft horizontal.

Values of the thrust deduction fraction t, the wake fraction w based on thrust identity, the relative rotative efficiency η_R, and the hull efficiency η_h are given in Figs. 17-20 in terms of the speed/length ratio $V/\sqrt{L}$. These show that the thrust deduction fraction t tends to vary much as the resistance coefficient ⓒ , with a maximum near $V/\sqrt{L} = 1.5$ and
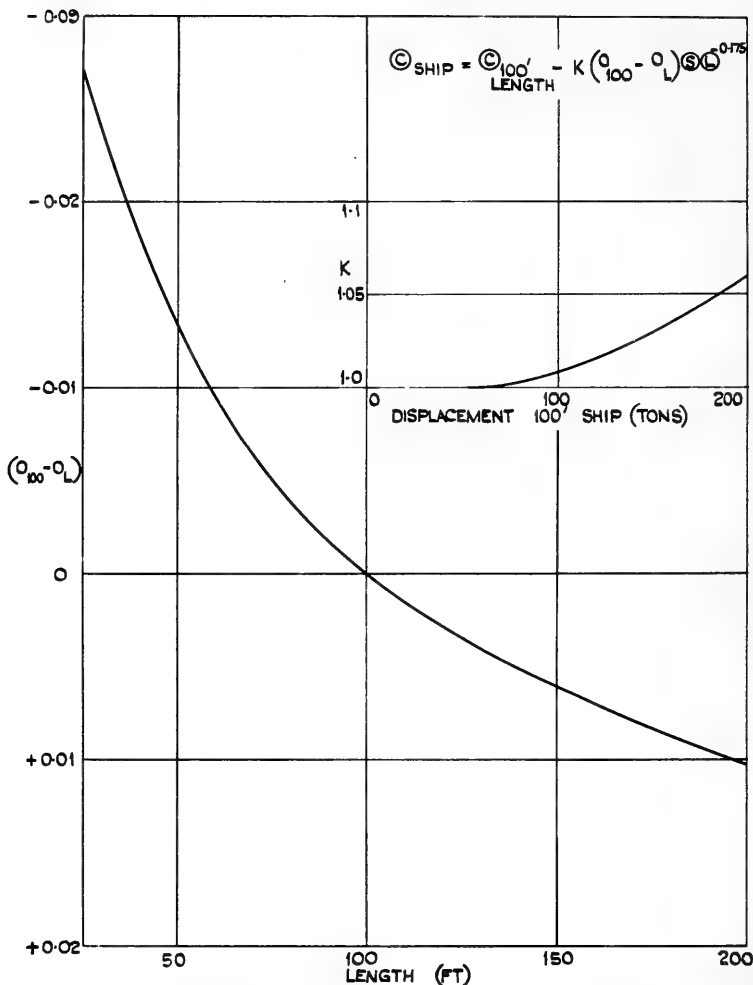
Fig. 16. Values of k and of Froude's "0" for a round-bilge boat

decreasing at higher speeds, finally approaching open water conditions. The wake fraction w is small, as expected, and slightly negative at high speeds.

From these factors and the propeller open water efficiency η_o, which depends principally on the permissible propeller diameter or the engine-propeller gear ratio, the quasi-propulsive coefficient η can be estimated as

$$\eta = \eta_o \eta_R \eta_h.$$

Ship-Model Comparison

Good data from full-scale trials under ideal conditions are required to determine the correlation factors linking predicted performance from model experiments with that measured on shipboard. Little reliable data for high speed displacement-type forms are available, and
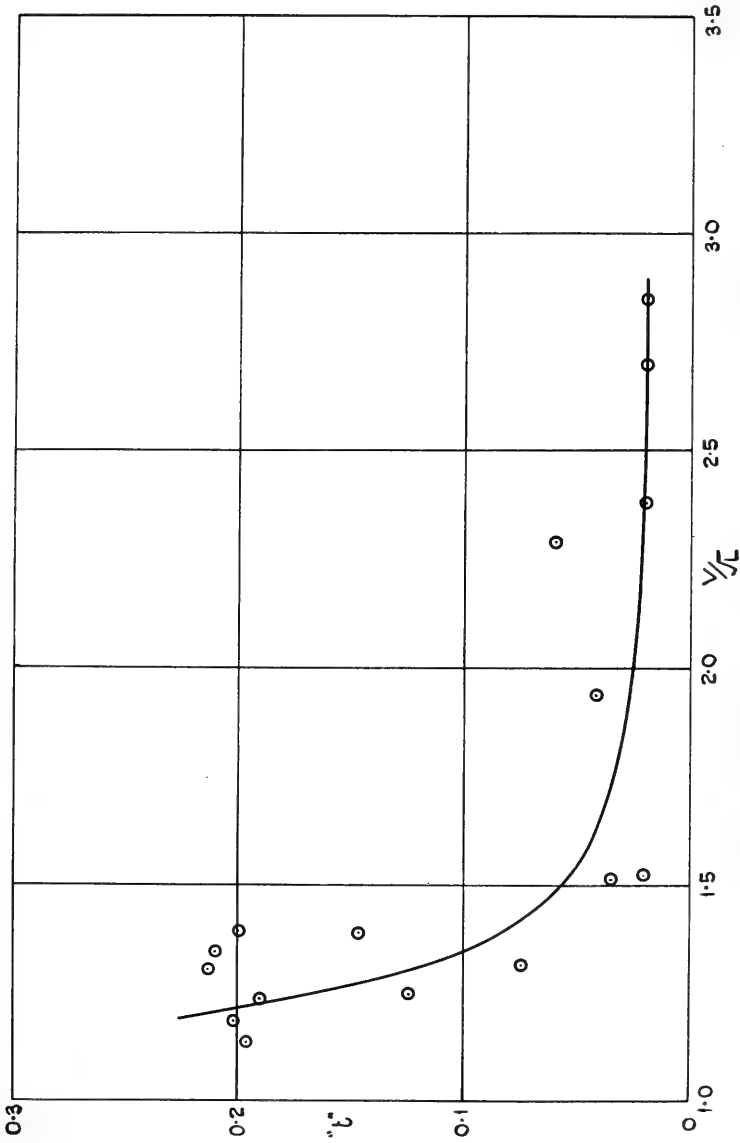
Fig. 17. Variation of the thrust deduction fraction t with $V/\sqrt{L}$ for a round-bilge boat
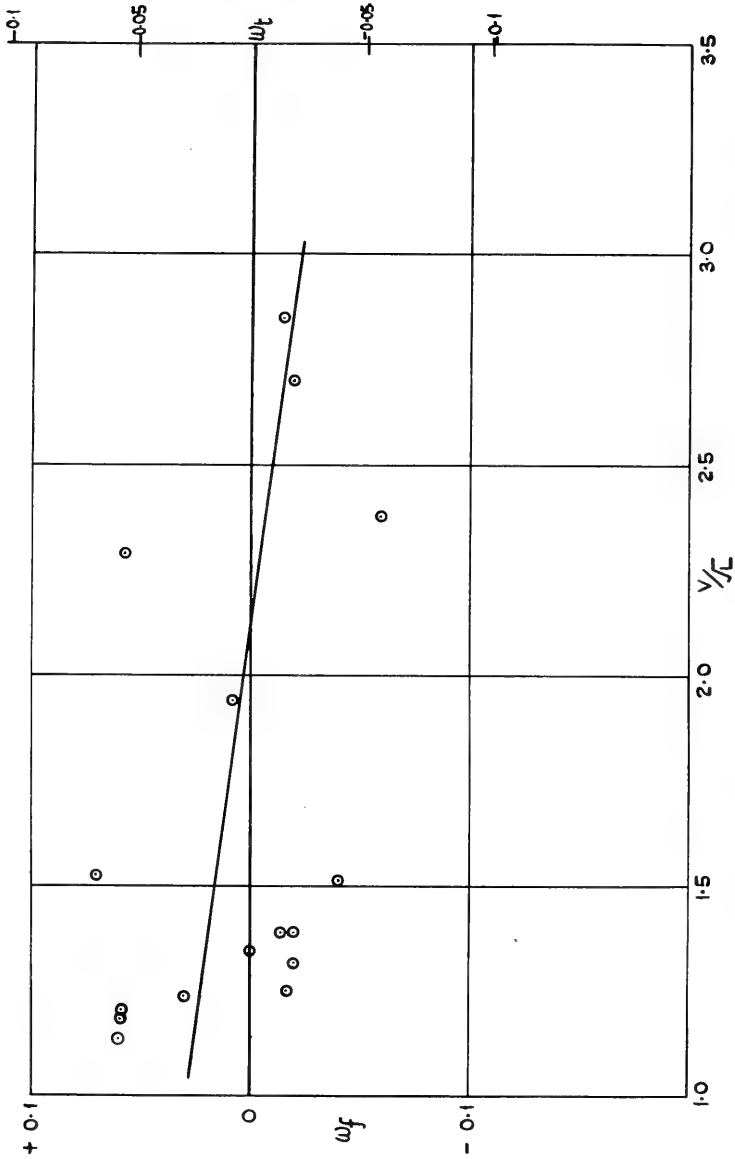
Fig. 18. Variation of the wake factor w_f with $V/\sqrt{L}$ for a round-bilge boat
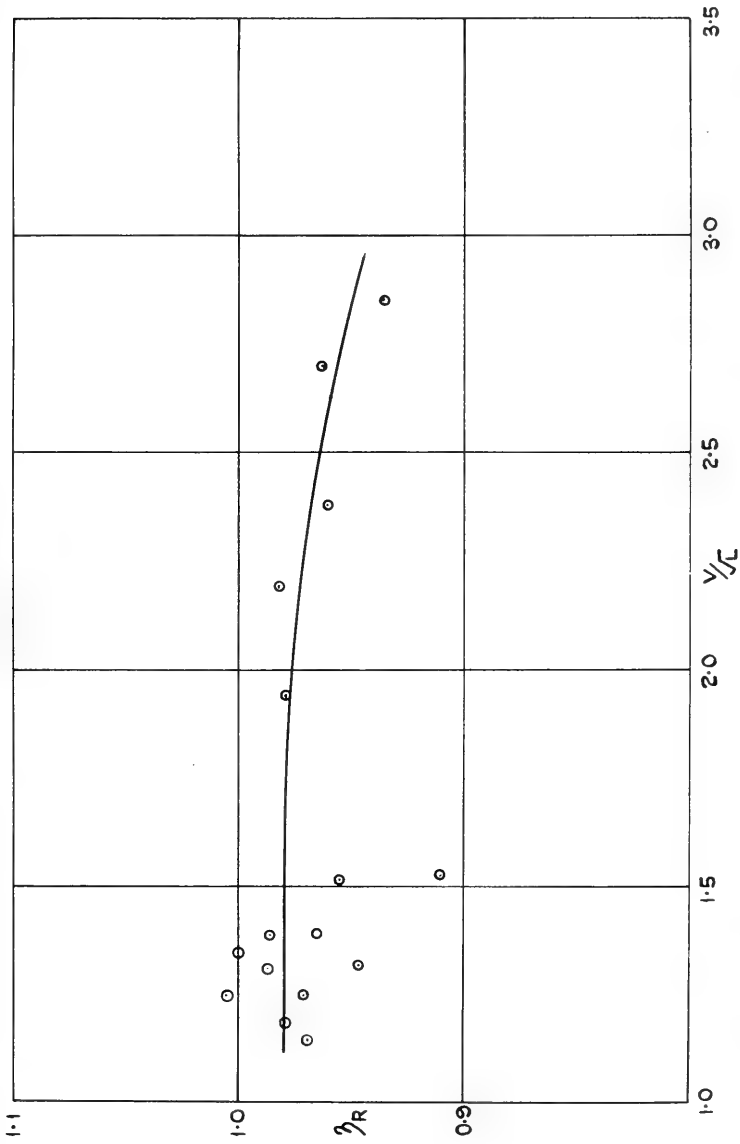
Fig. 19. Variation of the relative rotative efficiency η_R with $V/\sqrt{L}$ for a round-bilge boat
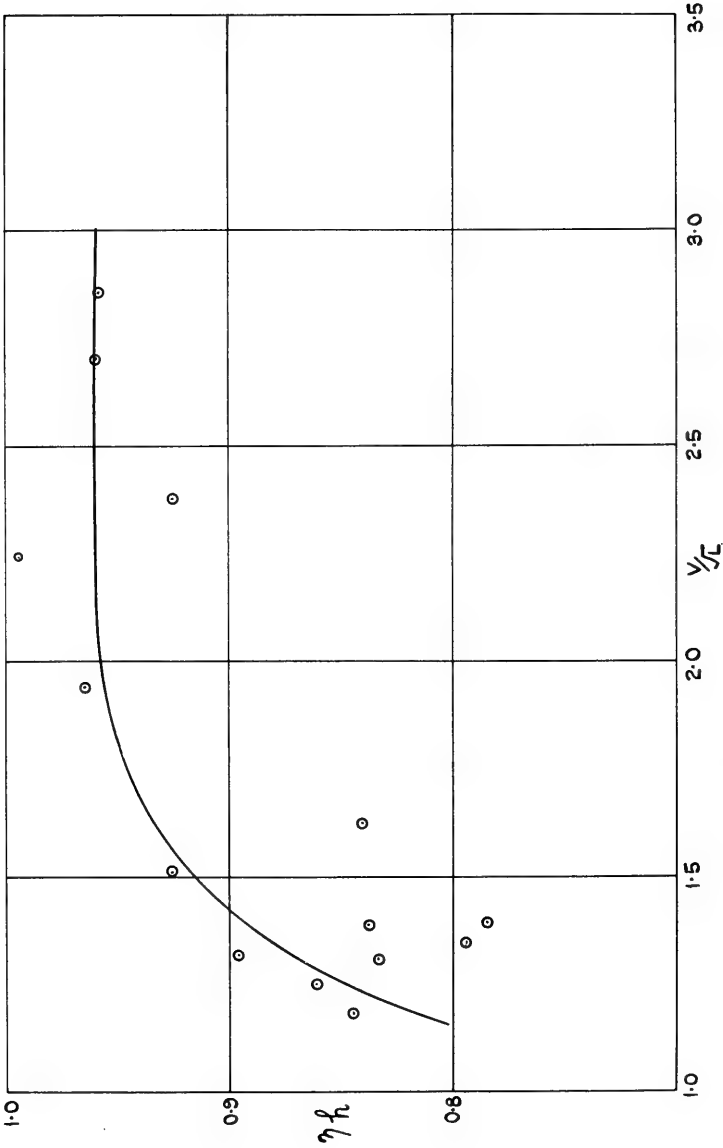
Fig. 20. Variation of the hull efficiency η_R with $V/\sqrt{L}$ for a round-bilge boat

an attempt to obtain further results is being made by the Ship Division, NPL. For this purpose two portable torque meters, of strain gauge type, have been designed and constructed at NPL to fit propeller shafts having diameters from 1-1/4 inches to 6 inches. A description of the first of these is given in Appendix A.

Using this torque meter, good trial results have recently been obtained for two twin-screw launches, one 71 feet in length and the other 51 feet. Resistance experiments were made at NPL with both forms, and propulsion experiments with the model of the smaller vessel.

The results of the trials with the 71-foot launch are given in Fig. 21; this shows the measured power for one shaft (only one torque meter was available) and also calculated
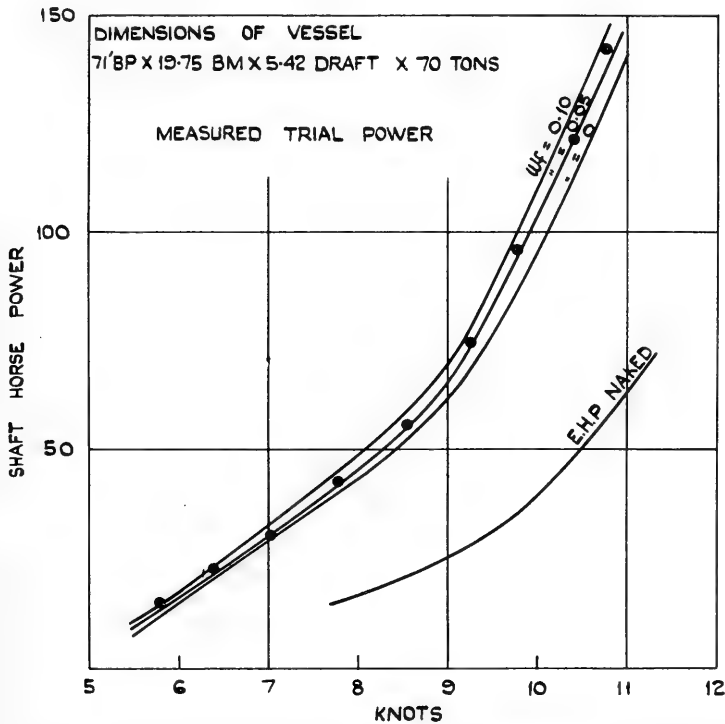
Fig. 21. Results of trials with a 71-foot round-bilge launch in a water depth of 50 feet

values of the power absorbed by the propeller for assumed wake fractions w_f of 0, 0.05, and 0.10. Closest agreement between measured and calculated power occurs for $w_f = 0.05$; the estimated value was 0.03. The measured power at the highest speed is greater than the absorbed power calculated for $w_f = 0.05$; this may have been caused by a 2-1/2 percent difference in the shaft revolutions. Had both shafts run at the higher speed of that with the torque meter, the total power, and consequently the speed, would have been slightly higher. In this case $w_f = 0.05$ would have given close agreement at the highest speed.

The full-scale power was estimated directly from the model results, taking $\eta_R = 0.99$, $\eta_o = 0.65$, $\eta_h = 0.83$, and appendage resistance of 0.20 ⓒ corresponding to a factor of 0.10. This gave a delivered horsepower (dhp) equal to 118 for a speed of 10.77 knots; wind resistance estimated from measured velocities increased this by 3 percent to $dhp = 121.5$. The measured power was 138; the correlation factor (ratio of measured to estimated power) is thus 1.135, slightly higher than the current NPL value 1.10 for this type of vessel. Part of the discrepancy may be due to a small difference in trim between model and full scale. These trials were run in water of depth about 50 feet, considered sufficient not to introduce any depth effect.

The trials with the 51-foot launch were run in water of depth 20 feet or less while the model experiments were made in water of 45-foot equivalent depth. A possible shallow water effect thus confuses the ship-model comparison; Fig. 22 shows that the greatest discrepancy between measured and predicted powers occurs at speeds close to the critical speed for water of depth 17 feet. In this trial also only one torque meter was fitted, but it was here assumed that both propellers absorbed equal powers. A power estimate based on
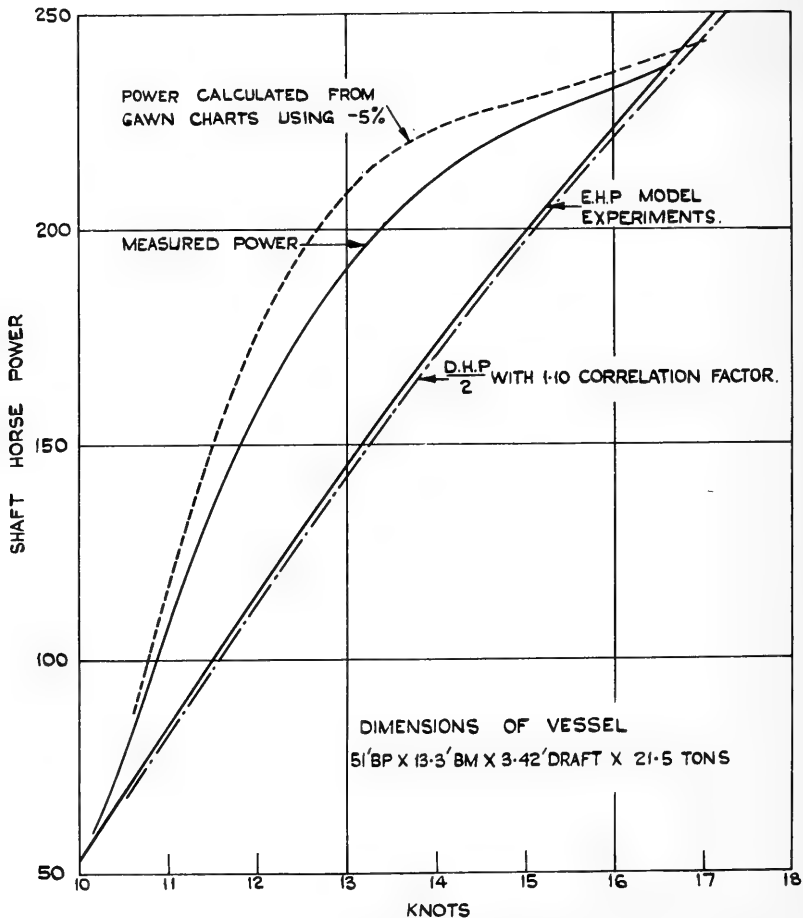
Fig. 22. Results of trials with a 51-foot round-bilge launch in a water depth
of 20 feet or less

a correlation factor of 1.10 and a measured model wake fraction of 0.05 gave good agreement with the measured power, particularly at higher speeds.

The results of these two trials suggest that a ship-model power correlation factor of 1.10 is reasonable; further trial data are needed to confirm this estimate.

RUNNING PERFORMANCE

Effect of Spray Strips

At speed/length ratios of 3.5 and above ($F_n \geqq 1.2$), a round-bilge displacement-type hull develops a troublesome bow wave. This occurs at about 25 to 40 percent of the length aft of the bow, and for a 100-foot vessel can be 4 to 5 feet above the still water level. Unfortunately, this wave often is covered by a fine spray film which starts at the bow profile and in still water clings to the hull above the main wave profile. In bad or windy weather this film breaks away from the hull as spray which can cause considerable wetness of the afterstructure.

Model experiments were made with spray strips in an effort to combat this effect. On the form shown in Fig. 23 a strip 1 inch × 1 inch (for a 100-foot vessel) was fitted at about 3 feet above the still water line from the bow to midships. This prevented the film rising to the top side of the model, and enabled the speed to be raised from 30 to 42 knots without serious trouble.
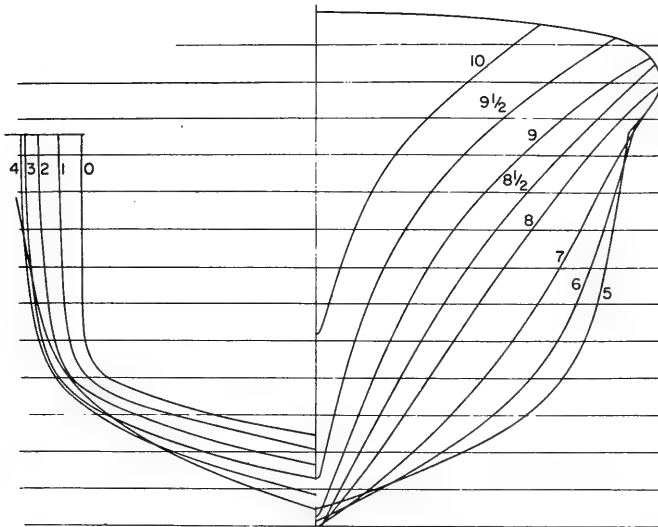
Fig. 23. Model 2084; 100 feet × 16 feet × 5.48 maximum
draft × 100 tons

It has been found that spray strips either reduce the resistance of a model or have no measurable effect. Model trim is increased by about 0.5 degrees at the highest speeds.

Design of a Round-Bilge Form for Good Seakeeping

For a small vessel, less than 100 feet in length, designed to operate at sea, the performance in waves can be more important than in smooth water. Near-synchronous pitching conditions may well be met, and waves no more than 3 feet in height can cause slamming decelerations up to 9 g, injurious to both structure and personnel, as recorded at sea [3] and observed in model experiments.

The requirements for a small vessel with good seakeeping qualities include: (a) a dry deck, especially forward of the wheelhouse so as not to interfere with navigation, and (b) avoidance of slamming, and (c) minimum resistance so that available power is efficiently used in maintaining speed in a seaway. Other qualities are also required, but these are not discussed here.

An attempt to design a hull form with these qualities was made some time ago at NPL. Initial experiments were carried out with models of hard chine forms similar to those used on wartime air-sea rescue launches. However, for a design maximum speed/length ratio of 3.4, it was soon found that a round-bilge form with a fine bow and a transom stern had a superior smooth water resistance. Such a form, designated Model 2084, was designed as shown in Fig. 23, and for comparison a hard chine form, designated Model 2117, shown in Fig. 24, was also evolved; boats with this hard chine form were known to have had
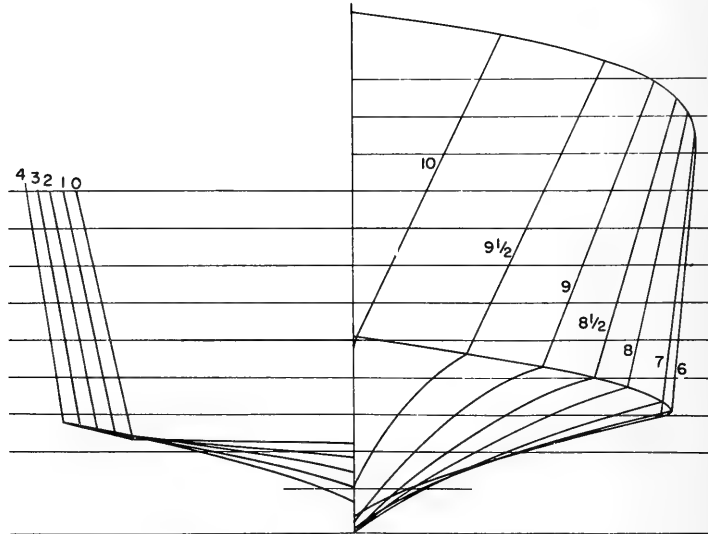
Fig. 24.   Model 2117, 100 feet × 18.8 feet × 4.80 maximum
draft × 100 tons

to reduce speed considerably in moderate seas. These two forms had the following main dimensions:

Type	Model	LWL (ft)	B on WL (ft)	Max. d (ft)	Δ (tons)
Round bilge	2084	100	16.0	5.48	100
Hard chine	2117	100	18.8	4.8	100

Smooth water resistance data for the two forms are given in Fig. 25; the round-bilge form behaved well up to 30 knots ($V/\sqrt{L}$ = 3.0), and a spray strip fitted as described previously helped to keep the hull clear at higher speeds.

Experiments with 1/15 scale models were also made in head seas. In these each model was towed by a bridle held by hand on the towing tank carriage. Hand towing was preferred to a rigid attachment to allow slight retardation of the model when its resistance increased in passing through a wave.

Figures 26-28 show extracts from continuous film records taken of both hulls in the wave conditions indicated in the figures. These film extracts have been chosen to show the vessels in their worst position, low in the wave with spray being thrown upwards or to the side.

The chine form is "stiff" in waves and tends to slam violently. The low chine forward throws water forward and up, obscuring wheelhouse vision and producing a wet ship. The round bilge form pitches more but this reduces slamming. The flare forward, which was designed with particular care, is very effective in throwing water away from the hull. The film records clearly show the superior wave-performance of the chineless, round-bilge form. Although the behaviour of the hard chine form could be improved by raising the chine line forward, it was not possible to reduce its resistance to that of the round-bilge form. It is hoped that a vessel having this round-bilge form will shortly be built.

SHALLOW WATER EFFECTS

Many builders of small boats do not appear to be aware of the marked effect of depth of water on wavemaking resistance. Trials are frequently run in river estuaries over accurately measured distances in water between 10 feet and 15 feet deep, which is considered to be ample for vessels with drafts of 2 feet to 3 feet. Not surprisingly, often the designed maximum speed is not achieved.

The 51-foot twin screw launch mentioned earlier demonstrates this shallow water effect. Its draft was 3.42 feet, and trials were run in about 20 feet of water, for which the critical speed ($v = \sqrt{gD}$) is about 15 knots. Figure 22 shows that the measured and predicted power curves differ most at about 13-1/2 knots. Saunders [2] quotes a method for assessing the depth of water effect both below and above the critical speed; this is based on data from trials of a German destroyer, the only available information for speeds above the critical value. Using this method, and taking the depth of water as 20 feet for the 51-foot launch, the shallow water effect given in Table 2 has been calculated.

The considerable differences between the power ratios directly measured for the 51-foot launch and those deduced from Saunders' data are not surprising, since Saunders states that other model and full-scale data do not agree with the German results. It is clear that further information is necessary, and a series of NPL trials in different depths of water with a 27-foot launch are being completed.
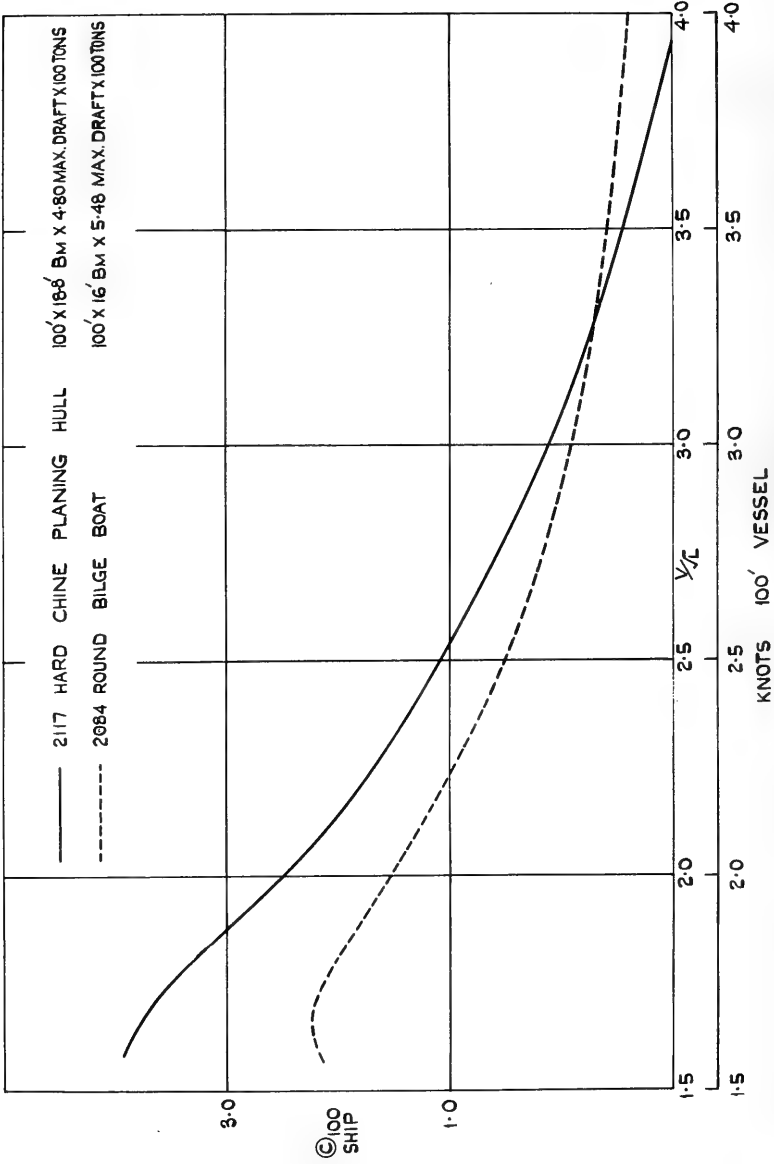
Fig. 25. Comparison of the resistance coefficient ⓒ for a round-bilge boat and a hard chine boat
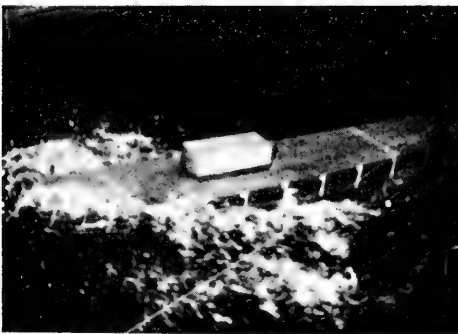
MODEL 2117   MODEL 2084

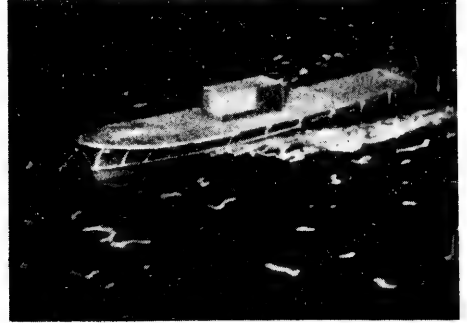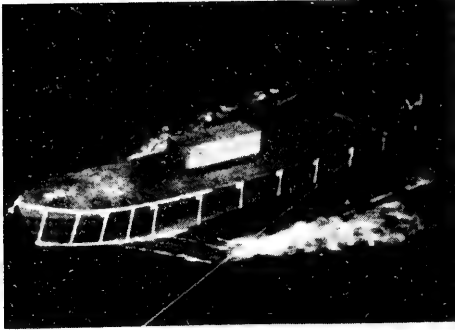

MODELS OUT OF WATER

SMOOTH WATER
SPEED 15 KNOTS

WAVES – LENGTH 130 FT HEIGHT 5 FT
SPEED 15 KNOTS

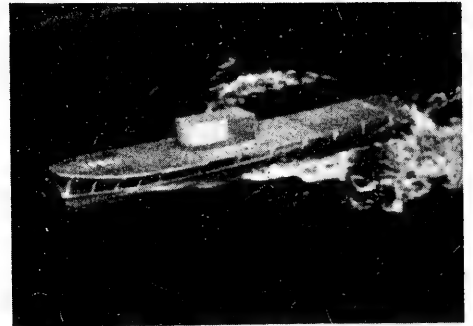Fig. 26. Behaviour of the two models of Figs. 23 and 24 in waves

SPEED   34   KNOTS
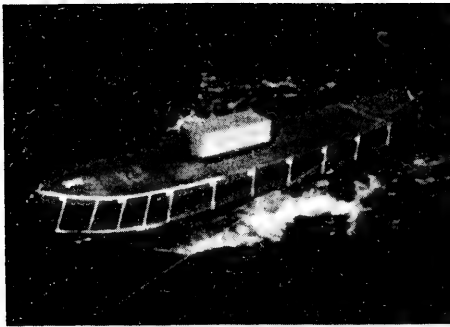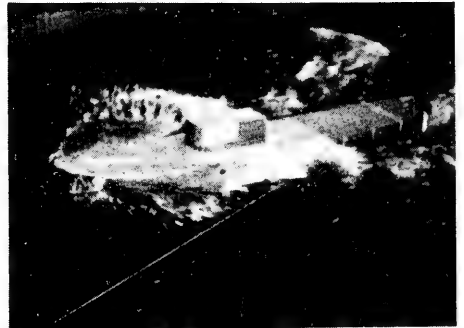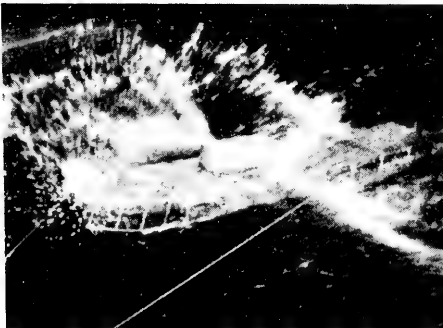
MODEL   2117   MODEL   2084

SMOOTH   WATER
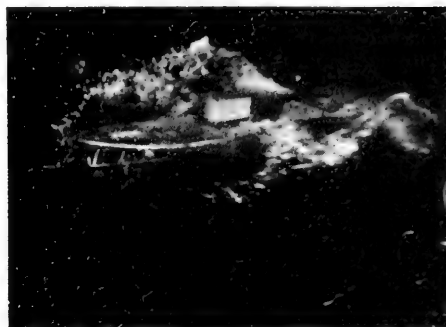

WAVES — LENGTH   45 FT   HEIGHT   4·5 FT
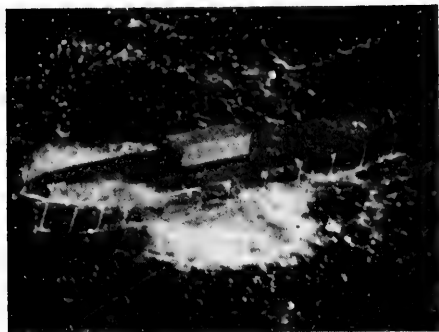

WAVES — LENGTH   95 FT   HEIGHT   4·5 FT

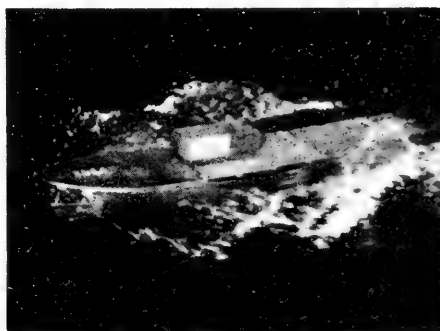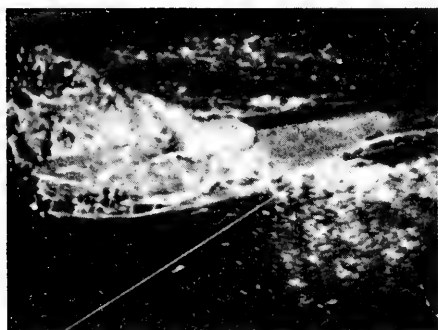Fig. 27. Behaviour of the two models of Figs. 23 and 24 in waves
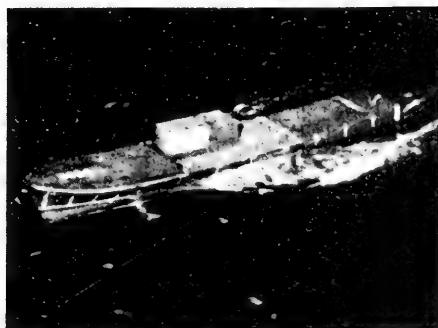
SPEED 34 KNOTS

MODEL 2117 MODEL 2084

WAVES — LENGTH 130 FT HEIGHT 4·5FT

WAVES — LENGTH 190 FT HEIGHT 4·5 FT

WAVES — LENGTH 315 FT HEIGHT 4·5FT

Fig. 28. Behaviour of the two models of Figs. 23 and 24 in waves

Table 2
Shallow Water Effect for a 51-Foot Launch in 20 Feet of Water

Speed/Depth Ratio $v/\sqrt{gD}$	Power in Shallow Water / Power in Deep Water	
	Predicted	Measured
0.720	1.0	1.285
0.850	1.25	1.364
0.867	1.5	1.330
0.885	2.00	1.313
0.915	2.50	1.270
1.010	2.50	1.120
1.080	2.00	1.035
1.170	1.50	Probably
1.230	1.25	becoming
1.370	1.00	< 1
1.400	0.95	
1.500	0.90	

FUTURE WORK ON ROUND-BILGE FORMS

While it is hoped that the preceding summary of data will be of use to the designer, it has also emphasized the scanty nature of the information presently available. Consequently, systematic investigations into high speed round-bilge forms are to be carried out as part of the research programme of the Ship Division, NPL.

The round-bilge form Model 2084 has been taken as the parent form. Systematic changes in form will cover variations in displacement, beam/draft ratio, and position of LCB, and features such as the depth and width of transom and the slope of afterbuttocks will also be varied. The displacement range will cover that shown in Fig. 7, and speed/length ratios from 1.2 to 3.5, and to 4.0 in certain cases, will be investigated.

Most of the model experiments will be made in the new large No. 3 tank at the Ship Hydrodynamics Laboratory of NPL. Its greater depth will allow higher speed/length ratios to be reached without encountering serious interference at the critical speed $v/\sqrt{gD}$, its greater size will enable larger models to be run so that reasonable size propellers can be fitted for propulsion experiments, and the wavemaker control system will facilitate experiments in irregular head and following sea conditions. The propulsion experiments will be made with at least three propellers of different pitch and diameter for each form so that data appropriate to different engine-propeller gear ratios will be obtained. Some detailed measurements of hull pressures are also planned.

DISPLACEMENT HULLS WITH PARTIAL HYDROFOIL SUPPORT

Recent studies of hydrofoil supported craft have included some interesting comparisons with high speed displacement-type hulls (e.g., Ref. 4). These naturally show that the effective lift/drag ratio, or displacement/resistance ratio, is higher for displacement hulls at low speed/length ratios, and then significantly higher for hydrofoil craft at high speed/length

ratios (say above $V/\sqrt{L} = 4.0$). The hydrofoil craft considered in these comparisons have been those in which the complete hull is above the water at the design operating speed, only a minimum of foil and support structure remaining immersed.

It seems worthwhile to consider whether a mixed-type craft has any advantages. In this the total weight of the craft and any foil support structure would be balanced partly by buoyancy, as in a conventional displacement vessel, and partly by dynamic lift generated by hydrofoils below the surface. Such a mixed type craft would thus move through the water rather as though it were a displacement vessel operating at a lighter draft than in its deep load condition. It seems possible that such a craft might have operating advantages compared with a fully supported hydrofoil craft, and consequently some preliminary estimates of the resistance of such a craft are given here.

Among the available NPL data for high speed displacement hulls are some results for one form at different displacements. These indicate that, at a fixed speed/length ratio the displacement/resistance ratio is approximately constant between full and half displacement. This enables an estimate to be made of the variation of resistance with displacement over this range. For any assumed reasonable value of the lift/drag ratio for a hydrofoil support system (which could closely resemble the simple arrangement familiar in ship roll stabilisers), it is then possible to estimate the total resistance of the partly supported mixed-type craft. Making a reasonable allowance for the additional weight of the foil support structure, it is then possible to compare the total resistances of a series of partly supported craft based on a single parent normal displacement-type hull. This simple analysis may be expressed thus:

$$r + D = R$$
$$\Delta + L = W + S$$
$$L/D = \epsilon$$
$$S = kL$$

where r — Resistance of hull remaining in water
  Δ — Displacement of hull remaining in water
L, D — Lift, drag respectively of hydrofoil system
  ϵ — Lift/drag ratio of hydrofoil system
  R — Total resistance of "mixed" craft
  W — Weight of vessel excluding foil and support structure
  S — Weight of hydrofoil and support structure
  k — Weight ratio of hydrofoil and support structure to lift of foil system.

Figure 29 shows a group of resistance curves derived on this basis from the data obtained from a model of a displacement-type craft having a full displacement of 80 tons and length 100 feet. At each speed/length ratio selected, estimates have been made for $L/D = 10$, 15, and 20 for the hydrofoil unit, and for $k = 0.15$. Variations in L/D significantly affect the result, but reasonable variations in k have little effect.

The shaded areas in Fig. 29 represent regions in which resistance, and thus power reductions are achieved. It is obvious that as L/D increases, so the possible reductions also increase. It is also clear that if displacement-type hulls can be designed so that the displacement/resistance ratio decreases with the displacement, then significant gains may also be achieved; this is now being investigated.
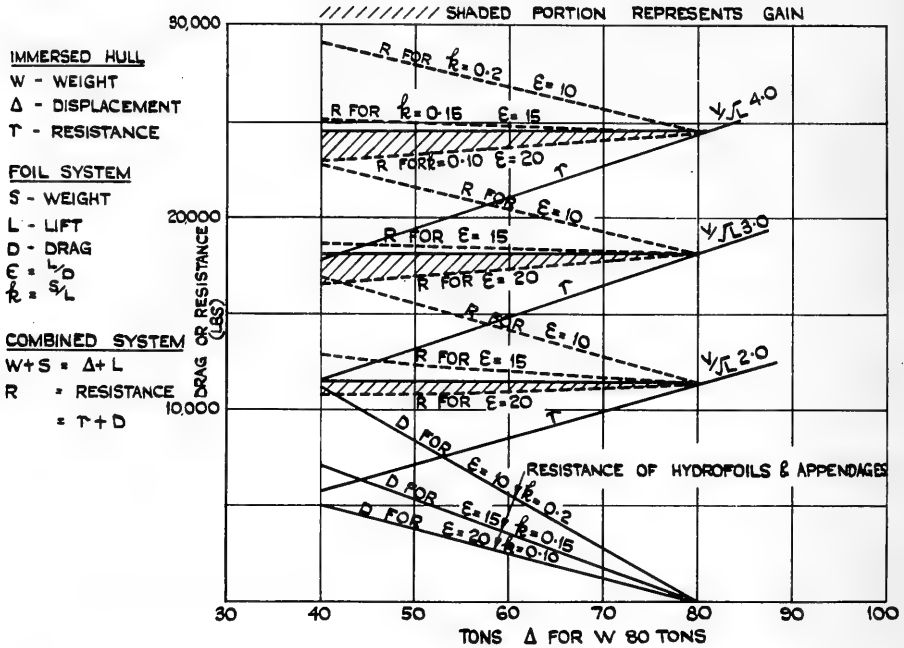
Fig. 29. Possible performance of a partially immersed 100-foot boat and fully
immersed hydrofoils

Preliminary calculations suggest that hydrofoil support systems to carry half the weight of a conventional displacement type vessel should present no serious hydrodynamic or structural design problems, even if the foils are restricted to noncavitating types.

ACKNOWLEDGMENTS

NOMENCLATURE

General

Δ = Displacement

L = Length (waterline), feet

V = Speed, knots

v = Speed, ft/sec

d = Draft, feet

B = Beam (waterline), feet

g = Gravitational constant, ft/sec^2

D = Depth of water, feet

C_B = Block coefficient

Resistance

$V/\sqrt{L}$ = Speed/length ratio

F_n = Froude number $V/\sqrt{gL}$

0_{100} = Froude skin friction coefficient for 100-foot ship

0_L = Froude skin friction coefficient for L-foot ship

Ⓢ = Wetted surface $\times 0.09346 / \Delta^{2/3}$

Ⓛ = Froude speed/length ratio = $1.055\ V/\sqrt{L}$

r/Δ = $\dfrac{Ⓒ}{1.319} \left(\dfrac{V}{\sqrt{L}}\right)^2 \dfrac{L}{\Delta^{1/3}}$

r = Resistance, pounds

Ⓒ = $\dfrac{ehp \times 427.1}{V^3 \Delta^{2/3}}$

Propulsion

t = Thrust deduction

η_h = Hull efficiency

η_r = Relative rotative efficiency

η_o = Open water propeller efficiency

η = Quasi-propulsive coefficient

w_f = Froude wake fraction

w_t = Tayler wake fraction

dhp = Delivered horsepower at propeller

ehp = Effective horsepower = Ⓒ $V^3 \Delta^{2/3} / 427.1$

Note: The constants used above are for ships in salt water.

REFERENCES

[1] Kafali, K., "The Powering of Round Bottom Motor Boats," International Shipbuilding Progress, Vol. 6, No. 54, Feb. 1959

[2] Saunders, H.E., "Hydrodynamics in Ship Design," Vol. 2, p. 408

[3] DuCane, P., "The Planing Performance, Pressures and Stresses in a High-Speed Launch," Trans. I.N.A. 98:469 (1956)

[4] Crewe, P.R., "The Hydrofoil Boat; Its History and Future Prospects," Trans. I.N.A. 100:329, Oct. 1958

APPENDIX A

NPL Small Portable Torsionmeter No. 1

This torque meter (Fig. A1) was designed to be readily portable, and to fit shafts having diameters from 1 to 6 inches without any need for removing any part of the propeller shaft. To meet these requirements a strain-guage-type meter was designed, with the gauges mounted directly on the shaft and their output leads taken through a readily dismountable slip ring assembly.

Four small resistance strain gauges are bonded to the shaft by an appropriate strain gauge cement at a position close to, and inboard of the stern gland. The gauges lie on 45-degree helices on the shaft surface, so placed that there is symmetry relative to the shaft axis and also to a plane normal to the shaft. Hence gauges respond only to torsion in the shaft and the gauge output is not affected by bending or thrust in the shaft. The gauge
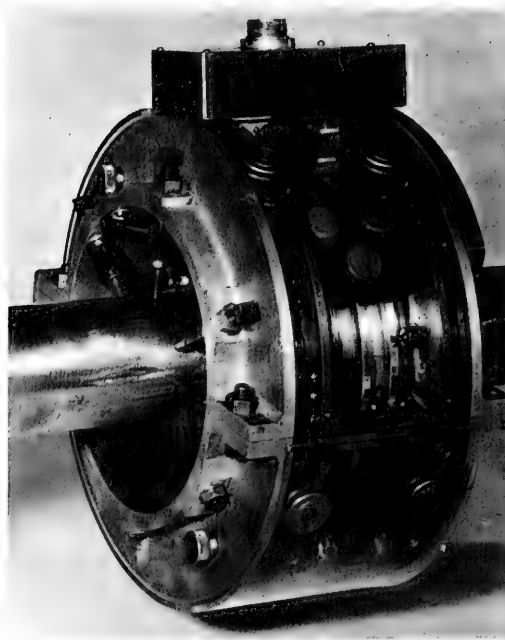

Fig. A1. Torsionmeter No. 1

leads are taken to a terminal block fixed to the shaft which is, in turn, connected to the inner unit of the slip ring assembly.

This slip ring assembly has two main units: an inner unit fixed to the shaft which carries the slip rings themselves, and which rotates with the shaft, and a fixed outer ring which carries the pickup brushes. Both units are made in two halves, so that they may each be placed around the shaft and bolted together. The inner unit of the slip ring assembly is large enough to fit around a 6-inch-diameter shaft; it is fitted to shafts of smaller diameter by inserting a distance piece in one half, and clamping the other half in place by adjustable, screwed feet. The outer unit carrying the pickup brushes is kept in position by rubber-tired rollers both radially and axially.

The five slip rings are of silver-plated brass, accurately scarphed at the joints of the two half units. Four rings are used for gauge leads, and the fifth for counting revolutions of the shaft. The brushes are of silver graphite. The gauge outputs are measured either on a Baldwin and Southwark SR 4 or a Siemens strain indicator. The complete meter is calibrated statically by applying known torques to the shaft close to the propeller when the vessel is out of the water.

The system has proved very reliable. The slip rings have behaved well, the strain readings are steady, and there is no appreciable zero drift.

DISCUSSION

Peter du Cane (Vosper Limited, Portsmouth)

We at Vosper have been interested in this paper as it discusses the range of high speed craft in which we have specialised over the last 25 years.

Within reason we agree that for $V/\sqrt{L} = 3.4$ a round-form hull as suggested by the authors would be our selection though only because if 3.4 is assumed as a maximum the probability is that for continuous cruising $V/\sqrt{L} = 2.5$ might be expected. At $V/\sqrt{L} = 3.4$ we could certainly produce a hard chine planing form with better resistance qualities than the round form and in our opinion with at least comparable seakeeping qualities.

It may be conceded that the subject of the relative merit of hard chine versus round form in waves is very relevant to this Symposium so that it is proposed to discuss it at some length:

Reference 4, which is a paper I submitted to the R.I.N.A. in 1956 and which was mainly concerned in recording extreme values, is quoted in justification of the following judgement on the qualities of the hard chine planing form: "waves no more than 3 feet in height can cause slamming decelerations up to 9 g, injurious to both structure and personnel, as recorded at sea."

It is felt there must be some misunderstanding of the data recorded in Ref. 4. Certainly there was no question of 9 g being recorded in 3-foot waves. If this is inferred

anywhere it is incorrect, though it is conceivable that such an acceleration could be recorded at say the stem in exceptional conditions of speed and irregular wave formation.

In the particular case of this reported research in Ref. 4, however, the objective was to find extremely adverse conditions which did not prove easy and eventually resulted in a slightly hazardous attempt to run across the bow wave train of the "Nieuw Amsterdam" at 35 knots.

As this bow wave train was approaching us at a speed estimated to be 14 knots the conditions of encounter were equivalent to the launch meeting the waves at (35 + 14) = 49 knots.

Under these circumstances it is not surprising that 6 g was experienced in the wheelhouse. The maximum acceleration at the stem was recorded as 8.28 g but this was in exceptionally adverse conditions.

The relative merits of the round form and the planing form (so called) are discussed at some length in Ref. 4 and in the discussion thereto.

In this connection it is interesting to mention N.P.L. Report S.H.MV. 5 of Feb. 28, 1955, where a hard chine and round form were tested in waves. It was reported that there was little to choose as regards vertical accelerations between the hard chine and the round form. If anything the accelerations appeared less in the case of the planing form and certainly the spray on decks was reported as less in the case of the planing form.

This, of course, does not accord with the comment in the paper we are now discussing which reads as follows:

"The chine form is 'stiff' in waves and tends to slam violently. The low chine forward throws water forward and up, obscuring wheelhouse vision and producing a wet ship. The round bilge form pitches more but this reduces slamming. The flare forward, which was designed with particular care, is very effective in throwing water away from the hull. The film records clearly show the superior wave performance of the chineless, round-bilge form. Although the behaviour of the hard chine form could be improved by raising the chine line forward, it was not possible to reduce its resistance to that of the round-bilge form. It is hoped that a vessel having this round-bilge form will shortly be built."

Among other comparisons between planing and hard chine craft which are available in Ref. 4 is a closely reasoned and cautious judgement made in the course of the discussion by Dr. Gawn based on his great experience at the Haslar Tank and his collated data from sea reports. His contribution is offered verbatim:

"The author makes no secret of his preference for a hard chine hull and it does appear this type can be drier and generally no less satisfactory at sea than the round bilge. There is a need for firm fact to replace some of the contentious opinions often expressed on sea behaviour, and the author's tests go some way in this direction. However, the issue is not clear cut in a general sense but depends on the size and speed of the craft. If, for example, the speed-length coefficient is less than about 3.7 there is much to be said for the round-bilge form because of its resistance advantage in calm water. If, on the other hand, as in the launch dealt with in the paper the speed is much greater, then the hard chine hull can have a clear advantage as regards resistance in calm water and in my judgement is to be recommended, provided there is no overriding emphasis on economic cruising at low speed."

Since the date of that paper, quite a lot more evidence on this matter has reached me, both from actual seagoing experience and model tests in waves. In particular and resulting from model tests carried out in irregular waves at the Davidson Laboratory of the Stevens Institute in 1959, Figs. D1 and D2 were reproduced in a report of the "Development and Running of the 'Brave' Class Fast Patrol Boat" read at Göteborg in February 1960.
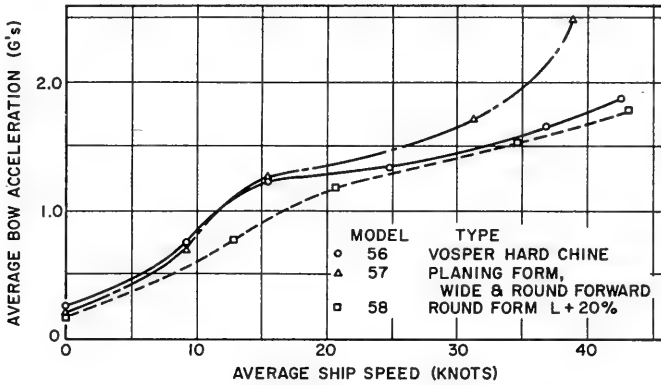

Fig. D1. Average bow acceleration versus average ship speed in an irregular head sea; Beaufort scale sea state 5; average height, 5.16 feet; signal height, 8.10 feet
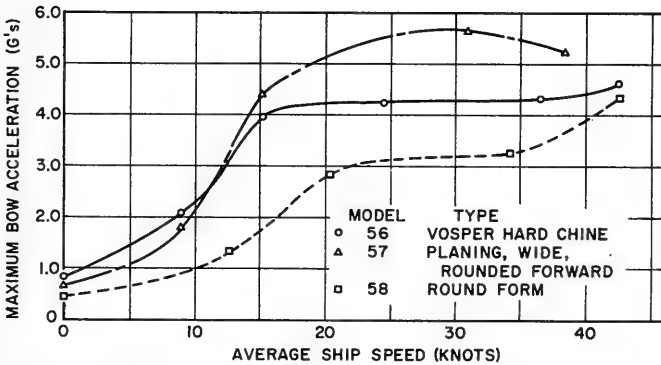
Fig. D2. Average bow acceleration versus average ship speed in an irregular head sea; Beaufort scale sea state 5; average height, 5.16 feet; signal height, 8.10 feet

This shows remarkably little difference between the round form 58 and the Vosper hard chine 56, especially when it is realised the round form was 20 percent longer for the same displacement.

To summarise, there is little to choose between the forms for speed/length ratios between say $V/\sqrt{L} = 2.5$ to 3.8. After this the hard chine planing form is a "must" for reasons of resistance.

The planing form probably *can* be made to slam more unless trim is adjustable by transom flap or similar device. Equally the round form can undoubtedly be made to bury her forecastle in the waves and wash down her bridge. Directional stability is much better in the planing form and there is less liability to yaw and broach in a following sea. In head seas the hard chine craft will lose more speed due to the energy lost in generating spray which undergoes an acceleration relatively forward and outward from rest. This feature tends to keep the decks and bridge dry.

So far we have only discussed the relative merits of the round form and hard chine planing craft and it may be appropriate to point out here that in the light of development over the years the difference between the two classes of craft which used to be clearly defined are becoming very much less.

For instance, both types are in fact planing craft in the generally accepted sense. In both types it is fully appreciated that the waves must be met from ahead by relatively soft V-shaped or rounded sections. Equally, to obtain good resistance qualities the aft sections in both types are relatively flat and wide and run to a "chine" at the sides. To control the amount of spray on deck both types work a substantial flare in forward sections leading to a "knuckle" or chine.

In fact it is probably fair to say that in theory the optimum would be represented by a rather wide form incorporating the forward sections of a round-form craft with the aft sections of a planing form. The draw-back here is that the round form leads to wetness on deck and width leads to rather excessive slamming.

Such a compromise form is represented in Figs. D1 and D2 by model 57.

As the subject of the Symposium covers high speed craft it may not be out of place here to state the admittedly personal opinion that no hydrofoil craft of the surface piercing type has given any real evidence of being able to deal with substantially rough conditions in the open sea more successfully than the round form or hard chine.

It seems possible the submerged foil arrangement as demonstrated by Dr. Hoerner during this Symposium may be superior in this respect but at the moment this awaits practical proof at sea, at least in the larger sizes.

The ground effect machine may seem to be limited at the present state of the art by the very severe effect upon lifting efficiency likely to be experienced if cushion heights suitable for passage over the ocean waves are to be generated.

Finally as a constructive suggestion we should like to suggest to the authors that we could submit for trial a hard chine planing form which would prove a much more serious competitor to the round form proposed than is the form exemplified in model 2117.

It would also be most valuable to run a hydrofoil configuration of comparable dimensions and load-carrying capacity in comparison with the above forms.

D. Savitsky (Davidson Laboratory, Stevens Institute of Technology)

I would like to comment on the interpretation given by the authors to the relative seakeeping abilities of the so-called hard chine and round-bilge boats. It is the authors'

contention that the round-bilge boat exhibits superior performance (less pitching motions and considerably less bow spray) than the hard chine boat. The point that I would like to clearly emphasize is that the existence of a hard chine or round bilge per se has no relevance to its behavior in waves. Heavy bow spray and large pitch motions are primarily dependent upon the fullness of the bow. For very sharp bow forms (high deadrise forward) the rough water behavior will be relatively mild and the development of bow spray very small. The reverse is true for a full bow (low deadrise forward). It is to be noted from the authors' paper that their round-bilge boat, which exhibited relatively mild rough water motions was indeed designed with large deadrise forward while their poorly performing hard chine boat was designed with low deadrise forward. With such design features it is expected in advance that the hard chine boat will perform poorly in waves. If the full bow is, for reasons of construction, necessarily inherent in a hard chine boat then the authors' general comments on the relative merits of each boat are correct. However, if this is not the case, that is, if high deadrise forward can be designed into each boat, then general conclusions on rough water behavior of round-bilge versus hard chine boats cannot yet be made.

In reply to the authors' plea for basic force data on planing boats, I would like to suggest the many reports prepared by the Davidson Laboratory of the Stevens Institute of Technology on this very subject. These basic experimental and analytical studies were sponsored at our laboratory by the Office of Naval Research.

E. V. Telfer (Technical University of Norway)

All I want to say is once more in connexion with presentation. In this paper the authors make the very positive statement that "again there is no clear evidence of any predominant form parameter." Against this I would like to suggest that what the authors really mean to say, but clearly do not, is that because they have adopted a basic presentation in terms of the displacement of the 100-foot ship, which is of course the Froude $Ⓜ = L/\nabla^{1/3}$ value in another form, this is clearly in itself the dominant form parameter and any other usual form parameter is likely to be of minor importance. Had the authors' diagrams such as Fig. 8 been presented in terms of $Ⓜ$ the importance of relative length on constant displacement would have been more evident and the distribution of the individual spots would have more uniformly covered the $Ⓜ$ base.

The issue is, however, not quite as simple as this. It should be noted that while at any constant displacement the $Ⓒ$ values correctly grade the corresponding powers, a comparison of the $Ⓒ$ value at one displacement does not give a direct comparison of the corresponding power ratio at any other displacement. The authors have made their $Ⓒ$ comparisons under the condition of constant $V/\sqrt{L}$, or since $L = 100$ feet, under the condition of constant speed. It follows therefore that to get the relative power ratios P_1 and P_2 for two different displacements Δ_1 and Δ_2, the respective $Ⓒ$ values must first be multiplied by the two-thirds power of their displacements. Alternatively to express the true relative power per ton displacement over the displacement range covered the $Ⓒ$ values first require multiplication by $Ⓜ$. When values of $Ⓒ$ $Ⓜ$ are plotted to the displacement base, then the comparison is both correct and compatible. The authors' presentation is neither. For example, in Fig. 8 for 200 tons displacement a $Ⓒ$ value of 4.9 may be indicated, while at 50 tons the $Ⓒ$ value is probably only 2.45 at most for the same B/d ratio. The corresponding $Ⓒ$ $Ⓜ$ comparison is thus $4.9 \times 17.1 = 84$ against $2.45 \times 27.2 = 66.6$. The 50-ton boat thus requires 79.4 percent of the power per ton displacement needed by the 200-ton boat.

The authors' presentation might have tempted the unwary to believe that the 50-ton boat was twice as efficient as the 200-ton boat. It follows therefore, since the authors' presentation has very seriously exaggerated the apparent importance of ⓜ value, that the influence of other factors will not necessarily have quite the insubordinate influence which the authors are led to believe. I am not, of course, suggesting that the authors themselves in their specialised tank practice would be at all unwary; but I do feel very strongly that all data presentation for general professional consumption should be visually correct, so that he who runs may read, and read quickly and accurately.

R. N. Newton (Admiralty Experiment Works)

Any paper which provides data which can be usefully employed by a designer is very welcome at any time or place. This paper by Messrs. Marwood and Silverleaf is just such a paper and any opportunity to add to the information they present should not be missed, for the same reason.

Experiments on high speed planing forms having been carried out at A.E.W. for many years, with forms of different lengths and coefficients, in calm water and in waves, and with various devices for improving performance, I will attempt to take this opportunity to qualify some of the statements in the paper and add to them, in a general way, in terms of the ratio of length of wave to length of craft and in terms of Froude number.

Here let me hasten to add that while I incline very much to Prof. Telfer's opinion that we should use more rational performance coefficients and parameters to show the trends arising from changes in form and displacement for the present purpose I must adhere to the commonly used ones, such as Froude number and length of wave to length of ship ratio.

First, then, speaking generally, on the effectiveness of steps in the bottom, a large number of resistance experiments conducted at A.E.W. between 1935 and 1944 led to the general conclusion that although stepped hulls had advantages over unstepped hulls in some ways, they also had inherent disadvantages and particularly increase of resistance at low speeds.

Experiments conducted with two, three, and five steps in the bottom, at different spacings and positions along the bottom indicated that these gave generally inferior performance to a single step on the same form, particularly as regards an increased tendency to porpoise and, judged by tests of one form in waves, inferior behaviour in waves.

There is an optimum position for the step which effects a comparison between reduction in resistance above planing speed, increase in resistance below planing speed, and the liability to porpoise. The risk of porpoising increases as the step is moved forward. As the step is moved aft the speed at which planing starts increases until when the step is well aft the craft can hardly be said to be planing at all in the usual sense of the word.

Secondly as regards resistance in calm water, the position of the center of gravity is critical and a small movement has a marked effect. Generally speaking a moderate stern trim in still water is an advantage at planing speeds but adds to resistance at lower speeds.

Too large a dihedral angle amidships adds to resistance due to increased running incidence and reduced rise. A low dihedral angle is good for calm water performance but detracts from behaviour in waves.

A narrow transom gives increased running trim but the effect on resistance is complicated. There is an optimum transom width depending on speed, trim, loading, and other form parameters. For high speed a wide transom is desirable, but if the width is excessive stern trim is impeded. If the width exceeds 0.8 of the maximum beam the sides of the hull may not be "clean" at top speed.

Running attitude at a given speed is mainly governed by loading and static trim, although chine dihedral, curvature, and width of transom can have appreciable effects as noted previously. Excessive trim causes high hump resistance which can lead to "locking up" of the engines. The effect of propellers is to increase the running trim by as much as 1 degree.

Next as regards resistance and motion in waves, as the authors have shown, a form which has a low calm water resistance by virtue of high running trim can be a poor boat in a seaway, particularly as regards pitch and slamming. On the other hand too small a trim leads to wetness and pounding even though slamming and motion may be reduced.

In $L/30$ waves maximum motion in ahead seas usually occurs at λ/L between 2.5 and 3.0 when the pitch is about 1.1 to 1.2 × maximum wave slope, out to out, and the heave about 1.1 × wave height.

In $L/20$ waves the maximum motion occurs at λ/L about 2.0 or less, pitch being about 1.35 × maximum wave slope and heave 0.9 × wave height.

The motion is characterised, at planing speeds, by notably small movement at the stern.

Mention is made in the paper of accelerations as high as 9 g and this has been referred to by previous speakers. Such accelerations can be produced of course but conditions on board would hardly be tenable and there would be grave risk of structural damage. Local accelerations of this order occur of course when the craft slams.

For a given maximum acceptable acceleration, which may be decided for strength or other reason, there is a limiting speed and wave slope; e.g., in a 70-foot boat if the maximum acceptable acceleration is 2 g the boat should not be driven into seas steeper than $L/20$ at speeds greater than $F_n = 0.7$. Steeper waves can only be encountered, to keep below 2 g, if they are shorter than ship length.

Now as regards the advantages of round bilge and hard chine forms there is much that can be added to the information given in the paper and among some of the more important facts are these.

In calm water the round bilge form is less resistful than the hard chine form up to at least $V/\sqrt{L} = 3.2$ ($F_n = 0.96$). Thereafter the hard chine form shows to advantage. This agrees with Fig. 25 of the paper being discussed.

In waves the resistance of the round bilge form is still less than the hard chine form up to $V/\sqrt{L} = 3.7$ ($F_n = 1.1$), but only in waves up to $3.0L$ when the difference is of small magnitude only.

As regards motion in waves it is necessary, I think, to qualify the statement in the subsection of the paper titled "Design of a Round-Bilge Form for Good Seakeeping" in terms of F_n and L_w/L_s.

Up to a certain speed, usually about $F_n = 0.7$, both pitch and heave in ahead seas are greater for the round-bilge boat, and less than the hard chine boat beyond this speed. This applies in waves up to 1.5 or 2.0L. In longer waves the round-bilge form continues to pitch more but there is little difference in heave between the two forms.

In the following seas the pitch of the round-bilge form is slightly greater in waves up to 2.0L and slightly less in longer waves. The reverse is true of heave.

In shallow seas the accelerations at the fore end of the round-bilge form are slightly higher than for the hard chine design, and this corresponds with the slightly greater pitch and heave. Accelerations at the after end are much the same for both designs. In steeper seas the accelerations of the hard chine form are greater both at the fore end and at the after end.

Slamming is generally more pronounced in the hard chine form for the same still-water loading condition as regards displacement and running trim.

With regard to wetness, as would be expected the water is thrown low and clear by the hard chine forms and higher and nearer the hull in the round bilge form, although both are generally dry in seas dead ahead. The effect of wind on the bow is to increase the degree of wetness, and the round-bilge form is wetter than the hard chine in this condition.

Finally there is one feature of high speed craft, of which the paper makes no mention, which I should like to remark on briefly, viz., the use of a transom flap in the form of a plate hinged at the lower edge of the transom so as to be adjustable and generally about 1/20th the length of the craft in width.

Model experiments show that in calm water running, stern trim and rise are reduced by the use of a transom flap at all speeds, from which it might be expected that the resistance would also be reduced at all speeds. In fact the measured model resistance is reduced by the use of a flap only up to a moderate speed, beyond which it increases, compared with no flap.

Nevertheless sea trials have shown that the flap improves the speed up to full power due to the change in interaction between hull and propellers having a favourable effect upon the hull efficiency elements. For a model of a 70-foot-long hull the augment of resistance was reduced and the wake increased to give an increase in hull efficiency of 8% at top speed, for a flap angle of 5 degrees.

Both model experiments and sea trials have demonstrated, however, that as the maximum speed increases, or as displacement decreases, the flap becomes less effective and smaller angles of incidence of the flap are required to obtain maximum effect. Ultimately a condition will be reached when the flap is of no propulsive advantage. One explanation, or part explanation, for this may be that in designs with high top speed, not fitted with a flap, the running trim ceases to increase above a certain speed and then begins to reduce, although rise may still continue to increase. Full consideration must be given to this fact when contemplating the incorporation of a transom flap in a new design.

As regards behaviour in a seaway in waves less than ship length and height, in the region of $L/30$ the flap has an appreciable effect upon pitch or heave at any speed. In waves of critical length about 2.5L when motion is usually severe the flap reduces the pitch and heave by about 10 percent.

In longer and steeper waves around 2 ship lengths and height $L/20$ and at F_n greater than 1.1 there is a more significant decrease in both pitch and heave of the order of 30 percent and 45 percent respectively.

At these high speeds, however, there is a grave danger of the craft plunging. In fact during one experiment with a model at $F_n = 1.4$ the model buried so deeply into the slope of the oncoming wave as to cause it to sink. Obviously in such conditions the ship would suffer grave damage or loss.

In following seas the use of a flap or wedge introduces a distinct tendency of the model to bury into the slope of the wave — much more so than in ahead seas. For instance, in the case mentioned previously the same model, in waves $1.5L$ using 5-degree flap incidence, plunged and sank at $F_n = 1.4$. The same occurred also at the same speed in waves $2.5L$. In longer wavelengths the model could only be controlled with difficulty and then only up to $F_n = 1.06$, when there was still a tendency to broach-to.

As a result of close study of films of models in waves and experimental data a general conclusion can be drawn. This is that whereas a transom flap can prove of advantage propulsively in calm weather, the degree of this advantage being determined by consideration of the top speed and displacement, before the flap can be used to improve the motion in waves, i.e., to make conditions on board more comfortable, it is essential for the operators to be able to recognise the sea conditions at the time, or to be provided with some scientific indication that the craft might be in danger. There is no doubt that with long experience of such craft, judgment can be placed upon the "average" length and height of sea which may be running, but this is very different from being able to predict the length and height of oncoming waves. For the time being, therefore, until much more research has been done into the statistics of wave spectra in a given ocean area, and until such time as the spectrum can be indicated with some degree of reliability, the use of transom flaps in rough weather cannot be recommended — at least not for craft designed for really high speed, say beyond 45 knots.

In conclusion it is perhaps pertinent to remark, in the light of these general observations that any change of form, or device, introduced into a new design, although it may improve performance from one aspect, may well detract from it in another aspect, and a compromise is very often necessary, and can only be found by careful model experiments.

K. C. Barnaby (John I. Thornycroft Company, Southampton)

The authors of this interesting paper referred to the difficulty of finding a suitable parameter for expressing their data. It is, of course, obvious that a conventional constant such as Ⓒ is quite unsuitable. Once dynamic lift has taken charge, the wetted surface is no longer constant, but must diminish rapidly since the product $C_1 \tfrac{1}{2} \rho S V^2$ must always be less than the original displacement *weight*, by at least the amount of submerged hydrostatic buoyancy. Also, the resistance to motion increases with approximately V and very definitely not with V^2. Thus both the terms $\Delta^{2/3}$ and V^3 become incorrect at high speeds.

The one factor that cannot change as the speed increases is the actual weight and this forms the basis of a suitable parameter. If one plots the ratio $R/\Delta V$, that is, the total resistance expressed in pounds per ton divided by the speed in knots, for a common parent form at various displacement ratios and speeds, a family of curves is obtained that, at sufficiently high speed/length ratios will merge into one line that is nearly independent of

displacement ratio and varies only slightly with speed. In general, there will be a slight increase with speed, except in the case of round-form hulls, which usually show a slight falling off.

This parameter $R/\Delta V$ is conveniently expressed in the modified form of $K = V/\sqrt{bhp/\Delta}$, where K is a constant depending on the type of craft and the static waterline length (or perhaps more correctly the beam as being an unaltered dimension). I have examined several hundred cases. Those giving $R/\Delta V$ directly have mainly come from tests at Mr. Thornycroft's Fort Steyne Model Basin. The more numerous K values have come from trial results and from published data. In no case have I found any wide discrepancy from Table D1. These latter are of course only approximate, but in naval architecture practice it is often more useful to have an approximation that can be made in a few minutes than a more elaborate method which takes a considerable time. The approximation can at least show whether a proposal is feasible or quite impossible.

Table D1
Values of the Constant K in the Formula* $K = V/\sqrt{bhp/\Delta}$
for Planing and Semiplaning Types

Length (ft)	Value of K for Various Types of Hull and Limits of Speed/Length Ratio			
	Round bottom, transom stern, very flat aft	V-Chine, stepless	Stepped	Hydrofoil
	$V/\sqrt{L} = 2.5\text{-}3.5$	$V/\sqrt{L} = 2.75\text{-}4.5$	$V/\sqrt{L} = 3.5\text{-}6.5$	Up to 60 knots
20	2.25	2.75	3.6	5.3
30	2.60	3.10	3.96	5.5
40	3.05	3.65	4.3	5.7
50	3.34	4.00	4.6	5.9
60	3.45	4.20	4.8	6.1

*Δ in tons and V in knots.

Surprise may be expressed at the inclusion of round-bottom craft in the table. It is however necessary for such a type to have a transom stern and a very flat stern in order to reach speed length ratios of over $V/\sqrt{L} = 2.5$. Under these circumstances, the stern lines are not very different from those of a normal V-chine type and a nearly comparable amount of dynamic lift can be obtained at high speeds. The increased drag due to the round bilge is however reflected in lower K values. It is assumed in all cases that the form is suitable for the speed and runs cleanly with a suppressed bow wave that does not lap high up the side but is deflected outwards. It is also assumed that the propulsive efficiency is normal, say, about 0.6.

Powering figures stated by Mr Rader, during the meeting, give a K of 4.76 at 40 knots, increasing to 4.90 at 55 knots. These were for a 100-ton V-chine hull of about 50 percent increased length over the maximum table length. They are thus in line with the table values.

J. B. Hadler and E. P. Clement (David Taylor Model Basin)

The authors have suggested that a high speed displacement-type hull combined with partial hydrofoil support may show performance which is superior to that of a conventional boat. A number of years ago the Model Basin gave consideration to the same suggestion and established a program of investigation under our Bureau of Ships Fundamental Hydro-mechanics Research Program. A partial support hydrofoil system, composed of two sub-merged foils, each on a strut attached to the side of the hull were installed on a model of the U.S. Navy 52-foot aircraft rescue boat. These foils were arranged such that their fore and aft location could be varied as well as their angle of attack. The optimum location for these foils was 32.7 percent of the length forward of the center of gravity, and at a minus 3-1/2 degree angle to the keel of the boat. At this condition the resistance was reduced throughout most of the higher speed range. For speeds below 15 knots, the resistance of the hybrid craft was somewhat greater. Between 15 knots and 30 knots the resistance decreased to about 75 percent of that of the conventional craft. Between 30 knots and 40 knots, the average reduction in resistance was about 25 percent. Although these results indicated favorable performance for the hybrid craft, no further work was undertaken at the Model Basin because of the urgency of the hydrofoil program itself. Further research should be continued in this area, particularly in investigating the performance of the hybrid craft in seaways and with foils of the surface-piercing type. The full details of this work are contained in a Model Basin report entitled, "Tests of a Planing Boat Model with Partial Hydrofoil Support," TMB Report 1254 dated August 1958.

The resistance data for high speed displacement-type hulls which are made available in the paper are very welcome. A similar presentation was made by H. F. Nordstrom in his 1951 publication, "Some Tests with Models of Small Vessels," but in that paper the maximum speeds are considerably below the maximum speeds for which data are given in the present paper. The data on the components of propulsive efficiency are particularly interesting and valuable, since little information of this kind has been previously made available. It is noted that there is considerable scatter in the plots of these data, however, presumably because of significant difference in the hull forms and appendages of the boats represented. The usefulness of the data would be enhanced considerably if the authors would provide some additional information on those designs which were self-propelled. A profile drawing of the stern, including the appendages, would be particularly helpful. This would make it possible for designers to select values of wake and thrust deduction for the design most like the one with which they were concerned at the moment, and thereby obtain assistance in making accurate predictions of performance.

W. J. Marwood and A. Silverleaf

The authors first wish to thank all those who contributed to the discussion of this paper; their comments have greatly enhanced its value.

Several contributors have discussed the relative merits of round-bilge and hard chine hull forms; however, the aim of the paper was solely to provide data on high speed displacement-type hulls, and there was no desire to make comparisons of a general nature between different basic forms. Commander du Cane's views on this important practical point naturally deserve close attention, but it is necessary to use carefully defined terms when comparing hull forms. The round-bilge form as defined and described in the paper is without any chine or knuckle line which could affect the flow, and is in extreme contrast to the hard chine form used in some of the experiments in waves. Forms of these two types

can be designed to differ much less, and the differences between them in performance will then also be much less. Indeed, the round-bilge form as quoted by Cdr. du Cane retains a chine line forward and aft intended to influence the flow pattern.

There seems to be some doubt as to the correct interpretation of some of the results given by Cdr. du Cane in Ref. 4. Table IV of that paper gives for Run 35 the maximum acceleration in the fore peak (position A1) as 8.36 g in waves 2 to 3 feet high. On the other hand, Table III gives a value of 2.86 g for the same run; this may be an average value of the measured acceleration, and agrees well with model values measured at N.P.L.

The experiments quoted by Dr. Graff, carried out in Duisburg with high power round-bilge forms in deep and shallow water, are of considerable interest. A full account of these experiments has been given,* and the results show the same characteristics as those given here for similar experiments. However, detailed comparison shows some differences in the absolute values of resistance coefficients, and these discrepancies emphasise the need for further investigations of shallow water effects.

Mr. Newton's contribution is a most valuable addition to the paper, for which we are very grateful. In drawing on the extensive store of information available at Haslar he has raised many points which we are not qualified to discuss, and we shall restrict our comments to four of the topics he mentions. First, we agree that a narrow transom does give increased running trim, but only for speed/length ratios $V/\sqrt{L}$ greater than 1.8, and it then also increases the resistance. However, at lower speeds, particularly below the resistance hump around $V/\sqrt{L} = 1.5$, when there is little or no hydrodynamic lift, a narrow transom is found to decrease resistance. Indeed, at lower speeds still it becomes advantageous to fit a cruiser stern. Second, we are slightly surprised at Mr. Newton's statement that propellers increase running trim significantly. Provided the model is towed along the shaft axis when the resistance and trim are measured, we should not expect the trim to alter appreciably when it is self-propelled, unless the propellers have a marked influence on the average surface pressures over the after body. Third, we agree that at planing speeds the pitching centre is well aft; indeed, it can be aft of the transom. Fourth, experiments made at N.P.L. support Mr. Newton's views about transom flaps. Attempts to turn or "hook" the extreme afterbuttock lines have also succeeded in reducing calm water resistance. However, we believe that, in a vessel designed to operate mostly at one speed, transom flaps are only needed when the basic hull design is faulty. For a vessel intended to operate at several different speeds, the fitting of flaps is more easily justified. Some interesting effects of flaps on heave and pitch have been observed in experiments at N.P.L., and these agree well with the comments made by Mr. Newton.

Mr. Savitsky points out that the terms round bilge and hard chine are not satisfactory descriptions for comparing ship performance in waves. We agree with this criticism, and agree also that the deadrise angle forward is a more realistic criterion to adopt. The principal justification for the descriptive terms used in this paper is that they are commonly employed by naval architects, and it was hoped that they would be sufficiently precise for the purposes of this preliminary report. We must also apologise for not referring explicitly to the Davidson Laboratory reports on planing craft.

---

* W. Sturtzel and W. Graff, "Systematische Untersuchungen von Kleinschiffsformen auf Flachem Wasser im Unter- und Uberkritischen Geschwindigkeitsbereich," Report 617, Versuchsanstalt für Binnenschiffbau, Duisburg, 1958.

Professor Telfer rightly draws attention to our statement that "again there is no clear evidence of any predominant form parameter." We agree that, for clarity, this would have been better if qualified by the important reservation "apart from displacement/length ratio or its equivalent Ⓜ ." We also agree that a presentation based on Ⓜ would be better than one with displacement alone as basis. Professor Telfer's advocacy of Ⓒ Ⓜ as the best criterion for power comparisons at different displacements also has much to commend it. However, we were primarily concerned with presenting the basic information as simply as possible, and presumed that those who used it would know how to do so correctly.

Mr. Barnaby also advocates an alternative basis of comparison. However, his factor $K = V\sqrt{\Delta}/P$ also has disadvantages. It has the dimensions of a velocity, and it seems that a nondimensional factor $K/\sqrt{V}$ would serve Mr. Barnaby's purpose better. This is closely related to what is sometimes called transport efficiency, and when the values quoted by Mr. Barnaby are converted into this form the very valid practical advantages which he claims for this type of comparison factor are demonstrated more clearly. It is also worth pointing out that much of the data given in the paper are for speeds at which hydrodynamic lift is relatively unimportant, and to that extent Ⓒ is still a reasonable drag criterion.

The comments of Mr. Hadler and Mr. Clement also form a valuable addition to the paper. We hope that further work will be undertaken at DTMB and other establishments to examine the potentialities of hybrid craft with partial hydrofoil support. The additional information requested on details of propulsion arrangements will be included in a subsequent paper intended to give results of systematic propulsion experiments with models of high speed displacement-type hulls.

*   *   *

AUTHOR INDEX